EVOLUTION AND ONTOGENY OF HADROSAURS (DINOSAURIA: ORNITHISCHIA) IN THE JUDITH RIVER FORMATION (LATE CRETACEOUS: CAMPANIAN) OF NORTHCENTRAL MONTANA

by

Elizabeth Anne Freedman

A dissertation submitted in partial fulfillment
of the requirements for the degree

of

Doctor of Philosophy

in

Earth Sciences

MONTANA STATE UNIVERSITY
Bozeman, Montana

April 2015

©COPYRIGHT

by

Elizabeth Anne Freedman

2015

All Rights Reserved

DEDICATION

This dissertation is dedicated to the memory of Cliff Ulmen, longtime friend of Montana paleontology, who shared his kindness and his coulee, and inspired his family to continue building friendships that span generations.

ACKNOWLEDGEMENTS

Immeasurable thanks go to my advisor, Jack Horner, for inviting a freshly-graduated high school student to come to Montana and dig dinosaurs, and continuing to support me along every step leading to this dissertation. I am forever grateful to Jack for providing me the opportunity to work in the spectacular field area of Kennedy Coulee, and for introducing me to Dan and Lila Redding and their family. Thanks to Dan and Lila for many years of hospitality, friendship, and logistical support with their tractors, magical garage full of tools, and menagerie of animals. I appreciate all of the friendship and support from everyone in Rudyard and the surrounding communities. Great thanks to Dan and Lila for donating the "Rocky" *Gryposaurus* bonebed specimens to the Museum of the Rockies, and great thanks to Nolan and Cheryl Fladstol and John and Claire Wendland for donating the "Superduck" brachylophosaur specimen. Fieldwork and research funding was generously provided to Jack Horner by the Ameya Preserve, Nathan Myhrvold, Damaris Wagoner, David Sands, Ellis Short, and other generous donors to the Museum of the Rockies; and to the author by the Geological Society of America, Tampa Bay Fossil Club and the MSU Dept. of Cell Biology and Neuroscience. Travel funding was generously provided by the Welles Research Fund (UCMP), Fritz Travel Grant (ROM), Jackson School of Geosciences (SVP), and the College of Letters and Science (MSU). Thanks to my committee members Dave Varricchio, Don Brinkman, Matt Lavin, and Aleks Rebane for reading and editing these papers. Thanks also to my very patient family, Mark, Karen, Matt, and Kevin Freedman, and to my husband Denver for talking about dinosaurs 24 hours a day.

TABLE OF CONTENTS

1. INTRODUCTION TO DISSERTATION 1

Literature Cited 7

2. A NEW BRACHYLOPHOSAURIN HADROSAUR (DINOSAURIA: ORNITHISCHIA) WITH AN INTERMEDIATE NASAL CREST FROM THE CAMPANIAN JUDITH RIVER FORMATION OF NORTHCENTRAL MONTANA 9

Contribution of Authors and Co-Authors 9
Manuscript Information Page 10
Abstract 11
Background 11
Methodology/Principle Findings 11
Conclusions/Significance 12
Introduction 12
Institutional Abbreviations 14
Study Areas 14
Materials and Methods 18
Nomenclatural Acts 22
Systematic Paleontology 22
Brachylophosaurini Gates et al., 2011 23
Definition 23
Diagnosis 23
Referred Material 23
Horizon and Locality 23
Brachylophosaurus canadensis Sternberg, 1953 24
Holotype 24
Referred Material 24
Emended Diagnosis 24
Horizons and Localities 24
Probrachylophosaurus gen. nov. 25
Type Species 25
Etymology 25
Diagnosis 25
Probrachylophosaurus bergei sp. nov 25
Holotype 25
Referred Specimen 26
Etymology 26
Horizon and Locality 26
Diagnosis 27

TABLE OF CONTENTS - CONTINUED

Osteological Description....28
Skull....29
Maxillary/Facial Complex....29
Premaxilla....29
Maxilla....29
Jugal....31
Lacrimal....33
Nasal....33
Prefrontal....36
Frontal....36
Parietal....39
Postorbital....39
Squamosal....40
Quadrate....42
Quadratojugal....43
Braincase....43
Palate....45
Mandible....45
Predentary....45
Dentary....45
Surangular....48
Postcrania....48
Vertebrae....48
Pelvis and Hindlimb....49
Pathologies....49
Summary of Morphology Comparisons Among *Probrachylophosaurus* and Other Brachylophosaurins....50
Phylogenetic Analyses....53
Analyses based on matrix of Prieto-Márquez (2010a)....53
Analysis based on matrix of Gates et al. (2011)....57
Phylogenetic Relationships....58
Histology....61
Histologic Maturity....64
Discussion....66
Conclusions....71
Acknowledgements....73
Literature Cited....109

3. TAPHONOMY OF A *GRYPOSAURUS* HADROSAUR BONEBED FROM THE JUDITH RIVER FORMATION (CAMPANIAN) OF NORTHCENTRAL MONTANA....116

TABLE OF CONTENTS - CONTINUED

Contribution of Authors and Co-Authors 116
Manuscript Information Page 117
Abstract 118
Introduction 119
Geologic Setting 120
Methods 121
Lithology and Non-Hadrosaur Fossils 121
Size Classes 122
Skeletal Element Abundances 124
Skeletal Maturity 125
Results 127
Lithology and Non-Vertebrate Fossils 128
Vertebrate Microfossils 130
Bonebed Taphonomy 132
Size Classes 134
Skeletal Element Abundances 137
Immaturity of Individuals 140
Histology 141
Pathologies and Bone Modification 145
Discussion 146
Bonebed Age Structure 148
Cause of Death 154
Drought 154
Drowning 155
Predation 155
Disease 156
Bonebed Deposition 157
Debris Flow Deposition 157
Overbank Flood and Lacustrine Deposition 158
Conclusions 162
Acknowledgements 164
Literature Cited 180

4. A NEW SPECIES OF *GRYPOSAURUS* (DINOSAURIA: ORNITHISCHIA) FROM THE JUDITH RIVER FORMATION OF NORTHCENTRAL MONTANA 185

Contribution of Authors and Co-Authors 185
Manuscript Information Page 186
Abstract 187
Introduction 188
Study Area 189

TABLE OF CONTENTS - CONTINUED

Institutional Abbreviations 191
Materials and Methods 191
Systematic Paleontology 195
Gryposaurus Lambe, 1914 196
Type Species 196
Holotype 196
Referred Material 196
Horizons and Localities 196
Revised Diagnosis 196
Remarks 197
Gryposaurus reddingi sp. nov 197
Holotype 197
Referred Material 197
Etymology 197
Horizon and Locality 197
Diagnosis 198
Osteological Description 198
Size Classes 200
Maxillary/Facial Complex 202
Premaxilla 202
Nasal 203
Maxilla 207
Jugal 209
Lacrimal 211
Prefrontal 212
Postorbital 213
Braincase and Posterior Skull 214
Frontal 214
Parietal 220
Presphenoid 222
Orbitosphenoid 223
Laterosphenoid 223
Basisphenoid and Parasphenoid 223
Prootic 224
Opisthotic-Exoccipital 225
Supraoccipital 226
Basioccipital 227
Palatoquadrate Complex 227
Squamosal 227
Quadratojugal 228
Quadrate 228
Pterygoid 229

TABLE OF CONTENTS - CONTINUED

Ectopterygoid....229
Palatine....230
Vomer....230
Mandibular Complex....230
Predentary....230
Dentary....231
Surangular....233
Splenial....234
Angular....234
Articular....234
Morphologic Comparisons Summary....234
Phylogenetic Analysis....235
Geometric Morphometric Analysis....237
Discussion....238
Conclusion....242
Acknowledgements....243
Literature Cited....281

5. A PHOTOGRAPHIC ATLAS OF THE POSTCRANIAL ANATOMY OF *GRYPOSAURUS REDDINGI* (DINOSAURIA: HADROSAURIDAE)....286

Contribution of Authors and Co-Authors....286
Manuscript Information Page....287
Abstract....288
Introduction....288
Institutional Abbreviations....290
Materials and Methods....290
Osteological Description....293
Axial Skeleton....293
Pectoral Girdle....294
Forelimb....295
Pelvic Girdle....297
Hindlimb....300
Conclusion....301
Acknowledgements....302
Literature Cited....331

6. CONCLUSIONS....333

Literature Cited....335

TABLE OF CONTENTS - CONTINUED

REFERENCES CITED.....336

APPENDICES 351

APPENDIX A: Ray Teeth Identification.....352
APPENDIX B: Ray Teeth from Oldman Formation Equivalent Localities in the Judith River Formation of Montana.....356
APPENDIX C: Character Matrix Based on Prieto-Márquez (2010) with All Characters Included, in Nexus Format 358
APPENDIX D: Character Matrix Based on Prieto-Márquez (2010) with Some Characters Excluded, in Nexus Format 366
APPENDIX E: Character Matrix Based on Gates et al. (2011), in Nexus Format.....375
APPENDIX F: Phylogeny of Hadrosaurines Based on Prieto-Márquez (2010).....378
APPENDIX G: High Resolution Color Quarry Map of Excavated Bones in the JR-429 *Gryposaurus* bonebed 381
APPENDIX H: Taphonomic Data Table for All Specimens (MOR 2573) Collected from the JR-429 *Gryposaurus* bonebed.....383
APPENDIX I: Character Matrix Based on Prieto-Márquez (2014), in Nexus Format.....470

LIST OF TABLES

Table Page

2.1. Radiometric date recalibrations 75

2.2. List of Brachylophosaurini specimens examined in this paper 77

2.3. Size comparisons of MOR 2919 and other selected Brachylophosaurini specimens 79

3.1. Relative abundances of vertebrate microfossils from the JR-429 bonebed compared to other lower Oldman Formation microsites 166

3.2. Abrasion and completeness stages of prepared bones from the JR-429 bonebed....167

3.3. Relative sizes of bones from smaller size class versus larger size class....167

3.4. Abundances of skeletal element types....168

3.5. Tibial histology growth zone circumferences of MOR 2573 and comparative specimens....169

4.1. *Gryposaurus* and other Kritosaurini specimens used for morphologic comparisons, in approximate stratigraphic order 245

4.2. Dentary and maxilla measurements for *Gryposaurus* specimens....250

4.3. Frontal length and width measurements for *Gryposaurus* specimens....251

LIST OF FIGURES

Figure Page

2.1. Generalized regional cross section of the Judith River Formation and its stratigraphic equivalents, with brachylophosaurin distribution 80

2.2. Map of Brachylophosaurini localities in Montana and southern Alberta....81

2.3. Stratigraphic section at *Probrachylophosaurus bergei* holotype (MOR 2919) quarry, MOR locality JR-518....82

2.4. *Probrachylophosaurus bergei* skull reconstruction....83

2.5. Brachylophosaurinan maxillae 84

2.6. Brachylophosaurinan jugals....85

2.7. Brachylophosaurinan lacrimals....86

2.8. *Probrachylophosaurus bergei* nasals....87

2.9. Brachylophosaurinan nasals, posterior view 88

2.10. Subadult *Brachylophosaurus canadensis* braincase MOR 940 in dorsal view, with nasals that do not form an overhanging crest 89

2.11. Posterior migration of brachylophosaurinan nasofrontal suture with ontogeny and stratigraphic age 90

2.12. Posterior migration and enlargement of nasofrontal suture with growth in brachylophosaurinans 91

2.13. *Probrachylophosaurus bergei* postorbital and squamosal....92

2.14. *Probrachylophosaurus bergei* quadrates 93

2.15. *Probrachylophosaurus bergei* braincase 94

2.16. *Probrachylophosaurus bergei* mandible 95

LIST OF FIGURES – CONTINUED

Figure Page

2.17. Taxonomic distribution and ontogenetic development of caudodorsal point on coronoid process of dentary 96

2.18. *Probrachylophosaurus bergei* cervical and dorsal vertebrae 97

2.19. *Probrachylophosaurus bergei* caudal vertebrae 98

2.20. *Probrachylophosaurus bergei* pelvic elements 99

2.21. *Probrachylophosaurus bergei* hindlimb elements....100

2.22. Time-calibrated phylogeny of hadrosaurines based on Prieto-Márquez (2010a)....101

2.23. Time-calibrated phylogeny of hadrosaurines based on Gates et al. (2011)....102

2.24. Tibial histology of MOR 2919, mid-diaphyseal cross-section. 103

2.25. Outer cortical histology of MOR 2919 tibia....104

2.26. Growth curves of tibial cortical circumference at each line of arrested growth in *Probrachylophosaurus bergei* (MOR 2919) and *Maiasaura peeblesorum* (MOR 758 NC-7-4-96-16 "T46").....105

2.27. Remodeled "fountain" of secondary osteons on anterolateral side of cortex, MOR 2919 tibia 106

2.28. Outer cortical histology of MOR 794 *Brachylophosaurus canadensis* femur....107

2.29. Ontogenetic and anagenetic hypothesis of brachylophosaurin evolution....108

3.1. Stratigraphic section of Kennedy Coulee, northcentral Montana, Judith River Formation....170

LIST OF FIGURES – CONTINUED

Figure Page

3.2. Quarry map of excavated bones in the JR-429 *Gryposaurus* sp. bonebed 171

3.3. Quarry maps showing distribution of each skeletal element type. 172

3.4. Microfossil material from the JR-429 bonebed horizon 173

3.5. Fossil wood impression 174

3.6. Bidirectional rose diagram of elongate bone orientations 175

3.7. Size range of large rib heads 176

3.8. Size distribution histograms of specimens by element type 177

3.9. Tibial histology of *Gryposaurus* "subadult" MOR 2573-6-12-06-17 178

3.10. Coprolite floating clast taphonomy 179

4.1. Generalized regional cross sections of the Judith River Formation and its stratigraphic equivalents, with distribution of *Gryposaurus* species 252

4.2. Stratigraphic section of Kennedy Coulee, northcentral Montana, Judith River Formation. 253

4.3. Nasals of *Gryposaurus* and other Kritosaurini 254

4.4. Landmark selection points for geometric morphometric analysis. 256

4.5. Skull reconstruction of *Gryposaurus reddingi*, MOR 2573. 257

4.6. Premaxillae of *Gryposaurus reddingi*, MOR 2573 258

4.7. Nasals of *Gryposaurus reddingi*, MOR 2573 259

4.8. Maxillae of *Gryposaurus reddingi*, MOR 2573 260

LIST OF FIGURES – CONTINUED

Figure Page

4.9. Length of tooth battery versus number of tooth rows in *Gryposaurus* maxillae and dentaries 261

4.10. Jugals of *Gryposaurus reddingi*, MOR 2573.....262

4.11. Lacrimals of *Gryposaurus reddingi*, MOR 2573.....262

4.12. Prefrontals of *Gryposaurus reddingi*, MOR 2573 263

4.13. Postorbitals of *Gryposaurus reddingi*, MOR 2573.....264

4.14. Frontals and parietals of *Gryposaurus reddingi*, MOR 2573 264

4.15. Presphenoid of *Gryposaurus reddingi*, MOR 2573.....266

4.16. Laterosphenoids of *Gryposaurus reddingi*, MOR 2573 267

4.17. Basisphenoids of *Gryposaurus reddingi*, MOR 2573 268

4.18. Articulated prootic, exoccipital, and supraoccipital of *Gryposaurus reddingi*, MOR 2573-7-10-10-414.....269

4.19. Opisthotic-Exoccipitals of *Gryposaurus reddingi*, MOR 2573.....270

4.20. Squamosal of *Gryposaurus reddingi*, MOR 2573 271

4.21. Quadratojugal of *Gryposaurus reddingi*, MOR 2573.....272

4.22. Quadrates of *Gryposaurus reddingi*, MOR 2573 273

4.23. Vomer of *Gryposaurus reddingi*, MOR 2573 274

4.24. Dentaries of *Gryposaurus reddingi*, MOR 2573 275

4.25. Surangulars of *Gryposaurus reddingi*, MOR 2573 276

4.26. Splenial of *Gryposaurus reddingi*, MOR 2573 277

LIST OF FIGURES – CONTINUED

Figure Page

4.27. Strict consensus tree of the three most parsimonious phylogenetic trees....278

4.28. Geometric morphometric Principal Components Analysis of nasal shape of *Gryposaurus* and other Kritosaurini specimens....279

4.29. Ontogenetic and anagenetic hypothesis of *Gryposaurus* evolution....280

5.1. Cervical vertebrae of *Gryposaurus reddingi*, MOR 2573....303

5.2. Dorsal vertebrae of *Gryposaurus reddingi*, MOR 2573....304

5.3. Disarticulated caudal neural arches of *Gryposaurus reddingi*, MOR 2573....305

5.4. Caudal centra of *Gryposaurus reddingi*, MOR 2573....307

5.5. Chevrons of *Gryposaurus reddingi*, MOR 2573....309

5.6. Ribs of *Gryposaurus reddingi*, MOR 2573....310

5.7. Partial sternal of *Gryposaurus reddingi*, MOR 2573....311

5.8. Scapulae of *Gryposaurus reddingi*, MOR 2573....312

5.9. Humeri of *Gryposaurus reddingi*, MOR 2573....313

5.10. Ulnae of *Gryposaurus reddingi*, MOR 2573....315

5.11. Radii of *Gryposaurus reddingi*, MOR 2573....316

5.12. Metacarpals of *Gryposaurus reddingi*, MOR 2573....317

5.13. Manual phalanges of *Gryposaurus reddingi*, MOR 2573....318

5.14. Ilia of *Gryposaurus reddingi*, MOR 2573....320

5.15. Ischia of *Gryposaurus reddingi*, MOR 2573....321

LIST OF FIGURES – CONTINUED

Figure Page

5.16. Pubes of *Gryposaurus reddingi*, MOR 2573 321

5.17. Femora of *Gryposaurus reddingi*, MOR 2573 322

5.18. Tibiae of *Gryposaurus reddingi*, MOR 2573 323

5.19. Fibulae of *Gryposaurus reddingi*, MOR 2573.....324

5.20. Astragalus of *Gryposaurus reddingi*, MOR 2573 324

5.21. Metatarsal IIs of *Gryposaurus reddingi*, MOR 2573 325

5.22. Metatarsal IIIs of *Gryposaurus reddingi*, MOR 2573 325

5.23. Metatarsal IVs of *Gryposaurus reddingi*, MOR 2573 327

5.24. Pedal phalanges of digit II of *Gryposaurus reddingi*, MOR 2573 328

5.25. Pedal phalanges of digit III of *Gryposaurus reddingi*, MOR 2573 329

5.26. Pedal phalanges of digit IV of *Gryposaurus reddingi*, MOR 2573.....330

ABSTRACT

Hadrosaurs, the "duck-billed" dinosaurs, were abundant members of Campanian (Late Cretaceous) communities in the Western Interior of North America, and are thus an ideal group for studying high-resolution evolutionary trends. This dissertation describes two new hadrosaurine taxa from the Judith River Formation exposed in Kennedy Coulee, northcentral Montana. The localities are stratigraphically equivalent to Unit 1 of the Oldman Formation, a time interval with no previously described hadrosaurine species. Phylogenetic and geometric morphometric analyses, combined with recalibrated radiometric dates, demonstrate that the new taxa form morphologic and stratigraphic intermediates within the lineages of *Gryposaurus* and *Acristavus-Brachylophosaurus*. The new genus of brachylophosaurin has a short posteriorly-oriented nasal crest hypothesized as an intermediate evolutionary state between the stratigraphically lower crestless *Acristavus* (lower Two Medicine Formation) and the stratigraphically higher *Brachylophosaurus* (middle Oldman Formation), with its wide posteriorly elongated crest. The nasal crest of *Brachylophosaurus* elongates posteriorly ontogenetically (as the individual grows). Histologic analysis demonstrates that the holotype of the new genus is relatively more mature than the largest *Brachylophosaurus* specimen, so its smaller crest size is not due to the ontogenetic status of the holotype. The new species of *Gryposaurus* is from a monodominant bonebed of at least ten individuals and three size classes: juvenile, subadult, and adult. The taphonomy of the bonebed is interpreted as a mass death assemblage deposited along a lake margin. The abundant postcranial bones are illustrated in a photographic atlas. In the new Gryposaurus species, the shape and position of the nasal crest is morphologically intermediate between the stratigraphically lower *G. latidens* (lower Two Medicine Formation) and the stratigraphically higher *G. notabilis* (lower Dinosaur Park Formation). In *G. latidens*, the nasal crest is low and anterodorsal to the posterior narial fenestra. The nasal crest becomes progressively higher and more posteriorly located in stratigraphically younger species. A similar trend occurs ontogenetically within specimens of the same species. Thus, in *Gryposaurus* and *Acristavus-Brachylophosaurus* lineages, directional trends in nasal crest morphology are observed both through ontogeny and between stratigraphically separated non-overlapping taxa, suggesting that the new taxa may be transitional members of anagenetic evolutionary lineages.

CHAPTER ONE

INTRODUCTION TO DISSERTATION

Hadrosaurs, the "duck-billed" dinosaurs, were abundant members of Campanian (Late Cretaceous) communities in the Western Interior of North America, and are thus an ideal group for studying high-resolution evolutionary trends. Most genera of hadrosaurs possessed cranial crests composed at least partially of the nasals; these crests are generally interpreted as display structures (e.g, Padian and Horner, 2011). The nasal crests of Hadrosaurinae (Saurolophinae sensu Prieto-Márquez, 2010) are "solid" and generally less elaborate than the "hollow" crests of Lambeosaurinae. Nevertheless, the crests of hadrosaurines are the main basis for differentiating most hadrosaurine taxa. In this dissertation I studied the changes in hadrosaurine crests ontogenetically (as the individual grows) and stratigraphically in two major groups of hadrosaurine dinosaurs, the tribe Brachylophosaurini and the genus *Gryposaurus*, by describing a new morphologically and stratigraphically intermediate taxon from each of these two groups.

The two new taxa were collected from the Kennedy Coulee area of Hill County, northcentral Montana, near the Montana-Alberta border. Kennedy Coulee is a richly fossiliferous exposure of the Judith River Formation (Late Cretaceous: Campanian). In Alberta, Judith River Formation equivalent deposits are named the Belly River Group, and include the Foremost, Oldman, and Dinosaur Park Formations (Eberth, 2005). Although the Montanan Judith River Formation is not subdivided into the formal units of the Belly River Group, the depositional sequences that created the Foremost, Oldman,

and Dinosaur Park Formations can be identified in Montana outcrop. This dissertation uses the terminology of these Canadian formations and their members to enable detailed stratigraphic correlation of fossiliferous localities, facilitating comparison of the hadrosaurs and other fauna over time.

Exposures in and near Kennedy Coulee are equivalent to the uppermost Foremost Formation and lowermost Oldman Formation of Alberta. The base of the coulee exposes a thick coal, the Marker A Coal, equivalent to the top of the Taber Coal Zone of the Foremost Formation, capped by a white-gray amalgamated channel sandstone equivalent to the Herronton Sandstone Zone at the top of the Foremost Formation (sensu Eberth, 2005). The upper portion of Kennedy Coulee, where the two new hadrosaurine taxa were collected, is dominated by mudstones and corresponds to Unit 1 (the lowest unit) of the Oldman Formation. Although several other partial skeletons have been excavated from the Foremost and lower Oldman Formations and their Judith River Formation equivalents, no species-level diagnostic hadrosaur material has previously been collected near the Foremost-Oldman Formation boundary, resulting in a gap in our knowledge of Campanian hadrosaur evolution. This dissertation describes two new species from this stratigraphic interval in Kennedy Coulee, which are morphologically intermediate between stratigraphically older and younger taxa.

The new taxa are placed into a high-resolution stratigraphic framework to study evolutionary trends over time. If related taxa co-exist (overlap stratigraphically), this is evidence of an earlier cladogenic event that divided the original lineage into two descendent lineages. If the taxa do not overlap stratigraphically, and are from the same

geographic area, the most parsimonious hypothesis is that they represent an unbranching anagenetic evolutionary lineage. If the changes in morphology among related species are directional and correspond with their relative stratigraphic positions (e.g., nasal crest becoming larger over millions of years), this supports the hypothesis of the species forming an anagenetic lineage.

Ontogeny, the morphologic changes as an individual grows from juvenile to adult, is intimately tied to evolution, as in a very general sense, ontogeny recapitulates phylogeny (Haeckel, 1866, 1901). This is often expressed in juvenile dinosaurs, which may appear more similar to their adult ancestors than to adults of their own species (Rozhdestvensky, 1965). A heterochronic shift in the timing of development of traits such as nasal crests can result in hypertrophy (larger size) of the crests in later species; the earlier and/or faster a crest grows, the larger it can be in the adult. Because juveniles may retain ancestral characteristics, without proper stratigraphic data they may be mistaken as older, more basal taxa. Indeed, when juvenile specimens are coded into a phylogenetic matrix, they are placed more basally on the resulting cladogram than are adults of that taxon (Tsuihiji et al., 2011; Campione et al., 2012).

To truly understand morphologic changes and the diversity of taxa within a clade, one must consider and account for multiple sources of variation, termed the "Unified Frames of Reference" (Horner et al., 2011): geography, taphohistory, stratigraphy, phylogeny, and ontogeny. This combination of ontogenetic and stratigraphic research has already been applied successfully to *Edmontosaurus* (Campione and Evans, 2011) and *Triceratops* (Horner and Goodwin, 2006; Scannella and Horner, 2010; Scannella et al.,

2014). This dissertation applies similar methods to two clades of Campanian hadrosaurines, the tribe Brachylophosaurini and the genus *Gryposaurus*.

Chapter Two describes a new genus and species within the tribe Brachylophosaurini. The previously described members of Brachylophosaurini include: *Acristavus gagslarsoni*, which lacks a nasal crest; *Brachylophosaurus canadensis*, which possesses a flat paddle-shaped nasal crest projecting posteriorly over the dorsal skull roof; and *Maiasaura peeblesorum*, which possesses a dorsally-projecting nasofrontal crest. *Acristavus*, from the lower Two Medicine Formation of Montana, is hypothesized to be the ancestral member of the clade. *Brachylophosaurus* specimens are from the middle Oldman Formation of Alberta and equivalent beds in the Judith River Formation of Montana. The new genus described here from Montana deposits equivalent to the lower Oldman Formation has a short, posteriorly-oriented triangular nasal crest, and is stratigraphically and morphologically intermediate between *Acristavus* and *Brachylophosaurus*. Thus the new genus is hypothesized to represent a transitional taxon within the *Acristavus-Brachylophosaurus* lineage.

Chapter Three introduces a *Gryposaurus* bonebed from Kennedy Coulee deposits stratigraphically equivalent to the lower Oldman Formation, and describes the taphonomy of this fossil assemblage. The bonebed is a strongly monodominant assemblage containing more than 800 bones of at least ten *Gryposaurus* individuals of three discrete size classes: four juveniles, five subadults, and one adult. Although phalanges and vertebrae are underrepresented relative to large limb bones, the overrepresentation of skull material as well as the presence of small porous elements such as phalanges and

caudal centra suggests minimal transport or winnowing of the assemblage. Fossilized wood, organic debris, and tyrannosaur teeth are abundant in the bonebed mudstone horizon. Although mollusks are not common in the bonebed mudstone, the taxa present indicate an oxic, quiet-water environment. The assemblage is hypothesized to have originated as a mass death assemblage on a floodplain or along a lake margin. The carcasses were fed upon by tyrannosaurs, and then the bones are hypothesized to have been concentrated and deposited by a flood into a lake or other quiet-water environment on the floodplain.

Chapter Four describes the cranial material from this bonebed, which represents a new species of *Gryposaurus* with an arching nasal crest that is morphologically intermediate between that of the stratigraphically lower *G. latidens* and the stratigraphically higher *G. notabilis*. *Gryposaurus* is unusual among dinosaur genera in including multiple valid species spanning several million years. Because these species are stratigraphically separated, and the nasal crest becomes larger and more posteriorly positioned in a directional trend from stratigraphically older to younger species, they are hypothesized to represent an anagenetic lineage.

Chapter Five is a photographic atlas of postcranial material from the *Gryposaurus* bonebed. Because cranial elements are the most diagnostic for determining species in hadrosaurs, hadrosaur cranial material has been well figured in numerous publications. However, until recently, postcranial material has been less completely illustrated. This photographic atlas is intended as a comprehensive resource to aid future researchers in the identification of hadrosaur postcranial fossils. Specimens are illustrated in multiple

views and anatomical features are labeled. Multiple specimens of each skeletal element are included to illustrate the range in apparent morphologic variation within members of a single species from a single bonebed. The variation between specimens of the same skeletal element is due to one or more factors: differing amounts of taphonomic breakage, different directions of diagenetic compression, ontogeny, and intraspecific individual variation.

This dissertation describes these two new hadrosaurine taxa and places them into ontogenetic and evolutionary context using cranial and postcranial morphologic descriptions, phylogenetic analysis, geometric morphometric analysis, and osteohistology. The taphonomic history of the *Gryposaurus* bonebed is analyzed, and the postcranial skeletal material from the bonebed is illustrated in a photographic atlas to aid the identification of hadrosaur fossils by future researchers.

Literature Cited

Campione, N. E., and D. C. Evans. 2011. Cranial growth and variation in edmontosaurs (Dinosauria: Hadrosauridae): implications for latest Cretaceous megaherbivore diversity in North America. PLoS ONE 6:e25186.

Campione, N. E., K. S. Brink, E. A. Freedman, C. T. McGarrity, and D. C. Evans. 2012. '*Glishades ericksoni*', an indeterminate juvenile hadrosaurid from the Two Medicine Formation of Montana: implications for hadrosauroid diversity in the latest Cretaceous (Campanian-Maastrichtian) of western North America. Palaeobiodiversity and Palaeoenvironments August 24:1-11.

Eberth, D. A. 2005. The Geology; pp. 54-82 in P. J. Currie and E. B. Koppelhus (eds.), Dinosaur Provincial Park: A Spectacular Ancient Ecosystem Revealed. Indiana University Press, Bloomington, Indiana.

Haeckel, E. 1866. Generelle morphologie der organismen. Allgemeine grundzüge der organischen formen-wissenschaft, mechanisch begründet durch die von Charles Darwin reformirte descendenz-theorie. Georg Reimer, Berlin.

Haeckel, E. 1901. The Riddle of the Universe at the Close of the Nineteenth Century. Harper & Brothers, New York, 391 pp.

Horner, J. R., and M. B. Goodwin. 2006. Major cranial changes during *Triceratops* ontogeny. Proceedings of the Royal Society B 273:2757-2761.

Horner, J. R., M. B. Goodwin, and N. Myhrvold. 2011. Dinosaur census reveals abundant *Tyrannosaurus* and rare ontogenetic stages in the Upper Cretaceous Hell Creek Formation (Maastrichtian), Montana, USA. PLoS ONE 6:1-9. e16574.

Padian, K., and J. R. Horner. 2011. The evolution of 'bizzare structures' in dinosaurs: biomechanics, sexual selection, social selection, or species recognition? Journal of Zoology 283:3-17.

Prieto-Márquez, A. 2010. Global phylogeny of Hadrosauridae (Dinosauria: Ornithopoda) using parsimony and Bayesian methods. Zoological Journal of the Linnean Society 159:435-502.

Rozhdestvensky, A. K. 1965. Growth changes in Asian dinosaurs and some problems of their taxonomy. Paleontologischeskii Zhurnal 3:95-109.

Scannella, J. B., and J. R. Horner. 2010. *Torosaurus* Marsh, 1891, is *Triceratops* Marsh, 1889 (Ceratopsidae: Chasmosaurinae): synonymy through ontogeny. Journal of Vertebrate Paleontology 30:1157-1168.

Scannella, J. B., D. W. Fowler, M. B. Goodwin, and J. R. Horner. 2014. Evolutionary trends in *Triceratops* from the Hell Creek Formation, Montana. Proceedings of the National Academy of Sciences 111:10245-10250.

Tsuihiji, T., K. Watabe, K. Tsogtbaatar, T. Tsubamoto, R. Barsbold, S. Suzuki, A. H. Lee, R. C. Ridgely, Y. Kawahara, and L. M. Witmer. 2011. Cranial osteology of a juvenile specimen of *Tarbosaurus bataar* form the Nemegt Formation (Upper Cretaceous) of Bugin Tsav, Mongolia. Journal of Vertebrate Paleontology 31:497-517.

CHAPTER TWO

A NEW BRACHYLOPHOSAURIN HADROSAUR (DINOSAURIA: ORNITHISCHIA) WITH AN INTERMEDIATE NASAL CREST FROM THE CAMPANIAN JUDITH RIVER FORMATION OF NORTHCENTRAL MONTANA

Contribution of Authors and Co-Authors

Manuscript in Chapter 2

Author: Elizabeth A. Freedman

Contributions: Conceived the study, performed the analyses, interpreted results, and wrote the manuscript.

Co-author: John R. Horner

Contributions: Conceived the study, provided funding and access to specimens and workspace, discussed implications of results, and edited earlier drafts of this manuscript.

Manuscript Information Page

Elizabeth A. Freedman, John R. Horner
PLoS One
Status of Manuscript:
_x_ Prepared for submission to a peer-reviewed journal
___ Officially submitted to a peer-reviewed journal
___ Accepted by a peer-reviewed journal
___ Published in a peer-reviewed journal

Abstract

Background

Brachylophosaurini is a clade of hadrosaurine dinosaurs from the Campanian (Late Cretaceous) of North America. Its members include: *Acristavus gagslarsoni*, which lacks a nasal crest; *Brachylophosaurus canadensis*, which possesses a flat paddle-shaped nasal crest projecting posteriorly over the dorsal skull roof; and *Maiasaura peeblesorum*, which possesses a dorsally-projecting nasofrontal crest. *Acristavus*, from the lower Two Medicine Formation of Montana (~81-80 Ma), is hypothesized to be the ancestral member of the clade. *Brachylophosaurus* specimens are from the middle Oldman Formation of Alberta and equivalent beds in the Judith River Formation of Montana; the upper Oldman Formation is dated 77.8 Ma.

Methodology/Principle Findings

A new brachylophosaurin hadrosaur, *Probrachylophosaurus bergei* (gen. et sp. nov.) is described based on the skull and postcranium of a large individual from the Judith River Formation of northcentral Montana (79.8-79.5 Ma); the horizon is equivalent to the lower Oldman Formation of Alberta. Cranial morphology of *Probrachylophosaurus*, most notably the nasal crest, is intermediate between *Acristavus* and *Brachylophosaurus*. In *Brachylophosaurus*, the nasal crest lengthens and flattens ontogenetically, covering the supratemporal fenestrae in large adults. The smaller nasal crest of *Probrachylophosaurus* is strongly triangular in cross section and only minimally overhangs the supratemporal fenestrae, similar to an ontogenetically earlier stage of

Brachylophosaurus. Body size, sutural fusion, and tibial osteohistology reveal that the holotype of *Probrachylophosaurus* was slowing its growth and was relatively more mature than a large *Brachylophosaurus* specimen. *Probrachylophosaurus* was added to two recent character matrices to compare the results of the two phylogenetic analyses.

Conclusions/Significance

The small triangular posteriorly oriented nasal crest of *Probrachylophosaurus* is proposed to represent a transitional nasal morphology between that of a non-crested ancestor such as *Acristavus* and the large flat posteriorly oriented nasal crest of adult *Brachylophosaurus*. Because *Probrachylophosaurus* is stratigraphically and morphologically intermediate between these taxa, *Probrachylophosaurus* is hypothesized to be an intermediate member of the *Acristavus*-*Brachylophosaurus* evolutionary lineage.

Introduction

Hadrosaurid dinosaurs dominated Late Cretaceous Campanian ecosystems of North America with an abundance of diverse taxa. The later portion of the Campanian included solid-crested hadrosaurines coexisting with hollow-crested lambeosaurines, but earlier in the Campanian, hadrosaurines were the dominant herbivores. Extensive bonebeds in the Two Medicine and Judith River Formations of Montana preserve numerous individuals of hadrosaurine taxa such as *Maiasaura peeblesorum* and *Brachylophosaurus canadensis* (Varricchio and Horner, 1993; Prieto-Márquez, 2005). These genera are members of the clade Brachylophosaurini, which includes the recently described basal taxon *Acristavus gagslarsoni* (Gates et al., 2011).

Acristavus, named for its lack of nasal crest, is found in the lower Two Medicine Formation of Montana (Figure 2.1; Gates et al., 2011). *Maiasaura* and *Brachylophosaurus* are more typical hadrosaurines in having prominent nasal crests, and are found stratigraphically higher than *Acristavus*. *Maiasaura*, with its dorsally projecting nasofrontal crest, is known from the upper half of the Two Medicine Formation (Horner and Makela, 1979; Horner, 1983, 1984). *Brachylophosaurus* canadensis specimens have posteriorly oriented flat paddle-shaped nasal crests, and are likely all from the Comrey Sandstone Zone of the middle Oldman Formation of Alberta and its Judith River Formation equivalent in Montana (LaRock, 2001; Ryan and Evans, 2005). A previously published taxon from lower Oldman-equivalent deposits, "*Brachylophosaurus goodwini*" (Horner, 1988), has been referred to *Brachylophosaurus canadensis* (Prieto-Márquez, 2005) and is here considered referable only to Brachylophosaurini indet. due to the state of preservation of the holotype and the lack of a preserved nasal crest.

Stratigraphically intermediate deposits between *Acristavus* and *Brachylophosaurus* include the lower Judith River Formation of Montana, and the corresponding Foremost and lower Oldman Formations of Alberta. Although several partial skeletons have been excavated from the Foremost and lower Oldman Formations and their Judith River Formation equivalents, no species-level diagnostic hadrosaur material has previously been collected near the Foremost-Oldman Formation boundary, resulting in a gap in our knowledge of Campanian hadrosaur evolution. This paper describes Museum of the Rockies (MOR) 2919, a specimen with a relatively complete skull from this stratigraphic interval in Kennedy Coulee, northcentral Montana, which

fills in the gap with a transitional morphology between the known taxa *Acristavus gagslarsoni* and *Brachylophosaurus canadensis*.

Institutional Abbreviations

CMN/NMC, Canadian Museum of Nature, formerly National Museum of Canada, Ottawa, Ontario, Canada; **FMNH**, Field Museum of Natural History, Chicago, Illinois, U.S.A.; **GPDM**, Great Plains Dinosaur Museum, Malta, Montana, U.S.A.; **OTM**, Old Trail Museum, Choteau, Montana, U.S.A.; **MOR**, Museum of the Rockies, Bozeman, Montana, U.S.A.; **ROM**, Royal Ontario Museum, Toronto, Ontario, Canada; **TMP**, Royal Tyrrell Museum of Paleontology, Drumheller, Alberta, Canada; **UCMP**, University of California Museum of Paleontology, Berkeley, California, U.S.A.; **UMNHVP**, Utah Museum of Natural History Vertebrate Paleontology, Salt Lake City, Utah, U.S.A.; **YPM-PU**, Princeton University collection at the Yale Peabody Museum, New Haven, Connecticut, U.S.A.

Study Areas

Kennedy Coulee is a richly fossiliferous exposure of the Judith River Formation (Late Cretaceous: Campanian) located in Hill County, northcentral Montana, and joins the valley of the Milk River near the USA-Canada border (Figure 2.2). In Alberta, Judith River Formation equivalent deposits are named the Belly River Group, and include the Foremost, Oldman, and Dinosaur Park Formations (Figure 2.1). Although the Montanan Judith River Formation is not subdivided into the formal units of the Belly River Group,

the depositional sequences that created the Foremost, Oldman, and Dinosaur Park Formations can be identified in Montana outcrop. Using the terminology of these Canadian formations and their members enables detailed stratigraphic placement of fossiliferous localities, facilitating comparison of the hadrosaurs and other fauna over time.

Exposures in and near Kennedy Coulee are equivalent to the uppermost Foremost Formation and lowermost Oldman Formation of Alberta, according to multiple lines of evidence: lithologic, radiometric, and biostratigraphic. The base of the coulee exposes a thick coal, the Marker A Coal, equivalent to the top of the Taber Coal Zone of the Foremost Formation, capped by a white-gray amalgamated channel sandstone equivalent to the Herronton Sandstone Zone at the top of the Foremost Formation (sensu Eberth, 2005). The upper portion of Kennedy Coulee, where MOR 2919 was collected, is dominated by mudstones and corresponds to Unit 1 (the lowest unit) of the Oldman Formation. The ceratopsian *Medusaceratops* was also collected from this upper mudstone zone of Kennedy Coulee (Ryan et al., 2010).

To facilitate comparison of radiometric dates from various formations and publications, all relevant dates were recalibrated to the Fish Canyon sanidine standard of 28.305 ± 0.036 Ma using the method of Renne et al. (2010). Published and recalibrated dates for relevant portions of the Judith River Formation, Belly River Group, Two Medicine Formation, and Wahweap Formation are listed in Table 2.1, and recalibrated dates are plotted on Figure 2.1.

Published radiometric dates from the upper mudstone zone and lower coal zone of Kennedy Coulee constrain the age of MOR 2919 between 78.5 ± 0.2 Ma and 78.2 ± 0.2 Ma according to the old standard of 520.4 ± 1.7 Ma for MMhb-1 (Goodwin and Deino, 1989). Conversion and recalibration to the Fish Canyon sanidine standard mentioned above adjusts these dates to 79.8 ± 0.2 Ma and 79.5 ± 0.2 Ma. The proposed stratigraphic position of Kennedy Coulee is consistent with its radiometric age within the range of recalibrated dates from the lower Foremost (80.45 ± 0.16 Ma) and upper Oldman Formations (77.76 ± 0.51 Ma) of Alberta (Eberth and Hamblin, 1993; Eberth, 2005).

Ray teeth collected from microsites throughout Kennedy Coulee, from the Herronton Sandstone to Unit 1 of the Oldman Formation, possess smooth-sided crowns, and are thus referable to *Pseudomyledaphus* sp. (Appendix A, Appendix B; Kirkland et al., 2013). In Alberta, *Pseudomyledaphus* sp. are only found in the Foremost and lowermost Oldman Formations (Peng et al., 2001; Brinkman et al., 2004; Kirkland et al., 2013), supporting the assignment of MOR 2919's locality to the lowermost Oldman Formation.

Brachylophosaurus canadensis specimens collected in Alberta all likely originate from the Oldman Formation (Table 2.2). The holotype of *B. canadensis*, NMC 8893, was collected in 1936 from the Comrey Sandstone Zone (Unit 2) of the middle Oldman Formation near the Red Deer River, within what is now Dinosaur Provincial Park (Cuthbertson and Holmes, 2010; D. A. Eberth personal communication 2011). A partial skull, FMNH PR 862, had also been collected in Dinosaur Provincial Park in 1922 (Eberth and Evans, 2011). FMNH PR 862 was more recently erroneously associated with

the Two Medicine Formation (Prieto-Márquez, 2005, 2007), but outcrops along the Red Deer River include the Oldman and Dinosaur Park Formations, and so FMNH PR 862 was likely collected from a similar stratigraphic level as the holotype. A third skull and partial skeleton, TMP 1990.104.001, was collected from a sandstone at an unspecified level of the Oldman Formation near the Milk River outside of the towns of Onefour and Manyberries (Ryan and Evans, 2005). Of these three specimens, only the holotype is confirmed to be from the Comrey Sandstone Zone, but there is no evidence to suggest that the other two specimens originate from a different horizon.

Although Alberta was the source of the holotype, the majority of known *Brachylophosaurus canadensis* specimens, notably a complete adult skeleton (MOR 794) and a bonebed containing individuals of various sizes (MOR 1071), were collected from the Judith River Formation exposed near Malta, Montana. Malta is 200 km east of Kennedy Coulee, and thus more distal along the depositional wedge and closer to the Western Interior Seaway. In the Malta area, the base of the Judith River Formation is the shoreface Parkman Sandstone, which is overlain by tan colored, quartz-rich sandstones (LaRock, 2001) equivalent to the Comrey Sandstone Zone of the middle Oldman Formation. Strata equivalent to the Foremost Formation and lower Oldman Formation are not present in the distal wedge deposits of Malta (Figure 2.1). Ray teeth collected with MOR 1071 are referable to *Myledaphus bipartitus* (Appendix A), which, in Alberta, are only found in the Comrey Sandstone Zone and higher units (Brinkman et al., 2004), supporting the assignment of the Malta *B. canadensis* localities to the Comrey Sandstone Zone of the Oldman Formation. Thus, Kennedy Coulee and MOR 2919 are

stratigraphically older than *Brachylophosaurus canadensis* specimens from Alberta and Malta, Montana.

A second species of *Brachylophosaurus*, *B. goodwini*, was described from Kennedy Coulee, Hill County, northcentral Montana (Horner, 1988). The cranial material of the holotype, UCMP 130139, was fragmentary and missing the nasal crest, and so was deemed undiagnostic and referred to *B. canadensis* (Prieto-Márquez, 2005; Cuthbertson and Holmes, 2010). However, due to the lack of a preserved nasal crest as well as its severe frontal depressions, UCMP 130139 cannot be confidently referred to either *B. canadensis* or the new genus described here, and is assigned to Brachylophosaurini indet. (see Discussion).

Materials and Methods

MOR 2919 was collected by Museum of the Rockies and University of California Museum of Paleontology crews using standard paleontology field techniques (Leiggi et al., 1994) on privately owned land. MOR 2919 was generously donated to the Museum of the Rockies by Nolan and Cheryl Fladstol and John and Claire Wendland. No permits were required for the described study, which complied with all relevant regulations.

Terminology in this paper follows traditional conventions and definitions of Hadrosauridae and Hadrosaurinae (Horner et al., 2004) rather than the proposed alternate names of Saurolophidae and Saurolophinae (Prieto-Márquez, 2010a) for reasons of taxonomic stability as detailed in Gates et al. (2011).

MOR 2919 was compared morphologically to other hadrosaurine specimens and casts at MOR, ROM, TMP, and UCMP, as well as published descriptions. Measurements were taken directly from the specimens or casts using a tape measure or digital calipers.

MOR 2919 was coded into the phylogenetic matrices of Gates et al. (2011) and Prieto-Márquez (2010a). To simplify the analyses and focus on the clade of interest (Brachylophosaurini), as well as to make the taxon lists of these matrices as similar as possible, most lambeosaurine and basal hadrosauroid taxa were removed from Prieto-Márquez's (2010a) and Gates et al.'s (2011) matrices. Relationships within lambeosaurs and basal hadrosauroids are thoroughly investigated in Prieto-Márquez (2010a) and need not be repeated here. *Iguanodon bernissartensis* was retained for use as the outgroup, consistent with Prieto-Márquez (2010a) and Gates et al. (2011). *Bactrosaurus johnsoni* was retained as a representative hadrosauroid because it is the most complete hadrosauroid in the matrices. *Hadrosaurus foulkii*, although not included in the Gates et al. (2011) matrix, was retained in the Prieto-Márquez (2010a) matrix due to the taxon's variable position in different phylogenetic analyses and its importance in defining the terms Hadrosauridae and Hadrosaurinae. *Corythosaurus casuarius* was retained as a representative lambeosaurine, consistent with Gates et al. (2011). Several incomplete hadrosaurine taxa (coded with a high percentage of "?") outside of Brachylophosaurini were removed from both matrices to simplify the analysis and improve resolution of Brachylophosaurini and the other major, well-defined hadrosaurine clades. The removed taxa were: *Barsboldia sicinskii*, *Kerberosaurus manakini*, Sabinas OTU, Salitral Moreno OTU (*Willinakaqe*), *Shantungosaurus giganteus*, and UTEP OTU.

Several character states in the published Prieto-Márquez (2010a) matrix were recoded, and after initial analysis, some characters were amended or excluded in a second analysis (see Phylogenetic Analyses section). No character states were recoded in the Gates et al. (2011) matrix, and no characters were excluded. Thus, phylogenetic analyses were performed on a total of three matrices: 1) the matrix of Prieto-Márquez (2010a) with all characters included (19 taxa, 370 characters; Appendix C); 2) the matrix of Prieto-Márquez (2010a) with some characters amended or excluded (19 taxa, 367 characters; Appendix D); 3) the matrix of Gates et al. (2011) with all characters included (13 taxa, 116 characters; Appendix E).

The matrices were analyzed with parsimony in PAUP 4.0b10 (Swofford, 2002) within a heuristic search of 5,000 replicates using ACCTRAN optimization and tree bisection-reconnection swapping to produce a strict consensus tree, followed by a bootstrap analysis using a heuristic search of 5,000 replicates.. The complete PAUP settings used are provided in the nexus files (Appendices C-E). For the Gates et al. (2011) matrix, the bootstrap replicates were increased to 50,000 due to the support values for certain clades being extremely close to the cutoff value of 50%. Phylogeny figures were time-calibrated by drawing the cladograms using published age ranges for taxa; dates for members of Brachylophosaurini were recalibrated as in Table 2.1 and Figure 2.1, using the method of Renne et al. (2010).

The left tibia of MOR 2919 was histologically sampled using the techniques of Lamm (2013) for large specimens. The mid-diaphyseal segment with minimum circumference was removed, molded and cast, and embedded in resin for histological

sectioning. Given the large dimensions of the tibia (anteroposterior mid-diaphysis cross-sectional diameter maximum 13.35 cm, mediolateral diameter minimum 10.60 cm), the transverse cross-section was cut into three parts (anterior, posteromedial, and posterolateral) that were mounted on separate slides and ground to a thickness of 100 μm. The finished slides were imaged at 10x and 40x total magnification on a Nikon Optiphot-Pol polarizing microscope with a Nikon DS-Fi1 digital sight camera utilizing an automated stage to move the slide incrementally. The resulting photomicrographs were compiled with NIS-Elements BR 3.0 software into high-resolution TIFF image files. Adobe Photoshop CS2 was used to combine the images of the three slides and trace the circumference of each line of arrested growth (LAG). These circumferences were then measured with ImageJ 1.46r (Rasband, 1997-2014).

Because the tibia was slightly crushed, several cortical segments were displaced radially inward, resulting in the LAG tracings overestimating the true circumference due to the LAGs on either side of a displacement needing to be connected by a radially oriented line. This was corrected for each LAG individually by subtracting the length of these radial lines at the three areas of greatest displacement (anterolateral, posterolateral, posteromedial) from the total LAG circumference measured in ImageJ.

The left tibia of MOR 2919 was originally collected by UCMP in 1981 and curated as UCMP 137272. Limb bones prepared at UCMP at the time sometimes included a metal rebar rod and epoxy inserted into the medullary cavity for rigid support. After the tibia was transferred to MOR collections and sectioned for histology, the rebar was cut out of the tibia segments prior to mounting them on slides to avoid grinding

metal on histological equipment. This created the open space seen in the center of the medullary cavity on the finished slides.

Nomenclatural Acts

The electronic edition of this article conforms to the requirements of the amended International Code of Zoological Nomenclature, and hence the new names contained herein are available under that Code from the electronic edition of this article. This published work and the nomenclatural acts it contains have been registered in ZooBank, the online registration system for the ICZN. The ZooBank LSIDs (Life Science Identifiers) can be resolved and the associated information viewed through any standard web browser by appending the LSID to the prefix "http://zoobank.org/". The LSID for this publication is: urn:lsid:zoobank.org:pub:657DD0A4-799D-443A-BE9F-A2987DFABADD. The electronic edition of this work was published in a journal with an ISSN, and has been archived and is available from the following digital repositories: PubMed Central, LOCKSS.

Systematic Paleontology

Dinosauria Owen, 1842

Ornithischia Seeley, 1888

Ornithopoda Marsh, 1881

Hadrosauridae Cope, 1869

Hadrosaurinae Cope, 1869

Brachylophosaurini Gates et al., 2011

Definition. Modified from Gates et al. (2011): Hadrosaurine ornithopods more closely related to *Brachylophosaurus*, *Probrachylophosaurus*, *Maiasaura*, or *Acristavus* than to *Gryposaurus* or *Saurolophus*.

Diagnosis. As in Gates et al. (2011).

Referred Material. UCMP 130139, a partial skull and skeleton originally described as the holotype of *Brachylophosaurus goodwini* (Horner, 1988), and later assigned to *Brachylophosaurus canadensis* (Prieto-Márquez, 2005; Cuthbertson and Holmes, 2010). Due to the lack of a preserved nasal, and the presence of deep frontal depressions, the specimen cannot be confidently assigned to any current genus of Brachylophosaurini.

Horizon and Locality. UCMP 130139 was collected from the Judith River Formation of Kennedy Coulee, Hill County, northcentral Montana, in beds equivalent to the lower Oldman Formation, with a published height of approximately 15 m above the Marker A Coal of the Taber Coal Zone of the Foremost Formation (Horner, 1988). However, a remeasured section shows that the site was actually only a few meters above the Marker A Coal, and lies within the Herronton Sandstone Zone (Mark Goodwin and David Evans personal communication, 2014).

Brachylophosaurus canadensis Sternberg, 1953

Holotype. NMC 8893

Referred Material**.** FMNH PR 862 (partial skull); MOR 720 (braincase); MOR 794 (nearly complete articulated skeleton); MOR 940 (braincase); MOR 1071 (monodominant bonebed); TMP 90.104.01 (complete skull and articulated partial skeleton).

Emended Diagnosis. Nasal crest flat and paddle-shaped in adults, covering most or all of the supratemporal fenestrae; prefrontal as in Cuthbertson and Holmes (2010): "prefrontal projecting posteriorly over frontal, and more posteriorly, ventromedially directed to underlie nasal crest and contribute to anterior border of supratemporal fenestra."

Horizons and Localities. NMC 8893, FMNH PR 862, and TMP 90.104.01 were collected from the Oldman Formation of southeastern Alberta. NMC 8893 and FMNH PR 862 were collected in Dinosaur Provincial Park; TMP 90.104.01 was collected near Onefour and the Milk River. Of these Albertan specimens, the exact stratigraphic position is known only for NMC 8893: the Comrey Sandstone Zone (Unit 2) of the Oldman Formation. MOR 720 was collected from the upper Judith River Formation in badlands surrounding the Missouri River north of Winifred, Fergus County, central Montana. MOR 794, MOR 940, and MOR 1071 were collected from the Judith River Formation of

Malta, northern Montana, in beds equivalent to the Comrey Sandstone Zone of the Oldman Formation.

Probrachylophosaurus gen. nov.

urn:lsid:zoobank.org:act:7B7C87AC-2EFE-4587-9A24-A5D48C908941

Type species. *Probrachylophosaurus bergei* sp. nov.

Etymology. *Pro-* (Latin) before, *-brachylophosaurus* (Greek) short-crested lizard, in reference to the new taxon's stratigraphic position below that of *Brachylophosaurus canadensis*.

Diagnosis. As for type and only species.

Probrachylophosaurus bergei sp. nov.

urn:lsid:zoobank.org:act:49D503CB-7FA6-4D66-8FC0-0B4E2A3EE106

Holotype. MOR 2919, majority of a skull and skeleton, disarticulated. Cranial material includes a right premaxilla (fragmentary), both maxillae, left jugal, partial right lacrimal, left posterior nasal, partial mid-region of right nasal, articulated braincase (with articulated frontals, parietal, postorbitals, and exoccipitals), both squamosals, both quadrates, predentary, both dentaries, and right surangular (Figures 2.4-2.16). Postcranial material includes atlas fragments and at least 10 other cervical vertebrae, 11 dorsal vertebrae, 29 caudal vertebrae, 19 chevrons, approximately 19 ribs, both ilia, both pubes, both ischia, both tibiae, both fibulae, both astragali, right metatarsal II, and right

metatarsal IV (Figures 2.17-2.20). Forelimbs and sacral vertebrae are absent, although an isolated neural spine may belong to a sacral vertebra.

Referred Specimen. MOR 1097, fragmentary subadult skull material including the right posterior nasal crest, right jugal, left coronoid process of dentary, dentary tooth rows, maxilla tooth rows, partial left prefrontal, and dorsal and ventral condyles of right quadrate.

Etymology. Species name *bergei* in memory of Sam Berge, co-owner of the land where the specimen was discovered, and friend and relative of many members of the Rudyard, Montana community, who have supported paleontologic research for decades. Pronunciation: berg-ee-i.

Horizon and Locality. MOR 2919 was collected from private land north of Rudyard, Montana, just east of the mouth of Kennedy Coulee along the Milk River near the USA-Canada border, in exposures of the Judith River Formation. The site, MOR locality JR-518 ("Superduck"), is within a grey mudstone stratigraphically equivalent to Unit 1 of the Oldman Formation of Alberta. The bone horizon is 17.5 m above the top of the Marker A Coal of the Taber Coal Zone of the Foremost Formation, and 7.0 m above the top of the Herronton Sandstone Zone of the Foremost Formation (Figure 2.3), with a recalibrated age between 79.5 ± 0.2 Ma and 79.8 ± 0.2 Ma (Goodwin and Deino, 1989; Renne et al., 2010). The skeleton was completely disarticulated and there was no preferred orientation of the long bones. Associated microsite material was rare, but

dominated by tyrannosaur teeth. MOR 1097 was collected from state-owned land less than 1 km east of MOR 2919, and at a similar stratigraphic height.

The site was discovered by Kyoko Kishi and partially excavated by a UCMP crew led by Mark Goodwin in 1981 and 1994, which collected some postcranial material (UCMP locality V81232). Additional material became exposed in 2007, so a MOR crew continued excavation in 2007 and 2008, collecting the skull and extensive postcrania. Because all skeletal material at the site belongs to a single individual, UCMP graciously transferred its postcranial material to MOR. Consequently, the specimen numbers have been altered; all bones are now MOR 2919, and the old UCMP numbers are now treated as "field numbers" for purposes of identifying individual bones within MOR 2919. Original UCMP collections numbers were: left tibia UCMP 137272, right fibula UCMP 156955, right metatarsal IV UCMP 399999, right ilium UCMP 172484, left astragalus UCMP 172484, and caudal vertebra UCMP 400000. A jacket containing an unprepared and thus previously uncataloged right tibia was also transferred to MOR.

Diagnosis. *Probrachylophosaurus bergei* is a hadrosaurine hadrosaurid diagnosed by the following features: solid crest consisting entirely of the nasals that overhangs the supratemporal fenestrae by less than 2 cm in adults; nasal crest being extremely dorsoventrally thickened medially, resulting in a strongly triangular frontal plane cross section, with the dorsal angle formed by the paired nasals in posterior view being less than 130 degrees.

Osteological Description

The focus of this description is to highlight features of MOR 2919 that differ from other specimens of Brachylophosaurini, are phylogenetically significant, or that may be ontogenetically variable in hadrosaurs. Characters not mentioned are either unobservable in the preserved elements of MOR 2919, or are consistent with *Brachylophosaurus canadensis* and related hadrosaurs (Sternberg, 1953; Prieto-Márquez, 2005; Cuthbertson and Holmes, 2010), such that descriptions need not be duplicated here. The comparative specimens of *B. canadensis* used herein are identified by specimen number rather than simply genus and species name due to slight morphologic differences among specimens (Table 2.2). Generally, morphologic descriptions of *B. canadensis* are based on the holotype, NMC 8893, for characters observable on an articulated skull, and MOR 1071 for characters only observable on disarticulated specimens. Unless otherwise indicated, all morphologic descriptions of *Acristavus* are based on MOR 1155 (holotype; Gates et al., 2011), *Maiasaura* on YPM-PU 22405 (holotype; Horner and Makela, 1979), *Gryposaurus* on CMN 2278 (holotype of Gryposaurus notabilis; Lambe, 1914), and *Prosaurolophus* on MOR 454 (holotype of Prosaurolophus blackfeetensis; Horner, 1992). For features not preserved on the *Maiasaura* holotype, a referred specimen (OTM F138) of uncertain stratigraphic position is used for comparison (Trexler, 1995).

MOR 2919 (Figure 2.4) represents one of the largest brachylophosaurin specimens. Exact comparisons of cranial dimensions among specimens are difficult due to diagenetic compression affecting each specimen to a different degree and direction. However, for specimens with associated postcrania, comparisons are more

straightforward (Table 2.3). Although the relative size of individuals does not necessarily indicate the same degree of relative maturity, the larger size of MOR 2919 suggests that it is an adult, not merely an immature specimen of *B. canadensis*; this conclusion is supported by its axial fusion and osteohistology (see Discussion).

Skull

Maxillary/Facial Complex

Premaxilla. The premaxilla is severely crushed and fragmented, and so is of limited morphological use. The anterior portion is best preserved; the posterodorsal and posteroventral processes are absent. The oral margin is anteroposteriorly wide and ventrally deflected as in *Brachylophosaurus* (NMC 8893, MOR 1071) rather than dorsally reflected as in other hadrosaurines (e.g. *Gryposaurus*, *Prosaurolophus* MOR 447). The ventral margin is eroded; no denticles are preserved. Premaxillary foramina are unobservable, either due to crushing or true absence.

Maxilla. The maxillae of MOR 2919 are consistent in most respects with the morphology of *Brachylophosaurus* (Figure 2.5). The relative size and placement of the large maxillary foramen in MOR 2919 is consistent with all members of Brachylophosaurini (*Brachylophosaurus* MOR 1071, *Maiasaura* OTM F138, *Acristavus*), although the number and pattern of additional smaller maxillary foramina on the lateral surface can be variable between individuals of the same species. Maxillae from the MOR 1071 *Brachylophosaurus* bonebed have four to five smaller foramina in

differing patterns of arrangement. MOR 2919 has three of these smaller foramina on each maxilla. As in *Acristavus*, the posterior maxillary process is broken at its base on both maxillae, but if complete would likely have been similar to that of *Brachylophosaurus*. The anterodorsal maxillary process is also partially broken on both maxillae (anteriorly on the right and anterodorsally on the left), but if complete would resemble that of *Brachylophosaurus*. The ventral margin of the maxilla is nearly straight, with the anterior one-third only slightly ventrally deflected, similar to the condition seen in *Acristavus* and *Brachylophosaurus*.

The left maxilla possesses 52 tooth rows; the right maxilla tooth rows are obscured anteriorly. The occlusal plane of the left maxilla (30.5 cm) of MOR 2919 is slightly longer than that of *Brachylophosaurus* holotype NMC 8893 (right 29 cm, left 28.5 cm), which has 46 tooth rows (Cuthbertson and Holmes, 2010). In both specimens, tooth sizes are largest in the center of the maxilla, and decrease in size anteriorly and posteriorly (Cuthbertson and Holmes, 2010). MOR 2919 is able to accommodate its increased density of tooth rows by decreasing its anterior and posterior tooth sizes relatively more than in NMC 8893. Because the number of tooth rows in hadrosaurines increases ontogenetically, the high tooth count in MOR 2919 is likely due to its size and maturity rather than being taxonomically informative. Less than one-third of the teeth that had begun to wear on the occlusal plane remain, so the number of teeth per family exposed on the occlusal plane cannot be determined; most teeth preserved in the maxillae are unworn. Each tooth possesses a single median carina, many of which are subtly sinusoidal (Figure 2.5F), as in *Brachylophosaurus* (FMNH PR 862). The edges of the

crowns have papillae that are slightly smaller but more prominent than those of *Brachylophosaurus* (MOR 1071).

Jugal. On the medial surface of the rostral (maxillary) process of subadult and adult *Probrachylophosaurus* (Figure 2.6), the palatine joint is obliquely oriented, raised medially, and extends anteriorly to form a lip as in *Brachylophosaurus* and *Acristavus*. The adult MOR 2919 palatine process extends the farthest anteriorly, forming a narrow slot below its 10 mm overhang (Figure 2.6B), and most closely matches that of adult *Brachylophosaurus* MOR 1071-7-16-98-248-Q (Figure 2.6F, lip 5 mm). The anterior curvature that forms the lip in the subadult MOR 1097 is gentle and forms a small overhanging lip (Figure 2.6C, 3 mm) identical in size and morphology to *Acristavus*. The lip in *Maiasaura* is variably developed, overhanging 4 mm in the holotype YPM-PU 22405 but only 1 mm in OTM F138. The palatine joint does not form an overhanging lip in *Prosaurolophus* or *Gryposaurus* (MOR 478, *G. latidens*).

In *Brachylophosaurus* (NMC 8893, FMNH PR 862, MOR 794, MOR 1071), the caudodorsal and caudoventral apices of the rostral process are in line vertically when the rostral process is oriented horizontally. In MOR 1097, MOR 2919, and *Acristavus* (contra Prieto-Márquez, 2010a), the caudoventral apex is posterior to the caudodorsal apex when the rostral process is oriented horizontally (character 106/J4 in Prieto-Márquez, 2010a). In *Maiasaura* (YPM-PU 22405, OTM F138), the caudoventral apex is only slightly posterior to the caudodorsal apex. The lacrimal process on the dorsal rostral process is broken in MOR 2919, but intact in MOR 1097, where it resembles that of *Brachylophosaurus*, although it is relatively slightly larger in MOR 1097. The ventral

margin of the rostral process is straight in MOR 1097 and MOR 2919, as in *Acristavus*. The ventral margin is sigmoidal in lateral view in *Brachylophosaurus* (NMC 8893, MOR 1071) and somewhat sigmoidal in one *Maiasaura* specimen (OTM F138), although it is straight in the *Maiasaura* holotype (YPM-PU 22405).

The ascending postorbital process is broken at its base, but bone texture at the base indicates that the postorbital process would have been angled to the same degree as in *Brachylophosaurus*. The ventral margin of the orbit is wider than the ventral margin of the lateral temporal fenestra, as in *Brachylophosaurus*, *Acristavus*, and *Maiasaura*.

MOR 2919 has a relatively wider (dorsoventrally) caudal constriction of the jugal than do *Brachylophosaurus* (NMC 8893, MOR 1071-7-16-98-248-Q), *Acristavus*, and *Maiasaura*, although MOR 1097's caudal constriction is narrower than in these other taxa. The ratio of the depth of the caudal constriction to the anterior constriction in MOR 2919 is 1.42 (character 113/J11 in Prieto-Márquez, 2010a). The ratio of dorsoventral depth of the caudoventral flange to the caudal constriction is 1.45 (character 110/J8 in Prieto-Márquez, 2010a). These ratios are 1.40 and 1.61, respectively, in the *Brachylophosaurus* holotype (NMC 8893). The caudoventral flange of MOR 2919 is dorsoventrally deep, as in other brachylophosaurins, but relatively wider anteroposteriorly than in *Brachylophosaurus*.

The concavity of the posterior jugal margin between the quadratojugal process and caudoventral flange is weakly developed in MOR 2919, as in *Acristavus* and *Maiasaura*. The concavity is deeper in *Brachylophosaurus*. The medial side of the quadratojugal process is more gently excavated in MOR 2919 than in *Brachylophosaurus*

or *Maiasaura*. The excavation in *Acristavus* is slightly more pronounced than in MOR 2919, but less than in *Brachylophosaurus*.

Lacrimal. The posterior right lacrimal preserves part of the anterior orbital margin and anteroventrally oriented lacrimal duct (Figure 2.7). The medial portion of the lacrimal is not preserved, so only the lateral side of the lacrimal foramen is present; the foramen's original size and shape cannot be determined. However, the bone lateral to the foramen is robust (Figure 2.7E), over twice as mediolaterally thick as the corresponding region in *Brachylophosaurus* MOR 1071-7-10-98-171 (Figure 2.7F), consistent with the robusticity described for *Acristavus* (Gates et al., 2011). The posterior jugal contact is robust and ventrally convex, whereas it is strongly ventrally concave in *Brachylophosaurus*.

Nasal. The size and shape of the nasal crest is the main distinguishing character between *Probrachylophosaurus* and *Brachylophosaurus*. The nasal crest of *Probrachylophosaurus* (MOR 1097, MOR 2919; Figures 2.8-2.9) is shorter, and more triangular in cross-section, than *Brachylophosaurus*. The crest consists entirely of the nasals, and overhangs the supratemporal fenestrae by less than 1 cm in the adult (Figure 2.4). The nasal crest is extremely dorsoventrally thickened medially, and rapidly thins laterally. The dorsal angle formed by the paired nasals, in posterior view, is 112° in the adult (MOR 2919; Figure 2.9B) and 126° in the subadult (MOR 1097; Figure 2.9A). The crest tapers posteriorly in a "V" shape. The posteriormost dorsal surface of the nasal crest is rugose in MOR 2919 but smooth in MOR 1097 (Figure 2.8).

In adult *Brachylophosaurus*, the exposed nasal crest is composed entirely of the nasals, but the frontal and/or prefrontal platform does extend posteriorly over the supratemporal fenestrae to support the base of the nasal crest (see frontal description below). The flat, paddle-like nasal crest of *Brachylophosaurus* varies in size amongst individuals. Prieto-Márquez (2005) categorized specimens as "slender" or "robust". The nasal crest of slender specimens (MOR 1071-7-7-98-86, MOR 1071-7-16-98-248) covers most of the length of the supratemporal fenestrae, but does not reach their posterior or lateral margins. The crest tapers posteriorly in a "U" shape, resulting in the crest overhanging approximately 50% of the area of the supratemporal fenestrae. The crest is thickened medially; the dorsal angle of the paired nasals is 140° in MOR 1071-7-7-98-86 (Figure 2.9C). The nasal crest of the robust MOR 794 is much longer and wider, overhanging the entire supratemporal fenestrae and extending posteriorly past the supraoccipital; the dorsal angle of the paired nasals is 165° (Figure 2.9E). These slender and robust categories are not discrete; some *Brachylophosaurus* specimens (NMC 8893, FMNH PR 862, TMP 1990.104.001) possess intermediate morphologies, completely overhanging the supratemporal fenestrae posteriorly but not laterally. The crests of FMNH PR 862 and TMP 1990.104.001 are nearly robust, while NMC 8893 more closely resembles an enlarged slender morphology. These intermediate crest morphologies also have intermediate dorsal angles of the paired nasals: 151° in FMNH PR 862 (Figure 2.9D) and 157° in NMC 8893. The nasals of subadult *Brachylophosaurus canadensis* (MOR 940) appear to remain flat against the frontal and do not form a crest (Figure 2.10).

The nasofrontal articulation surface of MOR 2919 is rugose, and the posterior articulation is composed of deep pits (up to 12 mm) and projections to interlock with those of the frontal (Figure 2.8B). The nasofrontal articulation surface of MOR 1097 consists of anteroposterior striations and a single pit on the posterolateral margin (Figure 2.8F). The striations on the subadult MOR 1097 nasofrontal articulation surface correlate well to the striations on the frontals of subadult *Brachylophosaurus* (see frontal discussion below). No disarticulated nasals of *Brachylophosaurus* were available for comparison.

The anterior nasals are not preserved, and no part of the nasals or premaxilla preserves more than a few centimeters of possible narial margin, if any. However, the lateral middle region of the left nasal is preserved, with articulation surfaces for the prefrontal, lacrimal, and posteroventral process of the premaxilla. On the lateral nasal surface, dorsal to the lacrimal articulation, is a subcircular depression 2 cm in diameter that includes a small fenestra. On the medial side in the same location is an anteroventrally-posterodorsally oriented excavation 4 cm long, 1 cm wide, and 1 cm deep; the small fenestra opens halfway along the length of the excavation. This excavation may correspond to the "anteroposteriorly oriented groove terminating in elongated foramen" described for *Brachylophosaurus* (Prieto-Márquez, 2005). However, the excavation in MOR 2919 is located on the medial side of the lateral nasal anterior to the prefrontal, whereas in MOR 1071-7-7-98-86 it is on the ventral side of the dorsal nasal medial to the prefrontal. Alternatively, the excavation in MOR 2919 may be pathologic, and possibly associated with the pathologies on both dentaries.

Prefrontal. No prefrontals are preserved in MOR 2919. MOR 1097 includes a partial left prefrontal, missing the posterior orbital region. Its morphology is generally similar to that of *Brachylophosaurus*.

Frontal. In MOR 2919, the nasofrontal suture is rugose, composed of anteroposterior linear striations, with pits at its posterior margin. The suture covers approximately half (59%) of the dorsal frontal surface, resembling the subadult condition of *Brachylophosaurus* (Figure 2.11A; Figure 2.12). Two small subadult specimens of *Brachylophosaurus*, MOR 1071-7-13-99-87-I (Figure 2.11B) and MOR 1071-C-3-3 (Figure 2.11C), allot 69% and 60%, respectively, of their frontal surfaces to the nasofrontal suture; the suture surfaces are covered with anteroposterior linear striations but are not pitted posteriorly. A slightly larger subadult, MOR 1071-6-30-98-4, has a suture at least 64% the length of the frontals (frontals are slightly broken anteriorly), and the surface includes both anteroposterior linear striations and minor posterior pitting. Another subadult specimen, MOR 940, still has the nasals articulated onto the frontals; the nasals cover 54% of the dorsal frontal surface, and do not rise above the frontals in a crest (Figure 2.10).

The posteriormost margin of the nasofrontal articulation is mediolaterally straight in MOR 1071-C-3-3 and MOR 1071-6-30-98-4, but in MOR 1071-7-13-99-87-I and MOR 940 the medial portion is indented anteriorly (the “M-shape” of Prieto-Márquez, 2005). The margin is gently convex posteriorly in MOR 2919 with no medial indentation. The interfrontal-parietal articulation is posterodorsally elevated in MOR 2919, as noted

for *Brachylophosaurus* (Prieto-Márquez, 2005). In the MOR 1071 subadult braincases, a raised lip defines the posterior margin of the nasofrontal articulation. The posterior margin in MOR 2919 lacks any line or lip, and instead undulates with the rugosities and posterior pits.

In adult *Brachylophosaurus*, the nasofrontal suture covers the entire anteroposterior length of the frontals (Figure 2.11D-2.11E; Figure 2.12). The platform supporting the nasals is posteriorly elongated to overhang the supratemporal fenestrae by a short distance. In NMC 8893, FMNH PR 862, and MOR 1071-7-7-98-86, this projection appears to be composed entirely of the prefrontals, but in MOR 720, it is composed of the frontals. The longer the nasal crest, the more the prefrontals and/or frontals are elongated posteriorly. The gracile-crested MOR 1071-7-7-98-86 possesses prefrontals that overhang the supratemporal fenestra by 2 cm, whereas the more robust FMNH PR 862 possesses prefrontals that overhang by 4 cm. The posteriorly incomplete frontals of MOR 720, a larger individual than FMNH PR 862, would have overhung the fenestrae by at least 5 cm. In subadult specimens where the nasofrontal suture does not cover the entire frontals, the prefrontals and frontals do not protrude over the supratemporal fenestrae at all (MOR 1071-7-13-99-87-I, MOR 1071-C-3-3, MOR 1071-6-30-98-4).

Posterior to the nasofrontal articulation, the frontals of MOR 2919 are shallowly depressed by 5 to 7 mm. *Acristavus* also possesses shallow frontal depressions. Frontal depressions are not observed in adult *Brachylophosaurus* due to complete coverage by the nasofrontal articulation. The MOR 1071 subadult *Brachylophosaurus* specimens have

small anteroposteriorly elongated frontal depressions 3 to 4 mm deep near the frontal-postorbital sutures, more laterally than those of MOR 2919. The dorsal sutures between the frontals and postorbitals of MOR 2919 are faintly visible, but are fused and nearly completely remodeled.

The frontals of the holotype of *Brachylophosaurus goodwini*, UCMP 130139, are fragmented and poorly preserved, but UCMP 130139 remains unique among Brachylophosaurini specimens in possessing deep frontal depressions (at least 2 cm deep). Horner (1988) measured the frontal thickness at the deepest point of the depression in UCMP 130139 as 5 mm thick. The corresponding region in MOR 2919 is 26 mm thick on the right side and 22 mm thick on the left side (slightly crushed).

The frontals of MOR 2919 at the orbital margin are 2.2 cm thick, rugose, and contribute a length of 2.3 cm to the orbital margin with no indentation between the prefrontal and postorbital, similar to that of *Acristavus*. The area near the orbital margin of UCMP 130139 is too poorly preserved to observe the locations of sutures, and so the presence, absence, or extent of frontal contribution to the orbital margin cannot be determined; as in MOR 2919, there is no indentation between the prefrontal and postorbital regions. In *Brachylophosaurus*, the frontal margin may be partially or entirely recessed in a medial indentation (0 to 1 cm deep) in the dorsal orbital margin between the prefrontal and postorbital. The base of this indentation exposes a length of 0 to 3 cm of the frontal to the orbital margin (NMC 8893, FMNH PR 862, MOR 794, all MOR 1071 braincases).

The anterior margin of the frontals in MOR 2919 forms a posteriorly directed "V" (Figure 2.11), similar to that seen in the "slender" adult *Brachylophosaurus* MOR 1071-7-7-98-86. The anterior frontals in subadult *Brachylophosaurus* MOR 1071 braincases form posteriorly directed "U" shapes. Both are distinct from the rectangular anterior frontal margin of *Acristavus*, with its midline slight anterior projection. The adult *Brachylophosaurus* skull GPDM JRF.65 has the rectangular margin of *Acristavus* but without the midline anterior projection.

Parietal. The lateral suture between the parietal and laterosphenoid is fused but still faintly visible. The overall morphology of the parietal is consistent with that of *Brachylophosaurus* and *Acristavus* (Prieto-Márquez, 2005; Cuthbertson and Holmes, 2010; Gates et al., 2011).

Postorbital. The orbital margin of the postorbital in MOR 2919 is similarly rugose to that of the frontal (Figure 2.13A). The lateral surface of the jugal process varies amongst specimens of Brachylophosaurini, and is highly intraspecifically variable within *Brachylophosaurus canadensis*. Thus it may not be a character of taxonomic value. The lateral surface is rough and straight in MOR 2919. This surface is smooth and concave in some *Brachylophosaurus* (MOR 794, MOR 1071-7-7-98-86). In other *Brachylophosaurus* (FMNH PR 862), the superior portion of the jugal process is smooth and gently concave, but inferiorly becomes rough and straight, identical to the condition in *Maiasaura* and Brachylophosaurini indet. (UCMP 130139). Cuthbertson and Holmes (2010) describe the lateral surface of the *Brachylophosaurus* holotype (NMC 8893) as

"deeply pitted", which is more similar to FMNH PR 862 and MOR 2919 than to the specimens from Malta, Montana (MOR 794, MOR 1071-7-7-98-86). The right postorbital of *Brachylophosaurus* TMP 1990.104.001 has a circular pathologic depression, and should not be used for textural comparison. The lateral surface of the jugal process in *Acristavus gagslarsoni* is smooth and concave, matching the Malta specimens. MOR 2919 lacks the anteriorly directed sheet of bone in the posterodorsal corner of the orbit and jugal process depression present in *Acristavus* sp. (UMNHVP 16607).

The squamosal processes of the MOR 2919 postorbitals were fractured at their bases and reattached; these breaks combined with diagenetic deformation make it difficult to determine whether the squamosal processes projected somewhat dorsally as in most hadrosaurines, or remained in line with the anterior postorbitals as in *Brachylophosaurus* and *Acristavus* (Gates et al., 2011). The squamosal processes of MOR 2919 are broken posteriorly before the contact with the squamosal. The sutures between the postorbitals and parietal are completely fused and obscured.

Squamosal. The prequadratic process is stout and as mediolaterally wide as it is dorsoventrally high (Figure 2.13B), similar to that of subadult *Brachylophosaurus* (MOR 1071-7-13-99-87-H), but it is shorter and wider than that of adult *Brachylophosaurus* (NMC 8893, MOR 794, MOR 1071-7-7-98-86) and *Acristavus*. The prequadratic processes of MOR 2919, *Acristavus*, and *Brachylophosaurus* (MOR 1071-7-7-98-86, MOR 1071-7-13-99-87-H) are strongly anteroposteriorly compressed. Outside of Brachylophosaurini, the prequadratic process is nearly twice as dorsoventrally high as it

is mediolaterally wide, and is subcircular in cross section rather than compressed (e.g. *Prosaurolophus*). The prequadratic processes in *Maiasaura* specimens YPM-PU 22405 and OTM F138 are not preserved well enough for comparison. The postquadratic process in MOR 2919, *Acristavus*, and *Brachylophosaurus* (MOR 1071-7-7-98-86) is more mediolaterally compressed than in *Maiasaura* or *Prosaurolophus*.

The articulation for the squamosal process of the postorbital extends to a point on the squamosal above the middle of the quadrate cotylus in MOR 2919, some *Brachylophosaurus* (FMNH PR 862), and Brachylophosaurini indet. (UCMP 130139), and extends just posterior to the middle in other *Brachylophosaurus* (MOR 794, MOR 1071-7-7-98-86). The squamosal process of the postorbital extends just anterior to the middle of the quadrate cotylus in *Acristavus*.

Posteriorly, the parasagittal crest of the parietal appears to bifurcate, similar to the condition in *Acristavus*. In MOR 2919 and *Acristavus*, this apparent bifurcation is actually composed of the posteromedial processes of the squamosals, which contact each other directly (Figure 2.4C-2.4D). The posteromedial processes are broken off of the main bodies of both squamosals of MOR 2919, but a fragment of the left process remains attached to the parietal, with the suture to the parietal fused and nearly obliterated. On the right side, the squamosal was broken roughly at the fused suture. In *Brachylophosaurus*, the squamosals are separated by a narrow (MOR 1071-7-7-98-86) or thickened (NMC 8893; Cuthbertson and Holmes, 2010) extension of the parasagittal crest. In *Maiasaura* OTM F138, the parasagittal crest inserts partially between the posteromedial processes of

the squamosals so they are separated anteriorly but not posteriorly; this area is broken in the *Maiasaura* holotype YPM-PU 22405.

Quadrate. The posterodorsal process below the squamosal condyle is slightly more enlarged than in *Brachylophosaurus*. In MOR 2919 the process is 4 cm high and extends 1 cm posteriorly (Figure 2.14). In *Brachylophosaurus* (NMC 8893, FMNH PR 862, MOR 794, MOR 1071-8-13-98-559-D) the posterodorsal process is more pointed, with its base a maximum of 3 cm high and extending a maximum of 1 cm posteriorly. The posterodorsal process in Brachylophosaurini indet. (UCMP 130139) is more similar to that of *Brachylophosaurus* than to MOR 2919. The posterodorsal process in *Acristavus* is low and gently convex, with its base 2 cm high and extending 3 mm posteriorly. In *Maiasaura* (YPM-PU 22405 and OTM F138) the posterodorsal process is elongated (3-3.5 cm high) as in MOR 2919, but low, extending only 3-5 mm posteriorly, as in *Acristavus*. The posterodorsal process in *Prosaurolophus* has an elongate base 2.5 cm high and extends 3 mm posteriorly, resembling that of *Maiasaura* and *Acristavus*. In *Gryposaurus notabilis* ROM 873 the posterodorsal process is large, convex, and continuous with the posterior margin of the squamosal condyle; in the *G. notabilis* holotype CMN 2278 the posterodorsal process is less pronounced posteriorly, but is vertically straight and continuous with the posterior margin of the condyle.

The dorsal half of the quadrate curves slightly posteriorly in *Brachylophosaurus* (NMC 8893, FMNH PR 862, MOR 794, MOR 1071-8-13-98-559-D) (Sternberg, 1953), Brachylophosaurini indet. (UCMP 130139), and *Maiasaura*, but is straight in MOR 2919 and *Acristavus*. In *Brachylophosaurus* (MOR 1071-8-13-98-559-D) the flange above the

dorsal quadratojugal articulation is much larger anteriorly than the ventral flange to accommodate the posterior deflection of the dorsal quadrate, so that the dorsal quadratojugal articulation is directly above the ventral in life position. Specimens with straight quadrates (MOR 2919 and *Acristavus*) have shallow quadratojugal embayments, with the dorsal flange only slightly larger than the ventral flange. Although *Maiasaura* possesses the posterior deflection of the dorsal quadrate, its quadratojugal flanges are nearly equal in size.

As in *Brachylophosaurus*, the embayment for the quadratojugal in MOR 2919 has roughened articular surfaces for the dorsal and ventral quadratojugal contacts, and is smooth in between them, suggesting the presence of a paraquadratic foramen. The pterygoid flange has a slightly roughened surface where it articulates with the pterygoid; its extent is similar to that in *Brachylophosaurus* (FMNH PR 862, MOR 1071-8-13-98-559-D); the dorsal margin of the articulation in MOR 2919 is defined by a slight ridge also present in *Brachylophosaurus*. The articulation surfaces in *Acristavus* and *Maiasaura* (OTM F138) are very subtly roughened.

Quadratojugal. No quadratojugals are preserved.

Braincase

The braincase elements are fully fused and suture lines are either in the process of being remodeled or are already obliterated (Figure 2.15), making the contacts of individual elements difficult to define, as in NMC 8893 (Cuthbertson and Holmes, 2010). Crushing has obscured some cranial nerve foramina. Aside from the features noted

below, the overall morphology conforms to that of *Brachylophosaurus* (Prieto-Márquez, 2005).

The large alar process of the basisphenoid is extremely thin, as in *Brachylophosaurus* (MOR 1071-7-7-98-86); the proximal-distal striations are more prominent in MOR 2919. The posteroventral process of the basisphenoid is more pronounced in MOR 2919 than in *Maiasaura* (OTM F138), *Acristavus*, and some *Brachylophosaurus* specimens (MOR 1071-7-7-98-86), but smaller than in others (NMC 8893; Cuthbertson and Holmes, 2010). In *Brachylophosaurus* (MOR 1071-7-7-98-86) and *Acristavus* the pterygoid processes of the basisphenoid are directed nearly entirely laterally, and slightly anteriorly and ventrally. In MOR 2919 and *Maiasaura* (OTM F138) the pterygoid processes are directed more ventrally than laterally, and slightly posteriorly. Much of this difference may be diagenetic; the braincases of MOR 1071-7-7-98-86 and MOR 1155 are dorsoventrally compressed, MOR 2919 is laterally compressed, and OTM F138 is slightly laterally compressed. The direction of compression likely determines the relative degree of lateral or ventral orientation of the pterygoid processes, and may determine whether the pterygoid processes are directed slightly anteriorly or posteriorly. Thus, the angle between the pterygoid processes of the basisphenoid is not a useful phylogenetic character without first accounting for diagenetic influence on all specimens.

In MOR 2919 as in *Brachylophosaurus* (NMC 8893, MOR 1071-7-7-98-86), the opening for cranial nerve VII is slightly posteroventral to cranial nerve V, rather than directly posterior as in *Acristavus* (UMNHVP 16607) (Cuthbertson and Holmes, 2010; Gates et al., 2011). The groove in the opisthotic leading from cranial nerve VIII to the

exoccipital is much wider and deeper in *Brachylophosaurus* (MOR 1071-7-7-98-86) than in MOR 2919. The paraoccipital processes of the exoccipitals barely curve anteriorly, similar to *Brachylophosaurus* (NMC 8893, MOR 794), and unlike the strong anterior curvature in *Acristavus*. The region of the posteriormost contacts between the squamosals, supraoccipital, and exoccipitals is broken, but if intact the exoccipital roof would have been short as in *Brachylophosaurus* (MOR 1071-7-7-98-86).

Palate

The pterygoids, ectopterygoids, vomers, and palatines are not preserved in MOR 2919. A partial palatine in MOR 1097 is morphologically similar to that of *Brachylophosaurus* (MOR 1071-7-26-99-221).

Mandible

Predentary. The predentary is very poorly preserved, but its relative dimensions are similar to those of *Brachylophosaurus* (MOR 1071-7-28-98-299), being roughly twice as wide mediolaterally as anteroposteriorly, and having a squared anterolateral corner (Figure 2.16A). The denticles are not preserved, and the nutrient foramina are crushed and obscured.

Dentary. The dental lamina is extremely thin; in some regions there are ridges corresponding to the median carinae of the teeth, and in other areas the lamina is so thin that the median carinae are exposed, possibly due to postmortem abrasion of the lamina (Figure 2.16). In *Brachylophosaurus* (FMNH PR 862), *Acristavus*, and *Maiasaura*, the

dental laminae are similarly ridged superficial to the carinae. The left dentary of MOR 2919 is larger than any other brachylophosaurin dentary (Table 2.1), and preserves the complete series of 43 tooth rows. *Brachylophosaurus canadensis* dentaries contain up to 39 tooth rows (NMC 8893; Sternberg, 1953); other specimens have 33 tooth rows (MOR 1071-8-98-X) and 36 tooth rows (FMNH PR 862). Most dentary tooth rows in MOR 2919 contribute two teeth to the occlusal surface, which is less concave than in other Brachylophosaurini. Typically, each tooth row corresponds to one medial dental foramen. However, the 3rd and 4th anterior tooth rows share the same dental foramen; because the number of tooth rows in hadrosaurs increases ontogenetically (Horner and Currie, 1994), this could represent the origin of an additional tooth row, and an additional foramen would develop later. The ventromedial groove that leads to the Meckelian canal originates below or anterior to the first tooth row in *Brachylophosaurus* (FMNH PR 862, MOR 1071-8-98-W, NMC 8893) (Cuthbertson and Holmes, 2010) and the *Maiasaura* holotype YPM-PU 22405, but several rows posterior to the first tooth row in MOR 2919, *Acristavus*, and *Maiasaura* OTM F138.

The dentary teeth have a prominent median carina with no secondary carinae. The median carinae are straight or rarely extremely subtly sinusoidal in MOR 2919, but many median carinae are subtly sinusoidal in at least one *Brachylophosaurus* (FMNH PR 862). The edges of the crowns have faint papillae that are much less prominent than the papillae on the maxillary teeth.

MOR 2919 has five anterolateral dental foramina. *Brachylophosaurus canadensis* may be intraspecifically variable: NMC 8893 has four anterolateral dental foramina

(Cuthbertson and Holmes, 2010), but FMNH PR 862 has either four or five anterolateral dental foramina (preservation may be obscuring some foramina). *Maiasaura* is also intraspecifically variable: YPM-PU 22405 has five foramina, but OTM F138 only has four foramina. Acristavus has four foramina.

MOR 2919, *Maiasaura*, and *Acristavus* possess a relatively shorter proximal edentulous slope of the dentary than in *Brachylophosaurus* (NMC 8893, FMNH PR 862, MOR 1071-8-98-W). In *Brachylophosaurus* and *Maiasaura*, the edentulous slope is actually horizontal for a few centimeters just anterior to the first tooth row before sloping anteroventrally; in MOR 2919 and *Acristavus* the anteroventral slope begins immediately anterior to the first tooth row.

Maiasaura (OTM F138, ROM 44770; area broken in holotype YPM-PU 22405) and *Brachylophosaurus* (NMC 8893, FMNH PR 862) are unique in possessing a dentary coronoid process with a horizontally straight dorsal margin leading to a sharp caudodorsal point (Figure 2.17). MOR 2919 has the horizontally straight dorsal margin, although it is thin and slightly broken, and appears to lack the caudodorsal point. The caudodorsal point also appears absent in *Acristavus*, but the posterodorsal margin of the coronoid process is slightly broken, and so the presence or absence of a caudodorsal point cannot be confirmed. The caudodorsal point develops ontogenetically in *Maiasaura* and *Brachylophosaurus*; juveniles have the straight dorsal margin with no point (MOR 547-W-55-2P, MOR 1071-8-1-99-313), similar to the state of the stratigraphically older MOR 2919. The subadult *Probrachylophosaurus* specimen, MOR 1097, does include a coronoid process, but the dorsal end is broken, so the size and shape of its margins cannot

be observed. The presence or absence of a caudodorsal point may be a useful ontogenetic taxonomic character, but because the point is easily taphonomically broken, it may be difficult to determine whether the absence of a caudodorsal point is true or taphonomic in certain specimens.

Surangular. The surangular (Figure 2.16D-2.16E) conforms in all respects to the morphology described for *Brachylophosaurus* (Prieto-Márquez, 2005; Cuthbertson and Holmes, 2010). The surangular of *Acristavus* is also consistent with that of *Brachylophosaurus* (Gates et al., 2011). The articular, splenial, and angular are not preserved.

Postcrania

In nearly all respects, the postcrania of MOR 2919 are consistent with those of *Acristavus* and *Brachylophosaurus*.

Vertebrae. In all collected vertebrae of MOR 2919 (cervicals, dorsals, and caudals), the neural arches are fully fused to the centra, with the suture lines nearly completely obliterated (Figures 2.17-2.18). Small cervical, dorsal, and caudal vertebrae from the MOR 1071 bonebed either have unfused neural arches found disarticulated from their centra, or are unfused but remained connected. A broken surface on an adult (determined by relative size) *Brachylophosaurus canadensis* dorsal vertebra MOR 1071-8-18-98-593 demonstrates that internal fusion and remodeling are complete, but the external surface of the suture line is still being remodeled. A dorsal vertebra of MOR

2919 from a similar serial position exhibits very faint remodeled bone texture along the location of sutural fusion.

MOR 2919 includes atlas fragments, 10 well-preserved cervical vertebrae, and fragments of additional cervical vertebrae, for a total of at least 12 cervical vertebrae (Figure 2.18). One cervical is morphologically consistent with cervical 14 of NMC 8893, the holotype of *Brachylophosaurus canadensis* (Cuthbertson and Holmes, 2010). Because the cervical series of MOR 2919 is incomplete, it cannot be determined whether this is actually the 14th vertebra in the series. Prieto-Márquez (2007) describes the articulated *B. canadensis* specimen MOR 794 as having only 13 cervical vertebrae, but Cuthbertson and Holmes (2010) note that they may differ in their interpretation of whether the 14th vertebra is a cervical or a dorsal.

Pelvis and Hindlimb. In *Brachylophosaurus* MOR 1071 specimens, the ischial peduncle of the pubis flares at its tip. In *Acristavus* and MOR 2919, it is a more rounded enlargement (Figure 2.20). The lengths of the fully intact limb bones (tibia, fibula, and metatarsal II; Figure 2.21) are provided in Table 2.3.

Pathologies

Pathologies are present on both dentaries, at least six caudal vertebrae, and at least two metatarsals. The dentaries of MOR 2919 possess a total of three pathologic circular depressions each surrounded by a ring of raised bone (Figure 2.16). Six middle caudal vertebrae of MOR 2919 exhibit neural spine pathologies consistent with various degrees of breakage and healing. The pathologies are limited to a single region of the middle of

the tail (Figure 2.19); the caudal series is disarticulated and incomplete, so there may have been additional pathologic vertebrae within this region. The only two metatarsals recovered, the right II and IV, both exhibit pathologic rugose surface texture. The right metatarsal II has this rugose texture on much of its contact surface with metatarsal III, and nowhere else. The right metatarsal IV has the rugose texture concentrated on its medial contact surface with metatarsal III, as well as it distal posterolateral surface. Metatarsal III was not recovered, but presumably would have suffered from a similar pathology. The distal ends of both tibiae and both fibulae exhibit patches of pathologic surface texture, suggesting that both feet may have been similarly affected. The pathologies of MOR 2919 will be described and discussed in detail in a later paper.

Summary of Morphologic Comparisons Among *Probrachylophosaurus* and Other Brachylophosaurins

In cases where cranial morphology can be directly compared between *Probrachylophosaurus*, *Acristavus*, *Brachylophosaurus*, and *Maiasaura*, *Probrachylophosaurus* is always more similar to *Acristavus* or *Brachylophosaurus* than it is to *Maiasaura*. The cranial elements with the most useful features for comparing brachylophosaurins are the jugal, lacrimal, nasal, frontal, squamosal, quadrate, braincase, and dentary.

The palatine process of the jugal in subadult *Probrachylophosaurus* (MOR 1097) is identical to the stratigraphically older *Acristavus*, but the palatine process of the jugal in adult *Probrachylophosaurus* (MOR 2919) is most similar to the stratigraphically younger *Brachylophosaurus*. The palatine process in *Maiasaura* is more similar to

Acristavus and subadult *Probrachylophosaurus* than to *Brachylophosaurus* and adult *Probrachylophosaurus*. The caudoventral apex of the jugal is posterior to the caudodorsal apex in both *Probrachylophosaurus* and *Acristavus*; the apices are vertically aligned in *Brachylophosaurus*. *Maiasaura* possesses an intermediate condition. The ventral margin of the rostral process of the jugal is nearly straight in *Probrachylophosaurus*, *Acristavus*, and *Maiasaura*, but sigmoidal in *Brachylophosaurus*. The concavity of the posterior jugal margin is shallow in *Probrachylophosaurus*, *Acristavus*, and *Maiasaura*, but deeper in *Brachylophosaurus*. The medial excavation of the quadratojugal process of the jugal is shallowest in *Probrachylophosaurus*, less shallow in *Acristavus*, and deepest in *Brachylophosaurus* and *Maiasaura*. The mediolateral width of the lacrimal is more thick and robust in *Probrachylophosaurus* and *Acristavus* than in *Brachylophosaurus* and *Maiasaura*.

Probrachylophosaurus and *Brachylophosaurus* are united by having a solid nasal crest overhanging the dorsal skull roof; *Acristavus* lacks any crest, and *Maiasaura* has a crest formed by the dorsal projection of both the nasals and frontals (Sternberg, 1953; Horner and Makela, 1979; Horner, 1983; Gates et al., 2011). The nasal crest of the smaller adult ("slender") *Brachylophosaurus* resembles a hypermorphic form of a *Probrachylophosaurus* crest, extending the crest posteriorly and laterally. The larger adult ("robust") *Brachylophosaurus* crest continues this growth trajectory, with the posterolateral growth forming a flat paddle shape. These taxa have the same pattern in their nasofrontal articulation; subadult *Brachylophosaurus* and adult *Probrachylophosaurus* possess a nasofrontal articulation covering slightly over half of

the dorsal frontal surface, whereas adult *Brachylophosaurus* have a larger nasofrontal articulation that covers the entire dorsal frontal surface.

The frontal contribution to the orbital margin is more similar in *Probrachylophosaurus* and *Acristavus* than either is to that of *Brachylophosaurus*. The prequadratic process of the squamosal in *Probrachylophosaurus* is more similar to that of subadult *Brachylophosaurus* than adult *Brachylophosaurus* or *Acristavus*. The postquadratic process of the squamosal is similar in *Probrachylophosaurus*, *Acristavus*, and *Brachylophosaurus*, and different from that of *Maiasaura*. The posterior end of the postorbital-squamosal articulation occurs just anterior to the middle of the quadrate cotylus in *Acristavus*, in the middle of the cotylus in *Probrachylophosaurus* and some *Brachylophosaurus* specimens, and just posterior to the middle in other *Brachylophosaurus*. In *Probrachylophosaurus* and *Acristavus*, the squamosals contact each other. In *Maiasaura*, the squamosals are partially separated by the parietal, and in *Brachylophosaurus*, the squamosals are completely separated by the parietal. The location of cranial nerve VII and the curvature of the paraoccipital processes of the exoccipitals are more similar in *Probrachylophosaurus* and *Brachylophosaurus* than in *Acristavus*.

The size and shape of the posterodorsal process of the quadrate is similar in *Probrachylophosaurus* and *Brachylophosaurus*. The process in *Acristavus* is shorter and smaller; the process in *Maiasaura* is intermediate between *Probrachylophosaurus* and *Acristavus*. The quadrate is straight in *Probrachylophosaurus* and *Acristavus*, but curved in *Brachylophosaurus* and *Maiasaura*.

The position of the ventromedial groove of the dentary of *Probrachylophosaurus* is more similar to *Acristavus* and *Maiasaura* OTM F138 than to *Brachylophosaurus* or *Maiasaura* YPM-PU 22405. The proximal edentulous slope of the dentary is shorter in *Probrachylophosaurus*, *Maiasaura*, and *Acristavus* than it is in *Brachylophosaurus*. The proximalmost portion of the edentulous slope is immediately sloping in *Probrachylophosaurus* and *Acristavus*, but horizontal in *Brachylophosaurus* and *Maiasaura*.

Probrachylophosaurus exhibits a unique combination of characters that make it morphologically intermediate between *Acristavus* and *Brachylophosaurus*. *Probrachylophosaurus* is most similar to *Acristavus* in overall morphology of the jugal and lacrimal. The morphologies of the frontal, quadrate, and squamosal are more similar to *Acristavus* in some attributes, but more similar to *Brachylophosaurus* in others. The braincase of *Probrachylophosaurus* is most similar to *Brachylophosaurus*. The presence of a posteriorly-oriented nasal crest also unites *Probrachylophosaurus* with *Brachylophosaurus*. The dentary is more similar to that of *Acristavus* than to *Brachylophosaurus*. These relationships of morphological similarities and differences were analyzed in more detail using phylogenetic analyses.

Phylogenetic Analyses

Analyses Based on Matrix of Prieto-Márquez (2010a)

Probrachylophosaurus bergei was coded into two versions of the matrix of Prieto-Márquez (2010b). The first version included some recodings of previous taxa, with

all characters included. The second version included these same recodings, but excluded some characters as detailed below.

The first analysis using the Prieto-Márquez (2010a) matrix included recodings of eight characters for *Acristavus* based on reexamination of the material. See Prieto-Márquez (2010a) for complete descriptions of characters and abbreviation codes (e.g., J4 is the fourth jugal character). Character 106 (J4), the relative position of the caudoventral apex of the rostral process of the jugal, was changed from state 1 to 0. *Probrachylophosaurus* is also coded as 0; *Brachylophosaurus* and *Maiasaura* are state 1. The quadrate of the *Acristavus* holotype (MOR 1155) was not coded into the original matrix, so it has been added here, replacing characters 116-121 (Q1-Q6) ?????? with 011211. These are the same codings as the quadrate of *Probrachylophosaurus* and *Brachylophosaurus*; *Maiasaura* has states 001211. Character 259 (PB8), the length/width ratio of the ischial peduncle of the pubis, was recoded from 0 to 1 for *Acristavus*; *Probrachylophosaurus*, *Brachylophosaurus*, and *Maiasaura* are also state 1.

In *Brachylophosaurus*, Character 138 (F1) was originally coded as state 0, indicating the lack of bifurcation of the anterior frontal margin. However, this is only true for some adult specimens (e.g. GPDM JRF.65); the "slender" adult *Brachylophosaurus* MOR 1071-7-7-98-86 and subadults MOR 1071-7-13-99-87-I and MOR 1071-C-3-3 have bifurcated anterior frontal margins, so this was recoded to the multistate "01".

When *Probrachylophosaurus bergei* is added to Prieto-Márquez's (2010a) matrix, with extraneous taxa removed and some character states recoded (see above), but all characters included (Appendix C), four most parsimonious trees were produced. The

strict consensus tree recovers *Brachylophosaurus* and *Maiasaura* as sister taxa, with *Probrachylophosaurus* and *Acristavus* forming a basal polytomy within Brachylophosaurini (Appendix F). Characters responsible for the position of *Probrachylophosaurus* included: 1 (dtth1), number of dentary tooth positions; 15 (mxth1), number of maxillary tooth positions; 36 (dt4), angle of the ventral rostral margin of the dentary; 44 (dt13), lack of caudodorsal point on coronoid process of dentary; 106 (j4), relative positions of caudodorsal and caudoventral apices of rostral process of jugal; 110 (j8), size of caudoventral flange of jugal; 113 (j11), ratio of caudal and rostral constrictions of jugal; and 143 (f6), contribution of the frontal to the orbital margin. The bootstrap 50% majority-rule consensus tree (5,000 replicates) finds 55% support for a *Probrachylophosaurus-Brachylophosaurus-Maiasaura* clade, with *Acristavus* as the basal member of Brachylophosaurini, and 64% support for *Brachylophosaurus* and *Maiasaura* as sister taxa.

Three of Prieto-Márquez's (2010a) characters were then excluded from the second analysis. Characters 1 (dtth1) and 15 (mxth1) are based on the number of teeth in the dentary and maxilla, respectively. The number of teeth in hadrosaur jaws increases ontogenetically (Langston, 1960; Horner and Currie, 1994), so the high tooth counts in MOR 2919 are liable to be due to the specimen's size and maturity rather than a true phylogenetic signal separating it from *Brachylophosaurus* and *Maiasaura*. Character 123 (pf2) describes the shape of the prefrontal contribution to the orbital margin. Many specimens of Brachylophosaurini examined in this study are intermediate between the

character states, and so this character was excluded to avoid ambiguous state assignments.

Character 143 (f6) in Prieto-Márquez (2010a) is a modification of character 57 in Horner et al. (2004). The contribution of the frontal to the orbital margin is either present or absent in Horner et al. (2004), but Prieto-Márquez (2010a) divides presence into two states, frontal exposed and forming part of orbital margin, or forming a narrow triangular apex that may or may not reach the orbital margin between the prefrontal and postorbital. This division is problematic because the width of the orbital contribution of the frontal is intraspecifically variable in *Brachylophosaurus* (MOR 1071 braincases, FMNH PR 862), and potentially may vary similarly in other taxa that currently have smaller sample sizes. Also, the distinction between the two states (frontal forming part of orbital margin or doing so through a narrow triangular apex) is not well defined. Prieto-Márquez (2010a) codes *Acristavus*, *Brachylophosaurus*, and *Maiasaura* as having the narrow triangular apex, but their contribution to the orbital margin can be more than 1 cm and not triangular. Thus, the frontal contribution to the orbital margin, when present, forms a continuum rather than two discrete states. End members are clear, but most brachylophosaurin specimens fall in between the end points, and so the original version of the character (simply presence or absence of frontal contribution to the orbital margin) in Horner et al. (2004) is preferred. Consequently, character 143 (f6) was recoded to merge states 0 and 1, so there are only two states (presence or absence) rather than three.

After these exclusions and recodings (Appendix D), two most parsimonious trees were produced. The strict consensus tree recovers *Acristavus* as the basal member of

Brachylophosaurini, with *Brachylophosaurus* and *Maiasaura* as sister taxa, and *Probrachylophosaurus* in an intermediate position (Figure 2.22). *Probrachylophosaurus, Brachylophosaurus*, and *Maiasaura*, but not *Acristavus*, share one apomorphic character state: 134 (sq1), very short precotyloid process of the squamosal. *Probrachylophosaurus* differs from *Acristavus*, *Brachylophosaurus*, and *Maiasaura* in its state for three characters: 36 (dt4), angle of the ventral rostral margin of the dentary; 110 (j8), size of the caudoventral flange of the jugal; and 113 (j11), ratio of caudal and rostral constrictions of the jugal; these character states are homoplasies shared with non-brachylophosaurin hadrosaurine taxa. *Brachylophosaurus* and *Maiasaura* are united as sister taxa due to two characters: 44 (dt13), the autapomorphic presence of a caudodorsal point on the coronoid process of the dentary; and 106 (j4), relative positions of caudodorsal and caudoventral apices of the rostral process of the jugal. Compared to the previous result, this bootstrap 50% majority-rule consensus tree finds increased (66%, was 55%) support for a *Probrachylophosaurus-Brachylophosaurus-Maiasaura* clade, with *Acristavus* as the basal member of Brachylophosaurini, and decreased (56%, was 64%) support for *Brachylophosaurus* and *Maiasaura* as sister taxa.

Analysis Based on Matrix of Gates et al. (2011)

When *Probrachylophosaurus bergei* is added to Gates et al.'s (2011) matrix, with extraneous taxa removed (see Methods), but all characters included (Appendix E), two most parsimonious trees were produced. The strict consensus tree recovers *Probrachylophosaurus* and *Brachylophosaurus* as sister taxa, with *Acristavus* as the basalmost member of Brachylophosaurini (Figure 2.23). *Probrachylophosaurus,*

Brachylophosaurus, and *Maiasaura*, but not *Acristavus*, share two apomorphic character states: character 36 state 1, presence of solid nasal crest; and character 37 state 1, circumnarial fossa terminates anterior to nasal crest. *Acristavus*, *Probrachylophosaurus*, and *Maiasaura*, but not *Brachylophosaurus*, share one apomorphic character state: character 53 state 0, straight to slightly curved ventral margin of the rostral process of the jugal. *Probrachylophosaurus* and *Brachylophosaurus* are united as sister taxa due to one apomorphic character state: character 105 state 0, postacetabular process is less than 40 percent the total length of the ilium. *Probrachylophosaurus* differs from *Acristavus*, *Brachylophosaurus*, and *Maiasaura* in its state for one character: character 72 state 0, low basipterygoid transverse ridge of the basisphenoid. The bootstrap 50% majority-rule consensus tree (50,000 replicates) finds 50% support for *Probrachylophosaurus* and *Brachylophosaurus* as sister taxa, with the positions of *Acristavus* and *Maiasaura* having less than 50% support.

Phylogenetic Relationships

Brachylophosaurini is supported as a robust clade in all recent phylogenetic analyses, but the relationships amongst its members vary. Prior to the description of *Acristavus gagslarsoni*, this clade consisted solely of *Maiasaura peeblesorum* and *Brachylophosaurus canadensis* (Horner et al., 2004; Prieto-Márquez, 2005; Gates and Sampson, 2007). Prieto-Márquez (2010a) recovered *Maiasaura* and *Brachylophosaurus* as sister taxa, with *Acristavus* ("Two Medicine OTU") as the basal member of the clade. However, Gates et al. (2011) recovered *Acristavus* and *Maiasaura* as sister taxa.

When *Probrachylophosaurus* is added to the Prieto-Márquez (2010a) and Gates et al. (2011) matrices, it is recovered with confidence as a member of Brachylophosaurini (bootstrap support 87% in both analyses). *Acristavus* is recovered as the basal taxon in all analyses, consistent with its stratigraphic position; thus, *Acristavus* or a close relative was likely ancestral to the rest of Brachylophosaurini. The inclusion of *Probrachylophosaurus* in the Prieto-Márquez (2010a) matrix still results in *Maiasaura* and *Brachylophosaurus* as sister taxa, but with much weaker bootstrap support for the clade (56% vs. 69% in Prieto-Márquez, 2010a). *Probrachylophosaurus* is recovered as intermediate between *Acristavus* and the *Brachylophosaurus*-*Maiasaura* clade. The inclusion of *Probrachylophosaurus* in the Gates et al. (2011) matrix yields *Probrachylophosaurus* and *Brachylophosaurus* as sister taxa, with *Maiasaura* intermediate between them and *Acristavus.* The differing positions of *Maiasaura* relative to *Probrachylophosaurus* and *Brachylophosaurus* in each analysis leads to uncertainty regarding the timing of the cladogenic split between the *Brachylophosaurus* and *Maiasaura* lineages. The analysis based on the Gates et al. (2011) matrix suggests that *Maiasaura* diverged from the *Probrachylophosaurus*-*Brachylophosaurus* lineage sometime between the stratigraphic existence of *Acristavus* and *Probrachylophosaurus* (Figure 2.23). The analysis based on the Prieto-Márquez (2010a) matrix suggests that the *Maiasaura* lineage either diverged from the *Brachylophosaurus* lineage sometime between the stratigraphic existence of *Probrachylophosaurus* and *Brachylophosaurus*, or *Maiasaura* is derived from *Brachylophosaurus* (Figure 2.22).

In the analysis based on the Prieto-Márquez (2010a) matrix, *Brachylophosaurus* and *Maiasaura* are united by two characters: 44 (dt13) caudodorsal point on the coronoid process of the dentary and 106 (j4) position of the caudoventral apex of the rostral process of the jugal relative to the caudodorsal margin of the rostral process. The caudodorsal point on the coronoid process of the dentary is potentially very useful for taxon identification, but is also problematic. The caudodorsal margins of Brachylophosaurini coronoid processes are very thin, and are broken in many specimens. The caudodorsal margins of the coronoid processes of *Acristavus* and *Probrachylophosaurus* are extremely thin and partially broken; they do not preserve points, and the thinness of the bone seems to indicate that there could not have been a point, but this cannot be confirmed with absolute confidence. Also, the caudodorsal point enlarges ontogenetically in *Brachylophosaurus* and *Maiasaura*; small individuals lack the point entirely. Thus, the maturity of a specimen lacking the caudodorsal point must be considered before including it in phylogenetic analyses. The *Acristavus* and *Probrachylophosaurus* holotypes are from large enough individuals that they should display the adult condition for this character. Character 106 (j4) concerns the relative positions of the caudodorsal and caudoventral points of the rostral process of the jugal. *Maiasaura* is coded as having the same state as *Brachylophosaurus*; the caudoventral point is directly ventral to the caudodorsal point, rather than being posterior to the caudodorsal point as it is in *Acristavus* and *Probrachylophosaurus*. However, in *Maiasaura*, the caudoventral point is slightly posterior to the caudodorsal point, and so is actually intermediate between the states of *Acristavus*-*Probrachylophosaurus* and

Brachylophosaurus. In summary, the phylogenetic analyses concur in placing *Acristavus* as the basalmost member of the Brachylophosaurini, consistent with its relative stratigraphic position, but the relationships among *Probrachylophosaurus*, *Brachylophosaurus*, and *Maiasaura* vary depending on the cladistic matrix used.

Histology

The left tibia of MOR 2919 includes 14 lines of arrested growth (LAGs) (Figures 2.24-2.25). Because LAGs represent annual interruptions in bone growth (Köhler et al., 2012), this indicates that MOR 2919 was 14 years old at time of death. The outermost LAGS (11-14) are closely spaced, yet still retain vascularity, and so cannot be considered an External Fundamental System (EFS). This indicates that MOR 2919 was still increasing its tibia circumference, and therefore body length and body mass, at time of death.

Bone apposition rates in hadrosaurs are generally greater on the posteromedial side of the cortex than on the anterolateral cortex (H. N. Woodward, personal communication 2013). In MOR 2919, this produced thicker zones between early LAGs on the posteromedial side. Later, bone deposition continued on the posteromedial side while it had ceased on the lateral side, resulting in the highest number of LAGs (14) countable on the posteromedial side, with the number of LAGs decreasing along the posterolateral (12-8 LAGs) and anteromedial (13-11 LAGs) cortex, and the fewest number of LAGs (8) countable on the lateral cortex (Figure 2.24). LAGs 1-12 are well defined and visible at 10x total magnification. When present, LAGs 13 and 14 are visible

at 40x total magnification. LAG 13 is visible as a darkened band that sometimes contains one or more lines. Thus, LAG 13 may not actually be a LAG, but may instead be an annulus, which represents an annual marker of growth that slowed but did not actually stop as it would in a LAG. LAG 14, when present, is extremely close to the outer surface of the cortex.

Generally, the zone thickness (spacing between LAGs) decreased each year, indicating a faster growth rate in the first few years of life, followed by a gradual decrease in growth rate (Figure 2.26). However, LAGs 5, 6, and 7 are relatively closely spaced, with wider growth zones occurring between later LAGs. This may indicate that the two growing seasons in between LAGs 5 and 6, and 6 and 7, were stressful times of low access to resources, and so growth was limited.

LAG 8 is actually a zone of one to five closely spaced lines occurring after a zone of typical annual bone deposition (Figure 2.25). Similar to the locations of outermost LAG deposition, LAG zone 8 contains the most lines (five) on the posteromedial side of the tibia, decreasing incrementally around the circumference, with a single line along the anterolateral to posterolateral sides. This LAG zone is interpreted as the result of a mild "unfavorable season" (*sensu* Köhler et al., 2012), perhaps a mild winter, during which small increments of bone deposition occurred between multiple pauses in growth, rather than the typical single cessation of growth for the entire unfavorable season. The circumference of LAG 8 was measured at the outermost line of the zone, because the outer circumference of this line marks the resumption of growth in the favorable season, as it does for all other LAGs.

The bone is minimally remodeled, such that LAG 1 is clearly visible along most of its circumference, and still faintly visible on the anterior side where secondary osteons mostly obscure the original bone texture. Secondary osteons are mainly confined to the area between the medullary cavity and LAG 1. Isolated secondary osteons are also scattered sparsely throughout the cortex. The only area of intensive remodeling outside of LAG 1 occurs as a narrow "fountain" of secondary osteons leading from the medullary cavity to the anterolateral outer cortex (Figure 2.27). This location corresponds to the anterolateral border of the tibia, along which runs the M. tibialis anterior. Dilkes (1993; 2000) notes that in turtles, *Sphenodon*, and squamates, the M. tibialis anterior originates on the anterior, medial, and lateral sides of the diaphysis of the tibia, whereas in crocodilians it originates from the proximolateral surface of the tibia, and in birds it originates on the lateral outer cnemial crest of the tibia and the anterior external condyle of the femur. Dilkes (1993; 2000) reconstructed the M. tibialis anterior of *Maiasaura* as originating on the cnemial crest of the proximal tibia due to the presence of muscle scarring on the cnemial crest. If the origin of the M. tibialis anterior actually covered a larger area, continuing down the anterolateral tibial diaphysis, then the "fountain" of secondary osteons along the anterolateral border of MOR 2919 may be due to it being a muscle attachment area; however, the cortical surface is smooth, with no scarring indicative of muscle attachment. Alternatively, the anterolateral border of the tibia may simply be an area subjected to great compressive or extensive stress, triggering Haversian remodeling.

This remodeled region is possibly similar to the "anterolateral plug" in a *Dysalotosaurus* (Ornithischia: Dryosauridae) tibia (Hübner, 2012), but the "fountain" in MOR 2919 is a continuous band of fairly consistent width connecting the medullary cavity to the periosteal surface and is nearly entirely composed of secondary osteons; the "plug" in *Dysalotosaurus* is "whirl-like" and may not extend to the medullary cavity or the periosteal surface. The "plug" is initially composed of randomly oriented primary osteons, and later contains a higher density of secondary osteons than are found in other areas of the tibial cross-section; it is interpreted as forming due to this area being a muscle attachment site (Hübner, 2012). The "fountain" of MOR 2919 and "anterolateral plug" of *Dysalotosaurus* are similar in their location and presence of secondary osteons, but the radial extent and degree of remodeling are much greater in MOR 2919. Adult *Maiasaura* also have concentrations of secondary osteons on the anterior side of the tibia that remodel the radial vascularity of the primary bone tissue in this area; Woodward et al. (in press) hypothesize that this remodeling results from muscle insertion on the anterior tibial border.

Histologic Maturity

The growth inflection points (Figure 2.26) occur later in MOR 2919 than in *Maiasaura*, indicating later sexual and skeletal maturation. Whereas *Maiasaura* is hypothesized to reach sexual maturity between two and three years of age (Woodward et al., in press), the corresponding inflection point in the growth of MOR 2919 occurs at 5 years of age. This suggests that *Probrachylophosaurus* had delayed sexual maturity relative to *Maiasaura*.

At the second inflection point, *Maiasaura* begins depositing an external fundamental system (EFS), indicating skeletal maturity (Woodward et al., in press). MOR 2919 decreases its growth rate at the second inflection point, but does not deposit an EFS, so it has not yet reached true skeletal maturity. This second decrease in growth rate occurs later in MOR 2919 (10 years) than in the largest sampled *Maiasaura* tibia (8 years). The later achievement of the second inflection point, as well as the lack of an EFS, suggests that *Probrachylophosaurus* attained skeletal maturity later than *Maiasaura*. However, the age of skeletal maturity in *Maiasaura* is individually variable (Woodward et al. in review), so a greater sample size of *Probrachylophosaurus* is needed to determine whether the apparent delayed maturation relative to *Maiasaura* is real or simply reflects individual variation in growth rates. In either case, MOR 2919's histology suggests that *Probrachylophosaurus* is a larger-bodied taxon than *Maiasaura* at all growth stages.

Although MOR 2919 lacks an EFS, its histology confirms that its growth rate had greatly slowed and it was possibly somewhat near skeletal maturity. Thus, its "adult" status is supported by three independent lines of evidence: histology, large body size, and externally fused and remodeled axial sutures. The term "adult", as applied to MOR 2919, is used to indicate that this is not a subadult specimen that may reasonably be expected to grow a full paddle-shaped nasal crest as seen in *Brachylophosaurus canadensis*. Its skull and body size, compared to the size distribution of its close relative *B. canadensis*, clearly categorize it as an adult *sensu* Evans (2010). However, because MOR 2919 has not attained an EFS, it is technically not skeletally mature, and by some definitions (e.g.,

Horner et al., 2009) would not be considered an adult. In this paper, MOR 2919 is considered an adult, and a fully skeletally mature specimen with an EFS would be considered a "senescent adult".

MOR 794, a large "adult" *Brachylophosaurus canadensis*, is similar to MOR 2919 in that it also has not yet deposited an EFS (Figure 2.28). The LAGs in the outermost cortex of the femur of MOR 794 are more widely spaced than those of MOR 2919; the outermost 3 mm of the femur of MOR 794 contain only one LAG, whereas the outermost 3 mm of the tibia of MOR 2919 contain five LAGs (Figure 2.25). Thus, MOR 2919, with its smaller nasal crest, is at a slightly later ontogenetic stage than MOR 794, and so MOR 2919 cannot represent an immature stage of *Brachylophosaurus canadensis*.

Discussion

Ontogeny is intimately tied to evolution, as in a very general sense, ontogeny recapitulates phylogeny (Haeckel, 1866, 1901). This is often expressed in juvenile dinosaurs, which may bear morphologic traits of their adult ancestors (peramorphy) that are not expressed in the adults of the later taxon, e.g. juvenile *Bactrosaurus* dentition resembling that of iguanodonts (Rozhdestvensky, 1965). Because juveniles may retain ancestral characteristics, without proper stratigraphic data they may be mistaken as older, more basal taxa. Indeed, when juvenile specimens are coded into a phylogenetic matrix, they are placed more basally on the resulting cladogram than are adults of that taxon (Tsuihiji et al., 2011; Campione et al., 2012).

Within hadrosaurine and lambeosaurine skulls, the most drastic ontogenetic changes occur in the morphology of the premaxillae, nasals, and supraoccipitals (Horner, 1989). As the individual grows, its premaxillae and nasals generally enlarge and change shape to form the crest (Horner, 1989), with the crest typically moving posteriorly during ontogeny (Langston, 1960; Prieto-Márquez, 2010b). Bones far from the incipient crest (quadrates, dentaries, and maxillae) change the least (Horner, 1989). The number of tooth rows increases (Langston, 1960; Horner and Currie, 1994), articular surfaces become more rugose, and the relative size of the orbit decreases (Horner and Currie, 1994). These general trends are observed in both *Probrachylophosaurus* and *Brachylophosaurus*.

The nasal crest of *Brachylophosaurus canadensis* enlarges late in ontogeny. Prieto-Márquez (2005) separated *Brachylophosaurus* specimens into "slender" and "robust" morphotypes, and stated that these individuals were approximately the same size. Although specimens of the two morphotypes have roughly the same interorbital and postorbital widths (Prieto-Márquez, 2005; Cuthbertson and Holmes, 2010), these widths have been affected by diagenetic compression. The robust specimen MOR 794 is laterally compressed, decreasing its cranial width; the slender specimens MOR 1071-7-7-98-86 and MOR 1071-7-16-98-248 are dorsoventrally compressed, increasing their cranial widths. Thus, although their apparent sizes are similar, after accounting for differential compression slender *Brachylophosaurus* specimens are slightly smaller than robust specimens. Slender and robust *Brachylophosaurus* specimens are both found in nearly the same horizons at Malta, Montana, and are therefore most parsimoniously ontogenetic stages of the same species. Cuthbertson and Holmes (2010) noted that the slender and

robust morphotypes are not discrete; *Brachylophosaurus* specimens such as FMNH PR 862 and TMP 1990.104.001 possess crests of intermediate sizes. The presence of intermediate crest morphologies supports individual or ontogenetic variation. Also, individual variation in body size could account for the presence of specimens with different crest sizes at similar body sizes.

Like many dinosaur taxa, hadrosaurs reached nearly their full adult size relatively quickly, and then grew increasingly slowly for the rest of their lives (Horner et al., 2000). In modern animals such as cassowaries and hornbills, the cranial crest grows rapidly late in ontogeny, often after the rate of skeletal growth has greatly slowed and the individual is nearly at full adult size. A near-adult cassowary with a skull length of 165 mm possesses a small incipient crest, and after a mere 5 mm (3%) of additional growth in skull length, acquires a full adult casque that covers most of the dorsal skull (Dodson, 1975). *Pachycephalosaurus* and *Stegoceras* juveniles have flat skulls, gaining their distinctive frontoparietal domes later in ontogeny (Horner and Goodwin, 2009; Schott et al., 2010). Centrosaurine ceratopsids also developed their pronounced cranial ornamentation late in ontogeny (Sampson et al., 1997). The nasal crests of slender and robust *Brachylophosaurus* follow this pattern of rapidly increasing crest size with a very small increase in overall skull size.

In *Brachylophosaurus*, the nasal crest elongates and flattens posteriorly ontogenetically, and the posterior margin of the nasofrontal suture migrates posteriorly as well. In MOR 2919, the nasofrontal suture is anteriorly placed as in a subadult *Brachylophosaurus*, and the nasal crest is shorter than that of any adult

Brachylophosaurus. Yet, MOR 2919 is not a subadult; in addition to its large size, the braincase elements and vertebral neural arches are completely fused externally, with most sutures obliterated, and histology confirms that MOR 2919 was nearing skeletal maturity. In slender adult *Brachylophosaurus* (MOR 1071), cranial sutures are still clearly defined, and sutures are still visible in the robust morphology of adult *Brachylophosaurus* (MOR 794). Although all sutures of braincase elements of MOR 2919 are fused and nearly obliterated, the nasofrontal suture and internasal suture are disarticulated and show no indications of fusion. The nasofrontal suture in *Brachylophosaurus* becomes more rugose ontogenetically, stabilizing the suture as the nasal crest grows. The lack of nasofrontal fusion in MOR 2919 suggests that the nasal crest was still enlarging at time of death.

The holotype of *Brachylophosaurus goodwini* (UCMP 130139) and MOR 2919 were both collected from the Kennedy Coulee area, but the *Brachylophosaurus goodwini* holotype was located stratigraphically lower in the coulee. Unfortunately, UCMP 130139 does not preserve the posterior nasals, which are a critical character in defining *Probrachylophosaurus bergei*. UCMP 130139 is adult-sized, and its frontals exhibit an anteriorly-located nasofrontal suture that does not cover the entire frontals, similar to that of MOR 2919 and subadult *Brachylophosaurus canadensis*. This supports UCMP 130139 and MOR 2919 being more closely related than either is to *B. canadensis*. However, UCMP 130139 exhibits anomalously deep frontal depressions that preclude it from being referred to *P. bergei*. If the deep frontal depressions are not pathologic, taphonomic, diagenetic, or individual variation, then they may potentially be used as an autapomorphy to resurrect *B. goodwini*. Given the poor preservational condition of the frontals of

UCMP 130139, the specimen should be referred to Brachylophosaurini indet. pending additional specimens with similar frontal depressions.

The morphologies of elements of *Probrachylophosaurus* are consistently more similar to members of Brachylophosaurini than to other hadrosaurs. Within Brachylophosaurini, elements of *Probrachylophosaurus* are either most similar to *Brachylophosaurus* or *Acristavus*, or intermediate between these taxa, as predicted by their relative stratigraphic positions. This supports the hypothesis of *Probrachylophosaurus bergei* representing an intermediate taxon within the *Acristavus*-*Brachylophosaurus* lineage (Figure 2.29).

In some morphologic characters within Brachylophosaurini, the subadult morphology of the stratigraphically younger taxon matches the adult condition of the stratigraphically older taxon, illustrating a peramorphic trend of immature animals of a descendant taxon resembling adults of the ancestral taxon (Rozhdestvensky, 1965). The palatine process of the jugal in subadult *Probrachylophosaurus* resembles the condition of adult *Acristavus*. The nasal crest in *Brachylophosaurus* increases in size late in ontogeny: subadults lack any crest, similar to the adult form of their proposed ancestor *Acristavus*; small adults have a small crest reminiscent of their proposed ancestor *Probrachylophosaurus*; and large adults have a large broad paddle-shaped crest. The nasofrontal suture of small subadult *Brachylophosaurus* is similar to that of adult *Probrachylophosaurus*, although *Probrachylophosaurus* has the deep rugosities of a more mature suture. The prequadratic process of the squamosal of small subadult

Brachylophosaurus is also more similar to that of adult *Probrachylophosaurus* than to adult *Brachylophosaurus*.

Probrachylophosaurus bergei shares many morphologic similarities with *Brachylophosaurus canadensis*, but shares other similarities with *Acristavus gagslarsoni*. Thus, placing *P. bergei* as merely a new species of either genus would be problematic. Depending on the cladistic matrix used, *P. bergei* may be the sister taxon to *B. canadensis* and could be classified as a member of the same genus (Figure 2.23), or *Maiasaura peeblesorum* may be the sister taxon to *B. canadensis* (Figure 2.22), requiring *P. bergei* to be classified as a separate genus. Given this phylogenetic uncertainty, *Probrachylophosaurus bergei* should be considered a unique genus. Future discoveries of additional intermediate specimens will hopefully clarify evolutionary relationships within the Brachylophosaurini clade.

Conclusions

In the early years of dinosaur paleontology, specimens were collected as isolated points, each so morphologically unique that their evolutionary relationships were difficult to determine. As more fossil specimens are collected, the gaps in morphology that previously separated species are being filled. With larger sample sizes resulting in more continuous series of fossils with good stratigraphic resolution, variations in morphology can be analyzed in a more complete context, and attributed to ontogeny, evolution, taphonomic alteration, biogeography, or individual variation (Horner et al., 2011). A better understanding of stratigraphy and advancements in radiometric dating enable

precise temporal correlation of geographically separated localities. Taxa can then be placed in temporal sequence, allowing tests of evolutionary hypotheses.

A precise stratigraphic framework is critical for determining whether morphological variations of adult specimens are due to evolution or are variations within a roughly contemporaneous population. If closely related taxa do not overlap stratigraphically, the pattern is more parsimonious with anagenesis than cladogenesis. Recent research has greatly increased the sample size and stratigraphic resolution of specimens from the Judith River and Hell Creek Formations of Montana and their Canadian equivalents, revealing several potential anagenetic lineages in Campanian and Maastrichtian ornithischians (Ryan and Evans, 2005; Evans and Reisz, 2007; Ryan et al., 2007; Campione and Evans, 2011; Scannella et al., 2014).

Because *Probrachylophosaurus bergei* is stratigraphically older than all *Brachylophosaurus canadensis* specimens, it is hypothesized to represent a more basal brachylophosaur morphology, early in the evolution of this lineage from a non-crested ancestor. Thus, the small crest of *Probrachylophosaurus* would represent a transitional nasal morphology between a non-crested ancestor such as *Acristavus* and the larger crests of adult *Brachylophosaurus*. The fourth member of Brachylophosaurini, *Maiasaura*, would represent a cladogenic event, diverging from the lineage that led to *Brachylophosaurus* at a currently unknown point.

Acknowledgments

Fieldwork and research funding was generously provided to JRH by the Ameya Preserve, Damaris Wagoner, David Sands, and other generous donors to the Museum of the Rockies Student Fund and Horner Fund; and to EAF by the Tampa Bay Fossil Club and the Montana State University Department of Cell Biology and Neuroscience. Travel funding was generously provided to EAF by the Doris O. and Samuel P. Welles Research Fund (University of California Museum of Paleontology), the M.A. Fritz Travel Grant for the Advancement of Studies in Palaeontology (Royal Ontario Museum), the Jackson School of Geosciences Student Member Travel Grant (Society of Vertebrate Paleontology), and the College of Letters and Science Student Research Travel Grant (Montana State University). Many thanks to Mark Goodwin, Dave Varricchio, Don Brinkman, Matt Lavin, Denver Fowler, Ray Rogers, Dave Evans, Michael Ryan, Terry Gates, and Nick Campione for morphologic, stratigraphic, and cladistic advice and discussions. For specimen collection, thanks to the 2007-2008 MOR field crews, especially Brian Baziak, Holly Woodward, and Cary Woodruff, and 1981 and 1994 UCMP field crews, especially Mark Goodwin and Kyoko Kishi. For fieldwork support, hospitality, and land access, great thanks as always to Dan and Lila Redding. For land access and specimen donation, and for suggesting the species name, grateful thanks to Nolan and Cheryl Fladstol and John and Claire Wendland. Thanks to all members of the Rudyard, Montana community, whose continuing support of local paleontology makes this work possible. Excellent preparation was done by Carrie Ancell, Jamie Jette, Aleen Kienholz, Patsy Hookey, and volunteers at the MOR Bowman Prep Lab. For histological

assistance, thanks to Ellen Lamm, Holly Woodward, Brian Baziak, and Christian Heck. For specimen transport, thanks to Robert and Sarah Boessenecker and Daniel Traub. Thanks to Kevin Seymour and David Evans (ROM); Don Brinkman, Brandon Strillsky, and Graeme Housego (TMP); Pat Holroyd, Mark Goodwin, and Kevin Padian (UCMP); Sue Frary (GPDM); and Sharon Emond (Phillips County Museum) for comparative specimen access. Dave Varricchio, Don Brinkman, and Matt Lavin provided helpful comments on drafts of this paper.

Table 2.1. Radiometric date recalibrations. Published dates have been recalibrated to the Fish Canyon sanidine standard (28.305 +/- 0.036 Ma) of Renne et al. (2010). Unless specified, stratigraphic heights "above bottom" and "below top" refer to the bottom and top of the entire formation, not its members. Ages and errors are in Ma. FCs: Fish Canyon sanidine standard used for published ages. MMhb-1: McClure Mountain hornblende standard. References used in Table 2.1: (Goodwin and Deino, 1989; Thomas et al., 1990; Eberth and Hamblin, 1993; Rogers et al., 1993; Renne et al., 1998; Eberth, 2005; Jinnah et al., 2009; Varricchio et al., 2010).

		Published			Recalibrated				
Formation	Stratigraphic height	FCs age	Age	Error	FCs age	Age	Error	Source Publication	Notes
Judith River	Unit 1 of Oldman Formation, 31.8 m above top of Marker A Coal of Taber Coal Zone	*27.84	78.2	0.2	28.305	79.49	0.21	Goodwin and Deino, 1989	Upper Kennedy Coulee, equivalent to Unit 1 of Oldman Formation. Sanidine. *Original standard used was MMhb-1 = 520.4 +/- 1.7 Ma, which was equivalent to FCs = 27.84 (Renne et al., 1998).
Judith River	Taber Coal Zone of Foremost Formation, 4.8 m below top of Marker A Coal	*27.84	78.5	0.2	28.305	79.79	0.21	Goodwin and Deino, 1989	Lower Kennedy Coulee, equivalent to Taber Coal Zone of Foremost Formation. Sanidine. *Original standard used was MMhb-1 = 520.4 +/- 1.7 Ma, which was equivalent to FCs = 27.84 (Renne et al., 1998).
Dinosaur Park	middle, 44 m above bottom	*27.84	75.2	0.3	28.305	76.45	0.31	Eberth and Hamblin, 1993	Sample from Dinosaur Provincial Park area. *The standard used is not mentioned in Eberth and Hamblin (1993), but the paper cites the methods of Thomas et al. (1990), which used the standard of MMhb-1 = 520.4 +/- 1.7 Ma, which was equivalent to FCs = 27.84 (Renne et al., 1998).
Oldman	upper, 4 m below top	*27.84	76.5	0.5	28.305	77.76	0.51	Eberth and Hamblin, 1993	Sample from Dinosaur Provincial Park area. *The standard used is not mentioned in Eberth and Hamblin (1993), but the paper cites the methods of Thomas et al. (1990), which used the standard of MMhb-1 = 520.4 +/- 1.7 Ma, which was equivalent to FCs = 27.84 (Renne et al., 1998).

Table 2.1 continued.

Foremost	lower, 30 m above bottom	*27.84	79.14	0.15	28.305	80.45	0.16	Eberth, 2005 citing A. L. Deino personal communication, 1993	Sample from Dinosaur Provincial Park area. *The standard used is not mentioned in Eberth (2005), but in the early 1990s Deino's lab, part of the Berkeley Geochronology Center, was using the Fish Canyon sanidine standard of 27.84 Ma (P. R. Renne personal communication, 2011). The samples listed above were tested in the same lab using the same standard.
Two Medicine	upper, 10 m below top	27.84	74.08	0.05	28.305	75.30	0.07	Rogers et al., 1993	Sample TM-6 plagioclase.
Two Medicine	upper middle	28.03	75.92	0.32	28.305	76.66	0.32	Varricchio et al., 2010	Bentonite is associated with the MOR TM-003 *Maiasaura* bonebed.
Two Medicine	lower, 100 m above bottom	27.84	80.04	0.08	28.305	81.37	0.10	Rogers et al., 1993	Sample RT/TM-7 biotite. This original date was used to estimate age of ~79.43 Ma for MOR 1155, holotype of *Acristavus gagslarsoni* (Gates et al., 2011), which recalibrates to 80.74 Ma.
Wahweap	middle, 40 m above bottom	28.02	80.1	0.3	28.305	80.91	0.31	Jinnah et al., 2009	Sample CF05-B bentonite sanidine. This original date was used to estimate age of 79.34-78.91 Ma for UMNHVP 16607, referred specimen of *Acristavus gagslarsoni* (Gates et al., 2011), which recalibrates to 80.14-79.71 Ma.

Table 2.2. List of Brachylophosaurini specimens examined in this paper. Relative ontogenetic stages are estimated using the size-based definitions of Evans (2010); size alone should not be used to infer the sexual or skeletal maturity or immaturity of a specimen. Juveniles are less than 50% the size of the largest known specimen of that taxon; subadults are 50-85% the size of the largest specimen; adults are more than 85% the size of the largest specimen. For details and references of the recalibrated ages, see Table 2.1. *Abbreviations*: *Fm*, Formation.

Taxon	Specimen	Type	Material Preserved	Ontogenetic Stage	Stratigraphic Position	Recalibrated Age	Specimen References
Probrachylophosaurus bergei	MOR 2919	holotype	skull (partially articulated) and partial skeleton	adult	Judith River Fm equivalent to Unit 1 of Oldman Fm, 17.5 m above top of Taber Coal Zone of Foremost Fm	78.5-78.2 Ma	this paper
Probrachylophosaurus bergei	MOR 1097	referred	partial skull (disarticulated)	subadult	Judith River Fm equivalent to Unit 1 of Oldman Fm	78.5-78.2 Ma	this paper
Brachylophosaurus canadensis	NMC 8893	holotype	skull (articulated) and partial skeleton	adult	Unit 2 (Comrey Sandstone) of Oldman Fm, 7.5 m below top of fm	> 77.76 Ma	Sternberg 1953, Cuthbertson and Holmes 2010
Brachylophosaurus canadensis	GPDM JRF.65	referred	braincase	adult	Judith River Fm equivalent to Unit 2 (Comrey Sandstone) of Oldman Fm	> 77.76 Ma	
Brachylophosaurus canadensis	FMNH PR 862	referred	skull (partially articulated)	adult	possibly Oldman Fm (quarry not relocated)	unknown	
Brachylophosaurus canadensis	MOR 720	referred	braincase	adult	upper Judith River Fm	unknown	
Brachylophosaurus canadensis	MOR 794	referred	skull (articulated) and skeleton (articulated)	adult	Judith River Fm equivalent to Unit 2 (Comrey Sandstone) of Oldman Fm	> 77.76 Ma	Prieto-Márquez 2005

Table 2.2 continued.

Brachylophosaurus canadensis	MOR 940	referred	braincase	subadult	Judith River Fm equivalent to Unit 2 (Comrey Sandstone) of Oldman Fm	> 77.76 Ma	
Brachylophosaurus canadensis	MOR 1071	referred	bonebed including skulls (partially articulated and disarticulated) and skeletons	adults, subadults, juveniles	Judith River Fm equivalent to Unit 2 (Comrey Sandstone) of Oldman Fm	> 77.76 Ma	Prieto-Márquez 2005
Brachylophosaurus canadensis	TMP 1990.104.001	referred	skull (articulated) and partial skeleton	adult	Oldman Fm	unknown	Cuthbertson and Holmes 2010
Maiasaura peeblesorum	YPM-PU 22405	holotype	skull (partially articulated)	adult	upper Two Medicine Fm	~76.66 Ma	Horner and Makela 1979, Horner 1983
Maiasaura peeblesorum	OTM F138	referred	skull (partially articulated) and skeleton	adult	Two Medicine Fm	unknown	Trexler 1995
Maiasaura peeblesorum	ROM 44770	referred	skull (articulated) and partial skeleton	adult	Two Medicine Fm	unknown	
Acristavus gagslarsoni	MOR 1155	holotype	skull (mostly articulated) and partial skeleton	adult?	lower Two Medicine Fm	~80.74 Ma	Gates et al. 2011
Acristavus sp.	UMN HVP 16607	referred	braincase	adult?	upper Middle Mudstone Member of Wahweap Fm, 170 m above base of fm	80.14-79.71 Ma	Gates et al. 2011
Brachylophosaurini indet. "*Brachylophosaurus goodwini*"	UCMP 130139	holotype	partial skull (partially articulated) and partial skeleton	adult	Judith River Fm equivalent to Unit 1 of Oldman Fm	78.5-78.2 Ma	Horner 1988

Table 2.3. Size comparisons of MOR 2919 and other selected Brachylophosaurini specimens. The value "% MOR 794" indicates the specimen's size relative to that of MOR 794, the largest *Brachylophosaurus canadensis*, and its categorization as adult or subadult based solely on its size; those specimens 50-85% the size of MOR 794 are considered subadults (Evans, 2010). The size of MOR 1097 is also given relative to MOR 2919 (*76%), which categorizes MOR 1097 as a subadult. The height of incomplete quadrates was estimated. The MOR 1097 quadrate estimate was based on the width of the ventral condyle, which scales linearly with height ($R^2 = 0.999$) in these specimens. Because MOR 1071 specimens are from a disarticulated bonebed, most bones cannot be associated together as specific individuals. For each element, the largest specimen and a representative subadult specimen were included here. Field numbers of MOR 1071 specimens, largest followed by smaller for each element: quadrates, 8-13-98-559D, 6-30-98-1; dentaries, 8-98-X (part of skull 7-7-98-86), 8-1-99-313; tibiae, 672-L, 8-10-98-514; fibulae, 7-7-98-88, 7-23-99-181; metatarsal IIs, 7-19-99-131B, 8-7-99-470.
Abbreviations: *est*, estimated; *sub*, subadult.

		Quadrate		**Dentary**		**Tibia**		**Fibula**		**Metatarsal II**	
Taxon	**Specimen**	**Height**	**% MOR 794**	**Length**	**% MOR 794**	**Length**	**% MOR 794**	**Length**	**% MOR 794**	**Length**	**% MOR 794**
Probrachylophosaurus	MOR 2919	37.0 cm	114% (adult)	52.5 cm	102% (adult)	120.0 cm	105% (adult)	112.0 cm	109% (adult)	38.0 cm	115% (adult)
	MOR 1097	28.0 cm (est)	86% (*76% sub)	-	-	-	-	-	-	-	-
Brachylophosaurus	MOR 794	32.5 cm	100% (adult)	51.5 cm	100% (adult)	114.0 cm	100% (adult)	103.0 cm	100% (adult)	33.0 cm	100% (adult)
	FMNH 862	32.5 cm (est)	92% (adult)	45.0 cm	87% (adult)	-	-	-	-	-	-
	MOR 1071	32.5 cm	100% (adult)	45.5 cm	88% (adult)	103.5 cm	91% (adult)	94.0 cm	91% (adult)	36.5 cm	111% (adult)

Table 2.3 continued.

	MOR 1071	21.3 cm	66% (sub)	29.5 cm	57% (sub)	65.0 cm	57% (sub)	64.5 cm	63% (sub)	23.5 cm	71% (sub)

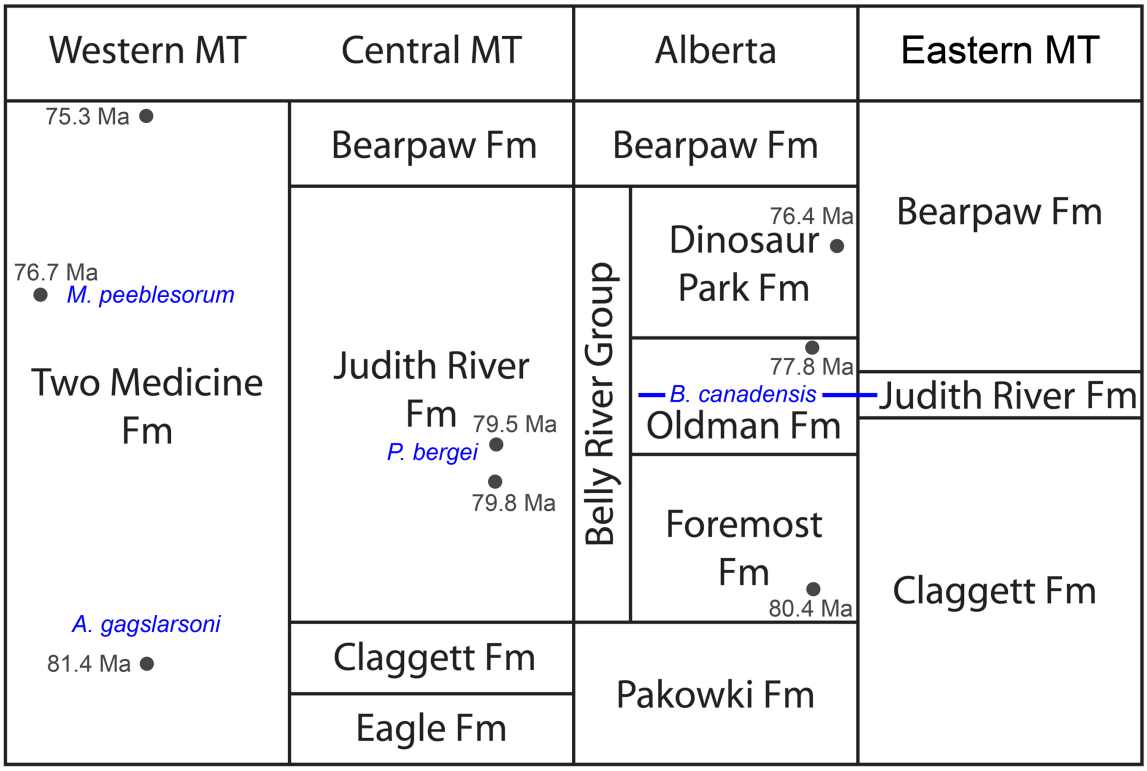


Figure 2.1. Generalized regional cross section of the Judith River Formation and its stratigraphic equivalents, with brachylophosaurin distribution. Members of Brachylophosaurini indicated in blue: *Acristavus gagslarsoni*, *Probrachylophosaurus bergei*, *Brachylophosaurus canadensis*, and *Maiasaura peeblesorum*. Radiometric dates are indicated in dark gray, and have been recalibrated to the Fish Canyon sanidine standard (28.305 ± 0.036 Ma) of Renne et al. (2010) from the originally published values (Goodwin and Deino, 1989; Eberth and Hamblin, 1993; Rogers et al., 1993; Eberth, 2005; Varricchio et al., 2010); see text and Table 1 for further recalibration details.

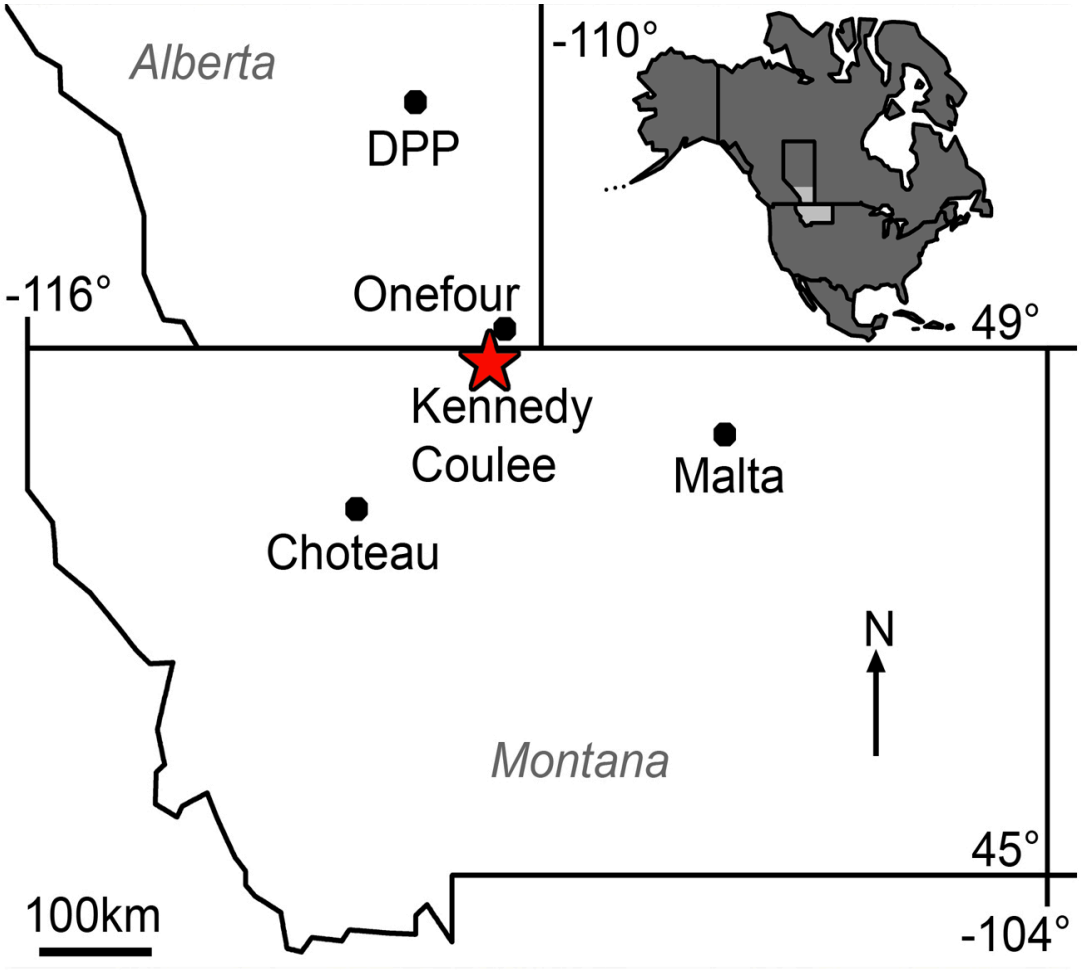


Figure 2.2. Map of Brachylophosaurini localities in Montana and southern Alberta. Inset shows North America in dark grey with Montana and southern Alberta in light grey. Kennedy Coulee, locality of *Probrachylophosaurus bergei*, marked with red star. Other Brachylophosaurini localities indicated with black dots: Malta, *Brachylophosaurus canadensis*; Onefour, *B. canadensis*; DPP (Dinosaur Provincial Park), *B. canadensis*; Choteau, *Acristavus gagslarsoni* and *Maiasaura peeblesorum*. Map adapted from maps.google.com.

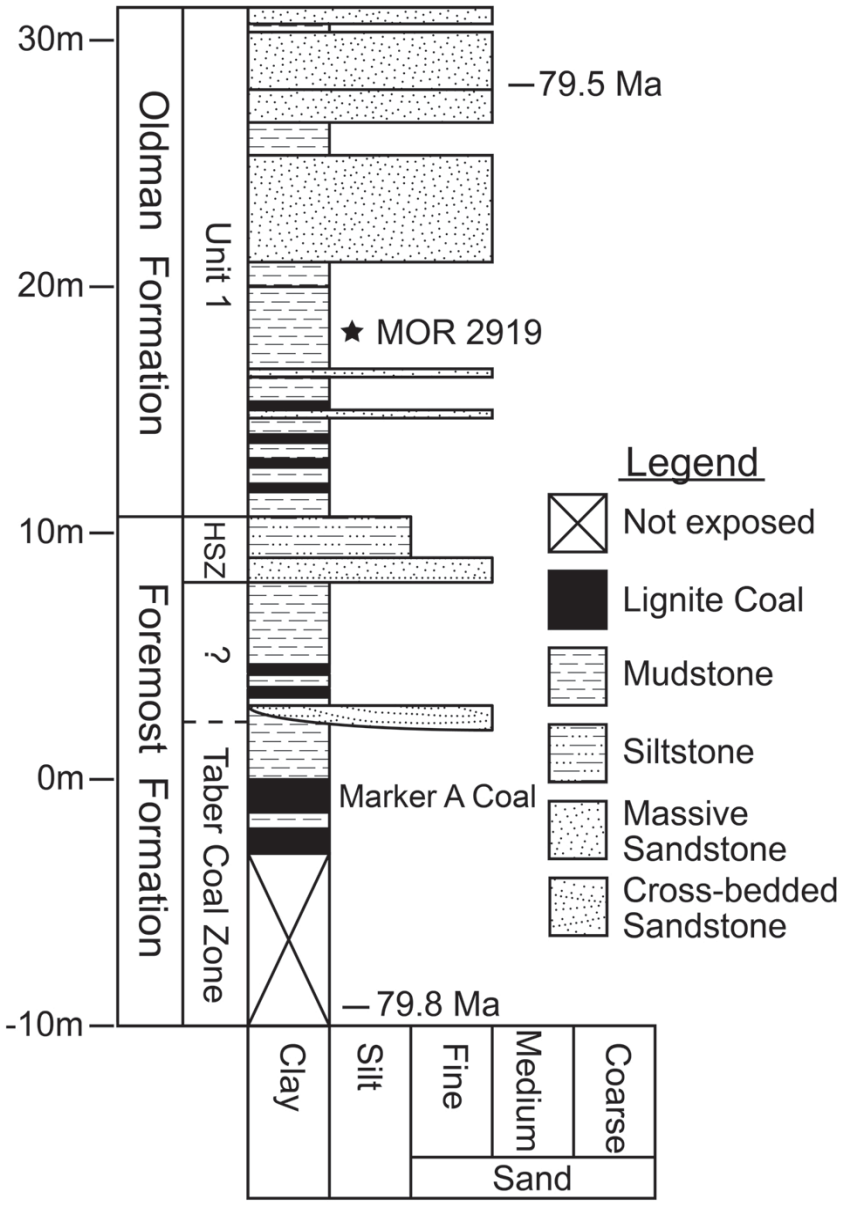


Figure 2.3. Stratigraphic section at *Probrachylophosaurus bergei* holotype (MOR 2919) quarry, MOR locality JR-518. Datum (0 m) is the top of the Marker A coal of the Taber Coal Zone of the Foremost Formation. Radiometric dates were recalibrated from Goodwin and Deino (1989) samples collected southwest of MOR JR-518 in Kennedy Coulee; their stratigraphic heights are indicated on the section. This section is atypical for Kennedy Coulee sections in that it has a relatively thin Herronton Sandstone Zone (HSZ) low in section, and more sandstones in the upper part of the section, whereas most of the coulee has a thick sandstone zone above the Marker A coal, and is dominated by mudstone in the upper regions. The region indicated with "?" below the HSZ may or may not be classified as a continuation of the Taber Coal Zone.

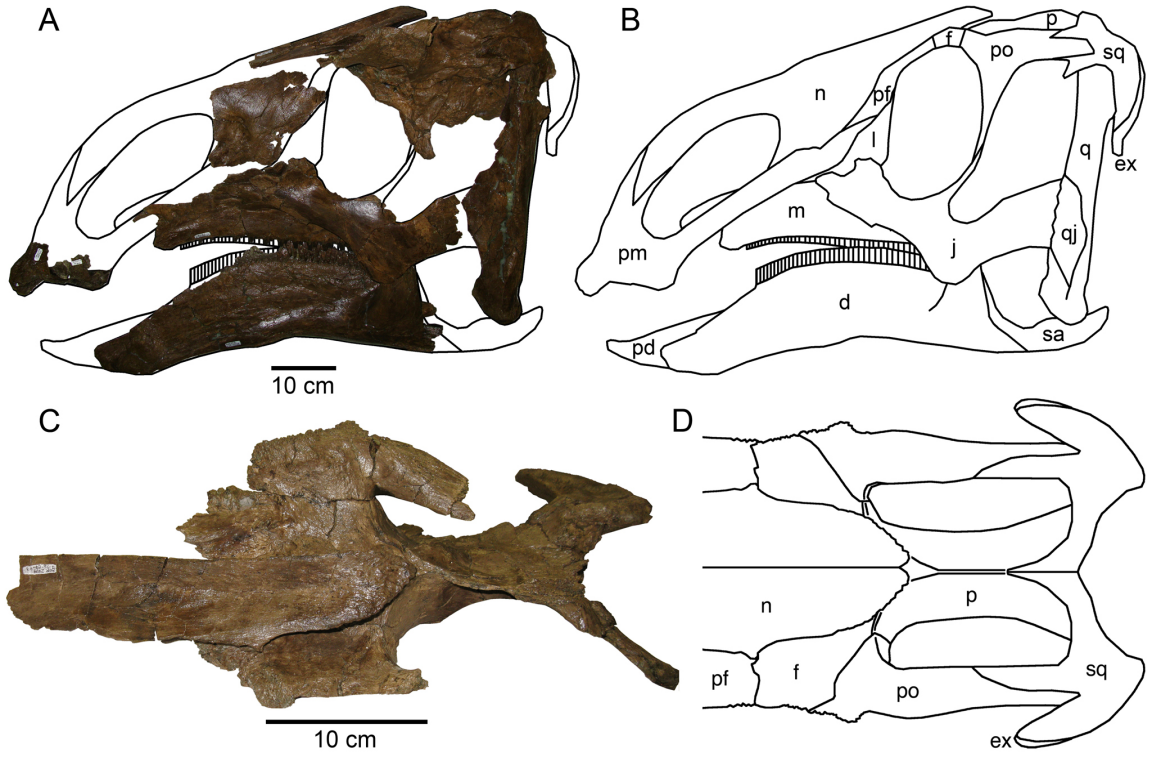


Figure 2.4. *Probrachylophosaurus bergei* skull reconstruction. (A) Preserved skull elements of MOR 2919, left lateral view. Predentary not included due to its poor preservation and diagenetic compression. (B) Outline of skull reconstruction, left lateral view. The outline accounts for diagenetic distortion of the posterior braincase, but otherwise does not correct for distortion of skull elements. Outlined regions where left skull material was not preserved are based on right bones when available. Regions with neither left nor right material preserved are hypothesized reconstructions based on *Brachylophosaurus canadensis* skulls. (C) Braincase with left nasal crest, dorsal view. (D) Outline of braincase reconstruction with nasal crest, dorsal view. Reconstruction accounts for diagenetic lateral compression and distortion of posterior braincase. *Abbreviations*: *d*, dentary; *ex*, exoccipital; *f*, frontal; *j*, jugal; *l*, lacrimal; *m*, maxilla; *n*, nasal; *p*, parietal; *pd*, predentary; *pf*, prefrontal; *pm*, premaxilla; *po*, postorbital; *q*, quadrate; *qj*, quadratojugal; *sa*, surangular; *sq*, squamosal.

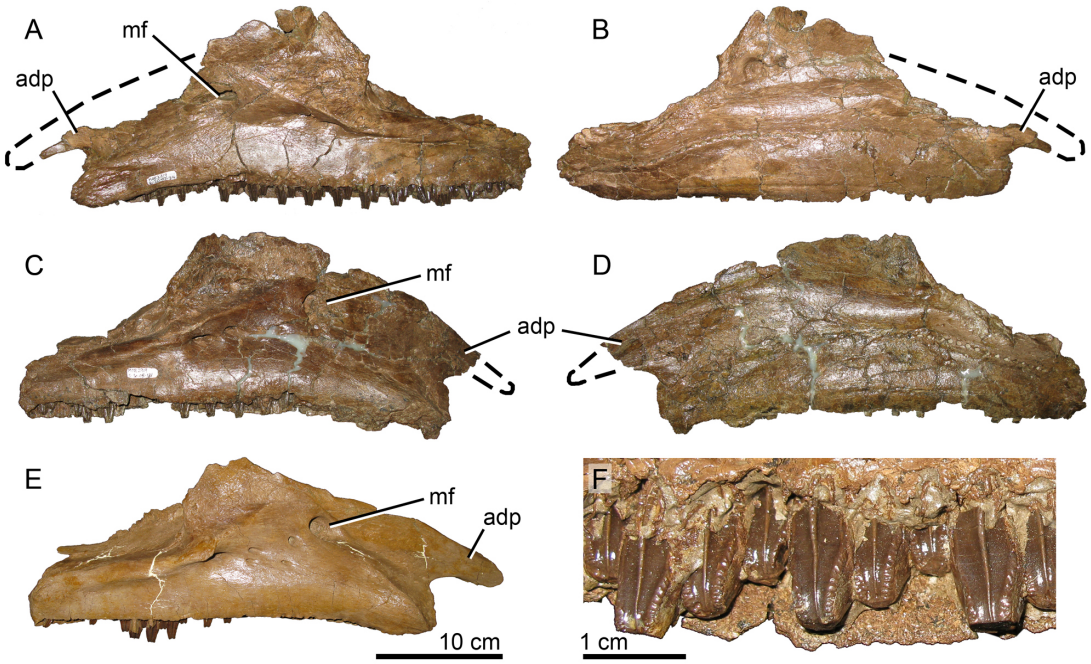


Figure 2.5. Brachylophosaurinan maxillae. (A-D, F) *Probrachylophosaurus bergei*, MOR 2919. Estimated reconstruction of anterodorsal process indicated with dashed line. (A) left maxilla, lateral view; (B) left maxilla, medial view; (C) right maxilla, lateral view; (D) right maxilla, medial view; (E) *Brachylophosaurus canadensis* right maxilla, lateral view MOR 1071-8-13-98-559; (F) teeth of MOR 2919 left maxilla demonstrating slight sinuosity of median carinae. *Abbreviations*: *adp*, anterodorsal process; *mf*, maxillary foramen.

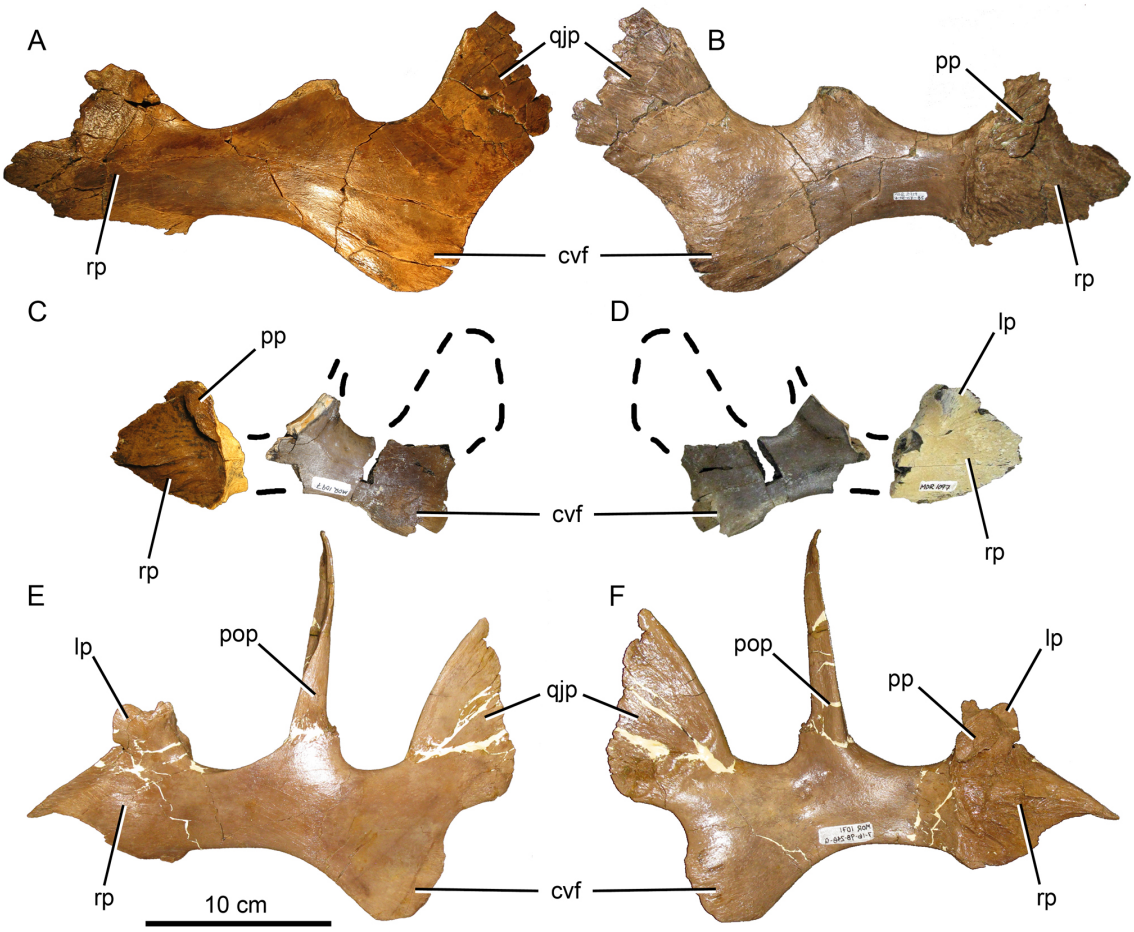


Figure 2.6. Brachylophosaurinan jugals. (A, B), *Probrachylophosaurus bergei* adult, MOR 2919, left jugal; (A) lateral view; (B) medial view. (C, D) *P. bergei* subadult, MOR 1097, right jugal reconstructed with dashed line; (C) medial view; (D) lateral view. (E, F) *Brachylophosaurus canadensis* adult, MOR 1071-7-16-98-248-Q, right jugal reversed. Note that the postorbital process was broken at its base and should be inclined more posteriorly; (E) lateral view; (F) medial view. *Abbreviations*: *cvf*, caudoventral flange; *lp*, lacrimal process; *pop*, postorbital process; *pp*, palatine process; *qjp*, quadratojugal process; *rp*, rostral process.

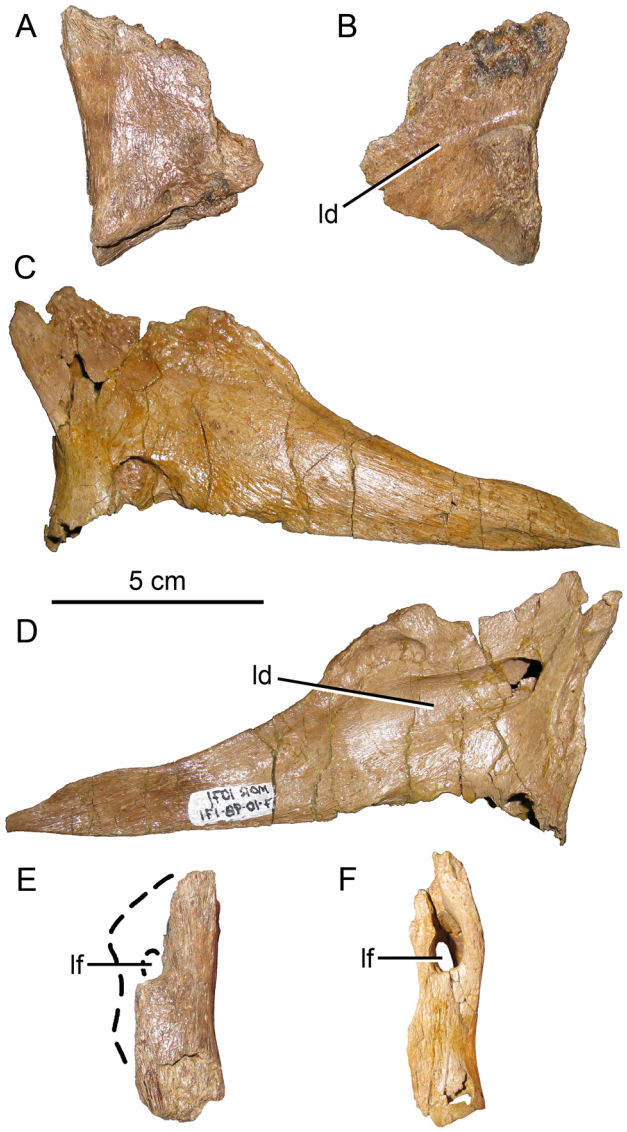


Figure 2.7. Brachylophosaurinan lacrimals. (A, B, E) *Probrachylophosaurus bergei*, MOR 2919, posterior right lacrimal; (A) lateral view; (B) medial view; (C, D, F) *Brachylophosaurus canadensis*, MOR 1071-7-10-98-171, left lacrimal reversed; (C) lateral view; (D) medial view; (E) posterior view MOR 2919, medial portion reconstructed with dashed line; (F) posterior view MOR 1071-7-10-98-171. *Abbreviations*: *ld*, lacrimal duct; *lf*, lacrimal foramen.

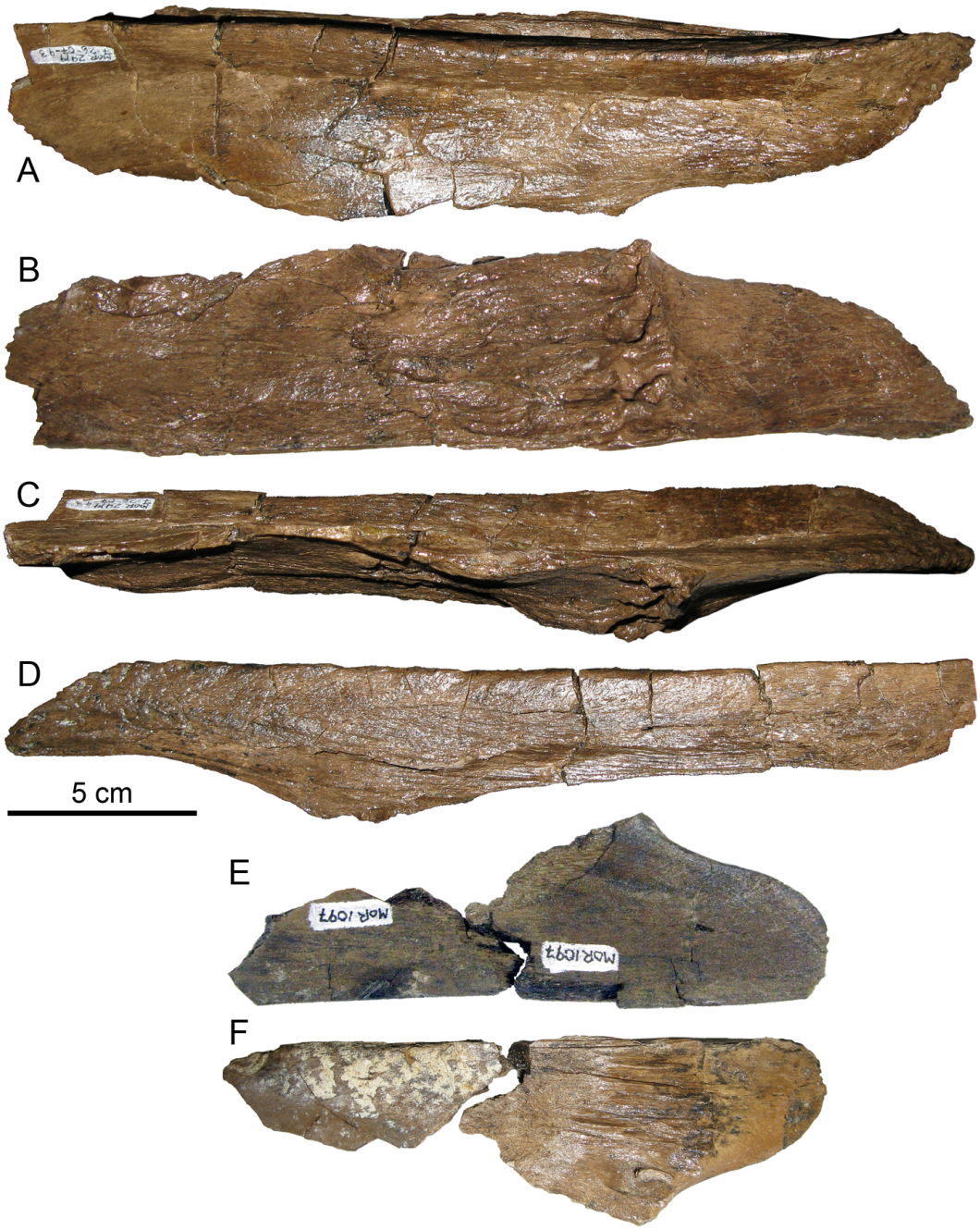


Figure 2.8. *Probrachylophosaurus bergei* nasals. (A-D) Adult, MOR 2919, posterior left nasal, crest pointing right except for (D); (A) dorsal view; (B) ventral view showing rugose nasofrontal suture; (C) lateral view; (D) medial view. (E, F) Subadult, MOR 1097, posterior right nasal; (E) dorsal view; (F) ventral view showing linearly striated nasofrontal suture.

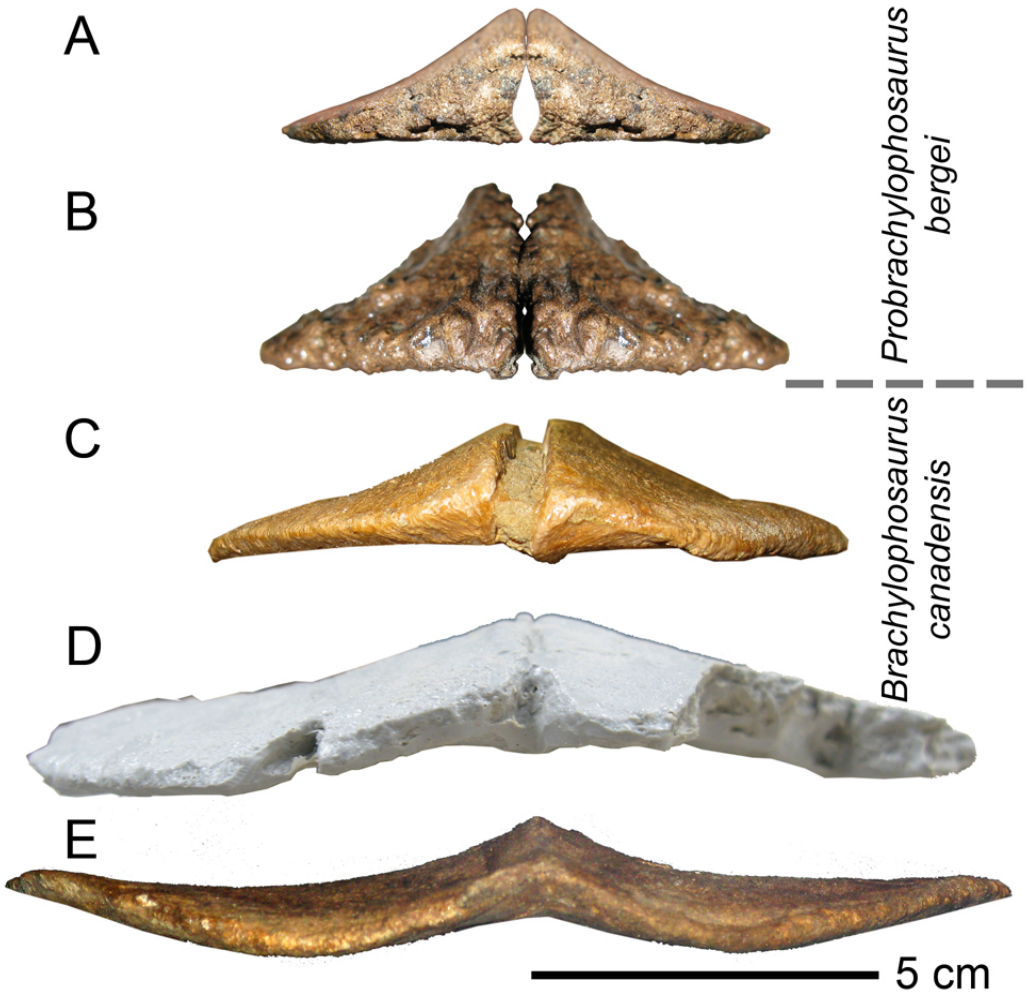


Figure 2.9. Brachylophosaurinan nasals, posterior view. In *Probrachylophosaurus bergei* and slender *Brachylophosaurus canadensis* morphotypes, the nasal crest is narrow and triangular in cross section. In *B. canadensis*, the nasal crest flattens as it grows wider. (A) *Probrachylophosaurus bergei* subadult, MOR 1097; (B) *P. bergei* adult, MOR 2919; (C) *Brachylophosaurus canadensis* slender morphotype, MOR 1071-7-7-98-86; (D) *B. canadensis* intermediate morphotype, FMNH PR 862; (E) *B. canadensis* robust morphotype, MOR 794.

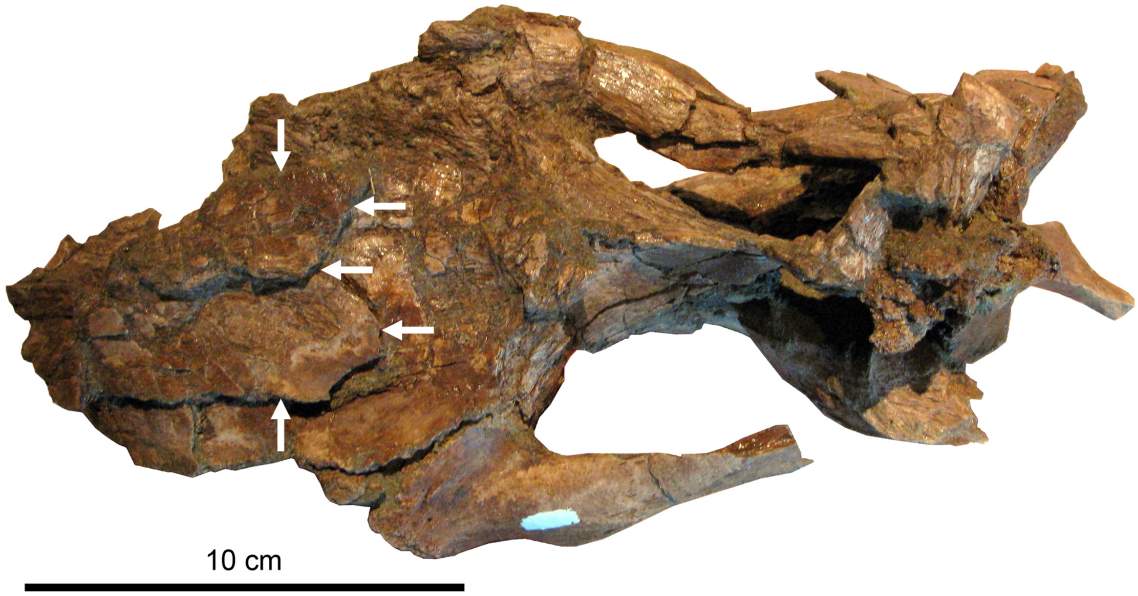


Figure 2.10. Subadult *Brachylophosaurus canadensis* braincase MOR 940 in dorsal view, with nasals that do not form an overhanging crest. Anterior is to the left. Specimen is from the Judith River Formation near Malta, Montana, in a horizon equivalent to the Comrey Sandstone Zone of the middle Oldman Formation. Borders of the nasals are indicated by white arrows. The specimen is heavily fractured, and the nasals are slightly elevated above the frontals, but this is due to fracturing; when undeformed, the nasals would have lain flush over the frontals, with no open space in between. There is no projection forming an overhanging, posteriorly oriented nasal crest as would be seen in larger *Brachylophosaurus canadensis* specimens.

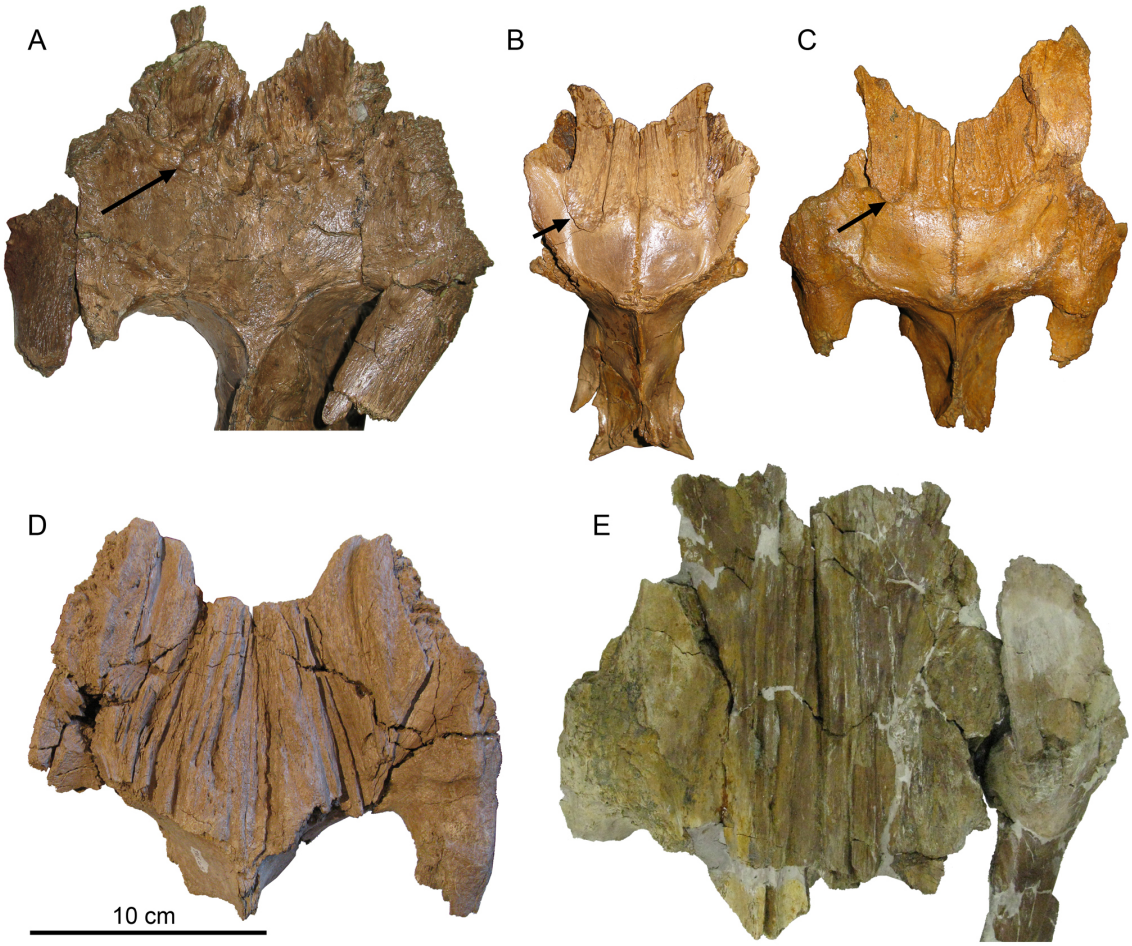


Figure 2.11. Posterior migration of brachylophosaurinan nasofrontal suture with ontogeny and stratigraphic age. In the stratigraphically oldest specimen, the adult *Probrachylophosaurus bergei*, (A) MOR 2919, from the Judith River Formation equivalent of Unit 1 of the lower Oldman Fm, the nasofrontal suture extends over less than half of the frontals. This suture extends over approximately half of the frontals in subadult *Brachylophosaurus canadensis* specimens (B) MOR 1071-7-13-99-87-I and (C) MOR 1071-C-3-3, from the Judith River Formation equivalent of the Comrey Sandstone of the middle Oldman Fm, and migrates posteriorly to completely cover the frontals in the adult (D) GPDM JRF.65, a condition also seen in adult *B. canadensis* from the upper Judith River Formation, (E) MOR 720. Border of nasofrontal suture in (A-C) indicated with arrows.

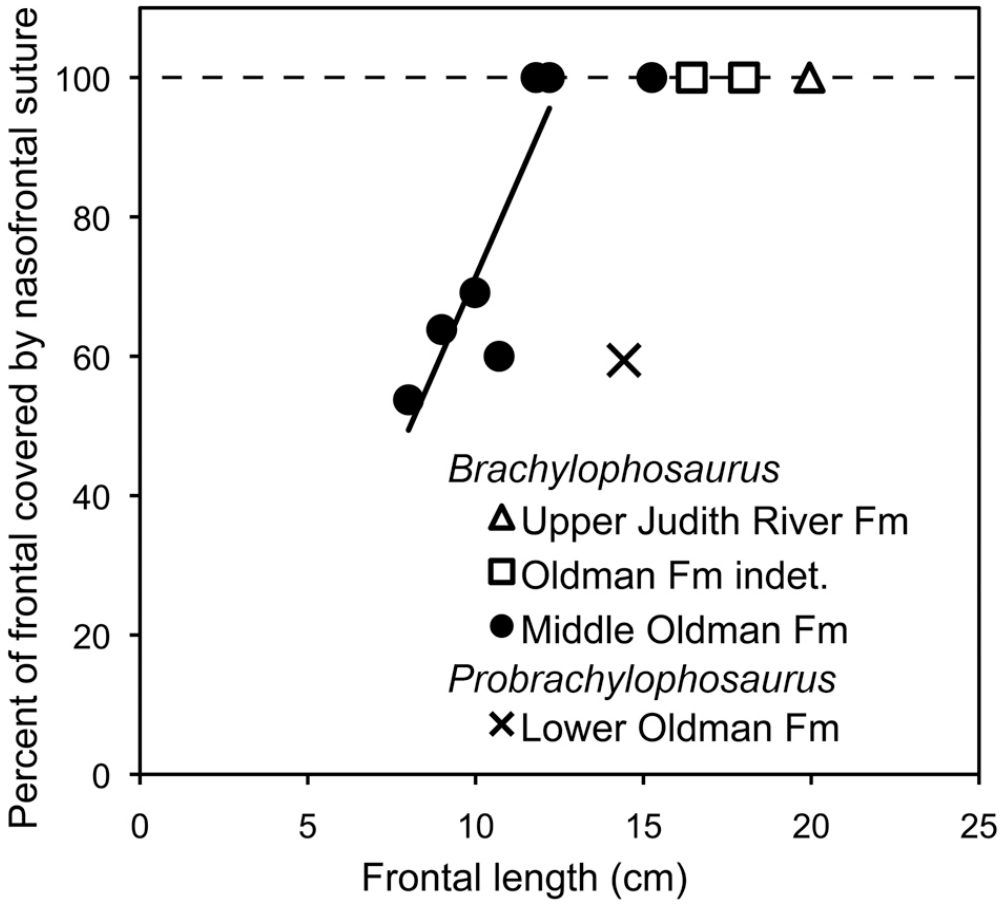


Figure 2.12. Posterior migration and enlargement of nasofrontal suture with growth in brachylophosaurinans. In subadult *Brachylophosaurus*, the nasofrontal suture covers 50-75% of the dorsal frontal surface; in adults, the nasofrontal suture covers the entire dorsal surface. In *Brachylophosaurus* specimens from the Comrey Sandstone Zone of the middle Oldman Formation and its Judith River Formation equivalent in Malta, Montana (solid black circles; NMC 8893, JRF.65, MOR 940, and MOR 1071 specimens C-3-3, 6-30-98-4, 7-13-99-87-I, and 7-7-98-86), the relative coverage of the nasofrontal suture increases with frontal length until the frontal is entirely covered by the nasofrontal suture. Larger adult *Brachylophosaurus* braincases from an unknown stratigraphic height in the Oldman Formation of Alberta (open squares; FMNH PR PR 862, TMP 1990.104.001) and the Upper Judith River Formation of central Montana (open triangle; MOR 720; stratigraphic height relative to Oldman Formation of Alberta unknown) also have the frontals entirely covered by the nasofrontal suture. *Probrachylophosaurus* from the Montana Judith River Formation equivalent of the lower Oldman Formation (black x; MOR 2919) differs from the *Brachylophosaurus* growth trajectory in having a subadult *Brachylophosaurus* degree of coverage in an adult sized skull.

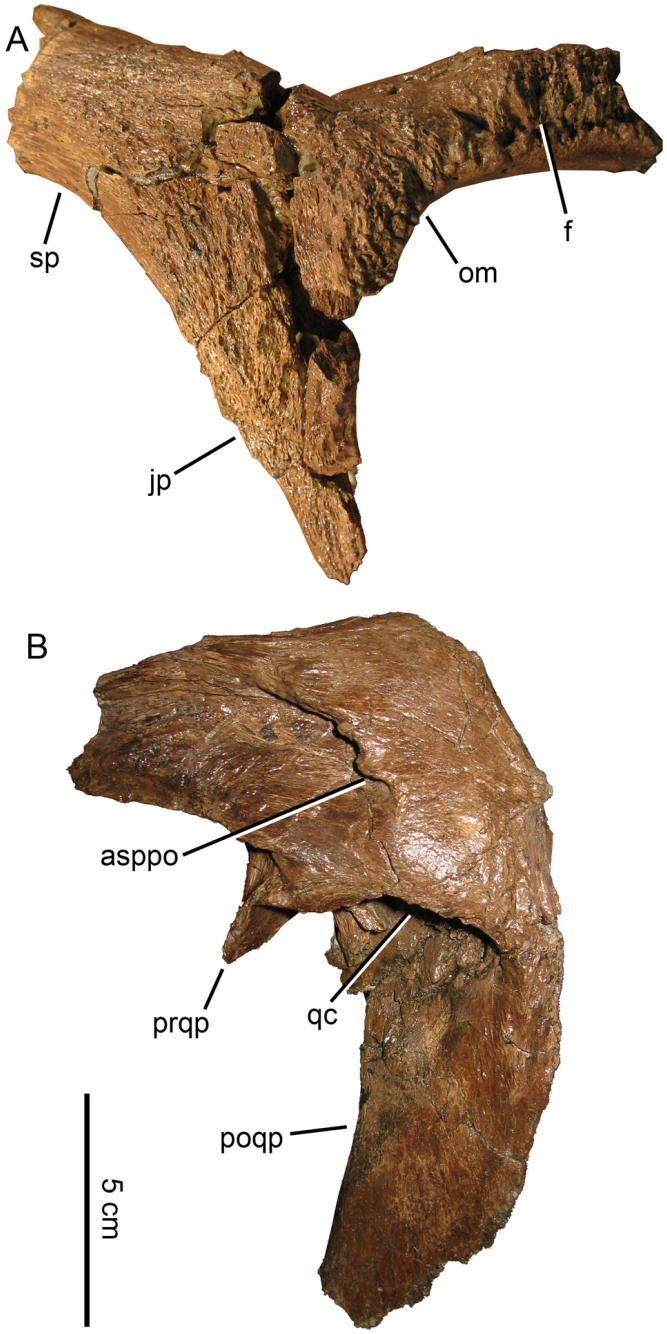


Figure 2.13. *Probrachylophosaurus bergei* postorbital and squamosal. MOR 2919 (A) right postorbital and orbital margin of frontal, lateral view; (B) left squamosal, lateral view. *Abbreviations*: *asppo*, articulation for the squamosal process of the postorbital; *f*, frontal; *jp*, jugal process; *om*, orbital margin; *poqp*, postquadratic process; *prqp*, prequadratic process; *qc*, quadrate cotylus; *sp*, squamosal process.

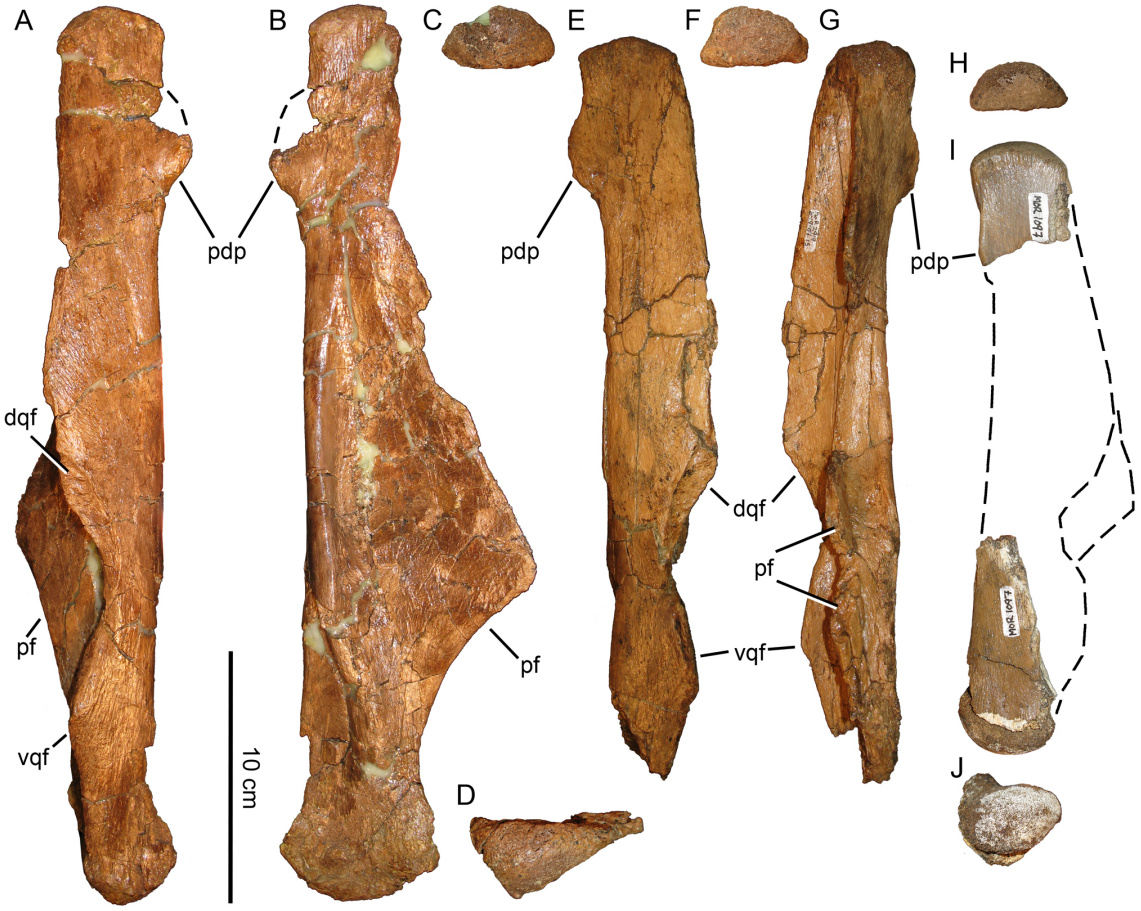


Figure 2.14. *Probrachylophosaurus bergei* quadrates. (A-D) Adult, MOR 2919, left quadrate; (A) lateral view; (B) medial view; (C) dorsal view of squamosal condyle; (D) ventral view of surangular condyle. (E-G) Adult, MOR 2919, right quadrate with broken pterygoid flange; (E) lateral view; (F) dorsal view of squamosal condyle; (G) medial view. (H-J) Subadult, MOR 1097, right quadrate; (H) dorsal view of squamosal condyle; (I) lateral view with missing portion reconstructed with dashed line; (J) ventral view of surangular condyle. Condyles are all oriented with the lateral side down. *Abbreviations*: *dqf*, dorsal quadratojugal flange; *pdp*, posterodorsal process; *pf*, pterygoid flange; *vqf*, ventral quadratojugal flange.

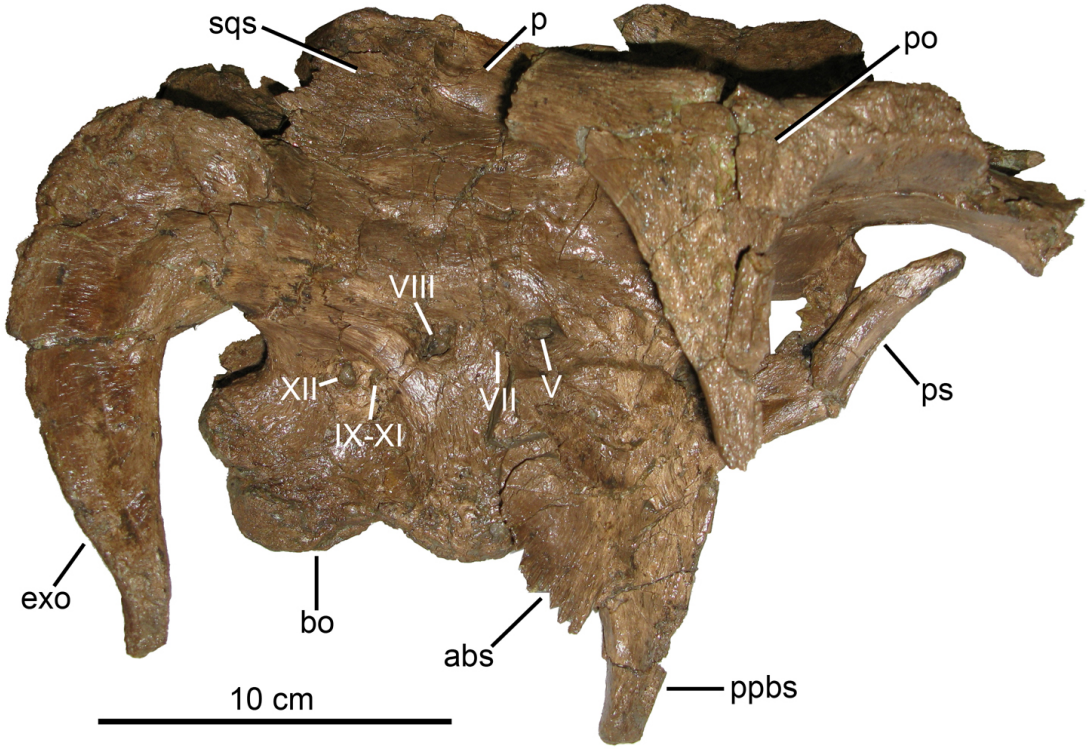


Figure 2.15. *Probrachylophosaurus bergei* braincase. MOR 2919, right lateral view. *Abbreviations*: *abs*, alar process of basisphenoid; *bo*, basioccipital; *exo*, exoccipital; *p*, parietal; *po*, postorbital; *ppbs*, pterygoid process of basisphenoid; *ps*, parasphenoid (broken and deflected dorsally); *sqs*, squamosal suture on parietal, broken; *V-XII*, cranial nerves.

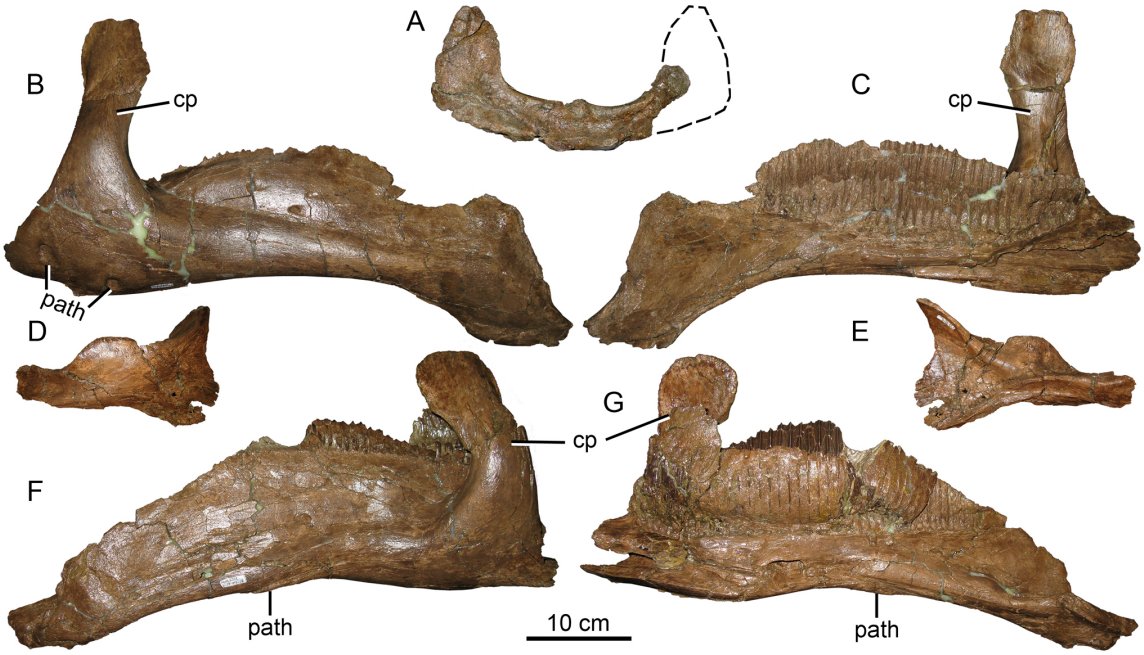


Figure 2.16. *Probrachylophosaurus bergei* mandible. MOR 2919 (A) predentary, ventral view; (B) right dentary, lateral view; (C) right dentary, medial view; (D) right surangular, lateral view; (E) right surangular, medial view; (F) left dentary, lateral view; (G) left dentary, medial view. The anterior portion of the right dentary was crushed mediolaterally, flattening the symphyseal region into a vertical orientation. The coronoid process of the left dentary was fractured, displacing the coronoid process anteromedially. *Abbreviations*: *cp*, coronoid process; *path*, pathology; pes, proximal edentulous slope.

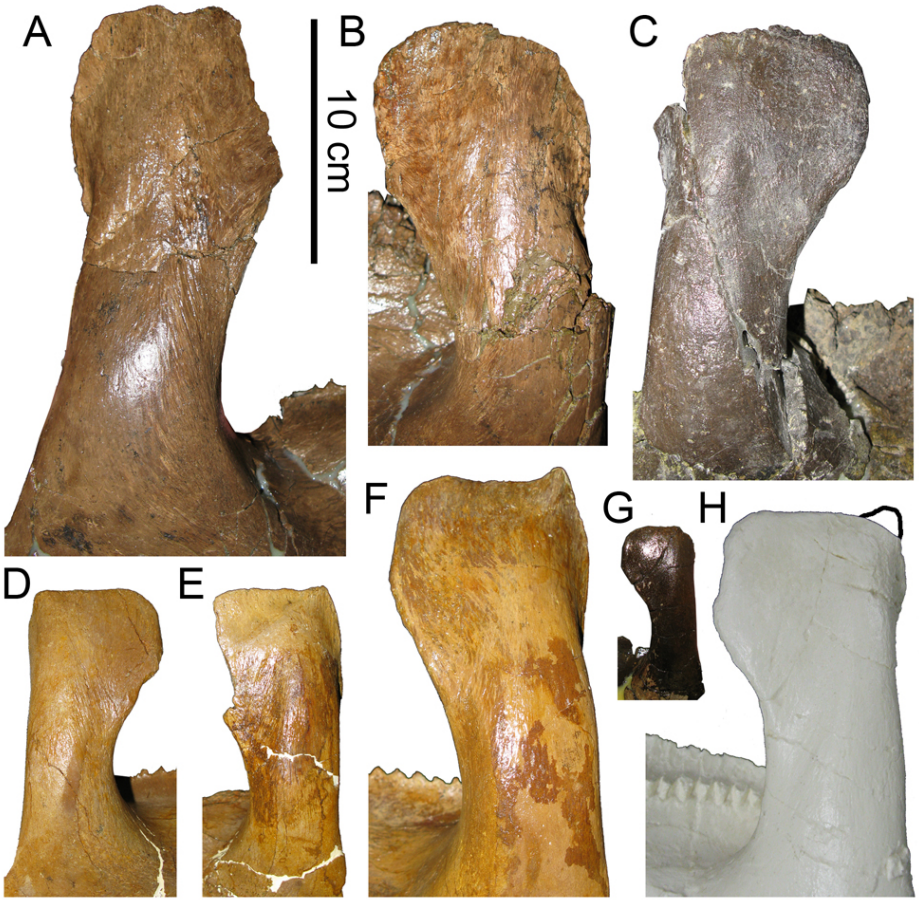


Figure 2.17. Taxonomic distribution and ontogenetic development of caudodorsal point on coronoid process of dentary. Caudodorsal point absent in: *Probrachylophosaurus* adult, MOR 2919, (A) right coronoid process, anterior margin broken, (B) left coronoid process, dorsal margin broken and entire process fractured and misaligned; (C) *Acristavus*, MOR 1155, right coronoid process, posterior margin broken. Caudodorsal point develops ontogenetically and with individual variation in *Brachylophosaurus*: (D) subadult, MOR 1071-8-1-99-313, right coronoid process; (E) subadult, MOR 1071-7-10-98-179, left coronoid process, anterior margin broken; (F) adult, MOR 1071-8-98-X, left coronoid process. Caudodorsal point develops ontogenetically in *Maiasaura*: (G) juvenile, MOR 547-W-55-2P, left coronoid process; (H) adult, OTM F138, left coronoid process of cast. The original description of OTM F138 (Trexler, 1995) includes a photograph of the left dentary with a complete caudodorsal point, but the cast at MOR does not include the caudodorsal point, suggesting that when the resin was poured into the mold, it did not completely fill this area. The missing caudodorsal point is indicated by a black outline traced from the left dentary photograph in Trexler (1995).

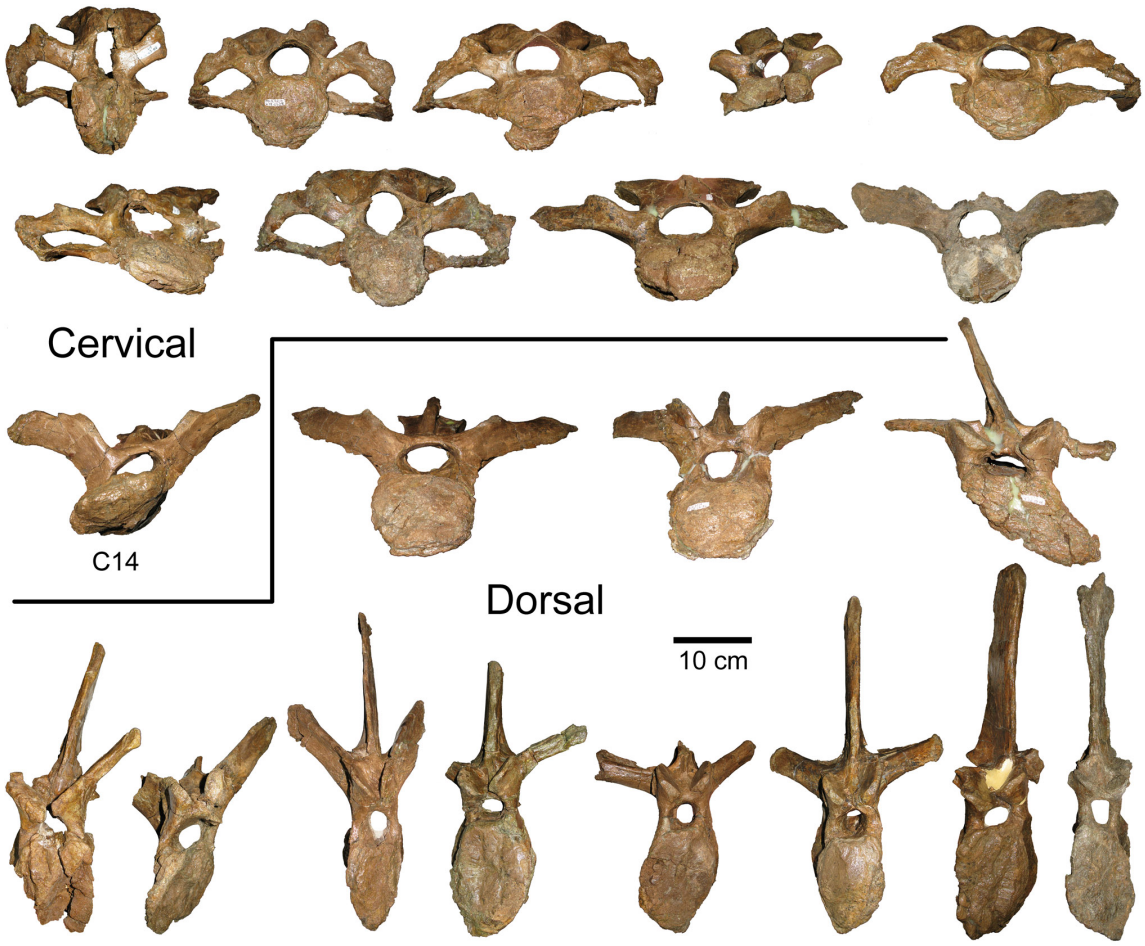


Figure 2.18. *Probrachylophosaurus bergei* cervical and dorsal vertebrae. MOR 2919 vertebrae are pictured in anterior view in their approximate order within their series. Serial position of vertebrae is not listed because the complete series of cervicals and dorsals were not preserved, and so their exact serial positions cannot be determined with confidence. However, the last cervical vertebra pictured, "C14", is consistent with the morphology of cervical 14 in NMC 8893, the holotype of *Brachylophosaurus canadensis* (Cuthbertson and Holmes, 2010). Atlas fragments and other vertebral fragments not pictured.

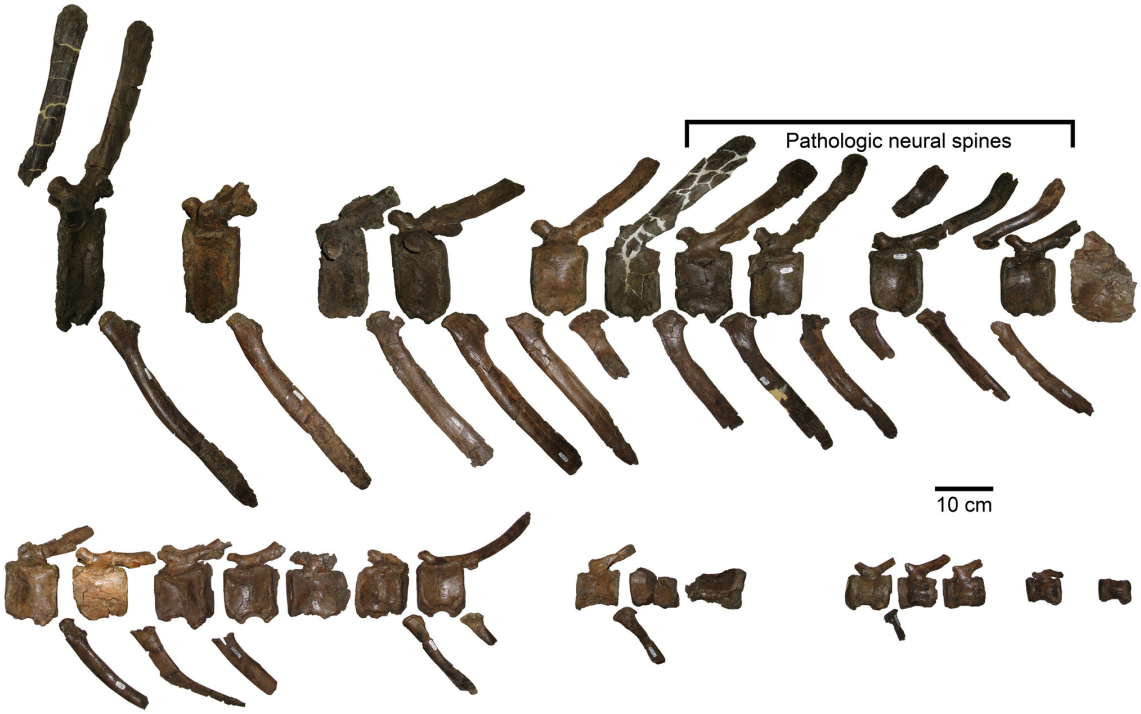


Figure 2.19. *Probrachylophosaurus bergei* caudal vertebrae. MOR 2919 vertebrae, neural spines, and chevrons are pictured in left lateral view in their approximate order within their series. Due to the disarticulated and incomplete nature of this caudal vertebral series, exact serial positions cannot be determined with confidence. Gaps between pictured vertebrae indicate noticeably missing segments of multiple vertebrae; additional vertebrae may be missing between any two vertebrae pictured here. Additional caudal vertebral fragments not pictured.

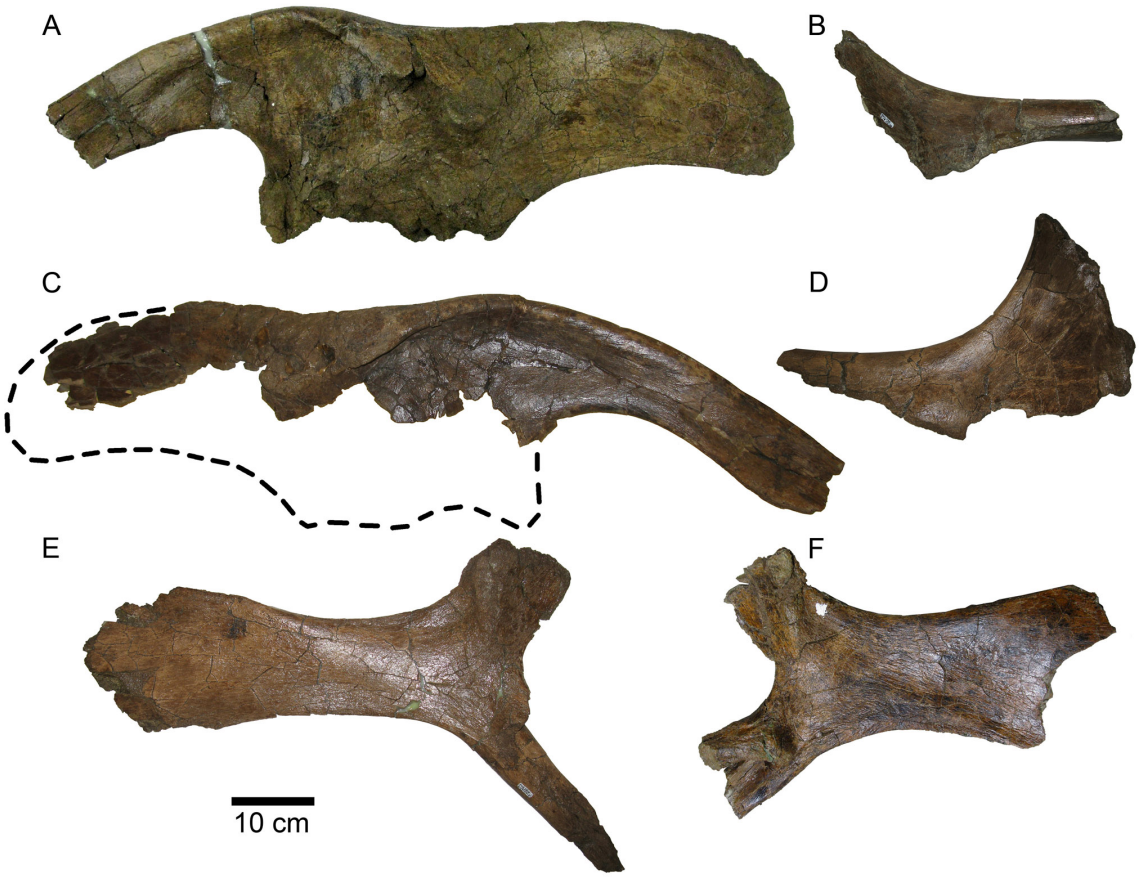


Figure 2.20. *Probrachylophosaurus bergei* pelvic elements. MOR 2919, all elements in lateral view; (A) left ilium; (B) partial proximal left ischium; (C) right ilium with dashed line indicating missing area; (D) partial proximal right ischium; (E) left pubis; (F) right pubis.



Figure 2.21. *Probrachylophosaurus bergei* hindlimb elements. MOR 2919 (A) left tibia, lateral view; (B) right tibia, lateral view; (C) left fibula, lateral view; (D) right fibula, lateral view; (E) left astragalus, anterior view; (F) right astragalus, anterior view; (G) right metatarsal II, medial view; (H) right metatarsal IV, medial view.

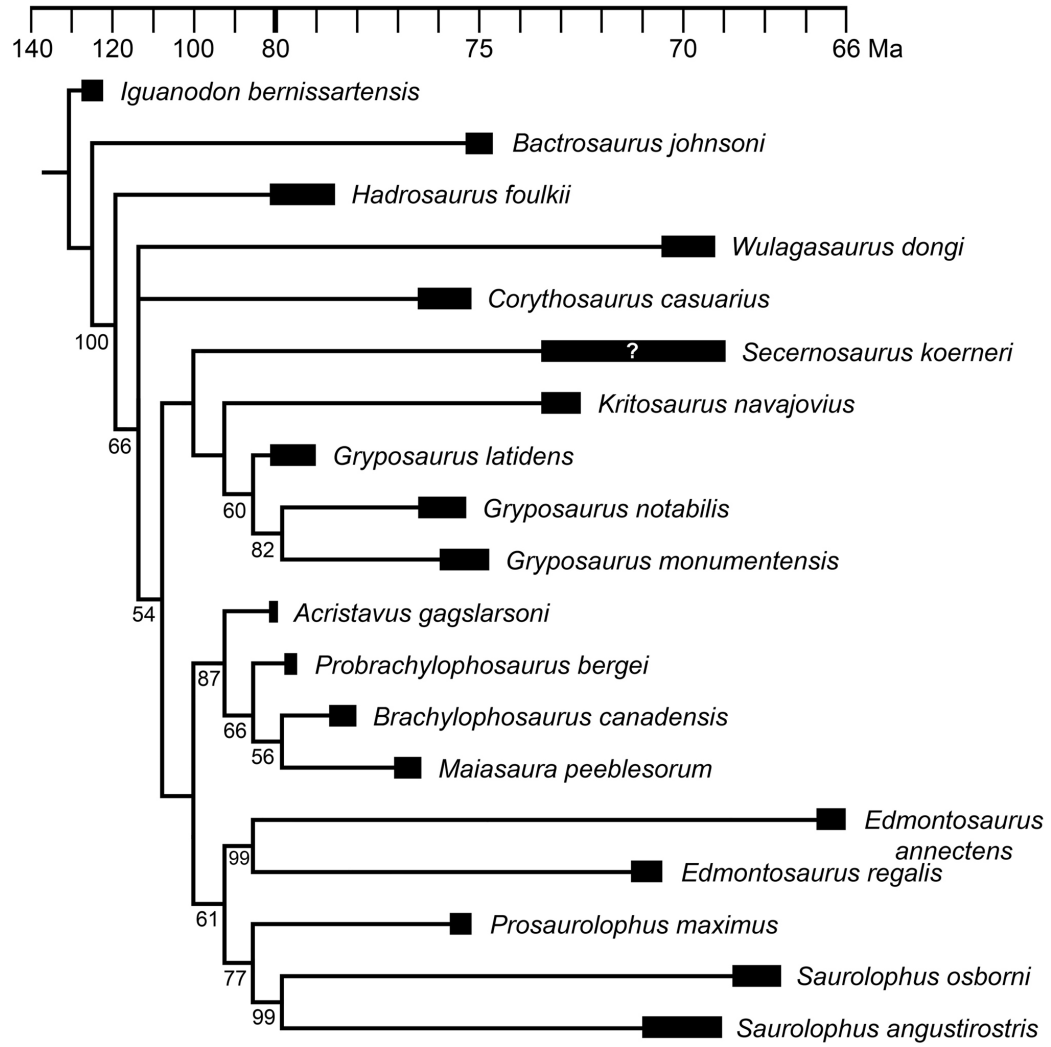


Figure 2.22. Time-calibrated cladogram of hadrosaurines based on Prieto-Márquez (2010a). The strict consensus of two most parsimonious trees resulting from adding *Probrachylophosaurus bergei* to Prieto-Márquez's (2010a) matrix with minor character recodings and exclusions as discussed in text was plotted using the age ranges for each taxon; branch lengths do not reflect the number of character state changes. Values on branches represent bootstrap support; branches without values had less than 50% support. Tree statistics: shortest tree length = 614, Consistency Index = 0.72, Retention Index = 0.68, Rescaled Consistency Index = 0.49. Age ranges of Brachylophosaurini are those recalibrated in Figure 1; age ranges of other taxa are approximate, and are based on unrecalibrated previously published dates (Rogers et al., 1993; Gallagher et al., 1996; Eberth, 2005; Roberts et al., 2005; Ryan and Evans, 2005; Gates and Sampson, 2007; Prieto-Márquez and Salinas, 2010; Bell, 2011b, a; Campione and Evans, 2011; Gates et al., 2011; Xing et al., 2012; McGarrity et al., 2013; Prieto-Márquez, 2014). Note that the age scale changes before and after 80 Ma. Also note that the age of *Bactrosaurus* has been variably proposed to be any time from late Turonian to early Maastrichtian in age (Van Itterbeeck et al., 2005; Sues and Averianov, 2009; Prieto-Márquez, 2011).

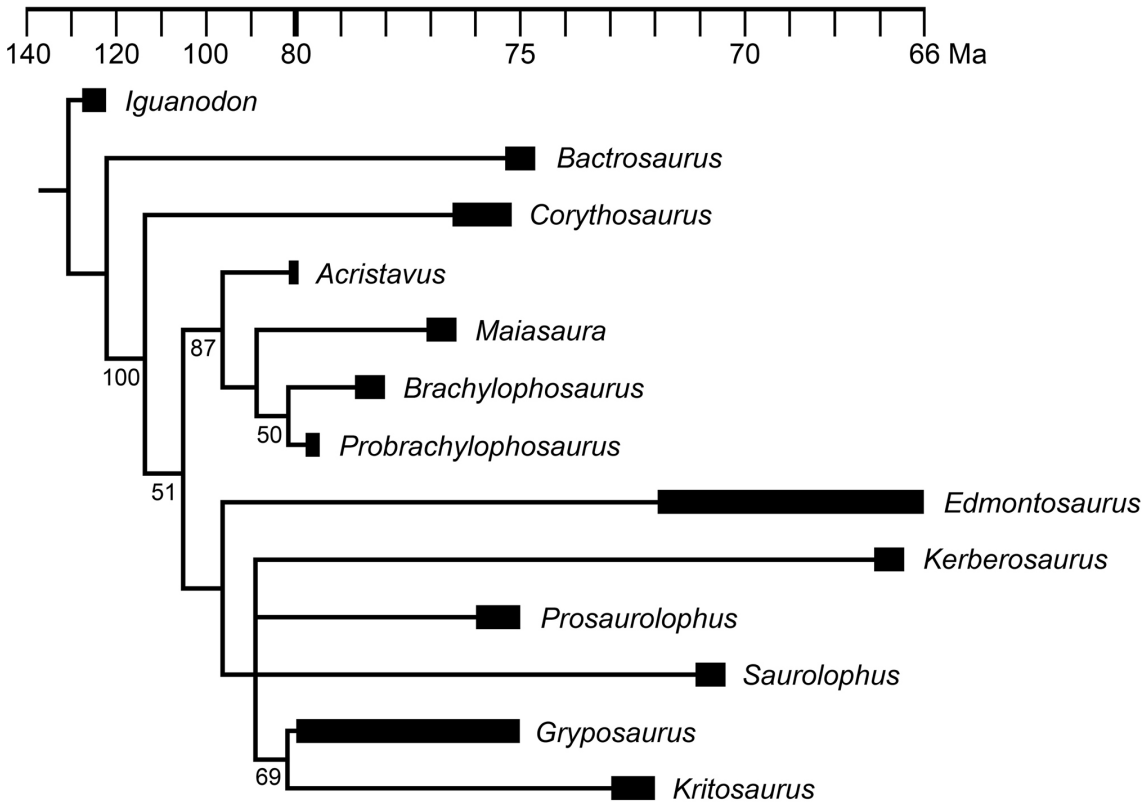


Figure 2.23. Time-calibrated cladogram of hadrosaurines based on Gates et al. (2011). The strict consensus of two most parsimonious trees resulting from adding *Probrachylophosaurus bergei* to Gates et al.'s (2011) matrix was plotted using the age ranges for each taxon; branch lengths do not reflect the number of character state changes. Because species within the same genus had the same codings, only genera are listed in the phylogeny. Values on branches represent bootstrap support; branches without values had less than 50% support. Tree statistics: shortest tree length = 188, Consistency Index = 0.70, Retention Index = 0.65, Rescaled Consistency Index = 0.45. Age ranges are approximate, and are based on those in Gates et al. (2011), aside from Brachylophosaurini, which have been recalibrated as in Figure 1. Note that the age scale changes before and after 80 Ma. Also note that the age of *Bactrosaurus* has been variably proposed to be any time from late Turonian to early Maastrichtian in age (Van Itterbeeck et al., 2005; Sues and Averianov, 2009; Prieto-Márquez, 2011).

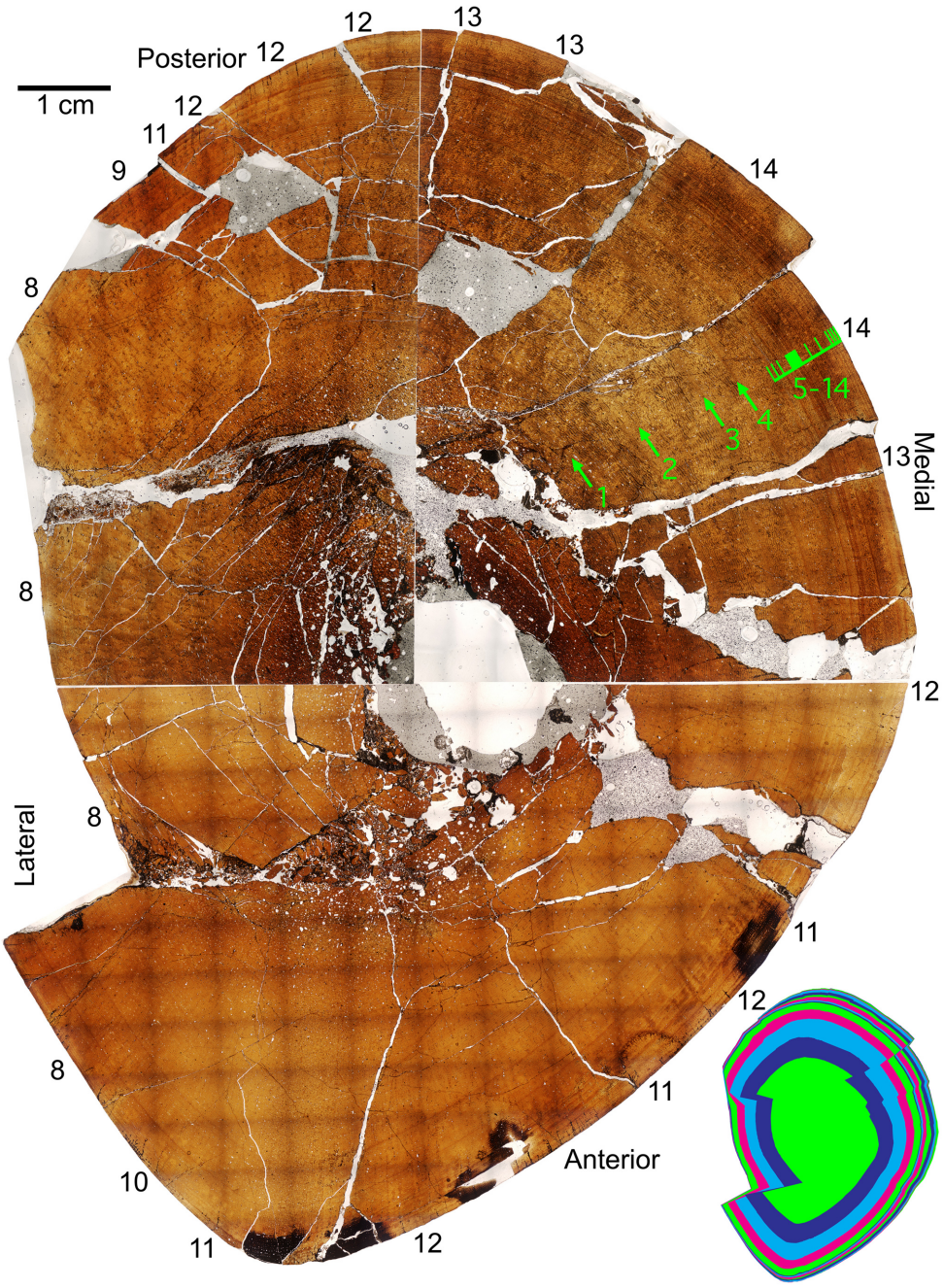


Figure 2.24. Tibial histology of MOR 2919, mid-diaphyseal cross-section. Numbered green arrows identify lines of arrested growth (LAGs). The closely spaced outer LAGs are indicated with tick marks along a green line. Numbers around the circumference of the cross-section indicate the number of LAGs preserved in that radial segment of the tibia. Note that diagenetic crushing has displaced several segments radially inward. Thumbnail image in lower right corner colors the area between each pair of LAGs to highlight locations of radial displacement as well as to indicate bone deposition between later LAGs occurring primarily along the posteromedial region.

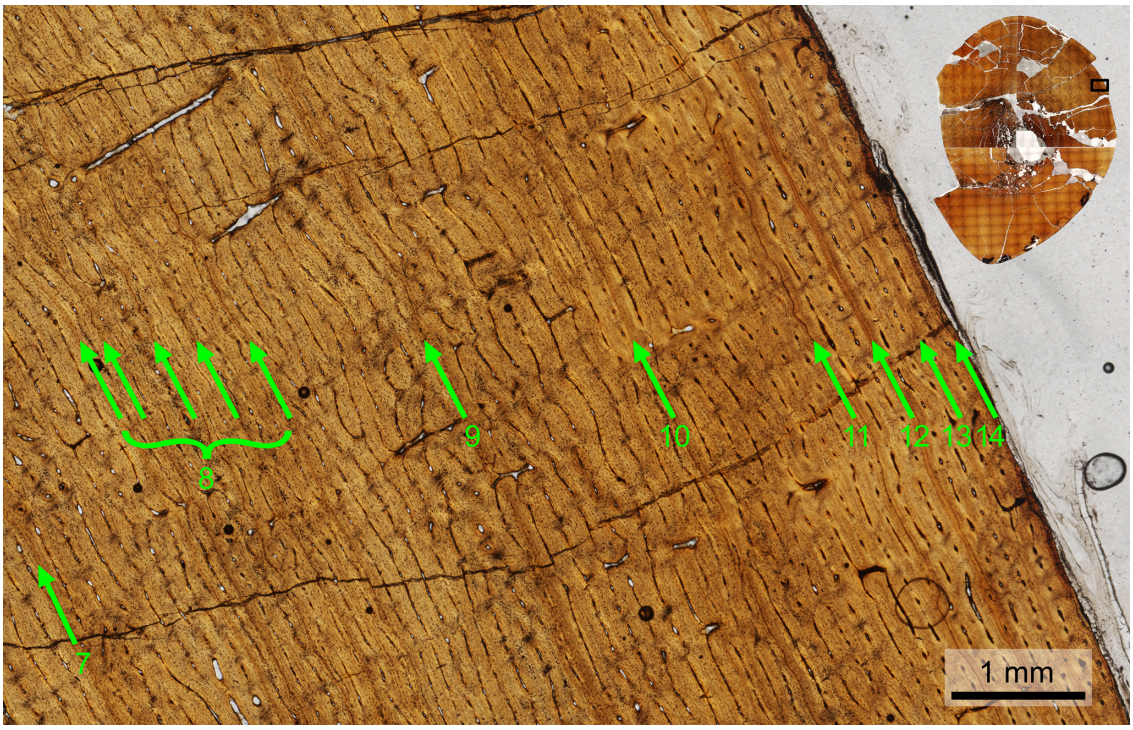


Figure 2.25. Outer cortical histology of MOR 2919 tibia. This is a higher-resolution image of the posteromedial cortex pictured in Figure 24, as indicated by the black box on the upper right thumbnail image of the entire mid-diaphyseal cross-section. Numbered green arrows identify lines of arrested growth (LAGs), including the multiple lines of LAG zone 8 (see text).

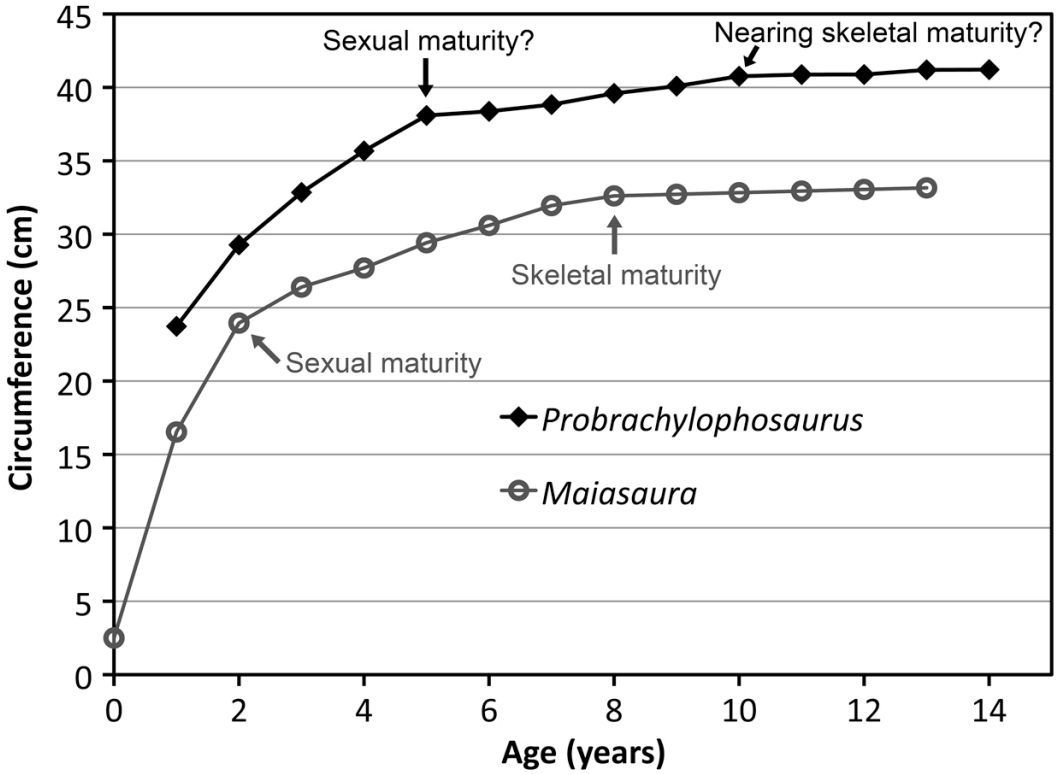


Figure 2.26. Growth curves of tibial cortical circumference at each line of arrested growth in *Probrachylophosaurus bergei* (MOR 2919) and *Maiasaura peeblesorum* (MOR 758 NC-7-4-96-16 "T46"). Age in years was determined by counting the number of lines of arrested growth within the tibial cortex. MOR 2919 left tibia is 119 cm long. *Maiasaura* data are taken from the largest tibia with complete histologic data (93 cm long) from Woodward et al. (in press). Inflection points in the growth of *Probrachylophosaurus* occur at 5 years and 10 years; these inflection points occur earlier in *Maiasaura*, at 2-3 years and 8 years. In Maiasaura, the first inflection point is interpreted as sexual maturity, and the second inflection point occurs at the initiation of the external fundamental system (EFS), representing skeletal maturity (Woodward et al., in press). Although MOR 2919 has an apparent second inflection point, it does not possess an EFS, so it is not skeletally mature.

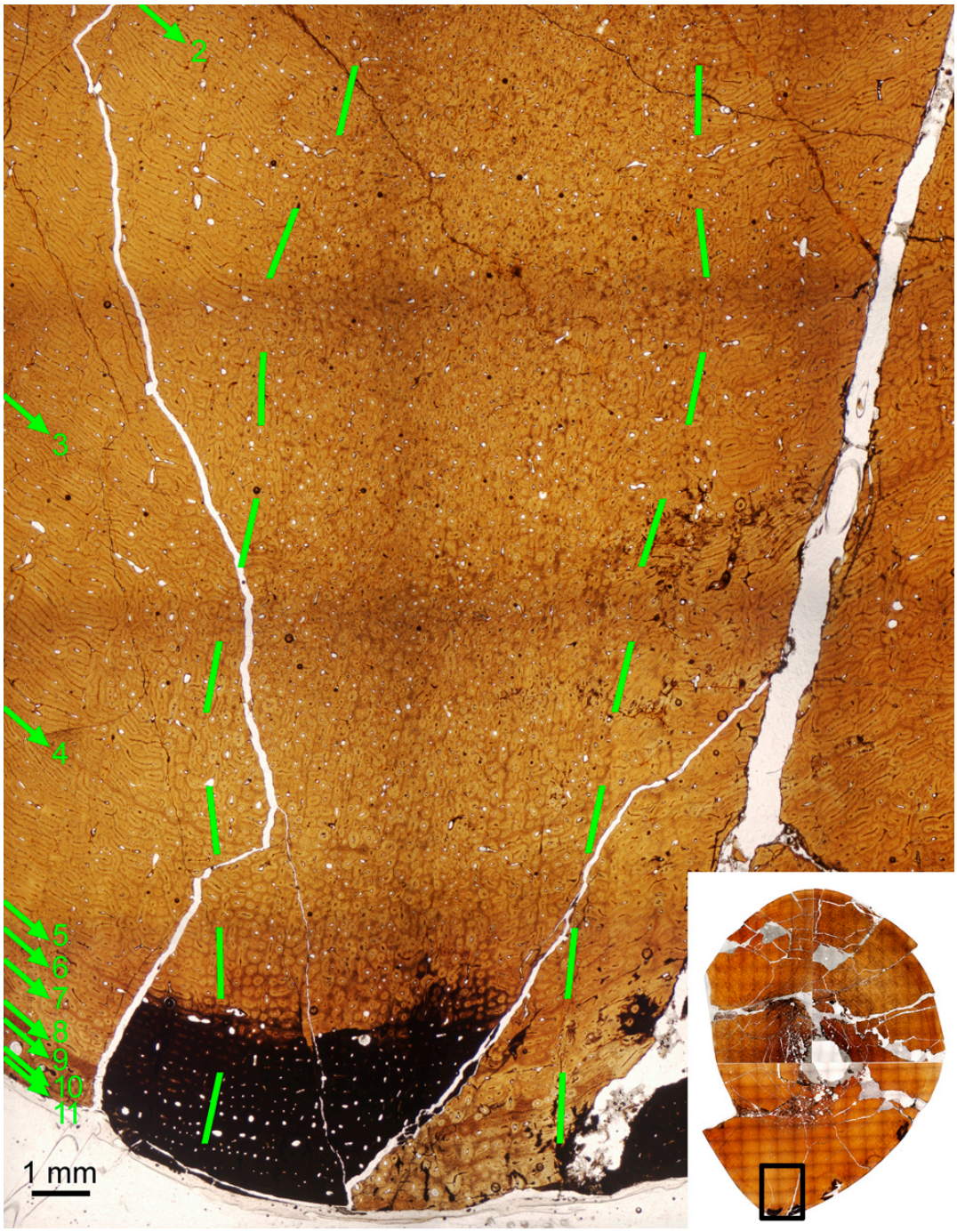


Figure 2.27. Remodeled "fountain" of secondary osteons on anterolateral side of cortex, MOR 2919 tibia. Margins of the remodeled region are indicated with dashed green lines. Numbered green arrows identify lines of arrested growth. Dark areas near edge of cortex are sections of bone that began to separate from the slide, requiring additional adhesive. Black box on the thumbnail image on lower right indicates location of Figure Z within the entire tibial cross-section.

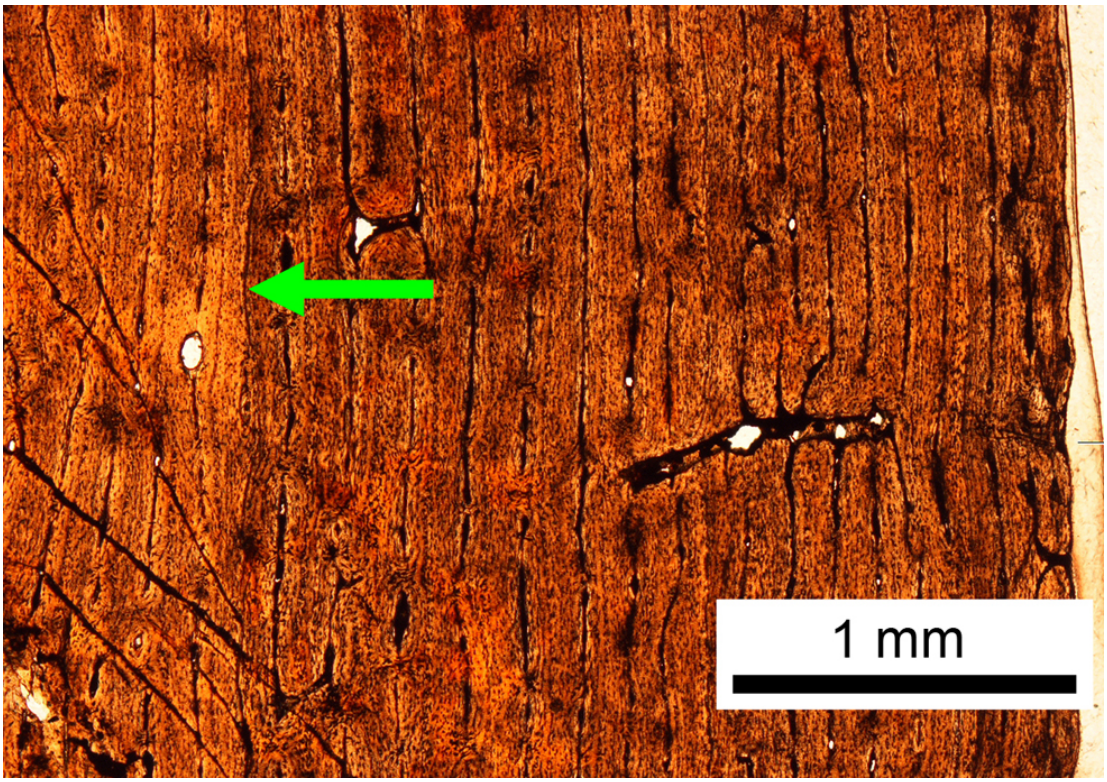


Figure 2.28. Outer cortical histology of MOR 794 *Brachylophosaurus canadensis* femur. The right femur (length 129.5 cm) of MOR 794 was histologically sampled using a core of the outer cortex of the anteromedial mid-diaphysis rather than a complete cross-section of the mid-diaphysis, so the complete LAG record was not sampled and the individual's age in years is unknown. Green arrow indicates the outermost LAG. Cortical surface is on the right.

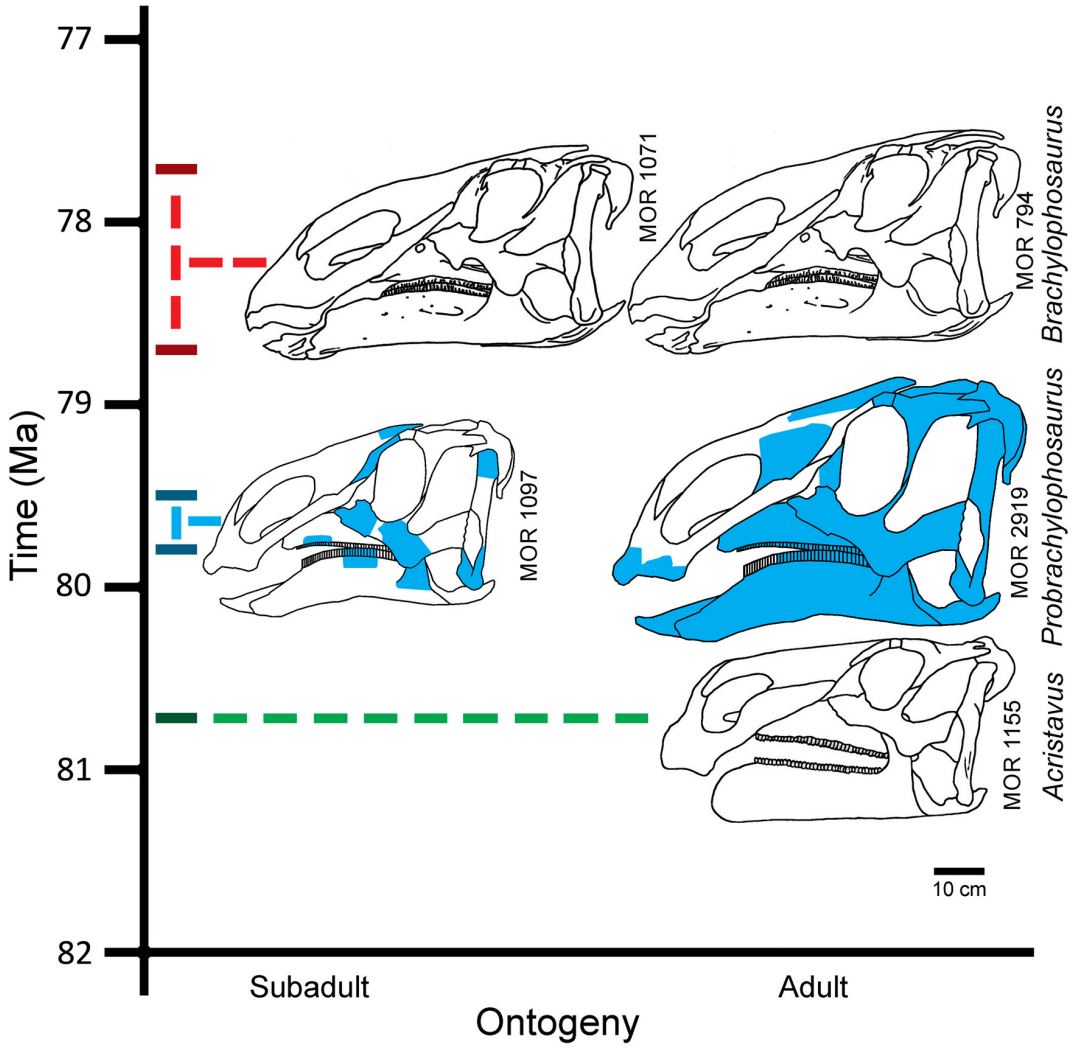


Figure 2.29. Ontogenetic and anagenetic hypothesis of brachylophosaurin evolution. *Probrachylophosaurus bergei* is proposed as an intermediate member of the lineage leading from *Acristavus gagslarsoni* to *Brachylophosaurus canadensis*. Shaded blue areas indicate known elements of *Probrachylophosaurus*. Skull outlines of *Acristavus* and *Brachylophosaurus* modified from Gates et al. (2011). The reconstruction of the MOR 1071 *Brachylophosaurus* skull is a composite of an articulated skull roof with a scaled-down copy of the MOR 794 skull outline. All skulls are scaled to the same 10 cm scale bar. The horizontal axis is not to scale; the MOR 1071 reconstruction is much closer to MOR 794 in size and hypothesized maturity than MOR 1097 is to MOR 2919. Radiometric ages have been recalibrated to the Fish Canyon sanidine standard (28.305 ± 0.036 Ma) of Renne et al. (2010) from the originally published values (Goodwin and Deino, 1989; Eberth and Hamblin, 1993; Eberth, 2005; Gates et al., 2011); see text and Table 1 for further recalibration details. The age of the *Acristavus* holotype was precisely estimated by Gates et al. (2011). The age of the Comrey Sandstone Zone of the Oldman Formation is not tightly constrained, leading to uncertainty in the exact age of *Brachylophosaurus*.

Literature Cited

Bell, P. R. 2011a. Cranial osteology and ontogeny of *Saurolophus angustirostris* from the Late Cretaceous of Mongolia with comments on *Saurolophus osborni* from Canada. Acta Palaeontologica Polonica 56:703-722.

Bell, P. R. 2011b. Redescription of the skull of *Saurolophus osborni* Brown 1912 (Ornithischia: Hadrosauridae). Cretaceous Research 32:30-44.

Brinkman, D. B., A. P. Russell, D. A. Eberth, and J. Peng. 2004. Vertebrate palaeocommunities of the lower Judith River Group (Campanian) of southeastern Alberta, Canada, as interpreted from vertebrate microfossil assemblages. Palaeogeography, Palaeoclimatology, Palaeoecology 213:295-313.

Campione, N. E., and D. C. Evans. 2011. Cranial growth and variation in edmontosaurs (Dinosauria: Hadrosauridae): implications for latest Cretaceous megaherbivore diversity in North America. PLoS ONE 6:e25186.

Campione, N. E., K. S. Brink, E. A. Freedman, C. T. McGarrity, and D. C. Evans. 2012. '*Glishades ericksoni*', an indeterminate juvenile hadrosaurid from the Two Medicine Formation of Montana: implications for hadrosauroid diversity in the latest Cretaceous (Campanian-Maastrichtian) of western North America. Palaeobiodiversity and Palaeoenvironments August 24:1-11.

Cuthbertson, R. S., and R. B. Holmes. 2010. The first complete description of the holotype of *Brachylophosaurus canadensis* Sternberg, 1953 (Dinosauria: Hadrosauridae) with comments on intraspecific variation. Zoological Journal of the Linnean Society 159:373-397.

Dilkes, D. W. 1993. Growth and locomotion in the hadrosaurian dinosaur *Maiasaura peeblesorum* from the Upper Cretaceous of Montana. PhD dissertation, Department of Zoology, University of Toronto, 447 pp.

Dilkes, D. W. 2000. Appendicular myology of the hadrosaurian dinosaur *Maiasaura peeblesorum* from the Late Cretaceous (Campanian) of Montana. Transactions of the Royal Society of Edinburgh-Earth Sciences 90:87-125.

Dodson, P. 1975. Taxonomic implications of relative growth in lambeosaurine hadrosaurs. Systematic Zoology 24:37-54.

Eberth, D. A. 2005. The Geology; pp. 54-82 in P. J. Currie and E. B. Koppelhus (eds.), Dinosaur Provincial Park: A Spectacular Ancient Ecosystem Revealed. Indiana University Press, Bloomington, Indiana.

Eberth, D. A., and A. P. Hamblin. 1993. Tectonic, stratigraphic, and sedimentologic significance of a regional discontinuity in the upper Judith River Group (Belly River wedge) of southern Alberta, Saskatchewan, and northern Montana. Canadian Journal of Earth Sciences 30:174-200.

Eberth, D. A., and D. C. Evans. 2011: Geology and Paleontology of Dinosaur Provincial Park, Alberta Field Trip Guidebook. International Hadrosaur Symposium, Drumheller, Alberta, 2011.

Evans, D. C. 2010. Cranial anatomy and systematics of *Hypacrosaurus altispinus*, and a comparative analysis of skull growth in lambeosaurine hadrosaurids (Dinosauria: Ornithischia). Zoological Journal of the Linnean Society 159:398-434.

Evans, D. C., and R. R. Reisz. 2007. Anatomy and relationships of *Lambeosaurus magnicristatus*, a crested hadrosaurid dinosaur (Ornithischia) from the Dinosaur Park Formation, Alberta. Journal of Vertebrate Paleontology 27:373-393.

Gallagher, W. B., P. J. Sugarman, and M. D. Feigenson. 1996. Strontium isotope age estimates for east coast dinosaur sites. Journal of Vertebrate Paleontology 16:36A.

Gates, T. A., and S. D. Sampson. 2007. A new species of *Gryposaurus* (Dinosauria: Hadrosauridae) from the late Campanian Kaiparowits Formation, southern Utah, USA. Zoological Journal of the Linnean Society 151:351-376.

Gates, T. A., J. R. Horner, R. R. Hanna, and R. C. Nelson. 2011. New unadorned hadrosaurine hadrosaurid (Dinosauria, Ornithopoda) from the Campanian of North America. Journal of Vertebrate Paleontology 31:798-811.

Goodwin, M. B., and A. L. Deino. 1989. The first radiometric ages from the Judith River Formation (Upper Cretaceous), Hill County, Montana. Canadian Journal of Earth Sciences 26:1384-1391.

Haeckel, E. 1866. Generelle morphologie der organismen. Allgemeine grundzüge der organischen formen-wissenschaft, mechanisch begründet durch die von Charles Darwin reformirte descendenz-theorie. Georg Reimer, Berlin, 462 pp.

Haeckel, E. 1901. The Riddle of the Universe at the Close of the Nineteenth Century. Harper & Brothers, New York, 391 pp.

Horner, J. R. 1983. Cranial osteology and morphology of the type specimen of *Maiasaura peeblesorum* (Ornithischia: Hadrosauridae), with discussion of its phylogenetic position. Journal of Vertebrate Paleontology 3:29-38.

Horner, J. R. 1984: Three ecologically distinct vertebrate faunal communities from the Late Cretaceous Two Medicine Formation of Montana, with discussion of evolutionary pressures induced by interior seaway fluctuations. Montana

Geological Society Field Conference and Symposium, Northwest Montana and Adjacent Canada, 1984.

Horner, J. R. 1988. A new hadrosaur (Reptilia, Ornithischia) from the Upper Cretaceous Judith River Formation of Montana. Journal of Vertebrate Paleontology 8:314-321.

Horner, J. R. 1989. The ontogenetic predictability of hadrosaur crania. Journal of Vertebrate Paleontology 9:25A.

Horner, J. R. 1992. Cranial morphology of *Prosaurolophus* (Ornithischia: Hadrosauridae) with descriptions of two new hadrosaurid species and an evaluation of hadrosaurid phylogenetic relationships. Museum of the Rockies Occasional Paper 2:1-119.

Horner, J. R., and R. Makela. 1979. Nest of juveniles provides evidence of family structure among dinosaurs. Nature 282:296-298.

Horner, J. R., and P. J. Currie. 1994. Embryonic and neonatal morphology and ontogeny of a new species of *Hypacrosaurus* (Ornithischia, Lambeosauridae) from Montana and Alberta. Dinosaur Eggs and Babies:312-336.

Horner, J. R., and M. B. Goodwin. 2009. Extreme cranial ontogeny in the Upper Cretaceous dinosaur *Pachycephalosaurus*. PLoS ONE 4:e7626 p. 1-11. doi:10.1371/journal.pone.0007626.

Horner, J. R., A. de Ricqlès, and K. Padian. 2000. Long bone histology of the hadrosaurid dinosaur *Maiasaura peeblesorum*: growth dynamics and physiology based on an ontogenetic series of skeletal elements. Journal of Vertebrate Paleontology 20:115-129.

Horner, J. R., D. B. Weishampel, and C. A. Forster. 2004. Hadrosauridae; pp. 438-463 in D. B. Weishampel, P. Dodson, and H. Osmólska (eds.), The Dinosauria. University of California Press, Berkeley.

Horner, J. R., M. B. Goodwin, and N. Myhrvold. 2011. Dinosaur census reveals abundant *Tyrannosaurus* and rare ontogenetic stages in the Upper Cretaceous Hell Creek Formation (Maastrichtian), Montana, USA. PLoS ONE 6:1-9. e16574.

Horner, J. R., A. de Ricqlès, K. Padian, and R. D. Scheetz. 2009. Comparative long bone histology and growth of the "hypsilophodontid" dinosaurs *Orodromeus makelai*, *Dryosaurus altus*, and *Tenontosaurus tillettii* (Ornithischia: Euornithopoda). Journal of Vertebrate Paleontology 29:734-747.

Hübner, T. R. 2012. Bone Histology in *Dysalotosaurus lettowvorbecki* (Ornithischia: Iguanodontia) - Variation, Growth, and Implications. PLoS ONE 7:e29958.

Jinnah, Z. A., E. M. Roberts, A. L. Deino, J. S. Larsen, P. K. Link, and C. M. Fanning. 2009. New 40Ar-39Ar and detrital zircon U-Pb ages for the Upper Cretaceous Wahweap and Kaiparowits formations on the Kaiparowits Plateau, Utah: implications for regional correlation, provenance, and biostratigraphy. Cretaceous Research 30:287-299.

Kirkland, J. I., J. G. Eaton, and D. B. Brinkman. 2013. Elasmobranchs from Upper Cretaceous freshwater facies in Southern Utah; pp. 153-194 in A. L. Titus and M. A. Loewen (eds.), At the Top of the Grand Staircase: the Late Cretaceous of southern Utah. Indiana University Press, Bloomington, Indiana.

Köhler, M., N. Marin-Moratalla, X. Jordana, and R. Aanes. 2012. Seasonal bone growth and physiology in endotherms shed light on dinosaur physiology. Nature 487:358-361.

Lambe, L. M. 1914. On *Gryposaurus notabilis*, a new genus and species of trachodont dinosaur from the Belly River Formation of Alberta, with a description of the skull of *Chasmosaurus belli*. The Ottawa Naturalist 27:145-155.

Lamm, E.-T. 2013. Preparation and sectioning of specimens; pp. 55-160 in K. Padian and E.-T. Lamm (eds.), Bone Histology of Fossil Tetrapods. University of California Press, Berkeley.

Langston, W., Jr. 1960. The vertebrate fauna of the Selma Formation of Alabama, part VI: the dinosaurs. Fieldiana: Geology Memoirs 3:314-363.

LaRock, J. W. 2001. Sedimentology and taphonomy of a dinosaur bonebed from the Upper Cretaceous (Campanian) Judith River Formation of north central Montana. unpublished M.S. thesis, Department of Earth Sciences, Montana State University, Bozeman, 61 pp.

Leiggi, P., C. R. Schaff, and P. May. 1994. Macrovertebrate collecting; pp. 59-77 in P. Leiggi and P. May (eds.), Vertebrate Paleontological Techniques. Cambridge University Press, Cambridge, UK.

McGarrity, C. T., N. E. Campione, and D. C. Evans. 2013. Cranial anatomy and variation in *Prosaurolophus maximus* (Dinosauria: Hadrosauridae). Zoological Journal of the Linnean Society 167:531-568.

Peng, J.-H., A. P. Russell, and D. B. Brinkman. 2001. Vertebrate microsite assemblages (exclusive of mammals) from the Foremost and Oldman Formations of the Judith River Group (Campanian) of Southeastern Alberta: an illustrated guide. Provincial Museum of Alberta Natural History Occasional Paper 25:1-54.

Prieto-Márquez, A. 2005. New information on the cranium of *Brachylophosaurus canadensis* (Dinosauria, Hadrosauridae), with a revision of its phylogenetic position. Journal of Vertebrate Paleontology 25:144-156.

Prieto-Márquez, A. 2007. Postcranial Osteology of the Hadrosaurid Dinosaur *Brachylophosaurus canadensis* from the Late Cretaceous of Montana; pp. 91-115 in K. Carpenter (ed.), Horns and Beaks: Ceratopsian and Ornithopod Dinosaurs. Indiana Press, Bloomington, IN.

Prieto-Márquez, A. 2010a. Global phylogeny of Hadrosauridae (Dinosauria: Ornithopoda) using parsimony and Bayesian methods. Zoological Journal of the Linnean Society 159:435-502.

Prieto-Márquez, A. 2010b. The braincase and skull roof of *Gryposaurus notabilis* (Dinosauria, Hadrosauridae), with a taxonomic revision of the genus. Journal of Vertebrate Paleontology 30:838-854.

Prieto-Márquez, A. 2011. Cranial and appendicular ontogeny of *Bactrosaurus johnsoni*, a hadrosauroid dinosaur from the Late Cretaceous of northern China. Palaeontology 54:773-792.

Prieto-Márquez, A. 2014. Skeletal morphology of *Kritosaurus navajovius* (Dinosauria: Hadrosauridae) from the Late Cretaceous of the North American south-west, with an evaluation of the phylogenetic systematics and biogeography of Kritosaurini. Journal of Systematic Palaeontology 12:133-175.

Prieto-Márquez, A., and G. C. Salinas. 2010. A re-evaluation of *Secernosaurus koerneri* and *Kritosaurus australis* (Dinosauria, Hadrosauridae) from the Late Cretaceous of Argentina. Journal of Vertebrate Paleontology 30:813-837.

Rasband, W. S. 1997-2014. ImageJ. U. S. National Institutes of Health, Bethesda, Maryland, USA, http://imagej.nih.gov/ij/,.

Renne, P. R., R. Mundil, G. Balco, K. Min, and K. Ludwig. 2010. Joint determination of 40K decay constants and 40Ar*/40K for the Fish Canyon sanidine standard, and improved accuracy for 40Ar/39Ar geochronology. Geochimica et Cosmochimica Acta 74:5349-5367.

Renne, P. R., C. C. Swisher, A. L. Deino, D. B. Karner, T. L. Owens, and D. J. DePaolo. 1998. Intercalibration of standards, absolute ages and uncertainties in 40Ar/ 39Ar dating. Chemical Geology 145:117-152.

Roberts, E. M., A. L. Deino, and M. A. Chan. 2005. 40Ar/39Ar age of the Kaiparowits Formation, southern Utah, and correlation of contemporaneous Campanian strata and vertebrate faunas along the margin of the Western Interior Basin. Cretaceous Research 26:307-318.

Rogers, R. R., C. C. Swisher, and J. R. Horner. 1993. 40Ar/39Ar age and correlation of the nonmarine Two Medicine Formation (Upper Cretaceous), northwestern Montana, USA. Canadian Journal of Earth Sciences 30:1066-1075.

Rozhdestvensky, A. K. 1965. Growth changes in Asian dinosaurs and some problems of their taxonomy. Paleontologischeskii Zhurnal 3:95-109.

Ryan, M. J., and D. C. Evans. 2005. Ornithischian Dinosaurs. Dinosaur Provincial Park: A Spectacular Ancient Ecosystem Revealed:312-348.

Ryan, M. J., R. B. Holmes, and A. P. Russell. 2007. A revision of the late Campanian centrosaurine ceratopsid genus *Styracosaurus* from the Western Interior of North America. Journal of Vertebrate Paleontology 27:944-962.

Ryan, M. J., A. P. Russell, and S. Hartman. 2010. A new chasmosaurine ceratopsid from the Judith River Formation, Montana. New Perspectives on Horned Dinosaurs:181-188.

Sampson, S. D., M. J. Ryan, and D. H. Tanke. 1997. Craniofacial ontogeny in centrosaurine dinosaurs (Ornithischia: Ceratopsidae): taxonomic and behavioral implications. Zoological Journal of the Linnean Society 121:293-337.

Scannella, J. B., D. W. Fowler, M. B. Goodwin, and J. R. Horner. 2014. Evolutionary trends in *Triceratops* from the Hell Creek Formation, Montana. Proceedings of the National Academy of Sciences 111:10245-10250.

Schott, R., D. C. Evans, M. B. Goodwin, C. M. Brown, and N. Longrich. 2010. Cranial ontogeny in *Stegoceras* and the evolution of cranial doming and ornamentation in Pachycephalosauria (Dinosauria: Ornithischia). Journal of Vertebrate Paleontology, SVP Program and Abstracts Book:159A.

Sternberg, C. M. 1953. A new hadrosaur from the Oldman Formation of Alberta: discussion of nomenclature. National Museum of Canada, Bulletin 128:275-286.

Sues, H.-D., and A. Averianov. 2009. A new basal hadrosauroid dinosaur from the Late Cretaceous of Uzbekistan and the early radiation of duck-billed dinosaurs. Proceedings of the Royal Society B 276:2549-2555.

Swofford, D. L. 2002. PAUP*. Phylogenetic analysis using parsimony (*and other methods). Version 4.0b10. Sinauer Associates, Sunderland, MA.

Thomas, R. G., D. A. Eberth, A. L. Deino, and D. Robinson. 1990. Composition, radioisotopic ages, and potential significance of an altered volcanic ash (bentonite) from the Upper Cretaceous Judith River Formation, Dinosaur Provincial Park, southern Alberta, Canada. Cretaceous Research 11:125-162.

Trexler, D. L. 1995. A detailed description of newly-discovered remains of *Maiasaura peeblesorum* (Reptilia: Ornithischia) and a revised diagnosis of the genus. Unpublished MS thesis. Department of Biological Sciences, University of Calgary, Calgary, Alberta, 235 pp.

Tsuihiji, T., K. Watabe, K. Tsogtbaatar, T. Tsubamoto, R. Barsbold, S. Suzuki, A. H. Lee, R. C. Ridgely, Y. Kawahara, and L. M. Witmer. 2011. Cranial osteology of a juvenile specimen of *Tarbosaurus bataar* form the Nemegt Formation (Upper Cretaceous) of Bugin Tsav, Mongolia. Journal of Vertebrate Paleontology 31:497-517.

Van Itterbeeck, J., D. J. Horne, P. Bultynck, and N. Vandenberghe. 2005. Stratigraphy and palaeoenvironment of the dinosaur-bearing Upper Cretaceous Iren Dabasu Formation, Inner Mongolia, People's Republic of China. Cretaceous Research 26:699-725.

Varricchio, D. J., and J. R. Horner. 1993. Hadrosaurid and lambeosaurid bonebeds from the Upper Cretaceous Two Medicine Formation of Montana: taphonomic and biologic implications. Canadian Journal of Earth Sciences 30:997-1006.

Varricchio, D. J., C. Koeberl, R. F. Raven, W. S. Wolbach, W. C. Elsik, and D. P. Miggins. 2010. Tracing the Manson impact event across the Western Interior Cretaceous Seaway. Geological Society of America Special Paper 465:269-299.

Woodward, H. N., E. A. Freedman Fowler, J. O. Farlow, and J. R. Horner. in press. *Maiasaura*, a model organism for extinct vertebrate population biology: a statistically robust assessment of growth dynamics and survivorship. Paleobiology.

Xing, H., A. Prieto-Márquez, W. Gu, and T.-X. Yu. 2012. Re-evaluation and phylogenetic analysis of *Wulagasaurus dongi*, a hadrosaurine dinosaur from the Maastrichtian of northeast China. Vertebrata PalAsiatica 50:160-169.

CHAPTER THREE

TAPHONOMY OF A *GRYPOSAURUS* HADROSAUR BONEBED FROM THE JUDITH RIVER FORMATION (CAMPANIAN) OF NORTHCENTRAL MONTANA

Contribution of Authors and Co-Authors

Manuscript in Chapter 3

Author: Elizabeth A. Freedman

Contributions: Conceived the study, performed the analyses, interpreted results, and wrote the manuscript.

Co-authors: none

Manuscript Information Page

Elizabeth A. Freedman
Status of Manuscript:
_x_ Prepared for submission to a peer-reviewed journal
___ Officially submitted to a peer-reviewed journal
___ Accepted by a peer-reviewed journal
___ Published in a peer-reviewed journal

Abstract

An extensive *Gryposaurus* bonebed from the Judith River Formation of northcentral Montana was preserved in an interchannel mudstone stratigraphically equivalent to the lower Oldman Formation of Alberta. The *Gryposaurus* bonebed is a strongly monodominant assemblage containing more than 800 bones of at least ten individuals of three discrete size classes: four juveniles, five subadults, and one adult. The discrete size classes with no intermediately sized individuals support a specific breeding season for *Gryposaurus*. The *Gryposaurus* bones are unweathered; abrasion on limb bones is minimal, but is present on some fractured bones such as ribs, vertebrae, and bone fragments. The majority of elongate bones are close to horizontal, with no preferred orientation. Although phalanges and vertebrae are underrepresented relative to large limb bones, the overrepresentation of skull material as well as the presence of small porous elements such as phalanges and caudal centra suggests minimal transport or winnowing of the assemblage. Wood, organic debris, and tyrannosaur teeth are abundant in the bonebed mudstone horizon. Although mollusks are not common in the bonebed mudstone, the taxa present indicate an oxic, quiet-water environment. The assemblage is hypothesized to have originated as a mass death assemblage on a floodplain or along a lake margin. The carcasses were fed upon by tyrannosaurs, and then the bones are hypothesized to have been concentrated and deposited by a flood into a lake or other quiet-water environment on the floodplain.

Introduction

Bonebeds offer glimpses into the behavior and ecology of fossil vertebrates, allowing insights into population structure, cause of death, and depositional environment. Campanian (Late Cretaceous) terrestrial deposits in Montana host multiple spectacular bonebeds of hadrosaurine dinosaurs. These include monodominant bonebeds such as *Maiasaura*, *Prosaurolophus*, and *Hypacrosaurus* bonebeds in the Two Medicine Formation of western Montana (Varricchio and Horner, 1993), and a *Brachylophosaurus* bonebed in the Judith River Formation of northeast-central Montana (Prieto-Márquez, 2005), as well as multitaxic bonebeds in the Two Medicine and Judith River Formations that contain multiple hadrosaur taxa and other dinosaurs (Fiorillo, 1991b; Varricchio, 1995). Many of these bonebeds contain a range of different sized individuals, while others are restricted to juveniles (Scherzer and Varricchio, 2010).

Although many individual *Gryposaurus* specimens have been collected from Montana, Alberta, and Utah, encompassing several species over a time period of five million years (Gates and Sampson, 2007), *Gryposaurus* bonebeds are rare. The bonebed described herein, Museum of the Rockies (MOR) locality JR-429, is one of only two known monodominant *Gryposaurus* bonebeds, both of which are found in mudstone horizons equivalent to the lower Oldman Formation (Scott et al., 2014). The only other documented *Gryposaurus* bonebed material is part of a multitaxic bonebed in the Two Medicine Formation of Montana (Varricchio, 1995). The JR-429 bonebed is the largest known *Gryposaurus* bonebed and preserves the greatest variety of skeletal elements, containing over 800 bones (MOR 2573) of two discrete non-adult size classes, with a rib

head providing the only evidence of a large adult. This paper analyzes the taphonomy of the JR-429 bonebed and proposes hypotheses for its origin and paleobiological significance.

Geologic Setting

Kennedy Coulee in northcentral Montana exposes part of the Judith River Formation corresponding to the upper Foremost Formation and lower Oldman Formation of the Belly River Group of Alberta. The Judith River Formation is the lowland complement to the roughly contemporaneous more upland Two Medicine Formation of western Montana (Rogers et al., 1993). Eberth's (2005) terms for the Albertan members of the Belly River Group are used here, as members of the Judith River Formation have not been formally defined. The lower exposures of Kennedy Coulee consist of the Taber Coal Zone and Herronton Sandstone Zone of the Foremost Formation, and the upper exposures consist of the mudstone-dominated Unit 1 of the Oldman Formation. The top of the uppermost major coal of the Taber Coal Zone, the Marker A Coal, is used as a regional correlation surface. The JR-429 bonebed is located in Unit 1 of the Oldman Formation, 26.6 m above the Marker A Coal (Figure 3.1). The bonebed was discovered by Dan Redding, and is located on private land. All fossil material from the JR-429 bonebed has been generously donated to the Museum of the Rockies (MOR), in Bozeman, Montana, by Dan and Lila Redding.

Methods

Specimens were collected during the summers of 2006 and 2010-2012 using standard vertebrate paleontological field techniques and taphonomic data collection methods (Leiggi et al., 1994; Eberth et al., 2007). The concreted sandstone horizon above the quarry was removed by cracking the rocks with Betonamit® non-explosive cracking agent, following the method of Mateus and Araújo (2008). Every bone in the bonebed horizon was collected, with the exception of small fragments of rib (<5 cm), ossified tendon (<3 cm), and unidentifiable poorly preserved bone fragments (<5 cm), unless these elements happened to be included in plaster jackets with other bones. Bones were assigned field numbers in the format MOR 2573-month-day-year-count (e.g. MOR 2573-7-22-10-447). Locations of bones were mapped, and trend and plunge was measured on elongate bones. Field notes recorded any noteworthy data for each specimen, such as its vertical position relative to other bones or wood, or to distinguish pre-burial fractures from more recent breaks.

Lithology and Non-Hadrosaur Fossils

A stratigraphic section was measured to the nearest 10 cm, and the detailed lithologies of the bonebed horizon as well as underlying and overlying layers were recorded. Within the bonebed horizon, the presence of mollusks, vertebrate microfossils, wood, and other organic material was noted, as was the absence of burrows, root traces, and sedimentary structures. All vertebrate microfossils and well-preserved mollusks encountered during the excavation were collected. Coalified wood trunks and branches

were highly abundant in the quarry; almost every plaster jacket included at least one segment of carbonized wood. The largest pieces of wood (generally >15 cm diameter) were included in the quarry map, but wood was so ubiquitous in the quarry, and fragile, that mapping every piece was not feasible.

Size Classes

Of the approximately 800 bones collected, 80% have been prepared and identified. Analyses here are generally limited to prepared bones, but in some analyses, unprepared bones that could be confidently identified in the field have been included. All prepared bones were identified to skeletal element as specifically as possible. The body side (left or right) was determined for skull bones and the appendicular skeleton, although the epiphyses of some limb bones (mostly radii) were not well preserved enough for side determination. The lengths of limb bones, dentaries, and maxillae were measured and used to construct size distribution histograms, which indicate whether the size distribution of individuals was continuous, skewed, or bimodal.

Specimens can be divided into two discrete size classes, termed “smaller” and “larger” size classes throughout this paper (see Results). The third and largest size class is represented only by a very large rib head. The size-based categorization of Evans (2010) was used to give approximate life-stage labels to these size classes. The largest individual of the taxon is used to represent 100% adult body size. Specimens with a skull length less than 50% of the largest individual are labeled juveniles; specimens 50%-85% of the largest individual are labeled subadults, and specimens larger than 85% are labeled adults. These are merely size-based categorizations used for convenience; size alone

should not be used as an indicator of ontogenetic stage or sexual or skeletal maturity. Other analyses of age and maturity are discussed below.

Material collected from the JR-429 bonebed does not include any elements of the large size class that are complete enough to be measured, but fortunately a large *Gryposaurus* partial skull, UM 5204, was previously collected from Kennedy Coulee. Due to its similar geographic and stratigraphic location, it is likely to be from the same taxon as MOR 2573, and is thus used as the proxy for maximum body size. Future discovery of a larger specimen would consequently make the MOR 2573 specimens relatively smaller. Next, the size of an element present in UM 5204 and both size classes of MOR 2573 is used to determine the sizes of the MOR 2573 specimens relative to UM 5204. Although the small size class of MOR 2573 is well represented by postcranial material, the small cranial material is more limited and mostly consists of dentaries. Unfortunately, UM 5204 is only represented by cranial material, and does not include a dentary. The most complete element preserved in UM 5204 as well as both the large and small size classes of MOR 2573 is the jugal. The length of the jugal was measured as the distance from the posteroventral point of the rostral process to the ventralmost point of the posteroventral flange, as this was complete on all three specimens measured.

The skeletal elements with the largest sample sizes of both the juvenile and subadult cohorts were used to determine the mean size and standard deviation of each size class. The mean juvenile size relative to the mean subadult size can then be used to predict the size of juvenile skeletal elements that have not yet been recovered.

The minimum number of identifiable specimens (NISP) was determined based on complete bones as well as whether fragmentary bones may or may not be parts of the same original bone. Then, the minimum number of individuals (MNI) was determined by the most abundant skeletal element from one side of the body (e.g. right maxillae); because the bonebed preserves three size classes of individuals, each size class could have MNIs based on different skeletal elements.

Skeletal Element Abundances

The relative abundances of collected skeletal elements (NISP of each bone type) were compared to the relative abundances of elements within a single complete *Gryposaurus* skeleton (based on an articulated subadult *G. notabilis*, ROM 764, and a mounted reconstruction of *G. monumentensis*, UMNH 20181) to determine which types of bones were most frequently preserved, similar to the method of Varricchio (1995). The expected distribution of bone types within a skeleton was determined by dividing the number of elements in a bone type group (e.g., number of skull bones) by the total number of bones in a skeleton. The observed distribution of bone types collected was determined by dividing the NISP in a bone type group (e.g., number of skull bones collected) by the total NISP of bones collected. Bone types with an observed percentage higher than the expected percentage are considered overrepresented; bone types with an observed percentage lower than the expected percentage are underrepresented. The significance of the difference between the observed and expected values was determined using a 1x2 Pearson's X^2 test for each bone type (e.g., skull bone abundance versus non-skull bone abundance). These abundance analyses were repeated for the bone type

distributions within the larger and smaller size classes; these size class analyses only included prepared specimens because subadult and juvenile sizes could have been misidentified in the field due to only part of the bone being exposed. Fragmentary specimens, especially ribs and vertebrae, could not always be assigned to a size class with confidence.

All prepared bones, including all collected bone fragments, were examined for abrasion and weathering stages (Fiorillo, 1988). Trends of long bones were plotted as a rose diagram using the package "Circular" in R 2.15.3 for Mac OS X (R_Core_Team, 2014). All other graphs were produced in Microsoft Excel 2008 for Mac.

Skeletal Maturity

Axial sutures and long-bone osteohistology were used to determine the degree of skeletal maturity of individuals. All skull elements and vertebrae, articulated or not, were examined to determine whether sutures were open and unfused, visible but possibly beginning to fuse, or fully fused and remodeled. Osteohistology was examined for all currently prepared tibiae from the JR-429 bonebed. Tibiae are the preferred element for histologic skeletochronology in hadrosaurs due to the tibia being a large weight-bearing bone that undergoes less remodeling than other large weight-bearing bones, because of the lack of a major trochanter or crest on the mid-diaphysis (Horner et al., 1999). The number of lines of arrested growth (LAGs), which mark annual pauses in bone apposition, (Köhler et al., 2012), is interpreted as the age, in years, of the animal at time of death. Similar markers called annuli are deposited annually but without a complete cessation of bone apposition (Hutton, 1986; Huttenlocker et al., 2013). The type of

vascularity in the bone tissue, as viewed in a transverse diaphyseal section, reflects the growth rate of bone apposition; bone tissue with radial or reticular vascularity indicates a higher growth rate than bone tissue with circumferential, laminar, or plexiform vascularity (Castanet et al., 2000; Chinsamy et al., 2012).

The JR-429 bonebed includes six tibiae of the larger size class, three of which have been prepared (MOR 2573-6-12-06-17, MOR 2573-7-08-10-396, and MOR 2573-7-31-10-497). These three tibiae were histologically sampled using the techniques of Lamm (2013) for large specimens. For each tibia, the mid-diaphyseal segment with minimum circumference was removed, molded and cast, and then embedded in resin for histological sectioning. Due to their sizes, each transverse cross-section was cut in half to better fit on slides, creating anterolateral and posteromedial halves for each tibia section. These half sections were mounted to glass slides and ground to a thickness of 100 μm. The finished slides were imaged at 10x total magnification on a Nikon Optiphot-Pol polarizing microscope with a Nikon DS-Fi1 digital sight camera utilizing an automated stage to move the slide incrementally. The resulting photomicrographs were compiled with NIS-Elements BR 3.0 software into high-resolution TIFF image files. Adobe Photoshop CS2 was used to combine the images of the two slide halves for each tibia and trace the zones of different bone tissue types in lieu of visible lines of arrested growth (LAGs). The circumferences of these growth zones were then measured with ImageJ 1.46r (Rasband, 1997-2014). These tibiae have relatively small medullary cavities, indicating that the first LAG, if one was deposited, has not been resorbed. The

relationship between growth zones and the presence or absence of LAGs is discussed in the Results section.

No tibiae of the smaller size class have yet been recovered, but their mean length can be predicted based on the size ratio of other bones in the smaller size class to those in the larger size class. The relationship between tibia length (x) and circumference (y) for *Maiasaura*, another hadrosaurine, was calculated as y=0.3685x-0.2654 by Woodward et al (in press). This equation was used to predict the mean circumference of bones in the smaller size class of the JR-429 bonebed. This mean circumference was then compared to the measured circumferences of LAGs in the tibiae of the larger size class, enabling estimation of the age at death for individuals in the smaller size class.

Results

MOR 2573 consists of over 800 bones that were collected from MOR locality JR-429. Appendix H lists each bone's identification, completeness, size, abrasion, weathering, and trend and plunge. The excavated area was 68 m^2, yielding an average bone density of over 11.8 bones per m^2 (Figure 3.2). The bonebed horizon extends laterally for at least an additional 36 m, as well as continuing into the hill, so the actual extent of the bonebed is likely to be at least four times the excavated area, and potentially even farther. The bone horizon is laterally uniform in its rates of breakage, abrasion, and weathering, and bone density does not taper at the edges of the excavated area.

Figure 3.3 and Appendix G show the distribution within the quarry of prepared bones from the smaller and larger size classes. There is no apparent pattern or clustering

of bones by size class; remains from each size class are fairly evenly distributed and intermingled. However, the overall distribution of bones is not continuous; there are many examples of bone "clusters", and patches of barren mudstone several tens of centimeters in diameter. Many of the densest clusters of bones contain a high percentage of large limb elements. The northwest end of the quarry has an especially high concentration of ribs, but ribs are evenly distributed at lower densities throughout the rest of the quarry. Skull elements, vertebrae, manus and pes elements, and bone fragments are fairly evenly distributed. Overall, the bone distribution indicates thorough disarticulation and intermixing of elements from multiple skeletons.

Lithology and Non-Vertebrate Fossils

Stratigraphy within the quarry contains four notable horizons, listed from lowest to highest: A) 4.3 m thick light grey silty mudstone, usually sharp upper contact with B) 0.5 m thick dark grey organic-rich well-sorted mudstone, gradational upper contact with C) 0.3 m thick light grey mudstone, sharp upper contact with D) 0.8 m thick poorly sorted silty fine sandstone layer. The main bone horizon is at the base of dark grey mudstone B, with some bones in the upper part of the underlying light grey mudstone A, and some small bones in the upper part of B as well as the overlying light grey mudstone C. Mudstones A-C lack internal laminations, suggesting periods of relative constancy within the depositional environment rather than numerous environmental fluctuations, or possibly a single depositional event for each of the three packages of sediment. None of these three mudstone horizons preserve sedimentary structures, caliche nodules, or evaporite surfaces.

The dark grey mudstone B of the main bone horizon contains large amounts of millimeter-scale fragmentary organic material. Coalified wood logs are abundant throughout mudstone B; most plaster jackets included at least some coalified wood. This wood matches the description of "compressed, coalified wood, showing conchoidal fractures and a vitreous luster" that was found in the northwest quarries of Jack's Birthday Site, a hadrosaur-dominated bonebed in the Two Medicine Formation (TM-068; Varricchio, 1995). The wood logs in the JR-429 bonebed were generally 5 to 15 cm wide, and ranged in length from 10 cm to at least 50 cm. Plunges of wood logs were less than 10°. The wood was randomly intermixed horizontally and vertically throughout the bone assemblage, sometimes forming vertical stacks of bone-wood-bone or wood-bone-wood.

The mudstone B main bone horizon does contain some whole mollusks, but does not contain the fragmented mollusk shell "hash" that is a common component of microsites in Kennedy Coulee. *Viviparus* and *Melanoides* gastropods are present but uncommon in the bone horizon (Figure 3.4A-B; J. H. Hartman personal communication, 2014). Small *Sphaerium* bivalves indicate a quiet-water environment such as a lake (Figure 3.4C; Varricchio, 1995). The exposed valves are parallel to bedding, not in life position. Due to being exposed on a flat fracture surface, the presence of single or paired valves cannot be determined. Small non-hadrosaurid coprolites are abundant (~1-6 cm long, n=90; Figure 3.4D).

These mudstones are capped by horizon D, a poorly sorted silty fine sandstone layer rich in mollusk shell, wood fragments, and vertebrate microfossils; in the northern half of the quarry this horizon is strongly cemented, forming an erosion-resistant

concreted layer of rock, leading to the site's nickname of "Rocky". This horizon is laterally extensive, cropping out in several locations in Kennedy Coulee, making it a useful horizon for correlating stratigraphic positions. It contains abundant unionid and *Sphaerium* bivalves and *Lioplacodes* gastropods (J. H. Hartman personal communication, 2014). Although grey when freshly broken, the rock weathers to an orange-tan color due to iron-rich cement, similar to an extensive unionid lithosome in the upper Oldman Formation of Dinosaur Provincial Park in Alberta (Johnston and Hendy, 2005).

The wood fragments in this concreted sandstone are fragile and weather out of the rock, leaving impressions in the sandstone. The surfaces of these wood impressions, whether from a small branch a few centimeters in diameter or a log over 30 cm in diameter, nearly all display a pattern of grain-parallel raised oblongs, which would have been depressions in the wood. These trace fossil oblongs are identical to those interpreted as mayfly burrows, *Asthenopodichnium* (Moran et al., 2010), but the near-ubiquity of this pattern in the surface of wood found in this horizon at multiple locations in Kennedy Coulee suggests a more mundane origin. The bark of modern conifers can have grain-parallel raised oblongs on its inner surface, with corresponding oblong depressions in the wood surface (Figure 3.5; D. A. Eberth personal communication, 2010).

Vertebrate Microfossils

Vertebrate microfossil material from the mudstone B main bone horizon of JR-429 includes 37 Tyrannosauridae teeth, representing 22.7% of total identifiable vertebrate microfossils (Table 3.1; Figure 3.5E). Ornithischian microfossil material includes 31 hadrosaur teeth, 13 ceratopsian teeth, and 16 tooth fragments small enough that they

cannot be confidently assigned to either hadrosaurs or ceratopsians. Thus, depending on the identities of these tooth fragments, hadrosaur teeth represent 19.0% to 28.8% of vertebrate microfossils. Of the teeth that are definitely hadrosaur, 22 are worn stubs that may have been shed during life, and only 9 are fairly complete teeth that would have left the jaw after death. Given that all eleven dentaries are missing their teeth, the low number of complete hadrosaur teeth in the bone horizon is intriguing.

For comparison, in five microsites sampled from Unit 1 of the Oldman Formation of Alberta along the Milk River (stratigraphically and geographically close to JR-429, ~30 km northwest), the relative abundance of tyrannosaur teeth ranges from 0% to 0.21% of total identifiable vertebrate microfossils, and the relative abundance of hadrosaur teeth ranges from 3.5% to 14.2% (Table 3.1; data from Brinkman et al., 2004). However, these percentages are based on screenwashed material, which recovered all microfossils above 0.85 mm (Brinkman et al., 2004). Collection of microfossil material in the JR-429 bonebed relied on the field crew member or preparator visually noticing the microfossil, biasing collection toward larger microfossils. Restricting the data to relatively larger elements that are also recovered in the JR-429 bonebed (teeth, scutes, and bones of turtles, champsosaurs, crocodilians, and dinosaurs), the Brinkman et al. (2004) data yields relative abundances of 15.1% to 70.6% hadrosaur teeth and 0% to 1.14% tyrannosaur teeth, much lower than the 24.7% abundance of tyrannosaur teeth in JR-429. Although this difference may still be due to size bias in collecting technique, the abundance of tyrannosaur teeth at JR-429 is so great that a hypothesis of tyrannosaurs feeding on the hadrosaur carcasses should be considered.

Bonebed Taphonomy

The bonebed is strongly monodominant; all but two of the non-microfossil bones are hadrosaurid, and all hadrosaurid bones are consistent with *Gryposaurus*. The two exceptions are the proximal femur of a theropod (ornithomimid or oviraptorid) and a badly crushed possible tyrannosaur centrum. Unidentifiable bone fragments are large enough that they must be dinosaurian, and are consistent with hadrosaur bone.

The vast majority of bones in the quarry exhibit abrasion stages 0 to 1 (Table 3.2). Of 659 prepared bones (508 identifiable bones and partial bones, and 150 unidentifiable bone fragments), 77.5% are abrasion stage 0 (sharp edges), 17.9% are stage 1 (minor rounding on edges), 4.3% are stage 2 (moderately rounded edges), and 0.3% are stage 3 (extremely well rounded bone fragment) (Fiorillo, 1988). Intact bones are generally stage 0, while broken bones may exhibit stages 0 or 1; stage 1 abrasion is most often observed on partial or fragmentary bones including ribs, neural arches, and skull elements. Abrasion stages 2 and 3 are restricted to bone fragments and one tibia diaphysis. Of these 659 prepared bones and fragments, all exhibit pre-burial weathering stage 0 (no sign of weathering) except one bone fragment that appears to exhibit pre-burial weathering stage 1 (surface cracking) (Behrensmeyer, 1978; Fiorillo, 1988).

Cancellous bone of epiphyses and vertebrae still contains open spaces not infilled with sediment or minerals, making it generally weaker than cortical bone when excavated. However, this is typical of bone preservation in this part of the Judith River Formation, and does not appear to be attributable to the “wet rot” of Scherzer and Varricchio (2010). Cervical neural arches are frequently found as isolated broken halves

(6 whole, 12 halves), and fragments of all types of neural arches are abundant (at least 43 pieces). Skull bones generally have their delicate processes at least slightly broken. Quadrates are usually found as isolated broken halves (1 whole, 10 halves). Ribs are nearly always broken into two or more pieces. Limb bones tend to be mostly intact, but some fibulae are fractured and incomplete, as are many pelvic elements: three ilia are only missing the ends of their processes, but three other ilia are broken in half; pubes can be missing most processes; proximal ischia are generally broken from their distal shafts.

Several pairs of broken bones may be halves of the same bone, but in most cases, the connection has been broken badly enough that it cannot be certain that they are actually the same bone. Halves of bones that definitely mend together were found 0 to 478 cm apart (n=14 pairs, mean 48.5 cm, standard deviation 126.5 cm). Specimens that are potentially halves of the same bone were found 20 to 575 cm apart (n=8 pairs, mean 122.8 cm, standard deviation 185.5 cm). However, if they are not halves of the same bone, this means that the true matching halves are located even farther away, in an unexcavated area of the bonebed.

Possible evidence for trampling includes three bones: a neural arch, scapula, and bone fragment. A caudal neural arch and spine (MOR 2573-7-03-06-102) was broken in half, with one half tilted down toward the break. This could have occurred if an animal had stepped on half of the bone, breaking it and pushing part of the bone flat down into the mud (trend 197°, plunge 2° S) while the other piece was rotated into a deep plunge (trend 162°, plunge 54° NW). A scapula (MOR 2573-7-09-10-407) was broken distally into multiple fragments; some fragments were displaced laterally, and others were tilted

vertically at 30-45° angles. Only one bone, an unnumbered fragment, exhibits parallel striations that may be trample marks.

Most of the bones are deposited in a single bone horizon (96.5% of 796 bones mapped in field), although 17.1% of bones within this main horizon overlap partially or completely, producing stacks two or three bones high. Bones in the main horizon have plunges close to horizontal; 71.1% of elongate bones plunged less than 10°, and a total of 89.3% of elongate bones plunged less than 20° (n=108 out of 121). The rose diagram of the trends of elongate bones reveals no overall preferred orientation (Figure 3.6). Twenty-nine bones were found 20-30 cm above the main bone horizon, in the same dark grey organic mudstone B. Two caudal centra and a basisphenoid were even higher, in the light grey mudstone C. Of these 32 high bones, 16 are caudal centra, other vertebral fragments, or phalanges: small elements that are composed mostly of cancellous bone and thus have low densities. Another 12 are pieces of rib, skull, or other bone fragments: small (<15 cm), but denser than vertebrae and phalanges. Only four of the 32 high bones are large: a complete dorsal vertebra, juvenile scapula, subadult metatarsal, and indeterminate limb bone. Only two bones were found below the main bone layer, by 10-20 cm: an abraded tibia diaphysis, and abraded bone fragment.

Size Classes

Size distribution histograms for the length of the dentary tooth row, maxilla tooth row, and limb bones (Figure 3.8) reveal two discrete size classes. Most prepared bones (skull and limb elements) are easily categorized into either the smaller or larger size class. Some vertebrae and ribs can be assigned to one of the two size classes, but many

partial vertebrae, caudal vertebrae, and rib fragments could not be assigned to a size class with great confidence, because they could be one of the larger ribs or vertebrae of a small individual, or one of the smaller ribs or vertebrae of a large individual.

To initially give each size class a convenient label that could be used prior to histologic maturity analysis, the method of Evans (2010) was used to determine the size of these individuals relative to an adult *Gryposaurus* from Kennedy Coulee, UM 5204. The length of a jugal (measured as the distance from the posteroventral point of the rostral process to the ventralmost point of the posteroventral flange) from each of the two size classes was compared to that of a large adult *Gryposaurus* skull, UM 5204 (14.6 cm). The larger size class jugal is 80.8% (11.8 cm) the length of the UM 5204 jugal, placing the larger size class of MOR 2573 in the upper range of the subadult category of Evans (2010). The smaller size class jugal is 42.5% (6.2 cm) the length of the UM 5204 jugal, placing the smaller size class of MOR 2573 in the upper range of the juvenile category of Evans (2010). Only a single completely-preserved jugal was available for each size class; because there is a range of individual sizes within each size class (Table 3.3), some individuals of each size class may be larger than the jugals used here, and so some individuals of the smaller size class may ultimately fall into the small end of the subadult category, and some individuals of the larger size class may potentially be labeled small adults. In this paper, the smaller size class will be referred to as “juveniles”, and the larger size class will be referred to as “subadults”, to make it clear that these specimens are not near adult size. The ontogenetic skeletal immaturity of the specimens will be discussed in the histology results below.

All prepared bones fit within the two discrete "juvenile" and "subadult" size categories except for a single very large rib head (Figure 3.7). Rib head MOR 2573-7-18-06-193 (Figure 3.7A) is noticeably larger than any other rib head in the JR-429 bonebed, including those from similar serial positions (Figure 3.7B-C) that are interpreted as belonging to the larger (subadult) size class. This extremely large rib head is morphologically consistent with other hadrosaur ribs, although the possibility remains that it could belong to another taxon. It is taphonomically consistent with the preservation of the other *Gryposaurus* bones within the JR-429 bonebed; there is no evidence to suggest that it had a different taphonomic history or origin than the other *Gryposaurus* bones.

This large rib head, MOR 2573-7-18-06-193, was compared to the size of a rib from a similar serial position from a specimen of known age and size: MOR 2919, an adult brachylophosaurinin hadrosaur from a nearby locality in the Kennedy Coulee area, also from the lower Oldman Formation. MOR 2919 has a tibia length of 120 cm; the tibia contains 14 lines of arrested growth, indicating that the individual was 14 years old at time of death (Freedman Fowler and Horner, Chapter Two). For comparison, the tibiae of the larger (subadult) size class in the JR-429 *Gryposaurus* bonebed are a maximum of 89.5 cm long, and are from individuals two to three years of age (see histology section below). Because rib head MOR 2573-7-18-06-193 (Figure 3.7A) is much larger than the equivalent rib head from MOR 2919 (Figure 3.7D), this individual would have been much larger than the adult MOR 2919.

Skeletal Element Abundances

The minimum number of individuals (MNI) was determined from the most abundant skeletal element of each size class that could be identified as left or right. For the larger (subadult) size class, the MNI is five, based on right maxillae (Figure 3.8). However, given the size distributions of the left and right maxillae, some of the left maxillae may be too small to pair with the larger right maxillae, indicating a higher MNI. For the smaller (juvenile) size class, the MNI is four, based on left metatarsal IIIs (Figure 3.8). The large rib head MOR 2573-7-18-06-193 indicates the presence of at least one individual in a third, largest (adult), size class, for a total MNI of ten individuals. These MNIs may increase as additional material is prepared and identified.

The abundances of each skeletal element type collected, based on the number of identifiable specimens (NISP), are presented in Table 3.4. Large limb (stylopodia and zeugopodia: humerus, femur, ulna, radius, tibia, fibula) and pelvic elements (ilium, ischium, pubis) are the most strongly overrepresented.

Hadrosaur skull elements generally suffer from preservation bias due to most skull bones being small, thin, and fragile, but skull material is overrepresented in the bonebed (Table 3.4). Within skull elements, the most strongly overrepresented are large, sturdy bones: dentaries, maxillae, and quadrates (often broken in half), which together comprise 32 of the 91 NISP of prepared skull elements. Other overrepresented skull elements include surangulars, premaxillae, nasals, jugals, frontals, parietals, laterosphenoids, basisphenoids, and exoccipitals. Underrepresented elements are mostly

small, thin bones (e.g., splenials, lacrimals, quadratojugals, vomers) as well as the remaining braincase and orbital elements.

Manus and pes elements (autopodia: carpals, metacarpals, tarsals, metatarsals, and phalanges) as a group are neither overrepresented nor underrepresented (Table 3.4). These elements are generally small and low-density, causing them to be easily transported away from an assemblage (Voorhies, 1969). Metatarsals, the largest pes elements, are overrepresented (29 of 65 total manus and pes elements), whereas manual and pedal phalanges, which are 8 times more abundant than metatarsals in a *Gryposaurus* skeleton, are underrepresented (28 of 65 total manus and pes elements). Although the relative abundance of phalanges is low, specimens from nearly all digits and both size classes have been recovered.

Vertebral elements are underrepresented to varying degrees, most notably in the strong underrepresentation of non-caudal centra. Aside from distal caudal vertebrae, the neural arches and centra are all unfused and are nearly all disarticulated. Non-caudal centra are extremely rare; only 6 have been collected: an isolated cervical centrum, an isolated dorsal centrum and dorsal centrum fragment, two dorsal vertebrae in which the centrum was still articulated with the neural arch, and a juvenile cervical centrum recovered within 30 cm of its neural arch. No sacral centra have been recovered. However, non-caudal neural arches were more commonly collected (NISP = 39). Caudal vertebrae display the opposite pattern; caudal centra are common (NISP = 38), but neural arches are less common (NISP = 26: 7 attached to distal caudal centra, 14 isolated arches, and fragments of at least 5 more arches), as are chevrons (only 6). Thus, non-caudal

neural arches are six times as abundant as non-caudal centra, but caudal centra are one and a half times as abundant as caudal neural arches.

Next, the prepared bones were divided into subadult and juvenile size classes to determine whether the pattern of preservation was similar for each size class; in general, the relative abundances followed similar patterns, but the low sample sizes of juvenile bones make many of the differences not statistically significant (Table 3.4). Juvenile bones were much less commonly recovered than subadult bones; the subadult MNI is 5 with a NISP of 262 bones, but the juvenile MNI is 4 with a NISP of only 88 bones. In both size classes, large limb material (humerus, radius, ulna, femur, tibia, fibula) is strongly overrepresented. For subadults, all large limb elements were collected with fairly similar frequency (n = 4 to 7 for each element). Juveniles, however, had a bias against the largest elements, with better recovery rates of the smaller of these limb elements: 3 radii, 1 ulna, half of a fibula, and no humeri, femora, or tibiae. Pelvic material is strongly overrepresented in subadults, but not in juveniles. Juvenile manus and pes elements were well represented, due mostly to a large number of juvenile metatarsals (10 of 19 total manus and pes elements). Juvenile skull material is generally considered to have low preservation potential due to juvenile skull elements being even smaller, thinner, and more fragile than their subadult counterparts, but skull material is slightly overrepresented among juvenile bones. Juvenile skull material (NISP = 13) is best represented by dentaries (NISP = 5) and a maxilla, which is expected due to these being relatively large sturdy bones within the skull.

Immaturity of Individuals

The non-adult status of individuals in the "smaller" and "larger" size classes of the bonebed is supported by their degree of axial fusion and osteohistology. Most skull elements were fully disarticulated and randomly distributed in the quarry. The only exceptions are certain braincase elements: two instances of frontals associated with parietals (although only one frontal-parietal pair was articulated), and one exoccipital articulated with a supraoccipital and prootic. The first set of frontals and parietal, MOR 2573-7-24-10-455 and -455A, was found ventral side up, with the right frontal fully articulated with the parietal, whereas the left frontal was in the correct anatomical position, but disarticulated and separated by a few millimeters from the other frontal and parietal. The suture surfaces on the left frontal are well preserved and indicate that this frontal was completely unfused from the right frontal, and almost certainly unfused from the parietal as well. The suture line between the right frontal and parietal is clearly visible; whether any fusion or remodeling has occurred internally is being investigated histologically (A. M. Bailleul and J. R. Horner personal communication, 2014). The second set of frontals and parietal, MOR 2573-7-23-11-574, -574A, and -575, was found with the three bones touching but rotated and shifted entirely out of anatomical position. The interfrontal suture was completely unfused, as was the medial portion of the fronto-parietal suture. However, a small flange of the anterolateral parietal broke off of the parietal and remained attached to the right frontal, with the suture contact still visible. Three isolated frontals were also found, indicating that not all frontals and parietals remained associated. Aside from frontals and parietals, the only articulated or even

closely associated bones are an exoccipital still articulated with a supraoccipital and prootic. The contact between the supraoccipital and prootic may be remodeling, but the sutures between these bones and the exoccipital are still clearly visible; whether any fusion has begun between these bones is unknown.

Of all vertebrae, only distal caudal vertebrae have fused neural arches with their centra. Although two dorsal vertebrae were found with articulated neural arches and centra, as mentioned above, their state of centrum preservation is poor and suture lines or fusion cannot be observed. Cervical and dorsal centra are rare, but isolated cervical and dorsal neural arches were all unfused, not broken from a fused centrum. Proximal caudal centra have unfused dorsal sutures, whereas distal caudal centra of both the juvenile and subadult size classes have fully fused neural arches with no suture visible.

Histology. The three sectioned subadult size class tibiae possess alternating zones of reticular fibro-lamellar and circumferential fibro-lamellar bone tissue. No lines of arrested growth (LAGs) or annuli are visible. The presence of alternating zones of tissue types, but lack of LAGs, leads to several explanatory hypotheses: 1) these three individuals were less than one year old at time of death; 2) these individuals were more than one year old, but did not deposit annual LAGs; or 3) LAGs were deposited but are not visible in the histological sections.

All three tibiae possess three sets of alternating zones of reticular and circumferential vascularity (Figure 3.9), although these zones are not always well defined. The boundary between reticular vascularity transitioning into circumferential vascularity is frequently irregular; some parts of the growing bone circumference began

depositing circumferential tissue while nearby areas continued depositing reticular tissue, resulting in a patchy vascular orientation appearance. The transition from circumferential tissue to reticular tissue is usually more linear. The circumferential zones sometimes include patches of sub-cirumferential to sub-plexiform vascularity, but their dominantly circumferentially-oriented vascularity is distinguishable from the multi-directional vascularity of the reticular zones.

Reticular fibro-lamellar tissue is deposited at a faster rate than circumferential fibro-lamellar tissue, which is a type of laminar fibro-lamellar tissue (Castanet et al., 2000; Chinsamy et al., 2012). Growth rates in modern ruminants are correlated with seasonal hormonal changes (Köhler et al., 2012). Thus, if hadrosaur growth rates are correlated with seasonal fluctuations in hormones and/or resource availability, then the reticular fibro-lamellar tissue was deposited at a time of year with higher growth rates and hypothesized better resource availability than when circumferential fibro-lamellar tissue was deposited. The circumferential fibro-lamellar tissue may have been deposited during the "unfavorable season" (sensu Köhler et al., 2012). If these alternating tissue zones reflect annual seasonal fluctuations, then these individuals would be between two and three years old. Lines of arrested growth (LAGs) represent a hiatus in bone deposition during the "unfavorable season". The lack of LAGs in the MOR 2573 tibiae, but presence of three sets of alternating tissue zones, indicates either that these individuals never fully paused growth, or that LAGs may have been deposited but are not visible for some reason. *Edmontosaurus* tibiae and femora from Alaska also lack

observable LAGs while possessing alternating reticular and circumferential vascularity (Chinsamy et al., 2012).

The alternate hypothesis that the lack of LAGs indicates that these individuals are less than one year of age is not supported for two reasons: 1) three sets of alternating growth zones are more parsimoniously interpreted as representing three years than as repeated fluctuations within a single year; 2) the sizes of these three sets of growth zones are consistent with the locations of annual LAGs in other hadrosaur tibiae (Table 3.5). The outer circumference of each zone of circumferential laminar tissue was used as a proxy for LAG location. The lengths of the three tibiae (MOR 2573-6-12-06-17, MOR 2573-7-08-10-396, and MOR 2573-7-31-10-497) range from 75.0 cm to 89.5 cm, and the circumferences of Zone 1 correspondingly range from 15.8 cm to 22.2 cm; the smallest tibia, MOR 2573-7-08-10-396, has the smallest Zone 1, and the largest tibia, MOR 2573-6-12-06-17, has the largest Zone 1. Because all three tibiae have the same number of zones, and the zone sizes correspond with tibia length, they are all interpreted to be from individuals of the same age. Thus, the different bone sizes are interpreted to represent individual variation in body size in animals that are between two and three years of age. Interestingly, the smallest tibia has the greatest amount of secondary remodeling and medullary cavity expansion, whereas the largest tibia has the least amount of secondary remodeling and medullary cavity expansion.

The spacing between zones of circumferential laminar tissue indicates that the MOR 2573 large size class tibiae were still greatly increasing their body size at time of death (Figure 3.9). The hadrosaurids *Maiasaura* and *Hypacrosaurus* reach skeletal

maturity at approximately 8 years (Horner et al., 1999; Woodward et al., in press); therefore, *Gryposaurus* individuals in the large size class of the JR-429 bonebed are far from being skeletally mature adults. *Maiasaura* are hypothesized to reach sexual maturity at 3 years of age (Woodward et al., in press); because these *Gryposaurus* subadults are still in their third year of growth, they may not have yet reached sexual maturity. Their histology will be described and analyzed in greater detail in a later study.

Depending on the skeletal element, the mean length of the smaller (juvenile) size class ranges between 57.8% and 68.2% the mean length of the larger (subadult) size class (Table 3.3). Thus, tibiae of the smaller size class would be expected to have a mean length between 46.6 cm and 55.0 cm (57.8-68.2% of 80.7 cm, the mean length of tibiae in the larger size class). These smaller size class tibiae would therefore be predicted to have a mean circumference between 16.9 cm and 20.0 cm, based on the relationship between tibia length and circumference of *Maiasaura* (Woodward et al., in press). In the three sectioned subadult tibiae from the JR-429 bonebed, the end of the first zone of laminar tissue occurred at a mean circumference of 19.7 cm. Therefore, the smaller size class tibiae are hypothesized to be from juvenile individuals nearly one year of age.

If the large rib head MOR 2573-7-18-06-193 does belong to a *Gryposaurus*, then this individual would be larger than any other currently recovered from the JR-429 bonebed. Based on the rib head's large size compared to another hadrosaur specimen, a 14 year old adult brachylophosaurinin (MOR 2919; Freedman Fowler and Horner, Chapter Two), the rib head is hypothesized to belong to a very large adult individual with

a tibia length greater than 120 cm; such a tibia is predicted to contain numerous LAGs and be approaching skeletal maturity.

Pathologies and Bone Modification

Out of the over 800 bones collected, only three had pathologies. One small fragment of rib or caudal neural spine, MOR 2573-7-14-06-168C, has at least three raised oval-shaped exostoses 1 cm apart in a straight line along the length of the bone. If this is a caudal neural spine, the locations of the exostoses could correspond to the locations of ossified tendons. A fragment of small limb bone, MOR 2573-7-11-06-154, has at least three irregularly shaped raised exostoses on its cortical surface. The other pathologic bone is an abrasion stage 2 (Fiorillo, 1988) fragment of a large limb or pelvic bone, MOR 2573-6-29-12-708A, that includes a raised exostosis over half of the fragment's periosteal surface, as well as a large gouge mark in the exostosis, and several fine parallel scratches that are most consistent with trample marks.

Three other small bone fragments have linear indentations that could be tooth or trample marks, but are likely to be tool marks from collection or preparation. There is no evidence of insect burrows, insect traces, or non-modern root traces on any of the bones from the level of the main bone horizon. However, the tibia diaphysis (MOR 2573-8-13-06-288) found 20 cm below the main bone horizon is missing areas of outer cortical bone and exhibits stage 2 abrasion, root traces, and trample marks. Due to this partial tibia's relatively high degree of taphonomic alteration, and location below the main bone horizon, it is possible that this bone was deposited prior to the rest of the bonebed.

Discussion

The 11.8 bones per m^2 density of bones in the JR-429 bonebed is comparable to that of the *Maiasaura* "Camposaur" bonebed (MOR locality TM-003) in the Two Medicine Formation, which has >10 bones per m^2 (Varricchio and Horner, 1993), but much less than the 130 bones per m^2 density of the juvenile lambeosaur Sun River Bonebed (MOR locality TM-260, also in the Two Medicine Formation (Scherzer and Varricchio, 2010).

Because the skeletons are completely disarticulated (with rare cranial exceptions) and bones from multiple individuals are thoroughly intermixed, the hadrosaur carcasses must have been exposed subaerially or subaqueously long enough for the removal or decay of soft connective tissues, but not long enough for bones to exhibit weathering effects. In modern mammal skeletons, weathering stage 0 can last for up to one year of subaerial exposure (Behrensmeyer, 1978; Fiorillo, 1988).

The majority of bones are non-abraded, but some fractured bones and bone fragments do exhibit varying stages of abrasion, which could indicate transport. Limb elements, which are composed of thick cortical bone, tend to be intact and unabraded. Bones that are smaller, thinner, or composed of more cancellous bone, such as neural arches, ribs, and many skull elements, are sometimes found intact and unabraded, or are found broken and may or may not have lightly abraded fracture surfaces, suggesting transport after the bones were broken. The highly abraded stage 2 and 3 bone fragments suggest extensive transport, whereas the stage 0 intact bones suggest minimal transport. Ryan et al. (2001) attributes such a disparity in abrasion stages to the bone fragments that

exhibit stage 2 or 3 abrasion, even if hadrosaurid, having a separate origin in time and/or space from the death or concentration event that accumulated the intact bones at this site. Bones that are fractured into two nearby halves suggest a second round of breakage after transport to the depositional location.

Large limb elements were the most overrepresented, as predicted due to their large size and composition of sturdy cortical bone (Behrensmeyer, 1975). Small elements comprised mostly of cancellous bone were more poorly represented; their size and low density makes them more prone to damage and transport (Behrensmeyer, 1975; Boaz and Behrensmeyer, 1976). However, smaller caudal centra had better recovery rates than larger cervical and dorsal centra, even though cervical and dorsal neural arches were commonly preserved. Some process must have removed the cervical and dorsal centra while leaving a higher percentage of caudal centra in the bone assemblage. This winnowing could be due to weathering or preferential transport; because the remaining centra show no signs of weathering or decomposition, selective hydraulic transport is more likely. Perhaps cervical and dorsal centra are less dense than caudal centra, so that despite their larger size, they are able to float away more easily.

The preservation rate of skull elements was higher than in most other hadrosaur bonebeds. Of the 630 prepared bones (whole or partial) of MOR 2573, 105 (16.7%) are cranial. Restricting the bones to NISP, 98 (22.5%) of 436 specimens are cranial. Interestingly, the MNIs for the subadult and juvenile size classes are based on maxillae and metatarsals, respectively, rather than large limb elements. The Sun River juvenile lambeosaurine bonebed TM-260 contains 9.8% cranial elements (Scherzer and

Varricchio, 2010), and the multitaxic hadrosaurid and theropod assemblage at Jack's Birthday Site (MOR locality TM-068) contains 12.1% cranial elements (Varricchio, 1995). The higher relative abundance of cranial elements in the JR-429 bonebed may reflect a gentler depositional history that allowed greater preservation of intact fragile skull bones. A *Prosaurolophus* bonebed (MOR localities TM-447 and TM-454) with the most similar ratio of cranial elements (21.7%; Rogers, 1990) to JR-429 was interpreted as a drought-killed assemblage buried by overbank flooding, a scenario that is very plausible for the formation of the JR-429 bonebed, as discussed below.

The only articulated bones in the JR-429 bonebed were frontals with parietals and a supraoccipital with exoccipital and prootic. The Sun River Bonebed TM-260 of juvenile lambeosaurs was also completely disarticulated aside from a few skull bones, although they were different cranial elements: a pair of exoccipitals and a frontal with prefrontal (Scherzer and Varricchio, 2010). The *Prosaurolophus* bonebed TM-447/454 was also fairly similar to JR-429 in containing a range of cranial preservation from fully disarticulated braincase and other skull elements to a complete articulated braincase, although the dentaries in TM-447/454 usually retained their tooth batteries (Rogers, 1990). The general ease of disarticulation and minimal, if any, fusion of cranial elements in the JR-429 bonebed is consistent with the non-adult status of collected specimens as inferred from their skeletal sizes.

Bonebed Age Structure

The presence of at least nine individuals of two discrete size classes, plus one extremely large rib head representing an additional, and large, individual, has interesting

taphonomic implications. As defined by Rogers et al. (2007), two or more skeletons at the same site constitute a bonebed, and some pre- or post-mortem process brought them to the same site. Perhaps they were animals that lived together, or just died in the same place, or died in different areas, and their remains were concentrated together at this site. The similar taphonomic signatures of most bones suggests that, whether or not these animals lived in a single social group, the individuals died within a single area over a relatively short period of time (less than one year, and perhaps much shorter). The fact that the three size classes are discrete, with no intermediate sized bones, supports a catastrophic hypothesis. If this were an attritional assemblage of animals dying throughout the year, a continuous sample of intermediate ages would be expected (e.g. 2.0 years old, 2.25 years, 2.5 years, etc.). However, a survey of hadrosaur specimens from multiple localities within the Dinosaur Park Formation of Alberta reveals discrete size classes, even though the isolated specimens from different localities represent an attritional sample (Brinkman, 2014). The Dinosaur Park Formation sample includes a size class of small hadrosaur individuals with tibiae and femora smaller than 20 cm. Such small individuals are not present in the JR-429 bonebed; the "juvenile" size class of the JR-429 bonebed is predicted to have tibia lengths ranging between 46.6 cm and 55.0 cm, falling within the middle size class of Brinkman (2014). The largest size class of hadrosaur elements in the Dinosaur Park Formation sample encompasses both the "subadult" and "adult" size classes of the JR-429 bonebed. This suggests that an attritional sample possesses a more continuous size distribution of subadult and adult individuals, and that the discrete subadult and adult size classes of the JR-429 bonebed

could be representative of a catastrophic origin to the assemblage. However, the sample size of adults in the JR-429 bonebed is very small, and additional specimens discovered in the future could possibly be intermediately sized.

The presence of three discrete size classes in the JR-429 bonebed, without intermediately sized and aged individuals, also supports a specific breeding season in hadrosaurs, rather than breeding randomly throughout the year; the discrete size classes may also support hypotheses of seasonal variations in mortality rates (Craig and Oertel, 1966; Varricchio and Horner, 1993; Brinkman, 2014). High growth rates are also required for cohorts of animals born in different years to form non-overlapping size classes.

The current dearth of adult-sized individuals, aside from a single very large rib head, collected from the JR-429 bonebed can be explained by one or a combination of three different hypotheses:

1) the life assemblage (biocoenose) consisted of only immature individuals;

2) the life assemblage included all ages of individuals, but immature individuals were most susceptible to the cause of death, resulting in an almost exclusively immature death assemblage (thanatocoenose);

3) all ages of individuals were present and susceptible to the cause of death, but due to an immature-dominated population structure, adults would be uncommon.

Hypothesis 1 would have interesting behavioral implications, indicating age-segregation of groups within the population. However, the single very large rib head is evidence of an adult being present, even if adults were rare overall in the life or death

assemblage. Ribs are one of the most common bones in a skeleton, so the only adult bone being a rib bone is not surprising. Hypothesis 2 is biologically plausible; some causes of death, such as drought, affect young and very old animals more severely than adults in their prime (Shipman, 1975; Varricchio, 1995), resulting in underrepresentation of adults in the death assemblage. Hypothesis 3 could be correct if the population structure is strongly dominated by immature individuals such that the sample size is simply not large enough to have collected more than a single rib of the uncommon adult material. Hypothesis 2 could easily combine with Hypothesis 3; if immature animals are more abundant than adults, and very old adults are rare, then despite very old adults having high mortality rates, they will still be relatively rare in the death assemblage compared to immature individuals. The presence of the large rib head falsifies Hypothesis 1 and supports Hypothesis 2 or 3, or a combination of Hypotheses 2 and 3.

Although Hypothesis 1 is not supported for the JR-429 *Gryposaurus* bonebed, some other hadrosaur bonebeds are currently interpreted as non-adult assemblages in which the living assemblage of individuals may have been age-segregated. However, caution must be used when interpreting a small sample size as representing an immature only assemblage; because dinosaurs laid large clutches of eggs, and took multiple years to reach sexual maturity, the population structure was likely dominated by small, immature individuals (Varricchio, 2011). If non-adult assemblages reflect a real biological signal and not a sampling artifact, such assemblages can be interpreted as social groups of immature animals that may have formed while adults were occupied with reproductive and parental activities (Varricchio, 2011). The Sun River late juvenile

lambeosaurine bonebed TM-260 lacks adults (Scherzer and Varricchio, 2010). However, the JR-429 bonebed differs from the Sun River bonebed in having both juvenile and subadult size classes. Another *Gryposaurus* sp. bonebed consisting of only juvenile and subadult elements is present in the Oldman Formation of Alberta (Scott et al., 2014), geographically and stratigraphically close to the JR-429 *Gryposaurus* sp. bonebed. Perhaps further excavation of this Alberta bonebed will reveal a large bone from an uncommon adult, like the large rib head of the JR-429 bonebed. However, if the identification or taphonomic analysis of the large rib head from the JR-429 bonebed is in error, and the large rib head does not represent a large *Gryposaurus* of the same biocoenose as the rest of the bonebed, then the JR-429 bonebed may be similar to these other non-adult bonebeds.

If Hypotheses 2 and/or 3 are correct, adults were present in the living assemblage, even though only a single adult rib head has so far been collected from the death assemblage. A catastrophic death event would provide a snapshot of the living population structure, and thus would be expected to yield the highest numbers of juveniles, with abundance decreasing with age; adults should be present but less abundant than subadults and juveniles (Voorhies, 1969; Varricchio and Horner, 1993). An attritional assemblage, consisting of animals dying of any cause over a period of time, should generally be dominated by young and old individuals, those with the highest mortality rates. Animals in their period of peak reproductive performance should be least represented in the death assemblage (Woodward et al., in press). Because an attritional assemblage forms over an extended time period, multiple taxa are likely to be included, but the JR-429 bonebed is

extremely monodominant. The excavated material from the JR-429 bonebed includes four juveniles, five subadults and one large adult, and so does not well match either the catastrophic or attritional age profile. Perhaps this is a catastrophic monodominant assemblage, with young animals most abundant, and the adults are present but rarely collected due to their relatively lower abundance.

To determine whether the current scarcity of adult bones might be an artifact of sample size, the age distribution of individuals in the JR-429 bonebed can be compared with that of the TM-003 *Maiasaura* bonebed. The JR-429 bonebed has a well-established total MNI of nine with the single large rib head increasing the MNI to ten: four juveniles that are likely approximately one year old, five subadults that are between two and three years old, and one large adult of unknown age. The TM-003 bonebed sample has MNI=32 based on right tibiae (Woodward et al., in press). Using these 32 right tibiae, the age distribution of the *Maiasaura* bonebed has 78.13% of individuals aged 0-2 years (n=25), none aged 3 years, and 21.88% aged 4-15 years (n=7). *Maiasaura* are hypothesized to attain sexual maturity at 3 years of age. If the JR-429 bonebed population is hypothesized to have the same age structure as the TM-003 *Maiasaura* bonebed population, then for a total MNI of ten in the JR-429 bonebed, 7.8 of the individuals would be predicted to be 0-2 years of age, and 2.2 of the individuals would be predicted to be adults 4 or more years of age. The actual age distribution of at least 9 young animals and 1 adult is consistent with the prediction of adults being uncommon in the bone assemblage.

Cause of Death

The most likely hypotheses for cause of death include drought, drowning, predation, disease, or a multi-cause attritional assemblage. A short-term catastrophic cause is supported more than a prolonged attritional one due to similar weathering, abrasion, and breakage patterns of the majority of elements, as well as the discrete size classes.

Drought. Droughts tend to concentrate herbivores near water sources, both for access to water and nearby vegetation (Shipman, 1975; Varricchio, 1995). Depending on the length and severity of a drought, it could catastrophically kill a group of animals in a short period of time, or it could attritionally kill the weakest, often youngest, animals over a longer period of time. A drought will generally affect many species in similar ways, producing a multitaxic death assemblage, but a large monospecific herd can dominate a particular area (Rogers, 1990; Varricchio and Horner, 1993). Thus, the extreme monodominance of *Gryposaurus* sp. in the JR-429 bonebed could be consistent with a drought. In modern mammals, young animals are more susceptible to drought than are adults (Varricchio, 1995 and references therein), so the scarcity of adults in the bonebed could simply be due to most adults surviving the stress of a drought. When a drought period ends, rain can produce significant runoff and entrain large amounts of sediment due to a decrease in living vegetation cover (Shipman, 1975). The light grey low-organic mudstone underlying the bone horizon could potentially have formed during a drier period, and then the environment became wetter, with a flood concentrating the bones and covering them with the dark grey highly organic saturated mud.

Other indicators of drought conditions, such as mud cracks and evaporites, are not present in the quarry sediments, but are not present at some other hypothesized drought-caused bonebeds either (Varricchio, 1995). Insect borings and traces on bones can be consistent with a drought hypothesis (Bader et al., 2009), but these were not found on the MOR 2573 bones. Drought conditions at a drying watering hole can result in miring (Varricchio et al., 2008), but this is not consistent with the JR-429 bonebed due to the complete disarticulation and mixing of skeletons, and the presence of some manus and pes elements higher than the main bone layer, rather than mired in situ in the mud below.

Drowning. In contrast to drought, mass assemblages can also perish by drowning. Most drowned assemblages contain multiple ages of individuals (Eberth and Getty, 2005). The lack of a nearby channel at the same stratigraphic horizon, the bones not being part of associated skeletons, as well as no preferred orientation of bones are all factors that do not support a mass drowning (Rogers, 1990). However, drowning is a very common cause of modern mass death assemblages (Ryan et al., 2001 and references therein), so a drowning hypothesis should still be considered.

Predation. The high abundance of shed tyrannosaur teeth relative to other vertebrate microfossils suggests that multiple tyrannosaurs fed upon the carcasses. Abundant tyrannosaur teeth are not always found in hadrosaur bonebeds; the Sun River Bonebed TM-260 of juvenile lambeosaurs lacked shed theropod teeth (Scherzer and Varricchio, 2010), but other hadrosaur and ceratopsian bonebeds did include shed theropod teeth (Rogers, 1990; Varricchio and Horner, 1993; Varricchio, 1995). Tooth-

marked bone is uncommon for dinosaurs, so the absence of tooth marks in the JR-429 bonebed does not help determine whether these tyrannosaurs were feeding as part of active predation or scavenging (Fiorillo, 1991a).

Disease. The possibility of dinosaur mass mortality resulting from botulism was investigated by Varricchio (1995). The botulism bacterium, *Clostridium botulinum*, can proliferate in dead invertebrates, killing most animals that feed upon these invertebrate carcasses. Because botulism can affect many species, especially carnivores that feed upon the accumulating carcasses, it tends to produce a multitaxic assemblage. The JR-429 bonebed is a monodominant herbivore assemblage, with only two theropod bones among the over 800 hadrosaur bones, and so is inconsistent with botulism deaths. Warm temperatures, shallow anoxic water, and rotting vegetation are often correlated with botulism outbreaks, which produce carcasses arranged linearly along the lake shore. The JR-429 bonebed lacks any linear arrangement, and although the invertebrate evidence supports a shallow water environment, the fact that the invertebrates are all gilled taxa indicates oxic, rather than anoxic, water. Other indicators of anoxic conditions are coalified plant material, which is abundant in JR-429, and finely laminated millimeter-scale beds which may contain articulated small vertebrates, neither of which are present in JR-429. Thus, botulism is unlikely to be the cause of death for these hadrosaurs.

Varricchio (1995) also considered the possibility of toxins released into drinking water from a cyanobacterial bloom. Algal blooms occur in warm, quiet, nutrient-rich water; invertebrates and organics in the JR-429 sediments indicate a quiet, nutrient-rich environment. Masses of cyanobacteria were not observed within the sediment, but they

may not have preserved. Thus, there is little evidence either to support or refute the hypothesis of cyanobacterial toxicosis; the likelihood and evidence supporting a drought-induced or drowning mortality is much stronger.

Bonebed Deposition

Hypotheses for the formation of bonebeds include debris flows, overbank deposition, lacustrine deposition, crevasse-splay deposition, and channel lags, any of which may include scavenging and trampling. The organic-rich mudstone is inconsistent with a crevasse splay or channel lag, and more consistent with overbank or lacustrine facies. Debris flows, overbank flooding, and lacustrine deposition, perhaps in a watering hole scenario, are most commonly invoked as the depositional origins of hadrosaur bonebeds in mudstone-dominated sediments (Rogers, 1990; Varricchio and Horner, 1993; Scherzer and Varricchio, 2010).

Debris Flow Deposition. Scherzer and Varricchio (2010) attributed the TM-260 juvenile lambeosaurine bonebed to a debris flow deposit based on normal grading of clasts, poor sediment sorting, preferred orientation of long bones, and steep plunge of many long bones. The JR-429 bonebed does exhibit normal grading of bones, with small elements sometimes found higher in the mudstone, but the sediment itself is well sorted, there is no preferred orientation of long bones, and the vast majority of bones are nearly horizontal. This suggests a more calm depositional history rather than a viscous debris flow, and is very similar to the flood-deposited TM-041 *Prosaurolophus* bonebed (Rogers, 1990). The TM-003 *Maiasaura* bonebed, which was interpreted as a debris

flow, is similar to JR-429 in the bones being disarticulated, normally graded, horizontally oriented, and randomly trending, underrepresentation of vertebrae and phalanges, and the presence of shed theropod teeth (Varricchio and Horner, 1993; Schmitt et al., 2014). However, most bones in the TM-003 bonebed have broken or weathered epiphyses, presumably due to violent transport in the debris flow, whereas most epiphyses are intact in JR-429, although ribs and neural arches are commonly broken. The TM-003 bonebed also includes abundant lithic clasts (Schmitt et al., 2014), which are not present in the JR-429 bonebed. The completeness or fracture patterns of elements in JR-429 are most similar to the flood-deposited TM-041 *Prosaurolophus* bonebed (Rogers, 1990).

Overbank Flood and Lacustrine Deposition. Given that the large elements in the main bone horizon are nearly horizontal, and include intact broad flat bones like scapulae and pubes, it is possible that this was the layer of deposition, and the small bones rose higher in the mud, rather than all bones originating at the top of the mud unit and the large bones being trampled or settling downward, which would have resulted in more non-horizontal plunges. Similar normal vertical grading of smaller bones higher in the deposits of two *Edmontosaurus* bonebeds were interpreted as evidence of viscous water columns in which the semi-cohesive fluid retarded their settling, possibly combined with bioturbation that disturbed small light bones that then resettled higher in the water-mud column (Gangloff and Fiorillo, 2010; Bell and Campione, 2014).

Ceratopsian bonebeds in overbank deposits also exhibit normal grading with small bones being found higher in the deposit (Eberth and Getty, 2005). In addition, these ceratopsian overbank deposits have most bones nearly horizontal, and can have matching

halves of broken bones located tens of centimeters apart, similar to the JR-429 bonebed. Overbank flood deposits incorporate large plant debris into the bonebed (Eberth and Getty, 2005), which is consistent with the high abundance of wood at this site. Overbank deposits may have root traces, but these are not present in the JR-429 bonebed.

Lacustrine and floodplain deposition are very low energy and disarticulation occurs mainly due to decay of soft tissues, subaqueously or subaerially. Hadrosaur and ceratopsian bonebeds interpreted as lake or floodplain deposition may have partial articulation or partial association of skeletons, but otherwise these bonebeds match the taphonomic signature of the JR-429 bonebed: horizontal bones with random trend, minimal breakage of most bone types, minimal or no weathering modification, possible underrepresentation of vertebrae and phalanges, and the presence of shed theropod teeth (Rogers, 1990; Varricchio and Horner, 1993). During a drought period, the sediment would have been consolidated, and trampling could easily break highly elongate but thin bones like ribs (Varricchio, 1995). After the muddy sediment covered the bones, further trampling could produce the few plunging bone orientations, broken bones in which the two halves are still nearby, and the striation marks found on at least one bone.

A lacustrine setting does not necessarily imply subaqueous immersion; bones may have accumulated subaerially around the lake margin before being buried in mud. It is possible that the concentration of bones represents a strand line along a lake margin (Varricchio, 1995), but there is no linear trend in the orientation of individual bones or wood, and no obvious linear trend in the overall distribution of bones within the bonebed horizon. The dark grey organic-rich mudstone of the JR-429 bonebed may indicate a low

energy reducing lake or other saturated environment (Rogers, 1990). The mudstone is massive and lacks laminations than can be found in lake sediment, but trampling bioturbation by large animals ("dinoturbation") within a lake or along a lake margin can homogenize the sediment (Lockley and Conrad, 1989; Varricchio, 1995).

The mollusk fauna in the JR-429 bonebed is consistent with a low energy aquatic environment such as a pond, lake, or slow-moving area of a river. The tiny *Sphaerium* clams indicate very low energy conditions. Modern *Sphaerium* often inhabit interchannel standing water environments with vegetation and muddy bottoms, such as ponds and lake margins, but their small size and shallow position in the substrate lead to their valves being easily transported (Johnston and Hendy, 2005). *Sphaerium* are also resistant to desiccation during drought conditions (Varricchio, 1995). The presence of *Melanoides* and *Viviparus* aquatic gilled gastropods also supports an aquatic depositional environment; however, these mollusks are not abundant. Modern *Viviparus* live in the portions of rivers where water movement is slow, and decaying organic material is plentiful. The gastropod assemblage at the multitaxic Jack's Birthday Site bonebed TM-068 is dominated by pulmonate gastropods, both terrestrial and aquatic, documenting a transition from floodplain to lake deposition, with the area of high *Sphaerium* bivalve abundance interpreted as a parautochthonous lacustrine assemblage (Varricchio, 1995). In the JR-429 bonebed, the lack of terrestrial or aquatic pulmonate gastropods, but presence of aquatic gilled gastropods and bivalves, is thus more consistent with lake deposition than with subaerial floodplain deposition.

This reducing saturated environment, and lack of bone weathering, is not obviously consistent with a drought scenario, but the time between death and burial may have been long enough for a drought to end and water levels to rise significantly. Due to decreased vegetation cover and possibly impermeable soil, a post-drought flood can be severe (Shipman, 1975). The JR-429 depositional environment lacks indicators of strong seasonality such as calcareous clasts and strongly color banded green and red mudstones, which are common in the more upland Two Medicine Formation (Scherzer and Varricchio, 2010). However, mudstone horizons within the quarry as well as elsewhere in Kennedy Coulee do vary in their shade of grey and associated organic content, indicating some variation in sediment saturation levels. These correspond to different depositional environments that may have been affected by long-term variations in weather. Therefore, drought and flood conditions are still possible even without strong seasonality in weather patterns.

A strong rainstorm can cause localized flooding capable of moving wood and bones. This fluid flow could rearrange and concentrate a bone assemblage while also mixing in other floating clasts such as logs and branches. This may also explain the abundance of small coprolites within the bonebed (n=90); coprolite and wood accumulations found near *Iguanodon* skeletons were interpreted as evidence of floods transporting and concentrating clasts (Fowler, 2000). In a modern semiarid prairie setting in eastern Montana, a severe rainstorm produced runoff that flattened grass and entrained dried herbivore fecal pellets (deer and/or rabbit) as floating clasts (E. A. Freedman and D. W. Fowler personal observation, 2009). A small stream flooded its banks, leaving a

strand line of herbivore fecal pellets and plant debris on the floodplain when the water level receded (Figure 3.10). The high content of plant material enabled these fecal pellets to float; however, the coprolites in the JR-429 bonebed are most likely produced by fish, turtles, or crocodilians, and do not contain fibrous plant material. Actualistic taphonomy experiments are needed to determine whether coprolites produced by aquatic organisms are capable of desiccating and then floating in a similar manner.

The JR-429 bonebed taphonomy best corresponds with floodplain or lake deposition due to the randomly horizontally oriented bones, low-energy aquatic mollusks, and abundant wood and small plant debris. The bonebed also shares some similarities with debris flow deposition, except that the limb bones are generally intact and only ribs and neural arches are commonly broken, and steeply plunging elements are rare. Therefore, the JR-429 bonebed is hypothesized to have formed through a combination of modes: death near a lake or other topographic low on the floodplain, with soft tissue decay (subaerial or subaqueous); if the bones were not yet immersed within the lake, then some degree of flow would have thoroughly mixed the bones of individual skeletons together and deposited them within the lake. Transport only needed to be great enough to mix and deposit the bones without causing significant abrasion, suggesting that this is an autochthonous or parautochthonous assemblage.

Conclusions

Although alternative hypotheses are possible, the following scenario is proposed for the formation of the JR-429 *Gryposaurus* bonebed. The hadrosaur individuals died,

perhaps due to drought or drowning, on a floodplain or near a lake or oxbow lake margin. They were exposed (subaerially or subaqueously) long enough for tyrannosaurs to feed upon the carcasses, the skeletons to disarticulate, and some bones to break from trampling, but not long enough for noticeable bone weathering to occur; perhaps a few months. Then the bones and wood logs were entrained by a flooding event that mixed bones from multiple skeletons and deposited them into a lake or topographic low on the floodplain. The flooding event would have had enough energy to move the bones and logs, but not as much energy and entrained sediment as a debris flow. This transport of carcasses may have occurred before or after subaerial decay and disarticulation; the remainder of decay and disarticulation would occur subaqueously. Some bones were broken during or after transport, possibly due to additional trampling, and the pieces remained near each other. Organic-rich sediment covered the bones; this sediment may have all been deposited during the same event that concentrated the bones, or it may have accumulated more gradually and been bioturbated. The sediment remained wet and soft enough for the small light elements such as centra and phalanges to rise upward in the sediment column, perhaps due to further bioturbation.

This monodominant *Gryposaurus* bonebed, like other monodominant hadrosaur bonebeds, is consistent with hypotheses of hadrosaur gregariousness, and the presence of discrete size classes supports previous hypotheses of seasonal breeding in hadrosaurs (Varricchio and Horner, 1993). The abundance and preservation quality of cranial material from two non-adult size classes make this site valuable for studies of

Gryposaurus ontogeny and evolution within the Late Cretaceous of western North America.

Acknowledgements

Grateful thanks to my advisor, Jack Horner, who provided the opportunity to work in a fantastic field area and made every aspect of this research possible. Additional thanks to Dave Varricchio, Don Brinkman, Matt Lavin, Denver Fowler, Holly Woodward, Dave Evans, Michael Ryan, Dave Eberth, Mark Goodwin, Ray Rogers, Karen Chin, and Joe Hartman for advice and discussions. For specimen collection, thanks to the 2006 and 2010-2012 MOR field crews, especially Brian Baziak, Bobby Ebelhar, Bob Harmon, and Cary Woodruff. For fieldwork support, hospitality, friendship, and specimen donation, great thanks as always to Dan and Lila Redding. Excellent preparation was done by Jamie Jette, Carrie Ancell, Aleen Kienholz, Susan Brewer, and volunteers at the MOR Bowman Prep Lab. Thanks to Ellen Lamm and Holly Woodward for histological assistance. Special thanks to Cary Woodruff for collecting the modern conifer bark sample, and Denver Fowler for observing the importance of, and documenting, the modern fecal pellet taphonomy. Fieldwork and research funding was generously provided to Jack Horner by: Nathan Myhrvold, David Sands and family, Ellis Short and family, Damaris Wagoner, and donors to the MOR Horner Fund and MOR Student Fund; and directly to the author by: the Geological Society of American Student Research Grant, the Royal Ontario Museum M. A. Fritz Travel Grant for the Advancement of Studies in Paleontology, and the Montana State University Department

of Cell Biology and Neuroscience. Doctoral committee members Jack Horner, Dave Varricchio, Don Brinkman, and Matt Lavin provided helpful comments on drafts of this paper.

Table 3.1. Relative abundances of vertebrate microfossils from the JR-429 bonebed compared to other lower Oldman Formation microsites. Column "JR-429" lists the abundances of all vertebrate microfossils recovered from the *Gryposaurus* bonebed. The other five columns list abundance data compiled from Brinkman et al. (2004) for five vertebrate microsites located in Unit 1 of the Oldman Formation of Alberta. The upper set of totals and percent abundances is based on all taxa, whereas the lower set of totals and percent abundances partially corrects for size bias in collection method by restricting the data set to taxa with relatively large bones and teeth: Testudines, Champsosaurus, Crocodylia, and Dinosauria. "Ornithischia indet." refers to tooth fragments that belong either to Hadrosauridae or Ceratopsidae, but cannot be confidently assigned to a family.

		Brinkman 2004				
Taxa	JR-429	HoS	WS	EZ	PHR93-2	PHS
Myledaphus	0	15	9	8	24	19
Non-Teleost Fish	8	1061	578	152	166	346
Teleostei	2	196	330	222	183	229
Amphibia	1	297	392	125	293	102
Squamata	2	8	45	60	11	25
Testudines	32	29	24	7	4	28
Champsosaurus	0	17	214	6	18	27
Crocodylia	16	31	82	13	20	51
Ankylosauria	0	2	0	1	0	2
Pachycephalosauridae	0	0	1	1	0	0
Ceratopsidae	13	3	8	11	10	2
Hadrosauridae	31	83	61	101	65	93
Ornithischia indet.	16	-	-	-	-	-
Tyrannosauridae	37	2	3	1	0	2
Maniraptoriformes	5	8	9	1	12	8
Aves	0	0	3	1	1	0
Mammalia	0	7	8	4	3	9
Total	163	1759	1767	714	810	943
% Tyrannosauridae	22.70	0.11	0.17	0.14	0.00	0.21
% Hadrosauridae	19.02	4.72	3.45	14.15	8.02	9.86
% Ceratopsidae	7.98	0.17	0.45	1.54	1.23	0.21
Total - large only	150	175	405	143	130	213
% Tyrannosauridae	24.67	1.14	0.74	0.70	0.00	0.94
% Hadrosauridae	20.67	47.43	15.06	70.63	50.00	43.66
% Ceratopsidae	8.67	1.71	1.98	7.69	7.69	0.94

Table 3.2. Abrasion and completeness stages of prepared bones from the JR-429 bonebed. Bone completeness categories are: Intact (>90% complete), Minor Fracture (76-90% complete), Major Fracture (25%-75% complete), and Fragment (<25% complete). Abrasion stages follow definitions of Fiorillo (1988).

	Abrasion					
Completeness	0	1	2	3	Total	Percent of all bones
Intact	145	1	0	0	146	22.15
Minor Fracture	36	2	0	0	38	5.77
Major Fracture	137	20	1	0	158	23.98
Fragment	193	95	27	2	317	48.10
Total	511	118	28	2	659	
Percent of all bones	77.54	17.91	4.25	0.30		

Table 3.3. Relative sizes of bones from smaller size class versus larger size class. Bones were grouped as belonging to the smaller size class or larger size class based on the bimodal bone size distribution histograms (Figure 3.8). Skeletal element types that are represented by multiple specimens of both size classes are included here. The mean length of the smaller size class was divided by that of the larger size class to express their relative sizes (last column). Abbreviations: n, number of specimens; sd, standard deviation.

	Smaller size class			Larger size class			Mean smaller size
Length of	n	Mean (cm)	sd (cm)	n	Mean (cm)	sd (cm)	as % of larger size
Dentary tooth row	5	19.1	0.9	6	28.4	1.4	67.2
Ulna	2	29.8	0.4	7	51.5	3.0	57.8
Radius	3	29.8	2.6	7	48.9	3.7	61.0
Metatarsal II	3	16.8	2.3	4	25.3	2.3	66.7
Metatarsal III	4	21.9	2.3	2	33.3	1.8	65.8
Metatarsal IV	3	18.3	1.2	5	26.9	1.8	68.2

Table 3.4. Abundances of skeletal element types. For each skeletal element type, the table lists: number of elements in a single *Gryposaurus* skeleton (based on Royal Ontario Museum 764 and the mounted reconstruction of Utah Museum of Natural History 20181), percent expected distribution of bone types (number of bones in group divided by total number of bones in skeleton), total NISP (minimum number of identifiable specimens) collected, and percent observed distribution (NISP of group divided by total NISP). Relative abundances of bone types are indicated with the following symbols: (+) overrepresented, percent observed is greater than expected; (=) approximately equal, percent observed and percent expected differ by less than 1; (-) underrepresented, percent observed is less than expected. Bone types that differ greatly from expected are indicated with double symbols: (++) strongly overrepresented, percent observed is more than twice the percent expected; (--) strongly underrepresented, percent observed is less than half the percent expected. The significance ("Sig.") of the difference between the observed and expected values was determined using a 1x2 Pearson's X^2 test for each bone type (e.g., skull bones versus non-skull bones). Abundances of bone types indicated with "ns" were not significantly different from expected ($p>0.1$). The "Total" NISP includes all prepared bones as well as unprepared bones with confident field identifications. Subadult and juvenile values only include prepared bones complete enough to confidently assign to a size category, so their totals are lower than the total of all bones. Chevrons were not assigned to size classes.

			Total				Subadult				Juvenile			
Bone Type	In 1 Skeleton	% Expected	NISP	% Observed	Abundance	Sig.	NISP	% Observed	Abundance	Sig.	NISP	% Observed	Abundance	Sig.
Skull	57	12.21	98	22.48	+	p<<0.001	74	28.24	++	p<<0.001	13	14.77	+	ns
Pectoral	6	1.28	9	2.06	=	ns	6	2.29	+	ns	1	1.14	=	ns
Pelvic	6	1.28	24	5.50	++	p<<0.001	12	4.58	++	p<<0.001	2	2.27	=	ns
Large limb	12	2.57	46	10.55	++	p<<0.001	33	12.60	++	p<<0.001	6	6.82	++	p=0.012
Manus pes	70	14.99	65	14.91	=	ns	36	13.74	-	ns	19	21.59	+	p=0.083
Ribs	60	12.85	79	18.12	+	p=0.001	43	16.41	+	p=0.085	24	27.27	++	p<<0.01
Non-caudal centra	40	8.57	6	1.38	--	p<<0.001	3	1.15	--	p<<0.001	1	1.14	--	p=0.013
Non-caudal neural arches	40	8.57	39	8.94	=	ns	33	12.60	+	p=0.021	4	4.55	-	ns
Caudal centra	63	13.49	38	8.72	-	p=0.004	16	6.11	--	p<<0.001	14	15.91	+	ns
Caudal neural arches	62	13.28	26	5.96	--	p<<0.001	6	2.29	--	p<<0.001	4	4.55	--	p=0.016
Chevrons	51	10.92	6	1.38	--	p<<0.001	-	-			-	-		
Total	467	100	436	100			262	100			88	100		

Table 3.5. Tibial histology growth zone circumferences of MOR 2573 and comparative specimens. The three sampled tibiae of MOR 2573 *Gryposaurus* sp. lack observable LAGs, so the outer circumference of each zone of circumferential laminar tissue is used as a proxy for LAGs. Comparative specimens of *Maiasaura peeblesorum* (MOR 005-T34) (Woodward et al., in press) and Brachylophosaurini nov. (MOR 2919) (Freedman Fowler and Horner, Chapter Two) do possess well-defined LAGs (7 LAGs and 14 LAGs respectively). Measurements for LAGs 5-13 of Brachylophosaurini nov. not included to simplify the table.

Taxon and Specimen	LAG or Zone	Circumference (cm)
Gryposaurus sp.	1	22.2
MOR 2573-6-12-06-17	2	Not Traceable
Tibia length = 89.5 cm	Surface	31.1
Gryposaurus sp.	1	15.8
MOR 2573-7-08-10-396	2	Not Traceable
Tibia length = 75.0 cm	Surface	27.9
Gryposaurus sp.	1	21.3
MOR 2573-7-31-10-497	2	26.3
Tibia length = 77.5 cm	Surface	29.7
Maiasaura peeblesorum	1	18.6
MOR 005-T34	2	22.8
Tibia length = 75.0 cm	3	26.0
	4	27.0
	5 to 7	Not Traceable
Brachylophosaurini nov.	1	23.7
MOR 2919	2	29.3
Tibia length = 120.0 cm	3	32.8
	4	35.7
	14	41.2

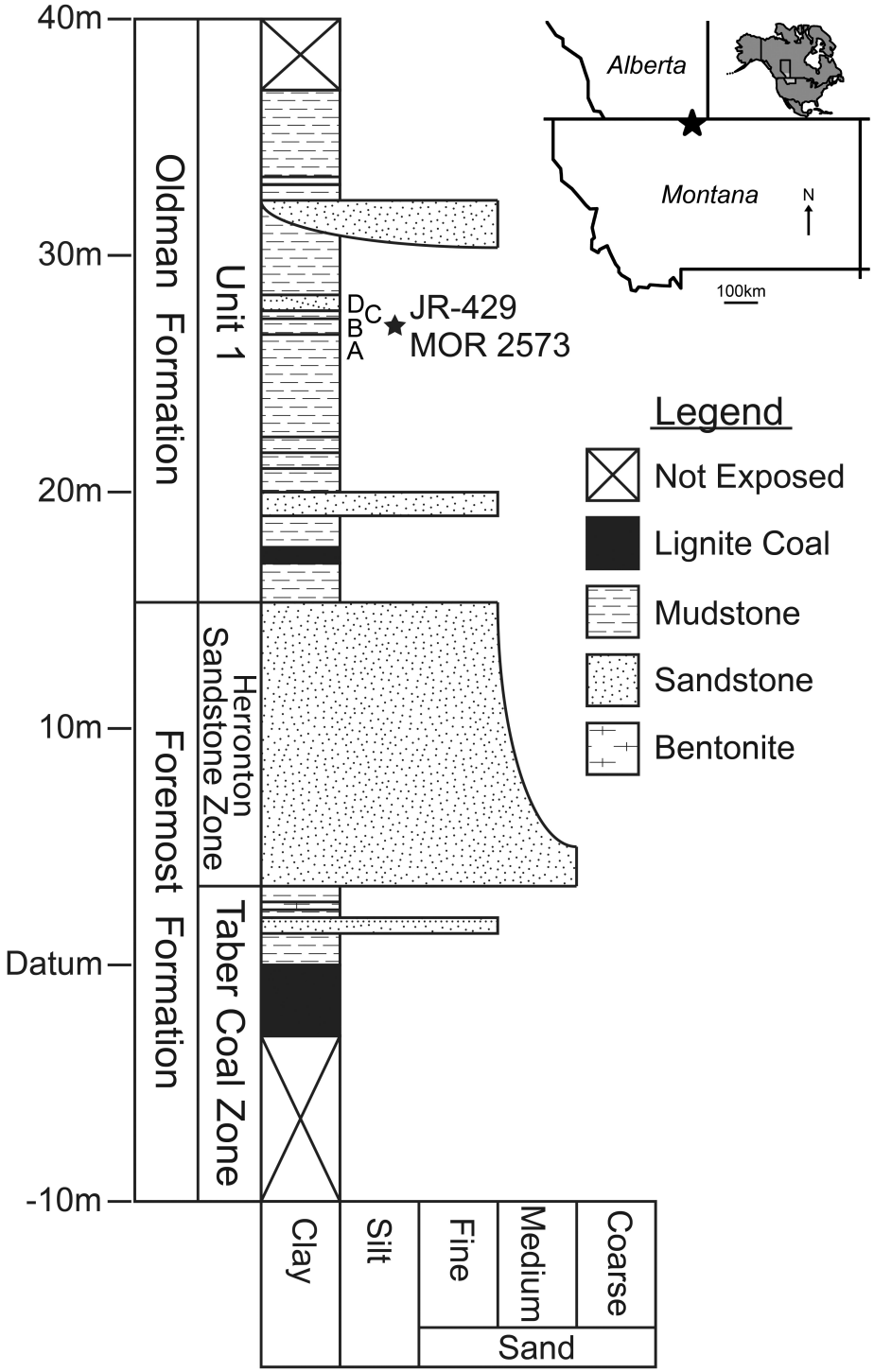


Figure 3.1. Stratigraphic section of Kennedy Coulee, northcentral Montana, Judith River Formation. Location of *Gryposaurus* sp. bonebed, MOR locality JR-429 (specimen MOR 2573), is indicated by black star on stratigraphic section and on inset map of Montana in upper right of figure. Letters ABCD indicate quarry horizons discussed in text.

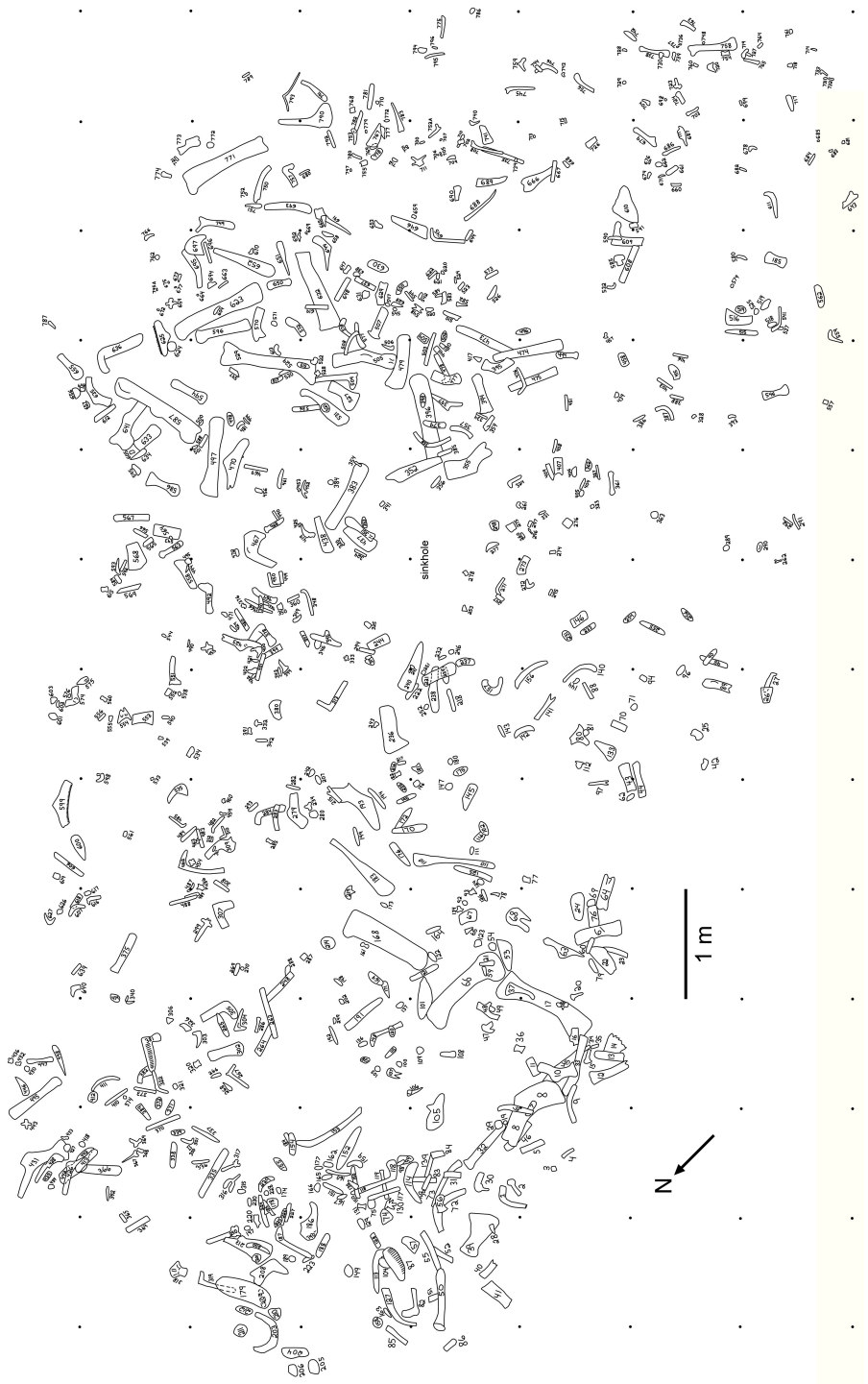


Figure 3.2. Quarry map of excavated bones in the JR-429 *Gryposaurus* sp. bonebed. Black dots denote 1 m grid system. Numbers labeling bones correspond to the field numbers listed in Appendix H. A higher resolution color version of this figure is available as Appendix G.

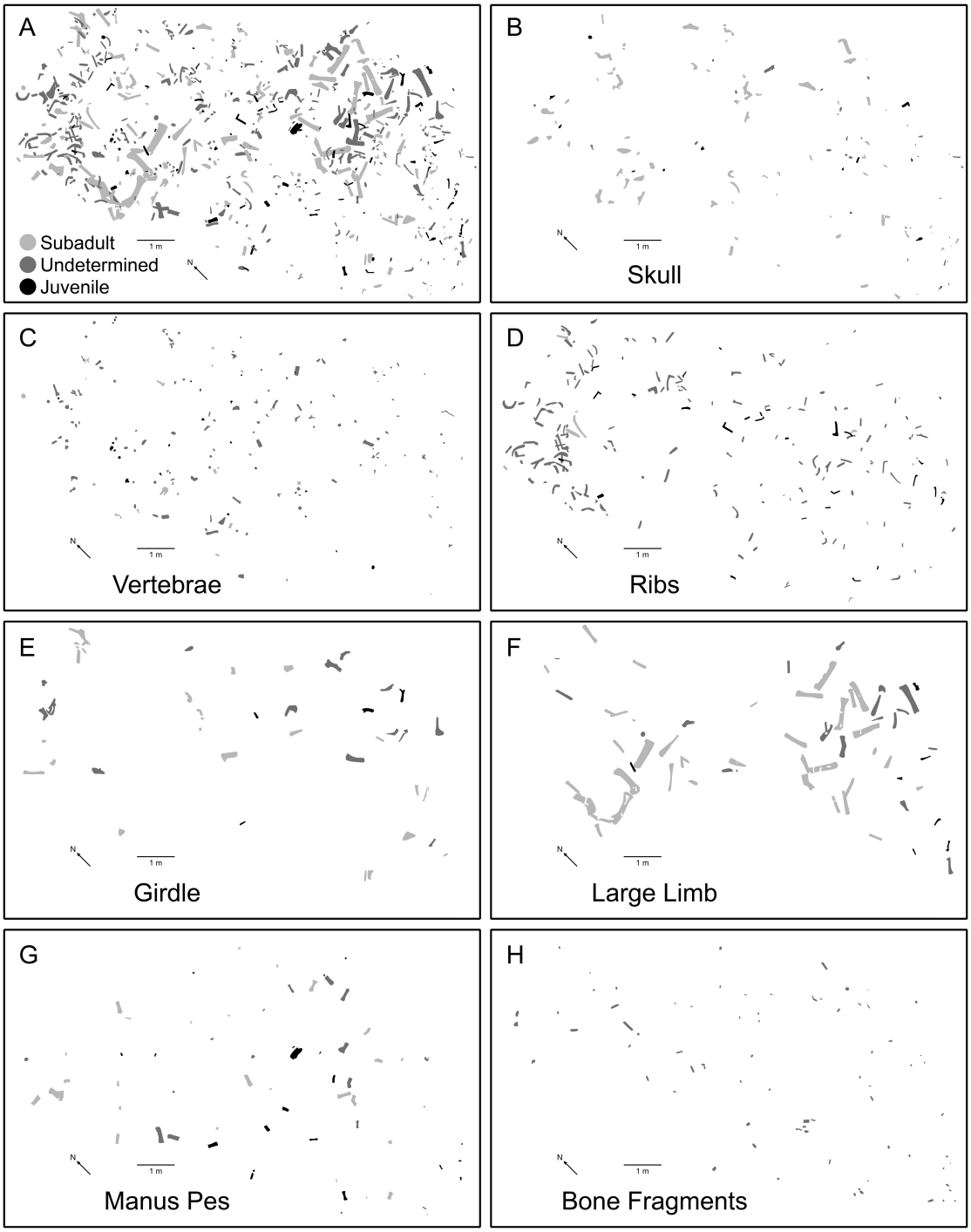


Figure 3.3. Quarry maps showing distribution of each skeletal element type. All maps use the same datum, scale, and color code: light grey represents subadult material, and black represents juvenile material. Dark grey indicates specimens of undetermined size class, which are generally unprepared, fragmentary, or are from ribs or vertebrae, which have only partially been identified into size classes. (A) All specimens of identifiable bone types. (B-H) Groups of bone types as labeled.

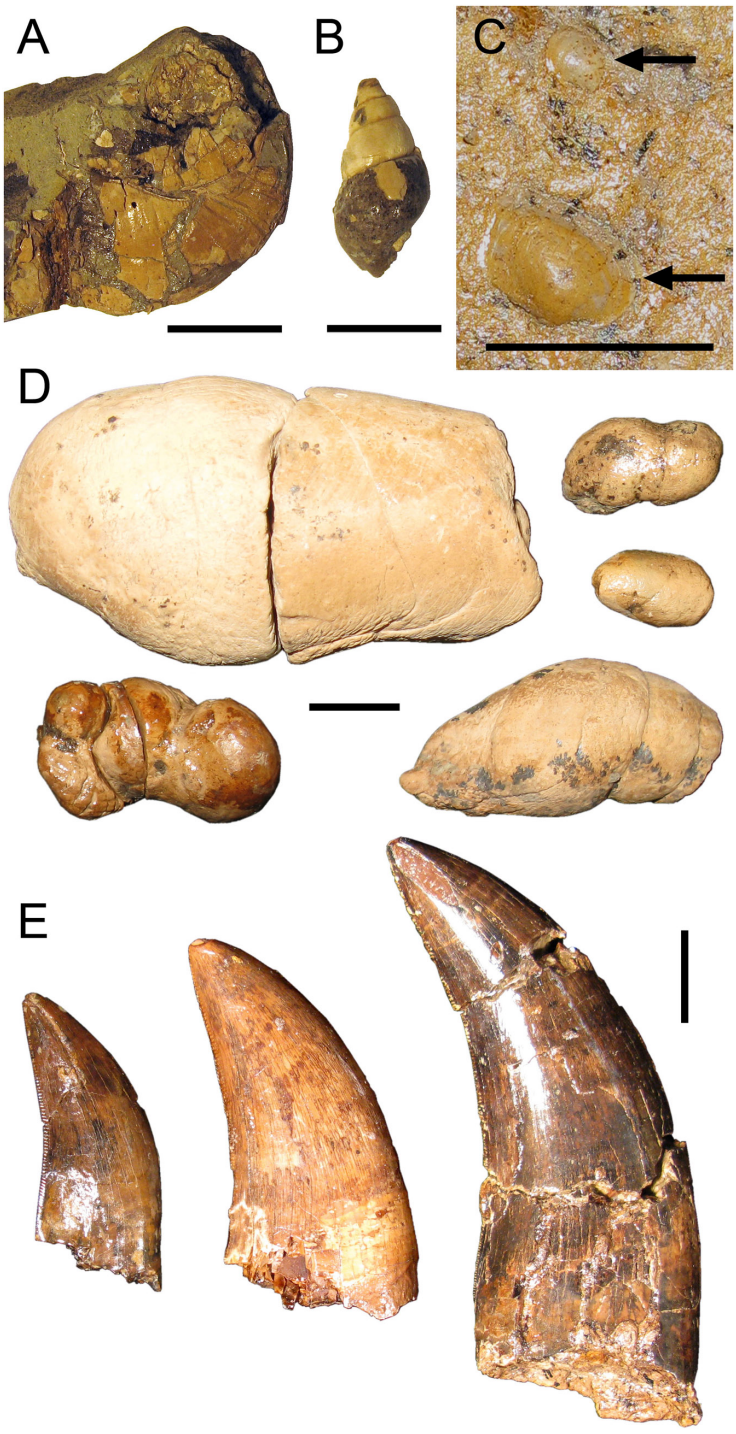


Figure 3.4. Microfossil material from the JR-429 bonebed horizon. (A) *Viviparus* gastropod. (B) *Melanoides* gastropod. (C) *Sphaerium* bivalves, indicated by arrows. (D) Non-dinosaurian coprolites representative of range in size and shape. (E) Tyrannosauridae teeth showing typical range in size. All scale bars equal 1 cm.

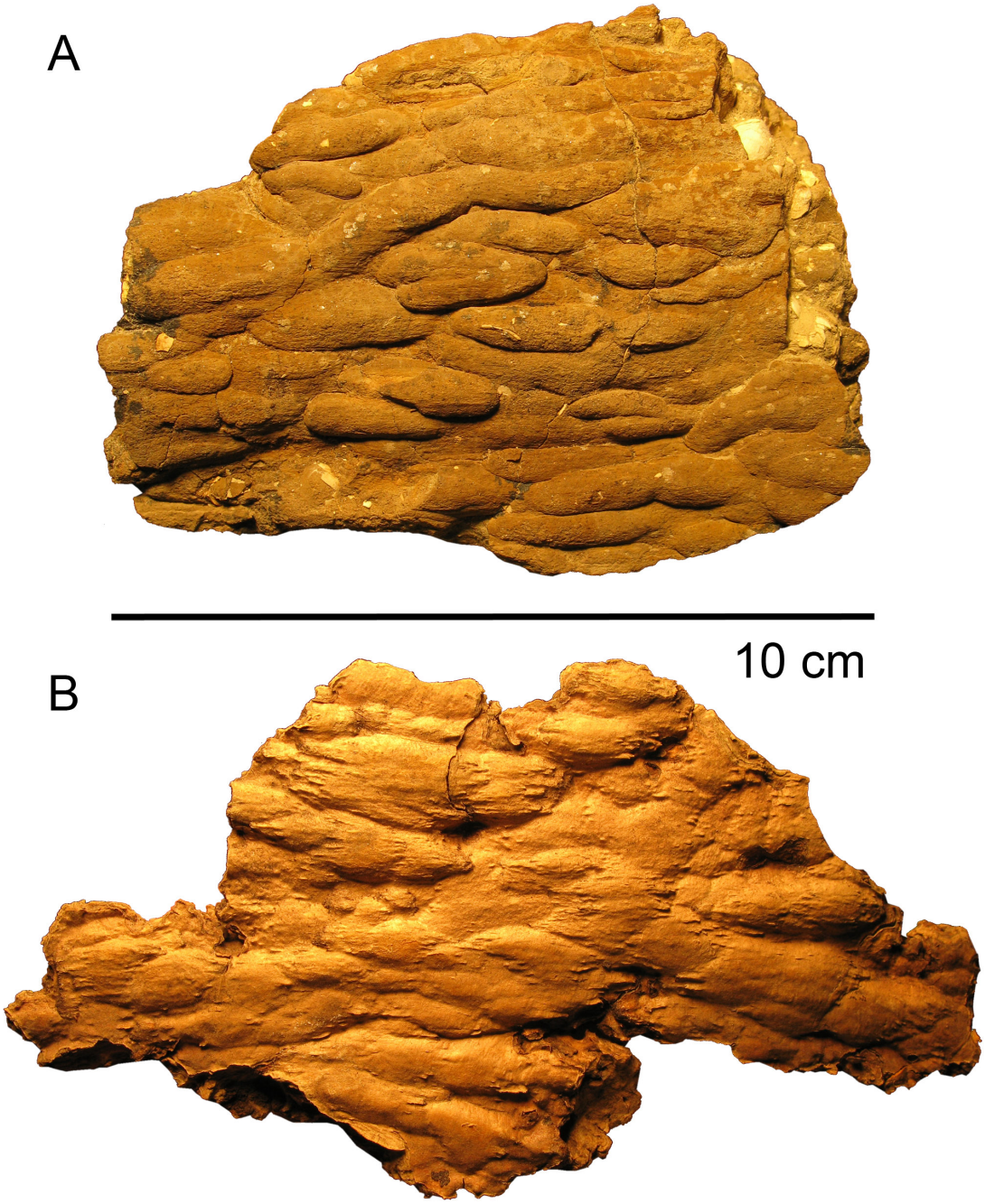


Figure 3.5. Fossil wood impression. Comparison of (A) wood impression trace fossil from concreted sandstone layer above the mudstone JR-429 bone horizon with (B) inner surface of bark from modern conifer (family Pinaceae).

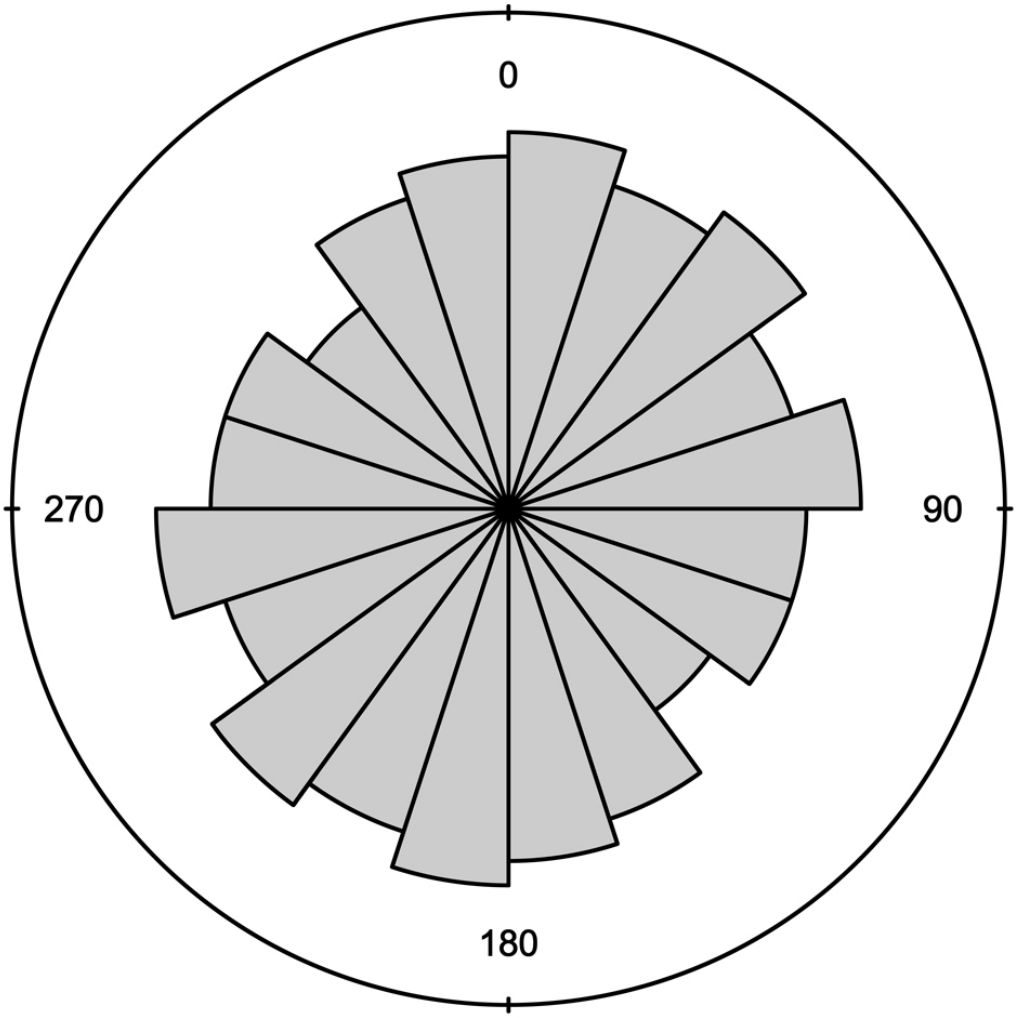


Figure 3.6. Bidirectional rose diagram of elongate bone orientations. Elongate bones included large limb bones (humeri, ulnae, radii, femora, tibiae, and fibulae), metacarpals, metatarsals, scapulae, ilia, ischia, pubes, elongate skull elements, rib shafts, neural spines, and large elongate fragments. N = 121. North corresponds to 0°.



Figure 3.7. Size range of large rib heads. A) MOR 2573-7-18-06-193, the largest rib head from the JR-429 *Gryposaurus* bonebed. B) MOR 2573-6-17-06-45A, the second largest rib head, although fragmentary, from a somewhat similar serial position as rib A. C) MOR 2573-7-11-06-152 (mirrored), the largest almost complete rib from a similar serial position as rib A. Ribs B and C are interpreted as belonging to the larger of the two main size classes of individuals in the JR-429 *Gryposaurus* bonebed. D) MOR 2919-6-20-07-25 (mirrored), a rib from a similar serial position as A, from a large (tibia length 120 cm) 14 year old individual of the hadrosaurine clade Brachylophosaurini from MOR locality JR-518, also from the lower Oldman Formation of Kennedy Coulee, Montana (Freedman Fowler and Horner, Chapter Two). Rib A is noticeably larger than ribs B, C, and D, indicating that rib A belongs to an individual larger than any other in the JR-429 *Gryposaurus* bonebed, and even larger than the 14 year old brachylophosaurin hadrosaur from a nearby locality.

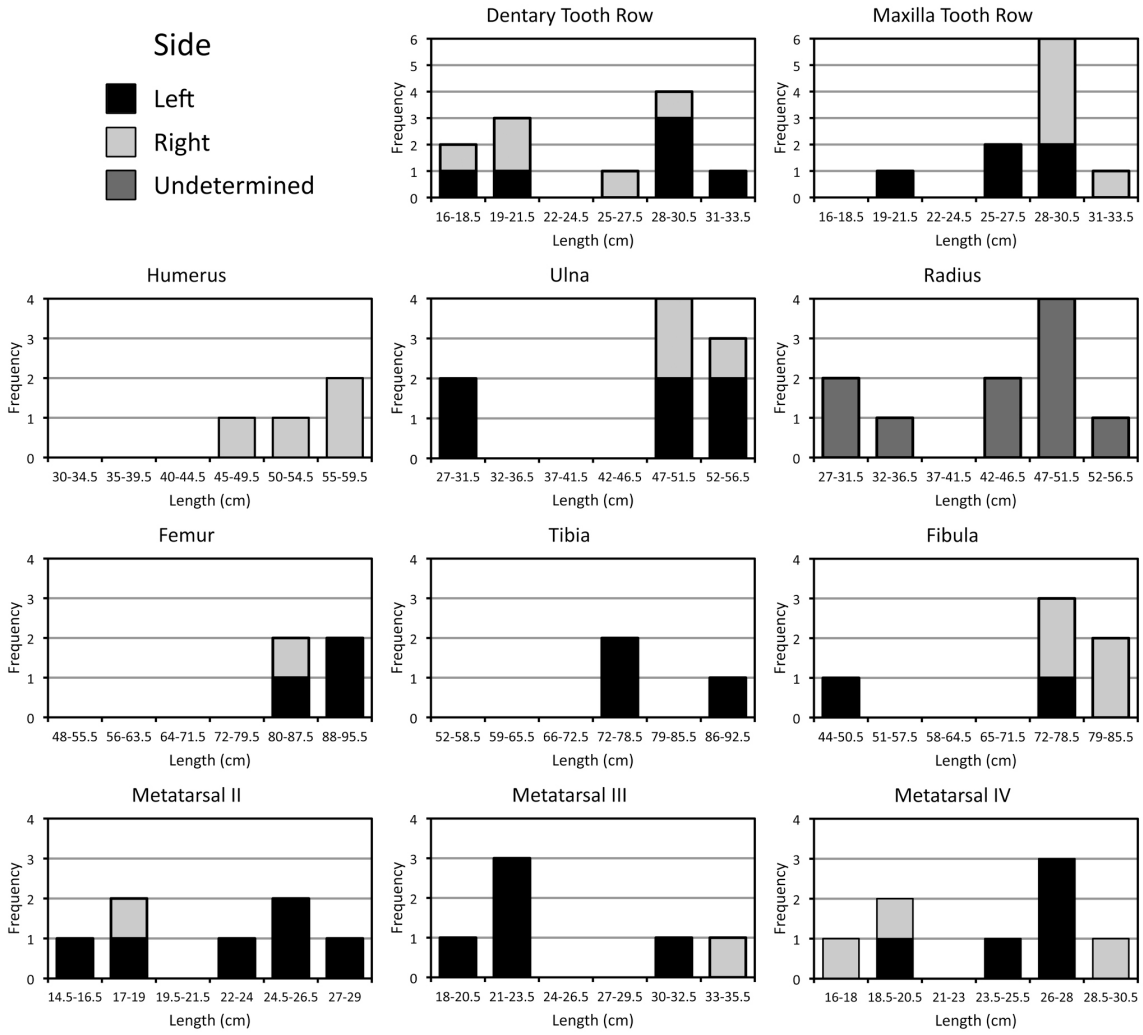


Figure 3.8. Size distribution histograms of specimens by element type. Note the overall bimodal distribution of two discrete size classes. All prepared limb elements were measured; the reconstructed lengths of partially broken elements were estimated by comparison to the complete element of the most similar size. Measured lengths and estimated lengths are available in Appendix H. Radii were not differentiated into left and right due to preservation of some elements making side determination difficult.

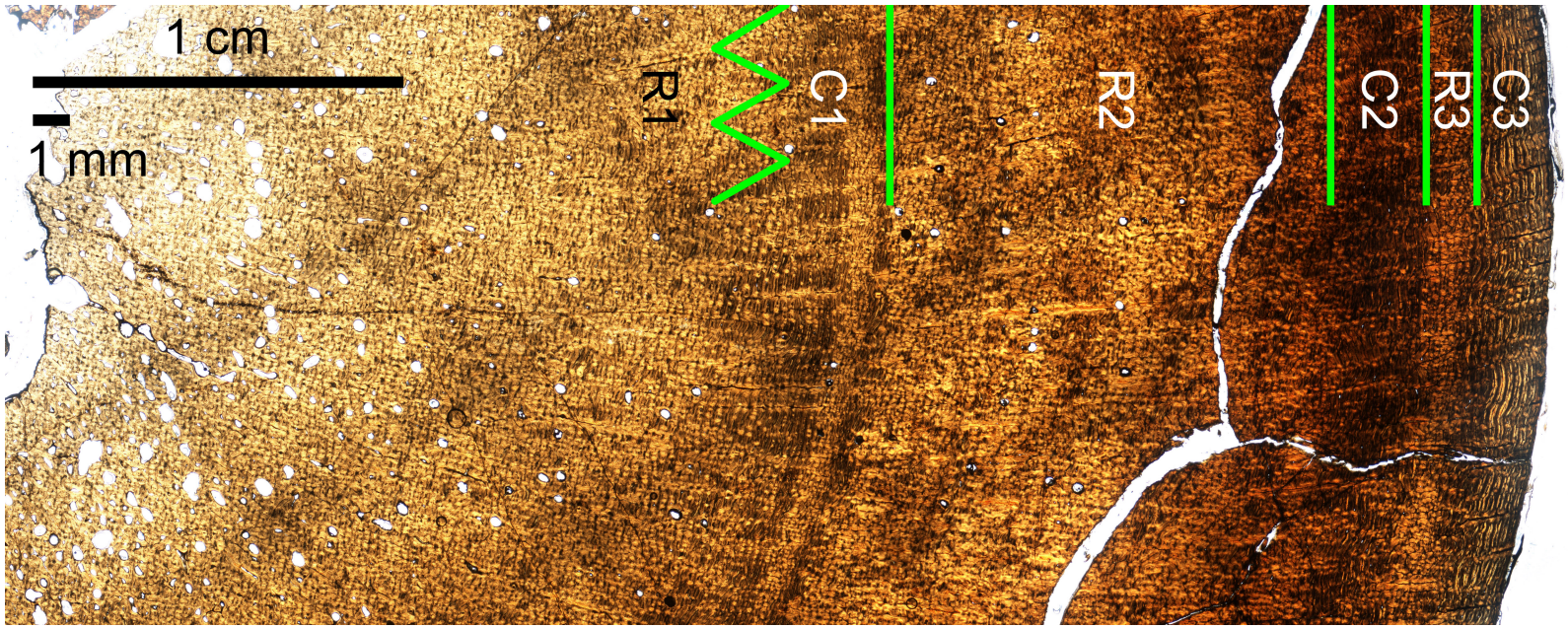


Figure 9. Tibial histology of *Gryposaurus* "subadult" MOR 2573-6-12-06-17. Radial section of posteromedial side of tibia mid-diaphysis. Medullary cavity is at the bottom of the figure; cortical surface is at the top. No lines of arrested growth (LAGs) are observable; instead, the bone tissue alternates between zones of reticular fibro-lamellar tissue (R1, R2, and R3) and circumferential fibro-lamellar tissue (C1, C2, and C3). The boundary between reticular vascularity transitioning into circumferential vascularity is irregular in some areas, especially between the first reticular zone and first circumferential zone; this irregular contact is indicated with a zig-zag line. The outermost extent of each zone of circumferential laminar tissue was used as a proxy for annual LAG location. Image taken using polarized light and one-quarter wave plate.

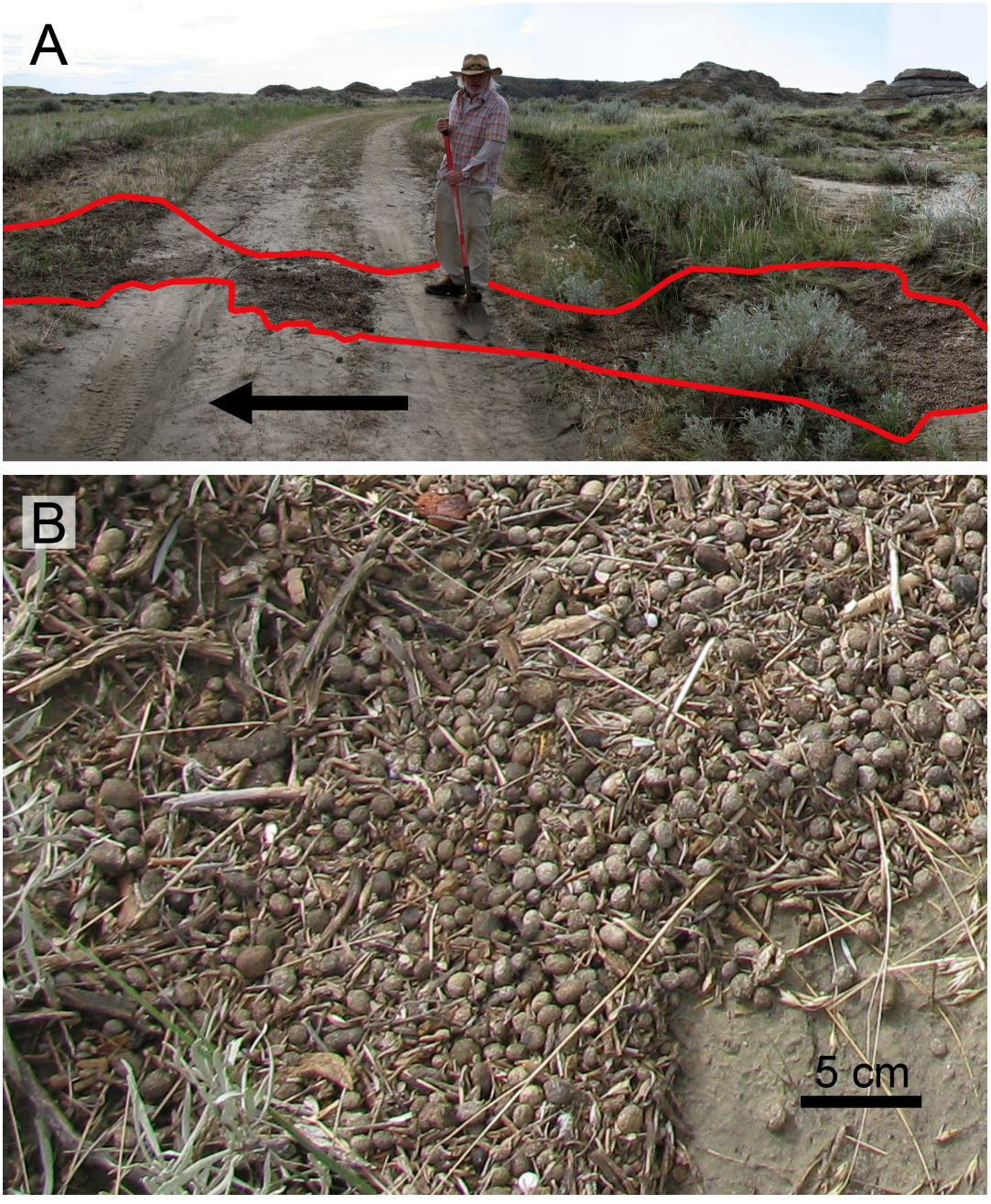


Figure 3.10. Coprolite floating clast taphonomy. A severe thunderstorm the night of July 13, 2009 northeast of Jordan, MT produced runoff that flattened grass and flooded small streams. (A) Dried herbivore fecal pellets and dried grass were transported as floating clasts and deposited as overbank strand lines as the water level receded. Borders of fecal pellet assemblage outlined in red. Arrow indicates flow direction. (B) Magnification of clasts in A, showing heterogeneous mixture of fecal pellets, dead grassy debris, and dead woody debris. Photographs courtesy of Denver Fowler.

Literature Cited

Bader, K. S., S. T. Hasiotis, and L. D. Martin. 2009. Application of forensic science techniques to trace fossils on dinosaur bones from a quarry in the Upper Jurassic Morrison Formation, northeastern Wyoming. Palaios 24:140-158.

Behrensmeyer, A. K. 1975. The taphonomy and paleoecology of Plio-Pleistocene vertebrate assemblages east of Lake Rudolf, Kenya. Bulletin Museum of Comparative Zoology 146:473-578.

Behrensmeyer, A. K. 1978. Taphonomic and ecological information from bone weathering. Paleobiology 4:150-162.

Bell, P. R., and N. E. Campione. 2014. Taphonomy of the Danek Bonebed: a monodominant *Edmontosaurus* (Hadrosauridae) bonebed from the Horseshoe Canyon Formation, Alberta. Canadian Journal of Earth Sciences 51:992-1006.

Boaz, N. T., and A. K. Behrensmeyer. 1976. Hominid taphonomy: transport of human skeletal parts in an artificial fluviatile environment. American Journal of Physical Anthropology 45:53-60.

Brinkman, D. B. 2014. The size-frequency distribution of hadrosaurs from the Dinosaur Park Formation of Alberta, Canada; pp. 416-421 in D. A. Eberth and D. C. Evans (eds.), Hadrosaurs. Indiana University Press, Bloomington, Indiana.

Brinkman, D. B., A. P. Russell, D. A. Eberth, and J. Peng. 2004. Vertebrate palaeocommunities of the lower Judith River Group (Campanian) of southeastern Alberta, Canada, as interpreted from vertebrate microfossil assemblages. Palaeogeography, Palaeoclimatology, Palaeoecology 213:295-313.

Castanet, J., K. Curry Rogers, J. Cubo, and J.-J. Boisard. 2000. Periosteal bone growth rates in extant ratites (ostriche and emu). Implications for assessing growth in dinosaurs. Comptes Rendus de l'Academie des Sciences Serie III Sciences de la Vie 323:543-550.

Chinsamy, A., D. B. Thomas, A. R. Tumarkin-Deratzian, and A. R. Fiorillo. 2012. Hadrosaurs were perennial polar residents. The Anatomical Record 295:610-614.

Craig, G. Y., and G. Oertel. 1966. Deterministic models of living and fossil populations of animals. Quarterly Journal of the Geological Society of London 122:315-355.

Eberth, D. A. 2005. The Geology; pp. 54-82 in P. J. Currie and E. B. Koppelhus (eds.), Dinosaur Provincial Park: A Spectacular Ancient Ecosystem Revealed. Indiana University Press, Bloomington, Indiana.

Eberth, D. A., and M. A. Getty. 2005. Ceratopsian bonebeds: occurrence, origins, and significance; pp. 501-536 in P. J. Currie and E. B. Koppelhus (eds.), Dinosaur Provincial Park: A Spectacular Ancient Ecosystem Revealed. Indiana University Press, Bloomington, Indiana.

Eberth, D. A., R. R. Rogers, and A. R. Fiorillo. 2007. A practical approach to the study of bonebeds; pp. 265-331 in R. R. Rogers, D. A. Eberth, and A. R. Fiorillo (eds.), Bonebeds: Genesis, analysis, and paleobiological significance. The University of Chicago Press, Chicago, Illinois.

Evans, D. C. 2010. Cranial anatomy and systematics of *Hypacrosaurus altispinus*, and a comparative analysis of skull growth in lambeosaurine hadrosaurids (Dinosauria: Ornithischia). Zoological Journal of the Linnean Society 159:398-434.

Fiorillo, A. R. 1988. Taphonomy of Hazard Homestead Quarry (Ogallala Group), Hitchcock County, Nebraska. Contributions to Geology, University of Wyoming 26:57-97.

Fiorillo, A. R. 1991a. Prey bone utilization by predatory dinosaurs. Palaeogeography, Palaeoclimatology, Palaeoecology 88:157-166.

Fiorillo, A. R. 1991b. Taphonomy and depositional setting of Careless Creek Quarry (Judith River Formation), Wheatland County, Montana, U.S.A. Palaeogeography, Palaeoclimatology, Palaeoecology 81:281-311.

Fowler, D. W. 2000. Vertebrate taphonomy of the plant debris beds from the Isle of Wight, UK: palaeoenvironmental and palaeoecological implications. Unpublished M.S. thesis, Department of Earth Sciences, University of Bristol, Bristol, UK, 117 pp.

Freedman Fowler, E. A., and J. R. Horner. Chapter Two. A new brachylophosaurinin (Dinosauria: Ornithischia) from the Judith River Formation of northcentral Montana.

Gangloff, R. A., and A. R. Fiorillo. 2010. Taphonomy and paleoecology of a bonebed from the Prince Creek Formation, North Slope, Alaska. Palaios 25:299-317.

Gates, T. A., and S. D. Sampson. 2007. A new species of *Gryposaurus* (Dinosauria: Hadrosauridae) from the late Campanian Kaiparowits Formation, southern Utah, USA. Zoological Journal of the Linnean Society 151:351-376.

Horner, J. R., A. de Ricqlès, and K. Padian. 1999. Variation in dinosaur skeletochronology indicators: implications for age assessment and physiology. Paleobiology 25:295-304.

Huttenlocker, A. K., H. N. Woodward, and B. K. Hall. 2013. The biology of bone; pp. 13-34 in K. Padian and E.-T. Lamm (eds.), Bone Histology of Fossil Tetrapods: Advancing Methods, Analysis, and Interpretation. University of California Press, Berkeley, California.

Hutton, J. M. 1986. Age determination of living Nile crocodiles from the cortical stratification of bone. Copeia 1986:332-341.

Johnston, P. A., and A. J. W. Hendy. 2005. Paleoecology of mollusks from the Upper Cretaceous Belly River Group; pp. 139-166 in P. J. Currie and E. B. Koppelhus (eds.), Dinosaur Provincial Park: A Spectacular Ancient Ecosystem Revealed. Indiana University Press, Bloomington, Indiana.

Köhler, M., N. Marin-Moratalla, X. Jordana, and R. Aanes. 2012. Seasonal bone growth and physiology in endotherms shed light on dinosaur physiology. Nature 487:358-361.

Lamm, E.-T. 2013. Preparation and sectioning of specimens; pp. 55-160 in K. Padian and E.-T. Lamm (eds.), Bone Histology of Fossil Tetrapods. University of California Press, Berkeley.

Leiggi, P., C. R. Schaff, and P. May. 1994. Macrovertebrate collecting; pp. 59-77 in P. Leiggi and P. May (eds.), Vertebrate Paleontological Techniques. Cambridge University Press, Cambridge, UK.

Lockley, M. G., and K. Conrad. 1989. The paleoenvironmental context, preservation and paleoecological significance of dinosaur tracksites in the western USA; pp. 121-134 in D. D. Gillette and M. G. Lockley (eds.), Dinosaur Tracks and Traces. Cambridge University Press, Cambridge.

Mateus, O., and R. Araújo. 2008. Stone-splitters and expansive demolition agents in vertebrate paleontological excavations. Journal of Paleontological Techniques 3:1-6.

Moran, K., H. L. Hilbert-Wolf, K. Golder, H. F. Malenda, C. J. Smith, L. P. Storm, E. L. Simpson, M. C. Wizevich, and S. E. Tindall. 2010. Attributes of the wood-boring trace fossil *Asthenopodichnium* in the Late Cretaceous Wahweap Formation, Utah, USA. Palaeogeography, Palaeoclimatology, Palaeoecology 297:662-669.

Prieto-Márquez, A. 2005. New information on the cranium of *Brachylophosaurus canadensis* (Dinosauria, Hadrosauridae), with a revision of its phylogenetic position. Journal of Vertebrate Paleontology 25:144-156.

R_Core_Team. 2014. R: A language and environment for statistical computing. R Foundation for Statistical Computing, Vienna, Austria. ISBN 3-900051-07-0, URL http://www.R-project.org/.

Rasband, W. S. 1997-2014. ImageJ. U. S. National Institutes of Health, Bethesda, Maryland, USA, http://imagej.nih.gov/ij/,.

Rogers, R. R. 1990. Taphonomy of three dinosaur bone beds in the Upper Cretaceous Two Medicine Formation of northwestern Montana: evidence for drought-related mortality. Palaios 5:394-413.

Rogers, R. R., C. C. Swisher, and J. R. Horner. 1993. 40Ar/39Ar age and correlation of the nonmarine Two Medicine Formation (Upper Cretaceous), northwestern Montana, USA. Canadian Journal of Earth Sciences 30:1066-1075.

Rogers, R. R., D. A. Eberth, and A. R. Fiorillo. 2007. Preface; pp. vii-x in R. R. Rogers, D. A. Eberth, and A. R. Fiorillo (eds.), Bonebeds: Genesis, analysis, and paleobiological significance. The University of Chicago Press, Chicago, Illinois.

Ryan, M. J., A. P. Russell, D. A. Eberth, and P. J. Currie. 2001. The taphonomy of a *Centrosaurus* (Ornithischia: Ceratopsidae) bone bed from the Dinosaur Park Formation (Upper Campanian), Alberta, Canada, with comments on cranial ontogeny. Palaios 16:482-506.

Scherzer, B. A., and D. J. Varricchio. 2010. Taphonomy of a juvenile lambeosaurine bonebed from the Two Medicine Formation (Campanian) of Montana, United States. Palaios 25:780-795.

Schmitt, J. G., F. D. Jackson, and R. R. Hanna. 2014. Debris flow origin of an unusual Late Cretaceous hadrosaur bonebed in the Two Medicine Formation of western Montana; pp. 486-501 in D. A. Eberth and D. C. Evans (eds.), Hadrosaurs. Indiana University Press, Bloomington, Indiana.

Scott, E. E., M. J. Ryan, and D. C. Evans. 2014. A *Gryposaurus* bone bed from the Oldman Formation (Campanian) of south-eastern Alberta with implications for dinosaur sociality. Geological Society of America Abstracts with Programs 46:13.

Shipman, P. 1975. Implications of drought for vertebrate fossil assemblages. Nature 257:667-668.

Varricchio, D. J. 1995. Taphonomy of Jack's Birthday Site, a diverse dinosaur bonebed from the Upper Cretaceous Two Medicine Formation of Montana. Palaeogeography, Palaeoclimatology, Palaeoecology 114:297-323.

Varricchio, D. J. 2011. A distinct dinosaur life history? Historical Biology 23:91-107.

Varricchio, D. J., and J. R. Horner. 1993. Hadrosaurid and lambeosaurid bonebeds from the Upper Cretaceous Two Medicine Formation of Montana: taphonomic and biologic implications. Canadian Journal of Earth Sciences 30:997-1006.

Varricchio, D. J., P. C. Sereno, Z. Xijin, T. Lin, J. A. Wilson, and G. H. Lyon. 2008. Mud-trapped herd captures evidence of distinctive dinosaur sociality. Acta Palaeontologica Polonica 53:567-578.

Voorhies, M. R. 1969. Taphonomy and population dynamics of an early Pliocene vertebrate fauna, Knox County, Nebraska. Contributions to Geology Special Paper No. 1, University of Wyoming 1:1-69.

Woodward, H. N., E. A. Freedman Fowler, J. O. Farlow, and J. R. Horner. in press. *Maiasaura*, a model organism for extinct vertebrate population biology: a statistically robust assessment of growth dynamics and survivorship. Paleobiology.

CHAPTER FOUR

A NEW SPECIES OF *GRYPOSAURUS* (DINOSAURIA: ORNITHISCHIA) FROM THE JUDITH RIVER FORMATION OF NORTHCENTRAL MONTANA

Contribution of Authors and Co-Authors

Manuscript in Chapter 4

Author: Elizabeth A. Freedman

Contributions: Conceived the study, performed the analyses, interpreted results, and wrote the manuscript.

Co-author: John R. Horner

Contributions: Conceived the study, provided funding and access to specimens and workspace, discussed implications of results, and edited earlier drafts of this manuscript.

Manuscript Information Page

Elizabeth A. Freedman, John R. Horner
Status of Manuscript:
_x_ Prepared for submission to a peer-reviewed journal
___ Officially submitted to a peer-reviewed journal
___ Accepted by a peer-reviewed journal
___ Published in a peer-reviewed journal

Abstract

A new species of *Gryposaurus* (Dinosauria: Ornithischia) is described from the Judith River Formation of northcentral Montana. Specimens were collected from a monodominant bonebed in a horizon equivalent to Unit 1 of the lower Oldman Formation of Alberta, stratigraphically intermediate between the positions of *G. latidens* and *G. notabilis*. The abundant cranial material is described, illustrated, and compared to the morphology of other *Gryposaurus* specimens, as well as being analyzed phylogenetically. *Gryposaurus reddingi*, sp. nov., is differentiated from other *Gryposaurus* species by a unique combination of characters: a wide posterior margin of the narial fenestra, as in *G. latidens* but not *G. notabilis*; and dentary tooth crowns with a height to width ratio of 2.07 to 2.39, intermediate between that of *G. latidens* and *G. notabilis*. The subadult nasal crest of *G. reddingi* is intraspecifically variable; two specimens have a gently curved nasal crest positioned dorsal to the posterior nasal fenestra, similar to adult *G. latidens*, and one specimen of *G. reddingi* has a more angled and anteriorly positioned nasal crest, similar to subadult *G. notabilis*. Changes in the position and shape of the nasal crest in *Gryposaurus* specimens are analyzed using geometric morphometrics, and the results are interpreted stratigraphically and ontogenetically. In the stratigraphically lowest *Gryposaurus* specimens, *G. latidens*, the nasal crest is low and anterior or dorsal to the posterior narial fenestra. The nasal crest is progressively higher and more posteriorly positioned in stratigraphically higher specimens. A similar trend is observed ontogenetically; small specimens have relatively anteriorly positioned low nasal crests that grow higher and migrate posteriorly in larger specimens of the same taxon. The

evolutionary trend of more posteriorly positioned nasal crests is continued in non-*Gryposaurus* members of the Kritosaurini such as *Naashoibitosaurus ostromi* and *Kritosaurus horneri*.

Introduction

Hadrosaur dinosaurs were one of the dominant groups of herbivores in Late Cretaceous ecosystems of western North America. Most genera of hadrosaurs possessed cranial crests composed at least partially of the nasals; these crests are generally interpreted as display structures (e.g, Padian and Horner, 2011). The hadrosaurine dinosaur *Gryposaurus* is distinguished by a nasal crest that forms an arch or peak above the posterior narial region of the skull. Unlike most other hadrosaurine genera, which include only one or two species, *Gryposaurus* contains three currently recognized species, and spans a time interval of more than four million years (Figure 4.1; Roberts et al., 2013).

The type species of the genus, *Gryposaurus notabilis*, was collected from the Dinosaur Park Formation in what is currently Dinosaur Provincial Park, Alberta, by Charles H. Sternberg in 1913, and described by Lambe (1914). In 1918, another *Gryposaurus* specimen was collected from the same area and described as *"Kritosaurus incurvimanus*" (Parks, 1919, 1920); this taxon is now considered to represent subadult *G. notabilis* (Prieto-Márquez, 2010a). A stratigraphically lower species, *G. latidens*, was collected by Brown et al. and Horner et al. in the lower Two Medicine Formation of Montana (Horner, 1992). The stratigraphically highest species, *G. monumentensis*, was

collected in the middle Kaiparowits Formation of Utah (Gates and Sampson, 2007). *Gryposaurus* is a member of the Kritosaurini, a clade that includes *Kritosaurus navajovius*, *Kritosaurus* ("*Anasazisaurus*") *horneri*, and *Naashoibitosaurus ostromi* (Brown, 1910; Lapparent and Lavocat, 1955; Hunt and Lucas, 1993; Prieto-Márquez, 2014).

This paper describes a new species of *Gryposaurus* that is stratigraphically and morphologically intermediate between *G. latidens* and *G. notabilis*. A monodominant bonebed in the Judith River Formation of Montana, Museum of the Rockies (MOR) locality JR-429, contains at least ten individuals of this new species; all specimens are curated under the number MOR 2573 and identified by their field numbers (e.g. MOR 2573-7-14-11-535). The large amount of disarticulated cranial material provided by the bonebed enables the first study of intraspecific variation within a single assemblage of *Gryposaurus* individuals, as well as elucidating aspects of *Gryposaurus* morphology that are inaccessible on fully articulated skulls. The stratigraphically intermediate position of this new species helps complete our understanding of the evolution of the *Gryposaurus* lineage.

Study Area

The JR-429 *Gryposaurus* bonebed is located in Kennedy Coulee, a fossiliferous exposure of the Judith River Formation (Late Cretaceous: Campanian) in Hill County, northcentral Montana, near the Milk River and the USA-Canada border. In Alberta, the Judith River Formation is termed the Belly River Group, and includes the Foremost,

Oldman, and Dinosaur Park Formations. These Albertan formations are further subdivided into members. The Judith River Formation deposits of northcentral Montana are not formally subdivided, but due to Kennedy Coulee's geographic proximity to Alberta and lithologic similarities of the deposits on both sides of the border, the terminology of the Albertan formations and their members can be used in Kennedy Coulee for high resolution stratigraphic correlations to localities in Alberta.

Kennedy Coulee exposes portions of the Judith River Formation equivalent to the uppermost Foremost Formation and lowermost Oldman Formation of Alberta. The lower third of the Kennedy Coulee section contains a thick coal, termed the Marker A Coal, which is used as a datum horizon throughout Kennedy Coulee. The Marker A Coal is equivalent to the top of the Taber Coal Zone of the Foremost Formation. The middle portion of the Kennedy Coulee section is a thick white-gray amalgamated channel complex equivalent to the Herronton Sandstone Zone that forms the top of the Foremost Formation (sensu Eberth, 2005). The JR-429 *Gryposaurus* bonebed is located in the mudstone-dominated upper portion of the Kennedy Coulee section, which is equivalent to Unit 1 of the lower Oldman Formation (Figure 4.2). These correlations are supported by the biostratigraphy of freshwater ray teeth. All ray teeth collected throughout Kennedy Coulee are referable to *Pseudomyledaphus* sp. (Freedman Fowler and Horner, Chapter Two); in Alberta, this taxon is only found in the Foremost and lowermost Oldman Formations (Peng et al., 2001; Brinkman et al., 2004; Kirkland et al., 2013).

Institutional Abbreviations

AMNH FARB, American Museum of Natural History (Fossil Amphibians, Reptiles, and Birds collection), New York, New York, U.S.A.; **BYU**, Brigham Young University, Provo, Utah, U.S.A.; **CMN/NMC**, Canadian Museum of Nature, formerly National Museum of Canada, Ottawa, Ontario, Canada; **MOR**, Museum of the Rockies, Bozeman, Montana, U.S.A.; **MSNM**, Museum Civico di Storia Naturale di Milano, Milan, Italy; **NMMNH**, New Mexico Museum of Natural History and Science, Albuquerque, New Mexico, U.S.A.; **RAM**, Raymond M. Alf Museum, Claremont, California, U.S.A.; **ROM**, Royal Ontario Museum, Toronto, Ontario, Canada; **TMP**, Royal Tyrrell Museum of Paleontology, Drumheller, Alberta, Canada; **UM**, University of Montana, Missoula, Montana, U.S.A.; **UMNH VP**, Utah Museum of Natural History Vertebrate Paleontology, Salt Lake City, Utah, U.S.A..

Materials and Methods

The MOR 2573 *Gryposaurus* specimens were collected from the JR-429 bonebed by Museum of the Rockies crews using standard paleontology field techniques (Leiggi et al., 1994) on privately owned land. MOR 2573 was generously donated to the Museum of the Rockies by Dan and Lila Redding. No permits were required for the described study, which complied with all relevant regulations.

The MOR 2573 material consists of approximately 800 hadrosaur fossil specimens; all diagnostic specimens are referable to *Gryposaurus*. There is no evidence for a second hadrosaur taxon within the bonebed. Aside from vertebrate microfossil

material, only two non-hadrosaur bones were present in the JR-429 bonebed: a theropod femur (Ornithomimidae or Oviraptorosauria) and a badly crushed tyrannosaur centrum. The taphonomy of the JR-429 *Gryposaurus* bonebed is described in a separate paper (Freedman Fowler, Chapter Three). The minimum number of *Gryposaurus* individuals within the bonebed is ten: four juveniles, five subadults, and one adult.

In this paper, the terms "juvenile", "subadult", and "adult" are applied to specimens based solely on their sizes, using the classification system of Evans (2010). Juveniles are less than 50% the size of the largest individual of the taxon. Subadults are 50-85% the size of the largest individual of the taxon. Adults are 85-100% the size of the largest individual of the taxon. These terms are used for convenience when discussing the relative sizes of specimens, but are merely hypotheses for the actual ontogenetic stages of specimens, and should not be used for interpretations of the sexual or skeletal maturity or immaturity of a specimen. Three MOR 2573 subadult tibiae have been histologically sectioned, and are interpreted as being two to three years of age (Freedman Fowler, Chapter Three). Aside from the MOR 2573 specimens, no other *Gryposaurus* specimens have been histologically examined for ontogenetic information.

Terminology in this paper follows traditional conventions and definitions of Hadrosauridae and Hadrosaurinae (Horner et al., 2004) rather than the proposed alternate names of Saurolophidae and Saurolophinae (Prieto-Márquez, 2010b) for reasons of taxonomic stability as detailed in Gates et al. (2011).

MOR 2573 was compared morphologically to other hadrosaurine specimens and casts at MOR, NMMNH, ROM, TMP, and UMNH, as well as published descriptions.

Measurements were taken directly from the specimens or casts using a tape measure or digital calipers. Museum of the Rockies specimens from multi-individual bonebeds are identified using a combination of specimen number and field number, e.g. MOR 2573-7-14-11-535, where MOR 2573 is the inclusive number for all hadrosaur specimens from the JR-429 bonebed, 7-14-11 is the date the bone was found, and 535 indicates that it was the 535th bone collected from the bonebed.

MOR 2573 was coded into the phylogenetic matrix of Prieto-Márquez (2014), which was a modification of his earlier matrix (2010b), with some character states for *Gryposaurus latidens* updated (Prieto-Márquez, 2012) and extraneous lambeosaurine taxa removed to simplify the analysis. *Equijubus normani* was used as the outgroup. The matrix contained 35 taxa and 265 unordered unweighted characters. One character state for *G. latidens* was altered: character 96 (J2) of Prieto-Márquez (2014), the caudodorsal height of the rostral process of the jugal, coded *G. latidens* as state 0, but the dorsal process is actually broken and the unbroken height of the specimen (MOR 478) would be state 1 as with all other hadrosaurines. One character state for *G. notabilis* was altered: character 124 (SQ3) of Prieto-Márquez (2014), the separation of the squamosals by the posterior parietal, coded *G. notabilis* as state 1, a narrow band of parietal separating the squamosals, but this is only true for AMNH FARB 5350. The holotype of *G. notabilis*, CMN 2278, has a wide parietal separation of the squamosals, state 1. Accordingly, the state for *G. notabilis* has been altered from only 1 to both 0 and 1.

The matrix was analyzed with parsimony in PAUP 4.0b10 (Swofford, 2002) within a heuristic search of 5,000 replicates using ACCTRAN optimization and tree

bisection-reconnection swapping to produce a strict consensus tree, followed by a bootstrap analysis using a heuristic search of 5,000 replicates.. The complete PAUP settings used are provided in the nexus file (Appendix I). The strict consensus tree was plotted using FigTree 1.4.0 (Rambaut, 2006-2012).

Landmark-based geometric morphometrics was used to analyze the shape of the nasal crest, its position relative to the external naris, and the width of the external naris. Geometric morphometric analysis was not performed on the whole skull because several *Gryposaurus* specimens are disarticulated, and some are simply isolated nasals. All geometric morphometric analyses were performed within the "geomorph" package (version 2.1.1; Adams and Otárola-Castillo, 2013) in the R language and environment for statistical computing, version 3.1.2 for Mac OSX (http://www.R-project.org/; R_Core_Team, 2014). The 19 specimens used in the geometric morphometric analysis are listed in Table 4.1 and illustrated in Figure 4.3. Left nasal images were flipped horizontally to appear as right nasals for comparative purposes, because slightly more of the nasals used in the geometric morphometric analysis were rights.

Because some specimens are articulated skulls and others are disarticulated, and sometimes isolated, nasals, landmark selection was restricted to points visible on both articulated and disarticulated nasals. Six landmark points were used in the geometric morphometric analysis (Figure 4.4). 1) Posteriormost extent of nasal in lateral view. 2) Lowest point between nasal crest and posteriormost extent of nasal. 3) Maximum extent of nasal crest, marked as the point of maximum curvature. 4) Contact point of nasal and posteroventral process of premaxilla along the external narial margin. 5)

Posterodorsalmost extent of the external naris, marked as the point of maximum curvature. 6) Point on opposite side of naris from point 4, representing the width of the external naris. If a line is drawn from point 4 to point 6, then a perpendicular line drawn from point 5 will bisect that line. A seventh point representing the dorsal contact between the nasal and posterodorsal process of the premaxilla was initially tested, but due to this area being broken in many specimens, it was not included in the final analysis.

The following functions within the "geomorph" package in R were utilized (Adams and Otárola-Castillo, 2013; R_Core_Team, 2014). Landmarks were digitized within the R program using "digitize2d". Because the narial margin of the *Gryposaurus monumentensis* holotype, RAM 6797, is broken, the missing points were estimated using "estimate.missing". Generalized Procrustes analysis using the function "gpagen" rotated and scaled nasals to the same orientation and centroid size, leaving only shape differences among specimens. The resulting Procrustes coordinates were analyzed in a Principal Components Analysis (function "plotTangentSpace").

Systematic Paleontology

Dinosauria Owen, 1842

Ornithischia Seeley, 1888

Ornithopoda Marsh, 1881

Hadrosauridae Cope, 1869

Hadrosaurinae Cope, 1869

Kritosaurini Lapparent and Lavocat, 1955

Gryposaurus Lambe, 1914

Type Species. *Gryposaurus notabilis* Lambe, 1914

Holotype. CMN 2278

Referred Material. AMNH FARB 5350, AMNH FARB 5465, CMN 8784, MOR 399, MOR 478, some of the MOR 553 specimens, MOR 2573, MSNM V345, RAM 6797, ROM 764, ROM 873, ROM 1939, TMP 1980.022.0001, UM 5204, UMNH 13970, UMNH 18568.

Horizons and Localities. The Campanian (Late Cretaceous) Dinosaur Park, Judith River, Kaiparowits, and Two Medicine Formations of Alberta, Montana, and Utah. See Table 4.1 for detailed locality information and references for each specimen.

Revised Diagnosis. Hadrosaurid dinosaur with the following autapomorphies listed in Prieto-Márquez (2010a), which were modified from those of Horner (1992) and Gates and Sampson (2007): "nasal bearing a protuberance anterior to the orbits, which is arcuate in many but not all specimens, and that rises above the level of the frontal in adults; dorsolateral flaring on the medial margin of the posteroventral process of the premaxilla; posterodorsal margin of the circumnarial depression gently incised and located dorsal to the anterior half of the lacrimal; and nasofrontal suture characterized by a small median nasal process inserting between the midline of the frontals." Note that the thickness of the paraoccipital process has been removed from the autapomorphy list of Prieto-Márquez (2010a).

Remarks. Prieto-Márquez (2010a) added the great thickness of the proximodorsal ridge of the paraoccipital process of the exoccipital to the diagnosis of *Gryposaurus*. However, the proximodorsal ridge of the paraoccipital process of the exoccipital in MOR 2573 specimens is not notably thick, and instead is similar to the thickness in *Naashoibitosaurus ostromi* NMMNH P-16106. Thus, this character is removed from the diagnosis of *Gryposaurus*.

Gryposaurus reddingi, sp. nov.

(Figures 4.5-4.8, 4.10-4.26)

Holotype. Left nasal MOR 2573-7-14-11-535 and its corresponding posterior fragment of the same element MOR 2573-7-14-11-534.

Referred Material. All *Gryposaurus* material MOR 2573 from the JR-429 bonebed.

Etymology. Species name *reddingi* in honor of Dan Redding, discoverer of the *Gryposaurus reddingi* bonebed JR-429, who with his wife Lila Redding and family donated the specimen and have been friends and supporters of paleontological research for decades.

Horizon and Locality. MOR 2573 was collected from a monodominant bonebed, JR-429, on private land north of Rudyard in Hill County, Montana. The site is located in Kennedy Coulee in the Judith River Formation, in a mudstone horizon equivalent to Unit 1 of the lower Oldman Formation of Alberta. The bonebed horizon is 26.6 m above the

top of the Marker A Coal that marks the top of the Taber Coal Zone of the Foremost Formation (Figure 4.2). The horizon is bracketed by published radiometric ages of 78.2 ± 0.2 Ma and 78.5 ± 0.2 Ma (Goodwin and Deino, 1989); these dates have been recalibrated to 78.71 ± 0.2 Ma and 79.02 ± 0.2 Ma by Roberts et al. (2013).

Diagnosis. Hadrosaurid dinosaur of the genus *Gryposaurus* that exhibits the following unique combination of characters intermediate between *Gryposaurus latidens* and *G. notabilis*: wide posterior margin of the narial fenestra as in *G. latidens* but not *G. notabilis*; dentary tooth crown height to width ratio ranging between 2.07 and 2.39, intermediate between the tooth dimensions of *G. latidens* and *G. notabilis*; and pronounced concavity of the ventral jugal margin similar to *G. notabilis* but not *G. latidens*.

Osteological Description

The intent of this morphologic description is threefold: 1) to document the differences between *Gryposaurus reddingi* and other *Gryposaurus* species; 2) to illustrate the intraspecific and taphonomic preservation variation among elements from the same bonebed; and 3) to note major differences between *Gryposaurus* and other hadrosaurine taxa. The previously published *Gryposaurus* species have been thoroughly described elsewhere: *G. latidens* (Horner, 1992; Prieto-Márquez, 2012); *G. notabilis* including *G.* "*incurvimanus*" (Lambe, 1914; Parks, 1920; Vialli, 1960; Pinna, 1979; Prieto-Márquez, 2010a); and *G. monumentensis* (Gates and Sampson, 2007). Thus, aspects of morphology that do not vary among *Gryposaurus* species, and are also present in *G. reddingi*, need

not be duplicated here. Instead, this description will highlight instances where *G. reddingi* differs from one or more *Gryposaurus* species.

Table 4.1 lists specimens of *Gryposaurus* and other Kritosaurini that include nasals and were used for comparative purposes. Because the nasal is an important bone in determining species within Kritosaurini, specimens without nasals, or with only partial nasals, are generally difficult to assign to a species. The TM-068 Jack's Birthday Site bonebed includes several disarticulated skull elements referable to *Gryposaurus* (all within the MOR 553 catalog number), but does not include elements diagnostic to a specific species of *Gryposaurus*, thus limiting its comparative utility. A single Kritosaurini nasal from the bonebed, MOR 553-7-2-8-26, is from a small individual of unique morphology and undetermined taxonomic affinity (see results of geometric morphometric analysis).

Table 4.1 also lists whether specimens are mostly articulated or disarticulated; the majority of described *Gryposaurus* specimens are fully or mostly articulated. Many characters used in cladistic analysis require the specimen to be either articulated or disarticulated. The morphology of a contact surface between two bones, such as the jugal-maxilla contact, requires a disarticulated specimen. In an articulated skull, many bones are only visible in limited views, e.g. lateral or dorsal view but not medial view. Characters relating to the shape of the skull or its regions, such as the shape of the infratemporal fenestra, require an articulated skull or the disarticulated remains of a single individual; a composite specimen assembled from a multi-individual bonebed may not be as accurate as an articulated skull. Morphologic comparisons are made with

holotypes as much as possible, but for many characters not preserved or observable on the holotypes, referred specimens have to be compared.

Thorough comparison of MOR 2573 to specimens of other *Gryposaurus* species would ideally be based on disarticulated skull material that includes nearly every element; such complete but disarticulated material, whether from a bonebed or a single individual, does not currently exist for any *Gryposaurus* specimen besides MOR 2573. Incomplete disarticulated specimens of described taxa include *G. latidens* MOR 478, *G. notabilis* ROM 1939, and *G. monumentensis* UMNH VP 13970. Incomplete disarticulated specimens currently assigned to *Gryposaurus* sp. include MOR 399, MOR 553, and UM 5204. As a result of the limited availability of disarticulated *Gryposaurus* material from described species, MOR 2573 specimens were also compared, when relevant, to disarticulated material of *Prosaurolophus blackfeetensis* (MOR 447 and holotype MOR 454) from the TM-041 bonebed (Horner, 1992). In the most recent phylogenetic analyses of *Gryposaurus* (Prieto-Márquez, 2012, 2014), the *Prosaurolophus-Saurolophus* clade is the sister clade to the Kritosaurini. Taxa such as *Edmontosaurus* and the Brachylophosaurini (*Acristavus*, *Maiasaura*, *Brachylophosaurus*) are more distantly related.

Size Classes

The JR-429 bonebed includes three size classes of individuals. The largest size class, termed “adult” only includes one bone, a very large rib head. Due to the lack of additional adult material for determining the relative sizes of individuals within the bonebed, a proxy for adult size is required. A partial large *Gryposaurus* skull, UM 5204,

was collected from another site in Kennedy Coulee, and represents the stratigraphically and geographically closest *Gryposaurus* specimen to the JR-429 bonebed. Although the specimen lacks a nasal and other elements diagnostic to the species level, it is the best proxy for the largest known adult size of the taxon found in the JR-429 bonebed, *G. reddingi* (MOR 2573).

As detailed in Freedman Fowler (Chapter Three), the jugal is the element that is best preserved in the smaller and larger non-adult size classes of MOR 2573 as well as UM 5204. The smaller size class jugal is 42.5% the size of UM 5204, and the larger non-adult size class jugal is 80.8% the size of UM 5204 (Freedman Fowler, Chapter Three). The quadrates of the smaller size class are all broken in half, so the height of a small quadrate cannot be measured. The smaller size class quadrate height range is estimated to be approximately 17 to 24 cm, making the smaller size class between 39.8% and 56.2% the height of the UM 5204 quadrate (42.7 cm). The most complete quadrate of the larger non-adult size class is 33.4 cm high, and therefore 78.2% the size of UM 5204. Thus, specimens of the smaller size class should most likely to be categorized as large juveniles in the size-based categorization of Evans (2010), and specimens of the larger non-adult size class are categorized as large subadults. The subadult status of the larger non-adult size class is supported by tibial osteohistology that suggests that members of this size class are approximately three years old and still rapidly growing (Freedman Fowler, Chapter Three). Most morphologic descriptions of MOR 2573 material will refer to specimens of the subadult size class, which has the most abundant cranial material (Figure 4.5). When juvenile specimens are described, they will be clearly labeled as such.

Maxillary/Facial Complex

Premaxilla. MOR 2573 includes four partial premaxillae (Figure 4.6). MOR 2573-6-10-10-304, a left premaxilla, is relatively the most complete. Two right premaxillae, MOR 2573-7-11-06-142A and MOR 2573-8-07-12-644 preserve the main anterior body of the premaxilla, but the distal processes are broken. MOR 2573-6-23-12-681 is a fragment of the main anterior body of a left premaxilla. These specimens are laterally compressed, so the width of the paired premaxillae in life is unknown; the compressed width of MOR 2573-6-10-10-304 paired with MOR 2573-7-11-06-142A is 10.4 cm. In dorsal view, the oral margins are gently curved.

The lateral compression and broken processes limit comparisons to other *Gryposaurus* taxa. The premaxillae of *G. latidens* AMNH FARB 5465 are dorsoventrally compressed, but even after accounting for their different compression directions, the MOR 2573 specimens could not have been as relatively wide as the premaxillae of *G. latidens* AMNH FARB 5465. Because the posteroventral processes are broken in MOR 2573 specimens, it is unknown whether a dorsal flange protruded into the naris midway along the posteroventral process of the premaxilla, as it does in *Gryposaurus* and *Rhinorex* (Gates and Sampson, 2007; Gates and Scheetz, 2014).

The anteroventral oral margin is rugose as in *G. monumentensis* RAM 6797 (Gates and Sampson, 2007). The double denticulate layer on the anteriormost ventral surface is similar to that in *G. latidens* AMNH FARB 5465 (Prieto-Márquez, 2012), but the denticles in MOR 2573 specimens are more prominent. There is an excavation on the anteriormost part of the medial surface of the MOR 2573 premaxillae.

Nasal. Multiple nasal specimens are present in MOR 2573 (Figure 4.7). Many of the nasals are broken into anterior and posterior portions, some of which were preserved in close proximity, whereas other nasal fragments were isolated. The holotype of *Gryposaurus reddingi* is the most complete and best preserved nasal (Figure 4.7A-4.7B), but it was found broken into two portions 25 cm apart in the bonebed deposit. MOR 2573-7-14-11-535 is the anterior portion, and MOR 2573-7-14-11-534 is the posterior portion. Due to their orientations in the sediment, the anterior portion was slightly mediolaterally compressed and the posterior portion was slightly dorsoventrally compressed, so although the contact surfaces demonstrate that the two pieces are certainly halves of the same bone, they are unable to be glued together as a single specimen. Another pair of nasal halves, anterior portion MOR 2573-7-18-06-186 and posterior portion MOR 2573-6-03-10-271 appear to match together, but were found 5.75 m apart in the bonebed, so it is not certain if they are truly halves of the same bone (Figure 4.7E-4.7F).

Three fragments of juvenile nasals are present in MOR 2573: two posterior fragments MOR 2573-7-10-10-412 and MOR 2573-6-29-12-709, and one fragment of the posterior narial region MOR 2573-7-16-11-539 (Figure 4.7K-4.7Q). This fragment of the narial region preserves a small amount (3.5 cm) of the nasal crest (Figure 4.7K). This is not enough to determine the shape of the nasal crest or position of its apex. However, the dimensions of this juvenile fragment are proportionately different than the subadult nasals. The juvenile fragment is preserved more three-dimensionally (Figure 4.7M) than the subadult nasals, which are mediolaterally compressed. The juvenile medial internasal

suture has an anteroposteriorly longitudinally oriented groove along its ventral margin merging with smaller subparallel grooves (Figure 4.7L). The dorsal part of the internasal suture has diagonal anteroventral to posterodorsal low ridges and shallow grooves. In the subadult nasals (Figure 4.7B, 4.7D, 4.7F), there is not a separate major longitudinal groove along the ventral margin of the internasal suture, and the suture is composed of many subparallel low ridges and shallow grooves oriented longitudinally along the nasal, similar to the nasals of *Gryposaurus latidens* AMNH FARB 5465 and MOR 478-7-2-7-3.

The juvenile specimens of MOR 2573 typically range from 58% to 68% the size of the subadult specimens (Freedman Fowler, Chapter Three). The size of the juvenile nasal fragment MOR 2573-7-16-11-539, measured as the vertical distance from the dorsal edge of the premaxillary articulation to the dorsal margin of the narial fenestra, is 49% that of subadult nasal MOR 2573 6-21-06-63. Although this lateral portion of the juvenile nasal is slightly smaller than the size predicted for juveniles, the dorsoventral thickness of the medial internasal suture is relatively much smaller than predicted. Directly dorsal to the posteriormost extent of the nasal margin, the internasal suture in juvenile MOR 2573-7-16-11-539 (13 mm high) is 43% of the suture in MOR 2573 6-21-06-63 (30 mm). However, more anteriorly, where the apex of the nasal crest is located in the subadult, the internasal suture in juvenile MOR 2573-7-16-11-539 (12 mm high) is 24% of the suture in MOR 2573 6-21-06-63 (51 mm). Anterior to this peak in the juvenile, the nasal rapidly thins dorsoventrally. Only the anterior tip is broken; most of the sharp decrease in nasal height anteriorly is accurate. This suggests that in the juvenile of *Gryposaurus reddingi*, the dorsoventral thickness of the nasal is relatively smaller than

in subadults, consistent with the trend of nasal crests becoming larger (dorsoventrally higher) ontogenetically.

The nasal crest in *Gryposaurus* species is a dorsal enlargement of the nasal that forms an arch or peak; the anteroposterior location of this arch, its dorsoventral height, being a smooth curve or more sharply angled, and the degree of curvature along the dorsal margin of the arch all vary (Figure 4.3). In two *G. reddingi* specimens, left nasal MOR 2573-7-14-11-535 with posterior fragment MOR 2573-7-14-11-534, and right nasal MOR 2573-7-18-06-186 and posterior fragment MOR 2573-6-03-10-271, the nasal arch is low, with its dorsal peak in lateral view located approximately between the dorsalmost and posteriormost extent of the narial fenestra. The third well preserved *G. reddingi* nasal, MOR 2573-6-21-06-63, has a nasal crest dorsal peak in lateral view located anterior to the dorsalmost extent of the narial fenestra. These three subadult nasals are approximately the same size, illustrating individual variation in the position of the peak of the nasal arch. Anterior to the peak of the nasal crest, the nasals of MOR 2573 are relatively dorsoventrally thicker than in any other *Gryposaurus* specimens.

The nasal crest in the *Gryposaurus latidens* holotype AMNH FARB 5465 is long, low, and gently curving, and its dorsal peak occurs approximately dorsal to the posteriormost extent of the narial fenestra. However, in the slightly smaller *G. latidens* specimen MOR 478-7-2-7-3, the nasal crest is more sharply angled, and its dorsal peak is located dorsal to the dorsalmost extent of the narial fenestra. In subadult *G. notabilis* specimens (ROM 764, TMP 1980.022.0001, ROM 1939), the first two of which were previously described as *G. incurvimanus*, the dorsal nasal is nearly horizontal, with a

peak located anterior to the dorsalmost extent of the narial fenestra. The peak is distinctly angled rather than being gently curved. Thus, two of the *G. reddingi* nasals are similar to adult *G. latidens*, and one of the *G. reddingi* nasals is similar to subadult *G. notabilis*.

In adult *G. notabilis* (CMN 2278, ROM 873, MSNM V345), and both subadult and adult *G. monumentensis* (RAM 6797, UMNH VP 13970), the nasal crest is relatively taller, with its dorsal peak located well posterior to the posterior extent of the narial fenestra; this results in a strong concavity at the posterior end of the nasal crest where its curve rises steeply from the posteriormost nasal. The dorsal nasal arch of *Rhinorex condrupus*, the taxon most closely related to *Gryposaurus* (Gates and Scheetz, 2014), is located posterior to the posteriormost margin of the narial fenestra; its dorsal curvature is most similar to that of *G. notabilis*. Other members of the Kritosaurini have distinctly different nasal crests from *Gryposaurus*. *Naashoibitosaurus ostromi* (NMMNH P-16106) has an elongated nasal crest located posterior to the posteriormost narial fenestra. The nasal crest in *Kritosaurus* ("*Anasazisaurus*") *horneri* (BYU 12950) is even more posteriorly elongated, and is unique among Kritosaurini in the peak of the nasal crest extending more posteriorly than its base, creating a posteriorly-directed nasal crest. For further comparisons of the nasal crests of *Gryposaurus* and other Kritosaurini, please see the geometric morphometrics results and discussion.

The posterior nasals do insert medially between the anterior frontals, but the exact shape of the articulation varies (see frontal description). The prefrontal articulation surface of the nasal is excavated slightly more deeply in all MOR 2573 specimens than it is in either specimen of *G. latidens* (AMNH FARB 5465, MOR 478-7-2-7-3).

The articulation surface on the subadult nasals of MOR 2573 for the posteroventral process of the premaxilla is a slightly medially depressed shelf. The ridge defining the dorsal edge of this shelf is most laterally prominent starting 2 cm posterior to the narial fenestra. In the juvenile nasal MOR 2573-7-16-11-539 as well as the adult *Gryposaurus latidens* holotype left nasal AMNH FARB 5465, the anteriormost portion of the dorsal shelf edge forms a ventrolaterally overhanging lip.

The circumnarial depression is not well defined in the MOR 2573 nasals, similar to other *Gryposaurus* species (Prieto-Márquez, 2010a). It is present as a slight depression or groove oriented anterodorsally to posteroventrally; the anterodorsal end nears the apex of the nasal crest, and the posteroventral end is located at least 1 cm posterior to the narial foramen. These two halves of the groove meet at a small foramen that is dorsal or caudodorsal to the posteriormost narial foramen.

Maxilla. Eight nearly complete maxillae (seven subadult, one juvenile) of MOR 2573 have been collected (Figure 4.8). Their shapes vary slightly due to some maxillae being laterally compressed, whereas others were compressed from a more dorsolateral direction. The effects of differential compression are especially noticeable in the orientation of the jugal articulation surface; in most specimens this surface is oriented more laterally than dorsally, but in MOR 2573-7-22-10-447 and the juvenile maxilla MOR 2573-7-31-10-359A the jugal articulation surface is mainly on the dorsal side of the specimens. Therefore, caution should be used when analyzing the orientation of this surface in an isolated maxilla specimen; diagenetic compression may be distorting the taxonomic signal.

The anterodorsal processes are broken on most MOR 2573 specimens, but those that are preserved are similar to the anterodorsal process of *Gryposaurus latidens* maxillae MOR 478-5-28-8-1 and MOR 478-5-24-8-7, and that of subadult *G. notabilis*, TMP 1980.022.0001. The complete length of the anterodorsal process is not preserved in any MOR 2573 specimen, and the premaxillary caudoventral processes are also broken, so it is unknown whether the anterodorsal process of the maxilla would have been visible in the narial fenestra in lateral view. Other described *Gryposaurus* specimens are articulated, so the anterodorsal process and jugal articulation surface cannot be easily observed.

The dorsal jugal tubercle is very prominent in MOR 2573 maxillae and protrudes relatively high (1 cm) from the jugal articulation surface, almost identical to the right maxilla of subadult *G. notabilis*, TMP 1980.022.0001. The dorsal jugal tubercle of *G. latidens* MOR 478-5-24-8-7 is also 1 cm high. That of *G. latidens* MOR 478-5-28-8-1, has also been described as "very prominent" (Prieto-Márquez, 2012) although it has been diagenetically compressed and is only elevated approximately 5 mm. The dorsal jugal tubercle is present but less pronounced (5 mm) in *Prosaurolophus blackfeetensis* (MOR 454). The maxillae of MOR 553 TM-068 bonebed that have been previously assigned to *Gryposaurus* sp. (Varricchio, 1995) have dorsal jugal tubercles that are as prominent as those of MOR 2573 and TMP 1980.022.0001, supporting their assignment to *Gryposaurus* rather than *Prosaurolophus*, which is also present in the bonebed. A dorsal jugal tubercle is also present in *Edmontosaurus* (MOR 601, MOR 1609), but it is a lower eminence that rises gradually from the articular surface rather than the distinct protrusion

of the tubercle in *Gryposaurus*. The dorsal jugal tubercle is small but present in *Acristavus gagslarsoni* (MOR 1155), but is reduced or absent in other members of the Brachylophosaurini: *Brachylophosaurus canadensis* (MOR 1071), *Maiasaura peeblesorum* (OTM F138), and MOR 2919 (Freedman Fowler and Horner, Chapter Two).

The height of the dorsal process of the maxilla is similar in the MOR 2573 specimens, *G. latidens* MOR 478-5-28-8-1, and subadult *G. notabilis* ROM 764 and TMP 1980.022.0001. The dorsal process of the maxilla is relatively higher dorsoventrally in adult *G. notabilis* CMN 2278 and ROM 873, and *G. monumentensis* RAM 6797.

MOR 2573 maxillae have five or six lateral maxillary fenestrae (ventral and anterior to the jugal articulation), and their positions are variable among specimens. The anteriormost fenestra is usually the largest, and the posteriormost is usually the second largest. The middle fenestrae vary in their spacing, dorsoventral position, and size.

The marginal denticles of the maxillary teeth are rounded papillae on the apical half of the diamond-shaped tooth crown. The subadult maxillae contain 34 to 39 tooth rows. The juvenile maxilla MOR 2573-7-31-10-359A is broken anteriorly and contains at least 20 tooth rows, and is estimated to have up to 25 tooth rows. Comparisons of the number of tooth rows to the total tooth battery length in *G. reddingi*, *G. latidens*, and *G. notabilis* are available in Table 4.2 and Figure 4.9. The relatively large sample size of *G. reddingi* maxillae illustrates the range of intraspecific variation in tooth row densities.

Jugal. MOR 2573 includes one well preserved subadult jugal, MOR 2573-6-18-06-48, one well preserved juvenile jugal, MOR 2573-7-17-06-181, and several partial

subadult jugals (Figure 4.10). The morphology of the subadult jugals is remarkably consistent. The juvenile jugal differs from the subadults in having a relatively narrower ventral margin of the infratemporal fenestra and slightly more concave ventral jugal margin. The rugosity of the maxillary articulation surface is also relatively greater in the juvenile. They also differ in their character states for character 103 (J11) in Prieto-Márquez (2014): the caudal constriction is notably thicker than the rostral constriction in the juvenile, with a ratio of 1.42, character state 2; these constrictions are relatively similar heights in the subadult, with a ratio of 0.96, character state 0. To avoid the ontogenetic complications of including juvenile specimens in a phylogeny, only the subadult character state (0) was used in the phylogenetic analysis. Because the ratio of 0.96 is so close to 1.00, the boundary between states 0 and 1, individual variation in additional specimens collected in the future from the same bonebed may incorporate both states 0 and 1.

The ratio of the height of the caudoventral flange to the minimum height of the caudal constriction, character 100 (J8) in Prieto-Márquez (2014), codes as three different states in the three measureable jugals of MOR 2573. The complete subadult jugal MOR 2573-6-18-06-48 has a ratio of 1.43, character state 1. MOR 2573-6-12-06-10, which is missing its anterior half but is otherwise well preserved, has a ratio of 1.59, character state 2. The juvenile jugal MOR 2573-7-17-06-181 has a ratio of 1.22, state 0. Only the subadult character states (1 and 2) were used in the phylogenetic analysis.

The MOR 2573 specimens differ from *Gryposaurus latidens* MOR 478-6-10-87-2 in having concave ventral jugal margins; the ventral margin is nearly straight in *G.*

latidens. The concavity of the ventral jugal margin in MOR 2573-6-18-06-48 and MOR 2573-6-12-06-10 is more similar to that of subadult and adult *G. notabilis* CMN 2278, ROM 873, ROM 764, and TMP 1980.022.0001, but is much more shallow than that of *G. monumentensis* RAM 6797.

The ventral margin of the rostral process of MOR 2573-6-18-06-48 is subtly sinusoidal, similar to that of *G. latidens* MOR 478-6-10-87-2, one adult *G. notabilis* CMN 2278, one subadult *G. notabilis* TMP 1980.022.0001, and *G. monumentensis* RAM 6797. However, the ventral margin of the rostral process is strongly sinusoidal in another adult *G. notabilis* ROM 873 and subadult *G. notabilis* ROM 764. The lacrimal process of the rostral process of MOR 2573-6-18-06-48 is similar to that of *G. latidens* MOR 478-6-10-87-2.

Lacrimal. Two left lacrimals of MOR 2573 are preserved (Figure 4.11). MOR 2573-6-21-06-74 displays a typical *Gryposaurus* lacrimal morphology of being a mediolaterally thin and anteriorly elongated triangle. MOR 2573 6-21-06-67 is slightly larger, and has an unusual outline due to the anterior process being broken along its dorsal, ventral, and anterior margins. Part of the jugal process on MOR 2573-6-21-06-74 is broken; this process is complete on MOR 2573 6-21-06-67.

The main morphologic difference between the two specimens that cannot be attributed to fracturing is the width of the ventral margin in ventral view. The ventral margin in MOR 2573-6-21-06-74 is mediolaterally wide with a flat to slightly concave ventral surface. It is, mediolaterally, the widest portion of the lacrimal. The only portion of the ventral edge of MOR 2573 6-21-06-67 that appears unbroken tapers mediolaterally

to a thin ventral margin. MOR 2573 6-21-06-67 also has a curving depression on its lateral surface leading dorsally from the ventral margin. No similar depressions are noted on other *Gryposaurus* lacrimals, suggesting that this may be pathologic. The broken edges of MOR 2573 6-21-06-67 are abraded, so the absence of a pathologic bone texture in the curving depression may be due to abrasion.

In posterior view, the lacrimals of MOR 2573 are widest ventrally, and narrowest dorsally. Their broken areas make detailed comparisons with other *Gryposaurus* specimens difficult, but the MOR 2573 lacrimal morphology is generally consistent with other *Gryposaurus* specimens.

Prefrontal. Two prefrontals of MOR 2573 are preserved (Figure 4.12). The lateral orbital margin of MOR 2573-7-05-06-122 is rugose along its entire length, whereas the lateral orbital margin of MOR 2573-6-05-10-290 is a simple ridge anteriorly, with increasing rugosity posteriorly. The anterodorsal corner of the orbit in each prefrontal forms an angle of 115 degrees. The angle is intraspecifically variable; it is 130 degrees in *Gryposaurus notabilis* CMN 2278, and 100 degrees in the prefrontal of *G. notabilis* AMNH 5350 (Prieto-Márquez, 2010a).

When articulated with the nasals in dorsal view, the prefrontals and nasals of MOR 2573 each represent approximately 50% the width of the skull roof, similar to the *G. notabilis* holotype CMN 2278. Other specimens of G. *notabilis*, AMNH FARB 5350 and TMP 1980.022.0001, have slightly wider nasals relative to the prefrontals. All of these *Gryposaurus* prefrontals are unlike the wide medial wings of the prefrontals in

Naashoibitosaurus NMMNH P-16106 that cover two-thirds of the skull width (Horner, 1992; Prieto-Márquez, 2014).

Postorbital. Two right postorbitals of MOR 2573 are preserved (Figure 4.13). The lateral orbital margin is rugose only along the dorsal orbital margin in both specimens. The lateral surface of the jugal process in each is very slightly concave, as in other *Gryposaurus* species. The ornamentation of the lateral surface of the jugal process is intraspecifically variable. MOR 2573-6-29-12-704 has a series of short (2 to 4 mm) raised vertical lines ornamenting the posterior half of the lateral surface of the jugal process. MOR 2573-7-11-06-144 has a partially damaged lateral surface, but the preserved portion suggests that the ornamentation did not extend as far dorsally, and was more subtle than that of MOR 2573-6-29-12-704. The lateral surface of the jugal process of the postorbital is intraspecifically variable in *G. notabilis* as well. The lateral surface is relatively smooth in CMN 2278 but rugose in ROM 873; the postorbital of TMP 1980.022.0001 is rugose in a small area of the posterior half of the lateral surface of the jugal process. In *G. latidens* MOR 478 6-20-7-13, the lateral surface of the jugal process is strongly concave, and the posterior half is strongly rugose.

The squamosal process (caudal ramus) is broken on both MOR 2573 postorbital specimens, but the only squamosal preserved (juvenile MOR 2573-7-18-06-185) indicates that the squamosal process of the postorbital was likely bifurcated, similar to *G. notabilis* CMN 2278 (Prieto-Márquez, 2010a).

The dorsal surface of the MOR 2573 postorbitals forms an almost straight line; the squamosal process rises from the body of the postorbital at a very shallow angle of

approximately 15 degrees (dorsal angle of 165 degrees). Farke and Herrero (2015) documented variation in the postorbital angle of *Gryposaurus* specimens. Large adult specimens such as *G. monumentensis* RAM 6797 and *G. notabilis* MSMN V345 and ROM 873 generally have relatively strongly angled postorbitals (dorsal angle 153 to 160 degrees), and smaller, younger specimens such as *G. notabilis* ROM 764 and TMP 1980.022.0001 have more horizontal postorbitals (163 to 170 degrees) (Gates and Sampson, 2007).

Braincase and Posterior Skull

The disarticulated braincase material of MOR 2573 offers a unique opportunity to examine the sutural surfaces of *Gryposaurus* braincase elements. Aside from a disarticulated frontal of *G. latidens*, MOR 478-7-20-7-12, braincase material of described species is generally fully articulated. External braincase anatomy is here compared to other *Gryposaurus* specimens, especially the well preserved braincase of *G. notabilis* AMNH FARB 5350 (Prieto-Márquez, 2010a). The *G. latidens* braincase is only known from a single referred frontal, and the *G. monumentensis* holotype RAM 6797 braincase is incomplete. The braincase is not exposed in the *G. notabilis* holotype CMN 2278 or referred specimens MSNM V345 and ROM 764, and poorly preserved in ROM 873 (Prieto-Márquez, 2010a). Interior sutural surfaces are compared to *Prosaurolophus blackfeetensis*: the holotype MOR 454 and disarticulated material of MOR 447.

Frontal. Two sets of paired frontals are preserved in association with their parietals (Figure 4.14). The frontals are disarticulated from each other, but one frontal

remains articulated with its parietal (MOR 2573-7-24-10-455). These frontals and parietals, along with a few other braincase elements discussed below, are the only associated or articulated specimens found anywhere in the JR-429 bonebed, suggesting that braincase elements are the last part of the skeleton to disarticulate. MOR 2573-7-24-10-455, the frontal that is still articulated with its parietal, is being examined histologically to determine if sutural fusion has occurred (Bailleul and Horner, personal communication 2015). The other set of frontals and parietal, MOR 2573-7-23-11-574, -574A, and -575, was disarticulated but the bones were still partially touching. Two isolated left frontals, MOR 2573-6-12-06-16 and MOR 2573-6-21-06-80, were also collected from the JR-429 bonebed. Frontal MOR 2573-6-21-06-80 is dorsoventrally thicker than the other MOR 2573 frontals. The frontals of MOR 2573 are elongated anteroposteriorly, with length to width ratios of 1.47 to 1.63, a more elongated ratio than *Gryposaurus latidens* or *G. notabilis* (Table 4.3).

The anterior frontals demonstrate that the posteriormost nasals inserted medially between the frontals for a short distance, which is an autapomorphy of *Gryposaurus* (Horner, 1992; Prieto-Márquez, 2010a). In paired frontals MOR 2573-7-23-11-574 and -574A, the nasals inserted 7 mm posteriorly into the medial frontals, with a paired nasal width of 17 mm; the shape of the insertion in dorsal view is subrectangular or semicircular. In paired frontals MOR 2573-7-24-10-455 and -455A, the nasals inserted 9 mm posteriorly into the medial frontals, with a paired nasal width of 23 mm. Narrow anterior tips of the medialmost frontals insert between the nasals, creating a “W” shaped articulation in dorsal view. Thus, the precise shape of the nasofrontal articulation in

dorsal view is intraspecifically variable between subrectangular and "W" shaped. The nasofrontal articulation is also "W" shaped in *Gryposaurus notabilis* CMN 2278, AMNH FARB 5350, ROM 764, and TMP 1980.022.0001 (Prieto-Márquez, 2010a). The nasofrontal articulation of *G. monumentensis* UMNH VP 13970 is described as "sigmoidal" (Gates and Sampson, 2007).

The lateral portion of the nasofrontal articulation consists of a short, sloped anterior process of the frontals that underlies the posterior nasal. This articulation surface is sloped anteroventrally at a 30 to 40 degree angle; the surface texture consists of anteroposteriorly oriented ridges. A disarticulated frontal of *G. latidens*, MOR 478-7-20-7-12, has a 35 degree slope of the nasofrontal articulation surface. In subadult *G. notabilis* TMP 1980.022.0001 the anterior frontal is relatively thinner, and the articulation surface slopes more gradually at a 15 degree angle.

The posteriorly-oriented fossa for the insertion of the conical shaped frontal process of the prefrontal is very deep, 27 mm in MOR 2573-7-24-10-455 and 24 mm in MOR 2573-7-23-11-574A measured from the dorsal side of the fossa. This area is either articulated, damaged, or not fully cleaned of sediment in other *Gryposaurus* frontals, so it cannot be determined with confidence whether this deep prefrontal articulation is common to all *Gryposaurus* species or only *G. reddingi*. In *G. notabilis* TMP 1980.022.0001 the anterolateral frontal is slightly damaged and the fossa is not entirely clear of sediment, but a fossa depth of 14 mm is preserved.

The frontal contributes to the orbital margin in all MOR 2573 specimens, but the length of frontal exposed along the lateral orbital margin is intraspecifically variable, as

well as asymmetrical within individuals. Left frontal MOR 2573-7-24-10-455A exposes 14 mm along the orbital margin; its partner right frontal MOR 2573-7-24-10-455 exposes 19 mm. Left frontal MOR 2573-7-23-11-574 exposes 10 mm along the orbital margin; its partner right frontal MOR 2573-7-23-11-574A exposes 9 mm. The orbital process is broken in the two isolated MOR 2573 frontals.

In the *G. notabilis* holotype CMN 2278 the frontal may or may not be entirely excluded from the orbit. A narrow triangular process separates the prefrontal from the postorbital on each side of the skull, but it is unclear whether this process is part of the frontal; Lambe (1914) interpreted this process as a separate supraorbital bone. The frontal is excluded from the orbit in *G. notabilis* MSNM V345 (Vialli, 1960; Pinna, 1979) and ROM 873. The frontal does contribute to the orbital rim in *G. notabilis* AMNH FARB 5350 and TMP 1980.022.0001, *G. latidens* MOR 478-7-20-7-12, and *G. monumentensis* RAM 6797; in *G. notabilis* ROM 764 the frontal is exposed along the orbital rim only at the base of a deep notch between the prefrontal and postorbital (Parks, 1920; Gates and Sampson, 2007; Prieto-Márquez, 2010a).

The paired frontals create a bowl-shaped depression on their dorsal surface. In frontals MOR 2573-7-24-10-455 and -455A this depression is very shallow, less than 5 mm. In frontals MOR 2573-7-23-11-574 and -574A this depression is deeper, between 5 and 10 mm. The depressions are deepest from the center of each frontal toward the anterior and medial margins, and shallower laterally and posteriorly. The posteromedial region is very slightly domed in both sets of frontals. A disarticulated frontal of *G. latidens*, MOR 478-7-20-7-12, has a relatively deep dorsal depression very similar to that

of MOR 2573-7-23-11-574 and -574A. Shallow frontal depressions similar to the frontals of MOR 2573-7-24-10-455 and -455A are present in *G. notabilis* CMN 2278, AMNH FARB 5350, and ROM 764 (Parks, 1920; Prieto-Márquez, 2010a). *Gryposaurus notabilis* TMP 1980.022.0001 also has similar shallow frontal depressions but the posteromedial doming is more pronounced than in MOR 2573.

The medial surface of the interfrontal suture has a similar structure in all MOR 2573 frontals. The posterior one-third of the interfrontal suture is composed of a series of vertically oriented ridges and grooves, some of which are connected by horizontal ridges. The anterior two-thirds of the suture contains antero-posteriorly oriented ridges and grooves. On three of the four left frontals (MOR 2573-7-24-10-455A, MOR 2573-6-12-06-16, and MOR 2573-6-21-06-80), the dorsalmost part of the articulation is a horizontal bar. This bar is vertically flat and 2 to 5 mm high in two specimens (MOR 2573-6-12-06-16, and MOR 2573-6-21-06-80) and is a simple medially oriented ridge in MOR 2573-7-24-10-455A. Ventral to this bar, there is a relatively deep horizontal groove. Ventral to this groove is a horizontal ridge with slightly rugose texture. Ventral to this ridge is a series of short ridges and groves oriented posterodorsally to anteroventrally. MOR 2573-7-24-10-455, the right frontal that pairs with MOR 2573-7-24-10-455A, displays the opposite pattern, with a dorsalmost groove, ridge in the middle, and another groove to interlock tightly with the left frontal. The other pair of frontals, MOR 2573-7-23-11-574 and -574A, has a suture pattern that is a mirror image of the other frontals; in this case the right frontal is the side with a dorsalmost ridge of the suture. Thus, the development of the asymmetry of the sutural surfaces is intraspecifically variable; in some individuals the

left frontal has a ridge-groove-ridge, and in other individuals the right frontal has that pattern.

In MOR 2573 frontals as well as *G. latidens* MOR 478-7-20-7-12, the articular surface for the presphenoid on the ventral side of the frontal is an oval fossa, deeper in some individuals than others. In MOR 2573-6-21-06-80, this fossa is divided by a ridge into anterior and posterior subfossae. In *Prosaurolophus blackfeetensis* MOR 454 and MOR 447 the articular surface for the presphenoid is not a fossa, but is a shallow sutural surface containing anteroposteriorly oriented ridges and grooves.

In MOR 2573 frontals, the articular surface for the orbitosphenoid on the ventral side of the frontal slopes anterodorsally to posteroventrally, so that it is more superior at its anterior end (the frontal is dorsoventrally thinner), and the orbitosphenoid articulation is more inferior at its posterior end (the frontal is dorsoventrally thicker). In *G. latidens* MOR 478-7-20-7-12 and *P. blackfeetensis* MOR 454 and MOR 447 the orbitosphenoid articulation is more horizontal. The orbitosphenoid articulation is mediolaterally wide in MOR 2573-7-23-11-574 and -574A, MOR 2573-6-21-06-80, and *G. latidens* MOR 478-7-20-7-12. The articulation is mediolaterally narrower in MOR 2573-7-24-10-455 and -455A and *P. blackfeetensis* MOR 454 and MOR 447. The laterosphenoid articulation surface is fairly similar in all MOR 2573 frontals, *G. latidens* MOR 478-7-20-7-12, and *P. blackfeetensis* MOR 454 and MOR 447.

On the frontals of MOR 2573, the posterolateral portion of the sutural surface for the parietal is composed of diagonal ridges and grooves oriented dorsolaterally to ventromedially. This area is missing from *G. latidens* frontal MOR 478-7-20-7-12. The

condition in MOR 2573 is similar to that observable on *P. blackfeetensis* MOR 447-4-8-9-86. The medial portion of the sutural surface for the parietal of MOR 2573 is a rugose suture that interlocks with the anteromedial process of the parietal. In MOR 2573-7-23-11-574 and -574A the posteriormost frontals are separated by a short rectangular anteromedial process of the parietal MOR 2573-7-23-11-575 in dorsal view (11 mm long, 15 mm wide). In ventral view this anteromedial process of the parietal is larger anteriorly and laterally. This area is difficult to observe in MOR 2573-7-24-10-455 and -455A due to the right frontal and parietal still being articulated and possibly fused. In isolated frontals MOR 2573-6-12-06-16 and MOR 2573-6-21-06-80, there is not a rectangular notch in the posteromedial frontal, so the anteromedial process of the parietal would have been a narrow triangular point. The frontals of *G. notabilis* CMN 2278 do not appear to be separated by an anteromedial process of the parietal. In *G. notabilis* AMNH FARB 5350 the posterior frontals are separated by a short triangular anteromedial process of the parietal. The interfrontal suture of *G. notabilis* ROM 873 is asymmetrical and deviates from the midsagittal plane; an anteromedial process of the parietal does not appear to be present in dorsal view. In the *P. blackfeetensis* holotype MOR 454 the frontals are separated by a very short rectangular anteromedial process of the parietal (5 mm long, 13 mm wide).

Parietal. Three parietals of MOR 2573 are preserved, all with various degrees of damage (Figure 4.14). The parietal still articulated with its frontal, MOR 2573-7-24-10-455, is well preserved anteriorly, and on its right side includes its complete articulation with the postorbital. However, the posterior half of this parietal is missing. Parietal MOR

2573-7-23-11-575 is complete except for its anterolateral processes, but this parietal is partially crushed, has an unusually concave dorsal margin (see next paragraph), and has a large hole in its posterolateral right side of unknown taphonomic or pathologic origin. Partial parietal MOR 2573-7-20-06-205 is severely water damaged due to its proximity to a modern sinkhole, but includes the best posterior parietal of the three specimens.

MOR 2573-7-24-10-455 preserves the anteriormost 55 mm of the dorsal midsagittal ridge of the parietal. The ridge is sharp, and at its anterior end the ridge bifurcates into sharp anterolateral ridges, forming a slightly depressed triangle on the anterodorsal parietal surface just posterior to the anteromedial process. This triangle is narrow, only 17 mm wide at its anteriormost margin. This dorsal triangle is very similar in *G. notabilis* CMN 2278, ROM 764, and TMP 1980.022.0001, and slightly wider in AMNH FARB 5350 (Parks, 1920; Prieto-Márquez, 2010a). In the *Prosaurolophus blackfeetensis* holotype MOR 454 this triangle is deeper and wider (30 mm), forming approximately one-third the width across the entire anterior parietal.

The dorsal midsagittal ridge of parietal MOR 2573-7-23-11-575 is not sharp, and although its anterior end is triangular, it is not bound by well-defined ridges. The anterodorsal triangle is 21 mm long, and posterior to the triangle the parietal ridge slopes steeply posteroventrally, with the lowest point of the concave ridge located 35mm from the anterior border of the triangle. If all MOR 2573 parietals had a concavity in the same location, then the preserved portion of MOR 2573-7-24-10-455 should have included it, but the dorsal midsagittal ridge of MOR 2573-7-24-10-455 is horizontal, with no evidence of a concavity. The dorsal midsagittal ridge of *G. notabilis* CMN 2278 is

completely straight and horizontal relative to the long axis of the parietal. The ridge is slightly concave in *G. notabilis* AMNH FARB 5350 (Prieto-Márquez, 2010a). Subadult *G. notabilis* ROM 764 and TMP 1980.022.0001 have a slight concavity of the dorsal midsagittal ridge in the same location as the deep concavity of MOR 2573-7-23-11-575, but this may be at least partly due to breakage of the sharp dorsal margin in each specimen. Parietals of *G. latidens* and *G. monumentensis* are not preserved (Gates and Sampson, 2007; Prieto-Márquez, 2012). The dorsal midsagittal ridge is sharp and horizontal in *P. blackfeetensis* (best preserved in MOR 447-7-14-7-8).

The posterior end of the dorsal midsagittal ridge in partial parietal MOR 2573-7-20-06-205 is a thin bar that barely separates the left and right squamosals. This region is either damaged or pathologic in MOR 2573-7-23-11-575; the squamosals appear to have touched posteriorly, although anteriorly they were still separated by a thin bar of parietal. The thin parietal bar separating the squamosals in MOR 2573-7-20-06-205 is similar to the state in some *G. notabilis* specimens, AMNH FARB 5350, ROM 764 and TMP 1980.022.0001, as well as *P. blackfeetensis* MOR 447-7-14-7-8 (Parks, 1920; Prieto-Márquez, 2010a). However, the posterior end of the dorsal midsagittal ridge in the *G. notabilis* holotype CMN 2278 widens to fully separate the left and right squamosals by 4 cm, demonstrating intraspecific variation in *G. notabilis*.

Presphenoid. Specimen MOR 2573-7-19-11-547 (Figure 4.15) is an abraded right presphenoid that articulates well with right frontal MOR 2573-7-23-11-574A. Some frontals have a transverse ridge in the presphenoid fossa; this corresponds to a groove in the dorsal articular surface of the presphenoid. The size and morphology of MOR 2573-

7-19-11-547 match closely with the right presphenoid of subadult *Gryposaurus notabilis* TMP 1980.022.0001. MOR 2573-7-19-11-547 and TMP 1980.022.0001 are both missing the subrectangular anterior projection of the ventral presphenoid seen in *G. notabilis* AMNH FARB 5350 (Prieto-Márquez, 2010a).

Orbitosphenoid. No orbitosphenoids are present in the MOR 2573 material.

Laterosphenoid. Two right subadult and two right juvenile laterosphenoids are present in MOR 2573 (Figure 4.16). They are morphologically similar to those of *G. notabilis* AMNH FARB 5350 and TMP 1980.022.0001 (Prieto-Márquez, 2010a). The lateral surface is strongly concave leading to the postorbital process of the laterosphenoid. The anteroposteriorly oriented groove for the ophthalmic branch of the trigeminal nerve (V1) is deep and well defined. The lateral surface ventral to the ophthalmic groove in the MOR 2573 specimens lacks the rugose surface texture described for *G. notabilis* AMNH FARB 5350 and *G. monumentensis* RAM 6797 (Prieto-Márquez, 2010a).

Basisphenoid and Parasphenoid. Basisphenoid MOR 2573-6-27-10-339 is fairly complete (Figure 4.17), but slightly water damaged from being located near a modern sinkhole in the bonebed. Another basisphenoid, MOR 2573-6-27-12-698, preserves the central core of the bone but is missing most of its processes. The anterior process of MOR 2573-6-27-10-339 is the cultriform process of the parasphenoid, which is fully fused with the basisphenoid. As in *G. notabilis* AMNH FARB 5350 and TMP 1980.022.0001, the dorsal surface of the cultriform process is mediolaterally concave

(Prieto-Márquez, 2010a). A median process was present on the ventral ridge between the basipterygoid processes of the basisphenoid MOR 2573-6-27-10-339, but the process was broken and so its shape and size are unknown. The basipterygoid processes of MOR 2573-6-27-10-339 are ventrolaterally oriented, more laterally then ventrally, as well as being slightly posteriorly oriented; the orientations of the basipterygoid processes may be influenced by a small amount of dorsoventral compression. In other *Gryposaurus* skulls with better three-dimensional preservation, the basipterygoid processes are oriented more ventrally than laterally, with varying anteroposterior orientations. In *G. notabilis* TMP 1980.022.0001, the basipterygoid processes are angled anteriorly. In *G. monumentensis* RAM 6797, the basipterygoid processes are slightly posteriorly oriented.

Prootic. A left prootic is preserved in articulation with a left exoccipital and supraoccipital, MOR 2573-7-10-10-414 (Figure 4.18). The prootic forms the posterior half or slightly more than half of the trigeminal foramen; in *Gryposaurus notabilis* AMNH FARB 5350 the prootic forms slightly less than half of the trigeminal foramen (Prieto-Márquez, 2010a). The trigeminal foramen is circular, as in *G. notabilis* AMNH FARB 5350, and unlike the more dorsoventrally elongated oval in the prootic of *Prosaurolophus blackfeetensis* MOR 447-8-3-87-24. The foramen for the facial nerve is not visible, but this area is poorly preserved in MOR 2573-7-10-10-414. The fenestra vestibuli (oval window, which connects the stapes to the inner ear) is an anteroposteriorly oriented oval rather than the heart shape seen in *G. notabilis* AMNH FARB 5350; the powdery preservation in this area of MOR 2573-7-10-10-414 prevents further comparisons to the morphology of the fenestra vestibuli in other specimens.

Opisthotic-Exoccipital. As in other hadrosaurs, the opisthotic and exoccipital of MOR 2573 are fused into a single element, commonly referred to as simply the exoccipital (Figure 4.19). The exoccipitals are large curving elements with numerous foramina visible medially and laterally near their condyloid bases. The mediolateral robusticity of the condyloid bases varies greatly among MOR 2573 specimens.

The anterodorsal surfaces of the MOR 2573 exoccipitals are generally flat to slightly convex mediolaterally. However, the exoccipital that is still articulated with its supraoccipital and prootic, MOR 2573-7-10-10-414, has a deep oval depression in its dorsal surface (Figure 4.18). There is also a deep circular depression on the ventral side where the exoccipital contacts the supraoccipital. In posterior view, the area connecting the condyloid base to the paraoccipital process is much wider mediolaterally than in the other MOR 2573 specimens. The proximal posterodorsal margin of the paraoccipital process is dorsoventrally thicker than in other MOR 2573 specimens, but it is also thick in some *Gryposaurus notabilis*, AMNH FARB 5350 and ROM 764 (Prieto-Márquez, 2010a). The paraoccipital process of MOR 2573-7-10-10-414 has a large tuberosity on its anterodorsal surface, and its posterior surface has several rugose excavations. The unusual morphology of MOR 2573-7-10-10-414 suggests that it does not represent typical exoccipital morphology for the species, and instead resulted from some combination of pathology (traumatic or infectious), perimortem feeding, or taphonomic or diagenetic distortion. Perhaps the pathology is responsible for the exoccipital remaining articulated with the prootic and supraoccipital; the bones may have partially fused.

As in *Gryposaurus notabilis* AMNH FARB 5350 (Prieto-Márquez, 2010a), the metotic foramen is subdivided into three foramina in lateral view, although in some MOR 2573 specimens only two subdivisions are easily visible; the spacing between the subdivisions is also intraspecifically variable. The dorsalmost foramen contained the vagus (X) nerve and possibly the glossopharyngeal (IX) nerve as well; the lower two foramina, and the larger foramen posterior to the metotic foramen, contained branches of the hypoglossal nerve (XII) (Prieto-Márquez, 2010a). This posteriormost hypoglossal canal is larger than the metotic foramin in MOR 2573 specimens, but it is smaller than the metotic foramen in AMNH 5350 (Prieto-Márquez, 2010a).

Supraoccipital. MOR 2573-7-10-10-414 includes a supraoccipital preserved articulated with its left exoccipital and prootic (Figure 4.18). A second supraoccipital is articulated with a partial parietal, MOR 2573-7-20-06-205, but it is poorly preserved and of limited morphologic use.

The posterodorsal surface of supraoccipital MOR 2573-7-10-10-414 is mediolaterally concave and anteroposteriorly elongated relative to that of *Prosaurolophus blackfeetensis* MOR 447-7-14-7-8, which is flatter and anteroposteriorly shorter. The ventral surface of supraoccipital MOR 2573-7-10-10-414 has prominent anteromedial to posterolateral striations, and the lateral portion of the ventral surface is dorsally elevated relative to the medial portion of the ventral surface. In *P. blackfeetensis* MOR 447-7-14-7-8, the striations are more subtle and the ventral surface is very flat horizontally.

Basioccipital. No basioccipitals are present in the MOR 2573 material.

Palatoquadrate Complex

Squamosal. Only a juvenile squamosal, MOR 2573-7-18-06-185, is preserved (Figure 4.20); no subadult squamosals have been collected from the JR-429 bonebed. The juvenile squamosal has been crushed so that the dorsal and lateral surfaces are almost in the same plane, rather than being perpendicular. The prequadratic process is flat on its posterior side and strongly convex on its anterior side, giving it a semicircular to semi-oval cross-section. The prequadratic process is dorsoventrally longer than the quadrate cotylus is anteroposteriorly wide. In lateral view, the posteroventral ramus is straight anteriorly and gently convex posteriorly. The posteroventral ramus is mediolaterally compressed; the medial surface is flat for contacting the paraoccipital process of the exoccipital, and the lateral surface is gently convex.

The overall morphology of MOR 2573-7-18-06-185 is very similar to that of *Gryposaurus notabilis* TMP 1980.022.0001. The squamosal of *G. latidens* MOR 478 7-2-7-2 is robust, and its prequadratic process is subtriangular in cross section rather than semicircular as in MOR 2573-7-18-06-185. The V-shaped articulation for the postorbital is similar in MOR 2573-7-18-06-185 and *G. latidens* MOR 478 7-2-7-2 (Prieto-Márquez, 2012). The precotyloid fossa of the juvenile MOR 2573-7-18-06-185 squamosal is shallow similar to that of the robust *G. latidens* squamosal MOR 478 7-2-7-2. This fossa is deeper in *G. notabilis* ROM 873, ROM 764, and TMP 1980.022.0001, and even deeper in *G. notabilis* CMN 2278 and *G. monumentensis* RAM 6797. Because only a juvenile

squamosal of MOR 2573 is preserved, it is unknown if the depth of the precotyloid fossa would have been relatively similar or deeper in the subadults of this species.

Quadratojugal. Only one quadratojugal is preserved, MOR 2573-6-30-12-720 (Figure 4.21). Like *Gryposaurus monumentensis* RAM 6797, MOR 2573-6-30-12-720 is more similar to other *Gryposaurus* species and to *Prosaurolophus* than to other hadrosaur genera (Gates and Sampson, 2007). Dorsally it tapers to a sharp triangular point. There is a similar dorsal point in *Gryposaurus notabilis* ROM 873, TMP 1980.022.0001, and ROM 764 (Parks, 1920). MOR 2573-6-30-12-720 is nearly identical in lateral view to *G. notabilis* TMP 1980.022.0001. The ventral point seen in other *Gryposaurus* specimens is broken from the MOR 2573-6-30-12-720 quadratojugal.

Posteriorly, where it contacts the quadrate, quadratojugal MOR 2573-6-30-12-720 is mediolaterally thick, and rapidly thins anteriorly. Due to most *Gryposaurus* skulls that include quadratojugals being articulated, MOR 2573-6-30-12-720 must be compared to a disarticulated quadratojugal of *P. blackfeetensis* MOR 447-6-14-7-11. The posterior portion of MOR 2573-6-30-12-720 is relatively much thicker mediolaterally than in *P. blackfeetensis* MOR 447-6-14-7-11.

Quadrate. Numerous halves and fragments of quadrates are present in MOR 2573, but only one quadrate, MOR 2573-7-01-10-345 is intact (Figure 4.22). The posterior margin is very straight, as in all other *Gryposaurus* quadrates. *Prosaurolophus blackfeetensis* MOR 454 has a similarly straight quadrate. The posterior margin of the

quadrate is concave in *Brachylophosaurus canadensis* (NMC 8893, FMNH PR 862, MOR 794, MOR 1071-8-13-98-559-D) and *Maiasaura peeblesorum* (YPM-PU 22405).

The posterodorsal process, also termed the quadrate buttress (Gates and Sampson, 2007), of the MOR 2573 quadrates is vertically oriented and continuous with the dorsal condyle. The height of the posterodorsal processes in the MOR 2573 subadult quadrates ranges between 40 mm and 47 mm. The posterodorsal processes of MOR 2573 quadrates are similar to those of other *Gryposaurus*: *G. notabilis* CMN 2278, ROM 764, and TMP 1980.022.0001; and *G. monumentensis* RAM 6797. The posterodorsal process in *G. notabilis* ROM 873 is convex and more posteriorly enlarged than in other *Gryposaurus* specimens. *Gryposaurus latidens* only includes a ventral quadrate, MOR 478-7-2-7-6, so the size and shape of the posterodorsal process are unknown. MOR 478-7-2-7-6 is larger than any of the MOR 2573 quadrates, and is morphologically very similar to them and other *Gryposaurus* quadrates.

The size and shape of the posterodorsal process varies in other hadrosaur genera. In *Prosaurolophus blackfeetensis* MOR 454, the posterodorsal process is a subtle tuberosity extending only 2 mm posteriorly, with its apex located 28 mm below the ventral margin of the dorsal condyle. In *Brachylophosaurus canadensis* (NMC 8893, FMNH PR 862, MOR 794, MOR 1071-8-13-98-559-D), the posterodorsal process is more pointed, extending up to 10 mm posteriorly.

Pterygoid. No pterygoids are present in the MOR 2573 material.

Ectopterygoid. No ectopterygoids are present in the MOR 2573 material.

Palatine. No palatines are present in the MOR 2573 material.

Vomer. One left vomer, MOR 2573-7-07-10-390 (Figure 4.23), and one left vomer fragment, MOR 2573-7-27-12-796, are preserved. The dorsal and posterior margins of MOR 2573-7-07-10-390 are broken along their full lengths, but the ventral margin is nearly completely preserved, aside from the broken posteroventralmost margin. The anterior process is elongated, and is mediolaterally wider dorsally and anteriorly. Its posterior half is a mediolaterally thin flat vertical plate. There is no evidence of the posterior vomer becoming mediolaterally wider dorsally, but it is possible that the widening occurred entirely in the missing dorsal region of the vomer, and that the complete vomer could have matched the morphology of *Kritosaurus* sp. YPM-PU 16970 (Horner, 1992). Considering the broken dorsal, posterior, and posteroventralmost edges, the lateral outline of MOR 2573-7-07-10-390 appears to have been similar to the vomer of *Gryposaurus monumentensis* UMNH VP 13970; the vomer of the *G. monumentensis* holotype RAM 6797 has a unique excavation forming a large hole in the main body of the vomer (Gates and Sampson, 2007).

Mandibular Complex

Predentary. No predentaries are present in the MOR 2573 material, so the shapes of the predentary denticles are unknown and cannot be compared to the large clover-shaped denticles unique to *Gryposaurus monumentensis* (Gates and Sampson, 2007).

Dentary. Dentaries are one of the most abundantly preserved cranial elements of MOR 2573 (Figure 4.24). Five subadult dentaries, four juvenile dentaries, and fragments of additional dentaries are preserved, although most of the juvenile dentaries are missing their coronoid processes and the anteriormost and posteriormost tooth rows. Unfortunately, the dental laminae and all dentary teeth are missing from all of the MOR 2573 dentaries. A few fragments of tooth roots remain in some alveoli, but they are not of diagnostic use. Considering the many hundreds of teeth that must have fallen out of these dentaries, the relative scarcity of hadrosaur teeth within the JR-429 bonebed is intriguing. Only 31 hadrosaur tooth fragments and 16 indeterminate ornithischian tooth fragments have been collected; in comparison, 37 tyrannosaur teeth have been collected from the bonebed (Freedman Fowler, Chapter Three). The hadrosaur tooth fragments may have originated from the same *Gryposaurus reddingi* individuals that are preserved in the bonebed, or some of the tooth fragments may have originated elsewhere and been transported with other vertebrate microfossils such as crocodile teeth and fish vertebrae.

In lieu of dentary teeth in confirmed association with the MOR 2573 dentaries, the morphologies of the most complete isolated teeth from the JR-429 bonebed are described here, while acknowledging that these hadrosaur teeth may be from a different taxon such as Brachylophosaurini, which is also known from Kennedy Coulee (Freedman Fowler and Horner, Chapter Two). Only a single tooth is completely preserved (Figure 4.24J), and five tooth fragments preserve half or more of the crown. The complete tooth is relatively wider than any of the tooth fragments, yet the complete tooth is still relatively less wide than almost every tooth in the dentary of *Gryposaurus latidens*

AMNH FARB 5465. In addition, no wide teeth similar to those of *G. latidens* have been collected from any vertebrate microsite in Kennedy Coulee.

The height (31 mm) divided by width (15 mm) ratio of the crown of the complete MOR 2573 tooth is 2.07. The partial tooth crowns have reconstructed estimated ratios of 2.09 to 2.39. In *G. latidens* AMNH FARB 5465, the dentary tooth crown height to width ratios range from 1.7 to 2.1 (Prieto-Márquez, 2012). The dentary tooth ratio of *G. notabilis* AMNH FARB 5350 is 3.1, but in *G. notabilis* TMP 1980.022.0001 and *G. monumentensis* RAM 6797 the ratio generally ranges from 2.75 to 2.80 (Prieto-Márquez, 2010a), but can be as low as 2.6 (Prieto-Márquez, 2012). Thus, although the widest tooth of MOR 2573 has a similar ratio to the narrowest tooth of *G. latidens*, their distributions barely overlap, and *G. latidens* remains unique among *Gryposaurus* species for the overall width of its dentary teeth. The average dentary tooth ratios of MOR 2573 are intermediate between those of *G. latidens* and those of *G. notabilis* and *G. monumentensis*.

The MOR 2573 teeth have a single median carina. The denticles on the MOR 2573 teeth are small papillae restricted to the dorsal half of the crown, similar to *G. notabilis* and *G. monumentensis*, and unlike the large denticles of *G. latidens* (Prieto-Márquez, 2012).

The MOR 2573 subadult dentaries contain 31 to 35 tooth rows. The only complete juvenile dentary contains 30 tooth rows despite its smaller size. Because hadrosaurs increase the number of tooth rows ontogenetically, this demonstrates the range of intraspecific variation in tooth row densities. Comparisons of the number of

tooth rows to the total tooth battery length in *G. reddingi*, *G. latidens*, and *G. notabilis* are available in Table 4.2 and Figure 4.9.

The coronoid processes of the MOR 2573 dentaries are only slightly anteriorly inclined, similar to *G. notabilis* CMN 2278, ROM 873, and TMP 1980.022.0001, and *G. monumentensis* RAM 6797 (Gates and Sampson, 2007). The coronoid process of *G. latidens* AMNH FARB 5465 is more strongly anteriorly inclined, but it is fractured at its base and this angle may not be accurate.

The rostral processes of the MOR 2573 are generally somewhat mediolaterally compressed and many are slightly broken, so comparisons of the shape and angles of the rostral processes to other *Gryposaurus* specimens would generally be inaccurate. The edentulous margin of all MOR 2573 dentaries appears to be gently concave, whereas it is more strongly concave in other *Gryposaurus* species; this difference may be due to a combination of broken margins and mediolateral compression in MOR 2573 specimens.

Surangular. The surangulars of MOR 2573 (Figure 4.25) are generally very similar to those of other *Gryposaurus* species as well as *Prosaurolophus blackfeetensis* MOR 454 and *Brachylophosaurus canadensis* MOR 1071. The median surangular process in MOR 2573 surangulars is semicircular as in *Gryposaurus latidens* MOR 478 surangulars. *Gryposaurus monumentensis* RAM 6797 has an anterior flange on the median surangular process (Gates and Sampson, 2007); a similar flange is present on *Brachylophosaurus canadensis* MOR 1071-8-98-EE, but not on any specimens of *G. reddingi* MOR 2573 or *G. latidens* MOR 478.

Splenial. One splenial, MOR 2573-6-24-10-326, is preserved (Figure 4.26). It is morphologically similar to that of *Gryposaurus latidens* (Prieto-Márquez, 2012).

Angular. No angulars are present in the MOR 2573 material.

Articular. No articulars are present in the MOR 2573 material.

Morphologic Comparisons Summary

Where there are morphologic differences among *Gryposaurus* species, *G. reddingi* is generally more similar to either *G. latidens* or *G. notabilis* than to *G. monumentensis* or other hadrosaur genera. In addition, when there is variation among specimens of *G. notabilis*, the *G. reddingi* subadults are more similar to the subadults of *G. notabilis* than to the adults of *G. notabilis*. Thus, some morphologic traits are shared by *G. latidens*, subadult *G. reddingi*, and subadult *G. notabilis*, with slightly different morphologies in adult *G. notabilis*. Such traits include the height of the dorsal process of the maxilla being lower in *G. latidens*, subadult *G. reddingi*, and subadult *G. notabilis* than in adult *G. notabilis* and *G. monumentensis*.

The concavity of the ventral jugal margin in *G. reddingi* is more similar to subadult and adult *G. notabilis* than to *G. latidens* or *G. monumentensis*. The frontals of the *G. reddingi* MOR 2573 specimens are more elongated anteroposteriorly (mediolaterally narrower) than in *G. latidens* or subadult or adult *G. notabilis*. In *G. notabilis* the frontals do grow relatively wider ontogenetically, but the *G. reddingi* MOR 2573 individuals are of a comparable size to the *G. notabilis* subadults, and yet the *G. reddingi* frontals are still narrower than those of the *G. notabilis* subadults. The slope of

the lateral nasofrontal articulation in *G. reddingi* is more similar to that of *G. latidens* than subadult *G. notabilis*. The prequadratic process of the squamosal of *G. reddingi* is more similar to that of subadult *G. notabilis* than *G. latidens*, but the shallowness of the precotyloid fossa of the squamosal of *G. reddingi* is more similar to that of adult *G. latidens* than subadult or adult *G. notabilis*. The height to width ratios of the dentary tooth crowns in *G. reddingi* are intermediate between those of *G. latidens* and *G. notabilis*. The denticles of the dentary tooth crowns in *G. reddingi* are more similar to those of *G. notabilis* and *G. monumentensis* than *G. latidens*.

Interestingly, the range of individual variation in nasals of *Gryposaurus reddingi* reveals similarities to both *G. latidens* and *G. notabilis*. Two of the *G. reddingi* subadult nasals, MOR 2573-7-14-11-535 and MOR 2573-7-18-06-186, are similar to the adult *G. latidens* nasal AMNH FARB 5465 in having a gently curving nasal crest that is not greatly dorsally elevated, with the peak of the crest located dorsal to the posterior narial fenestra. The third *G. reddingi* nasal, MOR 2573-6-21-06-63, has an arch more similar to that of subadult *G. notabilis* TMP 1980.022.0001, with the angular peak of the crest located anterior to the posterior narial fenestra. However, all three *G. reddingi* nasals differ from *G. notabilis* in having an extremely wide posterior margin of the narial fenestra, and are similar to the wide posterior narial fenestra of *G. latidens*.

Phylogenetic Analysis

The results of the phylogenetic analysis (Figure 4.27) based on the matrix of Prieto-Márquez (2014) with the addition of *Gryposaurus reddingi* are strikingly similar

to the results of Prieto-Márquez (2014). The topology is nearly identical; in the strict consensus tree of the current analysis, the only change outside of *Gryposaurus* is the destabilization of Brachylophosaurini (*Acristavus*, *Maiasaura*, and *Brachylophosaurus*) into a polytomy, and the bootstrap support values outside of *Gryposaurus* are only zero to two percent different from those of Prieto-Márquez (2014). The genus *Gryposaurus* is united as a monophyletic clade, although with only 54 percent bootstrap support in both this analysis and Prieto-Márquez (2014). Within *Gryposaurus*, *G. reddingi* is recovered as the sister taxon to *G. latidens*, although the bootstrap support for this clade is below 50 percent. In the Prieto-Márquez (2014) results, the sister taxa *G. notabilis* and *G. monumentensis* were united by 70 percent bootstrap support, which has decreased to 66 percent in the current analysis. Although the decrease is small, it may reflect the many similarities in character states between *G. reddingi* and *G. notabilis*.

There are four characters, only three of which are phylogenetically informative, that have the same character state in *Gryposaurus reddingi* and *G. latidens* but not *G. notabilis* and *G. monumentensis*. Using the labels of Prieto-Márquez (2014), these phylogenetically informative characters are: Character 76 (NS9), summit of the nasal arch located dorsal versus caudodorsal to the posterior margin of the narial foramen; Character 97 (J3), shape of the caudoventral corner of the rostral process of the jugal; and Character 103 (J11), the relative heights of the caudal and rostral constrictions of the jugal.

There are nine characters that have the same character state in *Gryposaurus reddingi* and *G. notabilis* but not *G. latidens*. These characters are: Character 5 (DTTH5),

height to width ratio of dentary tooth crowns; Character 8 (DTTH10), size of denticles on dentary teeth; Character 26 (DT1), relative length of proximal edentulous slope of the dentary; Character 27 (DT4), angle of ventral deflection of the rostral process of the dentary; Character 28 (DT5), anteroposterior position of the origin of the ventral deflection of the rostral process of the dentary along the ventral margin of the dentary; Character 102 (J10), degree of concavity between the caudoventral and quadratojugal flanges of the jugal; Character 206 (UL1), length of ulna relative to its diameter; Character 218 (IL5), anteroposterior position of the supraacetabular process of the ilium relative to the ischial peduncle of the ilium; and Character 223 (IL10), the posterior supraacetabular process having a well defined ridge or not.

Geometric Morphometric Analysis

The results of the geometric morphometric Principal Components Analysis (PCA) are presented in Figure 4.28. Axis 1 accounts for 67.4% of variation; Axis 2 accounts for 17.7% of variation. Specimens with positive values along Axis 1 tend to have anteriorly positioned nasal crests with the peak of the crest above the external naris, whereas specimens with negative values along Axis 1 tend to have more posteriorly positioned nasal crests with the peak of the crest posterior to the external naris. Specimens cluster somewhat by species, but *Gryposaurus notabilis* specimens are widely spread along Axis 1.

There are, however, stratigraphic and ontogenetic trends in the PCA results. Many of the specimens with positive values along Axis 1 are smaller (likely non-adult) and/or

have relatively low stratigraphic positions. The *Gryposaurus reddingi* specimens plot closest to the *G. notabilis* specimens TMP 1980.022.0001 and ROM 1939, which are the smallest *G. notabilis* specimens. *Gryposaurus reddingi* also plots near *G. latidens*, which is the stratigraphically lowest *Gryposaurus* species. The *Gryposaurus* sp. specimen UMNH VP 18569 from the lower Kaiparowits Formation (Gates et al., 2013) plots closest to *G. monumentensis* and adult *G. notabilis*, the taxa that stratigraphically bracket it. *Naashoibitosaurus ostromi* and *Kritosaurus* ("Anasazisaurus") *horneri* plot close together, and are both from the Kirtland Formation of New Mexico (Hunt and Lucas, 1993). Interestingly, a small individual (MOR 553-7-2-8-26) from the Jack's Birthday Site bonebed of the Upper Two Medicine Formation of Montana plots very close to *Naashoibitosaurus* and *K. horneri*.

Discussion

For nearly all morphologic characteristics of the skull material that differ among *Gryposaurus* species, *G. reddingi* is most similar to either *G. latidens* or *G. notabilis*. This is most notable in the intermediate morphologies of the dentary teeth and the nasals of *G. reddingi*. *Gryposaurus latidens* is defined, in part, by its wide dentary teeth, with tooth crown height to width ratios below 2.1. *Gryposaurus notabilis* has much narrower teeth, with ratios between 2.6 and 3.1. Tooth crowns of MOR 2573 found isolated within the JR-429 bonebed have height to width ratios between 2.07 and 2.39, intermediate between the dentary tooth crown ranges of *G. latidens* and *G. notabilis*. Although these MOR 2573 teeth were not found in situ within *G. reddingi* dentaries, there is no evidence

of wider dentary teeth being present anywhere within the bonebed, or at any other locality with the Kennedy Coulee area of the Judith River Formation, and thus no evidence of teeth with the *G. latidens* morphology.

In lieu of in situ dentary tooth batteries, the relative widths of dentary and maxillary alveoli (tooth battery length vs number of tooth rows) were compared among *Gryposaurus* specimens (Table 4.2; Figure 4.9). The *G. reddingi* subadult dentaries and maxillae have similar numbers of tooth rows as the similarly sized subadults of *G. latidens* and *G. notabilis*, indicating that relative alveolar width is consistent among species of *Gryposaurus*. The adult specimens of *G. latidens*, holotype AMNH FARB 5465 dentary and MOR 478-6-20-7-19 maxilla, are the largest *Gryposaurus* specimens and have the greatest number of tooth rows, but their alveolar widths are not outliers compared to adults of *G. notabilis*. Thus, the variations in tooth crown width among species are not reflected in alveolar width.

In the geometric morphometric Principal Components Analysis of Kritosaurini nasals (Figure 4.28), *Gryposaurus reddingi* plots closest to *G. latidens* and the smallest individuals of *G. notabilis* (TMP 1980.022.0001, ROM 1939). This is appropriate given the stratigraphic position and ontogenetic stage of the *G. reddingi* specimens (Figure 4.29). *Gryposaurus reddingi* is found stratigraphically above *G. latidens*, but below *G. notabilis*. *Gryposaurus reddingi* is somewhat similar in size and hypothesized subadult ontogenetic stage to the *G. notabilis* specimen TMP 1980.022.0001 (the holotype of *G.* "*incurvimanus*"; Table 4.1 specimen list).

Small specimens of *G. notabilis* were previously diagnosed as a distinct species, *G. incurvimanus*, but are currently interpreted as subadult *G. notabilis* (Wagner, 2001; Prieto-Márquez, 2010a). In *G. notabilis*, the nasal crest is low and anteriorly positioned in subadults (TMP 1980.022.0001), and enlarges and migrates posteriorly as the animal grows larger (Prieto-Márquez, 2010a). The nasal crest of *G. latidens* is also low and relatively anteriorly positioned, but this morphology is present in large adults (holotype AMNH FARB 5465). In some dinosaur taxa, juveniles of later species can be more similar to adults of the ancestral species than to adults of their own species (Rozhdestvensky, 1965). This trend appears to be true for *Gryposaurus*, in which the nasal crest of subadult *G. notabilis* resembles that of the stratigraphically older adult *G. latidens* more than that of adult *G. notabilis*.

The peaks of the nasal crests of the MOR 2573 subadult *Gryposaurus reddingi* specimens are positioned dorsally or anterodorsally to the dorsalmost extent of the external narial margin. This is more anterior than the nasal crests of adult *G. notabilis*, adult *G. monumentensis*, or subadult *G. monumentensis*, but not as anterior as the crests of subadult *G. notabilis*. The crest of *G. reddingi* is more anterior than that of the large holotype *G. latidens* (AMNH FARB 5465), but somewhat similar to the position of the crest in the *G. latidens* specimen MOR 478, which is larger than MOR 2573 but smaller than AMNH FARB 5465. Thus, within *G. latidens*, the crest migrates posteriorly with increasing body size as it does in *G. notabilis*. The subadult specimens of *G. reddingi* are therefore not unusual in having a relatively anteriorly positioned nasal crest as subadults.

Although the adult morphology of *G. reddingi* is unknown, the nasal crest is hypothesized to enlarge and migrate posteriorly as it does in *G. latidens* and *G. notabilis*.

Comparing *Gryposaurus reddingi* MOR 2573 subadult nasals to other specimens of similar size and thus potentially similar ontogenetic stage, the morphology of the MOR 2573 nasals is unique, supporting their diagnosis as a distinct species. MOR 2573 nasals share a wide posterior narial margin with the smallest *G. latidens* specimen, MOR 478 (a larger individual than any MOR 2573 specimens), but the peak of the crest of MOR 478 is higher and more strongly angled; the crests of *G. reddingi* specimens MOR 2573-7-14-11-535 and MOR 2573-7-18-06-186 are low and more gently curved. The *G. notabilis* juvenile (ROM 1939) and subadult (TMP 1980.022.0001) specimens have much narrower posterior narial margins than MOR 2573. The sharp angle of the peak of the nasal crest in the *G. notabilis* juvenile and subadult specimens is similar to that of the *G. reddingi* specimen MOR 2573-6-21-06-63, but not to the other, more gently curved specimens MOR 2573-7-14-11-535 and MOR 2573-7-18-06-186. The *G. monumentensis* subadult (UMNH VP 13970) has a narrower posterior nasal margin than MOR 2573 as well as a higher and more posteriorly positioned nasal crest. Thus, no other subadult or adult *Gryposaurus* nasals possess the combination of traits seen in *G. reddingi*: a wide posterior narial margin and low, relatively anteriorly placed nasal crest that is generally gently curved but may possess a sharper angle in some individuals.

Gryposaurus reddingi is morphologically intermediate between *G. latidens* and *G. notabilis* with the morphology of its nasal crest, width of dentary teeth, and other cranial characteristics. This is consistent with the relative stratigraphic positions of these

taxa (Figure 4.29). *Gryposaurus latidens*, *G. reddingi*, *G. notabilis*, and *G. monumentensis* specimens are stratigraphically separated; the species do not overlap stratigraphically, and so there is no evidence of cladogenesis within *Gryposaurus*. Instead, their stratigraphic distribution of morphologies is consistent with an anagenetic lineage. The species within the *Gryposaurus* lineage could be considered metaspecies (sensu Horner et al., 1992). The results of the phylogenetic analysis yield *G. latidens* and *G. reddingi* as sister taxa, but this clade is poorly supported (bootstrap value below 50 percent), and more character states are shared between *G. reddingi* and *G. notabilis* than between *G. reddingi* and *G. latidens*.

Of the non-*Gryposaurus* Kritosaurini specimens, the three stratigraphically highest specimens cluster tightly in the geometric morphometric Principal Components Analysis of Kritosaurini nasals (Figure 4.28): the holotypes of *Kritosaurus horneri* and *Naashoibitosaurus ostromi* from the Kirtland Formation of New Mexico are joined by the small Kritosaurini nasal MOR 553-7-2-8-26 from the upper Two Medicine Formation of Montana. These specimens are hypothesized to illustrate a continuation of the *Gryposaurus* evolutionary trend of the nasal crest being more posteriorly positioned in stratigraphically higher specimens.

Conclusion

Gryposaurus reddingi is described based on abundant disarticulated bonebed material, enabling examination of intraspecific variation and morphological details not accessible on articulated skulls. *Gryposaurus reddingi* is stratigraphically and

morphologically intermediate between *G. latidens* and *G. notabilis*. Phylogenetic analysis reveals the stratigraphically lowest *Gryposaurus* species, *G. latidens* and *G. reddingi*, as sister taxa, and the stratigraphically highest *Gryposaurus* species, *G. notabilis* and *G. monumentensis*, as sister taxa. In the geometric morphometric analysis, *G. reddingi* is most similar to *G. latidens* and subadult *G. notabilis*.

The differences between species of *Gryposaurus* are subtle; the genus changed relatively little over several million years. Species of *Gryposaurus* are stratigraphically separated, and the trends in morphology are aligned with the stratigraphic positions of the specimens. This suggests that the species of *Gryposaurus* represent an anagenetic lineage, and thus the individual species could actually be considered transitional metaspecies (sensu Horner et al., 1992) within the lineage.

Acknowledgments

Thanks to Dave Varricchio, Don Brinkman, Matt Lavin, Denver Fowler, Holly Woodward, John Scannella, Dave Evans, Michael Ryan, Dave Eberth, Mark Goodwin, and Ray Rogers for advice and discussions. For specimen collection, thanks to the 2006 and 2010-2012 MOR field crews, especially Brian Baziak, Bobby Ebelhar, Bob Harmon, and Cary Woodruff. For fieldwork support, hospitality, friendship, and specimen donation, great thanks as always to Dan and Lila Redding. Thanks to all members of the Rudyard, Montana community, whose continuing support of local paleontology makes this work possible. Excellent preparation was done by Jamie Jette, Carrie Ancell, Aleen Kienholz, Susan Brewer, and volunteers at the MOR Bowman Prep Lab. Fieldwork and

research funding was generously provided to JRH by: Nathan Myhrvold, David Sands and family, Ellis Short and family, Damaris Wagoner, and donors to the MOR Horner Fund and MOR Student Fund; and to EAFF by: the Geological Society of American Student Research Grant, the Royal Ontario Museum M. A. Fritz Travel Grant for the Advancement of Studies in Paleontology, the Tampa Bay Fossil Club, and the Montana State University Department of Cell Biology and Neuroscience. Thanks to Kevin Seymour and David Evans (ROM); and Don Brinkman, Brandon Strillsky, and Graeme Housego (TMP) for comparative specimen access. Thanks to Mark Norell, Carl Mehling, Danny Barta, and Channing Redford (AMNH) for the dentary measurement of AMNH FARB 5465. Training in R was provided to EAFF by the Paleobiology Database Intensive Summer Course in Analytical Paleobiology. Dave Varricchio, Don Brinkman, and Matt Lavin provided helpful comments on drafts of this paper.

Table 4.1. *Gryposaurus* and other Kritosaurini specimens used for morphologic comparisons, in approximate stratigraphic order. "Art." indicates whether a nasal was part of an articulated skull. "Nasal" lists which nasal of the specimen was used in the morphometric analysis (n=19); images of left nasals were flipped horizontally so all specimens appeared as right nasals. An asterisk (*) indicates that the opposite nasal is present in the specimen, but is either not as well preserved as the listed nasal, or was not available for observation. A hash symbol (#) indicates specimens that include only a partial nasal; these incomplete specimens were removed from the final morphometric analysis. The UM 5204 *Gryposaurus* sp. specimen does not have a nasal, but is included in this table because of its utility in size comparisons with MOR 2573. The quadrate height is used as a proxy for skull size because the height of the quadrate is easily measured in both articulated and disarticulated specimens. Because MOR 2573 specimens are disarticulated, the exact quadrate height for each nasal is unknown; the only intact quadrate MOR 2573-7-01-10-345 is 33.4 cm high. The juvenile quadrate height is estimated. The original published radiometric ages have been recalibrated by Roberts et al. (2013) to a Fish Canyon sanidine standard of 28.201 Ma. All ages are in Ma. Abbreviations: Art, articulated; Fm, formation; L, left; R, right. References used in Table 4.1: (Lambe, 1914; Parks, 1919, 1920; Vialli, 1960; Pinna, 1979; Horner, 1984; Goodwin and Deino, 1989; Horner, 1992; Hunt and Lucas, 1993; Rogers et al., 1993; Varricchio, 1995; Fassett and Steiner, 1997; Williamson, 2000; Horner et al., 2001; Currie and Russell, 2005; Ryan and Evans, 2005; Gates and Sampson, 2007; Prieto-Márquez, 2010a, 2012; Gates et al., 2013; Roberts et al., 2013; Gates and Scheetz, 2014; Prieto-Márquez, 2014; Tanke and Evans, 2014).

Taxon	Holotype	Specimen	Art.	Nasal	Quadrate	Locality	Stratigraphic Height	Age Published	Recalibrated (Roberts et al. 2013)	Taxonomic and Stratigraphic References
Naashoibitosaurus ostromi	yes	NMMNH P-16106	yes	L*	L: 32.5 cm, R: 32.1 cm	Willow Wash, New Mexico	base of De-na-zin Member, Kirtland Fm	73.04 ± 0.25 - 73.37 ± 0.18	72.66 ± 0.25 - 72.98 ± 0.18	Fasset & Steiner 1997; Hunt & Lucas 1993; Prieto-Márquez 2014; Williamson 2000
Kritosaurus ("*Anasazisaurus*") *horneri*	yes	BYU 12950	yes	R*	-	Farmington, New Mexico	Farmington Member, Kirtland Fm	73.37 ± 0.18 - 74.11 ± 0.62	72.98 ± 0.18 - 73.72 ± 0.62	Fasset & Steiner 1997; Hunt & Lucas 1993; Prieto-Márquez 2014

Table 4.1 continued.

Kritosaurini indet.	-	MOR 553-7-2-8-26	no	R	-	TM-068 Jack's Birthday Site, Glacier County, Montana	Upper Two Medicine Fm	~74.07 ± 0.72	~75.03	Varricchio 1995
Rhinorex condrupus	yes	BYU 13258	yes	R*	-	central Utah	Neslen Fm	~75	not recalibrated	Gates & Scheetz 2014
Gryposaurus monumentensis	yes	RAM 6797	yes	L	45 cm	Grand Staircase-Escalante National Monument, Utah	middle unit, Kaiparowits Fm	75.02 ± 0.15	75.51 ± 0.15	Gates & Sampson 2007; Prieto-Márquez 2014; Roberts et al. 2013
Gryposaurus monumentensis	no	UMNH VP 13970	no	L	-	Grand Staircase-Escalante National Monument, Utah	middle unit, Kaiparowits Fm	75.02 ± 0.15 - 75.96 ± 0.14	75.51 ± 0.15 - 76.46 ± 0.14	Gates & Sampson 2007; Roberts et al. 2013
Gryposaurus sp.	-	UMNH VP 18568	yes	R*	-	Wahweap Creek, Utah	lower unit, Kaiparowits Fm	~75.96 ± 0.14	~76.46 ± 0.14	Gates et al. 2013; Roberts et al. 2013
Gryposaurus notabilis	yes	CMN 2278	yes	R*	L: 42.5 cm, R: 43.5 cm	Dinosaur Provincial Park, Alberta	elevation 656 m	75.3 ± 0.3 - 76.5 ± 0.5	75.79 ± 0.24 - 77.00 ± 0.24	Lambe 1914; Currie & Russell 2005
Gryposaurus notabilis	no	ROM 873	yes	R*	R: 43.5 cm	Dinosaur Provincial Park, Alberta		75.3 ± 0.3 - 76.5 ± 0.5	75.79 ± 0.24 - 77.00 ± 0.24	Ryan & Evans 2005

Table 4.1 continued.

Gryposaurus notabilis	no	AMNH FARB 5350	yes	L*	-	Dinosaur Provincial Park, Alberta		75.3 ± 0.3 - 76.5 ± 0.5	75.79 ± 0.24 - 77.00 ± 0.24	Prieto-Márquez 2010
Gryposaurus notabilis	no	MSNM V345	yes	L	-	Dinosaur Provincial Park, Alberta	elevation 665 m	75.3 ± 0.3 - 76.5 ± 0.5	75.79 ± 0.24 - 77.00 ± 0.24	Currie & Russell 2005; Vialli 1960; Pinna 1979
Gryposaurus notabilis ("*incurvimanus*")	"yes"	ROM 764	yes	R#	34.5 cm	Dinosaur Provincial Park, Alberta	16 m above base of Dinosaur Park Fm	75.3 ± 0.3 - 76.5 ± 0.5	75.79 ± 0.24 - 77.00 ± 0.24	Parks 1919; Parks 1920; Prieto-Márquez 2010; Tanke & Evans 2014
Gryposaurus notabilis ("*incurvimanus*")	no	TMP 1980.022. 0001	yes	L*	L: 32.8 cm	Dinosaur Provincial Park, Alberta	elevation 670 m	75.3 ± 0.3 - 76.5 ± 0.5	75.79 ± 0.24 - 77.00 ± 0.24	Currie & Russell 2005; Prieto-Márquez 2010
Gryposaurus notabilis	no	ROM 1939	no	L	-	Dinosaur Provincial Park, Alberta	elevation 663.5 m	75.3 ± 0.3 - 76.5 ± 0.5	75.79 ± 0.24 - 77.00 ± 0.24	Currie & Russell 2005
Gryposaurus sp.	-	MOR 399	no	R	L: 36.3 cm	JR-027 Goffena Ranch, Musselshell County, Montana	Lower Judith River Fm	-	-	
Gryposaurus sp.	-	UM 5204	no	-	42.7 cm	Kennedy Coulee, Montana	Judith River Fm	78.2 ± 0.2 - 78.5 ± 0.2	78.71 ± 0.2 - 79.02 ± 0.2	Goodwin & Deino 1989; Horner 1992

Table 4.1 continued.

Gryposaurus reddingi	yes	MOR 2573-7-14-11-535 and -534	no	R	~33.4 cm	Kennedy Coulee, Montana	Judith River Fm equivalent to Unit 1, Oldman Fm	78.2 ± 0.2 - 78.5 ± 0.2	78.71 ± 0.2 - 79.02 ± 0.2	Goodwin & Deino 1989
Gryposaurus reddingi	no	MOR 2573-6-21-06-63	no	L	~33.4 cm	Kennedy Coulee, Montana	Judith River Fm equivalent to Unit 1, Oldman Fm	78.2 ± 0.2 - 78.5 ± 0.2	78.71 ± 0.2 - 79.02 ± 0.2	Goodwin & Deino 1989
Gryposaurus reddingi	no	MOR 2573-7-18-06-186 and -6-03-10-271	no	R	~33.4 cm	Kennedy Coulee, Montana	Judith River Fm equivalent to Unit 1, Oldman Fm	78.2 ± 0.2 - 78.5 ± 0.2	78.71 ± 0.2 - 79.02 ± 0.2	Goodwin & Deino 1989
Gryposaurus reddingi	no	MOR 2573-7-09-11-526	no	L#	~33.4 cm	Kennedy Coulee, Montana	Judith River Fm equivalent to Unit 1, Oldman Fm	78.2 ± 0.2 - 78.5 ± 0.2	78.71 ± 0.2 - 79.02 ± 0.2	Goodwin & Deino 1989
Gryposaurus reddingi	no	MOR 2573-7-16-11-539	no	L#	~17-24 cm	Kennedy Coulee, Montana	Judith River Fm equivalent to Unit 1, Oldman Fm	78.2 ± 0.2 - 78.5 ± 0.2	78.71 ± 0.2 - 79.02 ± 0.2	Goodwin & Deino 1989
Gryposaurus reddingi	no	MOR 2573-7-19-11-550	no	L#	~33.4 cm	Kennedy Coulee, Montana	Judith River Fm equivalent to Unit 1, Oldman Fm	78.2 ± 0.2 - 78.5 ± 0.2	78.71 ± 0.2 - 79.02 ± 0.2	Goodwin & Deino 1989

Table 4.1 continued.

Gryposaurus latidens	yes	AMNH FARB 5465	yes	L*	-	Two Medicine River near Shields Crossing, Glacier County, Montana	100m above Virgelle Sandstone, Lithofacies 3, lower Two Medicine Fm	79.6 ± 0.09 Ma	not recalibrated	Horner 1984; Horner 1992; Horner et al. 2001; Prieto-Márquez 2012; Rogers et al. 1993
Gryposaurus latidens	no	MOR 478-7-2-7-3	no	R	-	Shields Crossing area, Pondera County, Montana	Lithofacies 3, lower Two Medicine Fm	79.6 ± 0.09 Ma	not recalibrated	Horner 1992; Horner et al. 2001; Prieto-Márquez 2012; Rogers et al. 1993

Table 4.2. Dentary and maxilla measurements for *Gryposaurus* specimens. Stage indicates the relative ontogenetic stage of the specimens based solely on size, and should not be used to imply anything about sexual or skeletal maturity or immaturity. Because some specimens are damaged at the anterior or posterior end of the tooth row, a "~" symbol indicates that the value is a conservatively reconstructed estimate. In most cases, the missing portions were small and the estimates add only a few cm or tooth rows. The count of 40 tooth rows for AMNH FARB 5465 dentary is from Prieto-Márquez (2012). Posteriormost tooth rows were not visible on CMN 2278 due to coverage by the coronoid process of the dentary, so tooth counts and measurements are only for the exposed portions of the maxillary and dental tooth batteries, and the full measurement would be greater (>). The teeth and alveoli within MOR 2573-8-03-11-625 are too poorly preserved to count.

	Taxon	Specimen	Stage	Tooth Rows	Tooth Battery Length (cm)	Rows/Length
Maxilla	*G. reddingi*	MOR 2573-7-11-06-156	subadult	36	29.0	1.24
	G. reddingi	MOR 2573-7-13-06-167	subadult	38	27.5	1.38
	G. reddingi	MOR 2573-7-10-10-423	subadult	~39	31.5	1.24
	G. reddingi	MOR 2573-7-22-10-447	subadult	~39	30.5	1.28
	G. reddingi	MOR 2573-7-27-10-470	subadult	~39	28.0	1.39
	G. reddingi	MOR 2573-7-28-22-599	subadult	~34	28.5	1.19
	G. reddingi	MOR 2573-8-03-11-625	subadult	-	26.5	-
	G. reddingi	MOR 2573-7-01-10-359A	juvenile	~25	~20	1.25
	G. latidens	MOR 478-6-20-7-19	adult	~42	38.5	1.09
	G. latidens	MOR 478-5-28--8-1	subadult	~36	~28	1.29
	G. latidens	MOR 478-5-24-8-7	subadult	37	30	1.23
	G. notabilis	CMN 2278 (right)	adult	>42	>32	1.31
	G. notabilis	ROM 873 (left)	adult	~41	36.0	1.14
	G. notabilis	ROM 873 (right)	adult	~39	37.7	1.03
	G. notabilis	TMP 1980.022.0001 (left)	subadult	40	29.0	1.38
	G. notabilis	TMP 1980.022.0001 (right)	subadult	~39	28.0	1.39
Dentary	*G. reddingi*	MOR 2573-6-22-06-87	subadult	~34	~31	1.10
	G. reddingi	MOR 2573-7-05-10-378	subadult	31	27.0	1.15
	G. reddingi	MOR 2573-7-05-10-381	subadult	35	28.5	1.23
	G. reddingi	MOR 2573-8-03-11-636	subadult	~32	~28	1.14
	G. reddingi	MOR 2573-7-13-12-757	juvenile	30	19.0	1.58
	G. latidens	AMNH FARB 5465	adult	40	43.2	0.93
	G. notabilis	CMN 2278 (right)	adult	>32	>31	1.03
	G. notabilis	ROM 873 (left)	adult	38	35.8	1.06
	G. notabilis	ROM 873 (right)	adult	~38	36.5	1.04
	G. notabilis	TMP 1980.022.0001 (left)	subadult	37	27.5	1.35
	G. notabilis	TMP 1980.022.0001 (right)	subadult	~35	27	1.30
	G. notabilis	ROM 1939 (right)	juvenile	25	16.1	1.55

Table 4.3. Frontal length and width measurements for *Gryposaurus* specimens. Frontal length is measured as the longest anteroposterior length visible in dorsal view of an articulated specimen. Frontal width is measured from the orbital margin to the midsagittal plane.

Taxon	Specimen	Length (cm)	Width (cm)	Length/Width
Gryposaurus reddingi	MOR 2573-7-24-10-455	11.4	7.5	1.52
Gryposaurus reddingi	MOR 2573-7-24-10-455A	11.8	7.6	1.55
Gryposaurus reddingi	MOR 2573-7-23-11-574	12.2	8.3	1.47
Gryposaurus reddingi	MOR 2573-7-23-11-574A	11.9	7.3	1.63
Gryposaurus latidens	MOR 478-7-20-7-12	12.3	10.1	1.22
Gryposaurus notabilis	CMN 2278 (left)	11.5	11	1.05
Gryposaurus notabilis	CMN 2278 (right)	11.5	11	1.05
Gryposaurus notabilis	TMP 1980.022.0001 (left)	9.8	7.7	1.27
Gryposaurus notabilis	TMP 1980.022.0001 (right)	10.7	7.7	1.39

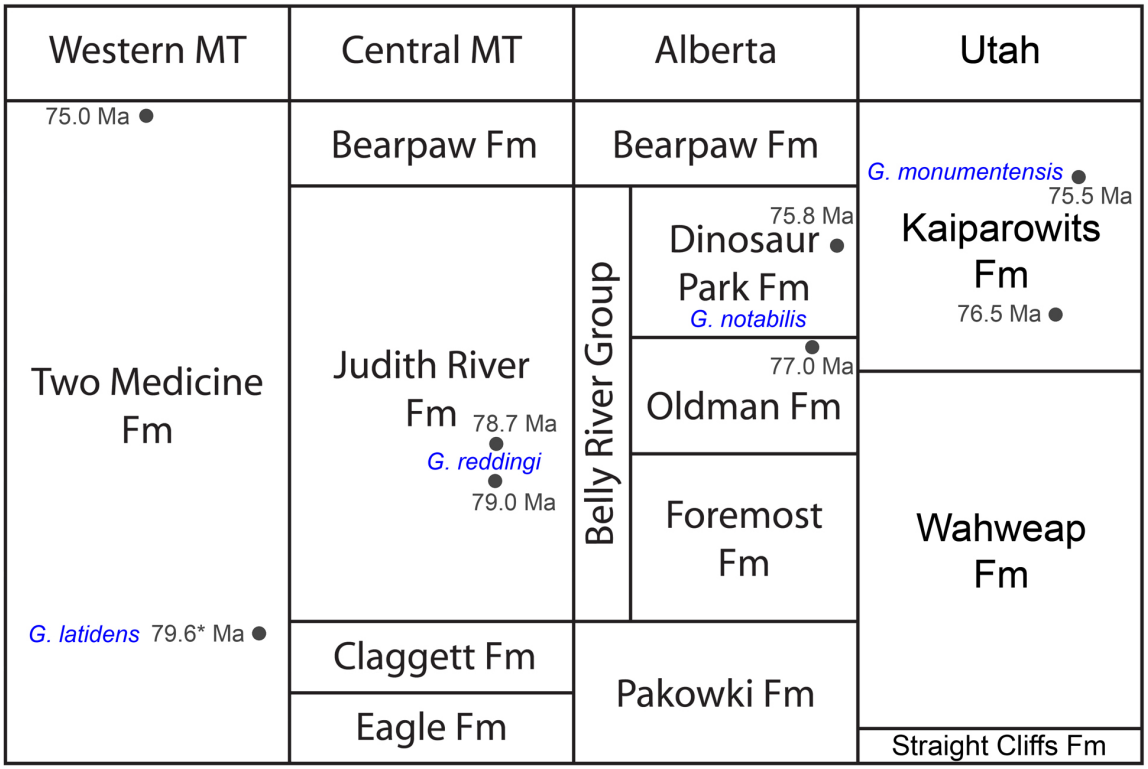


Figure 4.1. Generalized regional cross sections of the Judith River Formation and its stratigraphic equivalents, with distribution of *Gryposaurus* species. *Gryposaurus* species are indicated in blue: *G. latidens*, *G. reddingi*, *G. notabilis*, and *G. monumentensis*. Partial *Gryposaurus* specimens that have not been assigned to a species are not shown. Radiometric dates are indicated in dark gray, and have been recalibrated to a Fish Canyon Sanidine standard of 28.201 Ma by Roberts et al. (2013) based on previously published dates. However, the date of 79.6 Ma for the lower Two Medicine Formation was not recalibrated by Roberts et al. (2013), and thus appears younger than it would if recalibrated. See Table 4.1 for details on radiometric date recalibrations and references. Generalized correlations are based on Horner et al. (2001), Eberth (2005), and Jinnah (2013).

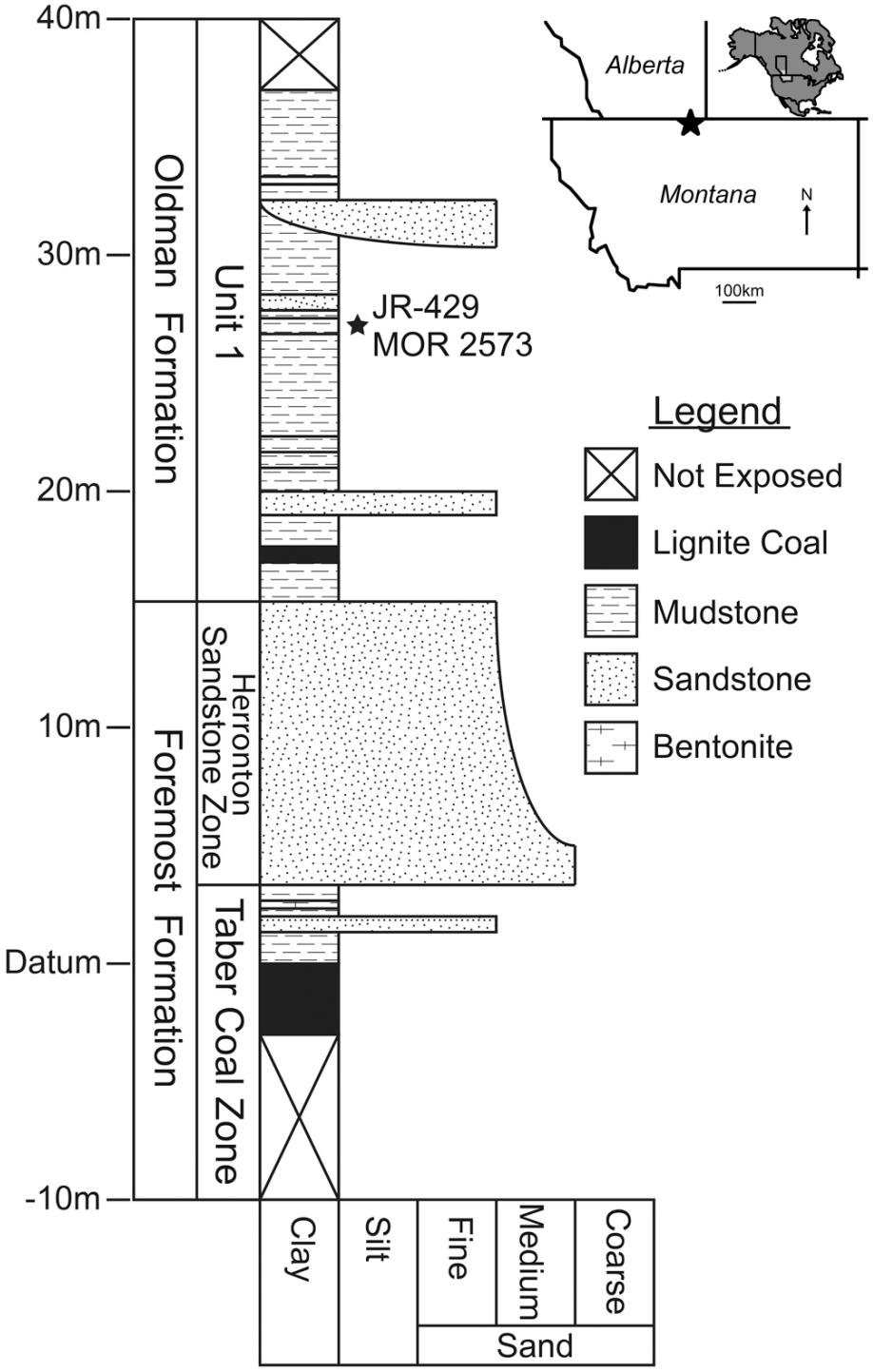
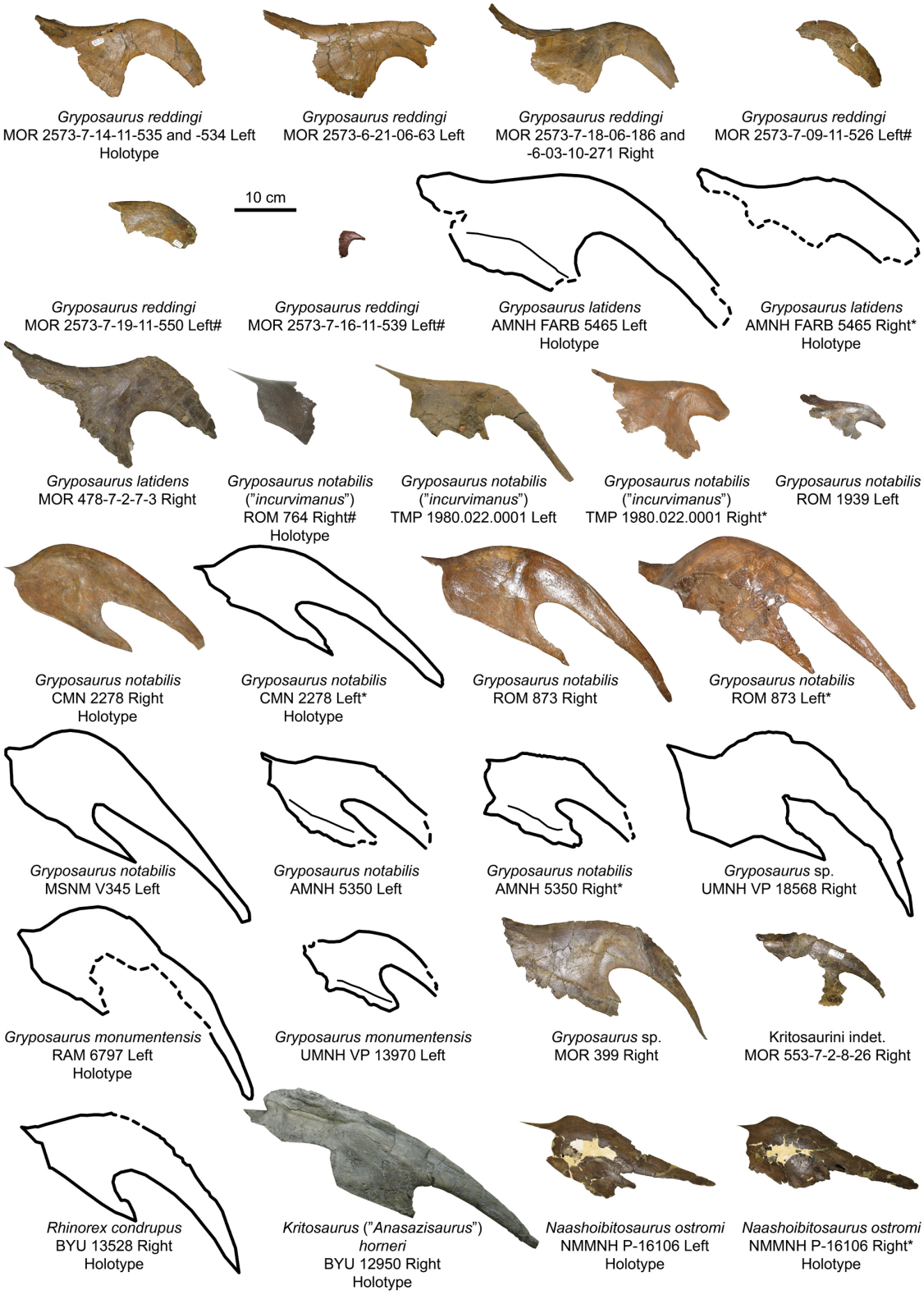


Figure 4.2. Stratigraphic section of Kennedy Coulee, northcentral Montana, Judith River Formation. Location of *Gryposaurus reddingi* bonebed, MOR locality JR-429 (specimen MOR 2573), is indicated by a black star on the stratigraphic section and on the inset map of Montana in upper right of figure.

(Figure 4.3 on next page)

Figure 4.3. Nasals of *Gryposaurus* and other Kritosaurini. Left nasal images have been flipped horizontally to appear as right nasals for comparative purposes, because slightly more of the nasals used in the geometric morphometric analysis were rights. When both nasals of a specimen are present, an asterisk (*) indicates the nasal that was excluded from the geometric morphometric analysis. A hash symbol (#) indicates partial nasals that were missing two or more landmark points and were excluded from the final morphometric analysis. The 19 nasals with neither symbol (* nor #) were the specimens used in the final morphometric analysis (Figure 4.28). Apparent variations in the shape of the ventral margin are generally related to articulation state: disarticulated nasals typically include the ventrolateral contact areas for the lacrimal and posteroventral process of the premaxilla, although they are partially broken in some disarticulated specimens; these areas are generally not visible on nasals within articulated skulls due to being covered by the lacrimal and premaxilla. In some cases, the contacts are obscured and the nasal ventral margins are difficult to determine. Due to these variations, the ventral margin of the nasal was not used in the geometric morphometric analysis. Specimen outlines were adapted from the literature: *Gryposaurus latidens* AMNH FARB 5465 left and right (Prieto-Márquez, 2012); *G. notabilis* CMN 2278 left (Lambe, 1914); *G. notabilis* MSNM V345 left (Pinna, 1979), *G. notabilis* AMNH 5350 left and right (Prieto-Márquez, 2010a), *G.* sp. UMNH VP 18568 right (Gates et al., 2013), *G. monumentensis* RAM 6797 left and UMNH VP 13970 left (Gates and Sampson, 2007). Dashed lines indicate broken edges. Thin line within outline indicates position of ventrolateral contact between nasal, premaxilla, and lacrimal. All images have been scaled to the same 10 cm.



Gryposaurus reddingi
MOR 2573-7-14-11-535 and -534 Left
Holotype

Gryposaurus reddingi
MOR 2573-6-21-06-63 Left

Gryposaurus reddingi
MOR 2573-7-18-06-186 and
-6-03-10-271 Right

Gryposaurus reddingi
MOR 2573-7-09-11-526 Left#

Gryposaurus reddingi
MOR 2573-7-19-11-550 Left#

Gryposaurus reddingi
MOR 2573-7-16-11-539 Left#

Gryposaurus latidens
AMNH FARB 5465 Left
Holotype

Gryposaurus latidens
AMNH FARB 5465 Right*
Holotype

Gryposaurus latidens
MOR 478-7-2-7-3 Right

Gryposaurus notabilis
("*incurvimanus*")
ROM 764 Right#
Holotype

Gryposaurus notabilis
("*incurvimanus*")
TMP 1980.022.0001 Left

Gryposaurus notabilis
("*incurvimanus*")
TMP 1980.022.0001 Right*

Gryposaurus notabilis
ROM 1939 Left

Gryposaurus notabilis
CMN 2278 Right
Holotype

Gryposaurus notabilis
CMN 2278 Left*
Holotype

Gryposaurus notabilis
ROM 873 Right

Gryposaurus notabilis
ROM 873 Left*

Gryposaurus notabilis
MSNM V345 Left

Gryposaurus notabilis
AMNH 5350 Left

Gryposaurus notabilis
AMNH 5350 Right*

Gryposaurus sp.
UMNH VP 18568 Right

Gryposaurus monumentensis
RAM 6797 Left
Holotype

Gryposaurus monumentensis
UMNH VP 13970 Left

Gryposaurus sp.
MOR 399 Right

Kritosaurini indet.
MOR 553-7-2-8-26 Right

Rhinorex condrupus
BYU 13528 Right
Holotype

Kritosaurus ("*Anasazisaurus*")
horneri
BYU 12950 Right
Holotype

Naashoibitosaurus ostromi
NMMNH P-16106 Left
Holotype

Naashoibitosaurus ostromi
NMMNH P-16106 Right*
Holotype

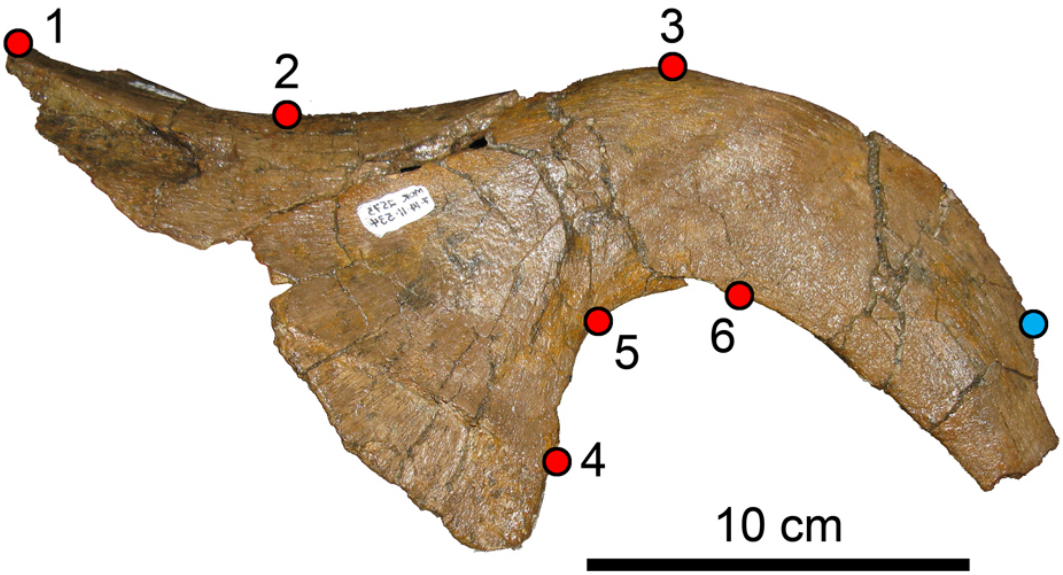


Figure 4.4. Landmark selection points for geometric morphometric analysis. The holotype nasal of *Gryposaurus reddingi*, MOR 2573-7-14-11-535 and -534, is used to illustrate landmark locations. The image was flipped horizontally so it appears as a right nasal for comparative purposes. Six points (red dots) were used in analysis. 1) Posteriormost extent of nasal in lateral view. 2) Lowest point between nasal crest and posteriormost extent of nasal. 3) Maximum extent of nasal crest, marked as the point of maximum curvature. 4) Contact point of nasal and posteroventral process of premaxilla along the external narial margin. 5) Posterodorsalmost extent of the external naris, marked as the point of maximum curvature. 6) Point on opposite side of naris from point 4, representing the width of the external naris. If a line is drawn from point 4 to point 6, then a perpendicular line drawn from point 5 will bisect that line. A seventh point (blue dot) representing the dorsal contact between the nasal and posterodorsal process of the premaxilla was initially tested, but due to this area being broken in many specimens, it was not included in the final analysis.

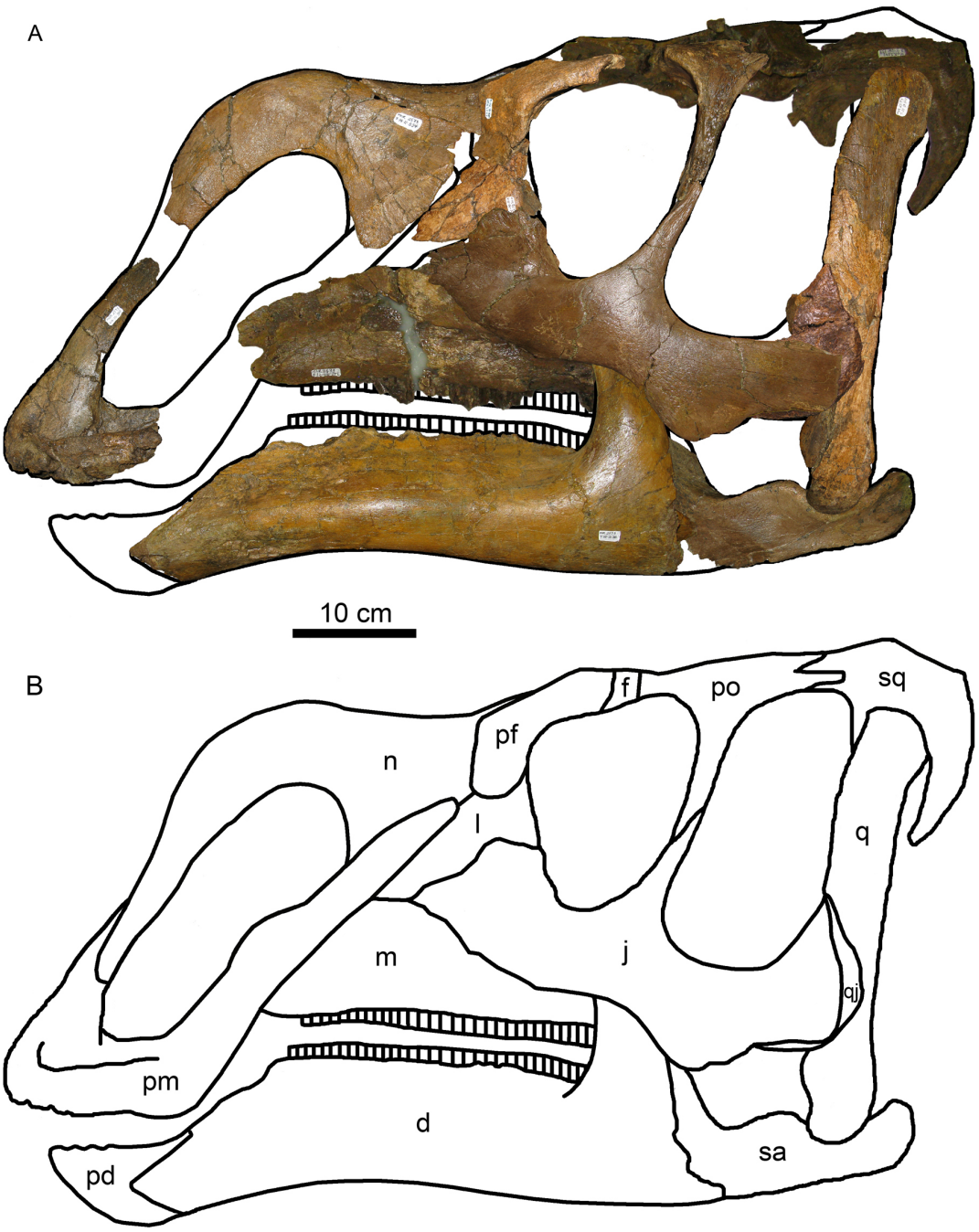


Figure 4.5. Skull reconstruction of *Gryposaurus reddingi*, MOR 2573. (A) Composite skull of MOR 2573 material from the JR-429 bonebed. Some right elements have been mirrored horizontally for use as left elements in the composite. (B) Outline of skull reconstruction of MOR 2573. Abbreviations: d, dentary; f, frontal; j, jugal; l, lacrimal; m, maxilla; n, nasal; p, parietal; pd, predentary; pf, prefrontal; pm, premaxilla; po, postorbital; q, quadrate; qj, quadratojugal; sa, surangular; sq, squamosal.

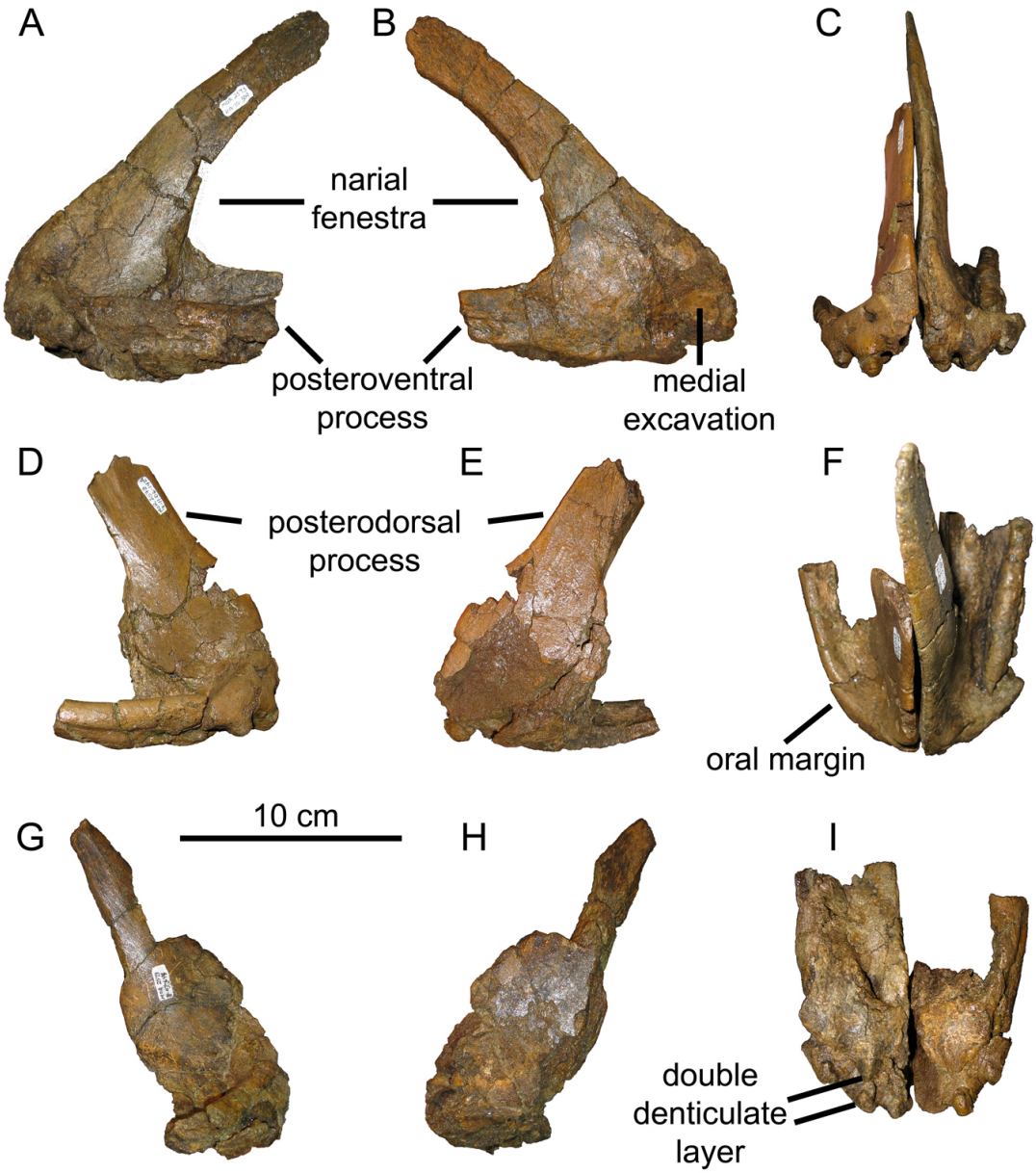


Figure 4.6. Premaxillae of *Gryposaurus reddingi*, MOR 2573. (A, B) Left premaxilla MOR 2573-6-10-10-304 in (A) lateral view and (B) medial view. (D, E) Right premaxilla MOR 2573-7-11-06-142A in (D) lateral view and (E) medial view. (G, H) Right premaxilla MOR 2573-8-07-12-644 in (G) lateral view and (H) medial view. (C, F, I) Premaxillae MOR 2573-6-10-10-304 and MOR 2573-7-11-06-142A illustrated together in (C) anterior view, (F) dorsal view, and (I) ventral view.

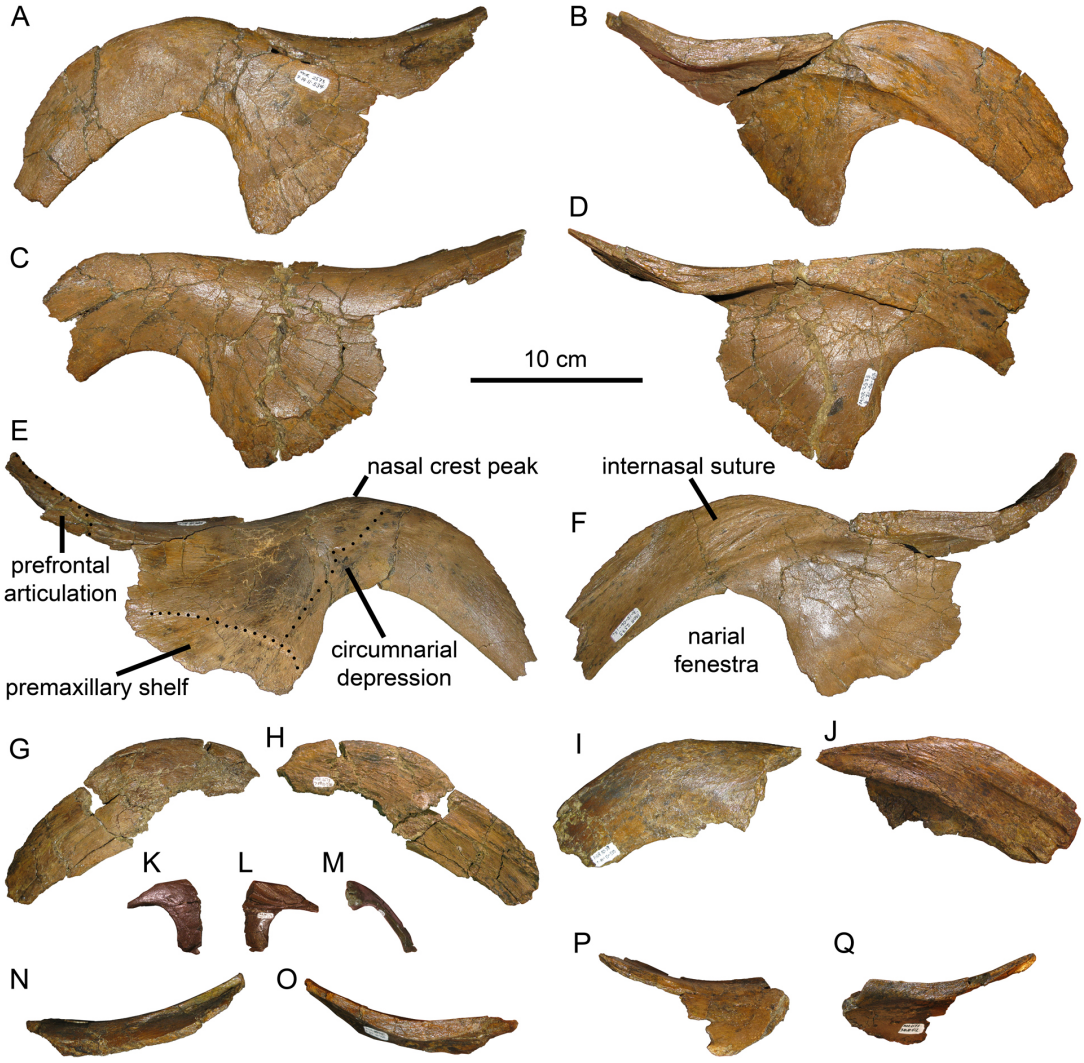


Figure 4.7. Nasals of *Gryposaurus reddingi*, MOR 2573. (A, B) Holotype of *Gryposaurus reddingi* left nasal MOR 2573-7-14-11-535 and posterior fragment MOR 2573-7-14-11-534 in (A) lateral view and (B) medial view. (C, D) Left nasal MOR 2573-6-21-06-63 in (C) lateral view and (D) medial view. (E, F) Right nasal MOR 2573-7-18-06-186 and posterior fragment MOR 2573-6-03-10-271 in (E) lateral view and (F) medial view. Dotted lines indicate locations of subtle ridges or grooves that mark the boundaries of the circumnarial depression and the articulations of the premaxilla and prefrontal. (G, H) Left nasal anterior fragment MOR 2573-7-09-11-526 in (G) lateral view and (H) medial view. (I, J) Left nasal anterior fragment MOR 2573-7-19-11-550 in (I) lateral view and (J) medial view. (K-M) Juvenile left nasal fragment of posterior narial fenestra region MOR 2573-7-16-11-539 in (K) lateral view, (L) medial view, and (M) anterior view demonstrating mediolateral width of narial region. (N, O) Juvenile left nasal posterior fragment MOR 2573-6-29-12-709 in (N) lateral view and (O) medial view. (P, Q) Juvenile right nasal posterior fragment MOR 2573-7-10-10-412 in (P) lateral view and (Q) medial view.

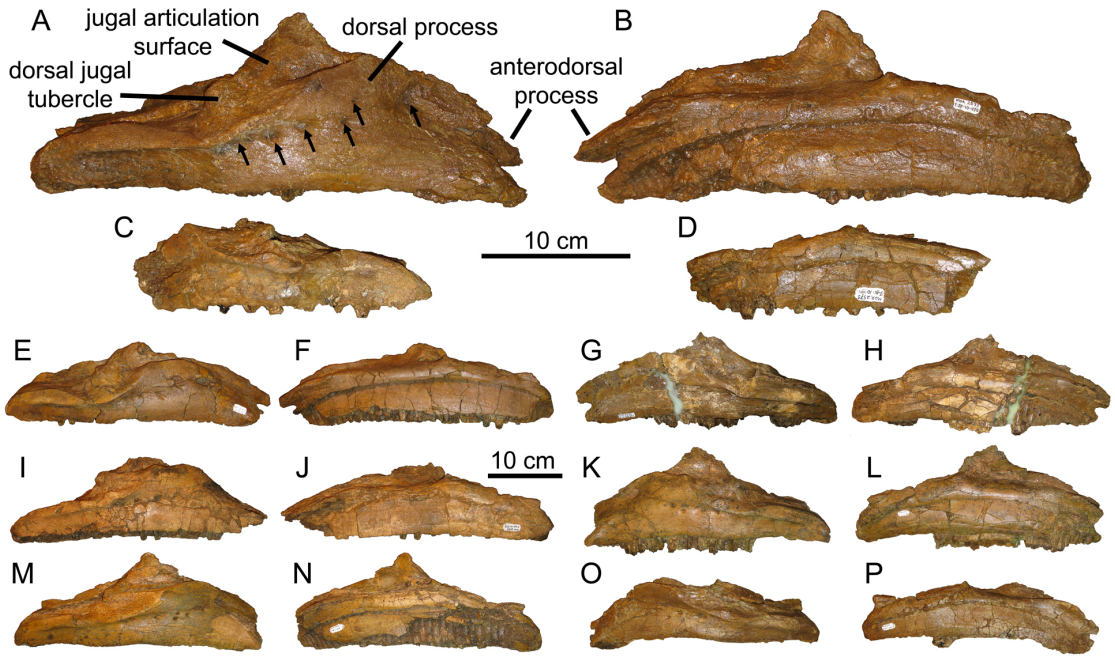


Figure 4.8. Maxillae of *Gryposaurus reddingi*, MOR 2573. Apparent morphologic differences are mostly due to differential diagenetic distortion. Note change in scale: (A-D) are double the scale size of (E-P). (A, B) Right maxilla MOR 2573-7-27-10-470 in (A) lateral view and (B) medial view. Arrows indicate positions of lateral maxillary fenestrae. (C, D) Left juvenile maxilla MOR 2573-7-01-10-359A in (C) lateral view and (D) medial view. (E, F) Right maxilla MOR 2573-7-10-10-423 in (E) lateral view and (F) medial view. (G, H) Left maxilla MOR 2573-7-11-06-156 in (G) lateral view and (H) medial view. (I, J) Right maxilla MOR 2573-7-22-10-447 in (I) lateral view and (J) medial view. (K, L) Left maxilla MOR 2573-7-13-06-167 in (K) lateral view and (L) medial view. (M, N) Right maxilla MOR 2573-7-28-22-599 in (M) lateral view and (N) medial view. (O, P) Left maxilla MOR 2573-8-03-11-625 in (O) lateral view and (P) medial view.

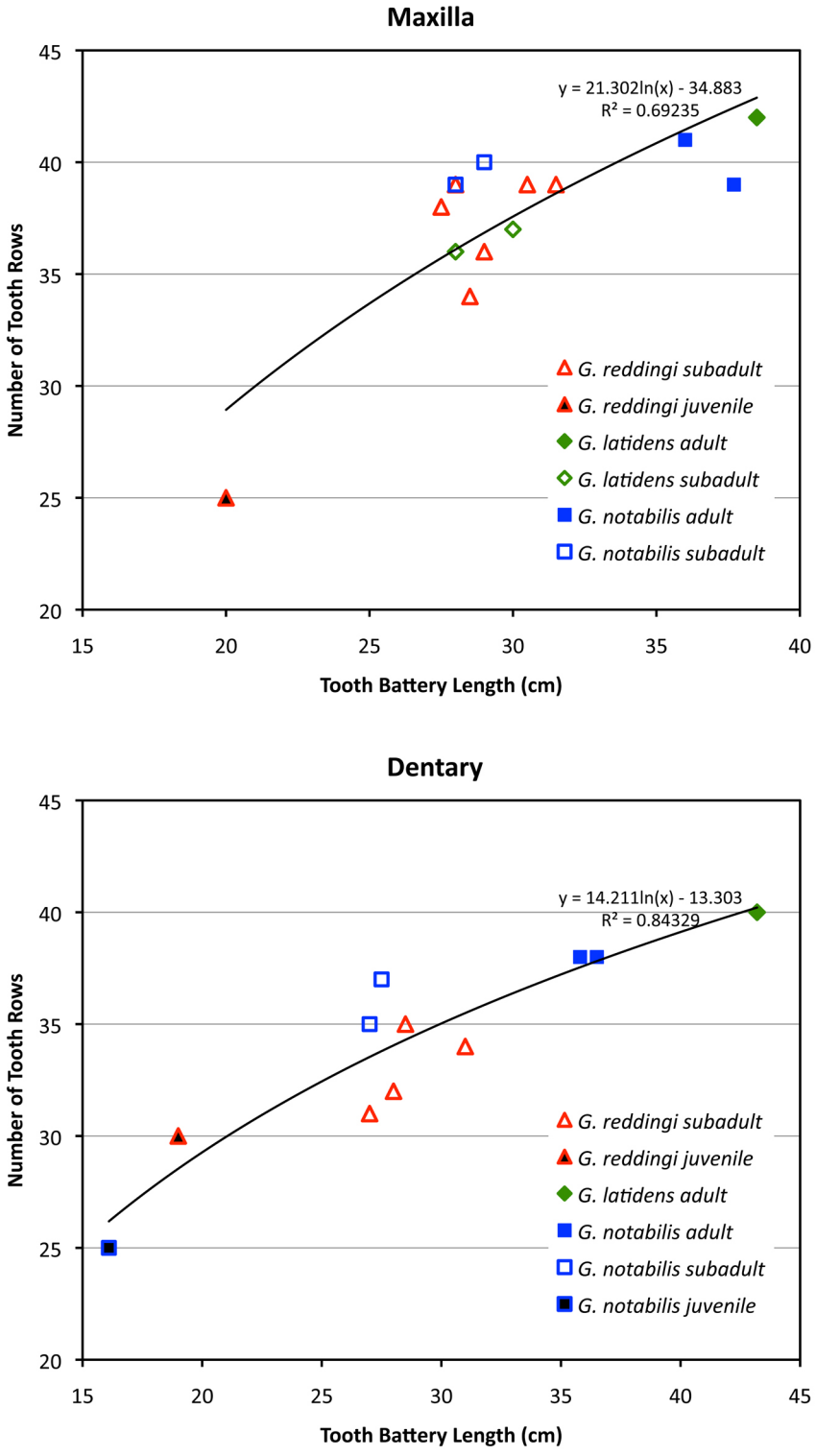


Figure 4.9. Length of tooth battery versus number of tooth rows in *Gryposaurus* maxillae and dentaries. Data are from Table 4.2.

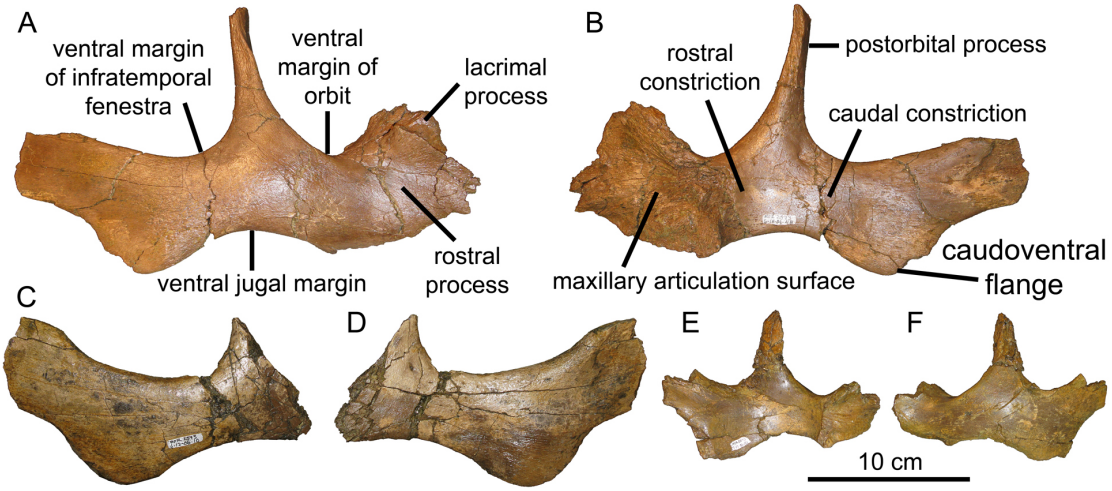


Figure 4.10. Jugals of *Gryposaurus reddingi*, MOR 2573. (A, B) Right jugal MOR 2573-6-18-06-48 in (A) lateral view and (B) medial view. (C, D) Right partial jugal MOR 2573-6-12-06-10 in (C) lateral view and (D) medial view. (E, F) Left juvenile jugal MOR 2573-7-17-06-181 in (E) medial view and (F) lateral view. The postorbital process of the juvenile jugal is fractured at its base and should be angled more posteriorly.

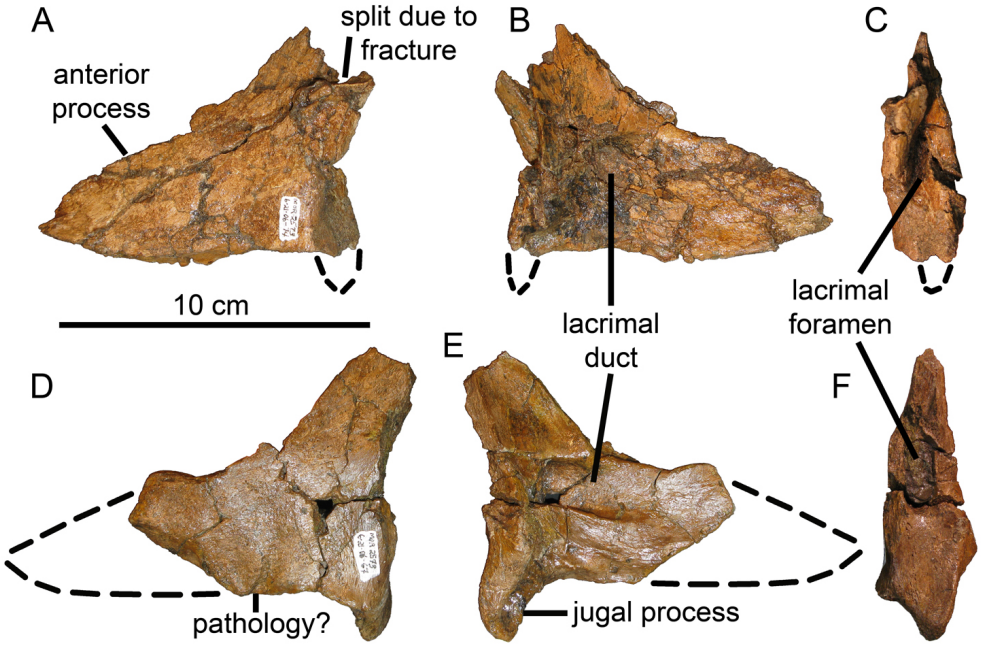


Figure 4.11. Lacrimals of *Gryposaurus reddingi*, MOR 2573. (A-C) Left lacrimal MOR 2573-6-21-06-74 in (A) lateral view, (B) medial view, and (C) posterior view. (D-F) Left lacrimal MOR 2573-6-21-06-67 in (D) lateral view, (E) medial view, and (F) posterior view. Dashed lines indicate approximate reconstructions of missing areas.

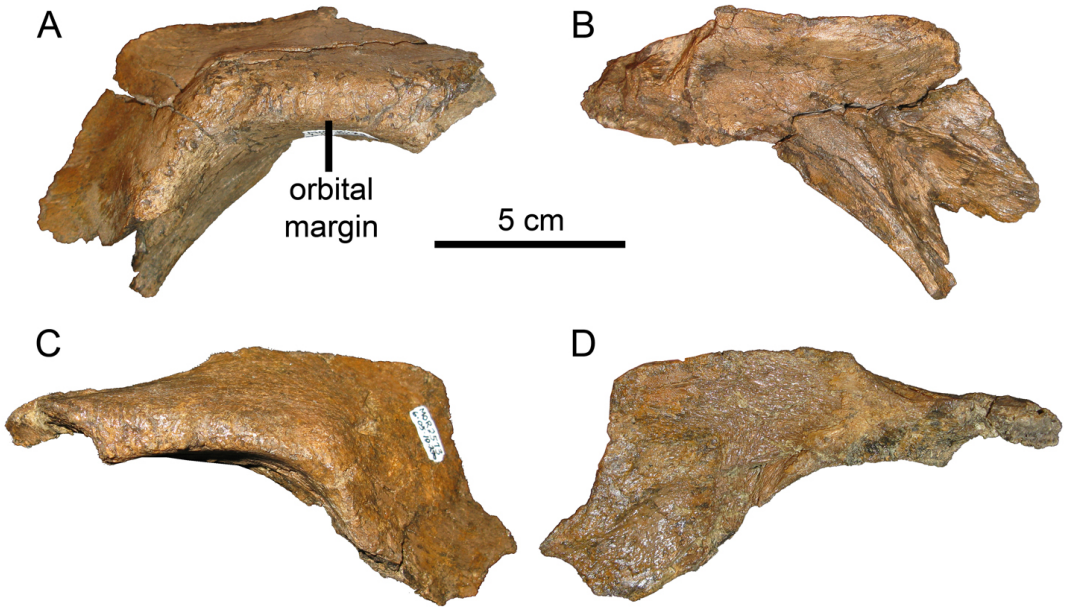


Figure 4.12. Prefrontals of *Gryposaurus reddingi*, MOR 2573. (A, B) Left prefrontal MOR 2573-7-05-06-122 in (A) lateral view and (B) medial view. (C, D) Right prefrontal MOR 2573-6-05-10-290 in (C) lateral view and (D) medial view.

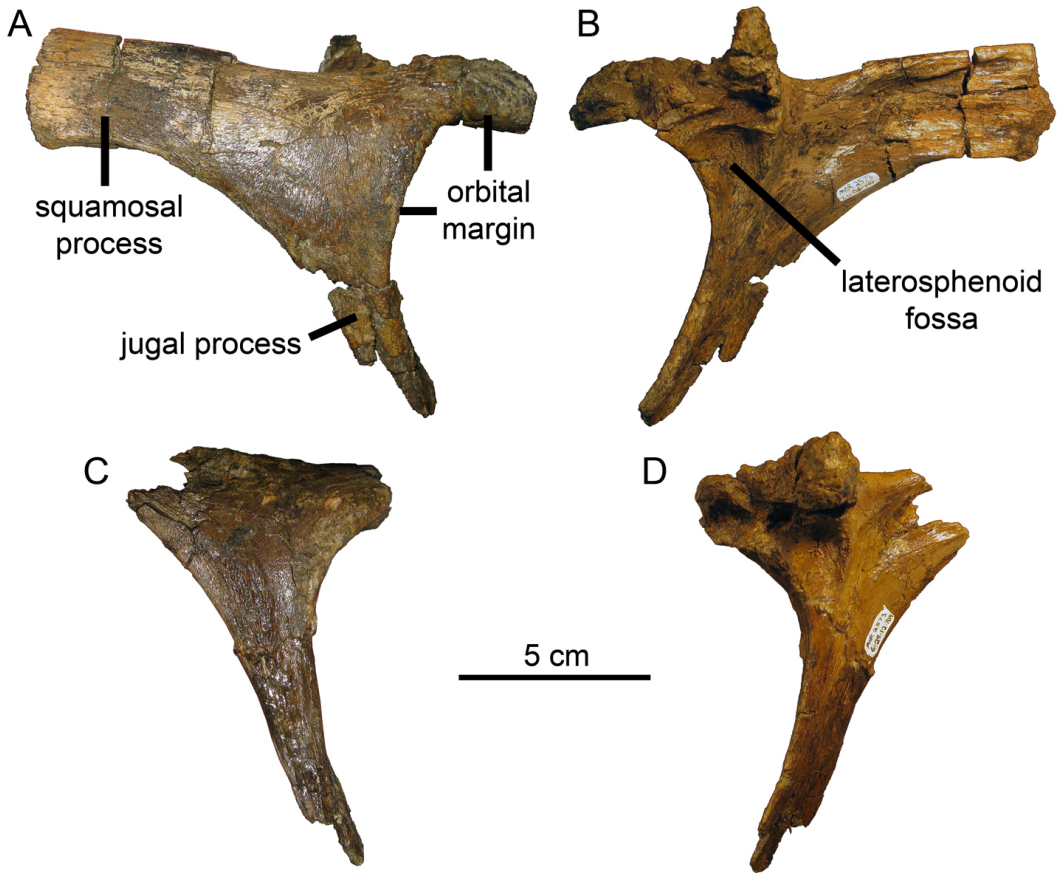
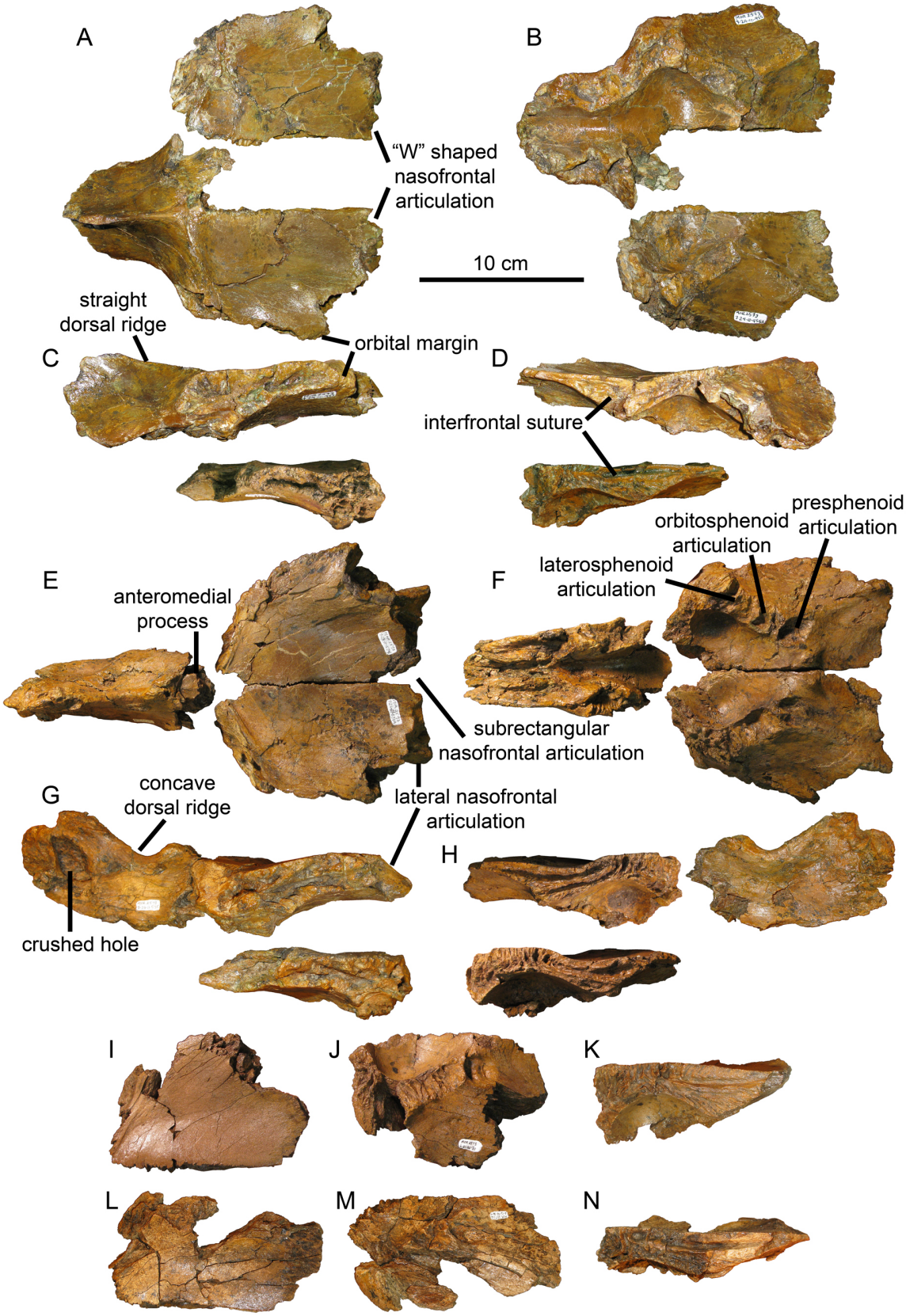


Figure 4.13. Postorbitals of *Gryposaurus reddingi*, MOR 2573. (A, B) Right postorbital MOR 2573-7-11-06-144 in (A) lateral view and (B) medial view. (C, D) Right postorbital MOR 2573-6-29-12-704 in (C) lateral view and (D) medial view.

(Figure 4.14 on next page)

Figure 4.14. Frontals and parietals of *Gryposaurus reddingi*, MOR 2573. Anterior is to the right in dorsal and ventral views. (A-D) Articulated right frontal and parietal MOR 2573-7-24-10-455 and associated left frontal MOR 2573-7-24-10-455A in (A) dorsal view, (B) ventral view, (C) lateral view, and (D) medial view. (E-H) Associated left frontal MOR 2573-7-23-11-574, right frontal MOR 2573-7-23-11-574A, and parietal MOR 2573-7-23-11-575. The right frontal articulates well with the left frontal and the parietal, but due to slight crushing of the parietal, the three cannot be articulated at the same time. (E) dorsal view, (F) ventral view, (G) lateral view of right frontal articulated with parietal, and lateral view of left frontal, and (H) medial views of frontals and left lateral view of parietal. (I-K) Isolated left frontal MOR 2573-6-21-06-80 in (I) dorsal view, (J) ventral view, and (K) medial view. (L-N) Isolated fragmented left frontal MOR 2573-6-12-06-16 in (L) dorsal view, (M) ventral view, and (N) medial view.


A
B
"W" shaped
nasofrontal
articulation
10 cm
straight
dorsal ridge
orbital margin
C
D
interfrontal suture
orbitosphenoid
articulation
presphenoid
articulation
laterosphenoid
articulation
E
F
anteromedial
process
subrectangular
nasofrontal articulation
G
concave
dorsal ridge
lateral nasofrontal
articulation
H
crushed hole
I
J
K
L
M
N

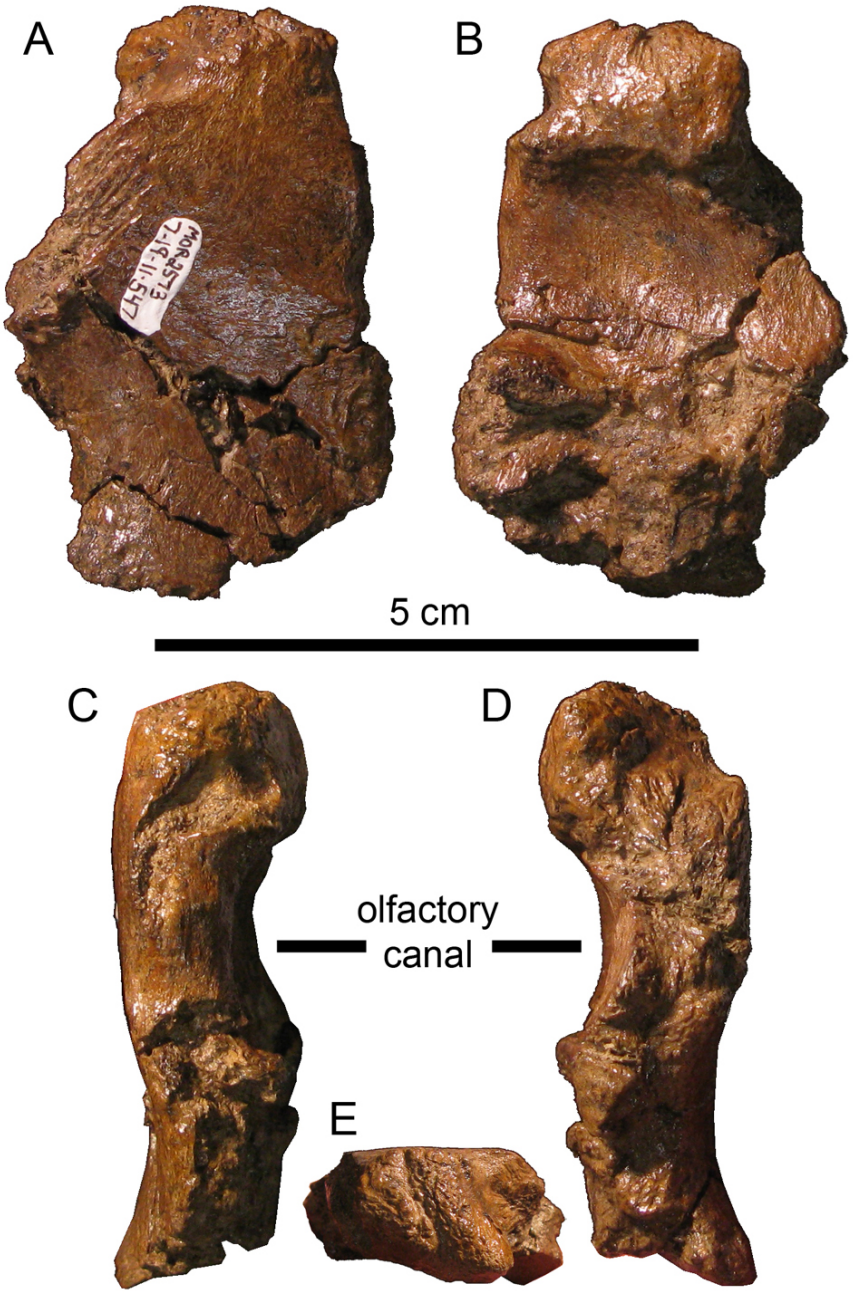


Figure 4.15. Presphenoid of *Gryposaurus reddingi*, MOR 2573. Right presphenoid MOR 2573-7-19-11-547 in (A) lateral view, (B) medial view, (C) anterior view, (D) posterior view, and (E) dorsal view.

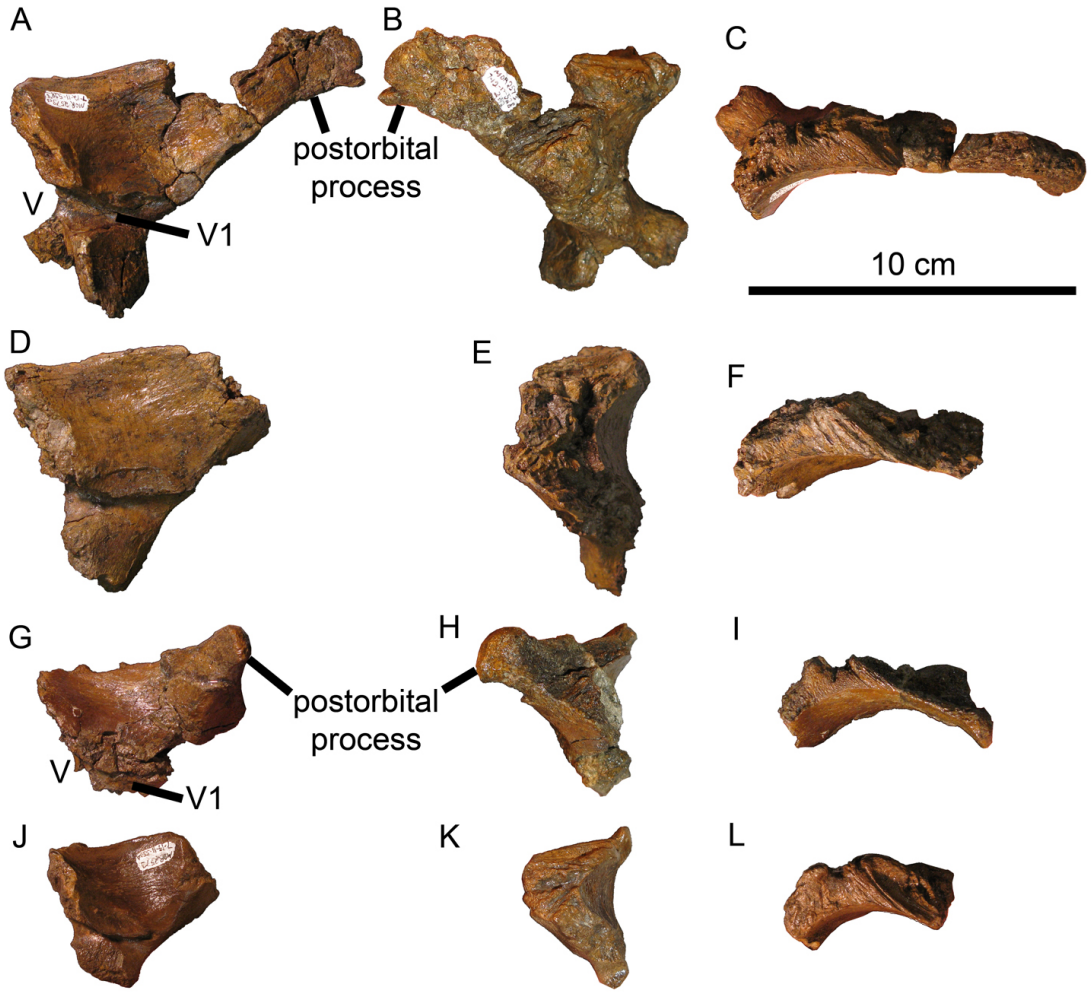


Figure 4.16. Laterosphenoids of *Gryposaurus reddingi*, MOR 2573. (A-C) Right laterosphenoid MOR 2573-7-12-11-528 in (A) posterolateral view, (B) anterior view, and (C) dorsal view. (D-F) Right laterosphenoid MOR 2573-7-21-11-560 in (D) posterolateral view, (E) anterior view, and (F) dorsal view. (G-I) Right juvenile laterosphenoid MOR 2573-7-31-10-499 in (G) posterolateral view, (H) anterior view, and (I) dorsal view. (J-L) Right juvenile laterosphenoid MOR 2573-7-19-11-550A in (J) posterolateral view, (K) anterior view, and (L) dorsal view. Abbreviations: V, trigeminal nerve foramen; V1, canal for ophthalmic branch of trigeminal nerve.

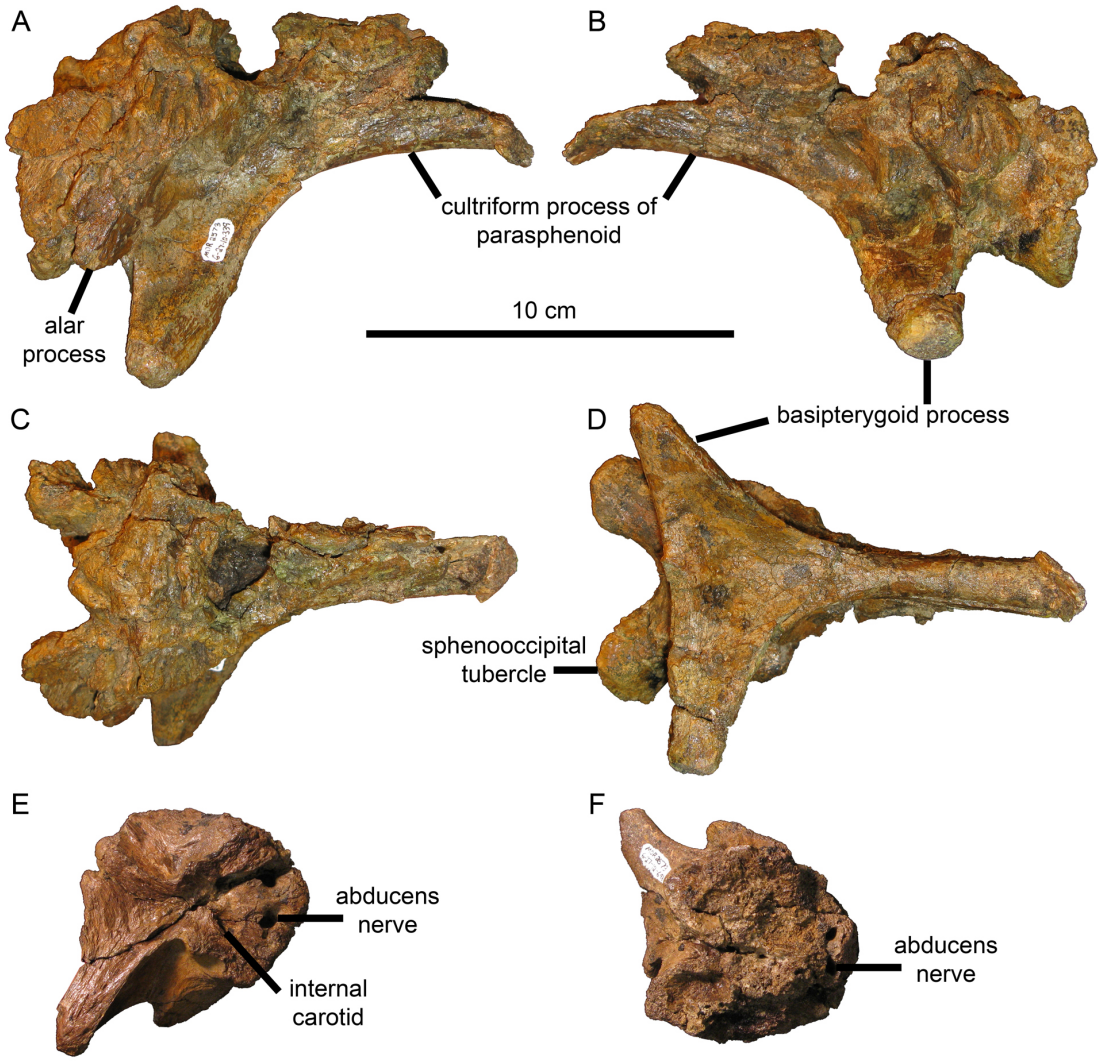


Figure 4.17. Basisphenoids of *Gryposaurus reddingi*, MOR 2573. The parasphenoid is fused with the basisphenoid into a single element. (A-D) Basisphenoid MOR 2573-6-27-10-339 in (A) right lateral view, (B) left lateral view, (C) dorsal view, and (D) ventral view. (E, F) Partial basisphenoid MOR 2573-6-27-12-698 in (E) dorsal view and (F) ventral view.

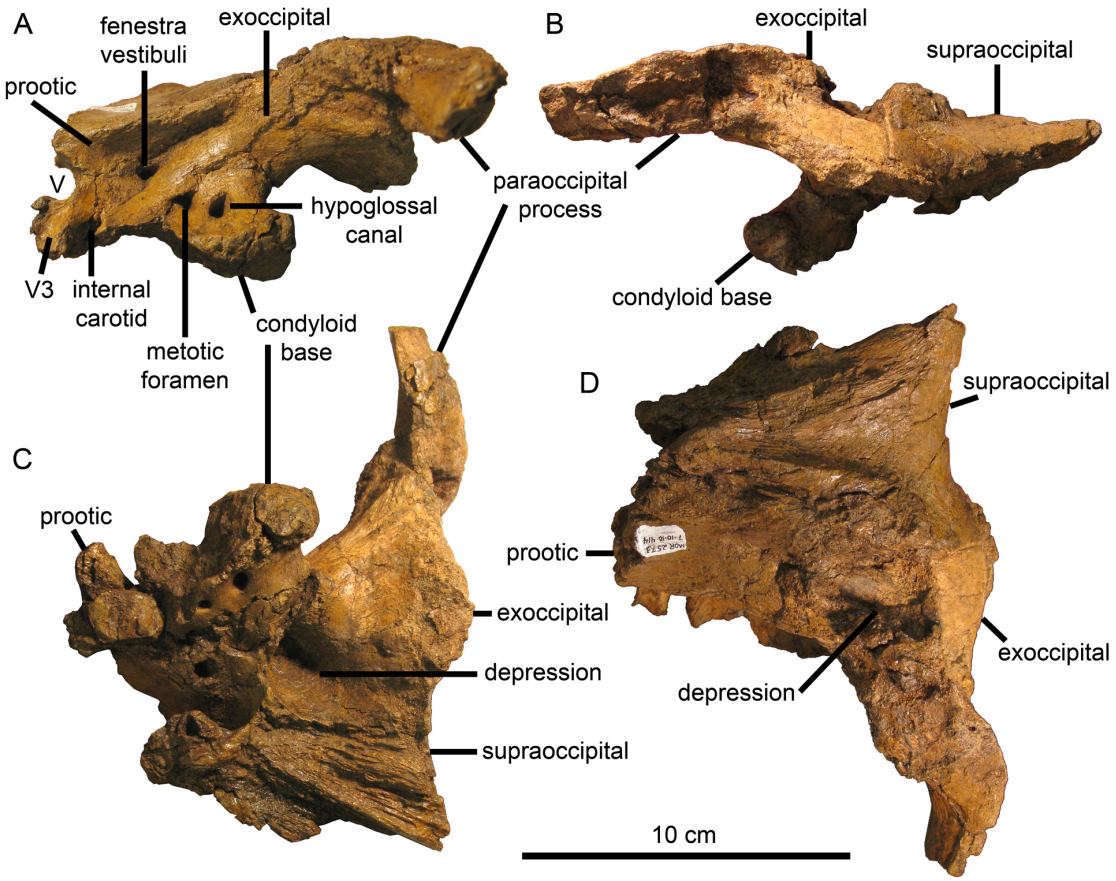


Figure 4.18. Articulated prootic, exoccipital, and supraoccipital of *Gryposaurus reddingi*, MOR 2573-7-10-10-414. Left prootic and left exoccipital articulated with the supraoccipital in (A) left lateral view, (B) posterior view, (C) ventral view, and (D) dorsal view. In ventral and dorsal views, anterior is to the left. The fenestra vestibuli (Prieto-Márquez, 2010a), also termed the oval window, is labeled as the auditory nerve (VIII) in some publications (Prieto-Márquez, 2005; Cuthbertson and Holmes, 2010). The metotic foramen includes subforamina for the vagus (X), hypoglossal (XII), and possibly glossopharyngeal (IX) cranial nerves (Prieto-Márquez, 2010a). Abbreviations: V, trigeminal nerve foramen; V3, canal for mandibular branch of trigeminal nerve.

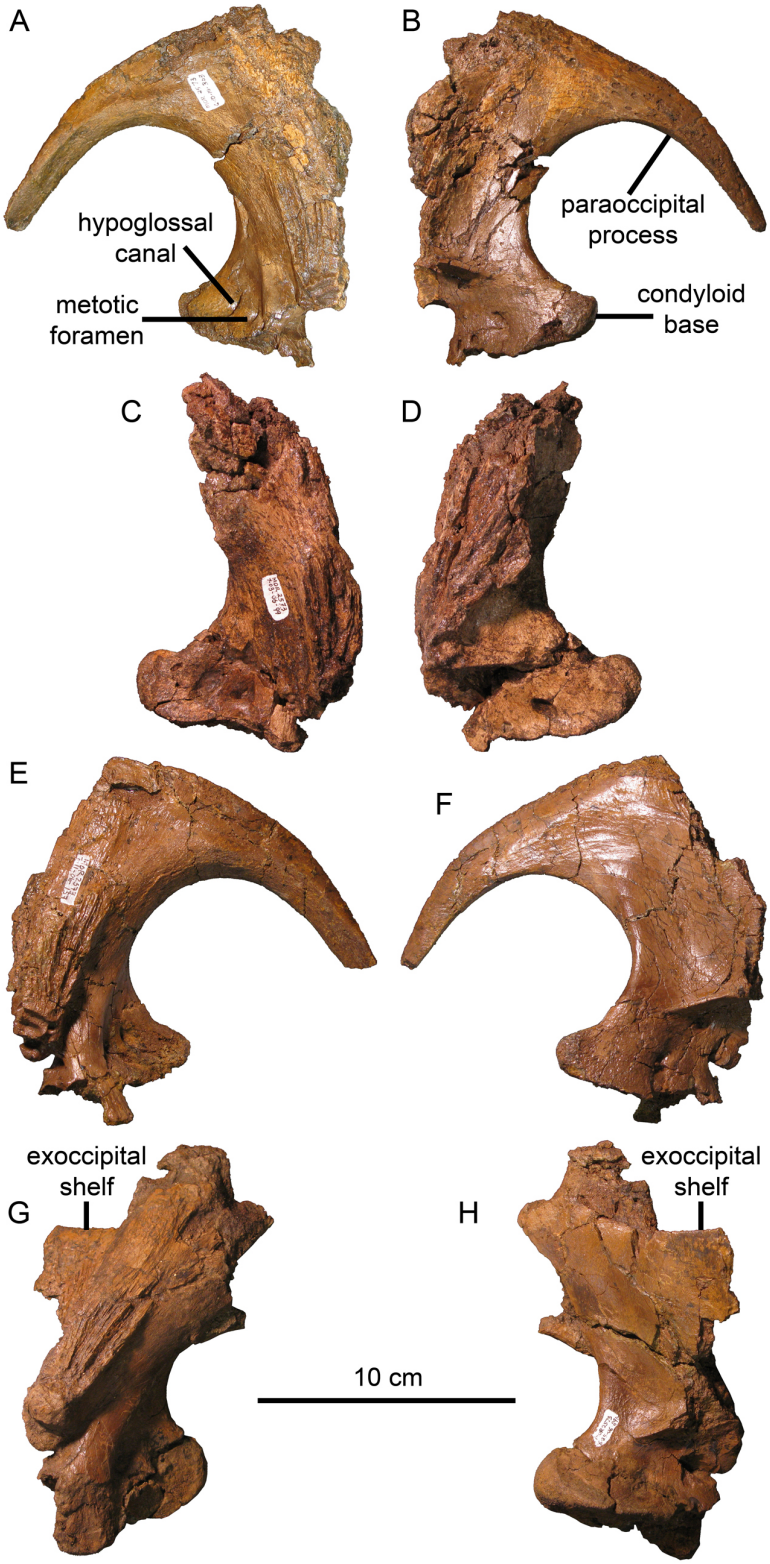


Figure 4.19. Opisthotic-Exoccipitals of *Gryposaurus reddingi*, MOR 2573. (A, B) Right opisthotic-exoccipital MOR 2573-6-10-10-303 in (A) anterolateral view and (B) posteromedial view. (C, D) Right partial opisthotic-exoccipital MOR 2573-7-03-06-99 in (C) anterolateral view and (D) posteromedial view. (E, F) Left opisthotic-exoccipital MOR 2573-7-11-06-157 in (E) anterolateral view and (F) posteromedial view. (G, H) Left partial opisthotic-exoccipital MOR 2573-6-25-06-89 in (G) anterolateral view and (H) posteromedial view.

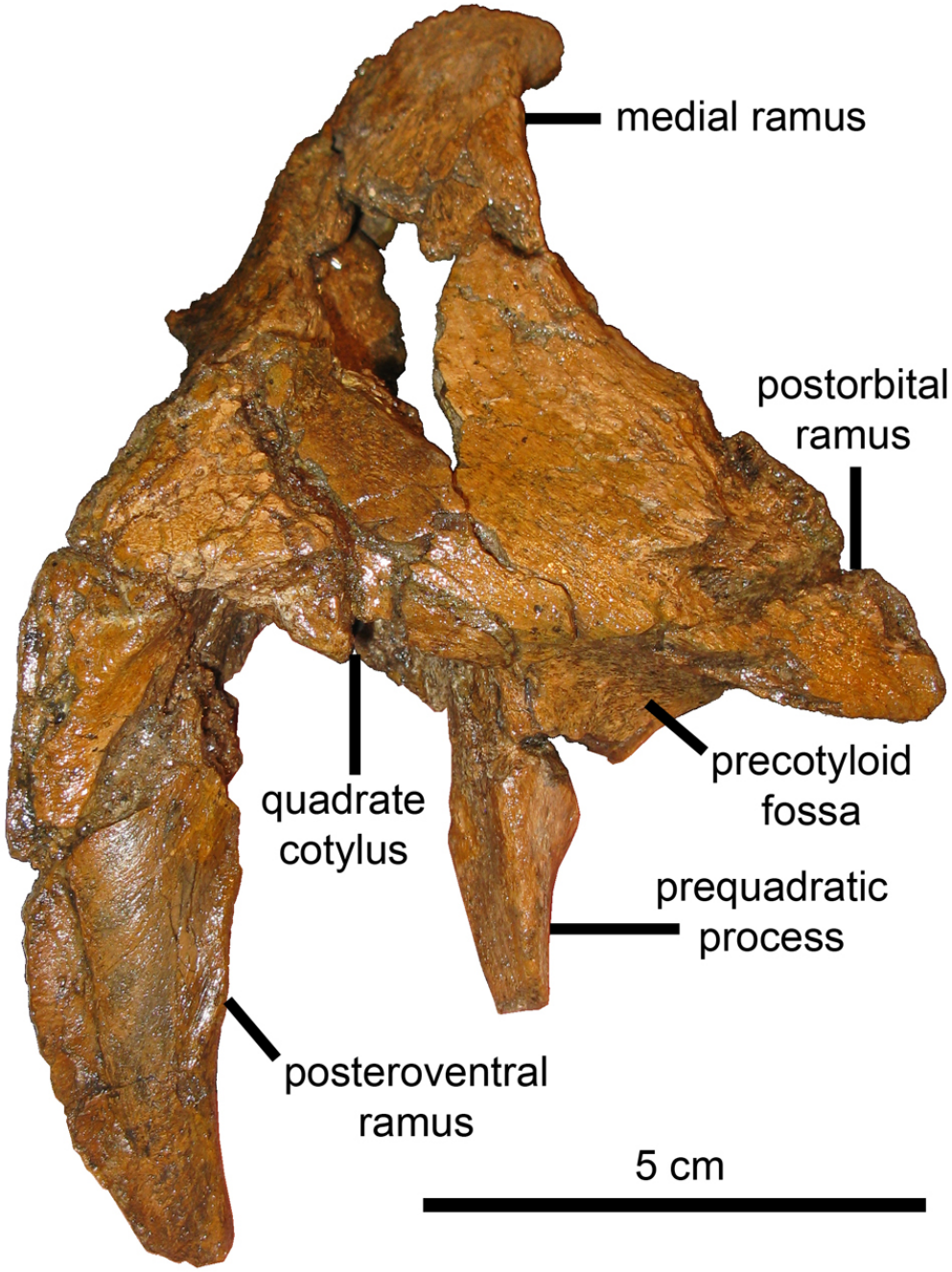


Figure 4.20. Squamosal of *Gryposaurus reddingi*, MOR 2573. Right juvenile squamosal MOR 2573-7-18-06-185 in dorsolateral view. The squamosal has been diagenetically distorted so that the dorsal and lateral surfaces are closer to being parallel than perpendicular.

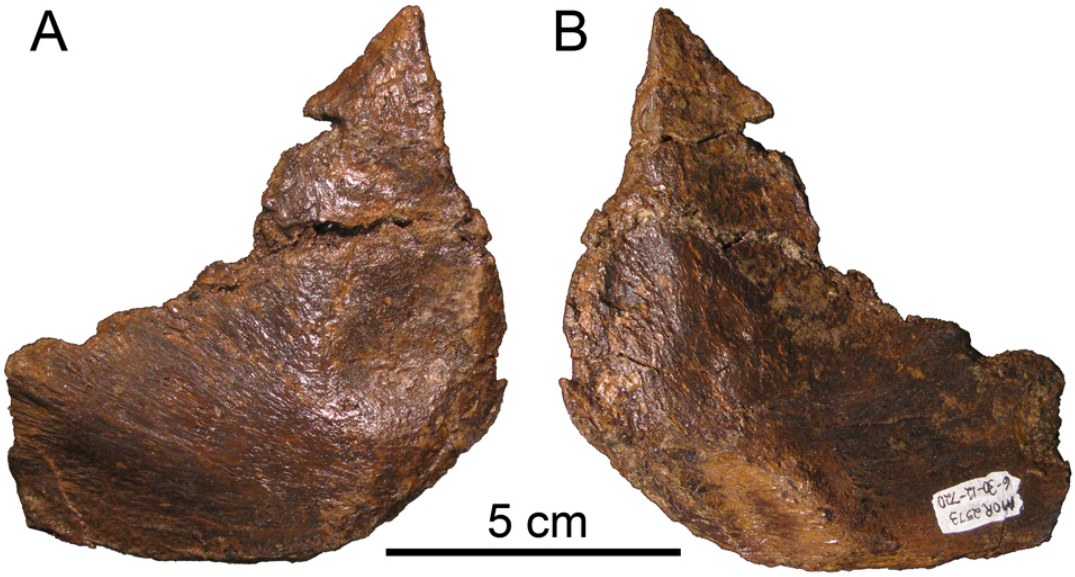


Figure 4.21. Quadratojugal of *Gryposaurus reddingi*, MOR 2573. Left quadratojugal MOR 2573-6-30-12-720 in (A) lateral view and (B) medial view.

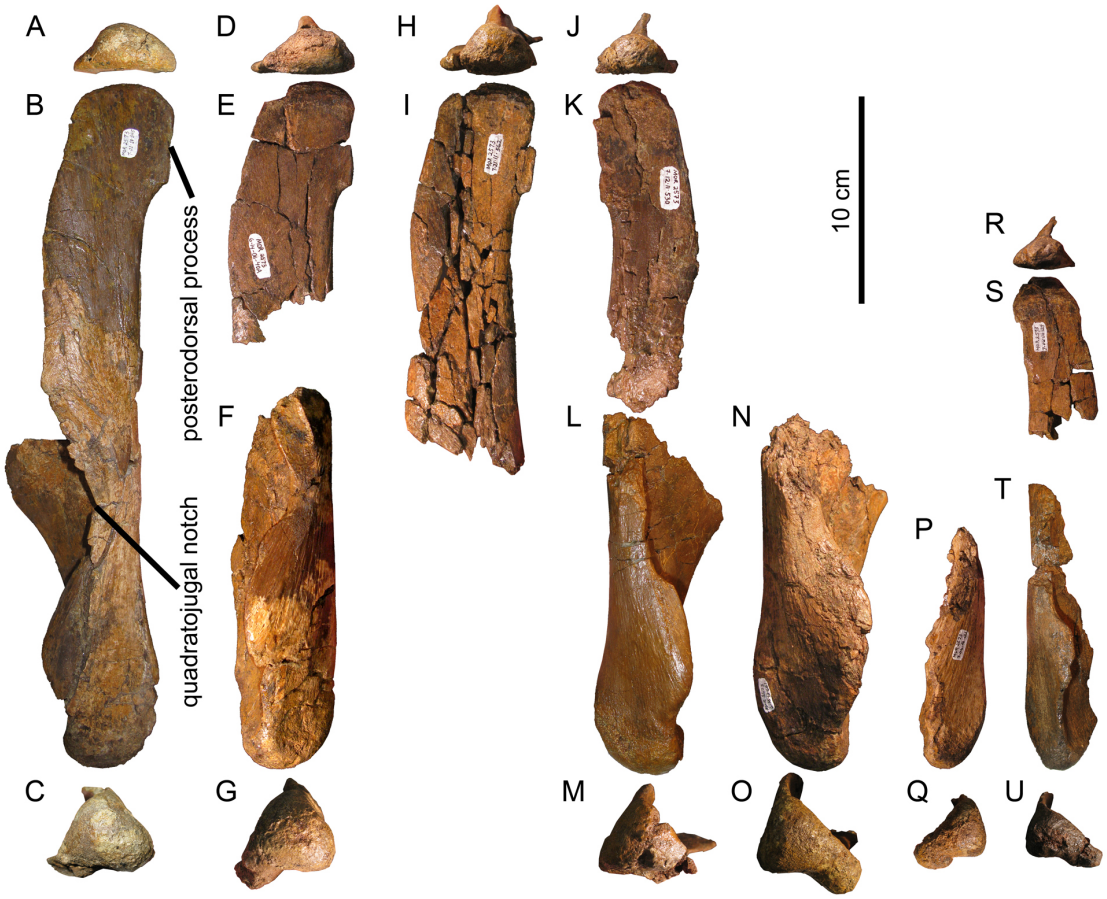


Figure 4.22. Quadrates of *Gryposaurus reddingi*, MOR 2573. In dorsal view, the lateral side is facing downward. In ventral view, the anterolateral side is facing upward. Quadrate halves illustrated together are not necessarily matching halves of the same individual bone. (A-C) Left quadrate MOR 2573-7-01-10-345 in (A) dorsal view, (B) lateral view), and (C) ventral view. (D, E) Left quadrate dorsal half MOR 2573-6-14-06-40A in (D) dorsal view and (E) lateral view. (F, G) Left quadrate ventral half MOR 2573-7-14-12-763 in (F) lateral view and (G) ventral view. (H, I) Left quadrate dorsal half MOR 2573-7-21-11-562 in (H) dorsal view and (I) lateral view. (J, K) Right quadrate dorsal half MOR 2573-7-12-11-530 in (J) dorsal view and (K) lateral view. (L, M) Right quadrate ventral half MOR 2573-8-11-11-650 in (L) lateral view and (M) ventral view. (N, O) Right quadrate ventral half MOR 2573-6-16-12-661 in (N) lateral view and (O) ventral view. (P, Q) Left juvenile quadrate ventral half MOR 2573-7-06-06-132 in (P) lateral view and (Q) ventral view. (R, S) Right juvenile quadrate dorsal half MOR 2573-7-06-06-124 in (R) dorsal view and (S) lateral view. (T, U) Right juvenile quadrate ventral half MOR 2573-6-21-06-59 in (T) lateral view and (U) ventral view.



Figure 4.23. Vomer of *Gryposaurus reddingi*, MOR 2573. Left vomer MOR 2573-7-07-10-390 in (A) lateral view and (B) medial view.

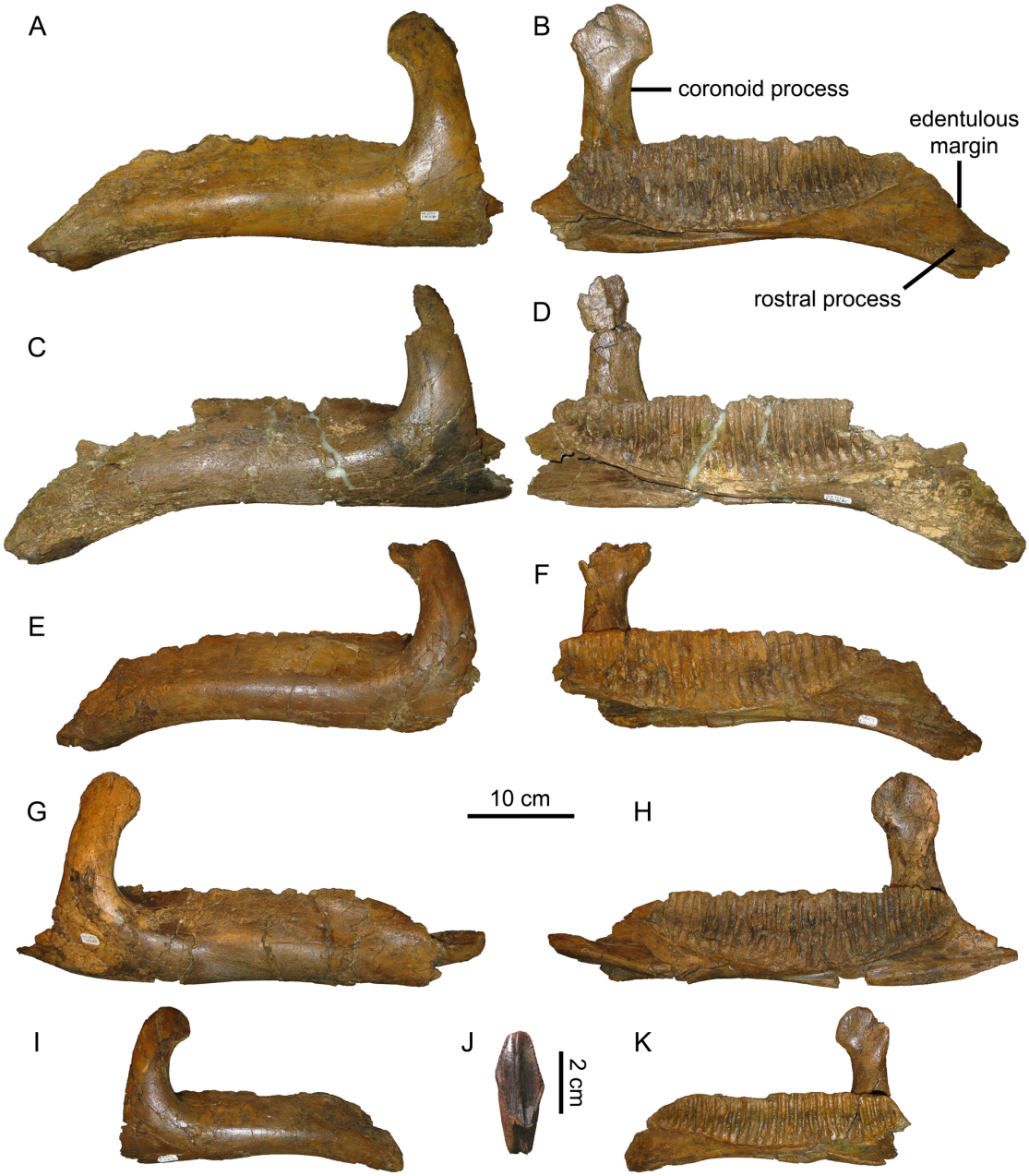


Figure 4.24. Dentaries of *Gryposaurus reddingi*, MOR 2573. (A, B) Left dentary MOR 2573-7-05-10-381 in (A) lateral view and (B) medial view. (C, D) Left dentary MOR 2573-6-22-06-87 in (C) lateral view and (D) medial view. (E, F) Left dentary MOR 2573-8-03-11-636 in (E) lateral view and (F) medial view. (G, H) Right dentary MOR 2573-7-05-10-378 in (G) lateral view and (H) medial view. (I, K) Right juvenile dentary MOR 2573-7-13-12-757 in (I) lateral view and (K) medial view. (J) Isolated dentary tooth from the JR-429 bonebed. It is the most complete tooth found in the bonebed, and it is also relatively wider than any of the partial teeth. The 10 cm scale bar applies to all dentaries; the 2 cm scale bar applies only to the tooth.

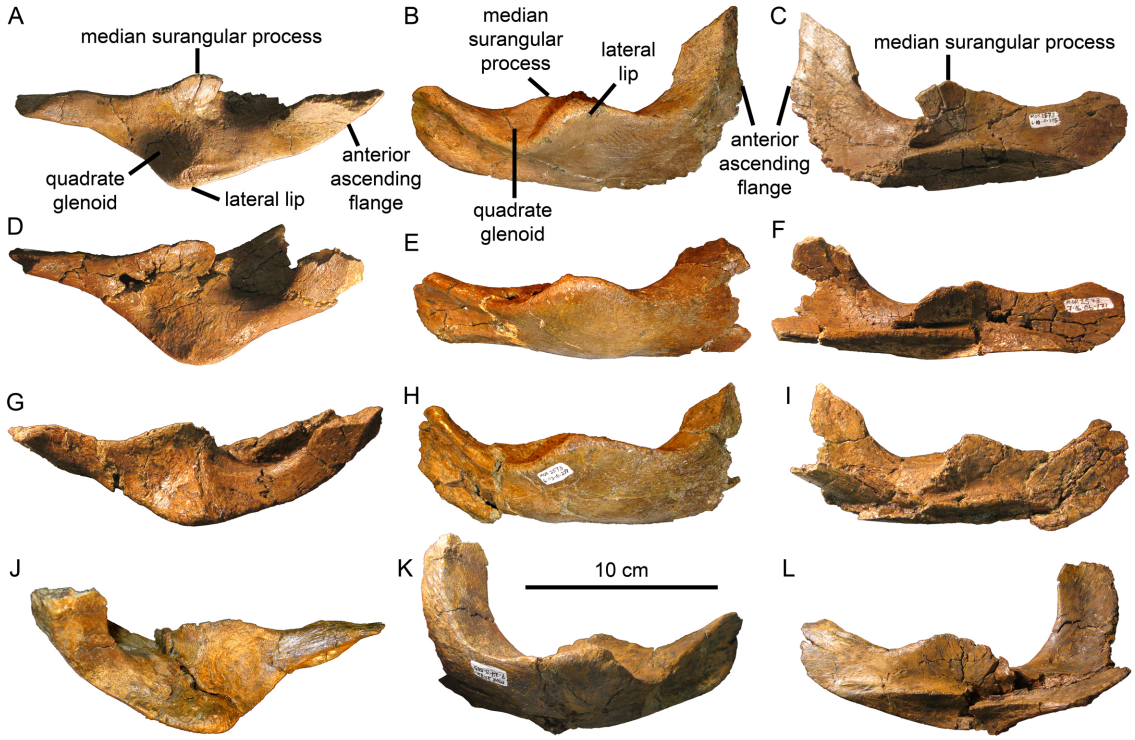


Figure 4.25. Surangulars of *Gryposaurus reddingi*, MOR 2573. (A-C) Right surangular MOR 2573-6-10-10-305 in (A) dorsal view, (B) lateral view, and (C) medial view. (D-F) Right surangular MOR 2573-7-16-06-171 in (D) dorsal view, (E) lateral view, and (F) medial view. (G-I) Right surangular MOR 2573-6-03-10-277 in (G) dorsal view, (H) lateral view, and (I) medial view. (J-L) Left surangular MOR 2573-7-24-11-583 in (J) dorsal view, (K) lateral view, and (L) medial view.

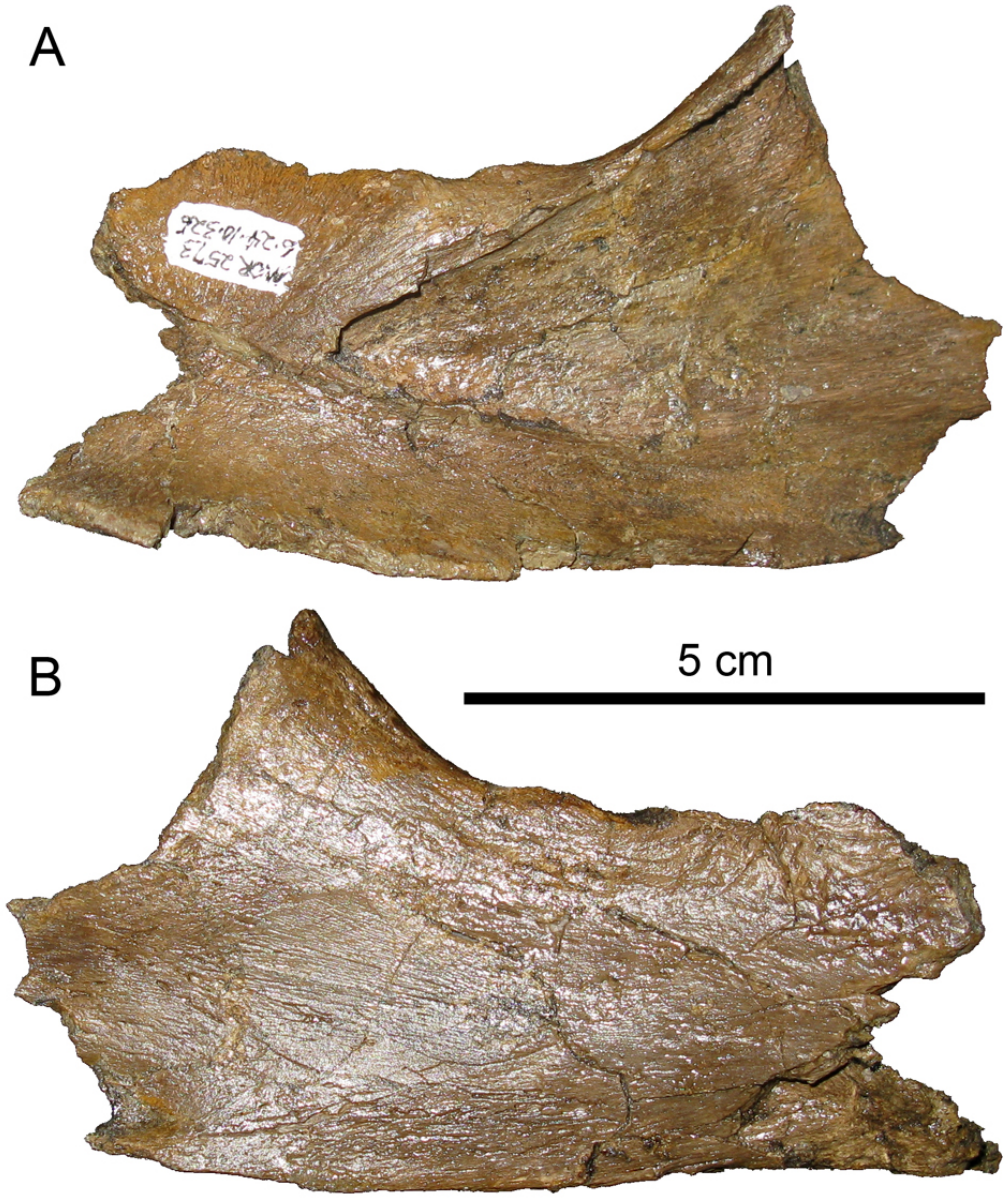


Figure 4.26. Splenial of *Gryposaurus reddingi*, MOR 2573. Right splenial MOR 2573-6-24-10-326 in (A) lateral view and (B) medial view.

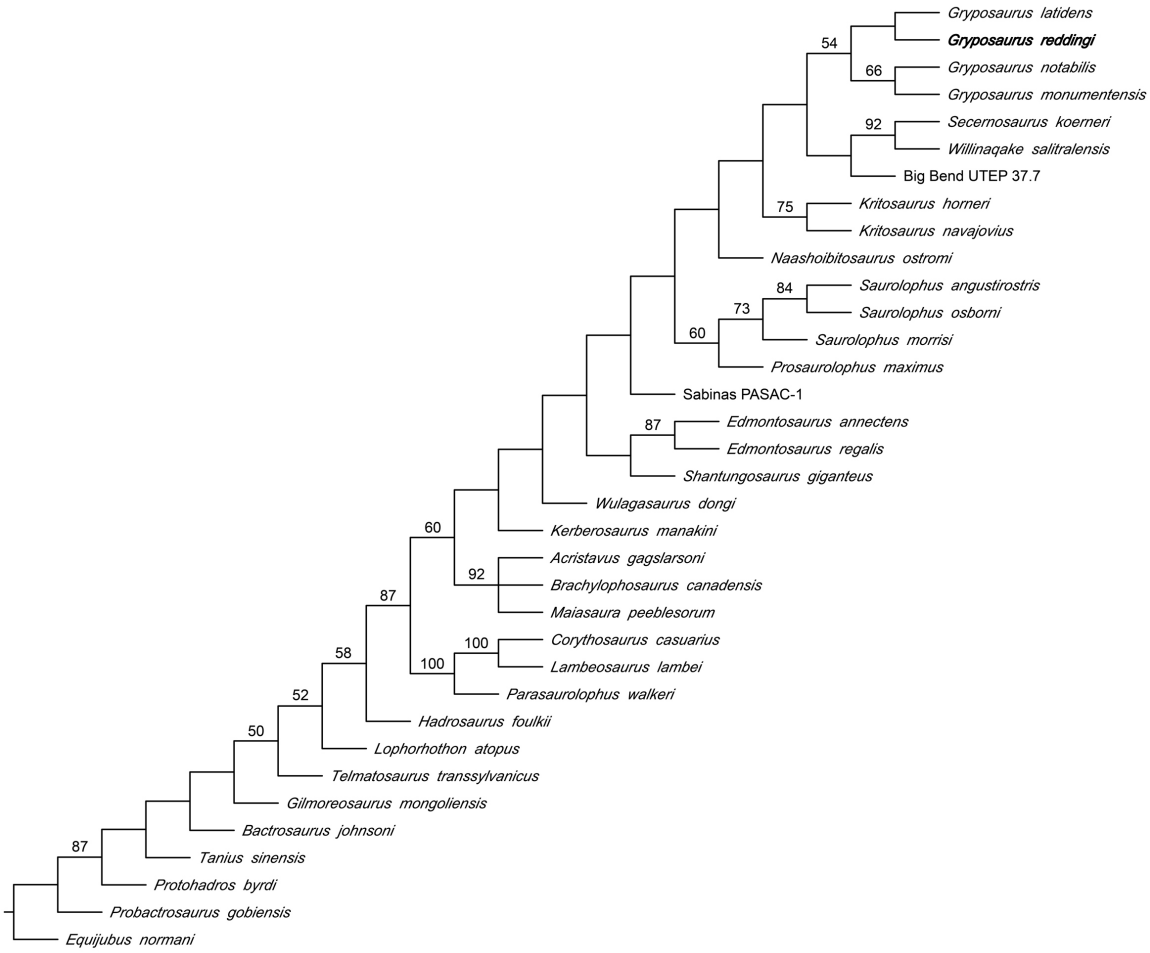


Figure 4.27. Strict consensus tree of the three most parsimonious phylogenetic trees. *Gryposaurus reddingi* was added to the matrix of Prieto-Márquez (2014); the resulting topology is nearly identical to that of Prieto-Márquez (2014), with the addition of *G. reddingi* as the sister taxon to *G. latidens*. Numbers on branches indicate bootstrap support values above 50 percent; branches without values had less than 50 percent support. Tree statistics: Tree Length = 668, Consistency Index = 0.61, Retention Index = 0.75, Rescaled Consistency Index = 0.46.

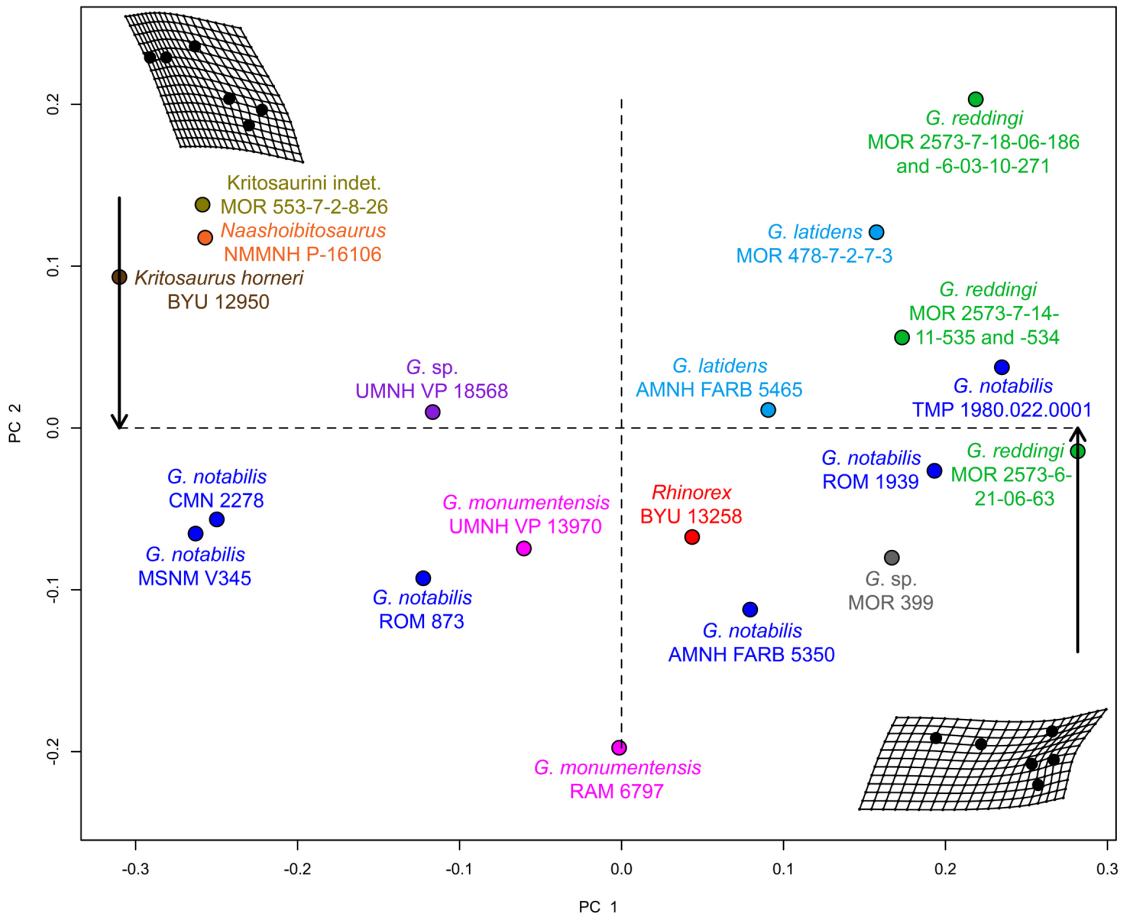


Figure 4.28. Geometric morphometric Principal Components Analysis of nasal shape of *Gryposaurus* and other Kritosaurini specimens. Deformation grids illustrate shapes of specimens at the endpoints of principal component axis 1. Axis 1 (x) accounts for 67.4% of variation; Axis 2 (y) accounts for 17.7% of variation. Abbreviations: PC, principal component axis.

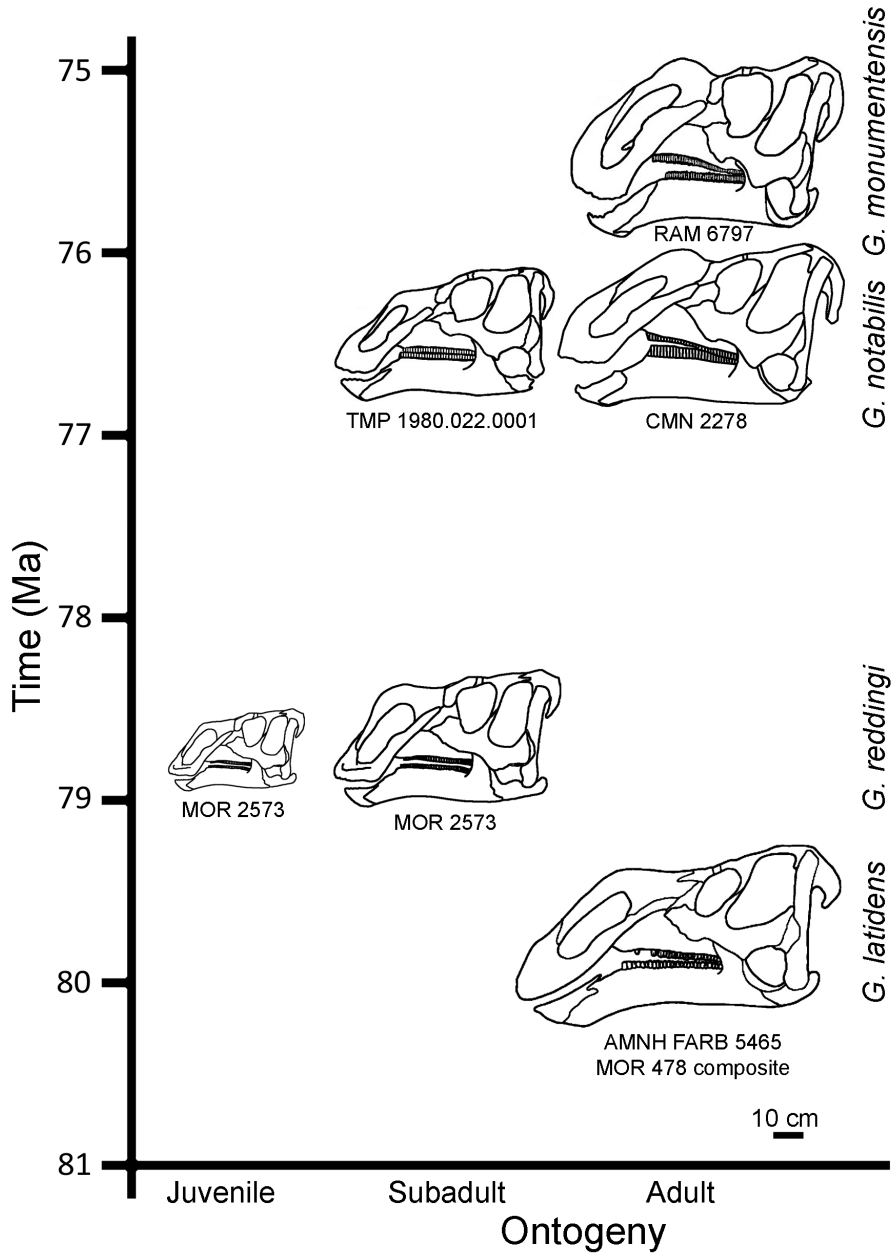


Figure 4.29. Ontogenetic and anagenetic hypothesis of *Gryposaurus* evolution. *Gryposaurus reddingi* is proposed as an intermediate member of the lineage leading from *G. latidens* to *G. notabilis* and *G. monumentensis*. Skull outlines of *G. latidens*, subadult *G. notabilis*, and *G. monumentensis* are modified from Gates and Sampson (2007) and Horner (1992). All skulls are scaled to the same 10 cm scale bar. The horizontal axis is not to scale. Positions of specimens along the vertical axis reflect the radiometric age ranges listed in Table 4.1 based on the recalibrations of Roberts et al. (2013) to a Fish Canyon sanidine standard of 28.201 Ma.

Literature Cited

Adams, D. C., and E. Otárola-Castillo. 2013. geomorph: an R package for the collection and analysis of geometric morphometric shape data. Methods in Ecology and Evolution 4:393-399.

Brinkman, D. B., A. P. Russell, D. A. Eberth, and J. Peng. 2004. Vertebrate palaeocommunities of the lower Judith River Group (Campanian) of southeastern Alberta, Canada, as interpreted from vertebrate microfossil assemblages. Palaeogeography, Palaeoclimatology, Palaeoecology 213:295-313.

Brown, B. 1910. The Cretaceous Ojo Alamo beds of New Mexico with description of the new genus *Kritosaurus*. Bulletin of the American Museum of Natural History 28:267-274.

Currie, P. J., and D. A. Russell. 2005. The geographic and stratigraphic distribution of articulated and associated dinosaur remains; pp. 537-569 in P. J. Currie and E. B. Koppelhus (eds.), Dinosaur Provincial Park: A Spectacular Ancient Ecosystem Revealed. Indiana University Press, Bloomington, Indiana.

Cuthbertson, R. S., and R. B. Holmes. 2010. The first complete description of the holotype of *Brachylophosaurus canadensis* Sternberg, 1953 (Dinosauria: Hadrosauridae) with comments on intraspecific variation. Zoological Journal of the Linnean Society 159:373-397.

Eberth, D. A. 2005. The Geology; pp. 54-82 in P. J. Currie and E. B. Koppelhus (eds.), Dinosaur Provincial Park: A Spectacular Ancient Ecosystem Revealed. Indiana University Press, Bloomington, Indiana.

Evans, D. C. 2010. Cranial anatomy and systematics of *Hypacrosaurus altispinus*, and a comparative analysis of skull growth in lambeosaurine hadrosaurids (Dinosauria: Ornithischia). Zoological Journal of the Linnean Society 159:398-434.

Farke, A. A., and L. Herrero. 2015. Variation in the skull roof of the hadrosaur *Gryposaurus* illustrated by a new specimen from the Kaiparowits Formation (late Campanian) of southern Utah; pp. 191-199 in D. A. Eberth and D. C. Evans (eds.), Hadrosaurs. Indiana University Press, Bloomington, Indiana.

Fassett, J. E., and M. B. Steiner. 1997. Precise age of C33N-C32R magnetic-polarity reversal, San Juan Basin, New Mexico and Colorado. New Mexico Geological Society Guidebook 48:239-247.

Freedman Fowler, E. A. Chapter Three. Taphonomy of a Gryposaurus hadrosaur bonebed from the Judith River Formation (Campanian) of northcentral Montana.

Freedman Fowler, E. A., and J. R. Horner. Chapter Two. A new brachylophosaurinin (Dinosauria: Ornithischia) from the Judith River Formation of northcentral Montana.

Gates, T. A., and S. D. Sampson. 2007. A new species of *Gryposaurus* (Dinosauria: Hadrosauridae) from the late Campanian Kaiparowits Formation, southern Utah, USA. Zoological Journal of the Linnean Society 151:351-376.

Gates, T. A., and R. D. Scheetz. 2014. A new saurolophine hadrosaurid (Dinosauria: Ornithopoda) from the Campanian of Utah, North America. Journal of Systematic Palaeontology:1-15. http://dx.doi.org/10.1080/14772019.2014.950614.

Gates, T. A., J. R. Horner, R. R. Hanna, and R. C. Nelson. 2011. New unadorned hadrosaurine hadrosaurid (Dinosauria, Ornithopoda) from the Campanian of North America. Journal of Vertebrate Paleontology 31:798-811.

Gates, T. A., E. K. Lund, C. A. Boyd, D. D. DeBlieux, A. L. Titus, D. C. Evans, M. A. Getty, J. I. Kirkland, and J. G. Eaton. 2013. Ornithopod dinosaurs from the Grand Staircase-Escalante National Monument region, Utah, and their role in paleobiogeographic and macroevolutionary studies; pp. 463-481 in A. L. Titus and M. A. Loewen (eds.), At the Top of the Grand Staircase: the Late Cretaceous of Southern Utah. Indiana University Press, Bloomington, Indiana.

Goodwin, M. B., and A. L. Deino. 1989. The first radiometric ages from the Judith River Formation (Upper Cretaceous), Hill County, Montana. Canadian Journal of Earth Sciences 26:1384-1391.

Horner, J. R. 1984: Three ecologically distinct vertebrate faunal communities from the Late Cretaceous Two Medicine Formation of Montana, with discussion of evolutionary pressures induced by interior seaway fluctuations. Montana Geological Society Field Conference and Symposium, Northwest Montana and Adjacent Canada, 1984.

Horner, J. R. 1992. Cranial morphology of *Prosaurolophus* (Ornithischia: Hadrosauridae) with descriptions of two new hadrosaurid species and an evaluation of hadrosaurid phylogenetic relationships. Museum of the Rockies Occasional Paper 2:1-119.

Horner, J. R., D. J. Varricchio, and M. B. Goodwin. 1992. Marine transgressions and the evolution of Cretaceous dinosaurs. Nature 358:59-61.

Horner, J. R., D. B. Weishampel, and C. A. Forster. 2004. Hadrosauridae; pp. 438-463 in D. B. Weishampel, P. Dodson, and H. Osmólska (eds.), The Dinosauria. University of California Press, Berkeley.

Horner, J. R., J. G. Schmitt, F. D. Jackson, and R. R. Hanna. 2001. Bones and rocks of the Upper Cretaceous Two Medicine-Judith River clastic wedge complex, Montana. Guidebook for the Field Trips, Society of Vertebrate Paleontology 61st Annual Meeting, Museum of the Rockies Occasional Paper 3:1-13.

Hunt, A. P., and S. G. Lucas. 1993. Cretaceous vertebrates of New Mexico. Bulletin - New Mexico Museum of Natural History and Science 2:77-91.

Jinnah, Z. A. 2013. Tectonic and sedimentary controls, age, and correlation of the Upper Cretaceous Wahweap Formation, Southern Utah; pp. 57-73 in A. L. Titus and M. A. Loewen (eds.), At the Top of the Grand Staircase: the Late Cretaceous of Southern Utah. Indiana University Press, Bloomington, Indiana.

Kirkland, J. I., J. G. Eaton, and D. B. Brinkman. 2013. Elasmobranchs from Upper Cretaceous freshwater facies in Southern Utah; pp. 153-194 in A. L. Titus and M. A. Loewen (eds.), At the Top of the Grand Staircase: the Late Cretaceous of southern Utah. Indiana University Press, Bloomington, Indiana.

Lambe, L. M. 1914. On *Gryposaurus notabilis*, a new genus and species of trachodont dinosaur from the Belly River Formation of Alberta, with a description of the skull of *Chasmosaurus belli*. The Ottawa Naturalist 27:145-155.

Lapparent, A. F., and R. Lavocat. 1955. Dinosauriens; pp. 785-962 in J. Piveteau (ed.), Traité de Paléontologie, Tome 5. Masson et Cie, Paris.

Leiggi, P., C. R. Schaff, and P. May. 1994. Macrovertebrate collecting; pp. 59-77 in P. Leiggi and P. May (eds.), Vertebrate Paleontological Techniques. Cambridge University Press, Cambridge, UK.

Padian, K., and J. R. Horner. 2011. The evolution of 'bizzare structures' in dinosaurs: biomechanics, sexual selection, social selection, or species recognition? Journal of Zoology 283:3-17.

Parks, W. A. 1919. Preliminary description of a new species of trachodont dinosaur of the genus *Kritosaurus*, *Kritosaurus incurvimanus*. Transactions of the Royal Society of Canada 3:51-59.

Parks, W. A. 1920. The osteology of the trachodont dinosaur *Kritosaurus incurvimanus*. University of Toronto Studies, Geological Series 11:1-76.

Peng, J.-H., A. P. Russell, and D. B. Brinkman. 2001. Vertebrate microsite assemblages (exclusive of mammals) from the Foremost and Oldman Formations of the Judith River Group (Campanian) of Southeastern Alberta: an illustrated guide. Provincial Museum of Alberta Natural History Occasional Paper 25:1-54.

Pinna, G. 1979. Osteologia dello scheletro di *Kritosaurus notabilis* (Lambe, 1914) del Museo Civico di Storia Naturale di Milano. Memorie della Società Italiana di Scienze Naturali e del Museo Civico di Storia Naturalle di Milano 22:33-56.

Prieto-Márquez, A. 2005. New information on the cranium of *Brachylophosaurus canadensis* (Dinosauria, Hadrosauridae), with a revision of its phylogenetic position. Journal of Vertebrate Paleontology 25:144-156.

Prieto-Márquez, A. 2010a. The braincase and skull roof of *Gryposaurus notabilis* (Dinosauria, Hadrosauridae), with a taxonomic revision of the genus. Journal of Vertebrate Paleontology 30:838-854.

Prieto-Márquez, A. 2010b. Global phylogeny of Hadrosauridae (Dinosauria: Ornithopoda) using parsimony and Bayesian methods. Zoological Journal of the Linnean Society 159:435-502.

Prieto-Márquez, A. 2012. The skull and appendicular skeleton of *Gryposaurus latidens*, a saurolophine hadrosaurid (Dinosauria: Ornithopoda) from the early Campanian (Cretaceous) of Montana, USA. Canadian Journal of Earth Sciences 49:510-532.

Prieto-Márquez, A. 2014. Skeletal morphology of *Kritosaurus navajovius* (Dinosauria: Hadrosauridae) from the Late Cretaceous of the North American south-west, with an evaluation of the phylogenetic systematics and biogeography of Kritosaurini. Journal of Systematic Palaeontology 12:133-175.

R_Core_Team. 2014. R: A language and environment for statistical computing. R Foundation for Statistical Computing, Vienna, Austria. ISBN 3-900051-07-0, URL http://www.R-project.org/.

Rambaut, A. 2006-2012. FigTree. 1.4.0. Institute of Evolutionary Biology, University of Edinburgh, Edinburgh, http://tree.bio.ed.ac.uk/software/figtree/

Roberts, E. M., S. D. Sampson, A. L. Deino, S. A. Bowring, and R. Buchwaldt. 2013. The Kaiparowits Formation: a remarkable record of Late Cretaceous terrestrial environments, ecosystems, and evolution in western North America; pp. 85-106 in A. L. Titus and M. A. Loewen (eds.), At the Top of the Grand Staircase: the Late Cretaceous of Southern Utah. Indiana University Press, Bloomington, Indiana.

Rogers, R. R., C. C. Swisher, and J. R. Horner. 1993. 40Ar/39Ar age and correlation of the nonmarine Two Medicine Formation (Upper Cretaceous), northwestern Montana, USA. Canadian Journal of Earth Sciences 30:1066-1075.

Rozhdestvensky, A. K. 1965. Growth changes in Asian dinosaurs and some problems of their taxonomy. Paleontologischeskii Zhurnal 3:95-109.

Ryan, M. J., and D. C. Evans. 2005. Ornithischian Dinosaurs. Dinosaur Provincial Park: A Spectacular Ancient Ecosystem Revealed:312-348.

Swofford, D. L. 2002. PAUP*. Phylogenetic analysis using parsimony (*and other methods). Version 4.0b10. Sinauer Associates, Sunderland, MA.

Tanke, D. H., and D. C. Evans. 2014. Relocating the lost *Gryposaurus incurvimanus* holotype quarry, Dinosaur Provincial Park, Alberta, Canada; pp. 385-395 in D. A. Eberth and D. C. Evans (eds.), Hadrosaurs. Indiana University Press, Bloomington, Indiana.

Varricchio, D. J. 1995. Taphonomy of Jack's Birthday Site, a diverse dinosaur bonebed from the Upper Cretaceous Two Medicine Formation of Montana. Palaeogeography, Palaeoclimatology, Palaeoecology 114:297-323.

Vialli, V. 1960. Uno scheletro di dinosauro del Museo Civico di Storia Naturale di Milano (*Kritosaurus notabilis* (Lambe)): osservazioni preliminari. Atti della Società Italiana di Scienze Naturali e del Museo Civico di Storia Naturale in Milano 99:169-185.

Wagner, J. R. 2001. The hadrosaurian dinosaurs (Ornithischia: Hadrosauria) of Big Bend National Park, Brewster County, Texas, with implications for Late Cretaceous Paleozoogeography. M.S. thesis, Texas Tech University, Lubbock, 417 pp.

Williamson, T. E. 2000. Review of Hadrosauridae (Dinosauria, Ornithischia) from the San Juan Basin, New Mexico. Bulletin - New Mexico Museum of Natural History and Science 17:191-213.

CHAPTER FIVE

A PHOTOGRAPHIC ATLAS OF THE POSTCRANIAL ANATOMY OF *GRYPOSAURUS REDDINGI* (DINOSAURIA: HADROSAURIDAE)

Contribution of Authors and Co-Authors

Manuscript in Chapter 5

Author: Elizabeth A. Freedman

Contributions: Conceived the study, performed the analyses, interpreted results, and wrote the manuscript.

Co-authors: none

Manuscript Information Page

Elizabeth A. Freedman
Status of Manuscript:
_x_ Prepared for submission to a peer-reviewed journal
___ Officially submitted to a peer-reviewed journal
___ Accepted by a peer-reviewed journal
___ Published in a peer-reviewed journal

Abstract

The abundance of hadrosaur fossil specimens in Late Cretaceous formations in the Western Interior of North America results in a need for reference materials for identification purposes and comparative anatomy. Because cranial elements are the most diagnostic for determining species in hadrosaurs, cranial material has been well figured in numerous publications. Until recently, postcranial material has been less completely illustrated. This photographic atlas depicts the postcranial material from a monodominant bonebed of *Gryposaurus reddingi* from the Campanian Judith River Formation of northcentral Montana. Specimens are illustrated in multiple views and anatomical features are labeled. Multiple specimens of each skeletal element are included to illustrate the range in apparent morphologic variation within members of a single species from a single bonebed. The variation between specimens of the same skeletal element is due to one or more factors: differing amounts of taphonomic breakage, different directions of diagenetic compression, ontogeny, and intraspecific individual variation.

Introduction

Hadrosaur fossils are abundant in Late Cretaceous formations in the Western Interior of North America, yet descriptions and illustrations of postcranial material are often overshadowed by those of cranial elements. Cranial elements are indeed more diagnostic for determining species, whereas postcranial elements have fewer differences among species and genera. However, subtle variations are present in the postcranial

material of different hadrosaur genera, making postcranial morphology useful in identifying the taxonomic identity of specimens that lack cranial material.

Most previously published hadrosaur postcranial material has only been partially figured; publications illustrating every postcranial element of the hadrosaur skeleton from multiple views are rare, and figures thoroughly labeling anatomical features of each element are even more rare. This paper builds on the excellently figured and labeled publications of *Edmontosaurus* hadrosaur postcrania by Campione (2014) and Prieto-Márquez (2014). Also of note is Zheng et al.'s (2011) complete photographic atlas of a hadrosaur foot, most likely *Edmontosaurus*, illustrating every pedal element in six orthogonal views.

This paper portrays the most completely figured and labeled hadrosaur postcranial material from a multi-individual hadrosaur bonebed ever published. The cranial material of *Gryposaurus reddingi* was described from a monodominant bonebed in the Judith River Formation of northcentral Montana, in a horizon stratigraphically equivalent to Unit 1 of the Oldman Formation of Alberta (Freedman Fowler and Horner, Chapter Two). This bonebed, MOR locality JR-429, includes abundant postcranial material, all catalogued under the specimen number MOR 2573. The best preserved specimens of this postcranial material are illustrated and described here.

In this photographic atlas, the inclusion of multiple specimens of each element is intended to illustrate the range of variation in the appearance of an element within a single bonebed. This variation may be due to intraspecific variation, or may be due to taphonomic or diagenetic differences in preservation. Other papers based solely on a

single specimen of each element may not be able to discriminate between taxonomically distinct morphological characteristics and intraspecifically or taphonomically variable characteristics. This is also the first paper to comprehensively figure bonebed material from multiple size classes. Prieto-Márquez (2014) noted ontogenetic differences in the postcranial material of *Edmontosaurus annectens*, but these specimens were from different localities.

Institutional Abbreviations

AMNH FARB, American Museum of Natural History (Fossil Amphibians, Reptiles, and Birds collection), New York, New York, U.S.A.; **CMN/NMC**, Canadian Museum of Nature, formerly National Museum of Canada, Ottawa, Ontario, Canada; **MOR**, Museum of the Rockies, Bozeman, Montana, U.S.A.; **RAM**, Raymond M. Alf Museum, Claremont, California, U.S.A.; **ROM**, Royal Ontario Museum, Toronto, Ontario, Canada; **SM**, Senckenberg Museum, Frankfurt, Germany; **TMP**, Royal Tyrrell Museum of Paleontology, Drumheller, Alberta, Canada; **UMNH VP**, Utah Museum of Natural History Vertebrate Paleontology, Salt Lake City, Utah, U.S.A..

Materials and Methods

The MOR 2573 *Gryposaurus* specimens were collected from the JR-429 bonebed by Museum of the Rockies crews using standard paleontology field techniques (Leiggi et al., 1994) on privately owned land. MOR 2573 was generously donated to the Museum of

the Rockies by Dan and Lila Redding. No permits were required for the described study, which complied with all relevant regulations.

The MOR 2573 material consists of approximately 800 hadrosaur bones and bone fragments; all diagnostic specimens are referable to *Gryposaurus reddingi*. Museum of the Rockies specimens from multi-individual bonebeds are identified using a combination of specimen number and field number, e.g. MOR 2573-7-17-10-432, where MOR 2573 is the inclusive number for all hadrosaur specimens from the JR-429 bonebed, 7-17-10 is the date the bone was found, and 432 indicates that it was the 432nd bone collected from the bonebed. Aside from vertebrate microfossil material, only two non-hadrosaur bones were present in the JR-429 bonebed: a theropod femur and a tyrannosaur centrum. The taphonomy of the JR-429 *G. reddingi* bonebed is described in Freedman Fowler (Chapter Three), and the cranial material is described in Freedman Fowler and Horner (Chapter Four). The minimum number of *G. reddingi* individuals within the bonebed is ten: four juveniles, five subadults, and one adult.

In this atlas, the terms “juvenile”, “subadult”, and “adult” are applied to specimens based solely on their sizes, using the classification system of Evans (2010), in which Juveniles are less than 50% the size of the largest individual of the taxon, subadults are 50-85% the size of the largest individual of the taxon, and adults are 85-100% the size of the largest individual of the taxon. These terms are simply used for convenience when discussing the relative sizes of specimens; they are merely hypotheses for the actual ontogenetic stages of specimens, and should not be used for interpretations of the sexual or skeletal maturity or immaturity of a specimen. The three subadult tibiae

of MOR 2573 have been histologically sectioned, and are interpreted as being two to three years of age (Freedman Fowler, Chapter Three). No juvenile or adult-sized tibiae are present in the MOR 2573 material, so their actual skeletal ages and relative maturity are unknown.

For each type of skeletal element, the most complete specimens of MOR 2573 are figured here. Partial specimens are figured when they represent the most complete example of that element from one of the size classes, or the best example of a particular anatomical feature. Specimens are figured in up to six different view orientations: generally lateral, medial, anterior, posterior, dorsal, and ventral. Flat two-dimensional elements or incompletely preserved elements are figured in fewer view orientations. Figure formatting style was inspired by the excellent figures of Campione (2014), Prieto-Márquez (2014), and Zheng et al. (2011). Names and locations of anatomical features were also derived mainly from those of Campione (2014) and Prieto-Márquez (2014). Length measurements for limb elements of MOR 2573 are listed in Freedman Fowler (Chapter Three) Supplementary Table 1 (Appendix H).

This photographic atlas is intended for use as a visual guide to identifying hadrosaur postcranial material. General aspects of hadrosaur postcranial anatomy that do not vary much among genera have already been well described (Prieto-Márquez, 2007; Campione, 2014; Prieto-Márquez, 2014) and need not be repeated here. Descriptions here will focus on morphological aspects of *Gryposaurus reddingi* that differ from other *Gryposaurus* species or other genera of hadrosaurs, as well as noting features that are

ontogenetically variable or that are subject to taphonomic alteration or diagenetic distortion.

The *Gryposaurus reddingi* MOR 2573 material is compared to other *Gryposaurus* specimens as much as possible. The holotype of *G. notabilis*, CMN 2278, does include postcranial material, but it is poorly preserved and incompletely prepared, and so is of little comparative use. However, two subadult specimens of *G. notabilis*, ROM 764 and TMP 1980.022.0001, do include nearly complete postcranial skeletons, and are similar sizes to the MOR 2573 subadult individuals. The *G. monumentensis* holotype RAM 6797 consists only of a skull; the *G. monumentensis* skeleton is best known from referred partial specimen UMNH VP 12265 (Gates et al., 2013). An additional postcranial skeleton from the Kaiparowits Formation, UMNH VP 20181, includes partial skull material but has not been assigned to a particular species of *Gryposaurus* (Gates et al., 2013). *Gryposaurus latidens* postcranial material is incompletely known from various elements preserved in AMNH FARB 5465 and MOR 478.

Osteological Description

Axial Skeleton

Aside from distal caudal vertebrae, the neural arches and centra are unfused and disarticulated. Non-caudal centra are rare in the JR-429 bonebed. Only the most complete neural arches are figured here (Figures 5.1-5.3); many more halves and fragments of neural arches are present in the MOR 2573 material. Numerous caudal centra are preserved, but they are all middle to distal caudal centra; no proximal caudal centra are

present in the MOR 2573 material (Figure 5.4). Chevrons are rare (Figure 5.5). Rib material is abundant in the JR-429 bonebed, but most rib specimens are fragmentary. Only the most complete ribs are figured here (Figure 5.6). Right sternal MOR 2573 6-20-06-57 is missing most of its anterior blade and part of its distal posterior process (Figure 5.7). If it were complete, the overall MOR 2573 sternal morphology would likely be consistent with that of *Gryposaurus notabilis* ROM 764 and TMP 1980.022.0001.

Pectoral Girdle

No coracoids are present in the MOR 2573 material, but several scapulae are preserved (Figure 5.8). In most MOR 2573 specimens, the distal scapular blade is broken, and the proximal processes are damaged. The most complete large scapula, MOR 2573-6-18-06-50, was preserved resting vertically along its dorsal edge, and so its proximal processes have been dorsoventrally compressed diagenetically. The other scapulae were preserved horizontally, and so they have been laterally compressed. As in juvenile *Edmontosaurus annectens* (Prieto-Márquez, 2014) and neonatal *Hypacrosaurus stebingeri* (Horner and Currie, 1994), the scapular blade of the juvenile MOR 2573-7-22-11-570 is narrow anteriorly and widens posteriorly, whereas the scapular blade of larger individuals has a less prominent anterior constriction. The orientation of the proximal scapula relative to the scapular blade is variable among MOR 2573 specimens. The ventral scapular margin appears to be most strongly angled in the juvenile MOR 2573-7-22-11-570, and most gently curved in MOR 2573-6-18-06-50, with intermediate curvature in MOR 2573-8-11-06-236. This variation is hypothesized to be at least partially due to differential diagenetic compression; MOR 2573-7-22-11-570 and MOR

2573-8-11-06-236 are mediolaterally compressed, making the proximal scapula appear dorsoventrally larger, whereas MOR 2573-6-18-06-50 is dorsoventrally compressed, making the proximal scapula appear dorsoventrally smaller.

Forelimb

The widths of the deltopectoral crests in MOR 2573 humeri (Figure 5.9) are more similar to those of other *Gryposaurus* (*G. latidens* AMNH FARB 5465 and MOR 478-5-25-8-5, *G. notabilis* ROM 764 and TMP 1980.022.0001, and *G. monumentensis* UMNH VP 12265) rather than the wider deltopectoral crests of *Edmontosaurus* (Campione, 2014; Prieto-Márquez, 2014). The ulnar condyle is slightly larger than the radial condyle in MOR 2573-6-12-06-8, but the condyles are subequally sized in MOR 2573-7-01-10-355 and MOR 2573-6-03-10-279. This differs from other *Gryposaurus* specimens (*G. latidens* AMNH FARB 5465 and MOR 478-5-25-8-5, and *G. monumentensis* UMNH VP 12265), in which the ulnar condyle is larger than the radial condyle (Prieto-Márquez, 2012; Gates et al., 2013). The ulnar and radial condyles are also subequally sized in *Edmontosaurus regalis* (Campione, 2014).

The robusticity of the ulnar diaphysis (diameter relative to length) varies among individuals of MOR 2573 (Figure 5.10). Depending on the in situ orientation of the ulna, the anterior angle between the medial and lateral processes may have been widened or compressed, but the relative sizes of the medial and lateral processes are consistent among specimens. The medial process of the ulna is more anteriorly elongated than the lateral process. The proximal ends of the juvenile ulnae are damaged, so the relative size of the proximal processes cannot be compared to those of the subadults.

The radii have slightly damaged or distorted proximal and distal ends, and are compressed in different orientations, making side determination difficult (Figure 5.11). As in *Edmontosaurus annectens* (Prieto-Márquez, 2014), the radial diaphysis becomes relatively more robust (larger diameter relative to length) ontogenetically in MOR 2573.

No carpals or metacarpal IIs are present in the MOR 2573 material. Metacarpals III, IV, and V are similar in morphology to those of *Gryposaurus notabilis* ROM 764 (Figure 5.12). Metacarpal III is relatively more robust (larger diameter relative to length) in the subadult MOR 2573-6-23-12-684 compared to the juvenile MOR 2573-6-28-12-703. However, the robusticity of the metacarpals is intraspecifically variable within *Edmontosaurus annectens* (Prieto-Márquez, 2014), so this may not be an ontogenetic character within *G. reddingi*.

Manual phalanx V-2 (Figure 5.13) is relatively shorter and wider in *Gryposaurus reddingi* MOR 2573-6-03-10-285 and MOR 2573-7-15-11-537 and *Gryposaurus notabilis* ROM 764 than in *Brachylophosaurus canadensis* MOR 794 or *Edmontosaurus annectens* LACM 23504 (Prieto-Márquez, 2014). Manual phalanx III-1 is relatively longer in *Gryposaurus reddingi* MOR 2573-7-06-06-131 and MOR 25733-7-12-06-161, *Gryposaurus notabilis* ROM 764, and *Brachylophosaurus canadensis* MOR 794 than in *Edmontosaurus annectens* LACM 23504 (Prieto-Márquez, 2014). Other preserved manual phalanges of MOR 2573 are fairly similar to the corresponding manual phalanges of *Gryposaurus notabilis* ROM 764 and *Brachylophosaurus canadensis* MOR 794, although not all manual phalangeal positions are represented in the MOR 2573 material.

Pelvic Girdle

Although the preacetabular process is slightly broken in most MOR 2573 ilia, the postacetabular process is completely missing from more than half of the ilia and partial ilia of MOR 2573, indicating that it is more frequently damaged before burial than the preacetabular process (Figure 5.14). The degree of ventral deflection of the preacetabular process of the ilium is intraspecifically variable in *Gryposaurus reddingi*. Although ilium MOR 2573-7-30-11-610 was fractured into three separate pieces prior to burial, the anterior portion is well preserved enough that its ventrally curved anterior half of the preacetabular process is unlikely to be purely a taphonomic artifact, regardless of whether the posterior pieces are reconstructed in their correct positions. In the other MOR 2573 ilia, the preacetabular process is straighter. The greater ventral deflection of the preacetabular process in adult *Edmontosaurus annectens* compared to juvenile *E. annectens* is interpreted as an ontogenetic character (Prieto-Márquez, 2014), but the subadult ilia of MOR 2573 are similar sizes, so intraspecific or taphonomic variation are more parsimonious hypotheses. The preacetabular process of the ilium is strongly ventrally deflected in *G. latidens* AMNH FARB 5465 (Prieto-Márquez, 2014), but no other complete preacetabular processes of *G. latidens* are available for determining the range of variation within this species. The preacetabular process of the ilium is strongly ventrally deflected in *G. monumentensis* UMNH VP 12265 as well (Gates et al., 2013). In subadult *G. notabilis* ROM 764 the preacetabular process is not strongly ventrally deflected. Thus, the preacetabular processes of *G. latidens* and *G. monumentensis* ilia are

similar to *G. reddingi* MOR 2573-7-30-11-610, but the preacetabular process of the *G. notabilis* ilium is similar to the other MOR 2573 ilia.

The lateral and ventral extension of the supraacetabluar crest of the ilium is highly variable within MOR 2573 specimens; this variation is attributable to taphonomic breakage of the crest and diagenetic compression. Ilium MOR 2573-7-21-10-442 is dorsoventrally compressed, making the supraacetabular crest appear to extend laterally and ventrally over much of the lateral body of the ilium. The other ilia are laterally compressed, making the body of the ilium taller dorsoventrally, with the supraacetabular crest broken and missing different amounts of its lateral extent, thus causing the supraacetabular crest to appear to not extend very far laterally and ventrally over the lateral body of the ilium.

The obturator foramen is not entirely enclosed by the obturator process in any MOR 2573 ischia (Figure 5.15). This may be due to breakage of the obturator process, but most likely the obturator foramen was never fully enclosed in *G. reddingi*, and should instead be termed the obturator notch. The obturator foramen in ischium MOR 2573-6-12-06-14 is oval shaped, but the obturator foramen in juvenile ischium MOR 2573-7-08-10-339 is slightly more circular, suggesting that the shape of the obturator foramen may change ontogenetically. The distalmost end of the posterior process of the ischium is slightly enlarged and downturned in MOR 2573-7-05-12-735, reminiscent of a very small version of the ischial process of lambeosaurines, and unlike hadrosaurines such as *Edmontosaurus regalis* and *E. annectens* (Campione, 2014; Prieto-Márquez, 2014). The slight distal enlargement is similar to that of *G. notabilis* ROM 764, but the distal end of

the ischium in ROM 764 is only very slightly ventrally curved; the ventral curvature is greater in MOR 2573-7-05-12-735. The size and curvature of the distal end of the ischium in MOR 2573-7-05-12-735 is similar to that of *Brachylophosaurus canadensis* MOR 794 (Prieto-Márquez, 2007).

Only two pubes of MOR 2573 are preserved, both missing most of the postpubic process (Figure 5.16). Right pubis MOR 2573 7-05-06-118 is well preserved and has a complete ischial peduncle, but the distal blade of the prepubic process is mostly missing. Left pubis MOR 2573-7-16-10-431 is severely fractured and expanded by modern sinkhole weathering, making its processes appear longer than they originally were. Its ischial peduncle is much longer and more narrow than that of right pubis MOR 2573 7-05-06-118; even considering the expansion from the modern weathering, the ischial peduncle of left pubis MOR 2573-7-16-10-431 would have been longer than that of MOR 2573 7-05-06-118. Although the distal blade of the prepubic process of left pubis MOR 2573-7-16-10-431 is broken distally, it does preserve the dorsal angle demonstrating that the distal blade would have been rectangular as it is in other *Gryposaurus* species.

The ischial peduncle branches dorsolaterally off of the postpubic process. The ischial peduncle of the pubis initiates more distally along the postpubic process in *G. reddingi* than it does in *G. latidens* AMNH FARB 5465 (Prieto-Márquez, 2012), *Brachylophosaurus canadensis* MOR 1071, and *Edmontosaurus regalis* CMN 2289 (Campione, 2014). However, the ischial peduncle of the pubis of *G. monumentensis* UMNH VP 12265 (Gates et al., 2013) does initiate more distally along the postpubic process, very similar to *G. reddingi*. *Gryposaurus notabilis* specimens ROM 764 and

TMP 1980.022.0001 are articulated, and so the ischial peduncle is difficult to access for comparison.

Hindlimb

The medial condyle of the femur is larger than the lateral condyle (Figure 5.17). The dorsal margin of the fourth trochanter slopes laterally more gradually than the ventral margin. No juvenile femora are present in the MOR 2573 material, so ontogenetic changes in femoral dimensions cannot be determined.

A transverse mid-diaphyseal section was sampled from each tibia of MOR 2573 (Figure 5.18) for osteohistology in a separate study (Prieto-Márquez, 2014). These subadult-sized tibiae preserve growth cycles rather than true lines of arrested growth, and are likely between two and three years of age. No juvenile-sized tibiae are present in the MOR 2573 material, so the age of this size class cannot be determined.

The proximal end of the fibula is slightly convex laterally and slightly concave medially (Figure 5.19). The cranial process of the proximal end extends anteriorly. The distal process also extends anteriorly. The distal end of the fibula is flat medially and convex laterally. The subadult fibulae of MOR 2573 are slightly more robust than the fibula of adult *G. latidens* AMNH FARB 5465 (Prieto-Márquez, 2012), but similar to those of subadult *G. notabilis* ROM 764 and TMP 1980.022.0001. Thus the fibula may become relatively more slender ontogenetically in *Gryposaurus*.

No calcanea are present in the MOR 2573 material, but one astragalus is well preserved (Figure 5.20). Metatarsals are relatively abundant in the MOR 2573 material (Figures 5.21-5.23), and most pedal phalanges are represented by at least one specimen

(Figures 5.24-5.26). The pes of *G. reddingi* is generally similar to that of *G. notabilis* ROM 764, *Brachylophosaurus canadensis* MOR 794, and c.f. *Edmontosaurus* (Zheng et al., 2011). The position of the medial tuberosity of metatarsal IV is variable among MOR 2573 specimens. It is relatively more dorsally positioned in MOR 2573-7-08-10-395 than in MOR 2573-8-03-11-629. Prieto-Márquez (2014) noted an ontogenetic increase in the relative size of the medial tuberosity and overall robusticity of metatarsal IV in *E. annectens*, but this is not the case for *G. reddingi*. The juvenile metatarsal IV MOR 2573-7-03-06-95 has similar proportions of the medial tuberosity and overall robusticity as the subadult metatarsal IVs. *Brachylophosaurus canadensis* and *Maiasaura peeblesorum* have a proximodistally-oriented ridge on the plantar surface of their pedal unguals, but this plantar ridge is not present in MOR 2573, other *Gryposaurus*, or *Edmontosaurus* (Prieto-Márquez, 2010).

Conclusion

Postcranial material of *G. reddingi* MOR 2573 from a monodominant bonebed, JR-429, is here figured and anatomically labeled in multiple views. Most elements are represented by multiple specimens, depicting the range in morphologic variation among specimens from the same taxon and locality. Some features that vary among specimens of MOR 2573 are attributable to taphonomic alteration or diagenetic distortion, whereas other features represent individual intraspecific variation. In elements where juvenile material is available for comparison to the subadult material, the morphologies are generally similar, although the robusticity of some elements varies ontogenetically. It is

hoped that this photographic atlas will be a useful asset to researchers in identifying hadrosaur postcranial material.

Acknowledgments

Grateful thanks to my advisor, Jack Horner, who provided the opportunity to work in a fantastic field area and made every aspect of this research possible. Additional thanks to Dave Varricchio, Don Brinkman, Matt Lavin, Denver Fowler, Holly Woodward, and John Scannella for advice and discussions. For specimen collection, thanks to the 2006 and 2010-2012 MOR field crews, especially Brian Baziak, Bobby Ebelhar, Bob Harmon, and Cary Woodruff. For fieldwork support, hospitality, friendship, and specimen donation, great thanks as always to Dan and Lila Redding. Thanks to all members of the Rudyard, Montana community, whose continuing support of local paleontology makes this work possible. Excellent preparation was done by Jamie Jette, Carrie Ancell, Aleen Kienholz, Susan Brewer, and volunteers at the MOR Bowman Prep Lab. Fieldwork and research funding was generously provided to Jack Horner by: Nathan Myhrvold, David Sands and family, Ellis Short and family, Damaris Wagoner, and donors to the MOR Horner Fund and MOR Student Fund; and to EAFF by: the Geological Society of American Student Research Grant, the Royal Ontario Museum M. A. Fritz Travel Grant for the Advancement of Studies in Paleontology, the Tampa Bay Fossil Club, and the Montana State University Department of Cell Biology and Neuroscience. Thanks to Kevin Seymour and David Evans (ROM); and Don Brinkman, Brandon Strillsky, and Graeme Housego (TMP) for comparative specimen access.

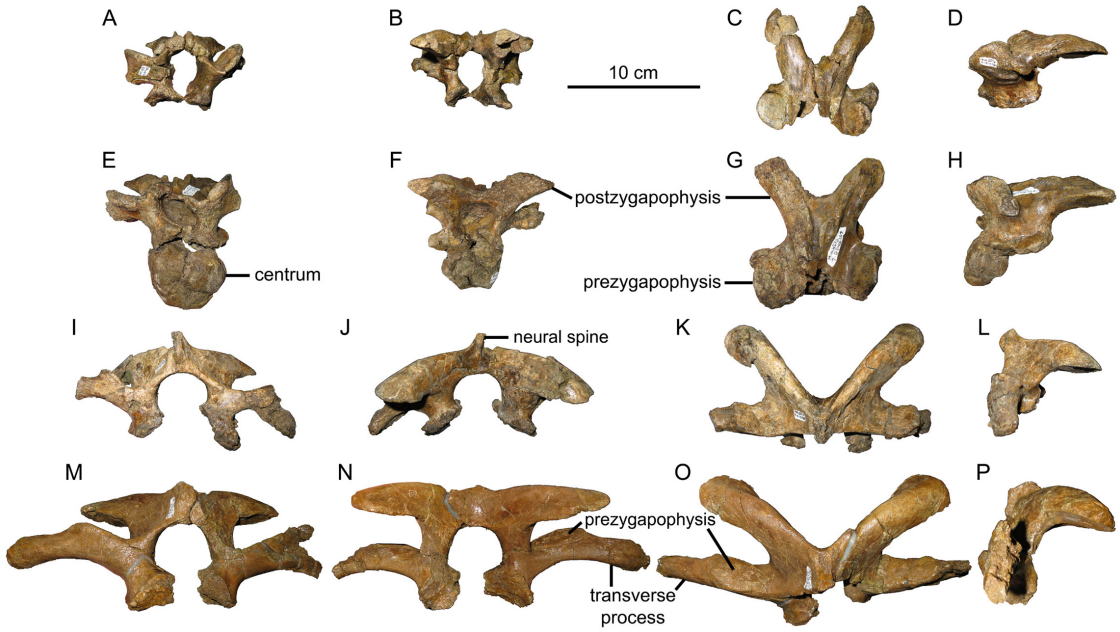


Figure 5.1. Cervical vertebrae of *Gryposaurus reddingi*, MOR 2573. (A-D) Anterior cervical neural arch MOR 2573-7-17-10-432 in (A) anterior, (B) posterior, (C) dorsal, and (D) left lateral views. (E-H) Anterior cervical neural arch MOR 2573-7-03-06-109 with associated disarticulated centrum MOR 2573-7-03-06-107 in (E) anterior, (F) posterior, (G) dorsal, and (H) left lateral views. (I-L) Posterior cervical neural arch MOR 2573-7-01-10-368 in (I) anterior, (J) posterior, (K) dorsal, and (L) left lateral views. (M-P) Posterior cervical neural arch MOR 2573-6-13-06-35 in (M) anterior, (N) posterior, (O) dorsal, and (P) left lateral views.

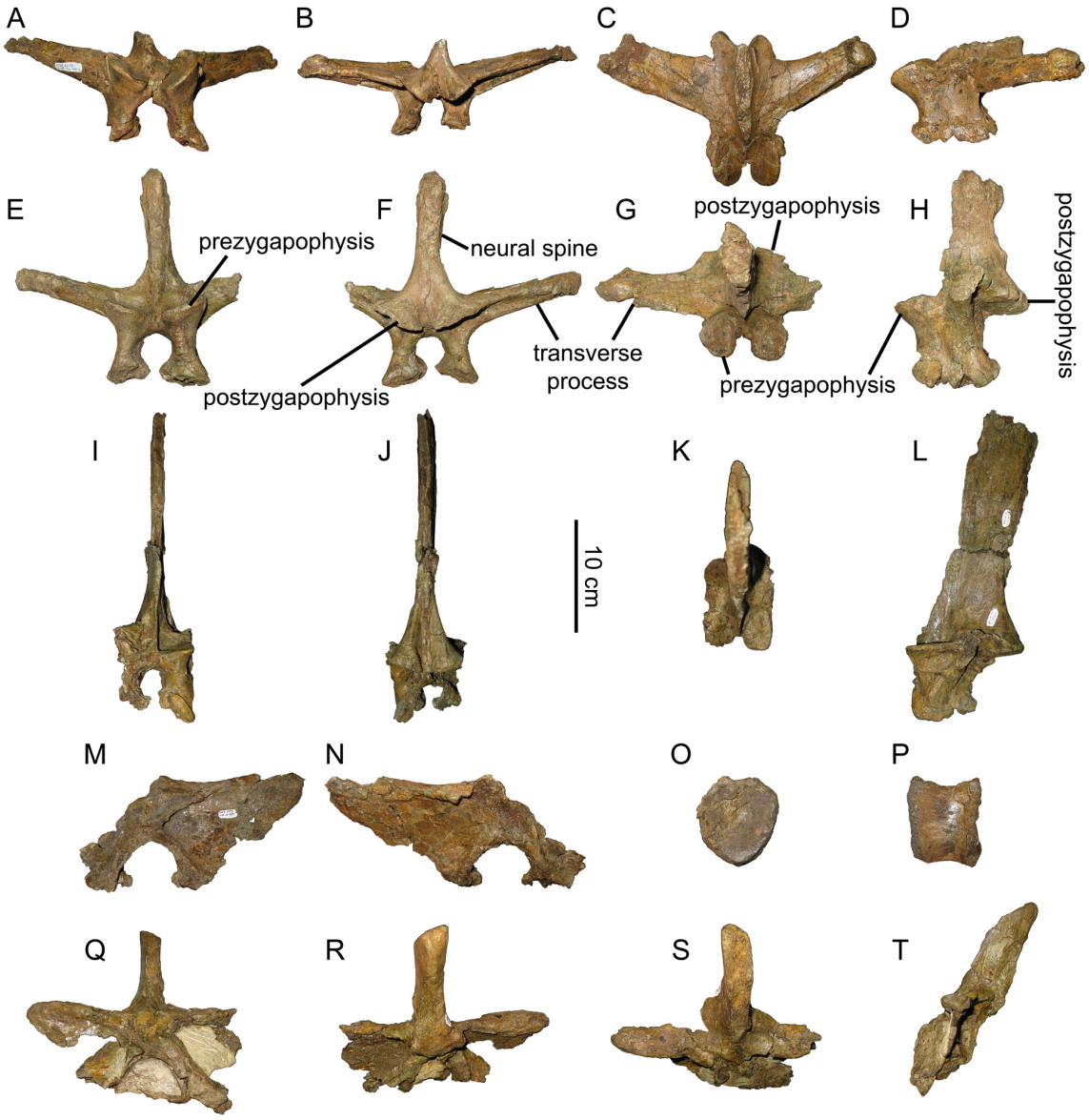
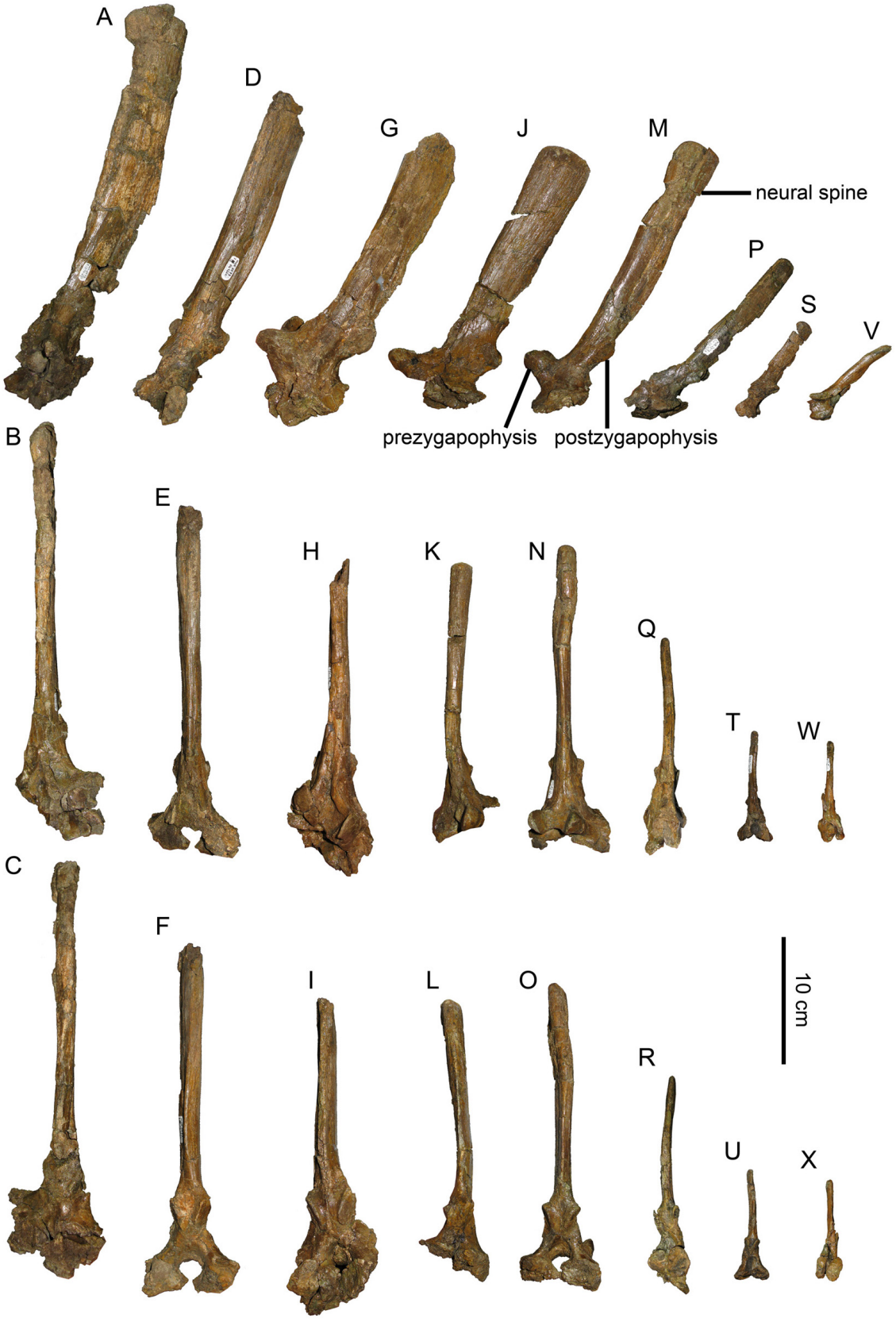


Figure 5.2. Dorsal vertebrae of *Gryposaurus reddingi*, MOR 2573. (A-D) Dorsal neural arch MOR 2573-7-18-06-186A in (A) anterior, (B) posterior, (C) dorsal, and (D) left lateral views. (E-H) Dorsal neural arch MOR 2573-6-10-10-316 in (E) anterior, (F) posterior, (G) dorsal, and (H) left lateral views. (I-L) Dorsal neural arch MOR 2573-7-13-06-166 in (I) anterior, (J) posterior, (K) dorsal, and (L) left lateral views. (M-N) Sacral neural arch MOR 2573-7-15-10-427 in (M) anterior and (N) posterior views. (O-P) Dorsal centrum MOR 2573-6-28-12-702 in (O) anterior and (P) left lateral views. (Q-T) Sacral neural arch MOR 2573-6-29-12-711 in (Q) anterior, (R) posterior, (S) dorsal, and (T) left lateral views.

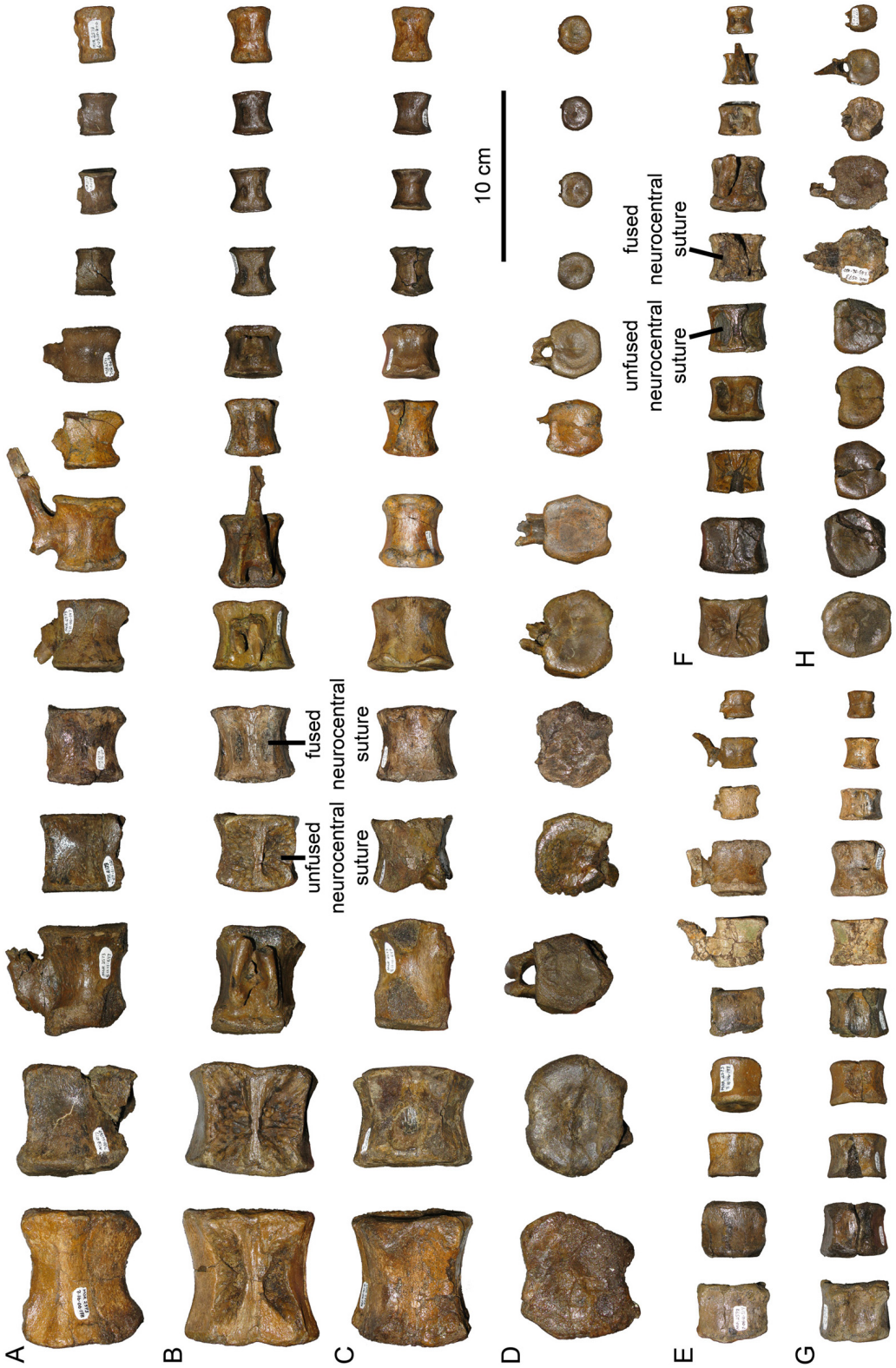
(Figure 5.3 on next page)

Figure 5.3. Disarticulated caudal neural arches of *Gryposaurus reddingi*, MOR 2573. The proximalmost neural arch is on the left side of the figure, and the distalmost neural arch is on the right. (A-C) Caudal neural arch MOR 2573-8-13-06-250A in (A) left lateral, (B) anterodorsal, and (C) posteroventral views. (D-F) Caudal neural arch MOR 2573-7-14-06-168A in (D) left lateral, (E) anterodorsal, and (F) posteroventral views. (G-I) Caudal neural arch MOR 2573-6-08-10-299 in (G) left lateral, (H) anterodorsal, and (I) posteroventral views. (J-L) Caudal neural arch MOR 2573-7-03-06-102 in (J) left lateral, (K) anterodorsal, and (L) posteroventral views. (M-O) Caudal neural arch MOR 2573-6-10-10-317 in (M) left lateral, (N) anterodorsal, and (O) posteroventral views. (P-R) Caudal neural arch MOR 2573-7-11-06-150A in (P) left lateral, (Q) anterodorsal, and (R) posteroventral views. (S-U) Caudal neural arch MOR 2573-6-21-06-64A in (S) left lateral, (T) anterodorsal, and (U) posteroventral views. (V-X) Caudal neural arch MOR 2573-6-21-06-65 in (V) left lateral, (W) anterodorsal, and (X) posteroventral views.


A
D
G
J
M
neural spine
P
S
V
prezygapophysis
postzygapophysis
B
E
H
K
N
Q
T
W
C
F
I
L
O
R
U
X
10 cm

(Figure 5.4 on next page)

Figure 5.4. Caudal centra of *Gryposaurus reddingi*, MOR 2573. (A-D) Caudal centra of MOR 2573 that are interpreted as subadult centra in (A) left lateral, (B) dorsal, (C) ventral, and (D) anterior views. Specimen numbers of subadult centra, from left to right, are: MOR 2573-7-16-06-178, MOR 2573-7-20-12-768, MOR 2573-8-11-11-647, MOR 2573-7-07-11-521, MOR 2573-6-12-06-29, MOR 2573-7-11-06-147, MOR 2573-8-12-11-654, MOR 2573-6-21-06-77, MOR 2573-7-02-06-92, MOR 2573-7-26-11-589, MOR 2573-7-19-11-545, MOR 2573-7-13-11-533, and MOR 2573-6-09-10-300. Caudal centra of MOR 2573 that are interpreted as juvenile centra in (E) left lateral, (F) dorsal, (G) ventral, and (H) anterior views. Specimen numbers of subadult centra, from left to right, are: MOR 2573-7-06-11-514, MOR 2573-7-16-11-538, MOR 2573-7-17-11-543, MOR 2573-7-18-06-197, MOR 2573-8-13-06-246, MOR 2573-7-03-06-100, MOR 2573-8-14-06-257, MOR 2573-6-21-06-81, MOR 2573-7-27-10-463, and MOR 2573-6-17-12-664.


A
B
C
D
E
F
G
H
unfused neurocentral suture
fused neurocentral suture
unfused neurocentral suture
fused neurocentral suture
10 cm

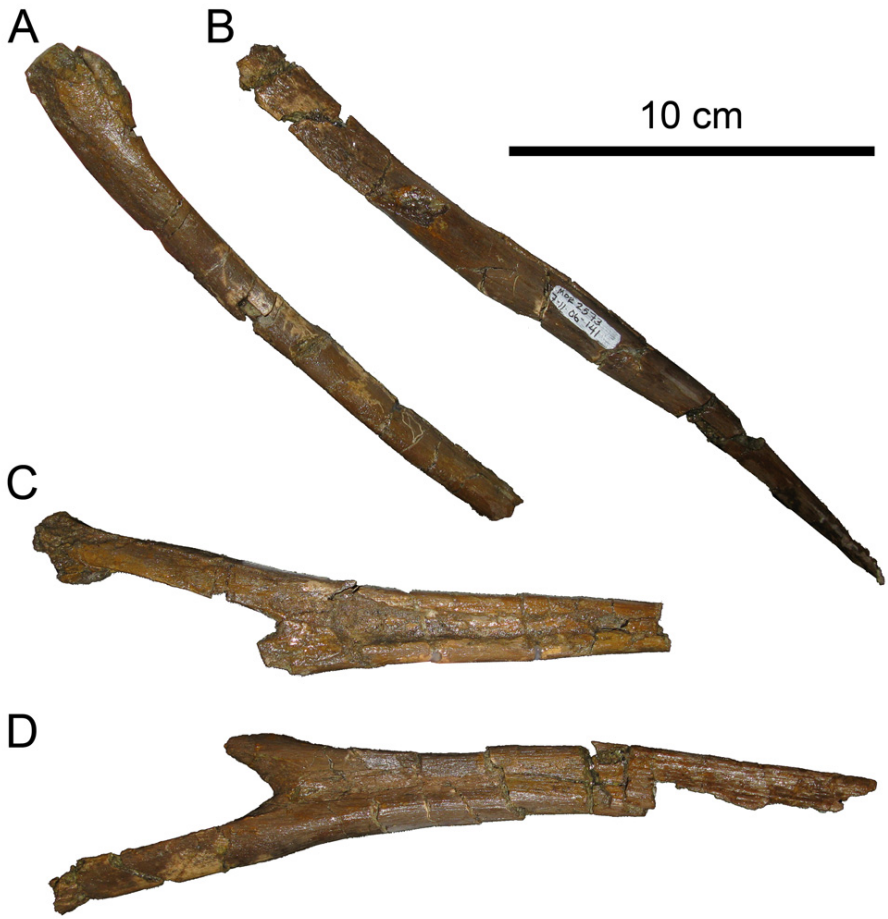


Figure 5.5. Chevrons of *Gryposaurus reddingi*, MOR 2573. (A, C) Chevron MOR 2573-7-27-06-215 in (A) left lateral and (C) anteroventral views. (B, D) Chevron MOR 2573-7-11-06-141 in (B) left lateral and (D) anteroventral views.

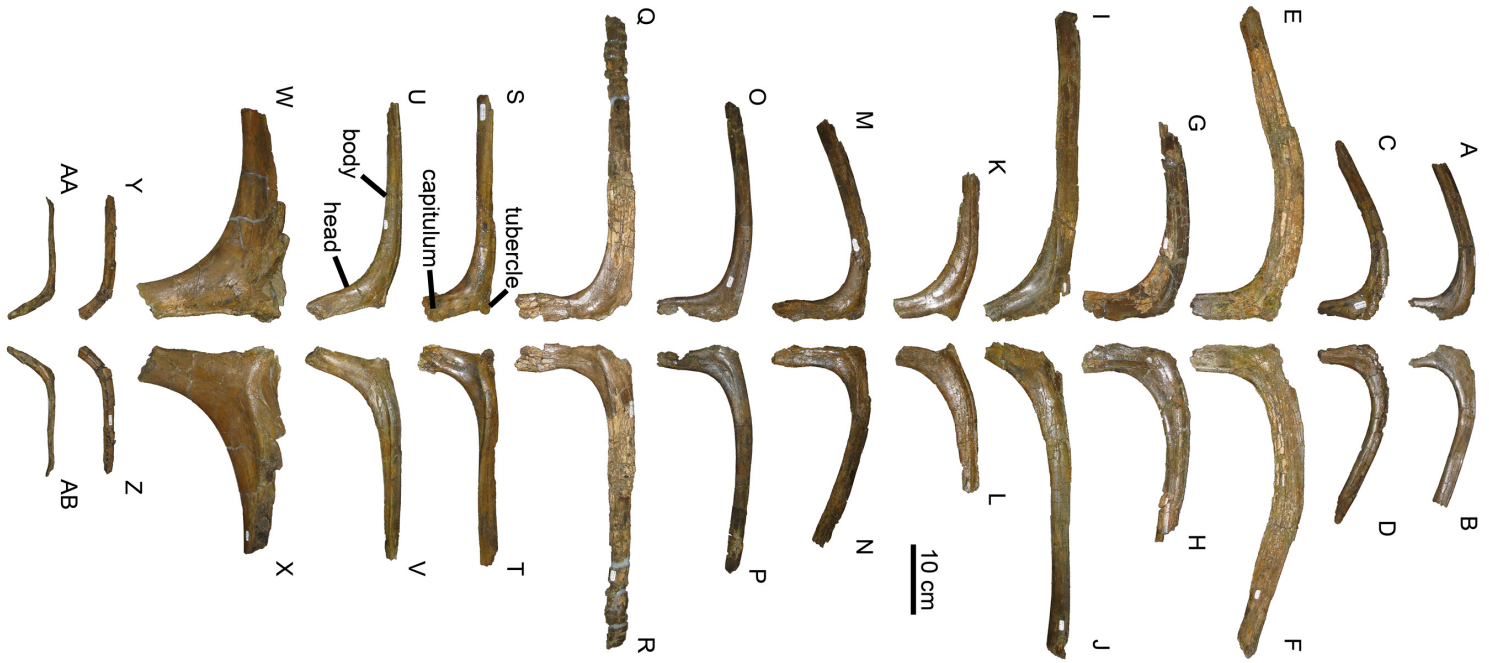


Figure 5.6. Ribs of *Gryposaurus reddingi*, MOR 2573. The sets of right ribs (A-L) and left ribs (M-AB) are each presented in their hypothesized approximate serial order within the ribcage, regardless of size. (A, B) Right rib MOR 2573-7-31-10-509 in (A) anterior and (B) posterior views. (C, D) Right rib MOR 2573-7-01-10-360 in (C) anterior and (D) posterior views. (E, F) Right rib MOR 2573-7-11-06-153 in (E) anterior and (F) posterior views. (G, H) Right rib MOR 2573-6-12-06-01 in (G) anterior and (H) posterior views. (I, J) Right rib MOR 2573-7-11-06-152 in (I) anterior and (J) posterior views. (K, L) Right rib MOR 2573-7-08-10-397 in (K) anterior and (L) posterior views. (M, N) Left rib MOR 2573-6-10-10-313 in (M) posterior and (N) anterior views. (O, P) Left rib MOR 2573-8-07-12-645 in (O) posterior and (P) anterior views. (Q, R) Left rib MOR 2573-7-5-06-113 in (Q) posterior and (R) anterior views. (S, T) Left rib MOR 2573-7-19-11-551 in (S) posterior and (T) anterior views. (U, V) Left rib MOR 2573-7-11-06-150 in (U) posterior and (V) anterior views. (W, X) Large left rib head MOR 2573-7-18-06-193 in (W) posterior and (X) anterior views. (Y, Z) Left rib MOR 2573-7-30-10-485 in (Y) posterior and (Z) anterior views. (AA, AB) Left rib MOR 2573-7-27-10-476 in (AA) posterior and (AB) anterior views.

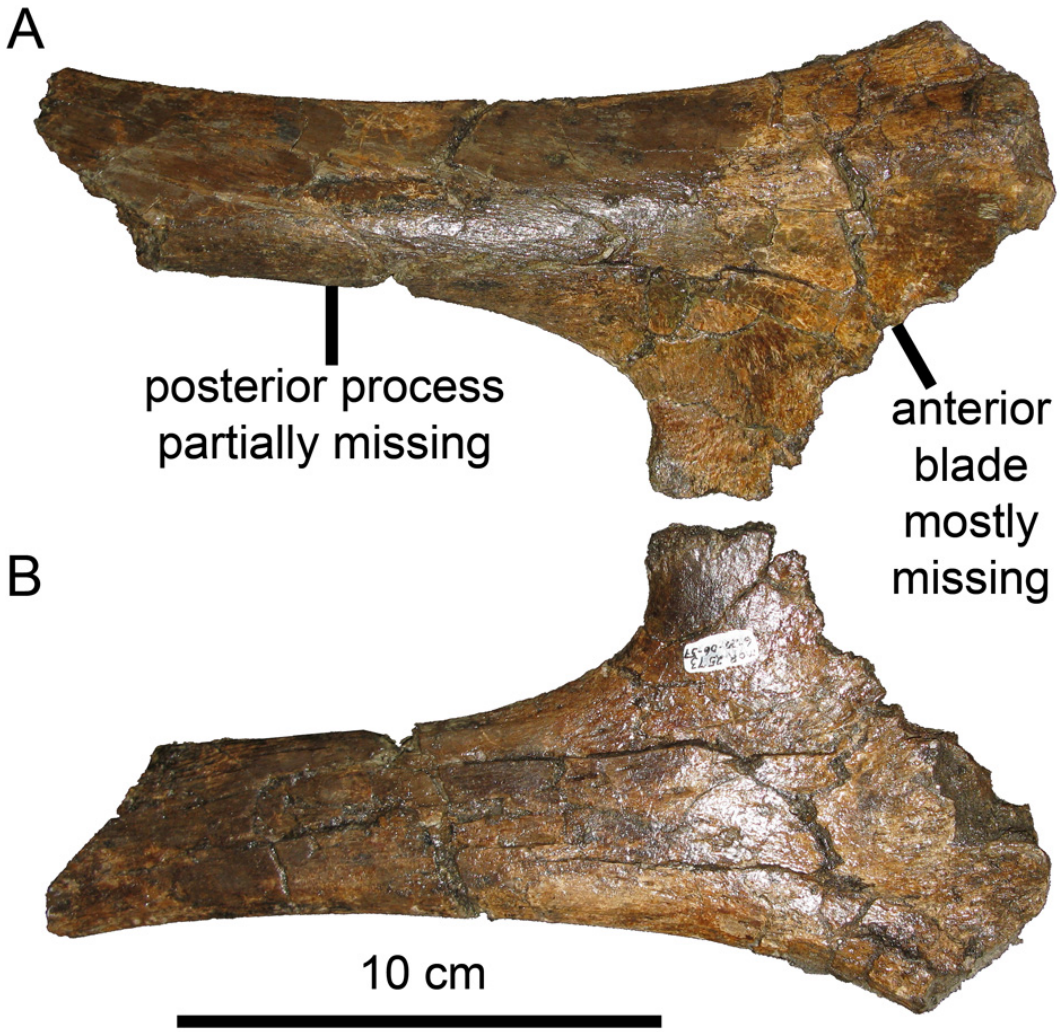


Figure 5.7. Partial sternal of *Gryposaurus reddingi*, MOR 2573. Right partial sternal MOR 2573-6-20-06-57 in (A) ventral and (B) dorsal views.

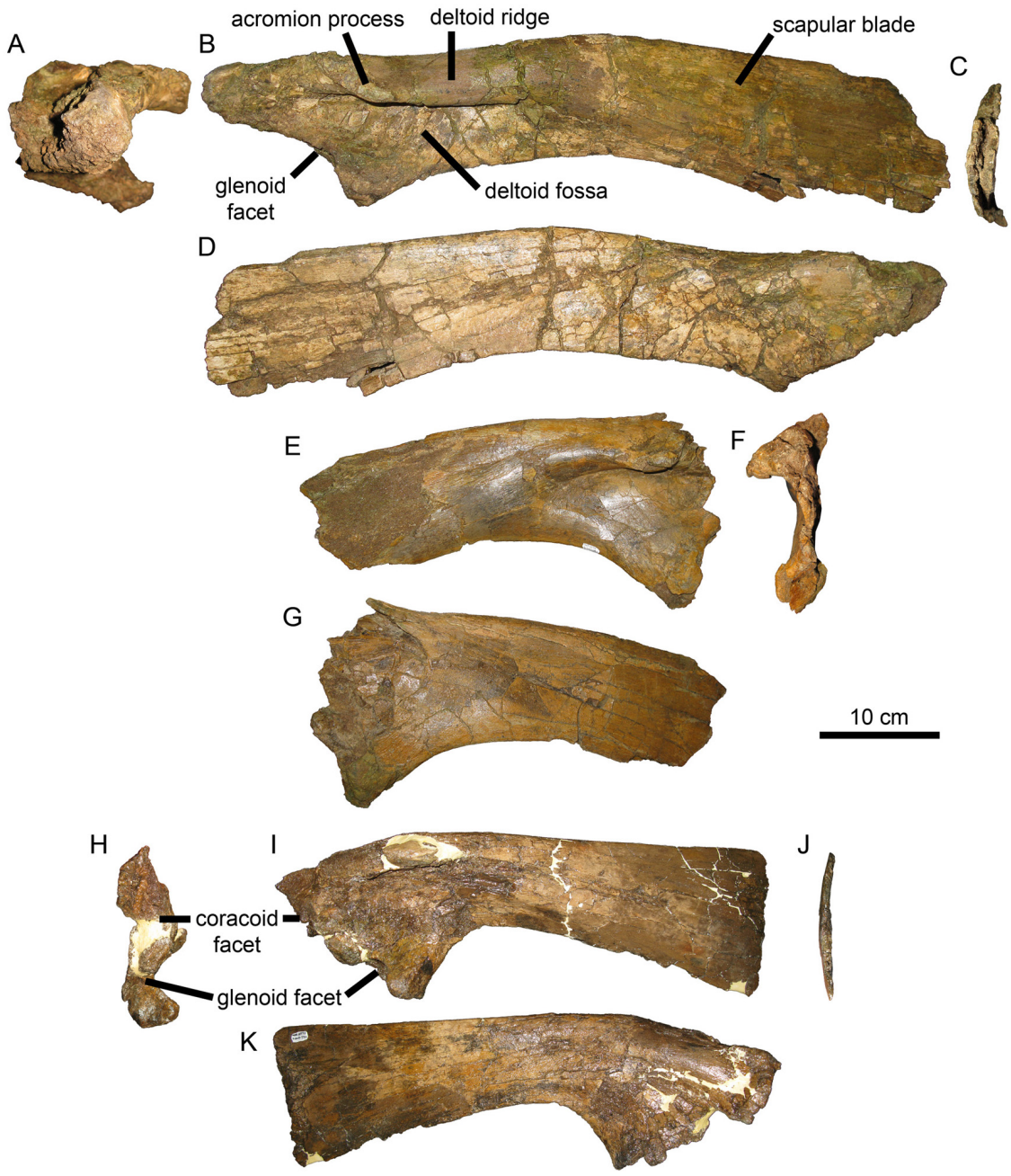
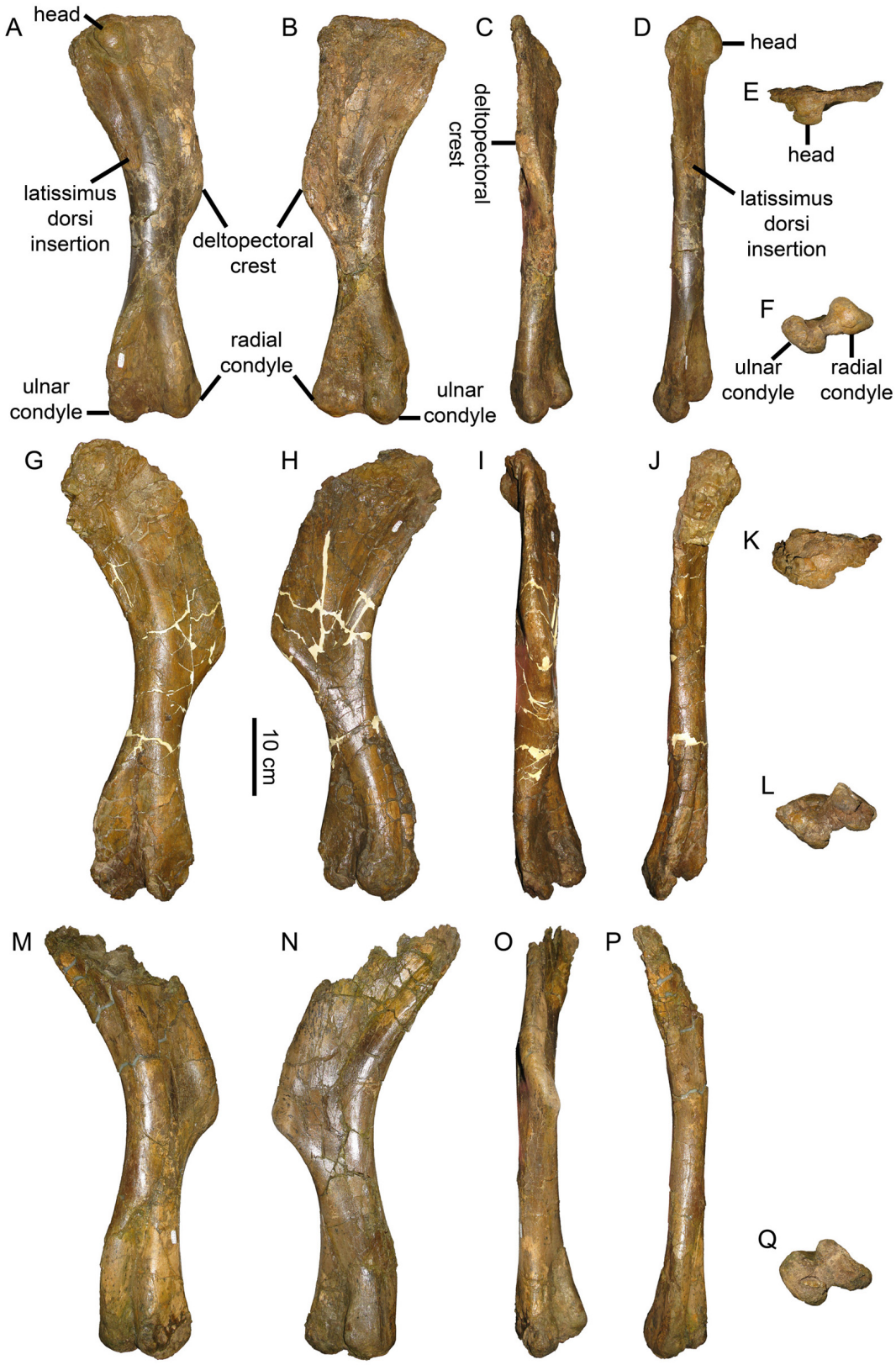


Figure 5.8. Scapulae of *Gryposaurus reddingi*, MOR 2573. (A-D) Left scapula MOR 2573-6-18-06-50 in (A) anterior, (B) lateral, (C) posterior, and (D) medial views. (E-G) Partial right scapula MOR 2573-8-11-06-236 in (E) lateral, (F) anterior, and (G) medial views. (H-K) Left juvenile scapula MOR 2573-7-22-11-570 in (H) anterior, (I) lateral, (J) posterior, and (K) medial views.

(Figure 5.9 on next page)

Figure 5.9. Humeri of *Gryposaurus reddingi*, MOR 2573. (A-F) Right humerus MOR 2573-7-01-10-355 in (A) posterior, (B) anterior, (C) lateral, (D) medial, (E) proximal, and (F) distal views. (G-L) Right humerus MOR 2573-6-12-06-8, with some mudstone matrix still attached to the proximal end, in (G) posterior, (H) anterior, (I) lateral, (J) medial, (K) proximal, and (L) distal views. (M-Q) Right humerus MOR 2573-6-03-10-279 in (M) posterior, (N) anterior, (O) lateral, (P) medial, and (Q) distal views.


A
head
latissimus dorsi insertion
deltopectoral crest
radial condyle
ulnar condyle
B
ulnar condyle
C
deltopectoral crest
D
head
latissimus dorsi insertion
E
head
F
ulnar condyle
radial condyle
G
H
10 cm
I
J
K
L
M
N
O
P
Q

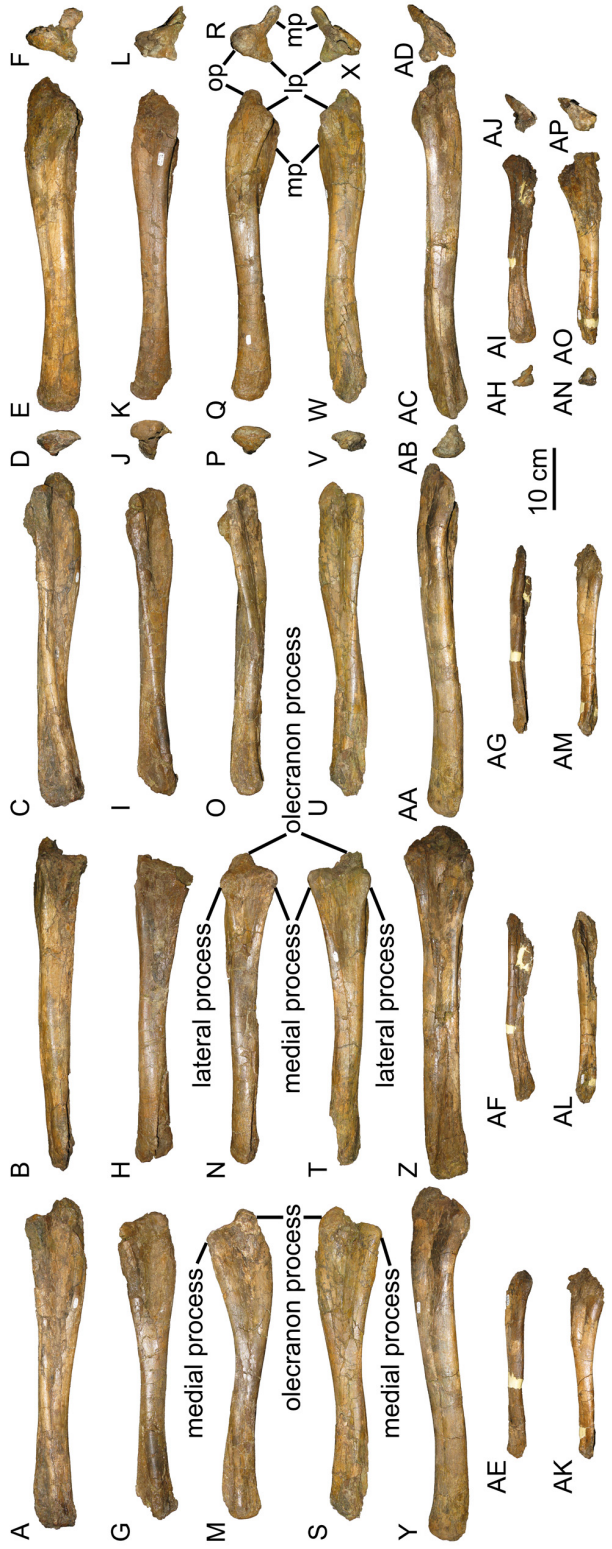


Figure 5.10. Ulnae of *Gryposaurus reddingi*, MOR 2573. (A-F) Right ulna MOR 2573-7-01-10-375 in (A) posterior, (B) anterior, (C) medial, (D) distal, (E) lateral, and (F) proximal views. (G-L) Right ulna MOR 2573-7-28-11-596 in (G) posterior, (H) anterior, (I) medial, (J) distal, (K) lateral, and (L) proximal views. (M-R) Right ulna MOR 2573-7-01-10-352 in (M) posterior, (N) anterior, (O) medial, (P) distal, (Q) lateral, and (R) proximal views. (S-X) Left ulna MOR 2573-8-11-06-240 in (S) posterior, (T) anterior, (U) medial, (V) distal, (W) lateral, and (X) proximal views. (Y-AD) Left ulna MOR 2573-6-03-10-263 in (Y) posterior, (Z) anterior, (AA) medial, (AB) distal, (AC) lateral, and (AD) proximal views. (AE-AJ) Left juvenile ulna MOR 2573-7-05-06-121 in (AE) posterior, (AF) anterior, (AG) medial, (AH) distal, (AI) lateral, and (AJ) proximal views. (AK-AP) Left juvenile ulna MOR 2573-7-12-12-756 in (AK) posterior, (AL) anterior, (AM) medial, (AN) distal, (AO) lateral, and (AP) proximal views. These juvenile ulnae have damaged proximal ends. Abbreviations: mp, medial process; lp, lateral process; op, olecranon process.

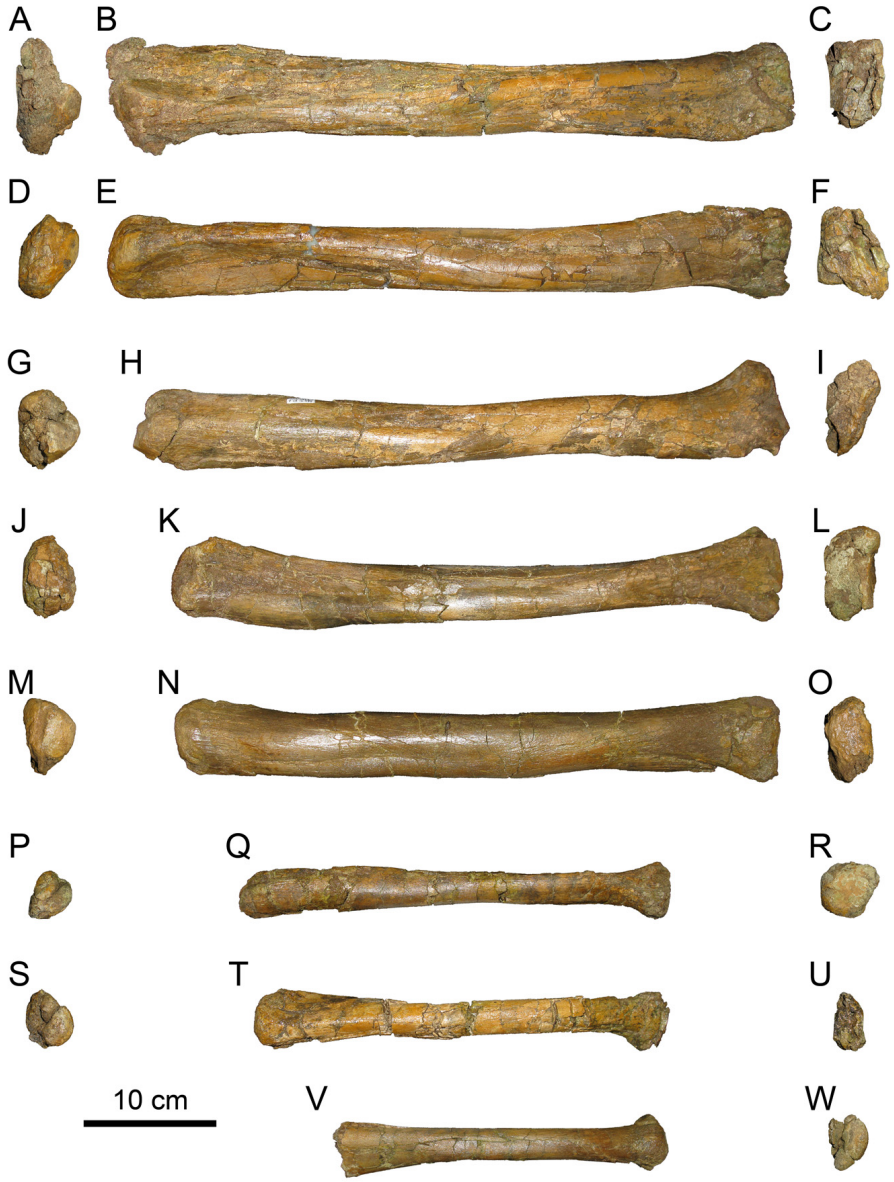


Figure 5.11. Radii of *Gryposaurus reddingi*, MOR 2573. (A-C) Radius MOR 2573-7-22-10-445 in (A) distal, (B) longitudinal, and (C) proximal views. (D-F) Radius MOR 2573-6-03-10-264 in (D) distal, (E) longitudinal, and (F) proximal views. (G-I) Radius MOR 2573-7-27-10-475 in (G) distal, (H) longitudinal, and (I) proximal views. (J-L) Radius MOR 2573-7-27-10-473 in (J) distal, (K) longitudinal, and (L) proximal views. (M-O) Radius MOR 2573-7-06-10-383 in (M) distal, (N) longitudinal, and (O) proximal views. (P-R) Juvenile radius MOR 2573-7-06-12-738 in (P) distal, (Q) longitudinal, and (R) proximal views. (S-U) Juvenile radius MOR 2573-6-24-12-686 in (S) distal, (T) longitudinal, and (U) proximal views. (V-W) Juvenile radius MOR 2573-7-25-12-783 with broken distal end in (V) longitudinal and (W) proximal views. Longitudinal view of radii is interpreted as anterior view; proximal ends are to the right.

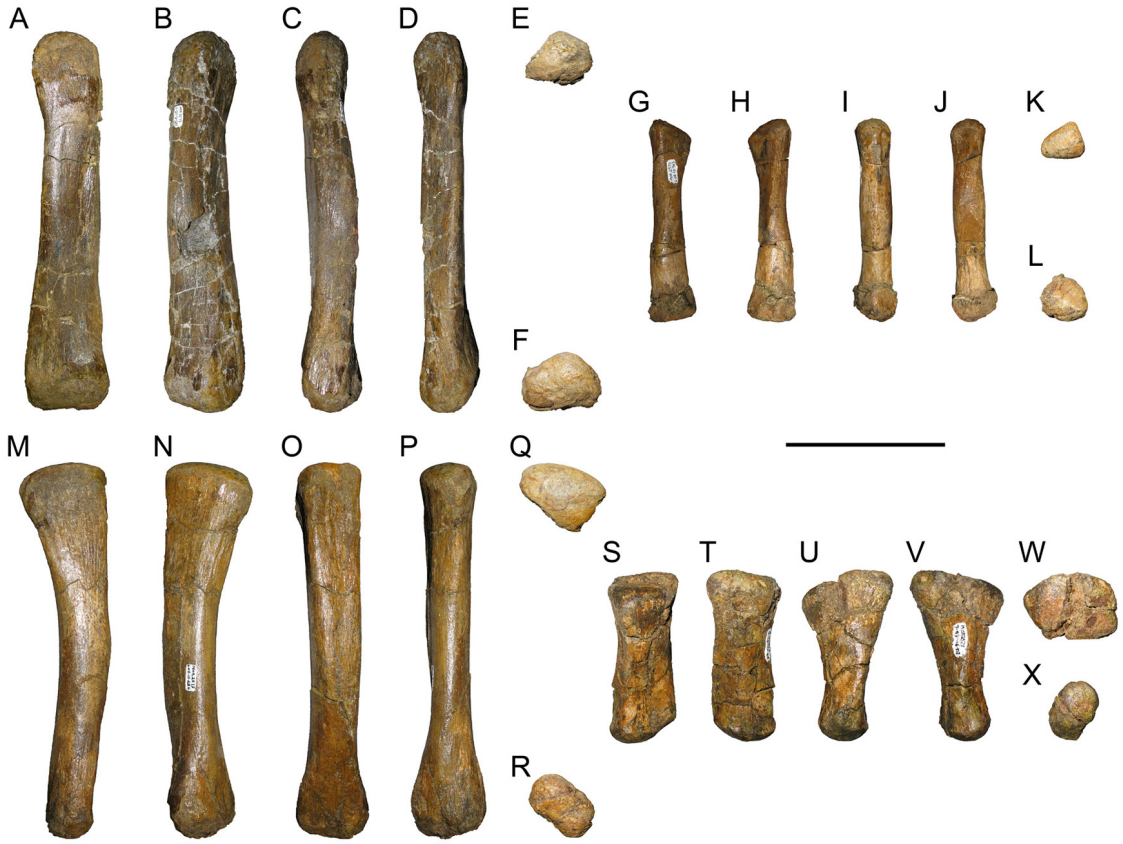
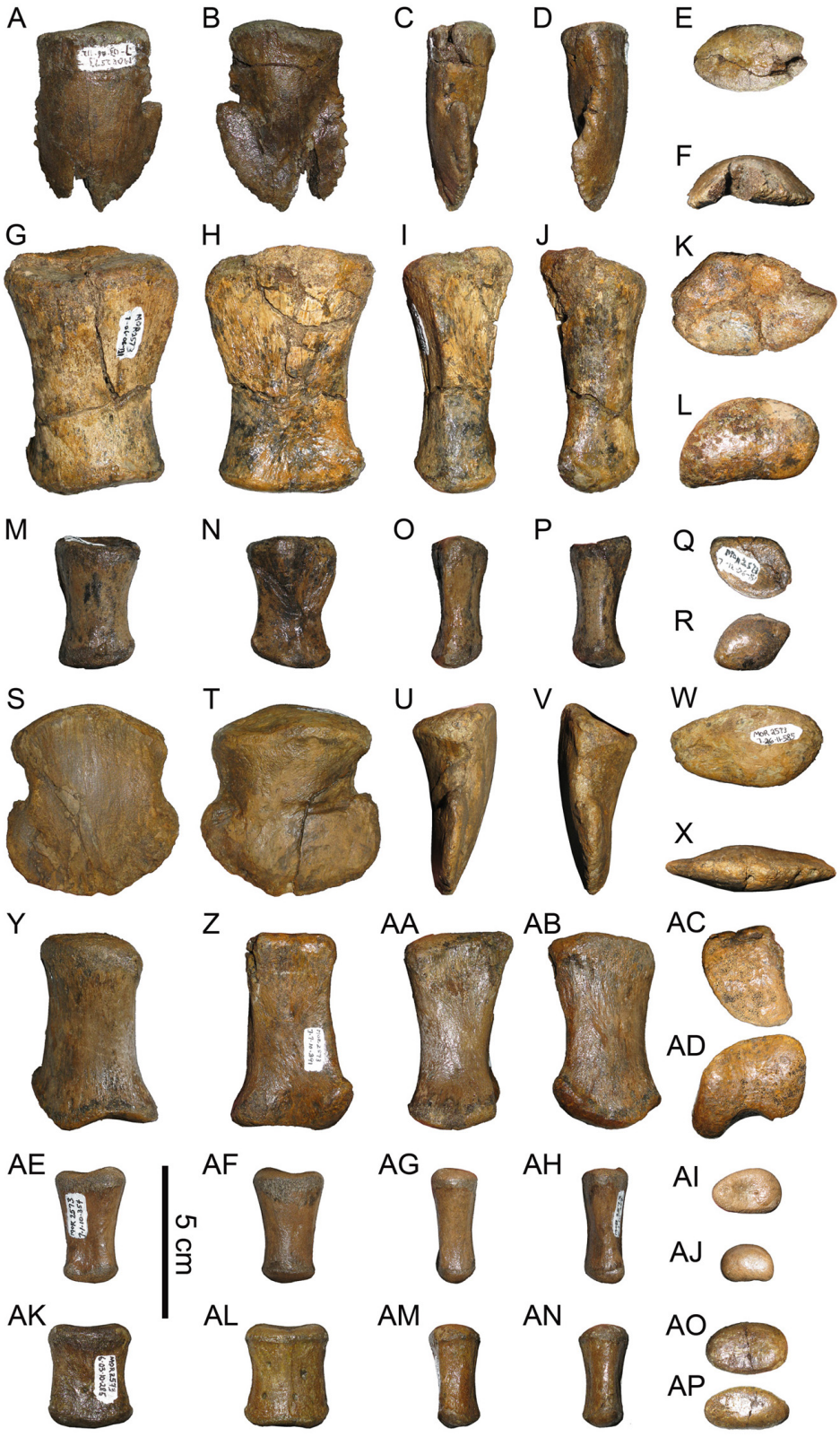


Figure 5.12. Metacarpals of *Gryposaurus reddingi*, MOR 2573. (A-F) Right metacarpal III MOR 2573-6-23-12-684 in (A) anterior, (B) posterior, (C) medial, (D) lateral, (E) proximal, and (F) distal views. (G-L) Right juvenile metacarpal III MOR 2573-6-28-12-703 in (G) anterior, (H) posterior, (I) medial, (J) lateral, (K) proximal, and (L) distal views. (M-R) Right metacarpal IV MOR 2573-6-04-10-286 in (M) anterior, (N) posterior, (O) medial, (P) lateral, (Q) proximal, and (R) distal views. (S-X) Right metacarpal V MOR 2573-7-03-06-108 in (S) anterior, (T) posterior, (U) medial, (V) lateral, (W) proximal, and (X) distal views.

(Figure 5.13 on next page)

Figure 5.13. Manual phalanges of *Gryposaurus reddingi*, MOR 2573. (A-F) Right manual ungual II-3 MOR 2573-7-03-06-112 in (A) anterior, (B) posterior, (C) medial, (D) lateral, (E) proximal, and (F) distal views. (G-L) Right manual phalanx III-1 MOR 2573-7-06-06-131 in (G) anterior, (H) posterior, (I) medial, (J) lateral, (K) proximal, and (L) distal views. (M-R) Left juvenile manual phalanx III-1 MOR 2573-7-12-06-161 in (M) anterior, (N) posterior, (O) medial, (P) lateral, (Q) proximal, and (R) distal views. (S-X) Left manual ungual III-3 MOR 2573-7-26-11-585 in (S) anterior, (T) posterior, (U) medial, (V) lateral, (W) proximal, and (X) distal views. (Y-AD) Right manual phalanx IV-1 MOR 2573-7-07-10-391 in (Y) anterior, (Z) posterior, (AA) medial, (AB) lateral, (AC) proximal, and (AD) distal views. (AE-AJ) Right juvenile manual phalanx V-1 MOR 2573-7-01-10-354 in (AE) anterior, (AF) posterior, (AG) medial, (AH) lateral, (AI) proximal, and (AJ) distal views. (AK-AP) Manual phalanx V-2 MOR 2573-6-03-10-285, interpreted as likely a right phalanx, in (AK) anterior, (AL) posterior, (AM) medial, (AN) lateral, (AO) proximal, and (AP) distal views.


A
B
C
D
E
F
G
H
I
J
K
L
M
N
O
P
Q
R
S
T
U
V
W
X
Y
Z
AA
AB
AC
AD
AE
AF
AG
AH
AI
AJ
AK
AL
AM
AN
AO
AP
5 cm

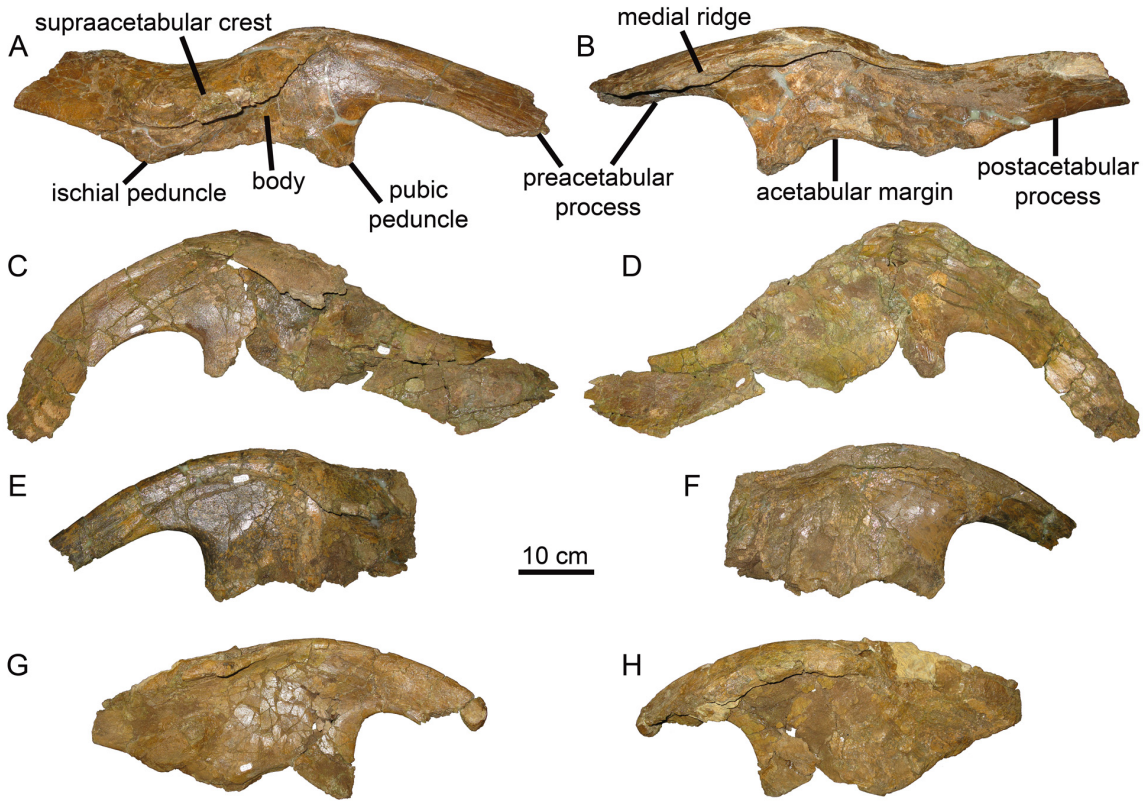


Figure 5.14. Ilia of *Gryposaurus reddingi*, MOR 2573. (A-B) Right ilium MOR 2573-7-21-10-442 in (A) lateral and (B) medial views. (C-D) Left ilium broken into three pieces prior to burial: MOR 2573-6-03-10-280, MOR 2573-6-03-10-284A, and MOR 2573-6-03-10-284B in (C) lateral and (D) medial views. (E-F) Left ilium MOR 2573-7-06-11-515 in (E) lateral and (F) medial views. (G-H) Right ilium MOR 2573-7-30-11-610 in (G) lateral and (H) medial views.

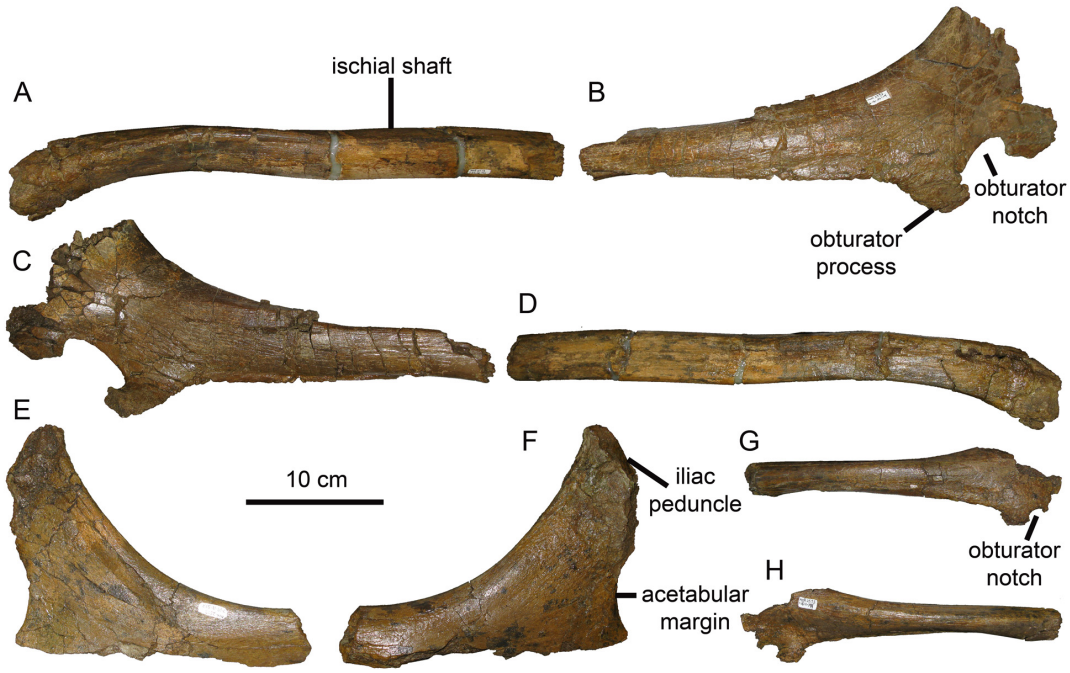


Figure 5.15. Ischia of *Gryposaurus reddingi*, MOR 2573. (A, D) Right ischial shaft MOR 2573-7-05-12-735 in (A) lateral and (D) medial views. (B-C) Right partial proximal ischium MOR 2573-6-12-06-14 in (B) lateral and (C) medial views. MOR 2573-7-05-12-735 and MOR 2573-6-12-06-14 may or may not be parts of the same ischium. Total ischial length is unknown. (E-F) Left partial proximal ischium MOR 2573-7-19-11-553 in (E) lateral and (F) medial views. (G-H) Right partial juvenile ischium MOR 2573-7-08-10-399 in (G) lateral and (H) medial views.

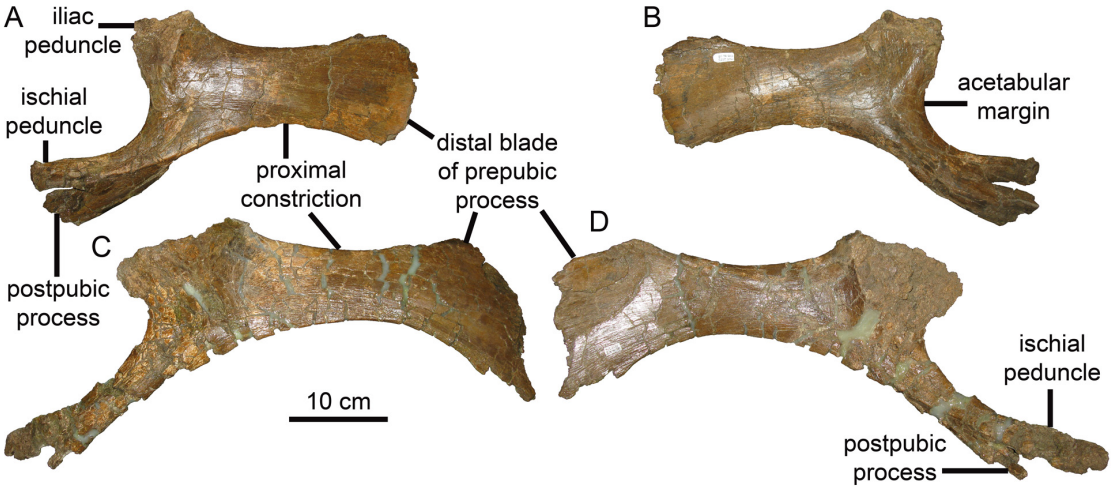


Figure 5.16. Pubes of *Gryposaurus reddingi*, MOR 2573. (A-B) Right pubis MOR 2573-7-05-06-118, missing most of distal blade, in (A) lateral and (B) medial views. (C) Left pubis MOR 2573-7-16-10-431, damaged and expanded by modern sinkhole weathering, in (C) medial and (D) lateral views.

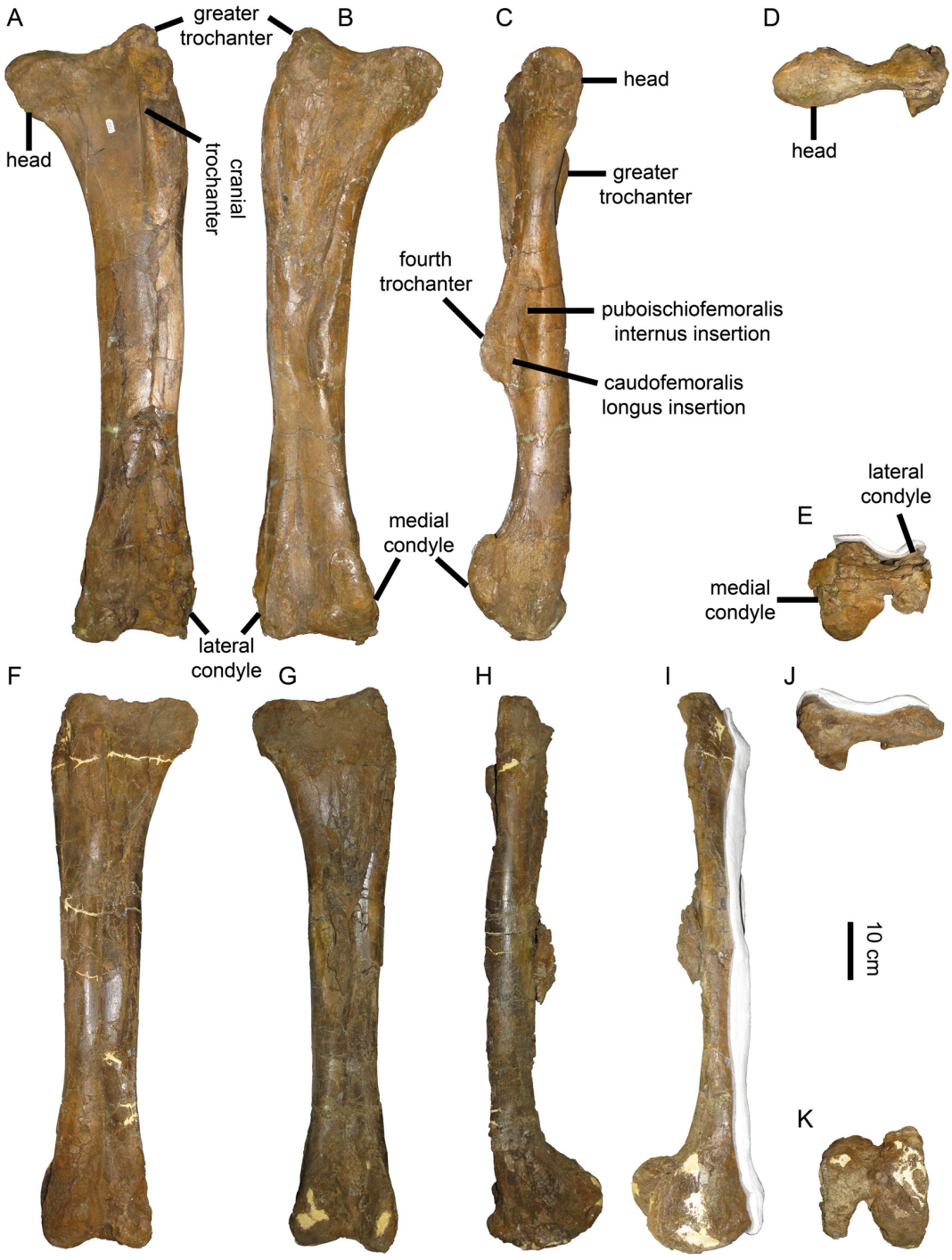


Figure 5.17. Femora of *Gryposaurus reddingi*, MOR 2573. (A-E) Left femur MOR 2573-7-14-06-168 in (A) anterior, (B) posterior, (C) medial, (D) proximal, and (E) distal views. (F-K) Right femur MOR 2573-7-12-11-529 in (F) anterior, (G) posterior, (H) medial, (I) lateral, (J) proximal, and (K) distal views. The femora are fragile and could not be removed from their supportive cradles in some lateral, proximal, and distal views.

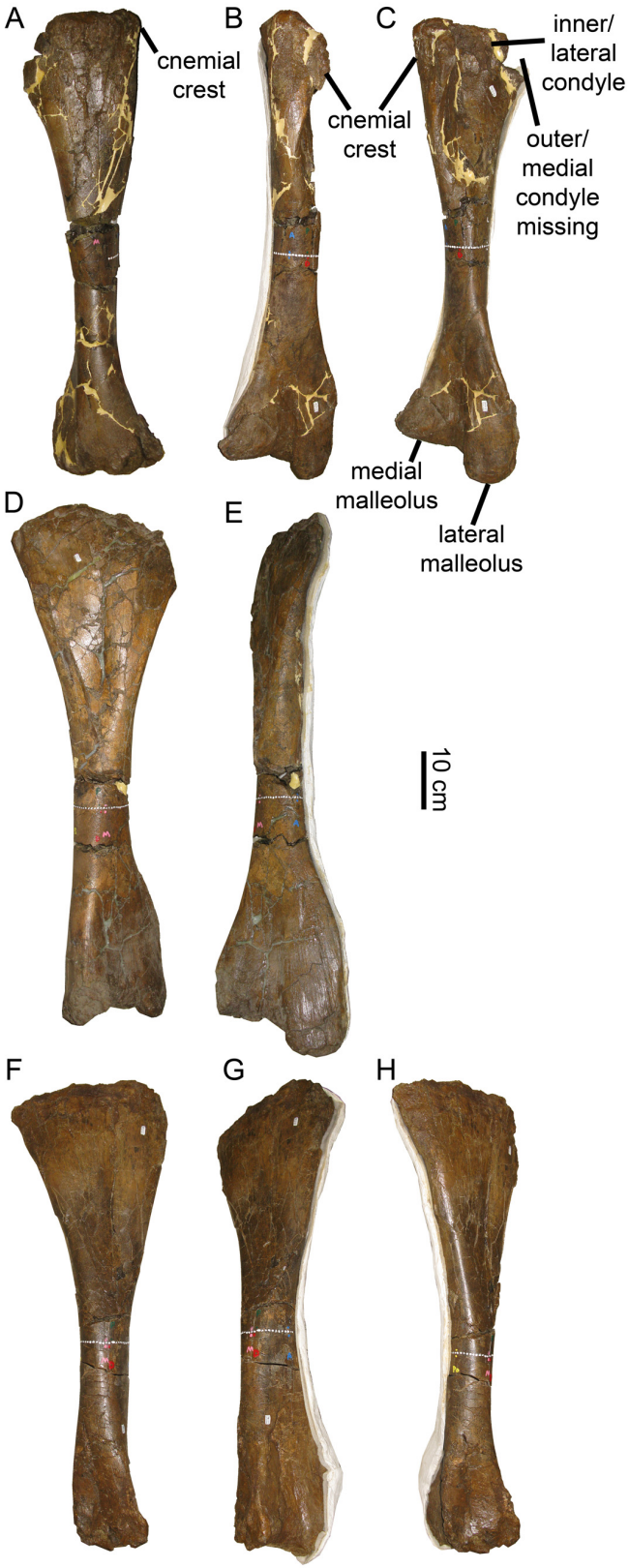


Figure 5.18. Tibiae of *Gryposaurus reddingi*, MOR 2573. (A-C) Left tibia MOR 2573-7-31-10-497 in (A) medial, (B) anterior, and (C) anterolateral views. (D-E) Left tibia MOR 2573-6-12-06-17 in (D) medial and (E) anteromedial views. (F-H) Left tibia MOR 2573-7-08-10-396 in (F) medial, (G) anteromedial, and (H) posteromedial views. The tibiae are fragile and could not be removed from their supportive cradles in several views. Dotted white lines indicate locations of transverse diaphyseal sections sampled for osteohistology (Freedman Fowler, Chapter Three).

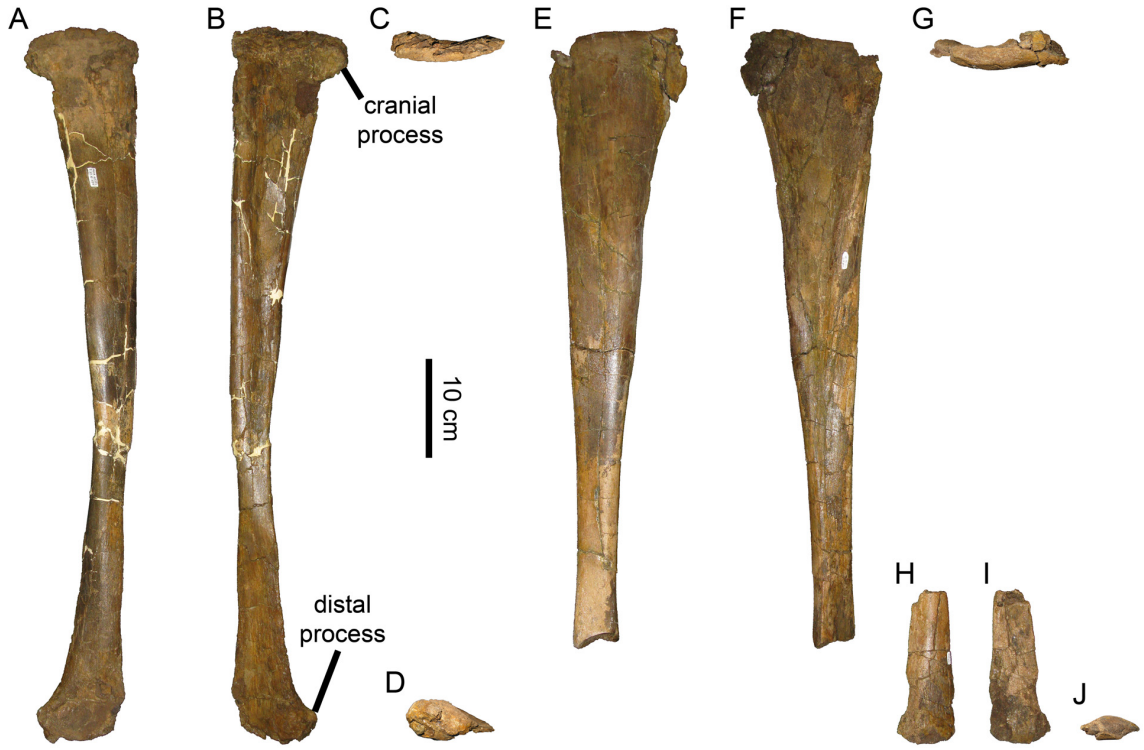


Figure 5.19. Fibulae of *Gryposaurus reddingi*, MOR 2573. (A-D) Left fibula MOR 2573 7-27-10-474 in (A) lateral, (B) medial, (C) proximal, and (D) distal views. (E-G) Right partial fibula MOR 2573-7-17-06-183 in (E) lateral, (F) medial, and (G) proximal views. (H-J) Left juvenile distal fibula MOR 2573-6-24-12-690 in (H) lateral, (I) medial, and (J) distal views.

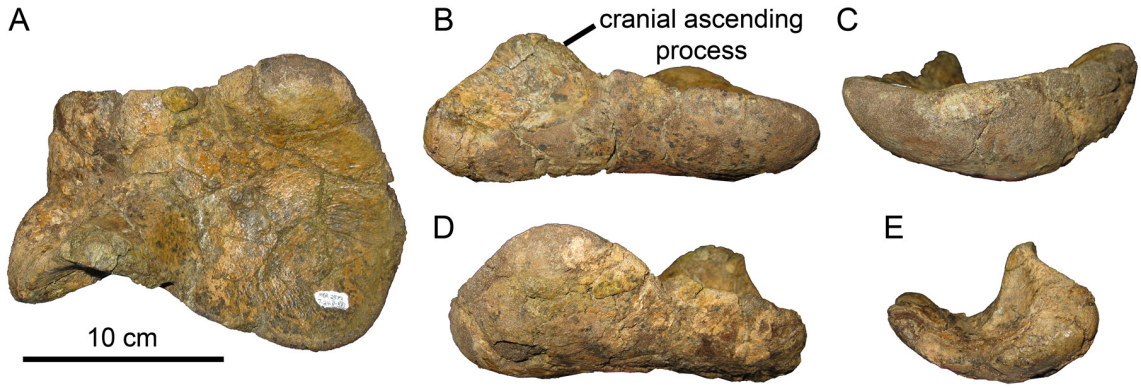


Figure 5.20. Astragalus of *Gryposaurus reddingi*, MOR 2573. Right astragalus MOR 2573-7-24-11-581 in (A) proximal, (B) anterior, (C) medial, (D) posterior, and (E) lateral views.

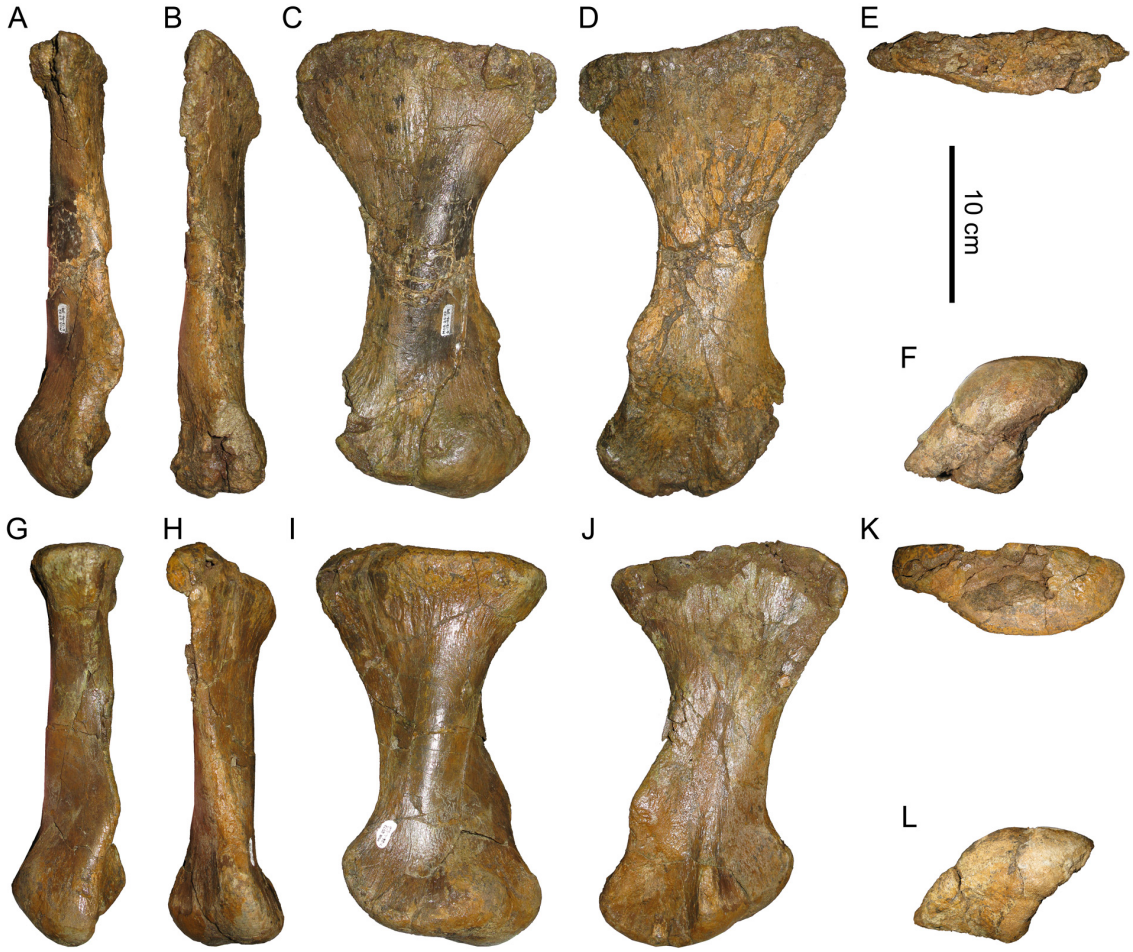


Figure 5.21. Metatarsal IIs of *Gryposaurus reddingi*, MOR 2573. (A-F) Left metatarsal II MOR 2573-6-13-06-39 in (A) anterior, (B) posterior, (C) medial, (D) lateral, (E) proximal, and (F) distal views. (G-L) Left metatarsal II MOR 2573-7-26-11-586 in (G) anterior, (H) posterior, (I) medial, (J) lateral, (K) proximal, and (L) distal views.

(Figure 5.22 on next page)

Figure 5.22. Metatarsal IIIs of *Gryposaurus reddingi*, MOR 2573. (A-F) Right metatarsal III MOR 2573-6-10-10-302 in (A) anterior, (B) posterior, (C) medial, (D) lateral, (E) proximal, and (F) distal views. (G-L) Left metatarsal III MOR 2573-7-08-10-394 in (G) anterior, (H) posterior, (I) medial, (J) lateral, (K) proximal, and (L) distal views. (M-R) Left juvenile metatarsal III MOR 2573-6-14-06-43 in (M) anterior, (N) posterior, (O) medial, (P) lateral, (Q) proximal, and (R) distal views. (S-X) Left juvenile metatarsal III MOR 2573-7-05-10-379 in (S) anterior, (T) posterior, (U) medial, (V) lateral, (W) proximal, and (X) distal views. Metatarsals MOR 2573-6-10-10-302 and MOR 2573-7-05-10-379 are anteroposteriorly compressed, whereas MOR 2573-7-08-10-394 is mediolaterally compressed.


A
B
C
D
E
F
G
H
I
J
K
L
M
N
O
P
Q
R
10 cm
S
T
U
V
W
X

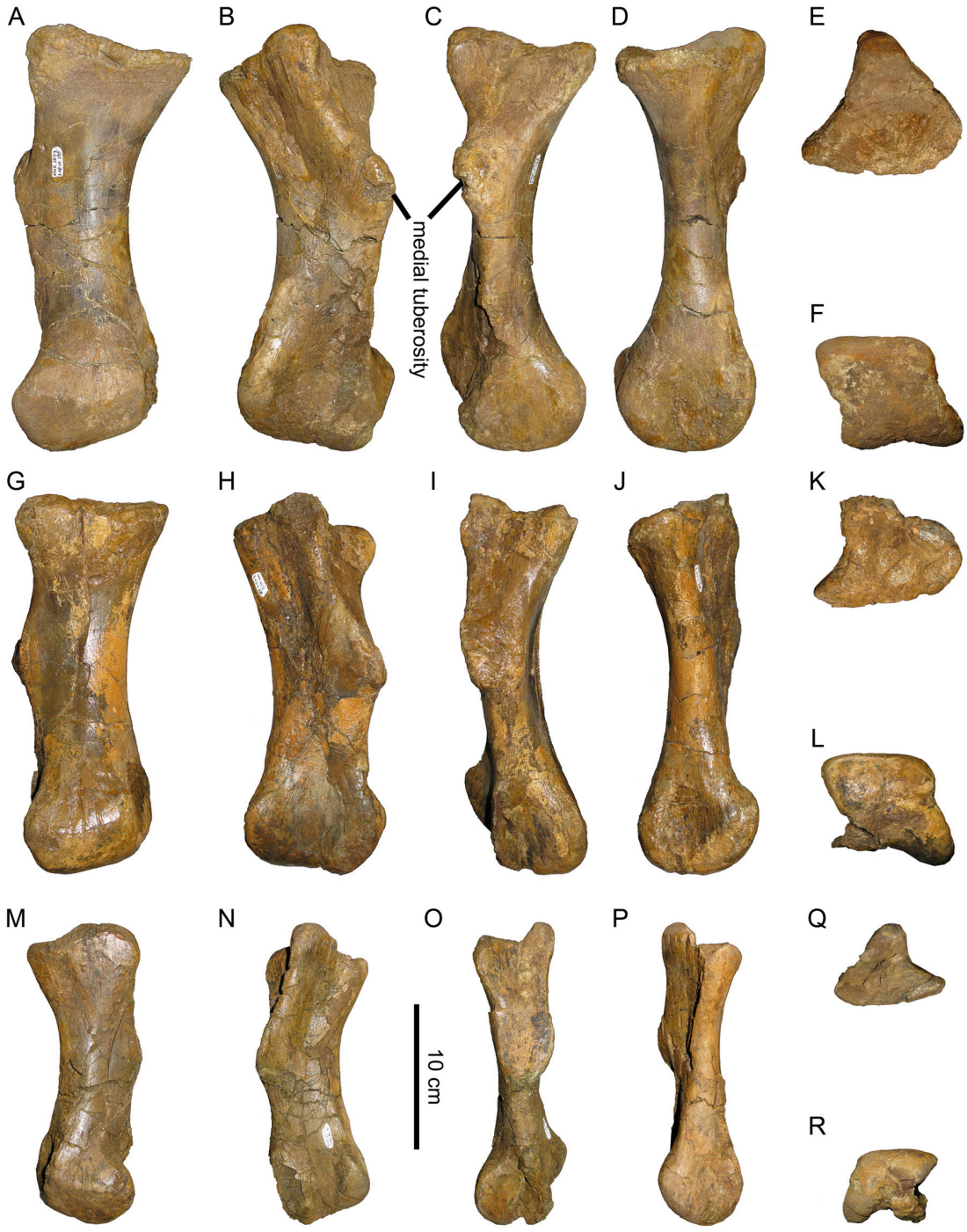


Figure 5.23. Metatarsal IVs of *Gryposaurus reddingi*, MOR 2573. (A-F) Left metatarsal IV MOR 2573-7-08-10-395 in (A) anterior, (B) posterior, (C) medial, (D) lateral, (E) proximal, and (F) distal views. (G-L) Left metatarsal IV MOR 2573-8-03-11-629 in (G) anterior, (H) posterior, (I) medial, (J) lateral, (K) proximal, and (L) distal views. (M-R) Right juvenile metatarsal IV MOR 2573-7-03-06-95 in (M) anterior, (N) posterior, (O) medial, (P) lateral, (Q) proximal, and (R) distal views.

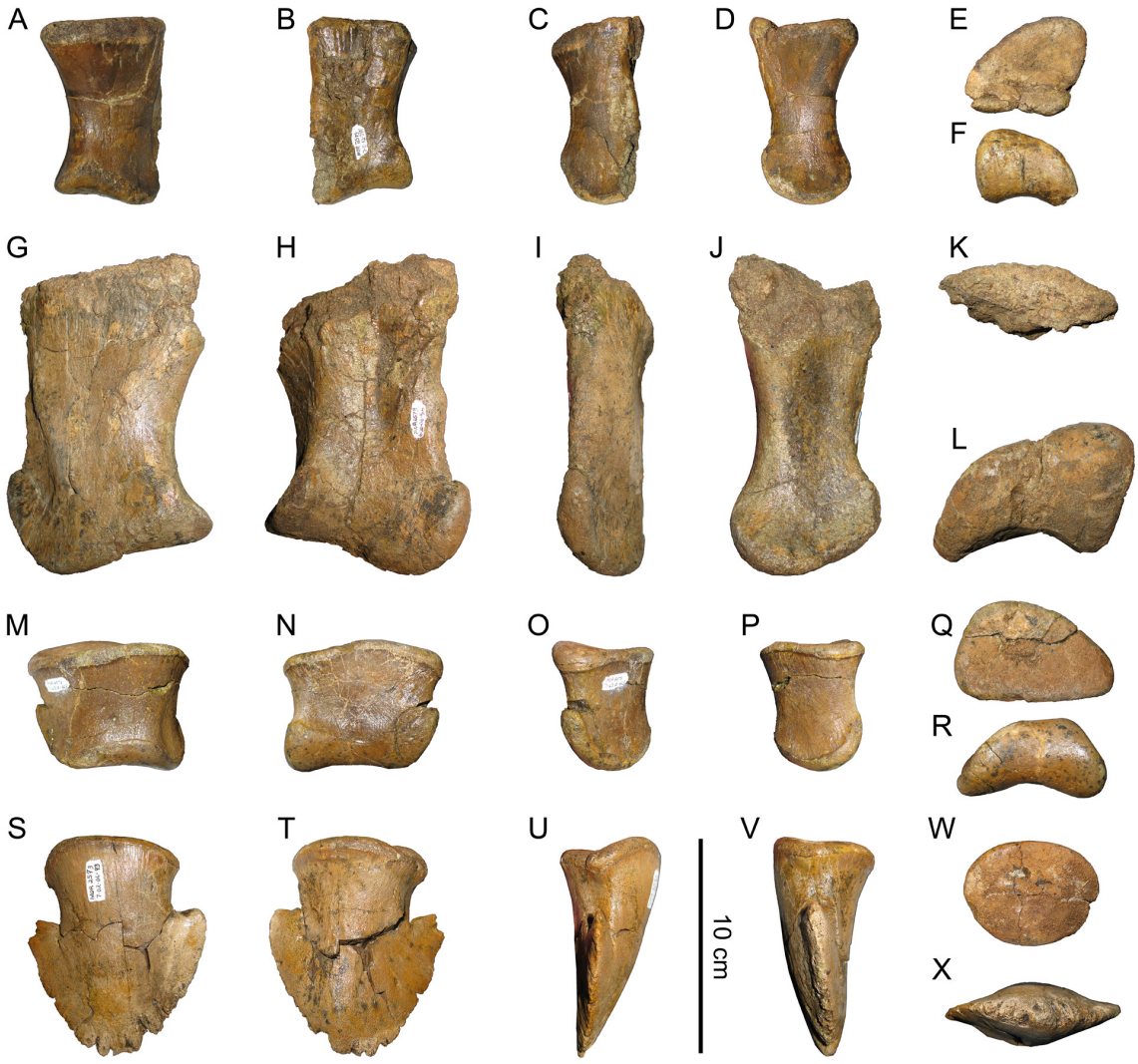


Figure 5.24. Pedal phalanges of digit II of *Gryposaurus reddingi*, MOR 2573. (A-F) Right juvenile pedal phalanx II-1 MOR 2573-7-11-12-754 in (A) dorsal, (B) plantar, (C) medial, (D) lateral, (E) proximal, and (F) distal views. (G-L) Left pedal phalanx II-1 MOR 2573-6-20-06-56 with damaged proximal end in (G) dorsal, (H) plantar, (I) medial, (J) lateral, (K) proximal, and (L) distal views. (M-R) Left pedal phalanx II-2 MOR 2573-7-28-11-603 in (M) dorsal, (N) plantar, (O) medial, (P) lateral, (Q) proximal, and (R) distal views. (S-X) Pedal ungual MOR 2573-7-02-06-93, possibly a left II-3, in (S) anterior, (T) posterior, (U) medial, (V) lateral, (W) proximal, and (X) distal views.

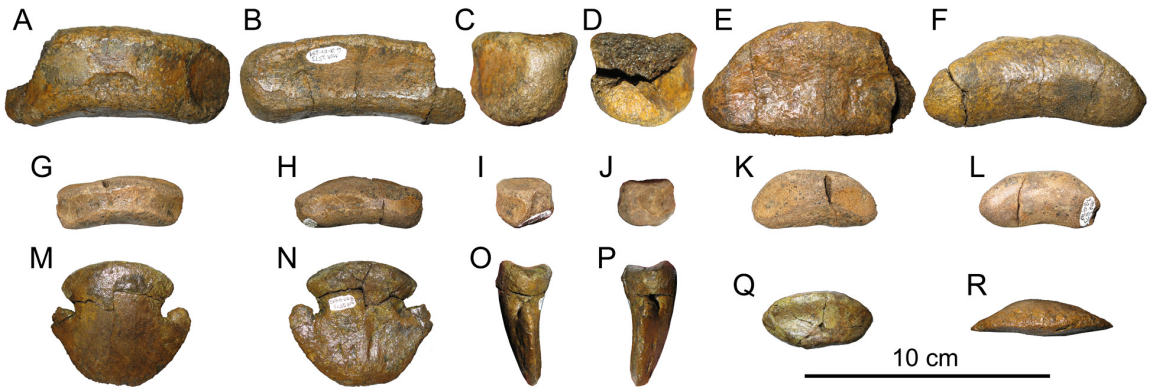


Figure 5.25. Pedal phalanges of digit III of *Gryposaurus reddingi*, MOR 2573. Pedal digit III elements are so symmetrical that left or right sides cannot be determined with confidence. (A-F) Pedal phalanx III-3 MOR 2573-6-18-07-259 with damaged right lateral side in (A) dorsal, (B) plantar, (C) left lateral, (D) right lateral, (E) proximal, and (F) distal views. (G-L) Juvenile pedal phalanx III-3 MOR 2573-7-3-12-728 in (G) dorsal, (H) plantar, (I) left lateral, (J) right lateral, (K) proximal, and (L) distal views. (M-R) Juvenile pedal ungual III-4 MOR 2573-8-07-11-642 in (M) dorsal, (N) plantar, (O) left lateral, (P) right lateral, (Q) proximal, and (R) distal views.

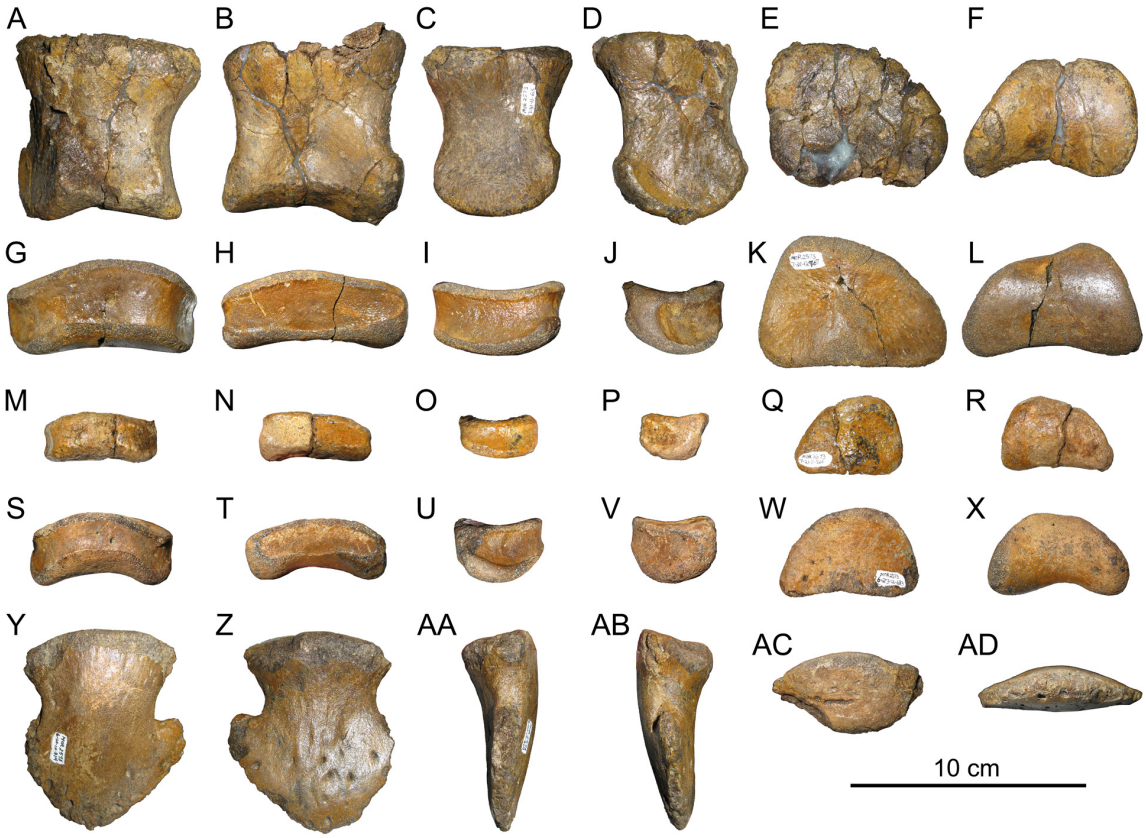


Figure 5.26. Pedal phalanges of digit IV of *Gryposaurus reddingi*, MOR 2573. (A-F) Right pedal phalanx IV-1 MOR 2573-7-31-11-615 in (A) dorsal, (B) plantar, (C) medial, (D) lateral, (E) proximal, and (F) distal views. (G-L) Right pedal phalanx IV-3 MOR 2573-7-20-12-769 in (G) dorsal, (H) plantar, (I) medial, (J) lateral, (K) proximal, and (L) distal views. (M-R) Left juvenile pedal phalanx IV-3 MOR 2573-7-21-11-561 in (M) dorsal, (N) plantar, (O) medial, (P) lateral, (Q) proximal, and (R) distal views. (S-X) Left pedal phalanx IV-4 MOR 2573-6-23-12-683 in (S) anterior, (T) posterior, (U) medial, (V) lateral, (W) proximal, and (X) distal views. (Y-AD) Pedal ungual MOR 2573-6-10-10-314, possibly a left IV-5, in (Y) anterior, (Z) posterior, (AA) medial, (AB) lateral, (AC) proximal, and (AD) distal views.

Literature Cited

Campione, N. E. 2014. Postcranial anatomy of *Edmontosaurus regalis* (Hadrosauridae) from the Horseshoe Canyon Formation, Alberta, Canada; pp. 208-244 in D. A. Eberth and D. C. Evans (eds.), Hadrosaurs. Indiana University Press, Bloomington, Indiana.

Evans, D. C. 2010. Cranial anatomy and systematics of *Hypacrosaurus altispinus*, and a comparative analysis of skull growth in lambeosaurine hadrosaurids (Dinosauria: Ornithischia). Zoological Journal of the Linnean Society 159:398-434.

Freedman Fowler, E. A. Chapter Three. Taphonomy of a Gryposaurus hadrosaur bonebed from the Judith River Formation (Campanian) of northcentral Montana.

Freedman Fowler, E. A., and J. R. Horner. Chapter Four. A new species of *Gryposaurus* (Dinosauria: Ornithischia) from the Judith River Formation of northcentral Montana.

Freedman Fowler, E. A., and J. R. Horner. Chapter Two. A new brachylophosaurinin (Dinosauria: Ornithischia) from the Judith River Formation of northcentral Montana.

Gates, T. A., E. K. Lund, C. A. Boyd, D. D. DeBlieux, A. L. Titus, D. C. Evans, M. A. Getty, J. I. Kirkland, and J. G. Eaton. 2013. Ornithopod dinosaurs from the Grand Staircase-Escalante National Monument region, Utah, and their role in paleobiogeographic and macroevolutionary studies; pp. 463-481 in A. L. Titus and M. A. Loewen (eds.), At the Top of the Grand Staircase: the Late Cretaceous of Southern Utah. Indiana University Press, Bloomington, Indiana.

Horner, J. R., and P. J. Currie. 1994. Embryonic and neonatal morphology and ontogeny of a new species of *Hypacrosaurus* (Ornithischia, Lambeosauridae) from Montana and Alberta. Dinosaur Eggs and Babies:312-336.

Leiggi, P., C. R. Schaff, and P. May. 1994. Macrovertebrate collecting; pp. 59-77 in P. Leiggi and P. May (eds.), Vertebrate Paleontological Techniques. Cambridge University Press, Cambridge, UK.

Prieto-Márquez, A. 2007. Postcranial Osteology of the Hadrosaurid Dinosaur *Brachylophosaurus canadensis* from the Late Cretaceous of Montana; pp. 91-115 in K. Carpenter (ed.), Horns and Beaks: Ceratopsian and Ornithopod Dinosaurs. Indiana Press, Bloomington, IN.

Prieto-Márquez, A. 2010. Global phylogeny of Hadrosauridae (Dinosauria: Ornithopoda) using parsimony and Bayesian methods. Zoological Journal of the Linnean Society 159:435-502.

Prieto-Márquez, A. 2012. The skull and appendicular skeleton of *Gryposaurus latidens*, a saurolophine hadrosaurid (Dinosauria: Ornithopoda) from the early Campanian (Cretaceous) of Montana, USA. Canadian Journal of Earth Sciences 49:510-532.

Prieto-Márquez, A. 2014. A juvenile *Edmontosaurus* from the late Maastrichtian (Cretaceous) of North America: implications for ontogeny and phylogenetic inference in saurolophine dinosaurs. Cretaceous Research 50:282-303.

Zheng, R., A. A. Farke, and G.-S. Kim. 2011. A photographic atlas of the pes from a hadrosaurine hadrosaurid dinosaur. PalArch's Journal of Vertebrate Paleontology 8:1-12.

CHAPTER SIX

CONCLUSIONS

This dissertation utilized the description of two new taxa that are stratigraphically intermediate between previously described species to illustrate how high-resolution stratigraphic correlation with consideration of ontogeny and taphonomic alteration can elucidate the evolutionary trends within hadrosaurine dinosaur lineages. The new genus of the tribe Brachylophosaurini reveals a hypothesized anagenetic lineage between *Acristavus gagslarsoni*, the new genus *Probrachylophosaurus bergei*, and *Brachylophosaurus canadensis*, with a directional evolutionary trend of increasing nasal crest size (posterior length and mediolateral width) in stratigraphically younger taxa; this trend is also observed ontogenetically in *Brachylophosaurus* individuals. The fourth member of Brachylophosaurini, *Maiasaura peeblesorum*, represents a cladogenic split from this lineage at an unknown point in time. The new species of *Gryposaurus*, *G. reddingi*, is described from a monodominant bonebed containing at least ten individuals of three size classes: juvenile, subadult, and adult. The bonebed is hypothesized to represent a mass death assemblage that was deposited along a lake margin and fed upon by tyrannosaurs. *Gryposaurus reddingi* is stratigraphically and morphologically intermediate between previously described species, forming a hypothesized anagenetic lineage between *G. latidens*, *G. reddingi*, *G. notabilis*, and *G. monumentensis*, with a directional evolutionary trend of increasing nasal crest height and more posterior position relative to the narial fenestra in stratigraphically younger species; this trend is also

observed ontogenetically in juvenile and subadult specimens of all four species. Finally, the postcranial material is thoroughly illustrated, with labeled anatomical features, in a photographic atlas intended to assist future researchers in the identification of hadrosaur postcranial specimens. This dissertation analyzed these hadrosaurine taxa using the "Unified Frames of Reference" of geography, taphohistory, stratigraphy, phylogeny, and ontogeny (Horner et al., 2011) to account for the multiple sources of morphologic variation among specimens. By understanding the ontogenetic changes within species, and the degrees of taphonomic alteration of different specimens, the underlying evolutionary trends within these dinosaur lineages are revealed.

Literature Cited

Horner, J. R., M. B. Goodwin, and N. Myhrvold. 2011. Dinosaur census reveals abundant *Tyrannosaurus* and rare ontogenetic stages in the Upper Cretaceous Hell Creek Formation (Maastrichtian), Montana, USA. PLoS ONE 6:1-9. e16574.

REFERENCES CITED

Adams, D. C., and E. Otárola-Castillo. 2013. geomorph: an R package for the collection and analysis of geometric morphometric shape data. Methods in Ecology and Evolution 4:393-399.

Bader, K. S., S. T. Hasiotis, and L. D. Martin. 2009. Application of forensic science techniques to trace fossils on dinosaur bones from a quarry in the Upper Jurassic Morrison Formation, northeastern Wyoming. Palaios 24:140-158.

Behrensmeyer, A. K. 1975. The taphonomy and paleoecology of Plio-Pleistocene vertebrate assemblages east of Lake Rudolf, Kenya. Bulletin Museum of Comparative Zoology 146:473-578.

Behrensmeyer, A. K. 1978. Taphonomic and ecological information from bone weathering. Paleobiology 4:150-162.

Bell, P. R. 2011a. Cranial osteology and ontogeny of *Saurolophus angustirostris* from the Late Cretaceous of Mongolia with comments on *Saurolophus osborni* from Canada. Acta Palaeontologica Polonica 56:703-722.

Bell, P. R. 2011b. Redescription of the skull of *Saurolophus osborni* Brown 1912 (Ornithischia: Hadrosauridae). Cretaceous Research 32:30-44.

Bell, P. R., and N. E. Campione. 2014. Taphonomy of the Danek Bonebed: a monodominant *Edmontosaurus* (Hadrosauridae) bonebed from the Horseshoe Canyon Formation, Alberta. Canadian Journal of Earth Sciences 51:992-1006.

Boaz, N. T., and A. K. Behrensmeyer. 1976. Hominid taphonomy: transport of human skeletal parts in an artificial fluviatile environment. American Journal of Physical Anthropology 45:53-60.

Brinkman, D. B. 2014. The size-frequency distribution of hadrosaurs from the Dinosaur Park Formation of Alberta, Canada; pp. 416-421 in D. A. Eberth and D. C. Evans (eds.), Hadrosaurs. Indiana University Press, Bloomington, Indiana.

Brinkman, D. B., A. P. Russell, D. A. Eberth, and J. Peng. 2004. Vertebrate palaeocommunities of the lower Judith River Group (Campanian) of southeastern Alberta, Canada, as interpreted from vertebrate microfossil assemblages. Palaeogeography, Palaeoclimatology, Palaeoecology 213:295-313.

Brown, B. 1910. The Cretaceous Ojo Alamo beds of New Mexico with description of the new genus *Kritosaurus*. Bulletin of the American Museum of Natural History 28:267-274.

Campione, N. E. 2014. Postcranial anatomy of *Edmontosaurus regalis* (Hadrosauridae) from the Horseshoe Canyon Formation, Alberta, Canada; pp. 208-244 in D. A. Eberth and D. C. Evans (eds.), Hadrosaurs. Indiana University Press, Bloomington, Indiana.

Campione, N. E., and D. C. Evans. 2011. Cranial growth and variation in edmontosaurs (Dinosauria: Hadrosauridae): implications for latest Cretaceous megaherbivore diversity in North America. PLoS ONE 6:e25186.

Campione, N. E., K. S. Brink, E. A. Freedman, C. T. McGarrity, and D. C. Evans. 2012. '*Glishades ericksoni*', an indeterminate juvenile hadrosaurid from the Two Medicine Formation of Montana: implications for hadrosauroid diversity in the latest Cretaceous (Campanian-Maastrichtian) of western North America. Palaeobiodiversity and Palaeoenvironments August 24:1-11.

Castanet, J., K. Curry Rogers, J. Cubo, and J.-J. Boisard. 2000. Periosteal bone growth rates in extant ratites (ostriche and emu). Implications for assessing growth in dinosaurs. Comptes Rendus de l'Academie des Sciences Serie III Sciences de la Vie 323:543-550.

Chinsamy, A., D. B. Thomas, A. R. Tumarkin-Deratzian, and A. R. Fiorillo. 2012. Hadrosaurs were perennial polar residents. The Anatomical Record 295:610-614.

Craig, G. Y., and G. Oertel. 1966. Deterministic models of living and fossil populations of animals. Quarterly Journal of the Geological Society of London 122:315-355.

Currie, P. J., and D. A. Russell. 2005. The geographic and stratigraphic distribution of articulated and associated dinosaur remains; pp. 537-569 in P. J. Currie and E. B. Koppelhus (eds.), Dinosaur Provincial Park: A Spectacular Ancient Ecosystem Revealed. Indiana University Press, Bloomington, Indiana.

Cuthbertson, R. S., and R. B. Holmes. 2010. The first complete description of the holotype of *Brachylophosaurus canadensis* Sternberg, 1953 (Dinosauria: Hadrosauridae) with comments on intraspecific variation. Zoological Journal of the Linnean Society 159:373-397.

Dilkes, D. W. 1993. Growth and locomotion in the hadrosaurian dinosaur *Maiasaura peeblesorum* from the Upper Cretaceous of Montana. PhD dissertation, Department of Zoology, University of Toronto, 447 pp.

Dilkes, D. W. 2000. Appendicular myology of the hadrosaurian dinosaur *Maiasaura peeblesorum* from the Late Cretaceous (Campanian) of Montana. Transactions of the Royal Society of Edinburgh-Earth Sciences 90:87-125.

Dodson, P. 1975. Taxonomic implications of relative growth in lambeosaurine hadrosaurs. Systematic Zoology 24:37-54.

Eberth, D. A. 2005. The Geology; pp. 54-82 in P. J. Currie and E. B. Koppelhus (eds.), Dinosaur Provincial Park: A Spectacular Ancient Ecosystem Revealed. Indiana University Press, Bloomington, Indiana.

Eberth, D. A., and A. P. Hamblin. 1993. Tectonic, stratigraphic, and sedimentologic significance of a regional discontinuity in the upper Judith River Group (Belly River wedge) of southern Alberta, Saskatchewan, and northern Montana. Canadian Journal of Earth Sciences 30:174-200.

Eberth, D. A., and M. A. Getty. 2005. Ceratopsian bonebeds: occurrence, origins, and significance; pp. 501-536 in P. J. Currie and E. B. Koppelhus (eds.), Dinosaur Provincial Park: A Spectacular Ancient Ecosystem Revealed. Indiana University Press, Bloomington, Indiana.

Eberth, D. A., and D. C. Evans. 2011: Geology and Paleontology of Dinosaur Provincial Park, Alberta Field Trip Guidebook. International Hadrosaur Symposium, Drumheller, Alberta, 2011.

Eberth, D. A., R. R. Rogers, and A. R. Fiorillo. 2007. A practical approach to the study of bonebeds; pp. 265-331 in R. R. Rogers, D. A. Eberth, and A. R. Fiorillo (eds.), Bonebeds: Genesis, analysis, and paleobiological significance. The University of Chicago Press, Chicago, Illinois.

Evans, D. C. 2010. Cranial anatomy and systematics of *Hypacrosaurus altispinus*, and a comparative analysis of skull growth in lambeosaurine hadrosaurids (Dinosauria: Ornithischia). Zoological Journal of the Linnean Society 159:398-434.

Evans, D. C., and R. R. Reisz. 2007. Anatomy and relationships of *Lambeosaurus magnicristatus*, a crested hadrosaurid dinosaur (Ornithischia) from the Dinosaur Park Formation, Alberta. Journal of Vertebrate Paleontology 27:373-393.

Farke, A. A., and L. Herrero. 2015. Variation in the skull roof of the hadrosaur *Gryposaurus* illustrated by a new specimen from the Kaiparowits Formation (late Campanian) of southern Utah; pp. 191-199 in D. A. Eberth and D. C. Evans (eds.), Hadrosaurs. Indiana University Press, Bloomington, Indiana.

Fassett, J. E., and M. B. Steiner. 1997. Precise age of C33N-C32R magnetic-polarity reversal, San Juan Basin, New Mexico and Colorado. New Mexico Geological Society Guidebook 48:239-247.

Fiorillo, A. R. 1988. Taphonomy of Hazard Homestead Quarry (Ogallala Group), Hitchcock County, Nebraska. Contributions to Geology, University of Wyoming 26:57-97.

Fiorillo, A. R. 1991a. Taphonomy and depositional setting of Careless Creek Quarry (Judith River Formation), Wheatland County, Montana, U.S.A. Palaeogeography, Palaeoclimatology, Palaeoecology 81:281-311.

Fiorillo, A. R. 1991b. Prey bone utilization by predatory dinosaurs. Palaeogeography, Palaeoclimatology, Palaeoecology 88:157-166.

Fowler, D. W. 2000. Vertebrate taphonomy of the plant debris beds from the Isle of Wight, UK: palaeoenvironmental and palaeoecological implications. Unpublished M.S. thesis, Department of Earth Sciences, University of Bristol, Bristol, UK, 117 pp.

Frampton, E. K. 2006. Taphonomy and paleoecology of mixed invertebrate-vertebrate fossil assemblage in the Foremost Formation (Cretaceous, Campanian), Milk River Valley, Alberta. Interdisciplinary Graduate Program, University of Calgary, Calgary, Alberta, 294 pp.

Freedman Fowler, E. A. Chapter Three. Taphonomy of a Gryposaurus hadrosaur bonebed from the Judith River Formation (Campanian) of northcentral Montana.

Freedman Fowler, E. A., and J. R. Horner. Chapter Four. A new species of *Gryposaurus* (Dinosauria: Ornithischia) from the Judith River Formation of northcentral Montana.

Freedman Fowler, E. A., and J. R. Horner. Chapter Two. A new brachylophosaurinin (Dinosauria: Ornithischia) from the Judith River Formation of northcentral Montana.

Gallagher, W. B., P. J. Sugarman, and M. D. Feigenson. 1996. Strontium isotope age estimates for east coast dinosaur sites. Journal of Vertebrate Paleontology 16:36A.

Gangloff, R. A., and A. R. Fiorillo. 2010. Taphonomy and paleoecology of a bonebed from the Prince Creek Formation, North Slope, Alaska. Palaios 25:299-317.

Gates, T. A., and S. D. Sampson. 2007. A new species of *Gryposaurus* (Dinosauria: Hadrosauridae) from the late Campanian Kaiparowits Formation, southern Utah, USA. Zoological Journal of the Linnean Society 151:351-376.

Gates, T. A., and R. D. Scheetz. 2014. A new saurolophine hadrosaurid (Dinosauria: Ornithopoda) from the Campanian of Utah, North America. Journal of Systematic Palaeontology:1-15. http://dx.doi.org/10.1080/14772019.2014.950614.

Gates, T. A., J. R. Horner, R. R. Hanna, and R. C. Nelson. 2011. New unadorned hadrosaurine hadrosaurid (Dinosauria, Ornithopoda) from the Campanian of North America. Journal of Vertebrate Paleontology 31:798-811.

Gates, T. A., E. K. Lund, C. A. Boyd, D. D. DeBlieux, A. L. Titus, D. C. Evans, M. A. Getty, J. I. Kirkland, and J. G. Eaton. 2013. Ornithopod dinosaurs from the Grand Staircase-Escalante National Monument region, Utah, and their role in paleobiogeographic and macroevolutionary studies; pp. 463-481 in A. L. Titus and M. A. Loewen (eds.), At the Top of the Grand Staircase: the Late Cretaceous of Southern Utah. Indiana University Press, Bloomington, Indiana.

Goodwin, M. B., and A. L. Deino. 1989. The first radiometric ages from the Judith River Formation (Upper Cretaceous), Hill County, Montana. Canadian Journal of Earth Sciences 26:1384-1391.

Haeckel, E. 1866a. Generelle morphologie der organismen. Allgemeine grundzüge der organischen formen-wissenschaft, mechanisch begründet durch die von Charles Darwin reformirte descendenz-theorie. Georg Reimer, Berlin.

Haeckel, E. 1866b. Generelle morphologie der organismen. Allgemeine grundzüge der organischen formen-wissenschaft, mechanisch begründet durch die von Charles Darwin reformirte descendenz-theorie. Georg Reimer, Berlin, 462 pp.

Haeckel, E. 1901. The Riddle of the Universe at the Close of the Nineteenth Century. Harper & Brothers, New York, 391 pp.

Horner, J. R. 1983. Cranial osteology and morphology of the type specimen of *Maiasaura peeblesorum* (Ornithischia: Hadrosauridae), with discussion of its phylogenetic position. Journal of Vertebrate Paleontology 3:29-38.

Horner, J. R. 1984: Three ecologically distinct vertebrate faunal communities from the Late Cretaceous Two Medicine Formation of Montana, with discussion of evolutionary pressures induced by interior seaway fluctuations. Montana Geological Society Field Conference and Symposium, Northwest Montana and Adjacent Canada, 1984.

Horner, J. R. 1988. A new hadrosaur (Reptilia, Ornithischia) from the Upper Cretaceous Judith River Formation of Montana. Journal of Vertebrate Paleontology 8:314-321.

Horner, J. R. 1989. The ontogenetic predictability of hadrosaur crania. Journal of Vertebrate Paleontology 9:25A.

Horner, J. R. 1992. Cranial morphology of *Prosaurolophus* (Ornithischia: Hadrosauridae) with descriptions of two new hadrosaurid species and an evaluation of hadrosaurid phylogenetic relationships. Museum of the Rockies Occasional Paper 2:1-119.

Horner, J. R., and R. Makela. 1979. Nest of juveniles provides evidence of family structure among dinosaurs. Nature 282:296-298.

Horner, J. R., and P. J. Currie. 1994. Embryonic and neonatal morphology and ontogeny of a new species of *Hypacrosaurus* (Ornithischia, Lambeosauridae) from Montana and Alberta. Dinosaur Eggs and Babies:312-336.

Horner, J. R., and M. B. Goodwin. 2006. Major cranial changes during *Triceratops* ontogeny. Proceedings of the Royal Society B 273:2757-2761.

Horner, J. R., and M. B. Goodwin. 2009. Extreme cranial ontogeny in the Upper Cretaceous dinosaur *Pachycephalosaurus*. PLoS ONE 4:e7626 p. 1-11. doi:10.1371/journal.pone.0007626.

Horner, J. R., D. J. Varricchio, and M. B. Goodwin. 1992. Marine transgressions and the evolution of Cretaceous dinosaurs. Nature 358:59-61.

Horner, J. R., A. de Ricqlès, and K. Padian. 1999. Variation in dinosaur skeletochronology indicators: implications for age assessment and physiology. Paleobiology 25:295-304.

Horner, J. R., A. de Ricqlès, and K. Padian. 2000. Long bone histology of the hadrosaurid dinosaur *Maiasaura peeblesorum*: growth dynamics and physiology based on an ontogenetic series of skeletal elements. Journal of Vertebrate Paleontology 20:115-129.

Horner, J. R., D. B. Weishampel, and C. A. Forster. 2004. Hadrosauridae; pp. 438-463 in D. B. Weishampel, P. Dodson, and H. Osmólska (eds.), The Dinosauria. University of California Press, Berkeley.

Horner, J. R., M. B. Goodwin, and N. Myhrvold. 2011. Dinosaur census reveals abundant *Tyrannosaurus* and rare ontogenetic stages in the Upper Cretaceous Hell Creek Formation (Maastrichtian), Montana, USA. PLoS ONE 6:1-9. e16574.

Horner, J. R., J. G. Schmitt, F. D. Jackson, and R. R. Hanna. 2001. Bones and rocks of the Upper Cretaceous Two Medicine-Judith River clastic wedge complex,

Montana. Guidebook for the Field Trips, Society of Vertebrate Paleontology 61st Annual Meeting, Museum of the Rockies Occasional Paper 3:1-13.

Horner, J. R., A. de Ricqlès, K. Padian, and R. D. Scheetz. 2009. Comparative long bone histology and growth of the "hypsilophodontid" dinosaurs *Orodromeus makelai*, *Dryosaurus altus*, and *Tenontosaurus tillettii* (Ornithischia: Euornithopoda). Journal of Vertebrate Paleontology 29:734-747.

Hübner, T. R. 2012. Bone Histology in *Dysalotosaurus lettowvorbecki* (Ornithischia: Iguanodontia) - Variation, Growth, and Implications. PLoS ONE 7:e29958.

Hunt, A. P., and S. G. Lucas. 1993. Cretaceous vertebrates of New Mexico. Bulletin - New Mexico Museum of Natural History and Science 2:77-91.

Huttenlocker, A. K., H. N. Woodward, and B. K. Hall. 2013. The biology of bone; pp. 13-34 in K. Padian and E.-T. Lamm (eds.), Bone Histology of Fossil Tetrapods: Advancing Methods, Analysis, and Interpretation. University of California Press, Berkeley, California.

Hutton, J. M. 1986. Age determination of living Nile crocodiles from the cortical stratification of bone. Copeia 1986:332-341.

Jinnah, Z. A. 2013. Tectonic and sedimentary controls, age, and correlation of the Upper Cretaceous Wahweap Formation, Southern Utah; pp. 57-73 in A. L. Titus and M. A. Loewen (eds.), At the Top of the Grand Staircase: the Late Cretaceous of Southern Utah. Indiana University Press, Bloomington, Indiana.

Jinnah, Z. A., E. M. Roberts, A. L. Deino, J. S. Larsen, P. K. Link, and C. M. Fanning. 2009. New 40Ar-39Ar and detrital zircon U-Pb ages for the Upper Cretaceous Wahweap and Kaiparowits formations on the Kaiparowits Plateau, Utah: implications for regional correlation, provenance, and biostratigraphy. Cretaceous Research 30:287-299.

Johnston, P. A., and A. J. W. Hendy. 2005. Paleoecology of mollusks from the Upper Cretaceous Belly River Group; pp. 139-166 in P. J. Currie and E. B. Koppelhus (eds.), Dinosaur Provincial Park: A Spectacular Ancient Ecosystem Revealed. Indiana University Press, Bloomington, Indiana.

Kirkland, J. I., J. G. Eaton, and D. B. Brinkman. 2013. Elasmobranchs from Upper Cretaceous freshwater facies in Southern Utah; pp. 153-194 in A. L. Titus and M. A. Loewen (eds.), At the Top of the Grand Staircase: the Late Cretaceous of southern Utah. Indiana University Press, Bloomington, Indiana.

Köhler, M., N. Marin-Moratalla, X. Jordana, and R. Aanes. 2012. Seasonal bone growth and physiology in endotherms shed light on dinosaur physiology. Nature 487:358-361.

Lambe, L. M. 1914. On *Gryposaurus notabilis*, a new genus and species of trachodont dinosaur from the Belly River Formation of Alberta, with a description of the skull of *Chasmosaurus belli*. The Ottawa Naturalist 27:145-155.

Lamm, E.-T. 2013. Preparation and sectioning of specimens; pp. 55-160 in K. Padian and E.-T. Lamm (eds.), Bone Histology of Fossil Tetrapods. University of California Press, Berkeley.

Langston, W., Jr. 1960. The vertebrate fauna of the Selma Formation of Alabama, part VI: the dinosaurs. Fieldiana: Geology Memoirs 3:314-363.

Lapparent, A. F., and R. Lavocat. 1955. Dinosauriens; pp. 785-962 in J. Piveteau (ed.), Traité de Paléontologie, Tome 5. Masson et Cie, Paris.

LaRock, J. W. 2001. Sedimentology and taphonomy of a dinosaur bonebed from the Upper Cretaceous (Campanian) Judith River Formation of north central Montana. unpublished M.S. thesis, Department of Earth Sciences, Montana State University, Bozeman, 61 pp.

Leiggi, P., C. R. Schaff, and P. May. 1994. Macrovertebrate collecting; pp. 59-77 in P. Leiggi and P. May (eds.), Vertebrate Paleontological Techniques. Cambridge University Press, Cambridge, UK.

Lockley, M. G., and K. Conrad. 1989. The paleoenvironmental context, preservation and paleoecological significance of dinosaur tracksites in the western USA; pp. 121-134 in D. D. Gillette and M. G. Lockley (eds.), Dinosaur Tracks and Traces. Cambridge University Press, Cambridge.

Mateus, O., and R. Araújo. 2008. Stone-splitters and expansive demolition agents in vertebrate paleontological excavations. Journal of Paleontological Techniques 3:1-6.

McGarrity, C. T., N. E. Campione, and D. C. Evans. 2013. Cranial anatomy and variation in *Prosaurolophus maximus* (Dinosauria: Hadrosauridae). Zoological Journal of the Linnean Society 167:531-568.

Moran, K., H. L. Hilbert-Wolf, K. Golder, H. F. Malenda, C. J. Smith, L. P. Storm, E. L. Simpson, M. C. Wizevich, and S. E. Tindall. 2010. Attributes of the wood-boring trace fossil *Asthenopodichnium* in the Late Cretaceous Wahweap Formation, Utah, USA. Palaeogeography, Palaeoclimatology, Palaeoecology 297:662-669.

Padian, K., and J. R. Horner. 2011. The evolution of 'bizzare structures' in dinosaurs: biomechanics, sexual selection, social selection, or species recognition? Journal of Zoology 283:3-17.

Parks, W. A. 1919. Preliminary description of a new species of trachodont dinosaur of the genus *Kritosaurus*, *Kritosaurus incurvimanus*. Transactions of the Royal Society of Canada 3:51-59.

Parks, W. A. 1920. The osteology of the trachodont dinosaur *Kritosaurus incurvimanus*. University of Toronto Studies, Geological Series 11:1-76.

Peng, J.-H., A. P. Russell, and D. B. Brinkman. 2001. Vertebrate microsite assemblages (exclusive of mammals) from the Foremost and Oldman Formations of the Judith River Group (Campanian) of Southeastern Alberta: an illustrated guide. Provincial Museum of Alberta Natural History Occasional Paper 25:1-54.

Pinna, G. 1979. Osteologia dello scheletro di *Kritosaurus notabilis* (Lambe, 1914) del Museo Civico di Storia Naturale di Milano. Memorie della Società Italiana di Scienze Naturali e del Museo Civico di Storia Naturalle di Milano 22:33-56.

Prieto-Márquez, A. 2005. New information on the cranium of *Brachylophosaurus canadensis* (Dinosauria, Hadrosauridae), with a revision of its phylogenetic position. Journal of Vertebrate Paleontology 25:144-156.

Prieto-Márquez, A. 2007. Postcranial Osteology of the Hadrosaurid Dinosaur *Brachylophosaurus canadensis* from the Late Cretaceous of Montana; pp. 91-115 in K. Carpenter (ed.), Horns and Beaks: Ceratopsian and Ornithopod Dinosaurs. Indiana Press, Bloomington, IN.

Prieto-Márquez, A. 2010a. The braincase and skull roof of *Gryposaurus notabilis* (Dinosauria, Hadrosauridae), with a taxonomic revision of the genus. Journal of Vertebrate Paleontology 30:838-854.

Prieto-Márquez, A. 2010b. Global phylogeny of Hadrosauridae (Dinosauria: Ornithopoda) using parsimony and Bayesian methods. Zoological Journal of the Linnean Society 159:435-502.

Prieto-Márquez, A. 2011. Cranial and appendicular ontogeny of *Bactrosaurus johnsoni*, a hadrosauroid dinosaur from the Late Cretaceous of northern China. Palaeontology 54:773-792.

Prieto-Márquez, A. 2012. The skull and appendicular skeleton of *Gryposaurus latidens*, a saurolophine hadrosaurid (Dinosauria: Ornithopoda) from the

early Campanian (Cretaceous) of Montana, USA. Canadian Journal of Earth Sciences 49:510-532.

Prieto-Márquez, A. 2014a. Skeletal morphology of *Kritosaurus navajovius* (Dinosauria: Hadrosauridae) from the Late Cretaceous of the North American south-west, with an evaluation of the phylogenetic systematics and biogeography of Kritosaurini. Journal of Systematic Palaeontology 12:133-175.

Prieto-Márquez, A. 2014b. A juvenile *Edmontosaurus* from the late Maastrichtian (Cretaceous) of North America: implications for ontogeny and phylogenetic inference in saurolophine dinosaurs. Cretaceous Research 50:282-303.

Prieto-Márquez, A., and G. C. Salinas. 2010. A re-evaluation of *Secernosaurus koerneri* and *Kritosaurus australis* (Dinosauria, Hadrosauridae) from the Late Cretaceous of Argentina. Journal of Vertebrate Paleontology 30:813-837.

R_Core_Team. 2014. R: A language and environment for statistical computing. R Foundation for Statistical Computing, Vienna, Austria. ISBN 3-900051-07-0, URL http://www.R-project.org/.

Rambaut, A. 2006-2012. FigTree. 1.4.0. Institute of Evolutionary Biology, University of Edinburgh, Edinburgh, http://tree.bio.ed.ac.uk/software/figtree/

Rasband, W. S. 1997-2014. ImageJ. U. S. National Institutes of Health, Bethesda, Maryland, USA, http://imagej.nih.gov/ij/,.

Renne, P. R., R. Mundil, G. Balco, K. Min, and K. Ludwig. 2010. Joint determination of 40K decay constants and 40Ar*/40K for the Fish Canyon sanidine standard, and improved accuracy for 40Ar/39Ar geochronology. Geochimica et Cosmochimica Acta 74:5349-5367.

Renne, P. R., C. C. Swisher, A. L. Deino, D. B. Karner, T. L. Owens, and D. J. DePaolo. 1998. Intercalibration of standards, absolute ages and uncertainties in 40Ar/39Ar dating. Chemical Geology 145:117-152.

Roberts, E. M., A. L. Deino, and M. A. Chan. 2005. 40Ar/39Ar age of the Kaiparowits Formation, southern Utah, and correlation of contemporaneous Campanian strata and vertebrate faunas along the margin of the Western Interior Basin. Cretaceous Research 26:307-318.

Roberts, E. M., S. D. Sampson, A. L. Deino, S. A. Bowring, and R. Buchwaldt. 2013. The Kaiparowits Formation: a remarkable record of Late Cretaceous terrestrial environments, ecosystems, and evolution in western North America; pp. 85-106 in A. L. Titus and M. A. Loewen (eds.), At the Top of the Grand Staircase:

the Late Cretaceous of Southern Utah. Indiana University Press, Bloomington, Indiana.

Rogers, R. R. 1990. Taphonomy of three dinosaur bone beds in the Upper Cretaceous Two Medicine Formation of northwestern Montana: evidence for drought-related mortality. Palaios 5:394-413.

Rogers, R. R., C. C. Swisher, and J. R. Horner. 1993. 40Ar/39Ar age and correlation of the nonmarine Two Medicine Formation (Upper Cretaceous), northwestern Montana, USA. Canadian Journal of Earth Sciences 30:1066-1075.

Rogers, R. R., D. A. Eberth, and A. R. Fiorillo. 2007. Preface; pp. vii-x in R. R. Rogers, D. A. Eberth, and A. R. Fiorillo (eds.), Bonebeds: Genesis, analysis, and paleobiological significance. The University of Chicago Press, Chicago, Illinois.

Rozhdestvensky, A. K. 1965. Growth changes in Asian dinosaurs and some problems of their taxonomy. Paleontologischeskii Zhurnal 3:95-109.

Ryan, M. J., and D. C. Evans. 2005. Ornithischian Dinosaurs. Dinosaur Provincial Park: A Spectacular Ancient Ecosystem Revealed:312-348.

Ryan, M. J., R. B. Holmes, and A. P. Russell. 2007. A revision of the late Campanian centrosaurine ceratopsid genus *Styracosaurus* from the Western Interior of North America. Journal of Vertebrate Paleontology 27:944-962.

Ryan, M. J., A. P. Russell, and S. Hartman. 2010. A new chasmosaurine ceratopsid from the Judith River Formation, Montana. New Perspectives on Horned Dinosaurs:181-188.

Ryan, M. J., A. P. Russell, D. A. Eberth, and P. J. Currie. 2001. The taphonomy of a *Centrosaurus* (Ornithischia: Ceratopsidae) bone bed from the Dinosaur Park Formation (Upper Campanian), Alberta, Canada, with comments on cranial ontogeny. Palaios 16:482-506.

Sampson, S. D., M. J. Ryan, and D. H. Tanke. 1997. Craniofacial ontogeny in centrosaurine dinosaurs (Ornithischia: Ceratopsidae): taxonomic and behavioral implications. Zoological Journal of the Linnean Society 121:293-337.

Scannella, J. B., and J. R. Horner. 2010. *Torosaurus* Marsh, 1891, is *Triceratops* Marsh, 1889 (Ceratopsidae: Chasmosaurinae): synonymy through ontogeny. Journal of Vertebrate Paleontology 30:1157-1168.

Scannella, J. B., D. W. Fowler, M. B. Goodwin, and J. R. Horner. 2014. Evolutionary trends in *Triceratops* from the Hell Creek Formation, Montana. Proceedings of the National Academy of Sciences 111:10245-10250.

Scherzer, B. A., and D. J. Varricchio. 2010. Taphonomy of a juvenile lambeosaurine bonebed from the Two Medicine Formation (Campanian) of Montana, United States. Palaios 25:780-795.

Schmitt, J. G., F. D. Jackson, and R. R. Hanna. 2014. Debris flow origin of an unusual Late Cretaceous hadrosaur bonebed in the Two Medicine Formation of western Montana; pp. 486-501 in D. A. Eberth and D. C. Evans (eds.), Hadrosaurs. Indiana University Press, Bloomington, Indiana.

Schott, R., D. C. Evans, M. B. Goodwin, C. M. Brown, and N. Longrich. 2010. Cranial ontogeny in *Stegoceras* and the evolution of cranial doming and ornamentation in Pachycephalosauria (Dinosauria: Ornithischia). Journal of Vertebrate Paleontology, SVP Program and Abstracts Book:159A.

Scott, E. E., M. J. Ryan, and D. C. Evans. 2014. A *Gryposaurus* bone bed from the Oldman Formation (Campanian) of south-eastern Alberta with implications for dinosaur sociality. Geological Society of America Abstracts with Programs 46:13.

Shipman, P. 1975. Implications of drought for vertebrate fossil assemblages. Nature 257:667-668.

Sternberg, C. M. 1953. A new hadrosaur from the Oldman Formation of Alberta: discussion of nomenclature. National Museum of Canada, Bulletin 128:275-286.

Sues, H.-D., and A. Averianov. 2009. A new basal hadrosauroid dinosaur from the Late Cretaceous of Uzbekistan and the early radiation of duck-billed dinosaurs. Proceedings of the Royal Society B 276:2549-2555.

Swofford, D. L. 2002. PAUP*. Phylogenetic analysis using parsimony (*and other methods). Version 4.0b10. Sinauer Associates, Sunderland, MA.

Tanke, D. H., and D. C. Evans. 2014. Relocating the lost *Gryposaurus incurvimanus* holotype quarry, Dinosaur Provincial Park, Alberta, Canada; pp. 385-395 in D. A. Eberth and D. C. Evans (eds.), Hadrosaurs. Indiana University Press, Bloomington, Indiana.

Thomas, R. G., D. A. Eberth, A. L. Deino, and D. Robinson. 1990. Composition, radioisotopic ages, and potential significance of an altered volcanic ash

(bentonite) from the Upper Cretaceous Judith River Formation, Dinosaur Provincial Park, southern Alberta, Canada. Cretaceous Research 11:125-162.

Trexler, D. L. 1995. A detailed description of newly-discovered remains of *Maiasaura peeblesorum* (Reptilia: Ornithischia) and a revised diagnosis of the genus. Unpublished MS thesis. Department of Biological Sciences, University of Calgary, Calgary, Alberta, 235 pp.

Tsuihiji, T., K. Watabe, K. Tsogtbaatar, T. Tsubamoto, R. Barsbold, S. Suzuki, A. H. Lee, R. C. Ridgely, Y. Kawahara, and L. M. Witmer. 2011. Cranial osteology of a juvenile specimen of *Tarbosaurus bataar* form the Nemegt Formation (Upper Cretaceous) of Bugin Tsav, Mongolia. Journal of Vertebrate Paleontology 31:497-517.

Van Itterbeeck, J., D. J. Horne, P. Bultynck, and N. Vandenberghe. 2005. Stratigraphy and palaeoenvironment of the dinosaur-bearing Upper Cretaceous Iren Dabasu Formation, Inner Mongolia, People's Republic of China. Cretaceous Research 26:699-725.

Varricchio, D. J. 1995. Taphonomy of Jack's Birthday Site, a diverse dinosaur bonebed from the Upper Cretaceous Two Medicine Formation of Montana. Palaeogeography, Palaeoclimatology, Palaeoecology 114:297-323.

Varricchio, D. J. 2011. A distinct dinosaur life history? Historical Biology 23:91-107.

Varricchio, D. J., and J. R. Horner. 1993. Hadrosaurid and lambeosaurid bonebeds from the Upper Cretaceous Two Medicine Formation of Montana: taphonomic and biologic implications. Canadian Journal of Earth Sciences 30:997-1006.

Varricchio, D. J., P. C. Sereno, Z. Xijin, T. Lin, J. A. Wilson, and G. H. Lyon. 2008. Mud-trapped herd captures evidence of distinctive dinosaur sociality. Acta Palaeontologica Polonica 53:567-578.

Varricchio, D. J., C. Koeberl, R. F. Raven, W. S. Wolbach, W. C. Elsik, and D. P. Miggins. 2010. Tracing the Manson impact event across the Western Interior Cretaceous Seaway. Geological Society of America Special Paper 465:269-299.

Vialli, V. 1960. Uno scheletro di dinosauro del Museo Civico di Storia Naturale di Milano (*Kritosaurus notabilis* (Lambe)): osservazioni preliminari. Atti della Società Italiana di Scienze Naturali e del Museo Civico di Storia Naturale in Milano 99:169-185.

Voorhies, M. R. 1969. Taphonomy and population dynamics of an early Pliocene vertebrate fauna, Knox County, Nebraska. Contributions to Geology Special Paper No. 1, University of Wyoming 1:1-69.

Wagner, J. R. 2001. The hadrosaurian dinosaurs (Ornithischia: Hadrosauria) of Big Bend National Park, Brewster County, Texas, with implications for Late Cretaceous Paleozoogeography. M.S. thesis, Texas Tech University, Lubbock, 417 pp.

Williamson, T. E. 2000. Review of Hadrosauridae (Dinosauria, Ornithischia) from the San Juan Basin, New Mexico. Bulletin - New Mexico Museum of Natural History and Science 17:191-213.

Woodward, H. N., E. A. Freedman Fowler, J. O. Farlow, and J. R. Horner. in press. *Maiasaura*, a model organism for extinct vertebrate population biology: a statistically robust assessment of growth dynamics and survivorship. Paleobiology.

Xing, H., A. Prieto-Márquez, W. Gu, and T.-X. Yu. 2012. Re-evaluation and phylogenetic analysis of *Wulagasaurus dongi*, a hadrosaurine dinosaur from the Maastrichtian of northeast China. Vertebrata PalAsiatica 50:160-169.

Zheng, R., A. A. Farke, and G.-S. Kim. 2011. A photographic atlas of the pes from a hadrosaurine hadrosaurid dinosaur. PalArch's Journal of Vertebrate Paleontology 8:1-12.

APPENDICES

APPENDIX A

RAY TEETH IDENTIFICATION

The ray teeth from Kennedy Coulee have a transverse crest on the occlusal surface of the crown that varies from barely present to strongly developed; in unworn teeth the crest is very well developed, with crenulations on the higher (lingual) half of the crown (Figure S2E). The sides of the crowns are straight and lack crenulations (Figure S2F, S2H, S2J). In the small hexagonal teeth, some roots are subequal in height to their crowns, while other roots are longer than their crowns; roots of the larger hexagonal teeth are distinctly longer than their crowns. The roots taper noticeably toward their tips. The nutritive groove of the root varies from arch shaped to keyhole shaped in side view. They cannot be *Myledaphus bipartitus* (sensu Kirkland et al., 2013) because the crenulations on the crowns of the Kennedy Coulee teeth do not cross the transverse crest, and do not have crenulated sides of the crowns.

Cristomylus cifellii and *Pseudomyledaphus madseni* teeth are both similar to the Kennedy Coulee teeth in having roots with tapering ends, and some teeth do have crenulations on the lingual side of the transverse crest of the crown (Kirkland et al., 2013). However, many *C. cifellii* small hexagonal teeth differ in the crowns being more oval shaped, with generally poorly defined sides of the crowns, whereas Kennedy Coulee small hexagonal teeth have well defined flat vertical sides of the crowns, similar to *P. madseni*. The midpoint of the root is wider in *C. cifellii* than in *P. madseni*; this character in the Kennedy Coulee teeth is more similar to that of *P. madseni*. Thus, the Kennedy Coulee teeth are more similar to *Pseudomyledaphus madseni* than to *Cristomylus cifellii*.

Kirkland et al. (2013) identified the "*Myledaphus* sp." teeth from the Foremost Formation of Alberta (Frampton, 2006; Peng et al., 2001) as being most similar to

Pseudomyledaphus madseni; these Foremost Formation teeth may represent a distinct species, so Kirkland et al. (2013) referred them to *Pseudomyledaphus* sp. Because the Kennedy Coulee teeth are not perfectly consistent with *P. madseni*, but are morphologically consistent with the "*Myledaphus* sp." teeth of the Foremost and lower Oldman formations of Alberta (Brinkman et al., 2004; Peng et al., 2001), they are here referred to *Pseudomyledaphus* sp. as well, supporting the stratigraphic assignment of Kennedy Coulee to the upper Foremost Formation and lower Oldman Formation.

Two ray teeth were found in the MOR 1071 (locality JR-224) *Brachylophosaurus canadensis* bonebed in the Comrey Sandstone Zone of Malta, Montana (Figure S2A-S2D). These large hexagonal teeth have well-worn occlusal surfaces of the crowns with the faint remains of a transverse ridge and possibly very faint crenulations. Crenulations are present on all sides of the crown. The roots are longer than the crowns, and the nutrient grooves of the roots are keyhole shaped. These teeth are referable to the emended diagnosis of *Myledaphus bipartitus* by Kirkland et al. (2013). In Alberta, *Myledaphus bipartitus* is only found in the Comrey Sandstone Zone and higher units (Brinkman et al., 2004). The presence of these two stratigraphically separated ray taxa in Kennedy Coulee and Malta supports their stratigraphic assignments to Unit 1 and Unit 2 (Comrey Sandstone Zone), respectively, of the Oldman Formation.

Literature Cited

Brinkman, D.B., Russell, A.P., Eberth, D.A. and Peng, J., 2004. Vertebrate palaeocommunities of the lower Judith River Group (Campanian) of southeastern Alberta, Canada, as interpreted from vertebrate microfossil assemblages. Palaeogeography, Palaeoclimatology, Palaeoecology, 213(3-4): 295-313.

Frampton, E.K., 2006. Taphonomy and paleoecology of mixed invertebrate-vertebrate fossil assemblage in the Foremost Formation (Cretaceous, Campanian), Milk River Valley, Alberta, University of Calgary, Calgary, Alberta, 294 pp.

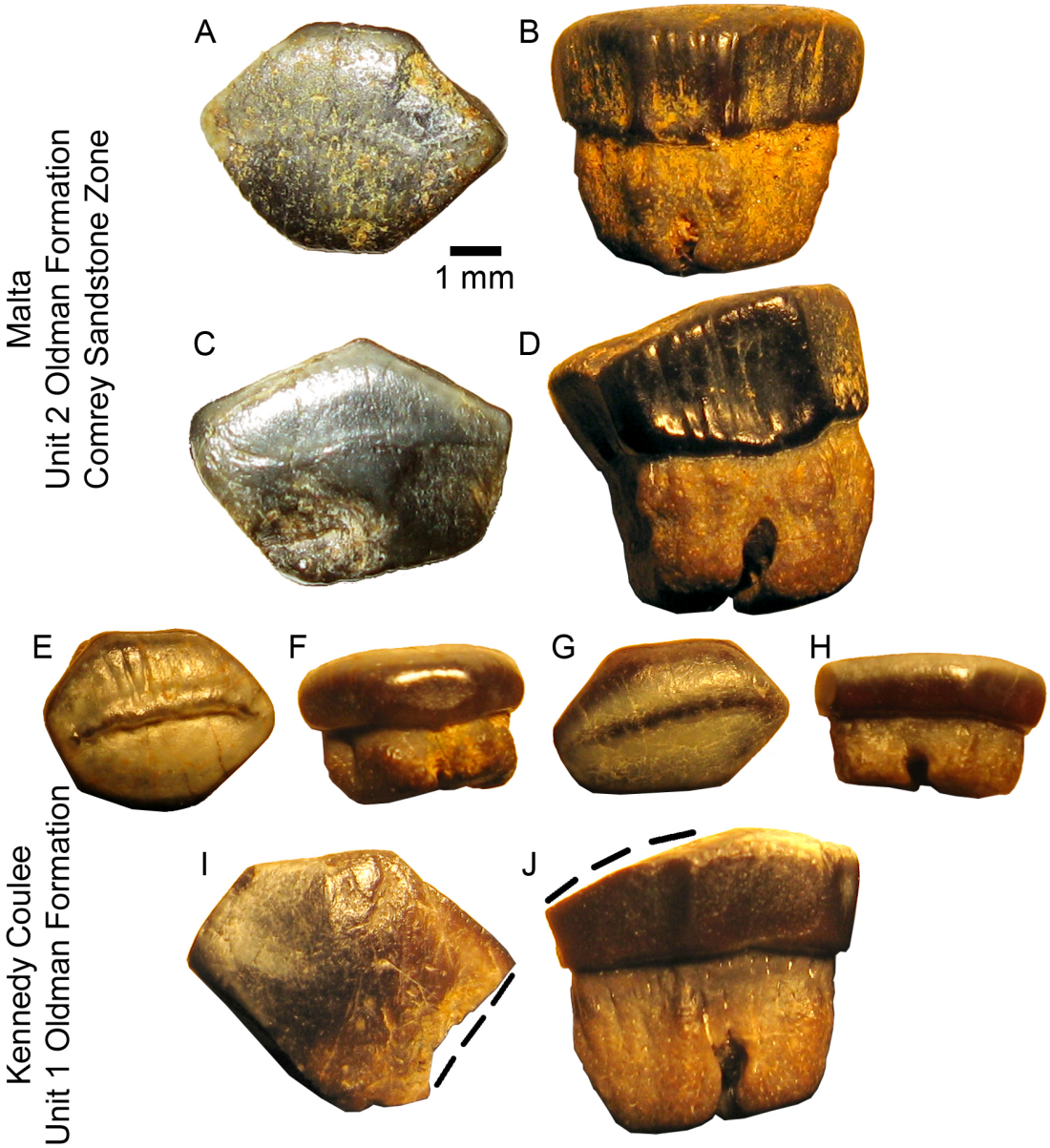
Kirkland, J.I., Eaton, J.G. and Brinkman, D.B., 2013. Elasmobranchs from Upper Cretaceous freshwater facies in Southern Utah. In: A.L. Titus and M.A. Loewen (Editors), At the Top of the Grand Staircase: the Late Cretaceous of southern Utah. Indiana University Press, Bloomington, Indiana, pp. 153-194.

Peng, J.-H., Russell, A.P. and Brinkman, D.B., 2001. Vertebrate microsite assemblages (exclusive of mammals) from the Foremost and Oldman Formations of the Judith River Group (Campanian) of Southeastern Alberta: an illustrated guide. Provincial Museum of Alberta Natural History Occasional Paper, 25: 1-54.

Prieto-Márquez, A., 2010. Global phylogeny of Hadrosauridae (Dinosauria: Ornithopoda) using parsimony and Bayesian methods. Zoological Journal of the Linnean Society, 159: 435-502.

APPENDIX B

RAY TEETH FROM OLDMAN FORMATION EQUIVALENT LOCALITIES IN THE JUDITH RIVER FORMATION OF MONTANA



Appendix B Figure. Ray teeth from Oldman Formation equivalent localities in the Judith River Formation of Montana. Upper half of figure (A-D): two *Myledaphus bipartitus* teeth in occlusal view (A, C) and side view (B, D) with worn occlusal surface of the crowns from the MOR 1071 (JR-224) *Brachylophosaurus canadensis* bonebed in Malta, Montana, at a horizon equivalent to Unit 2 (Comrey Sandstone Zone) of the Oldman Formation. Lower half of figure (E-J): three teeth tentatively attributed to *Pseudomyledaphus* sp. from the upper muddy zone of Kennedy Coulee, Montana, equivalent to Unit 1 of the Oldman Formation. (E-F) tooth with unworn occlusal surface of crown; (G-H) tooth with worn occlusal surface of crown; (I-J) tooth with extremely worn occlusal surface of crown. Dashed lines indicate partially broken crown.

APPENDIX C

CHARACTER MATRIX BASED ON PRIETO-MÁRQUEZ (2010) WITH ALL CHARACTERS INCLUDED, IN NEXUS FORMAT

#NEXUS

[Freedman Fowler and Horner, 2015, Appendix C]
[Formatted for PAUP 4.0b10 for MAC OS X]

[Matrix is modified from nexus file of Prieto-Márquez 2010 with character states for Probrachylophosaurus bergei added, as well as eight recodings for Acristavus (characters 106, 116-121, 259) and one for Brachylophosaurus (character 138). See main text for details.]
[Most hadrosauroid and lamebeosaurine taxa are excluded from Prieto-Márquez's 2010 matrix in order to simplify analysis and make taxon list more consistent with that of Gates et al. 2011.]

[Prieto-Márquez, A. 2010. Global phylogeny of Hadrosauridae (Dinosauria: Ornithopoda) using parsimony and Bayesian methods. Zoological Journal of the Linnean Society, 159:435-502.]

```
BEGIN TAXA;
	DIMENSIONS  NTAX=19;
	TAXLABELS
	Iguanodon_bernissartensis
	Hadrosaurus_foulkii
	Bactrosaurus_johnsoni
	Wulagasaurus_dongi
	Brachylophosaurus_canadensis
	Probrachylophosaurus_bergei
	Maiasaura_peeblesorum
	Acristavus_gagslarsoni
	Corythosaurus_casuarius
	Edmontosaurus_annectens
	Edmontosaurus_regalis
	Kritosaurus_navajovius
	Gryposaurus_notabilis
	Gryposaurus_latidens
	Gryposaurus_monumentensis
	Prosaurolophus_maximus
	Secernosaurus_koerneri
	Saurolophus_osborni
	Saurolophus_angustirostris;
END;

BEGIN CHARACTERS;
	DIMENSIONS  NCHAR=370;
```

```
        FORMAT SYMBOLS= " 0 1 2 3 4 5 6 7" MISSING=? GAP=- ;
        CHARSTATELABELS
                1 dtth1, 2 dtth3, 3 dtth4, 4 dtth5, 5 dtth6, 6 dtth7,
7 dtth8, 8 dtth9, 9 dtth10, 10 dtth11, 11 dtth12,
12 dtth13, 13 dtth14, 14 dtth15, 15 mxth1, 16 mxth3,
17 mxth4, 18 mxth5, 19 mxth6, 20 mxth7, 21 mxth8,
22 pdt1, 23 pdt2, 24 pdt3, 25 pdt4, 26 pdt5,
27 pdt6, 28 pdt7, 29 pdt8, 30 pdt9, 31 pdt11,
32 pdt13, 33 dt1, 34 dt2, 35 dt3, 36 dt4,
37 dt5, 38 dt6, 39 dt7, 40 dt9, 41 dt10,
42 dt11, 43 dt12, 44 dt13, 45 dt14, 46 dt15,
47 dt16, 48 dt17, 49 dt18, 50 dt19, 51 sa1,
52 sa2, 53 sa3, 54 sa4, 55 sa5, 56 sa6,
57 ang, 58 cob, 59 prar, 60 pmx1, 61 pmx2,
62 pmx3, 63 pmx5, 64 pmx6, 65 pmx7, 66 pmx8,
67 pmx9, 68 pmx10, 69 pmx11, 70 pmx12, 71 pmx13,
72 pmx14, 73 pmx15, 74 pmx16, 75 ns1, 76 ns2,
77 ns3, 78 ns4, 79 ns5, 80 ns6, 81 ns7,
82 ns8, 83 ns9, 84 mx1, 85 mx2, 86 mx3,
87 mx4, 88 mx5, 89 mx6, 90 mx7, 91 mx8,
92 mx9, 93 mx10, 94 mx11, 95 mx12, 96 mx13,
97 mx14, 98 mx15, 99 mx16, 100 mx17, 101 lc1,
102 lc2, 103 j1, 104 j2, 105 j3, 106 j4,
107 j5, 108 j6, 109 j7, 110 j8, 111 j9,
112 j10, 113 j11, 114 j12, 115 j13, 116 q1,
117 q2, 118 q3, 119 q4, 120 q5, 121 q6,
122 pf1, 123 pf2, 124 pf3, 125 pf4, 126 pf5,
127 pf6, 128 po1, 129 po2, 130 po3, 131 po4,
132 po5, 133 po6, 134 sq1, 135 sq2, 136 sq3,
137 sq4, 138 f1, 139 f2, 140 f3, 141 f4,
142 f5, 143 f6, 144 f7, 145 f8, 146 f9,
147 par1, 148 par2, 149 par3, 150 par4, 151 bo1,
152 bo2, 153 bo3, 154 bs1, 155 bs2, 156 bs3,
157 bs4, 158 bs5, 159 ls1, 160 ls2, 161 so1,
162 so2, 163 ex1, 164 ex2, 165 plt1, 166 plt2,
167 plt3, 168 rst2, 169 nps1, 170 nps2, 171 nps3,
172 nps4, 173 nps5, 174 nps6, 175 nps7, 176 nps8,
177 nps9, 178 cmn1, 179 cmn2, 180 cmn3, 181 crs1,
182 crs2, 183 crs3, 184 crs4, 185 crs5, 186 crs6,
187 plp, 188 orb, 189 pqf, 190 itf1, 191 itf2,
192 itf3, 193 stf, 194 sk1, 195 sk2, 196 sk3,
197 crv1, 198 crv2, 199 crv3, 200 drs1, 201 drs2,
202 scr, 203 cdl, 204 st, 205 cor1, 206 cor2,
207 cor3, 208 cor4, 209 cor5, 210 cor6, 211 scp1,
```

```
 212 scp2, 213 scp4, 214 scp5, 215 scp6, 216 scp7,
 217 scp8, 218 scp9, 219 hm1, 220 hm2, 221 hm3,
 222 hm4, 223 ul1, 224 ul2, 225 mn1, 226 mn2,
 227 mn3, 228 mn4, 229 mn6, 230 mn7, 231 mn8,
 232 il1, 233 il3, 234 il4, 235 il5, 236 il6,
 237 il7, 238 il8, 239 il9, 240 il10, 241 il11,
 242 il12, 243 il13, 244 il14, 245 il15, 246 il16,
 247 il17, 248 il18, 249 il19, 250 il20, 251 il21,
 252 pb1, 253 pb2, 254 pb3, 255 pb4, 256 pb5,
 257 pb6, 258 pb7, 259 pb8, 260 pb9, 261 pb10,
 262 pb11, 263 is1, 264 is2, 265 is3, 266 is4,
 267 is5, 268 is6, 269 is7, 270 is8, 271 is9,
 272 is10, 273 is11, 274 is12, 275 fm1, 276 fm2,
 277 tb, 278 fb, 279 as, 280 dsts, 281 pes1,
 282 pes2, 283 pes3, 284 pes4, 285 pes6, 286 pes7,
 287 Ig1, 288 Ig2, 289 Ig3, 290 Mt1, 291 Mt2,
 292 Eq1, 293 Eq2, 294 Eq3, 295 Eq4, 296 Pt1,
 297 Pt2, 298 Ba1, 299 Ba2, 300 Te1, 301 Te2,
 302 Te3, 303 Te4, 304 Te5, 305 Wu1, 306 Wu2,
 307 Wu3, 308 Sy1, 309 Sy2, 310 Sy3, 311 Am1,
 312 Am2, 313 Am3, 314 Ar1, 315 Ar2, 316 Br1,
 317 Ma1, 318 Ma2, 319 Ch1, 320 Ch2, 321 Cos1,
 322 Cos2, 323 Coi1, 324 Coi2, 325 Hy1, 326 Hy2,
 327 Hy3, 328 Lmm1, 329 Lmm2, 330 Lmm3, 331 Kb1,
 332 Kb2, 333 Kb3, 334 Kb4, 335 Kb5, 336 Np1,
 337 Np2, 338 Ve1, 339 Ve2, 340 Kr1, 341 Kr2,
 342 Grl1, 343 Grn1, 344 Grm1, 345 Grm2, 346 Ol1,
 347 Ol2, 348 Ol3, 349 Ol4, 350 Ol5, 351 Paw1,
 352 Paw2, 353 Pac1, 354 Pac2, 355 Pac3, 356 Pat1,
 357 Pat2, 358 Pat3, 359 Pr1, 360 Pr2, 361 Se1,
 362 Ph1, 363 Ts1, 364 Ts2, 365 Ts3, 366 Ts4,
 367 Ts5, 368 Ta1, 369 Lh1, 370 Lh2
                ;

MATRIX
[                      10     20     30     40     50     60     70     80     90
100    110    120    130    140    150    160    170    180    190    200
210    220    230    240    250    260    270    280    290    300    310
320    330    340    350    360    370]
[                        .      .      .      .      .      .      .      .      .      .
.      .      .      .      .      .      .      .      .      .      .      .      .      .
.      .      .      .      .      .      .      .      .      .      .      .]
```

Iguanodon_bernissartensis
00000000000000000000000000000000010000100001000000000000110000000000000
00000000000000000000000000000100000-0100100100010000000000110100?000-
000?1000000?00010000000?0001-00--0010-00----
10100000000001010000000000000000001000000100101000000001110000000000000
00011000000110000000001000001110000000000000000000000000000000000000000
00000000000000000000000000000000000000
Hadrosaurus_foulkii
???131011100 11???1101???
??????????????????2??
??????????????????????????-
??????????????????????????????????000110???????120123??012????10111?????11????01
11?00?0---
111???0??
???????????????
Bactrosaurus_johnsoni
011(12)10022?00110111(01)0100100010100012111012 0(01)0100011011010100100100
0000000000000?000-0?0100101000010110000000-
02100010111100000000000111000110 0-0000100011000111001001??100?-?0--0010-
00----
1010000?0?00?1?0?10200000010010101010 0??10?1?12001101011(01)110001000?120
01111111111102100111100?01101000000000000110000000000000000000000000000000
00000000?000000000000?0000000000000000000
Wulagasaurus_dongi
1?????????????????????????????????11101{01}?121??01?121????????????????????????
??????????0?01??211??2221??01?010??????1????????????????????????????????????
????????????????????????????????-?????????????????1??????110?1-
??1211???1???00?????????????????????0???0
00?00000111?0?0???0??0????????????000?0??0????0????00??????????0?0?????0??
Brachylophosaurus_canadensis
122231122?001111211(01)120211112211312(012)(012)111211101112111111001002131
1010000000000111000-
0101002021111222100011110122 11(01)1011211000010 0(01)(01)(12)11001100101100
02010111111120011111 01(12)00-10--0113010-2--
0101100(01)011111011112112 1111(01)1-
011011121111211120122031121000111111211111111101112211 0---
111001011011000000000000000000000000000000010000000000000000000000000000000
00000000000000000000000
Probrachylophosaurus_bergei
222231122200112 1?11112?2????{12}{23}?120221111211001112111110 0?0???3????0
???????00????00?0?0100202111?222100011010112120101121 1??????0?1??1002?0010
1000?20?0111?111?0?11{12}1??1?0?-?0--01??010-2--
01?11?00?1?1?10?1????????????????????????????1201220{23}11??000111111121?1111

11?01??221???????10????????0????00??0000?0???00????0???0???0?00000?0000???00
0?000?????0?00?000000000?0000??????
Maiasaura_peeblesorum
122231122?00111211??2021111221120211011211101112111110010021311010000000
0000111000-0101002021111222100011110122110100121100011000(01)11100210000-
100?(12)0101111111200111110110 0-00--0112011-4--
0101100001111101 1?1211?111111-
0110111111 1?2111201220311210001111112111111111011122110---
11100101?0110000000000000000000000000000011000000000000000000000000000000
000000000000000000000000
Acristavus_gagslarsoni
122231121?00111121111???????????202(01)0{01}11211?01112111110010 02?3?10100
00000000???000-
0?0100202111?222100011010122110101121101000001??1110210000-
100010001111111 20?1111??1?0?-?0--011??00----
010110010?????????????????????????1?11?????????????????????????????111111???
??????????11??????????0????000000000000000000000000000000000??0000000?00?00
0??0?00000?0000000000000000000
Corythosaurus_casuarius
12222112101111111211??01312111310111(12)(01)11121100111211111110011110000
112101-214--100-1-
00112121121232110212 1101(01)10111100001201002101011112110101211101111110
0110001101001(01)1-0-100120--
120621010102101101111101121111111101002210121111111120123120121000111110
11011111112111120210101111110101100000000000000000000000000000000000001100
000000000000000000000000000000000000000000000000
Edmontosaurus_annectens
232131(01)222001121211?21(01)111?11411(23)100(01)0103(12)100111211111001002
131111100000000022 1010-
0100012021111232100110010103021101 12(01)10100000120111011 1000-
000020201111011101112101 1000-10--0111100----0101100101011001111211211 1111-
01(12)111(01)11111111121123121121000111111310111101201212 2(01)00---
11100101101000000000000000000000000000000000000000000000000000000000000000
000000000000000000000000
Edmontosaurus_regalis
232231022200112121102101 11?11411(23)100(01)0103(12)100111211111001002131 11
11000000000221010-
0100012021111232100110010103021101120101000001201110111000-
000020201111011101112101 1000-10--0111100----0101100001011001111211111111 1-
012111111111111120123121121000111111310111101201212 1100---
11100100101000000000000000000000000000000000000000000000000000000000000000
000000000000000000000000
Kritosaurus_navajovius
1222210?2?00112121 10?001??11021?00120011211001112111110?100????????000000

000010010-000201202111?232100111010023110101121101000000111020 01?000-
100?10101111011100112 1?01?0?-?0--0112010-5--
010(01)010011?1??2????????????????????
????????????????????????0????000000000000000?00000?000000000??000000000?0
01100?00000?0000000000000000000
Gryposaurus_notabilis
132121012?001111211??00200010410(12)02(12)(01)011211001112111110010011211 0
10000000100010001100020130211102321011110110131102011211010000001110201 1
1000-100020001 11?0111001121001201-30--0111010-1--
010001001101100111121111100 11-
111(12)1(12)11111111111121121122???111?11411111???2011122100---
111101001110000000000000000000000000000000000000000000000000000000000001000
000000000000000000000000
Gryposaurus_latidens
132031111000111?211?????????????212220112110011121111100100212 11??0000000
?000100??000020130211102321??????1?????????????0??0?0?0????20????00????????
??????????????????1?0?-?0--0111010-1--0?0?0?????01?0?11112111110011-
111(01)1201??1????11?12112012200011111141111 1?012????????0---
???1??????10?00?0?0??0??00????000??????0?000??000000?000???00??00??100?0??0?
000000000000?00??0?
Gryposaurus_monumentensis
1321310?2?00111121102001110104102022101121?00111211111001001121101000000
010001000110002013021110232101111101?123111201121101000000111020?11000-
100?20?011?1?1110011?1001201-30--0111010-1--
010101001 1??2????????????????????
??????---
????????????0????000000000000000?000000000000000000000000000?00000011000
0?000?0000000000000000
Prosaurolophus_maximus
232231012?00112121 10?00(23)11011411110(01)00103(12)100111211111001002121 10
10000000000221010-
000(01)012021110232101110011 0(01)300120111010101(01)00111112011?000-
000020101111011000112100?102-20--0112110-5--
0101100(01)11?1100111121121111 11-
11111(12)1111111111211(23)212012200011111140111120120121221 10---
111001011110000000000000000000000000000000000000000000000000000000000000000
000000000000110000000000
Secernosaurus_koerneri
12?2310?2?001111?110????11??????002111112?100?112??1?1??100?????????0???????
???000-0?0201302????2121?????????????????????010000000????0?11000-
?000201011110 1?0001121??????-?0--0?????????-0?????0?1??1?1???111011110011-
11????1???1????111121020121131111111401111201201212212 0---
111???00??????0?0?0??????0000000?00?0000?0??000000???000000?00?00???0?00000
?00000000?01000??00?0

```
Saurolophus_osborni
23223101?2?0011212110?0031101041?2100001031100111211111001001121101000100
0000221000-
0001012021110232101110011003001(12)0111010001101212112121000112002??1?0111
?01?0001121001102-20--0113110-3--010110?111111011?12112111111-
01?21{01}01111??111211321211220001117?1141111??1101?1???10---
1110010011100000000000000000000000000000000000000000000000000000000000000000
0000000000000000000000000
Saurolophus_angustirostris
2321310?2?0011212117?00211010411(12)1000010311001112111110010011211010001
000000221000-
0001012021110232101110010003001(12)0111010001101212112121000112002?201011
1?0??0001121??1102-20--0113110-3--0101100111111011111212111111-
0122100111?111121132121122000111?11411111??11012112010---
111?0100111000000000000000000000000000000000000000000000000000000000000000
0000000000000000000000000
;
END;

BEGIN ASSUMPTIONS;
        OPTIONS  DEFTYPE=unord PolyTcount=MINSTEPS ;
        TYPESET * UNTITLED  = unord: 2 4-14 16 18-370, ord: 1 3 15 17;
END;

begin paup;
log file=PM2010sd_log.nex replace;
outgroup Iguanodon_bernissartensis;
set criterion=parsimony taxlabels=full torder=right maxtrees=5000 increase=no
root=outgroup outroot=monophyl storebrlens=yes warnreset=no warntree=no
warntsave=no warnroot=no warnredef=no autoclose=yes;
[delete [taxa];]
[exclude [characters];]
hsearch start=stepwise hold=2 addseq=simple limitperrep=no usenonmin=yes swap=tbr
steepest=yes multrees=yes; PSet MSTaxa=Variable opt=acctran;
describetrees 1/ root=outgroup plot=phylogram apolist=yes;
savetrees root=yes file=PM2010sd_tre.nex replace format=altnex brlens=yes;
contree all/strict=yes semistrict=no majrule=no adam=no root=outgroup
treefile=PM2010sd_tre.nex append=yes;
bootstrap nreps=5000 grpfreq=no conlevel=50 search=heuristic/ addseq=random nreps=1
swap=TBR steepest=no multrees=yes;
savetrees from=1 to=1 root=yes file=PM2010sd_tre.nex append=yes format=altnex
savebootp=brlens;
log stop;
end;
```

APPENDIX D

CHARACTER MATRIX BASED ON PRIETO-MÁRQUEZ (2010) WITH SOME CHARACTERS EXCLUDED, IN NEXUS FORMAT

#NEXUS

[Freedman Fowler and Horner, 2015, Appendix D]
[Formatted for PAUP 4.0b10 for MAC OS X]

[Matrix is modified from nexus file of Prieto-Márquez 2010 with character states for Probrachylophosaurus bergei added, as well as eight recodings for Acristavus (characters 106, 116-121, 259) and one for Brachylophosaurus (character 138). Three characters (1, 15, 123) are excluded. States of character 143 were changed for all taxa: the original three states (0 1 2) were reduced to two (0 1) by combining states 0 & 1 into 0, thus changing state 2 to 1. See main text for details.]
[Most hadrosauroid and lamebeosaurine taxa are excluded from Prieto-Márquez's 2010 matrix in order to simplify analysis and make taxon list more consistent with that of Gates et al. 2011.]

[Prieto-Márquez, A. 2010. Global phylogeny of Hadrosauridae (Dinosauria: Ornithopoda) using parsimony and Bayesian methods. Zoological Journal of the Linnean Society, 159:435-502.]

```
BEGIN TAXA;
        DIMENSIONS  NTAX=19;
        TAXLABELS
        Iguanodon_bernissartensis
        Hadrosaurus_foulkii
        Bactrosaurus_johnsoni
        Wulagasaurus_dongi
        Brachylophosaurus_canadensis
        Probrachylophosaurus_bergei
        Maiasaura_peeblesorum
        Acristavus_gagslarsoni
        Corythosaurus_casuarius
        Edmontosaurus_annectens
        Edmontosaurus_regalis
        Kritosaurus_navajovius
        Gryposaurus_notabilis
        Gryposaurus_latidens
        Gryposaurus_monumentensis
        Prosaurolophus_maximus
        Secernosaurus_koerneri
        Saurolophus_osborni
        Saurolophus_angustirostris;
END;
```

```
BEGIN CHARACTERS;
        DIMENSIONS  NCHAR=370;
        FORMAT SYMBOLS= " 0 1 2 3 4 5 6 7" MISSING=? GAP=- ;
        CHARSTATELABELS
                1 dtth1, 2 dtth3, 3 dtth4, 4 dtth5, 5 dtth6, 6 dtth7,
 7 dtth8, 8 dtth9, 9 dtth10, 10 dtth11, 11 dtth12,
 12 dtth13, 13 dtth14, 14 dtth15, 15 mxth1, 16 mxth3,
 17 mxth4, 18 mxth5, 19 mxth6, 20 mxth7, 21 mxth8,
 22 pdt1, 23 pdt2, 24 pdt3, 25 pdt4, 26 pdt5,
 27 pdt6, 28 pdt7, 29 pdt8, 30 pdt9, 31 pdt11,
 32 pdt13, 33 dt1, 34 dt2, 35 dt3, 36 dt4,
 37 dt5, 38 dt6, 39 dt7, 40 dt9, 41 dt10,
 42 dt11, 43 dt12, 44 dt13, 45 dt14, 46 dt15,
 47 dt16, 48 dt17, 49 dt18, 50 dt19, 51 sa1,
 52 sa2, 53 sa3, 54 sa4, 55 sa5, 56 sa6,
 57 ang, 58 cob, 59 prar, 60 pmx1, 61 pmx2,
 62 pmx3, 63 pmx5, 64 pmx6, 65 pmx7, 66 pmx8,
 67 pmx9, 68 pmx10, 69 pmx11, 70 pmx12, 71 pmx13,
 72 pmx14, 73 pmx15, 74 pmx16, 75 ns1, 76 ns2,
 77 ns3, 78 ns4, 79 ns5, 80 ns6, 81 ns7,
 82 ns8, 83 ns9, 84 mx1, 85 mx2, 86 mx3,
 87 mx4, 88 mx5, 89 mx6, 90 mx7, 91 mx8,
 92 mx9, 93 mx10, 94 mx11, 95 mx12, 96 mx13,
 97 mx14, 98 mx15, 99 mx16, 100 mx17, 101 lc1,
 102 lc2, 103 j1, 104 j2, 105 j3, 106 j4,
 107 j5, 108 j6, 109 j7, 110 j8, 111 j9,
 112 j10, 113 j11, 114 j12, 115 j13, 116 q1,
 117 q2, 118 q3, 119 q4, 120 q5, 121 q6,
 122 pf1, 123 pf2, 124 pf3, 125 pf4, 126 pf5,
 127 pf6, 128 po1, 129 po2, 130 po3, 131 po4,
 132 po5, 133 po6, 134 sq1, 135 sq2, 136 sq3,
 137 sq4, 138 f1, 139 f2, 140 f3, 141 f4,
 142 f5, 143 f6, 144 f7, 145 f8, 146 f9,
 147 par1, 148 par2, 149 par3, 150 par4, 151 bo1,
 152 bo2, 153 bo3, 154 bs1, 155 bs2, 156 bs3,
 157 bs4, 158 bs5, 159 ls1, 160 ls2, 161 so1,
 162 so2, 163 ex1, 164 ex2, 165 plt1, 166 plt2,
 167 plt3, 168 rst2, 169 nps1, 170 nps2, 171 nps3,
 172 nps4, 173 nps5, 174 nps6, 175 nps7, 176 nps8,
 177 nps9, 178 cmn1, 179 cmn2, 180 cmn3, 181 crs1,
 182 crs2, 183 crs3, 184 crs4, 185 crs5, 186 crs6,
 187 plp, 188 orb, 189 pqf, 190 itf1, 191 itf2,
 192 itf3, 193 stf, 194 sk1, 195 sk2, 196 sk3,
```

197 crv1, 198 crv2, 199 crv3, 200 drs1, 201 drs2,
202 scr, 203 cdl, 204 st, 205 cor1, 206 cor2,
207 cor3, 208 cor4, 209 cor5, 210 cor6, 211 scp1,
212 scp2, 213 scp4, 214 scp5, 215 scp6, 216 scp7,
217 scp8, 218 scp9, 219 hm1, 220 hm2, 221 hm3,
222 hm4, 223 ul1, 224 ul2, 225 mn1, 226 mn2,
227 mn3, 228 mn4, 229 mn6, 230 mn7, 231 mn8,
232 il1, 233 il3, 234 il4, 235 il5, 236 il6,
237 il7, 238 il8, 239 il9, 240 il10, 241 il11,
242 il12, 243 il13, 244 il14, 245 il15, 246 il16,
247 il17, 248 il18, 249 il19, 250 il20, 251 il21,
252 pb1, 253 pb2, 254 pb3, 255 pb4, 256 pb5,
257 pb6, 258 pb7, 259 pb8, 260 pb9, 261 pb10,
262 pb11, 263 is1, 264 is2, 265 is3, 266 is4,
267 is5, 268 is6, 269 is7, 270 is8, 271 is9,
272 is10, 273 is11, 274 is12, 275 fm1, 276 fm2,
277 tb, 278 fb, 279 as, 280 dsts, 281 pes1,
282 pes2, 283 pes3, 284 pes4, 285 pes6, 286 pes7,
287 Ig1, 288 Ig2, 289 Ig3, 290 Mt1, 291 Mt2,
292 Eq1, 293 Eq2, 294 Eq3, 295 Eq4, 296 Pt1,
297 Pt2, 298 Ba1, 299 Ba2, 300 Te1, 301 Te2,
302 Te3, 303 Te4, 304 Te5, 305 Wu1, 306 Wu2,
307 Wu3, 308 Sy1, 309 Sy2, 310 Sy3, 311 Am1,
312 Am2, 313 Am3, 314 Ar1, 315 Ar2, 316 Br1,
317 Ma1, 318 Ma2, 319 Ch1, 320 Ch2, 321 Cos1,
322 Cos2, 323 Coi1, 324 Coi2, 325 Hy1, 326 Hy2,
327 Hy3, 328 Lmm1, 329 Lmm2, 330 Lmm3, 331 Kb1,
332 Kb2, 333 Kb3, 334 Kb4, 335 Kb5, 336 Np1,
337 Np2, 338 Ve1, 339 Ve2, 340 Kr1, 341 Kr2,
342 Grl1, 343 Grn1, 344 Grm1, 345 Grm2, 346 Ol1,
347 Ol2, 348 Ol3, 349 Ol4, 350 Ol5, 351 Paw1,
352 Paw2, 353 Pac1, 354 Pac2, 355 Pac3, 356 Pat1,
357 Pat2, 358 Pat3, 359 Pr1, 360 Pr2, 361 Se1,
362 Ph1, 363 Ts1, 364 Ts2, 365 Ts3, 366 Ts4,
367 Ts5, 368 Ta1, 369 Lh1, 370 Lh2
;

MATRIX
[10 20 30 40 50 60 70 80 90 100 110
120 130 140 150 160 170 180 190 200 210 220
230 240 250 260 270 280 290 300 310 320 330
340 350 360 370]

[. . . . .
. . . .
. . . .]

Iguanodon_bernissartensis
0000000000000000000000000000000010000100001000000000000110000000000000
000000000000000000000000000100000-01001001000100000000001101000?000-
000?1000000?00010000000?0001-00--0010-00----
1010000000000101000000000000000000010000001001010000000011100000000000000
000110000000110000000001000001110000000000000000000000000000000000000000
000000000000000000000000000000000000000
Hadrosaurus_foulkii
???13101110011???1101??
??????????????????2??
????????????????????????-
???????????????????????????????000110???????120123??012????10111?????11????01
11?00?0---
111???0???
????????????????
Bactrosaurus_johnsoni
011(12)10022?00110111(01)0100100010100012111012O(01)010001101101010010O100
0000000000000?000-0?0100101000010110000000-
0210001011110000000000001110001100-000010001100011100100l??100?-?0--0010-
00----
1010000?0?00?1?0?10200000010010101010O??10?1?12001101011(01)110001000?120
0111111111110210011110O?0110100000000000011000000000000000000000000000
00000000?000000000000?00000000000000000000
Wulagasaurus_dongi
1??????????????????????????????11101{01}?121??01?121????????????????????????
??????????0?01??211??2221??01?010??????1??????????????????????????????????????
???????????????????????????????-?????????????????1??????110?1-
??1211???1???00???????????????????0???0
00?00000111?0?0???0??0????????????000?0??0????0????00?????????0?0?????0??
Brachylophosaurus_canadensis
122231122?001111211(01)120211112211312(012)(012)111211101112111110010021 31
1010000000000111000-
010100202111122210001111012211(01)10112110000100(01)(01)(12)11001100101000
0201011111112001111101(12)00-10--0113010-2--
0101100(01)0111110111121121111(01)1-
0110111211112111201220311210001111112111111111011122110---
1110010110110000000000000000000000000001000000000000000000000000000000
0000000000000000000000
Probrachylophosaurus_bergei
22223112220011 21?11112?2????{12}{23}?120221111211001112111110 0?0???3????0

???????00????00?0?0100202111?22210001101011212010112111?????0?1??1002?0010
1000?20?0111?111?0?11{12}1??1?0?-?0--01??010-2--
01?11?00?1?1?10?1?????????????????????????????1201220{23}11??000111111121?1111
11?01??221???????10????????0????00??0000?0???00????0???0???0?0000?0000???00
0?000?????0?00?000000000?0000??????
Maiasaura_peeblesorum
122231122?001111211??202111122112021101121110111211111001002131101000000
0000111000-0101002021111222100011110122110100121100011000(01)11100210000-
000?(12)0101111111200111110110 0-00--0112011-4--
0101100001111101 1?1211?111111-
011011111111?2111201220311210001111112111111111011122110---
11100101?0110000000000000000000000000000011000000000000000000000000000000
00000000000000000000000
Acristavus_gagslarsoni
122231121?001111211 1????????????202(01)0{01}11211?011121111100100 2?3?10100
00000000???000-
0?0100202111?22210001101012211010112110100000 1??1110210000-
000010001111111120?1111??1?0?-?0--011??00----
010110010?????????????????????????1?11?????????????????????????????111111???
??????????11??????????0????000000000000000000000000000000000??0000000?00?00
0??0?00000?00000000000000000
Corythosaurus_casuarius
12222112101111111211??01312111310111(12)(01)11121100111211111110011110000
112101-214--100-1-
00112121121232110212 1101(01)10111100001201002101011112110101111101111110
0110001101001(01)1-0-100120--
12062101010210110111110112111111110100221012111111112012312012100011111 0
11011111112111120210101111110101100000000000000000000000000000000001100
00000000000000000000000000000000000000000000000
Edmontosaurus_annectens
232131(01)222001121211?21(01)111?11411(23)100(01)0103(12)100111211111001002
13111110000000000221010-
0100012021111232100110010103021101 12(01)10100000120111011 1000-
000020201111011101112101 1000-10--0111100----0101100101011001111211211111 1-
01(12)111(01)11111111121123121121000111111310111101201212 2(01)00---
11100101101000000000000000000000000000000000000000000000000000000000000000
00000000000000000000000
Edmontosaurus_regalis
232231022200112121102101 11?11411(23)100(01)0103(12)100111211111001002131111
11000000000221010-
0100012021111232100110010103021101120101000001201110111000-
000020201111011101112101 1000-10--0111100----0101100001011001111211111111 1-
012111111111111120123121121000111111310111101201212 1100---

111001001010000000000000000000000000000000000000000000000000000000000
0000000000000000000000
Kritosaurus_navajovius
1222210?2?0011212110?001??11021?00120011211001112111110?100????????000000
000010010-000201202111?232100111010023110101121101000000011102001?000-
000?101011110111001121?01?0?-?0--0112010-5--
010(01)010011?1???2???????????????????
??????????????????????0????000000000000000?00000?00000000000??0000000000?0
01100?00000?0000000000000000000
Gryposaurus_notabilis
132121012?001111211??00200010410(12)02(12)(01)0112110011121111100100112110
1000000010001000110002013021110232101111011013110201121101000000011102011
1000-00002000111?0111001121001201-30--0111010-1--
01000100110110011112111110011-
111(12)1(12)111111111111121121122???111?11411111???2011122100---
1111010011100000000000000000000000000000000000000000000000000000001000
0000000000000000000000
Gryposaurus_latidens
132031111000111?211??????????????21222011211001112111110010021211??0000000
?000100??000020130211102321??????1???????????????0??0?0?0????20????00????????
?????????????????1?0?-?0--0111010-1--0?0?0?????01?0?11112111110011-
111(01)1201??1????11?121120122000111111411111?012?????????0---
???1??????10?00?0?0??0??00????000??????0?000??000000?000???00??00??100?0??0?
0000000000000?00??0?
Gryposaurus_monumentensis
1321310?2?00111121102001110104102022101121?00111211111001001121101000000
01000100011000201302111023210111101?1231112011211010000000111020?11000-
000?20?011?1?1110011?1001201-30--0111010-1--
0101010011??2??????????????????????
??????---
????????????0????000000000000000?0000000000000000000000000000?00000011000
0?000?0000000000000000
Prosaurolophus_maximus
232231012?0011212110?00(23)11011411110(01)00103(12)10011121111100100212110
1000000000221010-
000(01)0120211102321011100110(01)30012011010101(01)00111112011?000-
000020101111011000112100?102-20--0112110-5--
0101100(01)11?110011112112111111-
11111(12)11111111111211(23)21201220001111114011112012012122110---
1110010111100000000000000000000000000000000000000000000000000000000000
00000000000011000000000
Secernosaurus_koerneri
12?2310?2?001111?110???11??????002111112?100?112??1?1??100?????????0???????
???000-0?0201302????2121?????????????????????010000000????0?11000-

?000201011110l?0001121??????-?0--0?????????-0?????0?1??1?1???111011110011-
11????1???1????1111210201211311111114011112012012122120---
111???00??????0?0?0??????0000000?00?0000?0??000000???000000?00?00???0?00000
?00000000?01000??00?0
Saurolophus_osborni
232231012?00112121l0?00311010412100001031100111211111001001121101000100
0000221000-
000101202111023210111001100300l(12)0111010001101212112121000111002?1?0111
?01?0001121001102-20--0113110-3--010110?111111011l?12112111111-
01?21{01}01111??111211321211220001l1?11411111??1101?1???10---
111001001110000000000000000000000000000000000000000000000000000000000000
000000000000000000000000
Saurolophus_angustirostris
2321310?2?00112121l??00211010411(12)100001031100111211111001001121101000l
000000221000-
000101202111023210111001000300l(12)0111010001101212112121000111002?201011
1?0??0001121??1102-20--0113110-3--0101100111111011111211211111l-
012210011l1?111121132121122000111?11411111??11012112010---
111?010011100000000000000000000000000000000000000000000000000000000000000
000000000000000000000000
;
END;

BEGIN ASSUMPTIONS;
	OPTIONS DEFTYPE=unord PolyTcount=MINSTEPS ;
	TYPESET * UNTITLED = unord: 2 4-14 16 18-370, ord: 1 3 15 17;
END;

begin paup;
log file=PM2010sd_log.nex replace;
outgroup Iguanodon_bernissartensis;
set criterion=parsimony taxlabels=full torder=right maxtrees=5000 increase=no
root=outgroup outroot=monophyl storebrlens=yes warnreset=no warntree=no
warntsave=no warnroot=no warnredef=no autoclose=yes;
[delete [taxa];]
[exclude [characters];]
exclude 1 15 123;
hsearch start=stepwise hold=2 addseq=simple limitperrep=no usenonmin=yes swap=tbr
steepest=yes multrees=yes; PSet opt=acctran;
describetrees 1/ root=outgroup plot=phylogram apolist=yes;
savetrees root=yes file=PM2010sd_tre.nex replace format=altnex brlens=yes;

```
contree all/strict=yes semistrict=no majrule=no adam=no root=outgroup
treefile=PM2010sd_tre.nex append=yes;
bootstrap nreps=5000 grpfreq=no conlevel=50 search=heuristic/ addseq=random nreps=1
swap=TBR steepest=no multrees=yes;
savetrees from=1 to=1 root=yes file=PM2010sd_tre.nex append=yes format=altnex
savebootp=brlens;
log stop;
end;
```

APPENDIX E

CHARACTER MATRIX BASED ON GATES ET AL. (2011), IN NEXUS FORMAT

#NEXUS

[Freedman Fowler and Horner, 2015, Appendix E]
[Formatted for PAUP 4.0b10 for MAC OS X]

[Matrix is modified from nexus file of Gates et al. 2011 with character states for Probrachylophosaurus bergei added.]
[The taxa Lophorothon, Protohadros, and Telmatosaurus are excluded from Gates et al.'s 2011 matrix in order to simplify analysis and make taxon list more consistent with that of Prieto-Márquez 2010.]

[Gates, T.A., Horner, J.R., Hanna, R.R., and Nelson, R.C. 2011. New unadorned hadrosaurine hadrosaurid (Dinosauria, Ornithopoda) from the Campanian of North America. Journal of Vertebrate Paleontology, 31:798-811.]

BEGIN DATA;
	DIMENSIONS NTAX=13 NCHAR=116 ;
	FORMAT SYMBOLS= " 0 1 2 3" MISSING=? GAP=N ;
MATRIX

Iguanodon_bernissartensis
00000100000000000000000000000000000000000000000000000100000000000000000000?00000000000000000000000000000000000
Bactrosaurus
0?01?0111000??0?10001001 1??10001000000000?01010??000000010?0?0001?00?00200001??110?1101001100 10????1?000100?1110?1?1
Brachylophosaurus_canadensis
21110121121111111111120110110011110110011 0?2100011021120111001111111110100111101101011011110111111111110101101111111
Probrachylophosaurus_bergei
(23)11101211211111??1111?0???1??0?1??011?0?10?210??1102012011?0011?11{12}11100001?1?011??01?0??????????????1110?01??1?????
Corythosaurus
11111011111111111111111010010?1??0010001?11120100111021000001111111211112 12?11110111111111111011111111111110111111111
Edmontosaurus_spp.
31110121121011111111121111112011120000010?2100111012101000001111111110001010111011011101111101101111111111010111111111
Gryposaurus_spp.
21110121111110111111111111011101011012 00(02)10021001110111101100011111111 10001011101111111011100110111111111010111111 1
Kerberosaurus
111????11?????????????????????0?1120?110?100210??110?210?00?1?111??2????????1???1??????????????????????????????????????

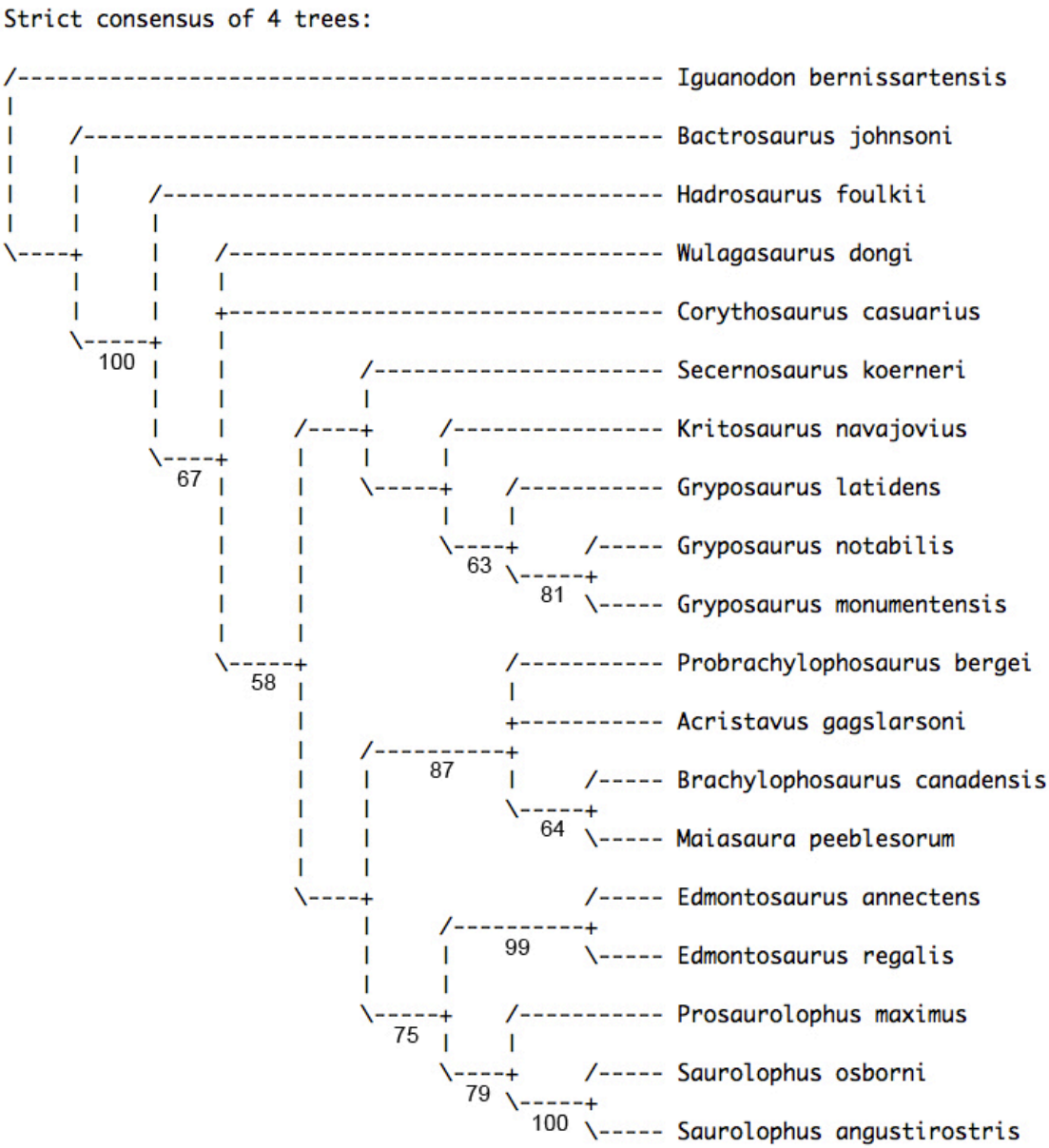
```
Maiasaura
21110121121111111111112011?10000011011001100210111102012011101111112111 01
?01?11011010110111100111111111111110110111111
Kritosaurus
2?????211?????????????????????0??1101210??0?2100011011110110 1?1111?111100?1?
?1?0111????????101?????????????????????????
Prosaurolophus_spp.
21110121111111111111111101?11201112012100100210101101210100011111111111 00
010111011011101111101101111111111110110111111
Saurolophus_spp.
31110121111111101111110000112011120121001002101011012100000111111121 11??
???011011011101111101101111111100011011 1111
Acristavus
1?110?2112101???11111?011011000110000001100210011102012011100111111111 01
001111011 1?01?0??????111??????????01??????11
;
END;

BEGIN ASSUMPTIONS;
        OPTIONS  DEFTYPE=unord PolyTcount=MINSTEPS ;
END;

begin paup;
log file=Gates2011_log.nex replace;
outgroup Iguanodon_bernissartensis;
set criterion=parsimony taxlabels=full torder=right maxtrees=5000 increase=no
root=outgroup outroot=monophyl storebrlens=yes warnreset=no warntree=no
warntsave=no warnroot=no warnredef=no autoclose=yes;
[delete [taxa];]
[exclude [characters];]
hsearch start=stepwise hold=2 addseq=simple limitperrep=no usenonmin=yes swap=tbr
steepest=yes multrees=yes; PSet opt=acctran;
describetrees 1/ root=outgroup plot=phylogram apolist=yes;
savetrees root=yes file=Gates2011_tre.nex replace format=altnex brlens=yes;
contree all/strict=yes semistrict=no majrule=no adam=no root=outgroup
treefile=Gates2011_tre.nex append=yes;
bootstrap nreps=50000 grpfreq=no conlevel=50 search=heuristic/ addseq=random
nreps=1 swap=TBR steepest=no multrees=yes;
savetrees from=1 to=1 root=yes file=Gates2011_tre.nex append=yes format=altnex
savebootp=brlens;
log stop;
end;
```

APPENDIX F

PHYLOGENY OF HADROSAURINES BASED ON PRIETO-MÁRQUEZ (2010)



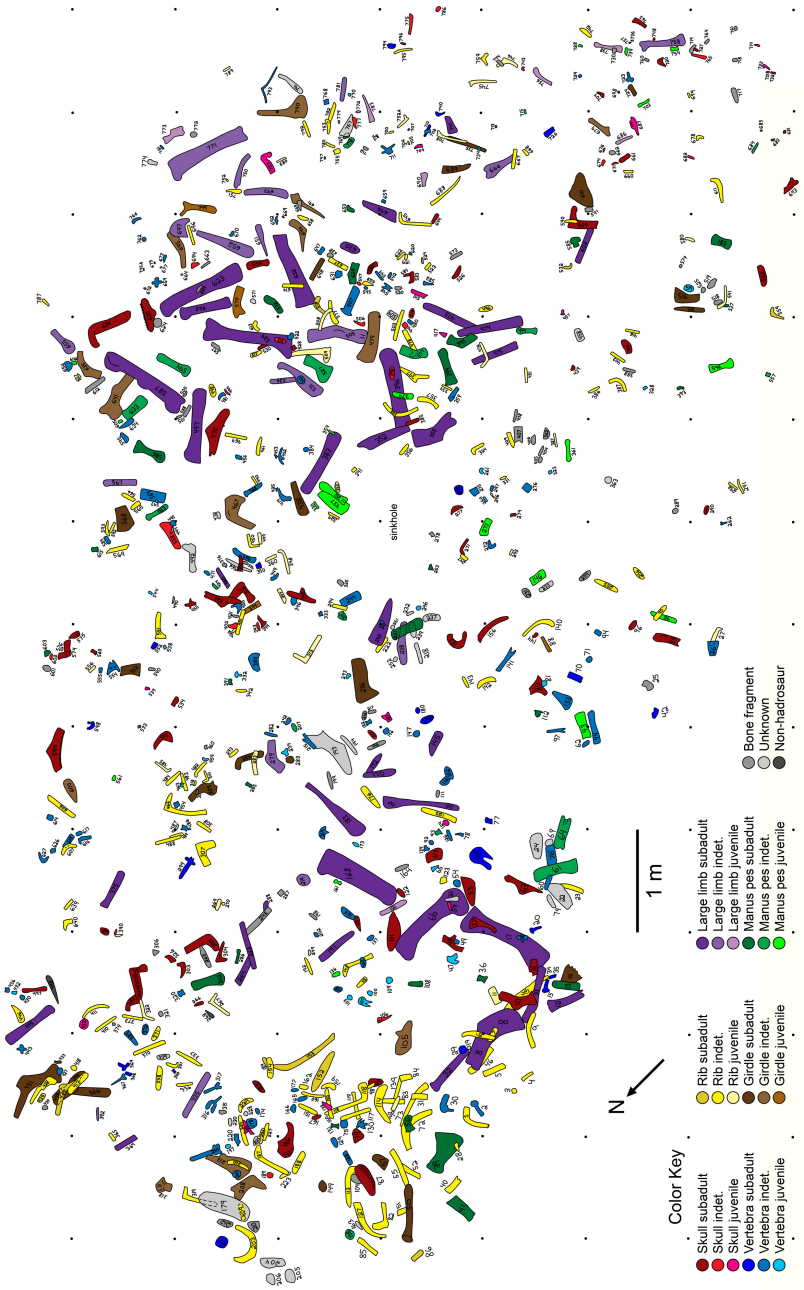
Appendix F Figure. Phylogeny of hadrosaurines based on Prieto-Márquez (2010). Strict consensus of two most parsimonious trees resulting from adding *Probrachylophosaurus bergei* to Prieto-Márquez's (2010) matrix with minor character recodings as discussed in text, but no excluded characters. Values on branches represent bootstrap support; branches without values had less than 50% support. Tree statistics: shortest tree length = 627, Consistency Index = 0.72, Retention Index = 0.68, Rescaled Consistency Index = 0.49. The clade of *Probrachylophosaurus*, *Brachylophosaurus*, and *Maiasaura* with the exclusion of *Acristavus* had 55% bootstrap support.

Literature Cited

Prieto-Márquez, A., 2010. Global phylogeny of Hadrosauridae (Dinosauria: Ornithopoda) using parsimony and Bayesian methods. Zoological Journal of the Linnean Society, 159: 435-502.

APPENDIX G

HIGH RESOLUTION COLOR QUARRY MAP OF EXCAVATED BONES IN THE JR-429 *GRYPOSAURUS* BONEBED



Appendix G Figure. High resolution color quarry map of excavated bones in the JR-429 *Gryposaurus* bonebed. Black dots denote 1 m grid system. Numbers labeling bones correspond to the field numbers listed in Appendix H. Bones are colored by element type and size category. “Indet.” indicates bones of indeterminate, not intermediate, size that could not be confidently assigned to either the subadult or juvenile size categories. This usually occurs for specimens that are not yet prepared, are fragmentary, or are ribs or vertebral fragments that might be small elements from a subadult, or large elements from a juvenile. “Unknown” indicates specimens that have not yet been prepared and could not be identified in the field.

APPENDIX H

TAPHONOMIC DATA TABLE FOR ALL SPECIMENS (MOR 2573)

COLLECTED FROM THE JR-429 *GRYPOSAURUS* BONEBED

Appendix H Table. Taphonomic data table for all specimens (MOR 2573) collected from the JR-429 bonebed. For bones that have not yet been prepared, field identifications are indicated within parentheses. Bone completeness categories are: Intact (>90% complete), Minor Fracture (76-90% complete), Major Fracture (25%-75% complete), and Fragment (<25% complete). Abrasion and weathering stages follow definitions of Fiorillo (1988). Duplicate field numbers are indicated by grey text.

Field Number	Element type	Identification	Completeness	Size Class	Left/ Right	Length (cm)	Abrasion	Weathering	Trend/ Plunge	Comments
6-12-06-01	rib	rib with head	major fracture	subadult?	-	-	0	0	-	
6-12-06-02	vertebra	caudal neural arch and spine	major fracture	subadult?	-	-	0	0	-	
6-12-06-03	rib	rib fragment	fragment	-	-	5	-	-	-	Not collected.
6-12-06-04	rib	rib fragment	fragment	-	-	-	-	-	Trend 169, Plunge 61 S	Not collected.
6-12-06-05	rib	rib fragment	fragment	-	-	20	-	-	-	Not collected. 20 cm above main bone layer.
6-12-06-06	rib	proximal rib shaft	major fracture	-	-	-	0	0	-	On top of #8 (humerus).
6-12-06-07	rib	partial rib head	fragment	-	-	-	0	0	-	
6-12-06-08	limb	humerus	intact	subadult	right	58.0	0	0	-	
6-12-06-08A	vertebra	partial caudal neural arch	major fracture	-	-	-	0	0	-	
6-12-06-09	rib	rib head	major fracture	-	-	-	0	0	-	
6-12-06-10	skull	jugal	major fracture	subadult	right	-	0	0	-	Unknown whether rostral process was lost pre-burial or due to modern erosion.
6-12-06-11	rib	small rib with head	major fracture	juvenile?	-	-	0	0	-	
6-12-06-12	limb	ulna	intact	subadult	left	~54.5	0	0	-	Distal end weathered away due to surface exposure.
6-12-06-13	pes	metatarsal IV	intact	subadult	right	29.5	0	0	-	
6-12-06-14	pelvis	ischium, proximal	major fracture	subadult	right	-	0	0	-	

Field Number	Element type	Identification	Completeness	Size Class	Left/ Right	Length (cm)	Abrasion	Weathering	Trend/ Plunge	Comments
6-12-06-15	vertebra	duplicate number for neural arch 35	-	-	-	-	-	-	-	Two different portions of a single bone were exposed in field, so it was given two field numbers.
6-12-06-16	skull	frontal	intact	subadult	left	13.2	0	0	-	
6-12-06-17	limb	tibia	intact	subadult	left	89.5	0	0	-	
6-12-06-18	vertebra	caudal neural arch	-	-	-	-	-	-	-	Not salvagable during preparation.
6-12-06-19	?	(?)	-	-	-	-	-	-	-	Small.
6-12-06-20	vertebra	cervical neural arch, left half of posterior cervical	major fracture	subadult	left	-	0	0	-	
6-12-06-21	fragment	bone fragment	fragment	-	-	-	-	-	-	Not salvagable during preparation.
6-12-06-22	?	(? Flat bone)	-	-	-	-	-	-	-	
6-12-06-23	rib	(rib?)	-	-	-	-	-	-	-	
6-12-06-24	fragment	fragment of wide flat bone such as part of the pelvic or pectoral girdle	fragment	-	-	-	0	0	-	
6-12-06-25	flat bone	flat bone fragment	fragment	-	-	-	-	-	-	Not collected.
6-12-06-26	vertebra	partial dorsal neural spine	fragment	-	-	-	0	0	-	
6-12-06-27	rib	small rib with partial head	major fracture	juvenile	-	-	0	0	-	
6-12-06-28	rib	rib fragment	fragment	-	-	-	-	-	-	Not collected.
6-12-06-29	vertebra	caudal centrum	intact	subadult	-	-	0	0	-	

Field Number	Element type	Identification	Completeness	Size Class	Left/ Right	Length (cm)	Abrasion	Weathering	Trend/ Plunge	Comments
6-13-06-30	vertebra	dorsal neural arch and base of spine	major fracture	subadult	-	-	0	0	-	
6-13-06-30A	vertebra	prezygapophysis - caudal?	fragment	subadult?	-	-	0	0	-	
6-13-06-31	rib	rib fragment	fragment	subadult?	-	-	1	0	-	
6-13-06-32	limb	radius	intact	subadult	-	~54	0	0	-	Epiphyses slightly damaged; cannot determine left or right.
6-13-06-33	limb	radius	intact	subadult	opposite side as 475	~51	0	0	-	
6-13-06-34	rib	rib fragment	fragment	-	-	-	1	0	-	
6-13-06-35	vertebra	cervical neural arch	intact	subadult	-	-	0	0	-	
6-13-06-36	pes	pedal phalanx II-2	intact	subadult	left	-	0	0	-	
6-13-06-37	skull	surangular	minor fracture	subadult	left	-	0	0	-	
6-13-06-37A	vertebra	tiny zygapophysis - dorsal?	fragment	juvenile?	-	-	0	0	-	
6-13-06-38	rib	fragment of small rib	fragment	juvenile	-	-	0	0	-	
6-13-06-39	pes	metatarsal II	intact	subadult	left	28.5	0	0	-	
6-14-06-40	rib	rib head and proximal shaft	major fracture	-	-	-	0	0	-	

Field Number	Element type	Identification	Completeness	Size Class	Left/ Right	Length (cm)	Abrasion	Weathering	Trend/ Plunge	Comments
6-14-06-40A	skull	left quadrate, dorsal portion	major fracture	subadult	left	4.1 cm width dorsal condyle	0	0	-	Smaller than 345, so probably too small to match ventral half 643, so could not go with any of the halves.
6-14-06-41	pes	metatarsal IV	intact	subadult	left	27	0	0	-	
6-14-06-42	vertebra	prezygapophysis - dorsal?	fragment	subadult	left	-	0	0	-	
6-14-06-43	pes	metatarsal III	intact	juvenile	left	18.5	0	0	-	
6-14-06-44	vertebra	dorsal neural arch and spine	intact	-	-	-	0	0	-	Was originally thought to be two bones; turns out 44 was the neural spine attached to 62 the neural arch
6-17-06-45	rib	rib with head	major fracture	-	-	-	0	0	-	Found under radius 33
6-18-06-46	rib	rib with head	major fracture	-	-	-	0	0	-	
6-18-06-47	vertebra	dorsal neural arch missing spine	major fracture	juvenile	-	-	0	0	-	
6-18-06-48	skull	jugal	intact	subadult	right	-	0	0	-	
6-18-06-49	vertebra	partial caudal neural arch and spine	minor fracture	-	-	-	0	0	-	
6-18-06-50	pectoral	scapula	intact	subadult	left	-	0	0	-	Upright, sitting on long edge, dorsal side down.
6-18-06-51	rib	rib fragment	fragment	-	-	-	0	0	-	
6-18-06-52	rib	rib fragment	fragment	-	-	-	0	0	-	
6-18-06-53	skull	(maxilla)	intact	subadult	left	-	-	-	-	
6-18-06-54	vertebra	caudal centrum	intact	subadult?	-	-	0	0	-	

Field Number	Element type	Identification	Completeness	Size Class	Left/ Right	Length (cm)	Abrasion	Weathering	Trend/ Plunge	Comments
6-20-06-55	rib	(rib)	-	-	-	-	-	-	-	
6-20-06-56	pes	(phalanx, large)	intact	subadult?	-	-	-	-	-	
6-20-06-57	pectoral	sternal	major fracture	subadult	right	-	0	0	-	
6-21-06-58	limb	duplicate number for femur 66	-	-	-	-	-	-	-	
6-21-06-59	skull	quadrate, ventral half	major fracture	juvenile	right	3.6 cm width ventral condyle	0	0	-	
6-21-06-60	vertebra	zygapophysis	fragment	-	-	-	0	0	-	
6-21-06-61	pes	(metatarsal)	-	-	-	-	-	-	-	
6-21-06-62	vertebra	duplicate number for neural arch 44	-	-	-	-	-	-	-	Two different portions of a single bone were exposed in field, so it was given two field numbers.
6-21-06-63	skull	nasal	minor fracture	subadult	left	-	0	0	-	
6-21-06-64	pes	(metatarsal)	-	-	-	-	-	-	-	
6-21-06-65	vertebra	caudal neural arch and spine, distal in tail	intact	juvenile?	-	-	0	0	-	
6-21-06-66	limb	(femur)	intact	-	-	-	-	-	Trend 12, Plunge 0	Small coprolite and tendon on top. Possible tooth mark.
6-21-06-67	skull	lacrimal	minor fracture	subadult	left	-	0	0	-	
6-21-06-68	vertebra	partial cervical neural arch, right half	major fracture	subadult	right	-	1	0	-	

Field Number	Element type	Identification	Completeness	Size Class	Left/ Right	Length (cm)	Abrasion	Weathering	Trend/ Plunge	Comments
6-21-06-69	?	(?)	-	-	-	-	-	-	-	
6-21-06-70	vertebra	dorsal neural spine	major fracture	subadult	-	-	1	0	-	
6-21-06-71	vertebra	neural arch fragment	fragment	-	-	-	1	0	-	
6-21-06-72	rib	(rib)	-	-	-	-	-	-	-	
6-21-06-73	rib	(rib)	-	-	-	-	-	-	-	
6-21-06-74	skull	lacrimal	intact	subadult	left	-	0	0	-	
6-21-06-75	vertebra	zygapophysis	fragment	-	-	-	0	0	-	
6-21-06-76	vertebra	(neural spine?)	-	-	-	-	-	-	-	
6-21-06-77	vertebra	caudal centrum	intact	subadult	-	-	0	0	-	
6-21-06-78	vertebra	(chevron?)	-	-	-	-	-	-	-	
6-21-06-79	?	(?)	-	-	-	-	-	-	-	
6-21-06-80	skull	frontal	intact	subadult	left	11.5 cm	0	0	-	
6-21-06-81	vertebra	caudal centrum	intact	juvenile	-	-	0	0	-	
6-21-06-82	rib	rib with partial head	major fracture	-	-	-	0	0	-	
6-21-06-83	rib	(rib)	-	-	-	-	-	-	-	
6-21-06-84	rib	(rib)	-	-	-	-	-	-	-	
6-21-06-85	rib	rib fragment	fragment	subadult?	-	-	-	-	-	Not salvagable during prep. Very damaged by modern roots and water.
6-22-06-86	rib	rib fragment	fragment	subadult?	-	-	0	0	-	
6-22-06-87	skull	dentary	minor fracture	subadult	left	tooth row estimated ~31.0	0	0	-	No teeth.

Field Number	Element type	Identification	Completeness	Size Class	Left/ Right	Length (cm)	Abrasion	Weathering	Trend/ Plunge	Comments
6-22-06-88	pelvis	ischium	major fracture	juvenile	right	-	1	0	-	
6-25-06-89	skull	exoccipital	minor fracture	subadult	left	-	0	0	-	Robust.
6-25-06-90	rib	(rib?)	-	-	-	-	-	-	-	
6-25-06-91	pes	duplicate number for metatarsal 95	-	-	-	-	-	-	-	
7-02-06-92	vertebra	caudal vertebra with neural arch but not spine	minor fracture	-	-	-	-	-	-	Higher up than other bones; most caudals were higher than rest, this was just the highest.
7-02-06-93	pes	pedal ungual	intact	-	-	-	0	0	-	High in quarry.
7-03-06-94	vertebra	caudal centrum	intact	-	-	-	0	0	-	Not higher than main bone layer, unlike other centra.
7-03-06-95	pes	metatarsal IV	intact	juvenile	right	19	0	0	-	
7-03-06-96	skull	quadrate, ventral fragment	fragment	subadult	right	-	0	0	-	Fragment of ventral flange, not part of any of the other partial quadrate specimens.
7-03-06-97	vertebra	chevron, missing one side of base	minor fracture	-	-	-	0	0	-	Small.
7-03-06-98	rib	fragment of small rib, may not be hadrosaur	fragment	-	-	-	0	0	-	May not be hadrosaur; may belong to microfossil assemblage.
7-03-06-99	skull	exoccipital, missing distal tip	major fracture	subadult	right	-	0	0	-	
7-03-06-100	vertebra	caudal vertebra	intact	juvenile	-	-	0	0	-	
7-03-06-101	skull	(surangular)	-	subadult	-	-	-	-	-	

Field Number	Element type	Identification	Completeness	Size Class	Left/ Right	Length (cm)	Abrasion	Weathering	Trend/ Plunge	Comments
7-03-06-102	vertebra	caudal neural arch and spine, includes 116	intact	-	-	-	0	0	Part 116: Trend 197, Plunge 2 S. Part 102: Trend 162, Plunge 54 NW.	Broken part of 116. Broken ends are touching. Evidence of trampling? After preparation, 102 and 116 were mended together, and whole bone is now called 102.
7-03-06-103	vertebra	caudal centrum half	major fracture	juvenile	-	-	0	0	-	
7-03-06-104	fragment	bone fragment	fragment	-	-	-	0	0	-	Found on top of dentary 87.
7-03-06-105	pelvis	(proximal ischium)	-	-	-	-	-	-	-	
7-03-06-106	skull	(skull?)	-	-	-	-	-	-	-	
7-03-06-107	vertebra	cervical neural arch	intact	subadult	-	-	0	0	-	Goes with centrum 109.
7-03-06-108	manus	metacarpal 5	intact	subadult	left?	-	0	0	-	
7-03-06-109	vertebra	cervical centrum, anterior half	major fracture	subadult	-	-	0	0	-	Goes with neural arch 107.
7-03-06-110	limb	(fibula)	-	subadult	-	~80	-	-	Trend 95, Plunge 3 W.	

Field Number	Element type	Identification	Completeness	Size Class	Left/ Right	Length (cm)	Abrasion	Weathering	Trend/ Plunge	Comments
7-03-06-111	fragment	bone fragment	fragment	-	-	-	-	-	-	Not collected.
7-03-06-112	manus	manual ungual	intact	subadult?	-	-	0	0	-	
7-05-06-113	rib	rib with head	intact	-	-	-	0	0	-	
7-05-06-114	rib	(rib head)	-	-	-	-	-	-	-	
7-05-06-115	rib	partial rib head	fragment	-	-	-	1	0	-	
7-05-06-116	vertebra	duplicate number for neural arch 102	-	-	-	-	-	-	-	102 and 116 were broken at angle in situ, but mended into single bone after preparation.
7-05-06-117	rib	(rib)	-	-	-	-	-	-	-	
7-05-06-118	rib	(rib with head)	-	-	-	-	1	0	-	Rib shaft has been prepared, now waiting for other jacket with rib head.
7-05-06-119	rib	(rib)	-	-	-	-	-	-	-	
7-05-06-120	vertebra	cervical neural arch, left half	major fracture	-	left	-	0	0	-	Could match with neural arch half 219.
7-05-06-121	limb	ulna	intact	juvenile	left?	~30	0	0	Trend 31, Plunge 12 N	
7-05-06-122	skull	prefrontal	intact	subadult	left	-	0	0	Trend 166, Plunge 88 N. Nearly vertical.	

Field Number	Element type	Identification	Completeness	Size Class	Left/ Right	Length (cm)	Abrasion	Weathering	Trend/ Plunge	Comments
7-05-06-123	rib	rib head fragment	fragment	-	-	-	0	0	-	
7-06-06-124	skull	quadrate, dorsal half	major fracture	juvenile	right	2.8 cm width dorsal condyle	0	0	-	Could match with ventral quadrate half 59.
7-06-06-125	rib	(rib)	-	-	-	-	-	-	Trend 97, Plunge 8 E	
7-06-06-126	vertebra	dorsal neural arch and spine	major fracture	-	-	-	0	0	-	
7-06-06-127	limb	humerus	intact	subadult	left	<63 cm	-	-	-	Fractured and expanded by modern sinkhole mud; too poorly preseved to determine abrasion level.
7-06-06-128	vertebra	dorsal neural arch	major fracture	-	-	-	0	0	-	
7-06-06-129	vertebra	transverse process of dorsal neural arch?	fragment	-	-	-	0	0	-	
7-06-06-130	vertebra	(neural arch)	-	-	-	-	-	-	-	
7-06-06-131	manus	manual phalanx III-1	intact	subadult	right	-	0	0	-	
7-06-06-132	skull	quadrate, ventral half	major fracture	juvenile	left	3.6 cm width ventral condyle	0	0		

Field Number	Element type	Identification	Completeness	Size Class	Left/ Right	Length (cm)	Abrasion	Weathering	Trend/ Plunge	Comments
7-06-06-133	vertebra	neural spine with partial arch	major fracture	-	-	-	0	0	-	
7-06-06-134	vertebra	neural arch fragment	fragment	-	-	-	1	0	-	
7-06-06-135	rib	rib fragment	fragment	-	-	<5	-	-	Trend 103, Plunge 38 E	Not collected.
7-07-06-136	manus	metacarpal half	major fracture	juvenile	-	-	0	0	-	
7-07-06-137	vertebra	caudal centrum	intact	-	-	-	0	0	-	
7-07-06-138	vertebra	dorsal neural spine	major fracture	-	-	-	0	0	-	
7-07-06-139	rib	(rib)	-	-	-	-	-	-	-	
7-11-06-140	rib	rib with head, in two pieces	minor fracture	-	-	-	1	0	-	Head of rib was rotated out of anatomical position so inner curvature was touching costal groove of rib shaft.
7-11-06-141	vertebra	chevron	minor fracture	-	-	-	0	0	-	
7-11-06-142	rib	rib head	major fracture	-	-	-	0	0	-	
7-11-06-142A	skull	partial premaxilla	major fracture	subadult	right	-	0	0	-	
7-11-06-143	rib	rib fragment	fragment	-	-	-	0	0	-	
7-11-06-143A	rib	small rib with head	major fracture	juvenile?	-	-	0	0	-	
7-11-06-144	skull	postorbital	minor fracture	subadult	right	-	0	0	Trend 105, Plunge 58 E	

Field Number	Element type	Identification	Completeness	Size Class	Left/ Right	Length (cm)	Abrasion	Weathering	Trend/ Plunge	Comments
7-11-06-145	limb	fibula? Part of same bone as 170. Epiphyses missing.	major fracture	subadult	-	if fibula, longer than 474	0	0	Trend 188, Plunge 42 N	Bones 145 and 170 part of same fibula. 170 was already merged with 172, which had broken pre-deposition.
7-11-06-146	pes	metatarsal II	intact	juvenile	right	est ~19, much larger than 739 or 330	0	0	-	Severely damaged during fieldwork. Bone was above the main bone layer.
7-11-06-147	vertebra	caudal centrum	minor fracture	-	-	-	0	0	-	
7-11-06-148	rib	rib head	major fracture	-	-	-	0	0	-	Under wood.
7-11-06-149	pelvis	ilium fragment - supra-acetabular process	fragment	subadult	left	-	0	0	-	
7-11-06-150	rib	rib with head	major fracture	-	-	-	0	0	-	
7-11-06-150A	vertebra	caudal neural arch and spine	major fracture	-	-	-	0	0	-	
7-11-06-151	rib	rib fragment	fragment	-	-	-	0	0	-	
7-11-06-152	rib	rib with head	minor fracture	subadult	-	-	0	0	-	
7-11-06-153	rib	rib with head	minor fracture	subadult	-	-	0	0	-	
7-11-06-154	fragment	fragment of small limb bone	fragment	-	-	-	1	0	-	Pathologies on surface.
7-11-06-155	skull	nasal fragment?	fragment	subadult?	left?	-	1	0	-	
7-11-06-156	skull	maxilla	intact	subadult	left	tooth row 29.0	0	0	-	

Field Number	Element type	Identification	Completeness	Size Class	Left/ Right	Length (cm)	Abrasion	Weathering	Trend/ Plunge	Comments
7-11-06-157	skull	exoccipital	intact	subadult	left	-	0	0	-	
7-12-06-158	pes	metatarsal fragment. Distal condyle of metatarsal II or III	fragment	-	-	-	0	0	-	
7-12-06-159	rib	rib head	major fracture	-	-	-	0	0	-	
7-12-06-160	rib	rib shaft, skinny	major fracture	juvenile?	-	-	0	0	-	
7-12-06-161	manus	manual phalanx III-1	intact	juvenile	left	-	0	0	-	
7-12-06-162	rib	rib fragment	fragment	-	-	-	0	0	-	
7-12-06-163	limb	duplicate number for humerus 127	-	-	-	-	-	-	-	Two different portions of a single bone were exposed in field, so it was given two field numbers.
7-13-06-164	fragment	long bone fragment - neural arch? Rib?	fragment	-	-	-	0	0	-	High in section, like most of the caudals.
7-13-06-165	vertebra	neural spine of dorsal neural arch 166	major fracture	-	-	-	0	0	-	Spine 165 and arch 166 were offset in the field, not connected.
7-13-06-166	vertebra	dorsal neural arch	major fracture	-	-	-	0	0	-	Spine 165 and arch 166 were offset in the field, not connected.
7-13-06-167	skull	maxilla	maxilla	subadult	left	tooth row 27.5	0	0	-	

Field Number	Element type	Identification	Completeness	Size Class	Left/ Right	Length (cm)	Abrasion	Weathering	Trend/ Plunge	Comments
7-13-06-167A	fragment	bone fragment with skully texture	fragment	-	-	-	0	0	-	Has maxilla-like texture, but doesn't seem to fit maxilla. Fragment was wrapped in foil in jacket.
7-14-06-168	limb	femur	intact	subadult	left	94.0	0	0	Trend 76, Plunge 6 E	
7-14-06-168A	vertebra	anterior caudal neural arch and spine	intact	-	-	-	0	0	-	
7-14-06-168B	fragment	limb bone fragment	fragment	-	-	-	2	0	-	
7-14-06-168C	rib	small rib fragment with 3-4 raised areas, equally spaced	fragment	-	-	-	0	0	-	Pathologies: 3-4 raised areas, equally spaced. May be a piece of neural spine, and raised areas might be tendon locations.
7-14-06-168D	vertebra	tiny caudal centrum	intact	juvenile?	-	-	0	0	-	
7-14-06-168E	fragment	limb fragment, or possibly extremely robust nasal fragment	fragment	-	-	-	1	0	-	
7-14-06-168F	fragment	bone fragment, probably part of 168E	fragment	-	-	-	0	1?	-	Possibly pre-burial weathering stage 1?

Field Number	Element type	Identification	Completeness	Size Class	Left/ Right	Length (cm)	Abrasion	Weathering	Trend/ Plunge	Comments
7-14-06-168G	fragment	bone fragment, probably part of 168E	fragment	-	-	-	0	0	-	
7-14-06-169	vertebra	partial caudal neural arch and spine	major fracture	-	-	-	0	0	Trend 97, Plunge 10 E	
7-14-06-170	limb	fibula? Part of same bone as 145. Epiphyses missing.	major fracture	subadult	-	if fibula, longer than 474	0	0	#170 Trend 64, Plunge 8 NE, part #172 rotated Trend 5, plunge 9 N.	Broken. Parts 170 and 172 were glued together and now labeled just 170. Likely part of same bone as 145.
7-16-06-171	skull	surangular	minor fracture	subadult	right	-	0	0	-	
7-16-06-172	rib	part of 170 (fibula?)	fragment	subadult	-	-	0	0	Trend 5, Plunge 9 N	Separate from 170 in field, but fit together in preparation.
7-16-06-173	vertebra	caudal centrum	intact	juvenile	-	-	0	0	-	Very high, in top of black mudstone.
7-16-06-174	vertebra	zygapophysis	fragment	-	-	-	0	0	-	
7-16-06-175	vertebra	cervical neural arch, left half	major fracture	subadult	left	-	0	0	-	

Field Number	Element type	Identification	Completeness	Size Class	Left/ Right	Length (cm)	Abrasion	Weathering	Trend/ Plunge	Comments
7-16-06-176	rib	(rib)	-	-	-	-	-	-	Trend 117, Plunge 2 W	Part of rib 125?
7-16-06-177	vertebra	neural arch fragment?	fragment	-	-	-	0	0	-	
7-16-06-178	vertebra	caudal centrum	intact	-	-	-	0	0	-	
7-16-06-179	pes?	metatarsal III?	intact	subadult?	right?	~41.5	-	-	-	Very high. Eaten by roots, and water-damaged by nearby sinkhole, resulting in poor preservation. Difficult to identify and measure due to modern crushing making it appear wider and longer, and poorly preserved ends missing length and morphology.
7-17-06-180	vertebra	duplicate number for neural arch 175	-	-	-	-	-	-	-	Two different portions of a single bone were exposed in field, so it was given two field numbers.
7-17-06-181	skull	jugal	minor fracture	juvenile	left	-	0	0	-	
7-17-06-182	vertebra	(centrum?)	-	-	-	-	-	-	-	High in layer.
7-17-06-183	limb	fibula, missing distal end	minor fracture	subadult	right	~80-82	0	0	-	

Field Number	Element type	Identification	Completeness	Size Class	Left/ Right	Length (cm)	Abra sion	Weath ering	Trend/ Plunge	Comments
7-17-06-184	rib	duplicate number for rib 153	-	-	-	-	-	-	-	Two different portions of a single bone were exposed in field, so it was given two field numbers.
7-18-06-185	skull	squamosal	intact	juvenile	right	-	0	0	-	
7-18-06-186	skull	nasal	major fracture	subadult	right	-	0	0	-	Posterior right nasal 271 probably completes this bone, but contacts are too worn to mend.
7-18-06-186A	vertebra	dorsal neural arch	major fracture	subadult	-	-	0	0	-	
7-18-06-187	rib	(rib with head)	-	-	-	-	-	-	-	
7-18-06-188	rib	rib fragment	fragment	-	-	-	0	0	-	
7-18-06-189	skull	skull fragment?	fragment	-	-	-	0	0	-	
7-18-06-190	skull	duplicate number for nasal 186	-	-	-	-	-	-	-	Two different portions of a single bone were exposed in field, so it was given two field numbers.
7-18-06-191	limb	fibula? Diaphysis only; epiphyeses broken	minor fracture	subadult	-	~60-65	0	0	-	
7-18-06-192	rib	duplicate number for limb bone 248	-	-	-	-	-	-	-	

Field Number	Element type	Identification	Completeness	Size Class	Left/ Right	Length (cm)	Abrasion	Weathering	Trend/ Plunge	Comments
7-18-06-193	rib	rib head, very large	major fracture	adult?	-	-	1	0	-	If correctly identified as a hadrosaur rib, this would be a very large adult hadrosaur. See main text.
7-18-06-194	rib	rib fragment	fragment	-	-	-	1	0	-	May be part of same bone as rib head 193.
7-18-06-195	fragment	bone fragment	fragment	-	-	-	-	-	-	Not collected.
7-18-06-196	vertebra	cervical neural arch, left half	major fracture	-	left	-	1	0	-	
7-18-06-197	vertebra	caudal centrum	intact	juvenile	-	-	0	0	-	Very high, like 179. Above black mudstone.
7-20-06-198	fragment	limb bone fragment, very dense diaphyseal section	fragment	-	-	-	0	0	-	Probably not part of this hadrosaur assemblage. Bone preservation is completely different, very solid and dense.
7-20-06-199	fragment	2 bone fragments	fragment	-	-	-	1	0	-	
7-20-06-200	rib	rib shaft	major fracture	-	-	-	0	0	Trend 78, Plunge 35 W	Higher than most bones, but not as high as 179.
7-20-06-201	vertebra	partial cervical neural arch, right half	major fracture	-	right	-	0	0	-	Higher than most bones, but not as high as 179.

Field Number	Element type	Identification	Completeness	Size Class	Left/ Right	Length (cm)	Abrasion	Weathering	Trend/ Plunge	Comments
7-20-06-202	vertebra	zygapophysis and neural arch fragments	fragment	-	-	-	0	0	-	-
7-20-06-203	rib	rib fragment	fragment	-	-	-	-	-	-	Not collected. Very poor preservation due to modern water damage.
7-20-06-204	?	(?)	-	-	-	-	-	-	-	Very poor preservation due to modern water damage.
7-20-06-205	?	(?)	-	-	-	-	-	-	-	Very poor preservation due to modern water damage.
7-20-06-206	?	(?)	-	-	-	-	-	-	-	Very poor preservation due to modern water damage.
7-21-06-207	pes	partial pedal ungual	fragment	-	-	-	0	0	-	
7-27-06-208	pelvis	(pubis?)	-	-	-	-	-	-	-	
7-27-06-209	rib	rib fragment	fragment	-	-	-	0	0	-	Under 179's jacket.
7-27-06-210	fragment	bone fragment	fragment	-	-	-	-	-	-	Not collected.
7-27-06-211	vertebra	partial cervical neural arch, left side, mostly just postzygapophysis	fragment	subadult	left	-	0	0	-	

Field Number	Element type	Identification	Completeness	Size Class	Left/ Right	Length (cm)	Abrasion	Weathering	Trend/ Plunge	Comments
7-27-06-212	fragment	bone fragment	fragment	-	-	-	-	-	-	Not collected.
7-27-06-213	pelvis	(proximal ischium)	-	-	-	-	-	-	-	Horizontal. Under 200 and 201's jacket
7-27-06-214	limb	proximal end of humerus	fragment	-	right	estimated ~45	0	0	-	
7-27-06-215	vertebra	chevron	major fracture	-	-	-	0	0	Trend 108, Plunge 4 NW	
7-27-06-216	fragment	bone fragment	fragment	-	-	-	0	0	-	Bone fragment with a plant impression touching it.
7-27-06-217	fragment	bone fragment	fragment	-	-	-	-	-	-	Very small fragment, not kept.
7-27-06-218	?	(?)	-	-	-	-	-	-	-	
7-27-06-219	vertebra	partial cervical neural arch, right half	major fracture	-	right	-	1	0	-	Could match with neural arch half 120.
7-27-06-219A	vertebra	zygapophysis, small	fragment	-	-	-	0	0	-	Too small for neural arch 219.
7-27-06-220	vertebra	(neural arch?)	-	-	-	-	-	-	-	
8-06-06-221	pes	metatarsal IV	intact	subadult	left	27	0	0	-	
8-06-06-222	rib	odd small rib or hyoid	minor fracture	-	-	-	0	0	-	
8-06-06-223	rib	(rib fragment)	fragment	-	-	-	-	-	-	
8-06-06-224	rib	(rib fragment)	fragment	-	-	-	-	-	-	
8-06-06-225	?	(?)	-	-	-	-	-	-	-	
8-06-06-226	rib	(rib fragment)	fragment	-	-	-	-	-	-	

Field Number	Element type	Identification	Completeness	Size Class	Left/ Right	Length (cm)	Abrasion	Weathering	Trend/ Plunge	Comments
8-06-06-227	rib	(rib fragment)	fragment	-	-	-	-	-	-	
8-06-06-228	?	(?)	-	-	-	-	-	-	-	
8-06-06-229	rib	(rib head)	-	-	-	-	-	-	-	Probably goes with rib fragment 224.
8-06-06-230	?	(?)	-	-	-	-	-	-	-	
8-06-06-231	fragment	bone fragment	fragment	-	-	-	0	0	-	
8-07-06-232	fragment	bone fragment	fragment	-	-	-	2	0	-	
8-09-06-233	skull	dentary, posteroventral fragment	fragment	subadult	right	tooth row estimated ~31.0	2	0	-	
8-10-06-234	vertebra	caudal neural arch	major fracture	juvenile	-	-	0	0	-	High in section, in black mudstone.
8-11-06-235	skull	skull bone fragment	fragment	-	-	-	-	-	-	
8-11-06-236	pectoral	scapula	minor fracture	subadult	right	estimated ~50 or more	0	0	Trend 125, Plunge 0	
8-11-06-237	?	(?)	-	-	-	-	-	-	Trend 223, Plunge 3 S	
8-11-06-238	limb	(limb bone)	-	-	-	-	-	-	Trend 145, Plunge 6 NW	

Field Number	Element type	Identification	Completeness	Size Class	Left/ Right	Length (cm)	Abrasion	Weathering	Trend/ Plunge	Comments
8-11-06-239	?	(?)	-	-	-	-	-	-	-	
8-11-06-240	limb	ulna	intact	subadult	left	49.5	0	0	Trend 176, Plunge 0	
8-11-06-241	vertebra	caudal neural arch and base of spine	major fracture	-	-	-	0	0	Trend 156, Plunge 3 NW	
8-13-06-242	vertebra	cervical neural arch fragment	fragment	-	right	-	2	0	-	High in black mudstone.
8-13-06-243	vertebra	partial neural arch	major fracture	juvenile	-	-	0	0	-	
8-13-06-244	vertebra	dorsal neural spine	major fracture	subadult?	-	-	0	0	Trend 201, Plunge 7 N	
8-13-06-244A	vertebra	dorsal neural spine half, split saggitally	fragment	-	-	-	1	0	-	
8-13-06-244B	fragment	bone fragment	fragment	-	-	-	1	0	-	
8-13-06-245	-	not bone	-	-	-	-	-	-	-	Initially looked like bone surface, but turned out to just be mudstone.
8-13-06-246	vertebra	caudal centrum	intact	juvenile	-	-	0	0	-	
8-13-06-247	rib	partial rib, split longitudinally	major fracture	-	-	-	-	-	-	Probably mends with rib 296, contact too worn to confirm.

Field Number	Element type	Identification	Completeness	Size Class	Left/ Right	Length (cm)	Abrasion	Weathering	Trend/ Plunge	Comments
8-13-06-248	fragment	bone fragment	fragment	-	-	-	2	0	-	
8-13-06-249	fragment	bone fragment	fragment	-	-	-	-	-	-	Not collected.
8-13-06-250	vertebra	proximal caudal neural arch and spine	minor fracture	-	-	-	0	0	Trend 188, Plunge 2 W	
8-14-06-251	?	(?)	-	-	-	-	-	-	-	
8-14-06-252	?	(?)	-	-	-	-	-	-	-	
8-14-06-253	pes	partial pedal ungual	major fracture	subadult	-	-	0	0	-	High in layer.
8-14-06-254	fragment	end of transverse process?	fragment	-	-	-	0	0	-	Very poor preservation due to modern water damage.
8-14-06-255	fragment	bone fragment	fragment	-	-	-	-	-	-	Very small fragment, not kept.
8-14-06-256	rib	rib w/ partial head	major fracture	-	-	-	0	0	-	Very poor preservation due to modern water damage.
8-14-06-257	vertebra	caudal centrum, with base of right neural arch	minor fracture	juvenile?	-	-	0	0	-	Found months earlier in hole behind quarry, indicating that bone layer extends several meters back. Nail left in place where centrum was to mark it for future mapping.

Field Number	Element type	Identification	Completeness	Size Class	Left/ Right	Length (cm)	Abrasion	Weathering	Trend/ Plunge	Comments
8-15-06-258	-	not bone	-	-	-	-	-	-	-	Initially looked like bone surface, but turned out to just be mudstone.
6-18-07-259	pes	pedal phalanx III-3	intact	subadult	-	-	0	0	-	High in layer.
6-18-07-260	vertebra	zygapophysis, cervical?	fragment	juvenile	-	-	0	0	-	High in layer. May be from same bone as 261.
6-18-07-261	vertebra	neural arch fragment - transverse process of juvenile cervical?	fragment	juvenile	-	-	1	0	-	High in layer. May be from same bone as 260.
6-03-10-262	vertebra	tiny chevron	major fracture	-	-	-	0	0	-	
6-03-10-263	limb	ulna	intact	subadult	left	55.0	0	0	-	
6-03-10-264	limb	radius	intact	subadult	same side as 475	-	0	0	-	
6-03-10-265	fragment	unkown robust bon fragmente with potential sutural surface	fragment	-	-	-	0	0	-	
6-03-10-266	skull	fragment of left premaxilla 304	fragment	subadult	left	-	0	0	-	Mends with left premaxilla 304, but contact not good enough to glue.

Field Number	Element type	Identification	Completeness	Size Class	Left/ Right	Length (cm)	Abrasion	Weathering	Trend/ Plunge	Comments
6-03-10-267	rib	small rib shaft, broken at bend for head	major fracture	juvenile?	-	-	0	0	-	Trend 234, Plunge 9 W
6-03-10-267A	rib	rib head	major fracture	-	-	-	0	0	-	
6-03-10-268	non-hadrosaur	unknown, has texture like tyrannosaur vertebra, not consistent with hadrosaur	-	-	-	-	-	-	-	Non-hadrosaur.
6-03-10-269	rib	small rib head? Unusual expansion on end; doesn't look like skull	major fracture	-	-	-	0	0	-	
6-03-10-270	rib	(rib fragment)	-	-	-	-	-	-	-	
6-03-10-271	skull	posterior nasal	fragment	subadult	right	-	0	0	-	Is match for missing part of right nasal 186, but contacts are not sharp, so can't be sure.
6-03-10-272	vertebra	partial cervical neural arch, left half	major fracture	-	left	-	0	0	-	
6-03-10-273	pes	metatarsal IV	intact	juvenile	right	17.0	0	0	-	

Field Number	Element type	Identification	Completeness	Size Class	Left/ Right	Length (cm)	Abrasion	Weathering	Trend/ Plunge	Comments
6-03-10-274	skull	maxilla fragment, tooth rows, left posterior lateral	fragment	subadult	left	tooth row estimated ~29.0	0	0	-	Maxilla fragment was washed down by modern sinkhole; cannot determine whether maxilla was more intact at time of deposition, and broken in modern times, or whether it was broken this much at time of deposition. Definitely not part of any other collected maxilla.
6-03-10-275	vertebra	flat bone chunk, part of dorsal neural spine?	fragment	-	-	-	0	0	-	
6-03-10-276	vertebra	dorsal centrum with transverse process. Centrum is poorly preserved.	major fracture	-	-	-	0	0	-	High in layer, 30 cm above rest of bones.
6-03-10-277	skull	surangular	minor fracture	subadult	right	-	0	0	-	
6-03-10-278	fragment	(bone fragment)	-	-	-	-	-	-	-	Curving surface texture like wood.
6-03-10-279	limb	humerus	intact	subadult	right	56.0	0	0	-	

Field Number	Element type	Identification	Completeness	Size Class	Left/ Right	Length (cm)	Abrasion	Weathering	Trend/ Plunge	Comments
6-03-10-280	pelvis	ilium, anterior half of ilium 284	major fracture	subadult	left	-	0	0	-	Rotated 180 degrees from proper orientation with the posterior half of the ilium 284.
6-03-10-281	-	not bone	-	-	-	-	-	-	-	Initially looked like bone surface, but turned out to just be mudstone.
6-03-10-282	tendon	tendon with attachment end	major fracture	-	-	-	0	0	-	
6-03-10-283	rib	small rib broken just distal to head	major fracture	juvenile	-	-	0	0	-	
6-03-10-284	pelvis	ilium, posterior half of ilium 280, in two pieces	major fracture	subadult	left	-	0	0	-	284 broken into two pieces, A and B, that are almost touching. Both are rotated 180 degrees from proper orientation with the anterior half of the ilium 280.
6-03-10-285	manus	manual phalanx V-2	intact	subadult	-	-	0	0	-	
6-04-10-286	manus	metacarpal IV	intact	subadult	right	22.4	0	0	-	
6-05-10-287	fragment	fragment of large limb bone	fragment	-	-	-	1	0	-	

Field Number	Element type	Identification	Completeness	Size Class	Left/ Right	Length (cm)	Abra sion	Weath ering	Trend/ Plunge	Comments
6-05-10-288	limb	tibia - diaphysis only	major fracture	subadult	-	-	2	0	-	Many root traces and trample marks. Missing patches of outer cortex. Found lower than main bone layer; if this bone predates the rest of the bonebed, it would explain why it is taphonomically different than all other tibiae.
6-05-10-289	fragment	bone fragment	fragment	-	-	-	-	-	-	Very small fragment, not kept.
6-05-10-290	skull	prefrontal	intact	subadult	right	-	0	0	-	
6-05-10-291	fragment	rib fragment	fragment	-	-	-	-	-	-	Very small fragment, not kept.
6-05-10-292	fragment	rib fragment	fragment	-	-	-	-	-	-	Very small fragment, not kept.
6-06-10-293	rib	(rib fragment)	fragment	-	-	-	-	-	-	
6-08-10-294	rib	rib shaft	major fracture	-	-	-	1	0	-	
6-08-10-295	rib	fragment of small rib shaft	fragment	juvenile?	-	-	1	0	-	
6-08-10-296	rib	partial rib, split longitudinally	fragment	-	-	-	0	0	-	Probably mends with rib 247, contact too worn to confirm.
6-08-10-297	vertebra	dorsal vertebra including centrum and neural arch	intact	-	-	-	0	0	-	

Field Number	Element type	Identification	Completeness	Size Class	Left/ Right	Length (cm)	Abrasion	Weathering	Trend/ Plunge	Comments
6-08-10-298	vertebra	cervical centrum	intact	subadult	-	-	0	0	-	Isolated, no indication which neural arch it should be associated with.
6-08-10-299	vertebra	caudal neural arch and spine	intact	subadult	-	-	0	0	-	
6-08-10-300	vertebra	distal caudal vertebra	intact	subadult	-	-	0	0	-	
6-08-10-301	rib	rib head	fragment	-	-	-	0	0	-	
6-08-10-301A	skull	skull bone fragment?	fragment	-	-	-	0	0	-	
6-10-10-302	pes	metatarsal III	intact	subadult	right	34.5	0	0	Trend 167, Plunge 0	
6-10-10-303	skull	exoccipital	intact	subadult	right	-	0	0	-	
6-10-10-304	skull	premaxilla	minor fracture	subadult	left	-	0	0	-	Mends with premaxilla fragment 266.
6-10-10-305	skull	surangular	intact	subadult	right	-	0	0	-	
6-10-10-306	fragment	bone fragment, epyphysis or centrum?	fragment	-	-	-	0	0	-	
6-10-10-307	pelvis	ilium, anterior fragment	fragment	subadult?	left	-	1	0	-	
6-10-10-308	rib	distal end of rib, nice tapering	fragment	-	-	-	0	0	-	
6-10-10-309	pelvis	ilium, anterior half	major fracture	subadult	right	-	0	0	-	

Field Number	Element type	Identification	Completeness	Size Class	Left/ Right	Length (cm)	Abra sion	Weath ering	Trend/ Plunge	Comments
6-10-10-310	rib	small rib or transverse process	fragment	-	-	-	0	0	-	
6-10-10-311	-	not bone	-	-	-	-	-	-	-	Initially looked like bone surface, but turned out to just be mudstone.
6-10-10-312	-	not bone	-	-	-	-	-	-	-	Initially looked like bone surface, but turned out to just be mudstone.
6-10-10-313	rib	rib with head	minor fracture	juvenile?	-	-	0	0	Trend 151, Plunge 4 S	
6-10-10-314	pes	pedal ungual II	intact	subadult	right	-	0	0		Ventral side up in field.
6-10-10-315	fragment	bone fragment	fragment	-	-	-	0	0	-	
6-10-10-316	vertebra	dorsal neural arch and spine	minor fracture	subadult	-	-	0	0	Trend 148, Plunge 1 S	
6-10-10-317	vertebra	caudal neural arch and spine	intact	-	-	-	0	0	Trend 174, Plunge 5 W	

Field Number	Element type	Identification	Completeness	Size Class	Left/ Right	Length (cm)	Abrasion	Weathering	Trend/ Plunge	Comments
6-10-10-318	pelvis	Very poorly preserved; perhaps partial ilium.	-	-	-	-	-	-	-	Very poor preservation due to modern water damage. Not kept.
6-10-10-319	rib	rib with head	-	-	-	-	-	-	Trend 53, Plunge 5 W.	Not collected. Very poor preservation due to modern water damage.
6-22-10-320	vertebra	fragment of centrum, lateral	fragment	-	-	-	-	-	-	
6-22-10-321	fragment	fragment of large bone, limb or pelvis	fragment	-	-	-	1	0	-	
6-22-10-322	rib	rib with head	major fracture	juvenile	-	-	0	0	-	
6-23-10-323	vertebra	caudal centrum, small	intact	juvenile	-	-	0	0	-	
6-23-10-324	rib	rib head missing outer edge	major fracture	-	-	-	0	0	-	
6-23-10-325	fragment	bone fragment	fragment	-	-	-	1	0	-	
6-24-10-326	skull	splenial, anterior half	major fracture	subadult	right	-	0	0	-	
6-24-10-327	rib	fragment of small rib	fragment	juvenile?	-	-	0	0	-	
6-24-10-328	vertebra	neural arch	major fracture	juvenile?	-	-	1	0	-	
6-25-10-329	rib	fragment of large rib	fragment	subadult?	-	-	1	0	-	
6-25-10-330	pes	metatarsal II	fragment	juvenile	left	estimated ~17	1	0	-	

Field Number	Element type	Identification	Completeness	Size Class	Left/ Right	Length (cm)	Abrasion	Weathering	Trend/ Plunge	Comments
6-25-10-331	rib	rib fragment	fragment	-	-	-	1	0	-	
6-27-10-332	vertebra	dorsal neural arch half with transverse process	major fracture	juvenile	-	-	0	0	-	
6-27-10-333	vertebra	3 fragments, possibly of neural arch. Possibly atlas vertebra?	fragment	-	-	-	0	0	-	
6-27-10-334	rib	rib fragment	fragment	-	-	-	0	0	-	
6-27-10-335	limb	limb diaphysis - fibula? ischium?	minor fracture	-	-	-	0	0	Trend 316, Plunge 0	
6-27-10-336	rib	odd small rib or hyoid	major fracture	-	-	-	0	0	Trend 4, Plunge 13 N	
6-27-10-337	rib	rib with head	major fracture	subadult	-	-	0	0	Trend 39, Plunge 5 SW	
6-27-10-338	rib	rib fragment	fragment	-	-	-	0	0	-	
6-27-10-338A	rib	rib fragment	fragment	-	-	-	0	0	-	
6-27-10-339	skull	basisphenoid	intact	subadult	-	-	0	0	-	
6-29-10-340	rib	small rib with head	major fracture	juvenile?	-	-	0	0	-	

Field Number	Element type	Identification	Completeness	Size Class	Left/ Right	Length (cm)	Abrasion	Weathering	Trend/ Plunge	Comments
6-29-10-340A	skull	skull bone fragment? Possibly fragment of premaxilla posterolateral process, juvenile?	fragment	-	-	-	0	0	-	
6-29-10-340B	skull	skull bone fragment	fragment	-	-	-	0	0	-	
6-29-10-341	rib	rib fragment	fragment	-	-	-	0	0	-	
6-29-10-342	rib	rib fragment	fragment	-	-	-	1	0	Trend 208, Plunge 47 SW	
6-29-10-343	skull	bone fragment. Possibly skull, rib, or vertebra fragment.	fragment	-	-	-	0	0	-	
6-29-10-344	skull	fragment of right dentary 609, posterior 6 tooth rows	fragment	subadult	right	tooth row estimated ~28.0	0	0	-	
7-01-10-345	skull	quadrate	minor fracture	subadult	left	height 33.4	0	0	-	Whole, not broken in half like other quadrates, but missing some of pterygoid flange.

Field Number	Element type	Identification	Completeness	Size Class	Left/ Right	Length (cm)	Abrasion	Weathering	Trend/ Plunge	Comments
7-01-10-346	vertebra	dorsal neural spine, distal portion	fragment	-	-	-	0	0	-	
7-01-10-347	rib	duplicate number for rib 360	-	-	-	-	-	-	-	
7-01-10-348	rib	rib with head	major fracture	juvenile?	-	-	0	0	-	
7-01-10-349	vertebra	sacral neural arch half	major fracture	subadult	-	-	0	0	-	
7-01-10-350	vertebra	partial neural arch with small prezygapophysis, left half. Anterior caudal?	major fracture	subadult?	left	-	0	0	-	
7-01-10-351	pes	metatarsal III	intact	juvenile	left	22.5	0	0	Trend 56, Plunge 0	Modern roots and water fractured bone longitudinally (horizontally in situ) and the halves were slid horizontally so they are slightly displaced, so it looked like two bones in the field (351 and 437).
7-01-10-352	limb	ulna	intact	subadult	right	49.0	0	0	Trend 177, Plunge 1 N	
7-01-10-353	rib	rib shaft, small, complete shaft but missing head	major fracture	juvenile?	-	-	0	0	-	

Field Number	Element type	Identification	Completeness	Size Class	Left/ Right	Length (cm)	Abrasion	Weathering	Trend/ Plunge	Comments
7-01-10-354	manus	manual phalanx V-1	intact	juvenile	right	-	0	0	-	High in layer.
7-01-10-355	limb	humerus	intact	subadult	right	51.0	0	0	-	
7-01-10-356	rib	rib fragment, split longitudinally	fragment	-	-	-	0	0	-	
7-01-10-357	rib	(rib head)	-	-	-	-	-	0	-	
7-01-10-358	rib	rib with head	major fracture	-	-	-	0	0	-	
7-01-10-359	vertebra	caudal neural arch and spine, left half	major fracture	-	left	-	0	0	-	
7-01-10-359A	skull	maxilla	minor fracture	juvenile	left	tooth row estimated ~19-20	0	0	-	
7-01-10-359B	vertebra	partial neural spine	fragment	-	-	-	0	0	-	
7-01-10-359C	rib	partial small rib head	fragment	juvenile?	-	-	0	0	-	
7-01-10-359D	rib	partial rib shaft from near head	fragment	-	-	-	1	0	-	
7-01-10-360	rib	rib with head	minor fracture	juvenile?	-	-	0	0	-	
7-01-10-361	pes	metatarsal IV	intact	juvenile	left	19	0	0	Trend 278, Plunge 0	
7-01-10-361A	rib	rib fragment	fragment	-	-	-	0	0	-	

Field Number	Element type	Identification	Completeness	Size Class	Left/ Right	Length (cm)	Abrasion	Weathering	Trend/ Plunge	Comments
7-01-10-361B	fragment	bone fragment	fragment	-	-	-	0	0	-	
7-01-10-361C	fragment	bone fragment	fragment	-	-	-	0	0	-	Small groove - potential tooth mark? Or tool mark?
7-01-10-362	skull	quadrate	intact?	subadult	left?	-	-	-	-	Poorly preserved and partially damaged during collection due to being in lightly concreted rock. Dorsal and ventral condyles are both partially preserved, but most of quadrate is severely damaged or missing; cannot determine its pre-collection taphonomic state or measure its size.
7-01-10-363	?	(?)	-	-	-	-	-	-	-	
7-01-10-364	limb	limb diaphysis - fibula? ischium?	major fracture	subadult?	-	-	0	0	Trend 324, Plunge 24 N	
7-01-10-365	rib	rib fragment	fragment	-	-	-	0	0	-	
7-01-10-366	pelvis	duplicate number for ilium 442	-	-	-	-	-	-	Trend 221, Plunge 16 E	Two different portions of a single bone were exposed in field, so it was given two field numbers.

Field Number	Element type	Identification	Completeness	Size Class	Left/ Right	Length (cm)	Abrasion	Weathering	Trend/ Plunge	Comments
7-01-10-367	vertebra	dorsal neural arch with left transverse process	major fracture	-	-	-	0	0	-	
7-01-10-368	vertebra	cervical neural arch	intact	subadult	-	-	0	0	-	
7-01-10-369	pelvis	duplicate number for neural arch 368	-	-	-	-	-	-	-	Two different portions of a single bone were exposed in field, so it was given two field numbers.
7-01-10-370	rib	(rib)	-	-	-	-	-	-	-	Trend 188, Plunge 13 W
7-01-10-371	rib	(rib fragment)	fragment	-	-	-	-	-	-	
7-01-10-372	vertebra	(neural arch)	-	-	-	-	-	-	-	
7-01-10-373	rib	(rib)	-	-	-	-	-	-	-	Trend 200, Plunge 7 E
7-01-10-374	fragment	bone fragment	fragment	-	-	-	1	0	-	
7-01-10-375	limb	ulna	intact	subadult	right	54.5	0	0	-	Trend 153, Plunge 12 N
7-05-10-376	fragment	bone fragment, or possibly a carpal	fragment	-	-	-	1	0	-	
7-05-10-377	non-hadrosaur	turtle femur - proximal	-	-	-	-	-	-	-	Non-hadrosaur vertebrate microfossil. Should not have been given a number.

Field Number	Element type	Identification	Completeness	Size Class	Left/ Right	Length (cm)	Abrasion	Weathering	Trend/ Plunge	Comments
7-05-10-378	skull	dentary	intact	subadult	right	tooth row 27.0	0	0	-	Main body of dentary was under other bones; only the coronoid process was visible at the main bone level. The chunk missing from the ventral margin (~2cm) was filled with mud in jacket; missing piece was never present in field. Looks like post-fossilization fracture, but must have occurred prior to burial. 30 tooth rows, but no teeth.
7-05-10-379	pes	metatarsal III	intact	juvenile	left	23.0	0	0	Trend 236, Plunge 18 W	
7-05-10-380	vertebra	sacral neural arch half	major fracture	subadult	-	-	0	0	-	
7-05-10-381	skull	dentary	intact	subadult	left	tooth row 28.5	0	0	-	No teeth.

Field Number	Element type	Identification	Completeness	Size Class	Left/ Right	Length (cm)	Abrasion	Weathering	Trend/ Plunge	Comments
7-06-10-382	skull	duplicate number for dentary 381	-	-	-	-	-	-	-	Two different portions of a single bone were exposed in field, so it was given two field numbers.
7-06-10-383	limb	radius	intact	subadult	opposite side as 475	44.0	0	0	Trend 147, Plunge 2 S	
7-06-10-384	vertebra	caudal centrum, dorsal half	major fracture	-	-	-	0	0	-	
7-06-10-385	skull	fragment of left dentary, posterior tooth rows near base of coronoid process	fragment	subadult	left	tooth row estimated ~28.0	2	0	-	Subadult, but looks small due to abrasion.
7-06-10-386	rib	(rib fragment?)	fragment	-	-	-	-	-	-	
7-06-10-387	rib	partial rib head	fragment	-	-	-	0	0	-	
7-06-10-388	fragment	skull fragment?	fragment	-	-	-	0	0	-	
7-07-10-389	vertebra	(neural spine?)	fragment	-	-	-	-	-	-	Trend 244, Plunge 0
7-07-10-390	skull	vomer	minor fracture	subadult	left	-	0	0	-	
7-07-10-391	manus	manual phalanx IV-1	intact	subadult	right	-	0	0	-	
7-07-10-392	limb	limb epiphysis?	fragment	-	-	-	0	0	-	High in layer.
7-08-10-393	pes	pedal phalanx IV-3?	intact	subadult	left	-	0	0	-	

Field Number	Element type	Identification	Completeness	Size Class	Left/ Right	Length (cm)	Abrasion	Weathering	Trend/ Plunge	Comments
7-08-10-394	pes	metatarsal III	intact	subadult	left	32	0	0	Trend 86, Plunge 16 W	
7-08-10-395	pes	metatarsal IV	intact	subadult	left	26.5	0	0	-	
7-08-10-396	limb	tibia	intact	subadult	left	75.0	0	0	Trend 108, Plunge 2 S	
7-08-10-397	rib	rib head with some proximal shaft	major fracture	-	-	-	0	0	Trend 194, Plunge 5 W	
7-08-10-398	skull	2 fragments: tip of coronoid process of dentary, and curving bone fragment	fragment	-	right	-	1	0	-	Potentially from same bone as 687 for MNI and NISP purposes. Size class difficult to determine; small subadult or large juvenile?
7-08-10-399	pelvis	ischium, proximal shaft to obturaor foramen	major fracture	juvenile	right	-	0	0	-	
7-08-10-400	vertebra	partial caudal neural arch, right prezygapophysis	major fracture	-	right	-	0	0	-	
7-08-10-401	rib	rib shaft	major fracture	-	-	-	0	0	Trend 144, Plunge 9 N	

Field Number	Element type	Identification	Completeness	Size Class	Left/ Right	Length (cm)	Abrasion	Weathering	Trend/ Plunge	Comments
7-08-10-402	skull	skull fragment?	fragment	-	-	-	0	0	-	High in layer.
7-08-10-403	rib	rib fragment	fragment	-	-	-	0	0	-	
7-09-10-404	rib	rib fragment	fragment	-	-	-	-	-	-	Poorly preserved and heavily fragmented small piece of rib; not kept after preparation. Could not determine its pre-collection taphonomic state.
7-09-10-405	fragment	bone fragment	fragment	-	-	-	-	-	-	Poorly preserved very small bone fragment; not kept after preparation. Could not determine its pre-collection taphonomic state.
7-09-10-406	skull	skull fragment?	fragment	subadult?	-	-	-	-	-	Poorly preserved due to being in lightly concreted rock; cannot determine its pre-collection taphonomic state.
7-09-10-407	pectoral	scapula	major fracture	subadult	left	-	0	0	-	Three different portions of a single bone were exposed in field, so it was given three field numbers.

Field Number	Element type	Identification	Completeness	Size Class	Left/ Right	Length (cm)	Abrasion	Weathering	Trend/ Plunge	Comments
7-09-10-408	pectoral	duplicate number for scapula 407	-	-	-	-	-	-	-	Three different portions of a single bone were exposed in field, so it was given three field numbers.
7-09-10-408A	vertebra	fragment of caudal neural spine	fragment	-	right	-	1	0	-	
7-09-10-409	pectoral	duplicate number for scapula 407	-	-	-	-	-	-	-	Three different portions of a single bone were exposed in field, so it was given three field numbers.
7-10-10-410	rib	(rib)	-	-	-	-	-	-	Trend 351, Plunge 4 N	
7-10-10-411	rib	(rib)	-	-	-	-	-	-	-	
7-10-10-412	skull	nasal fragment, middle/posterior portion (missing arch)	fragment	juvenile	right	-	0	0	-	
7-10-10-413	rib	rib shaft	fragment	-	-	-	0	0	Trend 152, Plunge 16 S	

Field Number	Element type	Identification	Completeness	Size Class	Left/ Right	Length (cm)	Abrasion	Weathering	Trend/ Plunge	Comments
7-10-10-414	skull	supraoccipital, exoccipital, prootic, articulated	minor fracture	subadult	left	-	0	0	-	Articulated skull bones. Only other articulated bones in bonebed are frontals with parietals.
7-10-10-415	skull	jugal, posterior half	major fracture	subadult	left	-	0	0	-	Could be same bone as 439 for MNI and NISP purposes.
7-10-10-416	rib	rib fragment	fragment	-	-	-	0	0	-	
7-10-10-417	skull	fragment of surangular?	fragment	juvenile?	-	-	0	0	-	
7-10-10-418	rib	duplicate number for rib 413	-	-	-	-	-	-	-	Two different portions of a single bone were exposed in field, so it was given two field numbers.
7-10-10-419	vertebra	(neural arch)	-	-	-	-	-	-	-	
7-10-10-420	limb	proximal end of fibula?	fragment	subadult?	right	estimated ~80-85	0	0	-	Size right for subadult fibula, but morphology not quite right for either end.
7-10-10-421	fragment	bone fragment	fragment	-	-	-	1	0	-	

Field Number	Element type	Identification	Completeness	Size Class	Left/ Right	Length (cm)	Abrasion	Weathering	Trend/ Plunge	Comments
7-10-10-422	rib	duplicate number for rib 401	-	-	-	-	-	-	-	Under rib 401 in field. Preparation revealed that it was a fragment of rib shaft 401, but had been slightly displaced from rest of rib, and is now glued back in place on 401.
7-10-10-423	skull	maxilla	intact	subadult	right	tooth row 31.5	0	0	-	
7-14-10-424	manus	metacarpal V, slight more than 1/4 of bone	major fracture	subadult	-	-	0	0	-	Was split longitudinally and transversely pre-burial; broken surfaces were all covered with mudstone, not lost during collection or preparation.
7-14-10-425	vertebra	(neural arch)	-	-	-	-	-	-	-	
7-15-10-426	rib	rib head, large	major fracture	subadult	-	-	0	0	-	Not likely same rib as shaft 413 because the proximal end of the head was pointing toward shaft 413.
7-15-10-427	vertebra	sacral neural arch	major fracture	subadult	-	-	0	0	-	
7-15-10-428	rib	rib with head	major fracture	-	-	-	0	0	-	

Field Number	Element type	Identification	Completeness	Size Class	Left/ Right	Length (cm)	Abrasion	Weathering	Trend/ Plunge	Comments
7-15-10-429	non-hadrosaur	Not part of this bonebed. Limb bone, not hadrosaur, element unknown.	-	-	-	-	-	-	-	Very high, at base of concreted layer, on mudstone/sandstone contact. Much larger and higher than the other small bones that floated up high in the bone layer (phalanges, caudal centra, etc). Likely not from this same bonebed event. Lying flat, not plunging.
7-16-10-430	vertebra	centrum fragment?	fragment	-	-	-	1	0	-	High in layer.
7-16-10-431	pelvis	pubis	intact	subadult	left	-	0	0	-	
7-17-10-432	vertebra	cervical neural arch	intact	subadult	-	-	0	0	-	
7-17-10-433	skull?	duplicate number for pubis 431	-	-	-	-	-	-	-	Two different portions of a single bone were exposed in field, so it was given two field numbers.
7-17-10-434	fragment	bone fragment	fragment	-	-	-	-	-	-	Very poor preservation due to modern water damage. Not kept.
7-17-10-435	rib	rib fragment	fragment	-	-	-	0	0	-	

Field Number	Element type	Identification	Completeness	Size Class	Left/ Right	Length (cm)	Abrasion	Weathering	Trend/ Plunge	Comments
7-17-10-436	vertebra	partial small caudal neural arch	fragment	-	-	-	0	0	-	
7-18-10-437	limb	duplicate number for metatarsal 351	-	-	-	-	-	-	Trend 57, Plunge 7 W	Modern roots and water fractured bone longitudinally (horizontally in situ) and the halves were slid horizontally so they are slightly displaced, so it looked like two bones in the field (351 and 437).
7-18-10-438	pectoral	scapula	major fracture	subadult	right	-	1	0	Trend 279, Plunge 3 E	
7-21-10-439	skull	jugal rostral process	fragment	subadult	left	-	0	0	-	Could be same bone as 415 for MNI and NISP purposes.
7-21-10-440	rib	rib fragment, probably, but could also be caudal neural spine	fragment	-	-	-	0	0	-	
7-21-10-441	skull	skull fragment, flat bone	fragment	-	-	-	0	0	-	
7-21-10-442	pelvis	ilium	intact	subadult	right	-	0	0	-	
7-21-10-443	vertebra	cervical neural arch	minor fracture	subadult	-	-	0	0	-	

Field Number	Element type	Identification	Completeness	Size Class	Left/ Right	Length (cm)	Abrasion	Weathering	Trend/ Plunge	Comments
7-21-10-444	pes	metatarsal II	intact	subadult	left	23	0	0	-	
7-22-10-445	limb	radius	intact	subadult	opposite side as 475	51.0	0	0	-	
7-22-10-446	rib	rib head	major fracture	-	-	-	0	0	-	
7-22-10-447	skull	maxilla	intact	subadult	right	tooth row 30.5	0	0	-	Tyrannosaur tooth found underneath maxilla.
7-22-10-448	non-hadrosaur	theropod proximal femur - ornithomimid?	-	-	-	-	-	-	-	
7-23-10-449	rib	fragment of small rib	fragment	juvenile?	-	-	1	0	-	
7-23-10-450	rib	(rib head)	-	-	-	-	-	-	-	
7-23-10-451	rib	fragment of small rib	fragment	juvenile?	-	-	0	0	-	
7-24-10-452	vertebra	dorsal neural arch with left transverse process	major fracture	-	left	-	0	0	-	
7-24-10-453	vertebra	duplicate number for neural arch 452	-	-	-	-	-	-	-	Two different portions of a single bone were exposed in field, so it was given two field numbers.
7-24-10-454	vertebra	(neural arch)	-	-	-	-	-	-	-	High in layer.

Field Number	Element type	Identification	Completeness	Size Class	Left/ Right	Length (cm)	Abrasion	Weathering	Trend/ Plunge	Comments
7-24-10-455	skull	parietal and right frontal, articulated	intact	subadult	right	11.8 cm (frontal)	0	0	-	Articulated.
7-24-10-455A	skull	frontal	intact	subadult	left	12.5 cm	0	0	-	Goes with parietal/frontal 455, but due to a bent part of the parietal, can't actually articulate them
7-24-10-456	vertebra	partial dorsal neural spine	fragment	-	-	-	0	0	-	
7-25-10-457	skull	coronoid process of dentary	fragment	juvenile	left	tooth row estimated ~18.0 maximum	0	0	-	Potentially from same bone as 733 for MNI and NISP purposes.
7-25-10-458	?	(?)	-	-	-	-	-	-	-	
7-25-10-459	vertebra	cervical neural arch half	major fracture	juvenile	-	-	1	0	-	
7-25-10-460	fragment	bone fragment	fragment	-	-	-	0	0	-	
7-25-10-461	rib	rib head	major fracture	-	-	-	0	0	-	
7-25-10-461A	rib	rib fragment	fragment	-	-	-	0	0	-	Found in concave area of rib head 461.

Field Number	Element type	Identification	Completeness	Size Class	Left/ Right	Length (cm)	Abrasion	Weathering	Trend/ Plunge	Comments
7-27-10-462	rib	(rib with head)	-	subadult	-	-	-	-	Trend 18, Plunge 4 W	
7-27-10-463	vertebra	tiny caudal vertebra, complete neural arch	intact	-	-	-	0	0	-	
7-27-10-464	vertebra	(neural spine?)	-	-	-	-	-	-	-	
7-27-10-465	fragment	(bone fragment)	fragment	-	-	-	-	-	-	
7-27-10-466	?	(?)	-	-	-	-	-	-	-	
7-27-10-467	pelvis	(proximal ischium)	-	-	-	-	-	-	-	
7-27-10-468	vertebra	(neural spine?)	-	-	-	-	-	-	-	
7-27-10-469	rib	(rib fragment)	fragment	-	-	-	-	-	-	
7-27-10-470	skull	maxilla	intact	subadult	right	tooth row 28.0	0	0	-	
7-27-10-471	vertebra	dorsal neural spine fragment	fragment	-	-	-	0	0	-	High in layer.
7-27-10-472	?	(?)	-	-	-	-	-	-	-	Very high in layer.
7-27-10-473	limb	radius	intact	subadult	-	44.5	0	0	Trend 224, Plunge 4 W	
7-27-10-474	limb	fibula	intact	subadult	left	72.5	0	0	Trend 179, Plunge 3 SW	

Field Number	Element type	Identification	Completeness	Size Class	Left/ Right	Length (cm)	Abrasion	Weathering	Trend/ Plunge	Comments
7-24-10-455	skull	parietal and right frontal, articulated	intact	subadult	right	11.8 cm (frontal)	0	0	-	Articulated.
7-24-10-455A	skull	frontal	intact	subadult	left	12.5 cm	0	0	-	Goes with parietal/frontal 455, but due to a bent part of the parietal, can't actually articulate them
7-24-10-456	vertebra	partial dorsal neural spine	fragment	-	-	-	0	0	-	
7-25-10-457	skull	coronoid process of dentary	fragment	juvenile	left	tooth row estimated ~18.0 maximum	0	0	-	Potentially from same bone as 733 for MNI and NISP purposes.
7-25-10-458	?	(?)	-	-	-	-	-	-	-	
7-25-10-459	vertebra	cervical neural arch half	major fracture	juvenile	-	-	1	0	-	
7-25-10-460	fragment	bone fragment	fragment	-	-	-	0	0	-	
7-25-10-461	rib	rib head	major fracture	-	-	-	0	0	-	
7-25-10-461A	rib	rib fragment	fragment	-	-	-	0	0	-	Found in concave area of rib head 461.

Field Number	Element type	Identification	Completeness	Size Class	Left/ Right	Length (cm)	Abrasion	Weathering	Trend/ Plunge	Comments
7-27-10-462	rib	(rib with head)	-	subadult	-	-	-	-	Trend 18, Plunge 4 W	
7-27-10-463	vertebra	tiny caudal vertebra, complete neural arch	intact	-	-	-	0	0	-	
7-27-10-464	vertebra	(neural spine?)	-	-	-	-	-	-	-	
7-27-10-465	fragment	(bone fragment)	fragment	-	-	-	-	-	-	
7-27-10-466	?	(?)	-	-	-	-	-	-	-	
7-27-10-467	pelvis	(proximal ischium)	-	-	-	-	-	-	-	
7-27-10-468	vertebra	(neural spine?)	-	-	-	-	-	-	-	
7-27-10-469	rib	(rib fragment)	fragment	-	-	-	-	-	-	
7-27-10-470	skull	maxilla	intact	subadult	right	tooth row 28.0	0	0	-	
7-27-10-471	vertebra	dorsal neural spine fragment	fragment	-	-	-	0	0	-	High in layer.
7-27-10-472	?	(?)	-	-	-	-	-	-	-	Very high in layer.
7-27-10-473	limb	radius	intact	subadult	-	44.5	0	0	Trend 224, Plunge 4 W	
7-27-10-474	limb	fibula	intact	subadult	left	72.5	0	0	Trend 179, Plunge 3 SW	

Field Number	Element type	Identification	Completeness	Size Class	Left/ Right	Length (cm)	Abrasion	Weathering	Trend/ Plunge	Comments
7-27-10-475	limb	radius	intact	subadult	-	48.0	0	0	Trend 165, Plunge 8 N	
7-27-10-476	rib	odd little rib with head	minor fracture	-	-	-	0	0	-	
7-29-10-477	pes	(metatarsal IV)	-	-	-	-	-	-	-	
7-29-10-478	rib	(rib with head)	-	-	-	-	-	-	-	
7-29-10-479	pectoral	(scapula?)	-	-	-	-	-	-	-	
7-29-10-480	vertebra	dorsal neural spine distal fragment	fragment	-	-	-	0	0	-	
7-29-10-481	vertebra	base of anterior caudal neural spine with postzygapophyses	fragment	-	-	-	1	0	-	
7-30-10-482	rib	rib shaft, proximal	fragment	-	-	-	1	0	-	
7-30-10-483	rib	rib shaft, distal	fragment	-	-	-	0	0	-	
7-30-10-484	rib	rib shaft, distal	fragment	-	-	-	0	0	-	
7-30-10-485	rib	rib with head	major fracture	juvenile?	-	-	0	0	-	
7-30-10-486	vertebra	(neural arch)	-	-	-	-	-	-	-	
7-30-10-487	?	(? Small and thin)	-	-	-	-	-	-	-	
7-30-10-488	rib	(rib)	-	-	-	-	-	-	-	
7-30-10-489	rib	(rib?)	-	-	-	-	-	-	-	Under rib 488.
7-30-10-490	fragment	bone fragment	fragment	-	-	-	-	-	-	Very small and poorly preserved fragment. Not kept.

Field Number	Element type	Identification	Completeness	Size Class	Left/ Right	Length (cm)	Abrasion	Weathering	Trend/ Plunge	Comments
7-30-10-491	-	not bone	-	-	-	-	-	-	-	Initially looked like bone surface, but turned out to just be mudstone.
7-30-10-492	?	(?)	-	-	-	-	-	-	-	powdery, 20cm long, curved width, like astragalus but not quite
7-30-10-493	?	duplicate number for 492	-	-	-	-	-	-	-	Two different portions of a single bone were exposed in field, so it was given two field numbers.
7-30-10-494	fragment	bone fragment	fragment	-	-	-	-	-	-	Not collected.
7-30-10-495	vertebra	small proximal caudal centrum (probably, could be distal phalanx)	major fracture	-	-	-	0	0	-	
7-31-10-496	rib	rib fragment	fragment	-	-	-	1	0	-	
7-31-10-497	limb	tibia	intact	subadult	left	77.5	0	0	Trend 290, Plunge 5 N	
7-31-10-498	rib	rib head with some proximal shaft	major fracture	-	-	-	0	0	-	Found in underside of jacket for tibia 497.
7-31-10-499	skull	laterosphenoid	minor fracture	juvenile	right	-	0	0	-	

Field Number	Element type	Identification	Completeness	Size Class	Left/ Right	Length (cm)	Abrasion	Weathering	Trend/ Plunge	Comments
7-31-10-500	fragment	bone fragment	fragment	-	-	-	-	-	-	Very small and poorly preserved fragment. Not kept.
7-31-10-501	fragment	duplicate number for fragment 588	-	-	-	-	-	-	-	
7-31-10-502	skull	(skull?)	-	-	-	-	-	-	-	
7-31-10-503	rib	(rib)	-	-	-	-	-	-	-	
7-31-10-504	?	(? Flat)	-	-	-	-	-	-	-	
7-31-10-505	limb	(humerus)	-	subadult	-	-	-	-	Trend 207, plunge 9 E	
7-31-10-506	skull	(skull?)	-	-	-	-	-	-	-	
7-31-10-507	vertebra	(neural arch and spine)	-	-	-	-	-	-	Trend 131, plunge 2 S	
7-31-10-508	rib	rib head	major fracture	juvenile?	-	-	-	-	-	Could not be collected.
7-31-10-509	rib	rib with head	major fracture	juvenile?	-	-	0	0	-	
7-31-10-510	skull	dentary, missing coronoid process	major fracture	juvenile	right	tooth row estimated ~18.5	0	0	-	
7-31-10-510A	rib	(rib fragment)	fragment	-	-	-	-	-	-	

Field Number	Element type	Identification	Completeness	Size Class	Left/ Right	Length (cm)	Abrasion	Weathering	Trend/ Plunge	Comments
7-05-11-511	limb	Not part of this bonebed. Hadrosaur radius.	-	-	-	-	-	-	Trend 110, Plunge 5 E	Very high, at base of concreted layer, on mudstone/sandstone contact. Much larger and higher than the other, small bones that floated up high in the bone layer (phalanges, caudal centra, etc). Likely not from this same bonebed event.
7-05-11-512	non-hadrosaur	Not part of this bonebed. Theropod phalanx.	-	-	-	-	-	-	-	In concreted sandstone layer of overburden. Not part of this bonebed; should not have been given a number.
7-06-11-513	skull	skull fragment, closest guess is left posterior coronoid process fragment?	fragment	-	left?	-	1	0	-	
7-06-11-514	vertebra	caudal centrum, proximal, small	intact	juvenile	-	-	0	0	-	
7-06-11-515	pelvis	ilium, missing posterior process	major fracture	subadult	left	-	0	0	-	

Field Number	Element type	Identification	Completeness	Size Class	Left/ Right	Length (cm)	Abra sion	Weath ering	Trend/ Plunge	Comments
7-06-11-516	pelvis	duplicate number for ilium 515	-	-	-	-	-	-	-	Two different portions of a single bone were exposed in field, so it was given two field numbers.
7-07-11-517	rib	rib fragment	fragment	-	-	-	1	0	-	
7-07-11-518	fragment	bone fragment, either rib or neural spine	fragment	-	-	-	2	0	-	
7-07-11-519	fragment	limb bone fragment	fragment	-	-	-	2	0	-	
7-07-11-520	fragment	limb bone fragment	fragment	-	-	-	2	0	-	
7-07-11-521	vertebra	caudal centrum, unfused	intact	-	-	-	0	0	-	
7-08-11-522	vertebra	neural arch fragment with 2 zygapophyses, dorsal?	fragment	-	-	-	1	0	-	
7-08-11-523	rib	rib fragment	fragment	-	-	-	1	0	-	
7-08-11-523	fragment	bone fragment	fragment	-	-	-	2	0	-	
7-08-11-524	fragment	bone fragment	fragment	-	-	-	0	0	-	
7-09-11-525	fragment	small fragment of large limb bone	fragment	-	-	-	2	0	-	
7-09-11-526	skull	nasal fragment, anterior	fragment	subadult	left	-	0	0	-	
7-12-11-527	pes	(metatarsal II)	-	-	-	-	-	-	-	
7-12-11-528	skull	laterosphenoid	intact	subadult	right	-	0	0	-	

Field Number	Element type	Identification	Completeness	Size Class	Left/ Right	Length (cm)	Abrasion	Weathering	Trend/ Plunge	Comments
7-12-11-529	limb	femur	intact	subadult	right	84.0	-	-	Trend 200, Plunge 2 W	Wood log was underneath femur.
7-12-11-530	skull	quadrate, dorsal half	major fracture	subadult	right	3.7 cm width dorsal condyle	0	0	-	
7-12-11-531	limb	(humerus)	-	-	-	50.0	-	-	Trend 48, Plunge 1 W	
7-13-11-532	rib	rib head with broken outer margin	fragment	-	-	-	0	0	-	
7-13-11-533	vertebra	caudal centrum, distal	intact	-	-	-	0	0	-	
7-14-11-534	skull	posterior nasal (goes with 535)	fragment	subadult	left	-	0	0	-	Part of same nasal as 535.
7-14-11-535	skull	nasal (goes with 534)	major fracture	subadult	left	-	0	0	-	Part of same nasal as 534.
7-12-11-536	limb	(rib or limb bone)	-	-	-	-	-	-	-	Accidentally had 2 532s, so this one became 536, but that's why 7-12 came after 7-14 in the field number dates.
7-15-11-537	manus	manual phalanx half, subadult V-2	major fracture	subadult	-	-	0	0	-	

Field Number	Element type	Identification	Completeness	Size Class	Left/ Right	Length (cm)	Abrasion	Weathering	Trend/ Plunge	Comments
7-16-11-538	vertebra	caudal centrum	intact	juvenile	-	-	1	0	-	Neural arch was unfused.
7-16-11-539	skull	nasal fragment of posterior naris	fragment	juvenile	left	-	1	0	-	
7-16-11-540	fragment	(thin flat bone fragment)	-	-	-	-	-	-	-	
7-16-11-541	rib	small rib with head	major fracture	juvenile?	-	-	0	0	Trend 279, Plunge 5 NW	
7-17-11-542	vertebra	(vertebral process?)	-	-	-	-	-	-	-	
7-17-11-543	vertebra	caudal centrum, proximal, small	intact	juvenile	-	-	0	0	-	
7-19-11-544	vertebra	dorsal vertebrae transverse process	fragment	juvenile?	-	-	1	0	-	
7-19-11-545	vertebra	caudal centrum	intact	-	-	-	0	0	-	small and distal, but not very elongated
7-19-11-546	pes	metatarsal III	intact	juvenile	left	23.5	0	0	Trend 8, Plunge 14 SW.	
7-19-11-547	skull	presphenoid	intact	subadult	right	-	1	0	-	
7-19-11-548	vertebra	dorsal neural arch, right half	major fracture	-	right	-	0	0	-	
7-19-11-549	tendon	tendon, thick	fragment	-	-	-	0	0	-	
7-19-11-550	skull	nasal fragment, left anterior-middle	fragment	subadult	left	-	1	0	-	

Field Number	Element type	Identification	Completeness	Size Class	Left/ Right	Length (cm)	Abrasion	Weathering	Trend/ Plunge	Comments
7-19-11-550A	skull	laterosphenoid	minor fracture	juvenile	right	-	1	0	-	
7-19-11-551	rib	rib with head	major fracture	-	-	-	0	0	Trend 296, Plunge 6 S	
7-19-11-552	vertebra	dorsal neural spine distal fragment	fragment	subadult	-	-	1	0	-	
7-19-11-553	pelvis	ischium, proximal	major fracture	subadult	left?	-	0	0	Trend 8, Plunge 8 W	
7-19-11-554	vertebra	dorsal neural arch	major fracture	juvenile?	-	-	0	0	-	
7-19-11-555	vertebra	duplicate number for neural arch 554	-	-	-	-	-	-	-	Two different portions of a single bone were exposed in field, so it was given two field numbers.
7-19-11-556	rib	rib with head	major fracture	juvenile?	-	-	0	0	-	
7-20-11-557	pes	phalanx, probably manual. Poorly preserved. If manual, subadult. If pedal, juvenile.	major fracture	subadult?	-	-	0	0	-	Poorly preserved and partially damaged during collection.
7-21-11-558	skull	(skull?)	-	-	-	-	-	-	-	
7-21-11-559	rib	rib head	major fracture	subadult?	-	-	0	0	-	
7-21-11-560	skull	laterosphenoid	minor fracture	subadult	right	-	0	0	-	
7-21-11-560A	vertebra	fragment of neural arch?	fragment	-	-	-	0	0	-	

Field Number	Element type	Identification	Completeness	Size Class	Left/ Right	Length (cm)	Abrasion	Weathering	Trend/ Plunge	Comments
7-21-11-561	pes	pedal phalanx IV-3	intact	juvenile	-	-	0	0	-	
7-21-11-562	skull	quadrate, dorsal half	major fracture	subadult	left	4.15 cm width dorsal condyle	0	0	-	Could be same bone as 643 for MNI and NISP purposes.
7-21-11-563	manus	(metacarpal?)	-	-	-	-	-	-	-	
7-21-11-564	vertebra	(neural spine?)	-	-	-	-	-	-	-	
7-21-11-565	rib	(rib fragment)	-	-	-	-	-	-	-	
7-21-11-566	rib	(rib fragment)	-	-	-	-	-	-	-	
7-21-11-567	limb	(radius?)	-	-	-	-	-	-	-	
7-21-11-568	pelvis	ilium (half prepared)	-	subadult?	-	-	1	0	-	
7-21-11-569	rib	(rib fragment)	-	-	-	-	-	-	-	
7-22-11-570	pectoral	scapula	intact	juvenile	left	41	0	0	Trend 305, Plunge 3 S	~25 cm higher than main bone layer.
7-22-11-571	?	(?)	-	-	-	-	-	-	-	~25 cm higher than main bone layer.
7-22-11-572	pes	metatarsal II	intact	subadult	left	~25 (crushed)	0	0	-	~25 cm higher than main bone layer.
7-23-11-573	fragment	fragment of small limb bone	fragment	-	-	-	0	0	-	
7-23-11-574	skull	frontal	intact	subadult	left	13.6 cm	0	0	-	Goes with parietal 575.

Field Number	Element type	Identification	Completeness	Size Class	Left/ Right	Length (cm)	Abrasion	Weathering	Trend/ Plunge	Comments
7-23-11-574A	skull	frontal	intact	subadult	right	13.6 cm	0	0	-	The two frontals were touching, making them seem like a single bone, which was labeled 574. Goes with parietal 575.
7-23-11-575	skull	parietal	intact	subadult	-	-	0	0	-	Goes with frontals 574 and 574A.
7-23-11-576	vertebra	cervical neural arch half	major fracture	juvenile?	right	-	0	0	-	Very tiny, too small for rest of the juveniles in bonebed. Not sure if this is just a random microfossil or if it is truly part of bonebed.
7-24-11-577	rib	(rib with head)	-	-	-	-	-	-	Trend 119, Plunge 11 S	
7-24-11-578	rib	rib head	major fracture	subadult?	-	-	0	0	-	
7-24-11-579	fragment	fragment of large limb bone	fragment	-	-	-	2	0	-	Possible tooth or trample marks.
7-24-11-580	rib	rib fragment	fragment	juvenile	-	-	-	-	-	Very small and damaged fragment, ~2 cm. Not kept after preparation.
7-24-11-581	pes	astragalus	intact	subadult	-	-	0	0	-	

Field Number	Element type	Identification	Completeness	Size Class	Left/ Right	Length (cm)	Abra sion	Weath ering	Trend/ Plunge	Comments
7-24-11-582	vertebra	dorsal neural arch with transverse process - right half	major fracture	-	right	-	0	0	-	
7-24-11-583	skull	surangular, anterior half	intact	subadult	left	-	0	0	-	Two halves of surangular (583 anterior, 584 posterior) were broken, rotated slightly, and shoved up against each other.
7-24-11-584	skull	surangular, posterior half	intact	subadult	left	-	0	0	-	Two halves of surangular (583 anterior, 584 posterior) were broken, rotated slightly, and shoved up against each other.
7-26-11-585	manus	manual ungual III-3	intact	subadult	left?	-	0	0	-	
7-26-11-586	pes	metatarsal II	intact	subadult	left	24.5	0	0	Trend 250, Plunge 3 NW	
7-26-11-587	limb	(femur)	-	-	-	90.0	-	-	Trend 244, Plunge 7 NW	
7-26-11-588	fragment	bone fragment	fragment	-	-	-	1	0	-	Was originally 501 but got renumbered.

Field Number	Element type	Identification	Completeness	Size Class	Left/ Right	Length (cm)	Abrasion	Weathering	Trend/ Plunge	Comments
7-26-11-589	vertebra	caudal centrum, elongated	major fracture	-	-	-	0	0	-	Neural arch missing, but was fused and broken off.
7-26-11-590	rib	rib fragment	fragment	-	-	-	1	0	-	
7-27-11-591	fragment	flat piece of cortical bone, probably from large flat girdle bone	fragment	-	-	-	0	0	-	
7-27-11-592	rib	rib shaft, probably goes with rib head 593	fragment	-	-	-	1	0	-	592 and 593 may be broken parts of same rib.
7-27-11-593	rib	rib head, probably goes with rib shaft 592	fragment	-	-	-	1	0	-	592 and 593 may be broken parts of same rib.
7-28-11-594	pes	(metatarsal?)	-	-	-	-	-	-	Trend 66, Plunge 4 NW	
7-28-11-595	vertebra	(transverse process)	fragment	-	-	-	-	-	-	
7-28-11-596	limb	ulna	intact	subadult	right	50.0	0	0	Trend 175, Plunge 5 SW	
7-28-11-597	fragment	bone fragment, like sternal or ischium but not	fragment	-	-	-	1	0	-	

Field Number	Element type	Identification	Completeness	Size Class	Left/ Right	Length (cm)	Abrasion	Weathering	Trend/ Plunge	Comments
7-28-11-598	vertebra	neural arch fragment - cervical?	fragment	subadult	-	-	0	0	-	Very poor preservation due to modern water damage.
7-28-11-599	skull	maxilla	intact	subadult	right	tooth row 28.5	0	0	-	
7-28-11-600	pelvis	ilium, anterior fragment	fragment	subadult	left	-	1	0	-	
7-28-11-601	fragment	fragment of medium-large limb bone	fragment	-	-	-	2	0	-	
7-28-11-602	skull	skull - braincase element with cranial nerve foramina, or possibly premaxilla or predentary	fragment	-	-	-	0	0	-	
7-28-11-603	pes	pedal phalanx II-2	intact	subadult	left	-	0	0	-	
7-28-11-604	rib	bone fragment	fragment	-	-	-	1	0	-	
7-29-11-605	manus	metacarpal V fragment, slightly more than 1/4 complete	major fracture	juvenile	-	-	1	0	-	Partially broken in field, but was not intact in mudstone prior to deposition
7-29-11-606	rib	rib shaft	fragment	-	-	-	0	0	-	
7-29-11-607	rib	partial rib head	fragment	-	-	-	0	0	-	

Field Number	Element type	Identification	Completeness	Size Class	Left/ Right	Length (cm)	Abrasion	Weathering	Trend/ Plunge	Comments
7-30-11-608	limb	ulna	intact	subadult	left	-	0	0	Trend 306, Plunge 7 S	
7-30-11-609	skull	dentary, anterior broken, goes with posterior fragment 344	major fracture	subadult	right	-	1	0	Trend of both parts 198, Plunge anterior 3 E, posterior 18 E.	Anterior end was missing pre-burial. Anterior part lying on top of limb 608, posterior end was crushed down over 608.
7-30-11-610	pelvis	ilium	major fracture	subadult	right	-	1	0	-	
7-30-11-611	rib	(rib with head)	-	-	-	-	-	-	-	
7-30-11-612	fragment	fragment of limb bone in two pieces	fragment	-	-	-	1	0	-	30 cm above main bone layer.
7-31-11-613	rib	rib head	major fracture	subadult?	-	-	-	-	-	Damaged due to being in concreted rock; cannot determine its pre-collection taphonomic state.
7-31-11-613A	vertebra	dorsal neural arch	major fracture	subadult?	-	-	-	-	-	Damaged due to being in concreted rock; cannot determine its pre-collection taphonomic state.

Field Number	Element type	Identification	Completeness	Size Class	Left/ Right	Length (cm)	Abra sion	Weath ering	Trend/ Plunge	Comments
7-31-11-613B	rib	rib fragment	fragment	-	-	-	-	-	-	Damaged due to being in concreted rock; cannot determine its pre-collection taphonomic state. Not sure of location in jacket; may or may not be same rib as other 613 rib fragments.
7-31-11-613C	rib	rib fragment	fragment	-	-	-	-	-	-	Damaged due to being in concreted rock; cannot determine its pre-collection taphonomic state. Not sure of location in jacket; may or may not be same rib as other 613 rib fragments.
7-31-11-613D	rib	rib fragment	fragment	-	-	-	-	-	-	Damaged due to being in concreted rock; cannot determine its pre-collection taphonomic state. Not sure of location in jacket; may or may not be same rib as other 613 rib fragments.

Field Number	Element type	Identification	Completeness	Size Class	Left/ Right	Length (cm)	Abrasion	Weathering	Trend/ Plunge	Comments
7-31-11-614	vertebra	centrum fragment, dorsal?	fragment	-	-	-	0	0	-	
7-31-11-615	pes	pedal phalanx IV-1	intact	subadult	right	-	0	0	-	
8-02-11-616	vertebra	caudal neural arch and spine	major fracture	-	-	-	0	0	-	616 and 617 not connected in field; parallel next to each other. Now glued back together.
8-02-11-617	vertebra	fragment of neural spine 616	fragment	-	-	-	-	-	-	617 and 617 not connected in field; parallel next to each other. Now glued back together.
8-02-11-618	vertebra	dorsal neural spine	fragment	-	-	-	0	0	-	Found near and may go with neural arch 627, but no contact surface.
8-02-11-619	rib	(rib fragment)	-	-	-	-	-	-	-	20 cm above main bone layer.
8-02-11-620	vertebra	prezygapophysis - dorsal?	fragment	-	-	-	0	0	-	
8-02-11-621	rib	rib fragment	fragment	-	-	-	-	-	-	Very small fragment. Not collected.
8-02-11-622	rib	rib fragment	fragment	-	-	-	-	-	-	Very small fragment. Not collected.
8-03-11-623	limb	femur	intact	subadult	left	85.0	0	0	Trend 162, Plunge 6 N.	

Field Number	Element type	Identification	Completeness	Size Class	Left/ Right	Length (cm)	Abrasion	Weathering	Trend/ Plunge	Comments
8-03-11-624	fragment	fragament of cancellous bone	fragment	-	-	-	-	-	-	Very small fragment. Not collected.
8-03-11-625	skull	maxilla	intact	subadult	left	tooth row 26.5	0	0	-	
8-03-11-626	vertebra	duplicate number for neural spine 618	-	-	-	-	-	-	-	Two different portions of a single bone were exposed in field, so it was given two field numbers.
8-03-11-627	vertebra	dorsal neural arch, right half	major fracture	-	right	-	0	0	-	Found near and may go with neural spine 618, but no contact surface.
8-03-11-628	rib	rib head	major fracture	-	-	-	0	0	-	
8-03-11-629	pes	metatarsal IV	intact	subadult	left	24.5	0	0	-	
8-03-11-630	limb	distal femoral condyle	fragment	subadult	-	-	-	0	-	Too poorly preseved to determine abrasion level.
8-03-11-631	vertebra	partial neural arch and transverse process	major fracture	-	-	-	0	0	-	
8-03-11-632	limb	(tibia)	-	subadult	-	73.0	-	-	Trend 73, Plunge 5 NW	

Field Number	Element type	Identification	Completeness	Size Class	Left/ Right	Length (cm)	Abrasion	Weathering	Trend/ Plunge	Comments
8-03-11-633	pes	(metatarsal II?)	-	-	-	-	-	-	Trend 0, Plunge 11 NE	
8-03-11-634	vertebra	(chevron)	-	-	-	-	-	-	-	
8-03-11-635	pelvis	(ischium?)	-	-	-	-	-	-	-	
8-03-11-636	skull	dentary	minor fracture	subadult	left	tooth row ~28.0	0	0	Trend 189, Plunge 2 W	
8-03-11-636A	fragment	small flat bone fragment	fragment	-	-	-	0	0	-	
8-04-11-637	rib	rib fragment	fragment	-	-	-	0	0	-	
8-04-11-638	fragment	bone fragment	fragment	-	-	-	1	0	-	
8-05-11-639	rib	rib fragment	fragment	-	-	-	0	0	-	
8-05-11-640	rib	(rib head?)	-	-	-	-	-	-	-	
8-07-11-641	pelvis	(ischium?)	-	-	-	-	-	-	-	
8-07-11-642	pes	pedal ungual III	intact	juvenile	-	-	0	0	-	
8-07-11-643	skull	quadrate, ventral half	major fracture	subadult	left	-	0	0	-	Flattened and distorted. Could be same bone as 562 for MNI and NISP purposes.
8-07-11-644	skull	premaxilla	major fracture	subadult	right	-	0	0	-	
8-07-11-645	rib	rib with head	minor fracture	-	-	-	0	0	Trend 35, Plunge 2 W	

Field Number	Element type	Identification	Completeness	Size Class	Left/ Right	Length (cm)	Abrasion	Weathering	Trend/ Plunge	Comments
8-07-11-646	limb	fibula, proximal half	major fracture	subadult	right	~72.0	0	0	Trend 229, Plunge 9 W.	
8-07-11-646A	vertebra	zygapophysis, from dorsal vertebra	fragment	-	-	-	0	0	-	
8-11-11-647	vertebra	caudal vertebra with neural arch but not spine	minor fracture	-	-	-	0	0	-	
8-11-11-648	pelvis	ischium shaft, partial	fragment	subadult	-	-	1	0	-	
8-11-11-649	pelvis	(ischium?)	-	-	-	-	-	-	Trend 255, Plunge 5 N	
8-11-11-650	skull	quadrate, ventral half	major fracture	subadult	right	4.7 cm width ventral condyle	0	0	-	Other half was always missing; filled with original mudstone, not broken during collection.
8-11-11-650A	fragment	bone fragment	fragment	-	-	-	0	0	-	
8-11-11-651	limb	(limb bone?)	-	-	-	-	-	-	Trend 264, Plunge 4 N	

Field Number	Element type	Identification	Completeness	Size Class	Left/ Right	Length (cm)	Abrasion	Weathering	Trend/ Plunge	Comments
8-11-11-652	limb	(limb bone)	-	-	-	-	-	-	Trend 218, Plunge 3 E	
8-11-11-653	pes	pedal phalanx IV-3	intact	subadult	left	-	0	0	-	
8-12-11-654	vertebra	caudal vertebra with neural arch	intact	-	-	~4.0	0	0	-	
8-12-11-655	limb	(distal epiphysis of humerus?)	-	-	-	-	-	-	-	
8-12-11-656	vertebra	(neural spine?)	-	-	-	-	-	-	-	
8-12-11-657	rib	(rib?)	-	-	-	-	-	-	-	
8-12-11-658	rib	(rib? Or may have been relabeled pubis 691?)	-	-	-	-	-	-	-	
8-12-11-659	vertebra	caudal centrum, small	intact	-	-	-	0	0	-	From the light gray mudstone above the organic black mudstone of the bone layer. Half of vertebra lost during collection.
6-16-12-660	rib	rib fragment	fragment	-	-	-	0	0	Trend 18, Plunge 6 W	

Field Number	Element type	Identification	Completeness	Size Class	Left/ Right	Length (cm)	Abrasion	Weathering	Trend/ Plunge	Comments
6-16-12-661	skull	quadrate, ventral half, robust	major fracture	subadult	right	5.5 cm width ventral condyle	0	0	Trend 350, Plunge 5 NE	~20 cm above main bone layer.
6-16-12-662	fragment	centrum or epiphysis, porous and fragmentary	fragment	-	-	-	1	0	-	~30 cm above main bone layer.
6-17-12-663	fragment	bone fragment	fragment	-	-	-	-	-	-	Very small fragment. Not kept.
6-17-12-664	vertebra	caudal centrum, small	intact	juvenile	-	-	0	0	-	
6-17-12-665	fragment	flat bone fragment	fragment	-	-	-	0	0	Trend 324, Plunge 54 N	
6-17-12-666	limb	(distal epiphysis of humerus?)	-	-	-	-	-	-	Trend 200, Plunge 7 N	
6-17-12-667	rib	(rib fragment)	fragment	-	-	-	-	-	Trend 135, Plunge 15 S	
6-17-12-668	rib	(rib fragment)	fragment	-	-	-	-	-	Trend 79, Plunge 5 W	
6-20-12-669	skull	skull or vertebra fragment	fragment	-	-	-	0	0	-	

Field Number	Element type	Identification	Completeness	Size Class	Left/ Right	Length (cm)	Abrasion	Weathering	Trend/ Plunge	Comments
6-20-12-670	vertebra	neural spine fragment?	fragment	-	-	-	1	0	-	
6-21-12-671	skull	skull fragment	fragment	-	-	-	0	0	Trend 24, Plunge 12 SW	
6-21-12-672	vertebra	caudal neural arch and spine, left half	major fracture	-	left	-	0	0	-	
6-21-12-673	vertebra	transverse process?	fragment	-	-	-	0	0	-	
6-21-12-674	skull	quadrate, ventral fragment, split longitudinally	fragment	-	right	-	1	0	-	Can't match with quadrate 96; they have overlapping parts.
6-21-12-675	vertebra	caudal centrum	intact	-	-	2.0	0	0	-	Damaged during collection.
6-21-12-676	skull	2 bone fragments, possibly skull	fragment	-	-	-	0	0	-	
6-21-12-677	fragment	shard of extremely thin bone - skull fragment?	fragment	-	-	-	0	0	-	
6-21-12-678	rib	partial rib head	fragment	-	-	-	0	0	-	
6-22-12-679	pelvis	pubis, all processes broken	major fracture	subadult	right	-	1	0	Trend 55, Plunge 6 SW	

Field Number	Element type	Identification	Completeness	Size Class	Left/ Right	Length (cm)	Abrasion	Weathering	Trend/ Plunge	Comments
6-23-12-680	rib	fragment of small rib	fragment	juvenile	-	-	0	0	Trend 357, Plunge 61 S	
6-23-12-681	skull	premaxilla, anterior medial portion	fragment	subadult	left	-	0	0	-	From edge of hill with lots of mud infilling cracks and displacing pieces.
6-23-12-682	skull	rostral process of jugal	fragment	subadult?	right	-	1	0	-	Breakage and abrasion may be making it appear smaller than it originally was.
6-23-12-683	pes	pedal phalanx IV-4	intact	subadult	left	-	0	0	-	
6-23-12-684	manus	metacarpal III	intact	subadult	right	22.7	0	0	Trend 130, Plunge 7 SE	
6-23-12-685	vertebra	caudal centrum fragment	fragment	-	-	-	0	0	-	
6-24-12-686	limb	radius	intact	juvenile	-	30.5	0	0	Trend 5, Plunge 2 SW	
6-24-12-687	skull	dentary, anterior half	major fracture	juvenile	right	tooth row estimated ~20.0	0	0	Trend 262, Plunge 4 W	

Field Number	Element type	Identification	Completeness	Size Class	Left/ Right	Length (cm)	Abrasion	Weathering	Trend/ Plunge	Comments
6-24-12-688	rib	rib fragment	fragment	-	-	-	0	0	Trend 259, Plunge 2 S	
6-24-12-689	pectoral	scapula	minor fracture	subadult	left?	estimated ~50 or more	0	0	Trend 15, Plunge 9 N	Was in light concretion, casued surface damage in field and prep
6-24-12-690	limb	fibula, distal end	major fracture	juvenile	left	estimated ~50	1	0	Trend 305, Plunge 1 SE	
6-24-12-690A	fragment	bone fragment	fragment	-	-	-	0	0	-	
6-27-12-691	pelvis	(ischium?)	-	-	-	-	-	-	Trend 230, Plunge 6 NE	
6-27-12-692	vertebra	(vertebral process)	-	-	-	-	-	-	-	
6-27-12-693	limb	(limb bone?)	-	-	-	-	-	-	-	
6-27-12-694	skull	(jugal)	-	-	-	-	-	-	Trend 198, Plunge 3 S	
6-27-12-695	pectoral	(scapula?)	-	-	-	-	-	-	Trend 264, Plunge 5 E	

Field Number	Element type	Identification	Completeness	Size Class	Left/ Right	Length (cm)	Abrasion	Weathering	Trend/ Plunge	Comments
6-27-12-696	rib	(rib)	-	-	-	-	-	-	Trend 265, Plunge 2 E	
6-27-12-697	limb	(limb bone?)	-	-	-	-	-	-	-	
6-27-12-698	skull	basisphenoid, missing most processes	major fracture	subadult	-	-	0	0	-	High in layer, right at contact between sandstone and mudstone. Missing processes, but they appear to have broken off in Cretaceous, not during collection.
6-27-12-699	rib	rib fragment	fragment	-	-	-	-	-	-	Very small fragment. Not kept.
6-28-12-700	rib	(rib)	-	-	-	-	-	-	-	
6-28-12-701	skull	base of exoccipital	fragment	-	-	-	0	0	-	
6-28-12-702	vertebra	dorsal centrum	intact	-	-	-	0	0	Trend 45, Plunge 14 NE	
6-28-12-703	manus	metacarpal III	intact	juvenile	right	12.3	0	0	Trend 337, Plunge 1 S	
6-29-12-704	skull	postorbital	major fracture	subadult	right	-	1	0	-	
6-29-12-704A	fragment	fragment of large bone	fragment	-	-	-	0	0	-	

Field Number	Element type	Identification	Completeness	Size Class	Left/ Right	Length (cm)	Abrasion	Weathering	Trend/ Plunge	Comments
6-29-12-705	rib	rib fragment	fragment	-	-	-	-	-	-	Very small fragment. Not kept.
6-29-12-706	rib	rib fragment	fragment	-	-	-	-	-	-	Very small fragment. Not kept.
6-29-12-707	skull	skull fragment	fragment	-	-	-	0	0	-	
6-29-12-708	rib	small rib with head, shaft split longitudinally and head missing outer edge	major fracture	juvenile?	-	-	0	0	Trend 42, Plunge 7 SW	
6-29-12-708A	fragment	fragment of large limb bone	fragment	-	-	-	2	0	-	Gouge mark, many small scratches, and possible healing pathology.
6-29-12-709	skull	nasal fragment, posterior	fragment	juvenile	left	-	1	0	-	
6-29-12-710	vertebra	cervical neural arch fragment: right transverse process of posterior cervical	fragment	subadult?	right	-	1	0	-	Very large.
6-29-12-711	vertebra	sacral neural arch and spine	major fracture	subadult	-	-	0	0	-	
6-29-12-712	fragment	limb bone fragment	fragment	-	-	-	1	0	-	
6-29-12-713	vertebra	prezygapophysis - dorsal? Maybe caudal?	fragment	-	-	-	1	0	-	
6-29-12-714	skull	nasal fragment, posterior	fragment	subadult?	right	-	0	0	-	Very fragmented, was close to edge of hill.

Field Number	Element type	Identification	Completeness	Size Class	Left/ Right	Length (cm)	Abrasion	Weathering	Trend/ Plunge	Comments
6-29-12-715	vertebra	partial neural arch lamina, dorsal?	fragment	juvenile	left	-	0	0	-	
6-30-12-716	non-hadrosaur	flat shard of tyrannosaur tooth, oddly split and abraded	-	-	-	-	-	-	-	Vertebrate microfossil material, should not have been given a number.
6-30-12-717	fragment	powdery small fragment	fragment	-	-	-	-	-	-	Very small and poorly preserved fragment of bone powder. Not kept.
6-30-12-718	fragment	bone fragment, lightly striated	fragment	-	-	-	1	0	-	
6-30-12-719	fragment	bone fragment, robust and curving	fragment	-	-	-	2	0	-	
6-30-12-720	skull	quadratojugal	intact	subadult	left	-	0	0	-	
6-30-12-721	vertebra	caudal centrum fragment	fragment	-	-	-	0	0	-	
6-30-12-722	non-hadrosaur	Not part of this bonebed. Ceratopsian metatarsal?	-	-	-	-	-	-	Trend 250, Plunge 15 E	~2.5 feet above main bone layer; likely not part of this bonebed.
6-30-12-723	vertebra	caudal neural arch and base of spine, proximal caudal	major fracture	-	-	-	0	0	-	
6-30-12-724	pelvis	ilium fragment, posterior	fragment	subadult	right	-	1	0	-	

Field Number	Element type	Identification	Completeness	Size Class	Left/ Right	Length (cm)	Abrasion	Weathering	Trend/ Plunge	Comments
6-30-12-725	skull	skull bone, thin strut- anterior nasal or posterior premaxilla fragment?	fragment	-	-	-	0	0	-	
6-30-12-726	vertebra	dorsal neural spine	major fracture	subadult	-	-	1	0	Trend 153, Plunge 15 S	
7-3-12-727	skull	fragment of posterior maxilla with ectopterygoid process	fragment	subadult	right	tooth row estimated ~28.5	0	0	Trend 225, Plunge 34 SW	Definitely not part of any other collected maxilla.
7-3-12-728	pes	pedal phalanx III-3	intact	juvenile	-	-	0	0	-	
7-3-12-729	vertebra	caudal centrum	intact	-	-	3.0	0	0	-	
7-3-12-730	fragment	bone fragment	fragment	-	-	-	2	0	-	Many marks on surface - unknown origin - tool/tooth/trample marks?
7-3-12-731	skull	skull fragment? Squamosal or parietal?	fragment	-	-	-	0	0	-	
7-3-12-732	skull	exoccipital base	fragment	subadult	right	-	0	0	-	

Field Number	Element type	Identification	Completeness	Size Class	Left/ Right	Length (cm)	Abrasion	Weathering	Trend/ Plunge	Comments
7-3-12-733	skull	dentary, missing posterior and coronoid process	major fracture	juvenile	left	tooth row estimated ~21.0	0	0	-	Potentially from same bone as 457 for MNI and NISP purposes.
7-3-12-733A	fragment	small squarish flat bone fragment, almost like tip of coronoid process but not	fragment	-	-	-	1	0	-	
7-5-12-734	pes	pedal phalanx	intact	-	-	-	0	0	-	
7-5-12-735	pelvis	ischium shaft, distal	major fracture	subadult	right	-	0	0	Trend 226, Plunge 9 SW	
7-6-12-736	fragment	small fragment of odd rib or skull	fragment	-	-	-	0	0	-	
7-6-12-737	skull	dentary, posterior tooth row fragment	fragment	juvenile	right	-	0	0	-	Potentially from same bone as 510 for MNI and NISP purposes.
7-6-12-738	limb	radius	intact	juvenile	same side as 783, opposite side from 686.	32.0	0	0	Trend 32, Plunge 14 NE	

Field Number	Element type	Identification	Completeness	Size Class	Left/ Right	Length (cm)	Abrasion	Weathering	Trend/ Plunge	Comments
7-6-12-739	pes	metatarsal II, distal half	major fracture	juvenile	left	estimated ~14.5 very rough	0	0	-	
7-6-12-740	vertebra	partial neural arch, late cervical or early dorsal	major fracture	subadult	right	-	0	0	-	
7-7-12-741	limb	fibula, proximal end	major fracture	subadult	right	-	1	0	Trend 70, Plunge 10 NE	
7-7-12-741A	fragment	bone fragment	fragment	-	-	-	1	0	-	
7-9-12-742	rib	rib fragment	fragment	-	-	-	1	0	-	
7-9-12-743	skull	skull fragment-concave cotyle-either subadult postorbital fragment or juvenile squamosal fragment	fragment	-	-	-	0	0	-	
7-9-12-744	fragment	bone fragment-flat bone such as pubis	fragment	-	-	-	1	0	-	
7-9-12-745	rib	small rib with partial head	major fracture	juvenile?	-	-	0	0	Trend 20, Plunge 4 NE	

Field Number	Element type	Identification	Completeness	Size Class	Left/ Right	Length (cm)	Abrasion	Weathering	Trend/ Plunge	Comments
7-10-12-745A	skull	tiny skull fragment or tiny rib head	fragment	-	-	-	0	0	-	
7-10-12-746	rib	small rib with head	major fracture	juvenile?	-	-	0	0	-	
7-10-12-747	skull	skull fragment?	fragment	juvenile?	-	-	0	0	-	
7-10-12-748	skull	frontal fragment	fragment	subadult	-	-	2	0	-	
7-11-12-749	pelvis	(pubis?)	-	(juvenile?)	-	-	-	-	-	
7-11-12-750	limb	(ulna?)	-	-	-	-	-	-	-	
7-11-12-751	rib	(rib fragment)	-	-	-	-	-	-	-	
7-11-12-752	rib	rib fragment	-	-	-	-	-	-	-	
7-11-12-752A	rib	small rib with head	major fracture	juvenile?	-	-	0	0	Trend 329, Plunge 7 SE	
7-11-12-753	rib	rib head	major fracture	-	-	-	0	0	-	
7-11-12-754	pes	pedal phalanx II-1	intact	juvenile	right	-	0	0	-	
7-12-12-755	rib	fragment of rib head	fragment	-	-	-	1	0	-	
7-12-12-755A	fragment	limb bone fragment	fragment	-	-	-	1	0	-	Found under jacket containing rib 745.
7-12-12-756	limb	ulna	intact	juvenile	left	-	0	0	Trend 253, Plunge 1 E	

Field Number	Element type	Identification	Completeness	Size Class	Left/ Right	Length (cm)	Abrasion	Weathering	Trend/ Plunge	Comments
7-13-12-757	skull	dentary	intact	juvenile	right	tooth row 19.0	0	0	Trend 260, Plunge 8 E	
7-14-12-758	limb	(tibia)	-	-	-	-	-	-	-	
7-14-12-759	rib	rib head	major fracture	-	-	-	0	0	-	
7-14-12-760	fragment	(bone fragment)	-	-	-	-	-	-	-	
7-14-12-761	fragment	bone fragment	fragment	-	-	-	0	0	-	
7-14-12-762	vertebra	dorsal neural arch	major fracture	-	-	-	0	0	-	
7-14-12-763	skull	quadrate, ventral half	major fracture	subadult	left	5.5 cm width ventral condyle	1	0	-	
7-18-12-764	fragment	(bone fragment)	-	-	-	-	-	-	-	
7-18-12-765	skull	(quadrate?)	-	-	-	-	-	-	-	
7-20-12-766	vertebra	caudal neural arch fragment	fragment	-	-	-	0	0	-	
7-20-12-766A	vertebra	cervical neural arch half, with postzygapophysis	major fracture	subadult	right	-	0	0	-	
7-20-12-767	fragment	limb bone fragment	fragment	-	-	-	1	0	Trend 212, Plunge 15 SE	
7-20-12-768	vertebra	caudal centrum	intact	-	-	~5.0	0	0	-	

Field Number	Element type	Identification	Completeness	Size Class	Left/ Right	Length (cm)	Abrasion	Weathering	Trend/ Plunge	Comments
7-20-12-769	pes	pedal phalanx IV-3	intact	subadult	right	-	0	0	-	
7-21-12-770	vertebra	fragment of small neural arch?	fragment	juvenile?	-	-	0	0	-	
7-21-12-771	limb	(femur)	-	-	-	-	-	-	Trend 2, Plunge 6 N	
7-21-12-772	fragment	(bone fragment)	-	-	-	-	-	-	-	
7-21-12-773	limb	(humerus?)	-	(juvenile?)	-	-	-	-	Trend 355, Plunge 1 N	
7-21-12-774	?	(limb fragment?)	-	-	-	-	-	-	Trend 24, Plunge 15 SW	
7-22-12-775	skull	unknown fragment-could just be curving rib shaft split longitudinally, but could be anterior nasal or dorsal premaxilla.	fragment	-	-	-	0	0	Trend 117, Plunge 10 NW	
7-24-12-776	vertebra	centrum fragment, elongate	fragment	-	-	-	0	0	-	

Field Number	Element type	Identification	Completeness	Size Class	Left/ Right	Length (cm)	Abrasion	Weathering	Trend/ Plunge	Comments
7-25-12-777	skull	(nasal fragment?)	-	-	(right ?)	-	-	-	Trend 255, Plunge 5 E	
7-25-12-778	pes	(pedal phalanx)	-	-	-	-	-	-	-	
7-25-12-779	fragment	(bone fragment)	-	-	-	-	-	-	-	
7-25-12-780	rib	(rib fragment)	-	-	-	-	-	-	-	
7-25-12-781	limb	(partial radius or ulna)	-	-	-	-	-	-	Trend 120, Plunge 23 SE	
7-25-12-782	rib	(rib fragment)	-	-	-	-	-	-	-	
7-25-12-783	limb	radius	intact	juvenile	same side as 738, opposite side from 686.	~27 cm long, end slightly broken	0	0	Trend 90, Plunge 2 SE	
7-25-12-784	fragment	bone fragment	fragment	-	-	-	-	-	-	Very small and poorly preserved fragment. Not kept.
7-25-12-785	pes	limb bone end, maybe small metatarsal?	fragment	-	-	-	0	0	-	Found directly under 775.
7-25-12-786	skull	maxillary tooth plate fragment	fragment	-	-	-	1	0	-	

Field Number	Element type	Identification	Completeness	Size Class	Left/ Right	Length (cm)	Abrasion	Weathering	Trend/ Plunge	Comments
7-26-12-787	rib	partial rib head	fragment	-	-	-	0	0	-	
7-26-12-788	fragment	fragment-end of limb bone or astragalus	fragment	-	-	-	0	0	-	
7-26-12-789	rib	fragment of small rib	fragment	juvenile?	-	-	0	0	-	
7-26-12-790	pelvis	(ischium?)	-	-	-	-	-	-	Trend 23, Plunge 4 SW	
7-26-12-791	?	(limb fragment?)	-	-	-	-	-	-	Trend 68, Plunge 14 NE	
7-26-12-792	rib	(rib fragment)	-	-	-	-	-	-	-	
7-26-12-793	tendon	tendon	fragment	-	-	-	-	-	-	
7-27-12-794	vertebra	short neural spine - axis?	fragment	subadult?	-	-	1	0	-	
7-27-12-795	rib	rib shaft, split longitudinally	fragment	-	-	-	0	0	-	
7-27-12-796A	skull	skull fragment	fragment	juvenile?	-	-	1	0	-	
7-27-12-796B	fragment	bone fragment	fragment	-	-	-	1	0	-	
7-27-12-796C	fragment	bone fragment	fragment	-	-	-	1	0	-	
7-27-12-796	skull	vomer fragment	fragment	subadult	left	-	1	0	-	
	fragments	82 unnumbered bone fragments: 44 abrasion stage 0, 25 abrasion stage 1, 11 abrasion stage 2, 2 abrasion stage 3								

APPENDIX I

CHARACTER MATRIX BASED ON PRIETO-MÁRQUEZ (2014), IN NEXUS FORMAT

```
#NEXUS

[Freedman Fowler and Horner, Chapter Four, Appendix I]
[Formatted for PAUP 4.0b10 for MAC OS X]

[Matrix is modified from nexus file of Prieto-Márquez 2014 with character states for Gryposaurus reddingi added, as well as one recoding for G. latidens (character 96) and one for G. notabilis (character 124). See main text for details.]

[Prieto-Márquez, A. 2014. Skeletal morphology of Kritosaurus navajovius (Dinosauria: Hadrosauridae) from the Late Cretaceous of the North American south-west, with an evaluation of the phylogenetic systematics and biogeography of Kritosaurini. Journal of Systematic Palaeontology, 12:133-175.]


BEGIN TAXA;
	TITLE Taxa;
	DIMENSIONS NTAX=35;
	TAXLABELS
		Bactrosaurus_johnsoni Equijubus_normani Gilmoreosaurus_mongoliensis
Hadrosaurus_foulkii Lophorhothon_atopus Probactrosaurus_gobiensis Protohadros_byrdi
Tanius_sinensis Telmatosaurus_transsylvanicus Acristavus_gagslarsoni
Kritosaurus_horneri Kritosaurus_navajovius Brachylophosaurus_canadensis
Edmontosaurus_annectens Edmontosaurus_regalis Shantungosaurus_giganteus
Gryposaurus_latidens Gryposaurus_reddingi Gryposaurus_notabilis
Gryposaurus_monumentensis Kerberosaurus_manakini Maiasaura_peeblesorum
Naashoibitosaurus_ostromi Prosaurolophus_maximus 'Sabinosaur PASAC-1'
Saurolophus_angustirostris Saurolophus_morrisi Saurolophus_osborni
Secernosaurus_koerneri Big_Bend_UTEP_37.7 Willinaqake_salitralensis
Wulagasaurus_dongi Corythosaurus_casuarius Lambeosaurus_lambei
Parasaurolophus_walkeri
	;

END;


BEGIN CHARACTERS;
	TITLE  'Matrix in file "PM2014RockyforPAUP4.nex"';
	DIMENSIONS  NCHAR=265;
	FORMAT DATATYPE = STANDARD GAP = - MISSING = ? SYMBOLS = "
0 1 2 3 4 5 6 7";
	CHARSTATELABELS
		1 DTTH1, 2 DTTH3, 3 DTTH4, 4 DTTH14, 5 DTTH5, 6 DTTH6, 7
DTTH7, 8 DTTH10, 9 DTTH12, 10 DTTH13, 11 MXTH1, 12 MXTH3, 13 MXTH4, 14
```

MXTH5, 15 MXTH6, 16 MXTH8, 17 PDT1, 18 PDT3, 19 PDT4, 20 PDT6, 21 PDT7, 22 PDT8, 23 PDT9, 24 PDT11, 25 PDT13, 26 DT1, 27 DT4, 28 DT5, 29 DT6, 30 DT7, 31 DT9, 32 DT11, 33 DT12, 34 DT13, 35 DT14, 36 DT15, 37 DT16, 38 DT17, 39 DT18, 40 DT19, 41 SA1, 42 SA2, 43 SA3, 44 SA4, 45 SA5, 46 ANG, 47 PRAR, 48 PMX1, 49 PMX2, 50 PMX3, 51 PMX5, 52 PMX8, 53 PMX9, 54 PMX6, 55 PMX7, 56 PMX10, 57 PMX11, 58 PMX12, 59 PMX13, 60 PMX14, 61 PMX15, 62 PMX16, 63 PMX17, 64 PMX18, 65 PMX19, 66 PMX20, 67 NS1, 68 NS2, 69 NS3, 70 NS4, 71 NS5, 72 NS6, 73 NS7, 74 NS8, 75 NS10, 76 NS9, 77 MX1, 78 MX2, 79 MX4, 80 MX5, 81 MX18, 82 MX7, 83 MX8, 84 MX9, 85 MX10, 86 MX11, 87 MX12, 88 MX13, 89 MX14, 90 MX15, 91 MX16, 92 MX17, 93 LC1, 94 LC2, 95 J1, 96 J2, 97 J3, 98 J4, 99 J5, 100 J8, 101 J9, 102 J10, 103 J11, 104 J13, 105 Q1, 106 Q2, 107 Q3, 108 Q4, 109 Q5, 110 Q6, 111 PF1, 112 PF2, 113 PF7, 114 PF3, 115 PF4, 116 PF6, 117 PO1, 118 PO2, 119 PO3, 120 PO5, 121 PO6, 122 SQ1, 123 SQ2, 124 SQ3, 125 SQ4, 126 F1, 127 F2, 128 F3, 129 F4, 130 F5, 131 F10, 132 F6, 133 F7, 134 F8, 135 F9, 136 F11, 137 PAR1, 138 PAR2, 139 PAR4, 140 BO1, 141 BO3, 142 BS2, 143 BS3, 144 BS4, 145 BS5, 146 LS1, 147 LS2, 148 EX1, 149 PLT1, 150 PLT2, 151 PLT3, 152 RST2, 153 NPS1, 154 NPS2, 155 NPS3, 156 NPS4, 157 NPS5, 158 NPS6, 159 NPS7, 160 NPS8, 161 NPS9, 162 CMN1, 163 CMN2, 164 CMN3, 165 CRS1, 166 CRS2, 167 CRS3, 168 CRS4, 169 CRS5, 170 CRS6, 171 PLP, 172 ORB, 173 PQF, 174 ITF1, 175 ITF2, 176 ITF3, 177 STF, 178 SK1, 179 SK2, 180 CRV1, 181 CRV2, 182 CRV3, 183 DRS1, 184 DRS2, 185 SCR, 186 CDL, 187 ST, 188 COR1, 189 COR2, 190 COR3, 191 COR4, 192 COR5, 193 COR6, 194 SCP1, 195 SCP2, 196 SCP4, 197 SCP5, 198 SCP6, 199 SCP7, 200 SCP8, 201 SCP9, 202 HM1, 203 HM2, 204 HM3, 205 HM4, 206 UL1, 207 UL2, 208 MN1, 209 MN2, 210 MN3, 211 MN4, 212 MN6, 213 MN7, 214 MN8, 215 IL1, 216 IL3, 217 IL4, 218 IL5, 219 IL6, 220 IL7, 221 IL8, 222 IL9, 223 IL10, 224 IL11, 225 IL12, 226 IL13, 227 IL14, 228 IL15, 229 IL16, 230 IL17, 231 IL18, 232 IL19, 233 IL21, 234 PB1, 235 PB2, 236 PB3, 237 PB4, 238 PB5, 239 PB6, 240 PB7, 241 PB8, 242 PB9, 243 PB10, 244 PB11, 245 IS1, 246 IS3, 247 IS4, 248 IS5, 249 IS6, 250 IS7, 251 IS8, 252 IS9, 253 IS10, 254 IS11, 255 IS12, 256 FM1, 257 FM2, 258 TB, 259 AS, 260 DSTS, 261 PES1, 262 PES3, 263 PES4, 264 PES6, 265 PES7 ;

MATRIX

Bactrosaurus_johnsoni 0110(1 2)102000111(0 1)101001010001100 10(0 1)0100011011011010010000000000010--0000?-00--1?10-
1010000101100000002100101111000000000011000111 00-
0100001001001110000??100?-?0--0010-00----
1010000?000?1?0?10200000010010101010 0??10?1?12001101111(0 1)11000100?120011111111111021001111 0?01010

Equijubus_normani
01??0000000??000010100 00?001?01000?0????0010?0?0000000000000000--00001-00-010?0-1??000000??000000000011000010000000000?010???000-0100?01000?0???0?0???100-00--0010-00----
001000?00000?00??????????????????????????????0000000010 00??000?0?????????????????????????????

Gilmoreosaurus_mongoliensis
01102?????01111100?00010?001001???10001?????????????????????????????0000?-
????1?10-
201000?111100?0?00??0??0111100????00?????????????010?????????????????????0?-??--
00????0----??????????0???????200000?00010101011{0
1}??1????12101101112011010 1)?????0???1111111011000111 0?01000
Hadrosaurus_foulkii
????131100???111???
??????????2??
????????-
??????????????????????????????????000110???????120123??112????1011?????11????011?
00?0---111??0????
Lophorhothon_atopus
????22110?0??111?????????????????????????????????????00000??????00???-011-
1?00-2????0?????0?00?00?????01111100000000?0??20001100-
0100001?01??????00?00?0?-?0--0?11010-5--0??1000?1???????001000000001-
00000210??10?1?12?02102?1??00010111??1101??11021????0---1010?01000
Probactrosaurus_gobiensis
011011000000??0??0?000010?00100100010001??0?0???000?000000000000??000??-
????10?????0???0?00???000000?????????????????000?00?001??00-
0100?0100??????0?0??0?0?-?0--0?1???0----
?0?100001?????0?00100000000000000011??01?11?000000001000110001000120 1???1
11100101100000????1000
Protohadros_byrdi 01??01(0
1)10011??11000??14101220110001001100010000?1100000000000000000--00?0?-
????1110-101010?1011??000001001201 00?0000?1????????00-
010000??????????????0101-00--0010-00----
0???00?0??????????????????????????000??
??????????????
Tanius_sinensis
??-00--
??????????????????????000000001 01??1????0?0001?1?0?11100-
0100?0100110??1000001???-??????????0----
0???000?11??2??????????1000000001 00?????????120101011111111010000?????????????
?????????1?????????
Telmatosaurus_transsylvanicus
01??1200110?1110?????????00000100000011 0?110010?0000000000000000--00???-00-
-1?10-2010?002111??0??00????001??11?????00?????00?1100-
0100?010?11???100???1101-00--0?1???0----
0?0?0000?01??
??????????????
Acristavus_gagslarsoni 1220231100112111?????????2(0
1)001111?01112111110102131101000000000?0-0001??-00--1110-
202111122210001111221 1????1?0100000111100200000-

1100001001111120?1??1?00-?0--0111?00----
010110000?????????????????????????1?11?????????????????????????????1110111?????
???????11????????

Kritosaurus_horneri
??2023120022?2?????????????????????1?????????????????????0000000????00010-10--
102213?211?02???0111101???0???????0100000111?0?0?000-
1?00?0100?????????????201-?0--0112010-5--
010001011???
???????????????

Kritosaurus_navajovius 1220231200211?01??1041?020010(0
1)1001112111110101121101000?000011000??0-10--10{1
2}213?211?0232???111012310201121107?00?00011120?0?000-
1100?01001??10?10??01201-?0--0?1????-?--
010001011???2?????????????????????
???????????????

Brachylophosaurus_canadensis 1220231200112111211122113(0 1 2)(0 1
2)011110111211111010213110100000000(0 1)0-000111-00--1110-
202111122210001111221110112110100000(0
1)11100100010111000020011112001101(1 2)00-10--0113010-2--
010110000111101111121121111(0 1)1-
011011211112111202220301210001111121111111101122110---1110101011

Edmontosaurus_annectens 2320131200212112011?1141130(0
1)010110011121111101021311110000000(0 1)0-000221-00--1101-
202111232100110010302101120101100001211010100 0-
010000200110111012011000-10--0111200----010110000011001111211211111 1-01(1
2)111(0 1)1111111112122312012100011111310111101202122(0 1)00---1110101010

Edmontosaurus_regalis 2320231200212112011?1141130(0
1)010110011121111101021311111000000000-000221-00--1101-
202111232100110010302101120101100001211010100 0-
010000200110111012011000-10--0111200----010110000011001111211111111-
012111111111111120223120121000111113101111011021211 00---1110101010

Shantungosaurus_giganteus
232013120022??11??2???0???2020101100??121?????10????????00000????-?00???-?0-
?1?01-
202111?2?21?????????????1112010??0000?111?0201?00?0100?02001???????2????0?-
?0--0?1??00----0????00?1?0?1110112111010011-
00211111??1????121223120121000111113?0111111002122110---1110?00010

Gryposaurus_latidens
13200311001?211??????????2210111100111211111010212 1?01?0000001010000010-
???0102203021110232 1??1100113002??????0???00?0??020?0??00?????????????????
??1?01-?0--0111010-1--0?0?0????01?0?11112111110011-111(0
1)1201??1????11?12112112200011111411111?012????????0---????????10

Gryposaurus_reddingi 1???13120011211{1 2}?????????1(1
2)00111100111211111 0????21??10000000?01??00010-

01?01?2203021110231O?11001(1 2)?10201121101000000110201010001100002?01?0111002??1201-30--0111010-1--010?010???1?0???1??????100(0 1)1-111(0 1)1(0 1)1{0 1}??11{1 2}1?1?122{0 1}?2012?000?11114??111?0??0?1????0---1110??1?10

Gryposaurus_notabilis 13201212001121l?020010410(1 2)(1 2)(0 1)01111001112111110101121101000000010110000010-01111022030211102321011110113112011211010000001102O(0 1)01000-11000020011011100200120l-30--0111010-1--0100010110110011112111110011-111(1 2)1(1 2)11111111111122112012O???1111141111l???201122100---1110101110

Gryposaurus_monumentensis 13201312001121120110104102210111?001112111110101121101000000010110000l0-01111022030211102321011110123112011211010000001102O?01000-1100?02001??11100?001201-30--0111010-1--010101011???2?????????????????????????---??????????

Kerberosaurus_manakini ??????????2?211???0?????????00???-????1?1??202111?1?21??11001030110l1??1010000??????0?01?00-??000?20011????0?2??1?0?-?0--0?11??????-0?0???

Maiasaura_peeblesorum 122023120011211?121112211211011111011121111101021311010000000010-000111-00--1110-202111122210001111221110112110100100011100200000-1100?0(1 2)0011111200110110O-00--0112011-4--0101100001111011?1211?111111-011011111l?2111202220301210001111121111111l101122110---111010?011

Naashoibitosaurus_ostromi ???023120?2?2112?????????????????1?????????????????????000????????000?0-10-0101202021110232100111011311101121101000000111201O?000-1000?010011?1?0002?01?0?-?0--0111110-1--0101000?1?11?????????????????????1??2???

Prosaurolophus_maximus 2321231200212l1?0(2 3)10114111(0 1)0010110011121111101021211010000000001010022l-10--10120202111023210111001(0 1)300201110101001001111201O?000-0100002001101100020O?002-20--0112110-5--010110001?110011112112111111-11111(1 2)1111111111212(2 3)21211220001111140111120120212211O---1110101110

'Sabinosaur PASAC-1' 232???????212l???????????1100101100111212?????10?????????00?????????????-????1?12?202?11?2321????????????0112110?????0?????0?0???????????20011?1101?2?0??0?-?0--0?????0----0?0????????1?1?1??111?2?0??01-11?????????????????222120121000111114011l1?11202122100---111???????

Saurolophus_angustirostris 2321131200212l1?02101041120001011001112111110101121101000100000201002l1-

00--10120202111023210111001030 0(1
2)0111010100101211121200011100 10?1210110??0002??1002-20--0113110-3--
0101100011110111112112111111-
012210011 11?111121232120122000111114111 11??1102112010---1110101110
Saurolophus_morrisi
23?11312002?211??????1??0201??0110011?21?11101??1211010????0??010100???-
???-
1??20202?1??2321??110010??020111?10?????0?1????2000?????10?1?0??????????2???0
00-?0--0????1?----?????000?????????1?????1??11-
?11211???11?1??1110
Saurolophus_osborni
232123120021211?0310104 1?2000101100111211111010112110100010000010100221-
00--10120202111023210111001030 0(1
2)0111010100101211121200011100?0?1?101101?0002001002-20--0113110-3--
010110?01111011 1?12112111111-01?21{0
1}01111??111212321201220001111141111 1??110?1???10---1110101110
Secernosaurus_koerneri
12??2312001 1?11???1??????0210111100?112??1?1?10?????????0?????????00???-
?10?1?20-??211??2121?????????????????????0100000?1???0?01000-
1100002001101?0002??????-?0--0??????-?--0?????0?1?1?1???111011110011-
11????1???1????1112210211211311111140111120120212212 0---111??0????
Big_Bend_UTEP_37.7
??
??
???????-?????????????0?????111111??01-1111111{1
2}??1??1?120221120121131101 1????111?01?0012??00---11???0???0
Willinaqake_salitralensis 1220231200112 11??????????0(1
2)1011110011121?1?1??0???1??10?0?????0?-?00???-????1?20-
??2111?2321?????????????????1???0?-?0--
01110??-??-??????????1?1???111011110011-
112111????1????1112210211211311111 1??1111??1202122020---1110?01?10
Wulagasaurus_dongi {1
2}??????????????????????????101??11??01?121????????????????????????????????????
?????211??2221???1??1???0101?2??????????????????????????????202??????0??????????
?????????????-?????????????????1????2?110?1-
?01111?????????12?223020?2????????1???????????0?1???00?????????????
Corythosaurus_casuarius 1220221111112 11?0311113101(1 2)(0
1)0111100111211111110111110000112101-01--214--100--0-01-2121121232110212 11(0
1)1011100001200102101111120101010011100111101100000 01(0 1)1-0-100120--
120621010102101011111011211111111101002210121111111120223121121000111101 1
011111112111202101011111 00110
Lambeosaurus_lambei 1(1 2)20(2 3)21111(1 2)121110(2 3)1011(3
4)1011011110011121111111011110000112211-01--213--000--0-01-(1
2)121121232110212 11(0

1)10111000012001011011111201010100111001111011010000111-0-110120--
122630010102101011111011211111110010??1{0 1}1{1
2}11111111202231211210001111012?0111111121112011010111110111
0
Parasaurolophus_walkeri
1220?????????111031?1141010201111001112111111101111000010000 4-01--2??--000-
-0-11-
11211?1232?1?3121101020100001200102121112120000100012100111?????0?0??121-
1-021220--12270-
010112101?11111??12111111110001221001111001112023312112000011?1011011111?
102111201 1?1111??1????0

;

END;
BEGIN ASSUMPTIONS;
OPTIONS DEFTYPE = unord PolyTcount = MINSTEPS;
TYPESET * UNTITLED = unord: 1 - 265;

END;

begin paup;
log file = PM2014Rocky_log.nex replace;
outgroup Equijubus_normani;
set criterion = parsimony taxlabels = full torder = right maxtrees = 5000 increase = no
root = outgroup outroot = monophyl storebrlens = yes warnreset = no warntree = no
warntsave = no warnroot = no warnredef = no autoclose = yes;
hsearch start = stepwise hold = 2 addseq = simple limitperrep = no usenonmin = yes swap
= tbr steepest = yes multrees = yes;
PSet MSTaxa = Variable opt = acctran;
describetrees 1 / root = outgroup plot = phylogram apolist = yes;
savetrees root = yes file = PM2014Rocky_tre.nex replace format = altnex brlens = yes;
contree all / strict = yes semistrict = no majrule = no adam = no root = outgroup treefile =
PM2014Rocky_tre.nex append = yes;
bootstrap nreps = 5000 grpfreq = no conlevel = 50 search = heuristic / addseq = random
nreps = 1 swap = TBR steepest = no multrees = yes;
savetrees from = 1 to = 1 root = yes file = PM2014Rocky_tre.nex append = yes format =
altnex savebootp = brlens;
log stop;

END;